

**FIELD, LABORATORY, AND ANALYTICAL INVESTIGATION OF
ANGLES-WITH-PLATE RETROFIT FOR DISTORTION-INDUCED
FATIGUE IN STEEL BRIDGES**

By

Kathleen S. McElrath

Submitted to the graduate degree program in
Civil, Environmental, and Architectural Engineering
and the Graduate Faculty of the University of Kansas
in partial fulfillment of the requirements for the degree of
Doctor of Philosophy.

Committee Co-Chairman _____
Dr. Caroline Bennett

Committee Co-Chairman _____
Dr. Adolfo Matamoros

Committee Members _____
Dr. Stanley Rolfe

Dr. Jian Li

Dr. Lisa Friis

Date Defended: _____

The Dissertation Committee for Kathleen S. McElrath certifies
that this is the approved version of the following dissertation:

**FIELD, LABORATORY, AND ANALYTICAL INVESTIGATION OF
ANGLES-WITH-PLATE RETROFIT FOR DISTORTION-INDUCED
FATIGUE IN STEEL BRIDGES**

Committee Co-Chairman _____
Dr. Caroline Bennett

Committee Co-Chairman _____
Dr. Adolfo Matamoros

Committee Members _____
Dr. Stanley Rolfe

Dr. Jian Li

Dr. Lisa Friis

Date Approved: _____

Executive Summary

Prior to the mid-1980s, steel girder bridges were designed with a detail susceptible to distortion-induced fatigue cracking. While a number of retrofit measures have been developed to repair this problem, many of those retrofits have long-term performance issues or are difficult and expensive to implement. Recent research at the University of Kansas has focused on the development of a new retrofit measure that could be effective in repairing distortion-induced fatigue cracking while also being inexpensive and easier to install than currently available retrofits. This new retrofit measure, referred to as the “angles-with-plate” retrofit, stiffens the problematic region and redistributes distortion-induced fatigue stresses away from cracking prone areas. By eliminating the need for cumbersome installation procedures, the angles-with-plate retrofit also provides a more economical repair that can be implemented with minimal traffic interruptions.

This dissertation is presented in three parts and appendices. Part I provides a brief overview of distortion-induced fatigue cracking and the development of the angles-with-plate retrofit. Part II gives details and findings of an experimental investigation of the performance of the angles-with-plate retrofit and a stiffened version of the angles-with-plate retrofit on a 9.1 m (30 ft.) laboratory test bridge. Part III describes field and analytical tests performed on an active steel girder bridge system near Park City, Kansas on which the angles-with-plate retrofit was used as a repair for distortion-induced fatigue cracking.

Acknowledgements

This dissertation would not have been possible without the support and contributions of many people at the University of Kansas. Special appreciation is due to Drs. Caroline Bennett and Adolfo Matamoros for the knowledge and guidance they provided throughout this research. I would also like to thank Drs. Stanley Rolfe, Jian Li, and Lisa Friis for their willingness to support me and be a part of this research. Several undergraduate students should be recognized for their hard work in helping me complete this research including, Riley Piles, Zach Olson, Patrícia Aguiar, Nick Crain, and Cody Gibbens. In addition, I would like to thank technicians Matt Maksimowicz, David Woody, and Eric Nicholson for their invaluable assistance in the laboratory. I am also indebted to the following graduate students for their contributions to this work: Amanda Hartman, Temple Richardson, Alisha Elmore, and Say Hak Bun.

I would also like to express gratitude for funding support provided by the Kansas Department of Transportation (KDOT), the University of Kansas Transportation Research Institute (KU TRI), and the Transportation Pooled Fund Study TPF 5(189).

Finally, I would like to thank my family for their unconditional encouragement and support.

Table of Contents

Part I: Introduction

Distortion Induced-Fatigue in Steel Bridges	1
Angles-with-Plate Retrofit.....	1

Part II: Experimental Investigation of Distortion-Induced Fatigue Repair in 9.1 m [30 ft.] Test System

Abstract.....	4
Introduction.....	5
Background	6
Objective and Scope.....	9
Experimental Program	9
<i>Girder Specifications</i>	<i>10</i>
<i>Loading</i>	<i>12</i>
<i>Instrumentation</i>	<i>12</i>
<i>Retrofit Specifications</i>	<i>15</i>
<i>Cracking and Inspection</i>	<i>16</i>
Test 1	17
Test 2	18
<i>Test Trials</i>	<i>18</i>
Results and Discussion.....	22
<i>Crack Initiation and Propagation.....</i>	<i>23</i>
Crack Initiation – Test 1	23
Crack Initiation – Test 2.....	24
Crack Propagation Pattern – Test 1	26
Crack Propagation Pattern – Test 2.....	27
Trials 1.1N-1.7N Crack Growth (North Girder Test 1 Trials)	29
Trials 1.1S-1.7S Crack Growth (South Girder Test 1 Trials)	33
Trials 2.1N-2.7N Crack Growth (North Girder Test 2 Trials)	35
Trials 2.1S-2.7S Crack Growth (South Girder Test 2 Trials)	41
<i>Girder Cross Frame Strains</i>	<i>42</i>
Test 1	42
Test 2	44
<i>Lateral Girder Deflection</i>	<i>47</i>
Test 1	47
Test 2	49
Conclusions.....	50
References	52

Part III: Field and Analytical Testing of Angles-With-Plate Retrofit for Distortion-Induced Fatigue in Kansas Bridge 135-87 (043/044)

Abstract.....	54
Introduction.....	55
Background	56
<i>Development of the Angles-With-Plate Retrofit.....</i>	<i>57</i>
<i>History of Kansas Bridge 135-87(043/044).....</i>	<i>62</i>
<i>Retrofit Recommendation for Kansas Bridge 135-87(043/044)</i>	<i>64</i>
Objective	67
Field Tests	68
<i>Instrumentation</i>	<i>69</i>
<i>Loading</i>	<i>74</i>
Finite Element Models.....	74
Top Web Gap Comparison	80
Results and Discussion.....	81
<i>Global Behavior – Field and FEM Investigations.....</i>	<i>81</i>
<i>Local Behavior - Field and FEM Investigations</i>	<i>85</i>
<i>Top Web Gap Behavior - FEM Investigation</i>	<i>89</i>
Conclusions.....	95
References	97

Appendix A: Test Specimen Specifications

Girders	99
Retrofit	104
Load Cells	106
Concrete Deck	107
Gage Placement.....	111
<i>Lateral Girder Deflections – LVDTs or String Potentiometers.....</i>	<i>111</i>
<i>Vertical Girder Deflections – LVDTs</i>	<i>111</i>
<i>Strain Gages.....</i>	<i>112</i>
<i>Strain Transducers.....</i>	<i>113</i>
<i>Gage Labeling.....</i>	<i>113</i>

Appendix B: Calibration Constants

Strain Transducers from Bridge Diagnostics Inc. (BDI)	115
Linear Variable Differential Transformer (LVDT)	115
String Potentiometers	116
Load Cells	116

Appendix C: Loading Protocol

Pump Protocol	117
<i>Turning the Pump On for 90 GPM Pump</i>	117
<i>Turning the Pump Off for 90 GPM Pump</i>	117
Actuator Warm-Up	118
Tuning	118
New Program	118
Testing	119

Appendix D: Finite Element Study

PARAMETRIC RETROFIT ANALYSIS FOR DISTORTION-INDUCED FATIGUE IN A 9.1 M (30 FT.) TEST BRIDGE	120
--	------------

Appendix E: Experimental Data

Concrete Material Properties	149
Crack Growth	150
<i>North Girder – Test 1</i>	150
<i>South Girder – Test 1</i>	152
<i>North Girder – Test 2</i>	155
<i>South Girder – Test 2</i>	158
Load Distribution	160
<i>Test 1</i>	160
<i>Test 2</i>	161
Experimental Data Plots	162
<i>Test 1</i>	163
<i>Test 2</i>	194
Experimental Log	213
<i>Test 1</i>	213
<i>Test 2</i>	244

Appendix F: Kansas Bridge 135-087 (043/044) Plans

Original Plans	267
Repair Plans	278

Appendix G: Filtered Field Test Data

Before Retrofit	289
After Retrofit	307

Appendix H: Field Test and Finite Element Analyses Results

Field Test and Complementary Finite Element Analyses	331
Top Web Gap Behavior Finite Element Analyses	340

List of Figures

Part I: Introduction

N/A

Part II: Experimental Investigation of Distortion-Induced Fatigue Repair in 9.1 m [30 ft.] Test System

Figure 1: Out-of-plane rotation causing distortion-induced fatigue.	6
Figure 2: Test set-up for 2.8 m [9.3 ft.] girder sub-assembly testing (Alemdar et al. 2013a; 2013b).	8
Figure 3: (a) Dimensions and schematic of test region cross frames. (b) Girder span and load application.	11
Figure 4: Instrumentation placements for (a) LVDTs, (b) string potentiometers, and (c) strain gages.	13
Figure 5: Retrofit as applied to top web gap in test specimen.	15
Figure 6: Stiffened angles-with-plate retrofit applied to exterior girders in Trials 1.7 and 2.2-2.7.	16
Figure 7: Crack definition for (a) interior side of girder web at cross frame connection plate and (b) exterior or fascia side of girder web.	17
Figure 8: Strains in top web gaps at (a) 0 cycles and (b) 15,000 cycles. Top web gap denoted by T in legend and bottom web gap denoted by B. Number denotes gage location from Figure 4(c).	24
Figure 9: Strains in top web gaps at (a) 15,000 cycles, (b) 30,000 cycles, and (c) 45,000 cycles. Top web gap denoted by T in legend and bottom web gap denoted by B. Number denotes gage location from Figure 4(c).	25
Figure 10: North girder crack growth around transverse connection plate in Test 1.	30
Figure 11: North cross frame failure during Trial 4N.	31
Figure 12: South girder crack growth around transverse connection plate in Test 1.	33
Figure 13: North girder crack growth along transverse connection plate in Test 2.	36
Figure 14: North girder crack growth along flange-web weld in Test 2.	36
Figure 15: Broken bolt at the end of Trial 2.3N.	38

Figure 16: Crack found in cross frame connection plate at the south face of the center girder. ..	39
Figure 17: South cross frame connection plate four-angle repair from (a) northeast, (b) northwest, (c) southeast and (d) southwest face of center girder.....	39
Figure 18: South cross frame tab plate failure from (a) east and (b) west side of cross frame. ...	40
Figure 19: South girder crack growth around transverse connection plate and flange-web weld in Test 2.....	41
Figure 20: Cross frame strains for (a) uncracked, unretrofitted at 0 cycles, (b) cracked at 150,000 cycles, (c) cracked, unretrofitted at 1.35 million cycles, and (d) cracked, retrofitted at 1.35 million cycles.	44
Figure 21: Cross frame strains for (a) uncracked, unretrofitted at 0 cycles, (b) cracked, unretrofitted at 1.25 million cycles, (c) cracked, unretrofitted at 2.45 million cycles, and (d) cracked, retrofitted at 2.45 million cycles.	45
Figure 22: Cross frame strains for (a) cracked, retrofitted at 3.05 million cycles, (b) cracked connection plate at 3.41 million cycles.....	46
Figure 23: Cross frame strains for (a) repaired connection plate at 3.41 million cycles, and (b) cracked cross frame tab at 3.59 million cycles.	47
Figure 24: Girder lateral displacements at 150,000 cycles (end of Trials 1S and 1N) for (a) unretrofitted and (b) retrofitted conditions.	48
Figure 25: Girder lateral displacements at 1.35 million cycles for (a) unretrofitted and (b) retrofitted conditions.	49
Figure 26: Girder lateral displacements at 50,000 cycles for (a) unretrofitted and (b) retrofitted conditions.....	50

Part III: Field and Analytical Testing of Angles-With-Plate Retrofit for Distortion-Induced Fatigue in Kansas Bridge 135-87 (043/044)

Figure 1: Test set-up for 2.8 m (9.3 ft.) girder subassembly test (Alemdar, Overman, et al. 2013a).	58
Figure 2: Test set-up for 9.1 m (30 ft.) three girder test bridge (Hartman 2013).	60
Figure 3: Cross-section of Kansas Bridge 135-87(043/044).	63
Figure 4: Plan of Kansas Bridge 135-87(043/044); circled areas indicate locations where cracks have been reported.	63

Figure 5: Types of cracks occurring in Kansas Bridge 135-87(043/044).....	64
Figure 6: Cross frame geometry of Kansas Bridge 135-87(043/044) (Richardson 2012).....	66
Figure 7: Angles-with-plate retrofit recommended to KDOT for repair of Kansas Bridge 135-87(043/044) (Richardson 2012).....	67
Figure 8: Details of retrofit applied to the bridges.....	68
Figure 9: Cracking at the instrumentation location on the (a) stiffener side (b) non-stiffener side.	69
Figure 10: Strain gage locations for both tests on the (a) stiffener side (b) non-stiffener side. Green highlighting indicates that the strain gage was placed in the same location for the second test, yellow highlighting indicates that the strain gage was moved for the second test, and red highlighting indicates that the strain gage was not applied for the second test.	71
Figure 11: BDI strain transducer locations for both tests in (a) section view (b) plan view.	72
Figure 12: Photograph of LVDT placement similar to that used in the first and second field test.	73
Figure 13: (a) Full scale model with concrete deck (b) Full scale model without concrete deck (c) stiffener side of Girder C with angles-with-plate retrofit (d) non-stiffener side of Girder C with angles-with-plate retrofit.....	75
Figure 14: Crack patterns modeled at (a) top web gap (b) bottom web gap.....	77
Figure 15: Truck tire contact area dimensions and placements, as measured in the field.	78
Figure 16: Truck load modeled in (a) west lane (b) bridge center (c) east lane.	79
Figure 17: Maximum principal stress paths (a) HSS 1 (b) HSS 2.....	81
Figure 18: Girder flange BDI results from field tests and FE analyses for (a) west truck load placement (b) center truck load placement (c) east truck load placement. Bottom flange BDIs are shown on the left side of the figure, while top flange BDIs are shown on the right. Legend stresses are in ksi. *FE analyses values.....	83
Figure 19: Cross frame BDI results from field tests and FE analyses for (a) west truck load placement (b) center truck load placement (c) east truck load placement. Legend stresses are in ksi. *FE analyses values.	84

Figure 20: String potentiometer results from field tests and FE analyses for (a) west truck load placement (b) center truck load placement (c) east truck load placement. *FE analyses values.	85
Figure 21: Maximum principal stresses for center load truck placement at (a) top web gap, before retrofit (b) top web gap, after retrofit (c) bottom web gap, before retrofit (d) bottom web gap, after retrofit. Legend stresses are in ksi.	87
Figure 22: Directional stresses for center load truck placement at (a) top web gap, before retrofit (b) top web gap, after retrofit (c) bottom web gap, before retrofit (d) bottom web gap, after retrofit. Legend stresses are in ksi. *FE analyses values.	87
Figure 23: Maximum principal stresses for west load truck placement at (a) top web gap, before retrofit (b) top web gap, after retrofit (c) bottom web gap, before retrofit (d) bottom web gap, after retrofit. Legend stresses are in ksi.	88
Figure 24: Directional stresses for west load truck placement at (a) top web gap, before retrofit (b) top web gap, after retrofit (c) bottom web gap, before retrofit (d) bottom web gap, after retrofit. Legend stresses are in ksi. *FE analyses values.	88
Figure 25: Maximum principal stresses at top web gap for west load truck placement when both the connection plate-to-web and flange-to-web weld cracks are present for (a) stiffener side, before retrofit (b) stiffener side, after retrofit (c) non-stiffener side, before retrofit (d) non-stiffener side, after retrofit. Legend stresses are in ksi.	90
Figure 26: Maximum principal stresses at top web gap for center load truck placement when both the connection plate-to-web and flange-to-web weld cracks are present for (a) stiffener side, before retrofit (b) stiffener side, after retrofit (c) non-stiffener side, before retrofit (d) non-stiffener side, after retrofit. Legend stresses are in ksi.	90
Figure 27: Maximum principal stresses at top web gap for east load truck placement when both the connection plate-to-web and flange-to-web weld cracks are present for (a) stiffener side, before retrofit (b) stiffener side, after retrofit (c) non-stiffener side, before retrofit (d) non-stiffener side, after retrofit. Legend stresses are in ksi.	91
Figure 28: Maximum principal stresses at top web gap when only connection plate-to-web weld crack is present for (a) west load truck placement, before retrofit (b) west load truck placement, after retrofit (c) center load truck placement, before retrofit (d) center load	

truck placement, after retrofit (e) east load truck placement, before retrofit (f) east load truck placement, after retrofit. Legend stresses are in ksi.....	92
Figure 29: Maximum principal stresses at top web gap when only flange-to-web weld crack is present for (a) west load truck placement, before retrofit (b) west load truck placement, after retrofit (c) center load truck placement, before retrofit (d) center load truck placement, after retrofit (e) east load truck placement, before retrofit (f) east load truck placement, after retrofit. Legend stresses are in ksi.....	93
Figure 30: Top web gap crack locations in Kansas Bridge 135-87(043/044) with crack types indicated.....	95

Appendix A: Test Specimen Specifications

Figure A. 1: Specimen plan.	99
Figure A. 2: Specimen girder elevations.....	100
Figure A. 3: Specimen cross frame elevations.....	101
Figure A. 4: Specimen stiffener details.....	102
Figure A. 5: Specimen splice details.....	103
Figure A. 6: $\frac{3}{4}$ in. Retrofit Dimensions.	104
Figure A. 7: $\frac{3}{4}$ in. Stiffened Retrofit Dimensions.....	105
Figure A. 8: Deck reinforcement.	107
Figure A. 9: Deck reinforcement for center panel.	108
Figure A. 10: Deck panel and hole layout.	109
Figure A. 11: Details for deck framing and attachment to girder flanges.	110
Figure A. 12: Lateral deflection monitoring for (a) LVDT placement and (b) String Potentiometer placement.....	111
Figure A. 13: Web gap strain gage placements.	112
Figure A. 14: BDI placements.	113

Appendix B: Calibration Constants

N/A

Appendix C: Loading Protocol

N/A

Appendix D: Finite Element Study

Figure 1: Girder sub-assembly set-up for 2.8 m [9 ft.] testing and finite element modeling (Alemdar et al. 2013a; 2013b).	122
Figure 2: Hot spot stress at (a) HSS-1 crack and (b) HSS-2 crack for no retrofit, F-F retrofit, and S-S retrofit (Przywara 2013).	123
Figure 3: (a) Overall model with concrete deck, (b) overall model without concrete deck, (c) deflected model with concrete deck, deflection scale=425, (d) deflected model without concrete deck, deflection scale=425, and (e) deflected section cut at mid-span, deflection scale=100.	125
Figure 4: (a) Dense mesh (2.54 mm [0.1 in.]) in web gap region transitions to coarse mesh (25.4 mm [1.0 in.]) and (b) mesh sensitivity study for changing dense region mesh.	127
Figure 5: Cracking and maximum principal hot spot stresses (Nagati 2012).	129
Figure 6: Hot Spot Stress Paths for (a) interior connection plate side or connection plate-web weld, (b) exterior fascia side or flange-web weld.	130
Figure 7: Views of various retrofits examined in finite element models: (a) angles-with- plate retrofit; (b) stiffened angles-with-plate retrofit; (c) positive attachment between transverse connection stiffener and top flange retrofit; and (d) full depth back-up stiffener bearing on top and bottom flanges.	131
Figure 8: Percentage of uncracked hot spot stresses with change in horseshoe crack length for connection plate-web weld and flange-web weld.	132
Figure 9: Percentage of uncracked hot spot stresses with change in longitudinal crack length for connection plate-web weld and flange-web weld.	133
Figure 10: Maximum principal stresses with scale from 0 MPa to 138 MPa [0 ksi to 20 ksi] for (a) unretrofitted model with normal deck stiffness and (b) unretrofitted model with reduced deck stiffness and a 51 mm [2 in.] crack. Legend stresses are in ksi.	135
Figure 11: Girder lateral deflections with unbroken cross frame elements and broken cross frame element framing into the north girder top web-gap.	137

Figure 12: Girder deflection profiles for (a) 25 mm [1 in.] cracked and retrofitted model and (b) 25 mm [1 in.] cracked and retrofitted model with broken north cross frame element. ..	138
Figure 13: Maximum principal stresses for model replicating Trial 2.3N under the stiffened angles-with-plate repair with (a) functioning bolt, shown from fascia side, (b) missing bolt, shown from fascia side, (c) functioning bolt, shown from stiffener side, and (d) missing bolt, shown from stiffener side. Legend stresses are in ksi.	140
Figure 14: Maximum principal stresses for model replicating Trial 2.7N under the stiffened angles-with-plate repair with (a) functioning bolt, shown from fascia side, (b) missing bolt, shown from fascia side, (c) functioning bolt, shown from stiffener side, and (d) missing bolt, shown from stiffener side. Legend stresses are in ksi.	141
Figure 15: Percent of uncracked stress at (a) connection plate-web weld and (b) flange-web weld for various retrofit techniques and crack lengths.	143
Figure 16: Percentage of uncracked hot spot stresses for connection plate-web weld and flange-web weld with various retrofit conditions and a 51 mm [2 in.] horseshoe crack.	144

Appendix E: Experimental Data

Figure E. 1: Deck Layout and Labeling.....	149
Figure E. 2: North girder crack growth.....	150
Figure E. 3: South girder crack growth.....	152
Figure E. 4: North girder crack growth.....	155
Figure E. 5: South girder crack growth.....	158
Figure E. 6: Static (0 Cycles) 5.24.2012.....	163
Figure E. 7: Static (15000 Cycles) 5.24.2012.....	164
Figure E. 8: Static (20000 Cycles) 5.25.2012.....	165
Figure E. 9: Static (30000 Cycles) 5.29.2012.....	166
Figure E. 10: Static (45000 Cycles) 5.31.2012.....	167
Figure E. 11: Static (60000 Cycles) 5.31.2012.....	168
Figure E. 12: Static (75000 Cycles) 6.01.2012.....	169
Figure E. 13: Static (90000 Cycles) 6.04.2012.....	170
Figure E. 14: Static (105000 Cycles) 6.05.2012.....	171

Figure E. 15: Static (120000 Cycles) 6.06.2012.....	172
Figure E. 16: Static (135000 Cycles) 6.06.2012.....	173
Figure E. 17: Static (150000 Cycles) 6.07.2012.....	174
Figure E. 18: Static (150000 Cycles) 7.24.2012.....	175
Figure E. 19: Static (150000 Cycles) 09.18.2012 - Without Retrofit.....	176
Figure E. 20: Static (150000 Cycles) 9.27.2012 – With Retrofit	177
Figure E. 21: Static (1350000 Cycles) 12.07.2012– Without Retrofit	178
Figure E. 22: Static (1350000 Cycles) 12.07.2012 – With Retrofit	179
Figure E. 23: Static (2550000 Cycles) 12.21.2012 – With Retrofit	180
Figure E. 24: Static (2550000 Cycles) 12.21.2012 – Without Retrofit	181
Figure E. 25: Static (2550000 Cycles) 01.03.2013 - Without Retrofit Drilled Holes	182
Figure E. 26: Static (2550000 Cycles) 01.04.2013 - With Retrofit Drilled Holes	183
Figure E. 27: Static (3611097 Cycles) 01.17.2013 - With Retrofit Cracked Cross Frame Drilled Holes	184
Figure E. 28: Static (3611097 Cycles) 01.22.2013- With Retrofit New Crossframe 0.5in Hole	185
Figure E. 29: Static (3611097 Cycles) 01.22.2013 - Without Retrofit New Crossframe 0.5in Hole.....	186
Figure E. 30: Static (3611097 Cycles) 01.22.2013 - Without Retrofit New Crossframe	187
Figure E. 31: Static (4811097 Cycles) 02.15.2013 - Without Retrofit.....	188
Figure E. 32: Static (4811097 Cycles) 02.15.2013 - With Retrofit	189
Figure E. 33: Static (6011097 Cycles) 04.16.2013 - With Retrofit	190
Figure E. 34: Static (6011097 Cycles) 05.20.2013 - Without Retrofit.....	191
Figure E. 35: Static (7211097 Cycles) 07.11.2013 - With Retrofit North Girder Weld Cracked Cross Frame	192
Figure E. 36: Static (7211097 Cycles) 07.11.2013 - Without Retrofit North Girder Weld Cracked Cross Frame	193
Figure E. 37: Static (0 Cycles) 07.15.2014.....	194
Figure E. 38: Static (15000 Cycles) 07.16.2014.....	195
Figure E. 39: Static (30000 Cycles) 07.17.2014.....	196
Figure E. 40: Static (45000 Cycles) 07.21.2014.....	197

Figure E. 41: Static (50000 Cycles) 07.28.2014 Without Retrofit Drilled Holes.....	198
Figure E. 42: Static (50000 Cycles) 07.28.2014 With Retrofit Drilled Holes.....	199
Figure E. 43: Static (1250000 Cycles) 08.29.2014 With Retrofit	200
Figure E. 44: Static (1250000 Cycles) 08.29.2014 Without Retrofit	201
Figure E. 45: Static (2450000 Cycles) 09.30.2014 With Retrofit	202
Figure E. 46: Static (2450000 Cycles) 10.02.2014 Without Retrofit	203
Figure E. 47: Static (2450000 Cycles) 10.02.2014 Without Retrofit Drilled Holes in North Girder	204
Figure E. 48: Static (2450000 Cycles) 10.02.2014 With Retrofit Drilled Holes in North Girder	205
Figure E. 49: Static (3050000 Cycles) 10.23.2014 With Retrofit	206
Figure E. 50: Static (3410000 Cycles) 11.14.2014 With Retrofit Cracked Connection Stiffener	207
Figure E. 51: Static (3410000 Cycles) 01.12.2015 With Retrofit Cracked Connection Stiffener Repair.....	208
Figure E. 52: Static (3410000 Cycles) 01.12.2015 Without Retrofit Cracked Connection Stiffener Repair.....	209
Figure E. 53: Static (3591092 Cycles) 01.27.2015 With Retrofit Cracked Cross Frame Tab....	210
Figure E. 54: Static (3591092 Cycles) 02.18.2015 Without Retrofit New Cross Frame	211
Figure E. 55: Static (3591092 Cycles) 02.24.2015 With Retrofit New Cross Frame.....	212

Appendix F: Kansas Bridge 135-087 (043/044) Plans

Figure F. 1: Contour map.....	267
Figure F. 2: Construction layout of southbound bridge.	268
Figure F. 3: Construction layout of northbound bridge.	269
Figure F. 4: Engineering geology.	270
Figure F. 5: Abutment details.	271
Figure F. 6: Auxiliary abutment details.	272
Figure F. 7: Pier details.....	273
Figure F. 8: Girder details.....	274

Figure F. 9: Concrete details.	275
Figure F. 10: Bearing device details.	276
Figure F. 11: Expansion device and miscellaneous details.....	277
Figure F. 12: Title sheet.	278
Figure F. 13: General notes and quantities.	279
Figure F. 14: General notes and quantities.	280
Figure F. 15: Construction layout.	281
Figure F. 16: Framing plan.	282
Figure F. 17: Existing girder details at cross frames.	283
Figure F. 18: Proposed girder web repair details at cross frames (single web stiffener locations).	284
Figure F. 19: Proposed girder web repair details at cross frames (single web stiffener locations).	285
Figure F. 20: Proposed girder web repair details at cross frames (double web stiffener locations).	286
Figure F. 21: Proposed girder web repair details at cross frames (double web stiffener locations).	287
Figure F. 22: Structural steel details.	288

Appendix G: Filtered Field Test Data

Figure G. 1: West Truck Load Placement 8-16 km/h (5-10 mph).	289
Figure G. 2: West Truck Load Placement 8-16 km/h (5-10 mph).	290
Figure G. 3: West Truck Load Placement 8-16 km/h (5-10 mph).	291
Figure G. 4: West Truck Load Placement 105-121 km/h (65-75 mph).	292
Figure G. 5: West Truck Load Placement 105-121 km/h (65-75 mph).	293
Figure G. 6: West Truck Load Placement 105-121 km/h (65-75 mph).	294
Figure G. 7: Center Truck Load Placement 8-16 km/h (5-10 mph).	295
Figure G. 8: Center Truck Load Placement 8-16 km/h (5-10 mph).	296
Figure G. 9: Center Truck Load Placement 8-16 km/h (5-10 mph).	297
Figure G. 10: Center Truck Load Placement 105-121 km/h (65-75 mph).	298

Figure G. 11: Center Truck Load Placement 105-121 km/h (65-75 mph).	299
Figure G. 12: Center Truck Load Placement 105-121 km/h (65-75 mph).	300
Figure G. 13: East Truck Load Placement 8-16 km/h (5-10 mph).	301
Figure G. 14: East Truck Load Placement 8-16 km/h (5-10 mph).	302
Figure G. 15: East Truck Load Placement 8-16 km/h (5-10 mph).	303
Figure G. 16: East Truck Load Placement 105-121 km/h (65-75 mph).	304
Figure G. 17: East Truck Load Placement 105-121 km/h (65-75 mph).	305
Figure G. 18: East Truck Load Placement 105-121 km/h (65-75 mph).	306
Figure G. 19: West Truck Load Placement 8-16 km/h (5-10 mph).	307
Figure G. 20: West Truck Load Placement 8-16 km/h (5-10 mph).	308
Figure G. 21: West Truck Load Placement 8-16 km/h (5-10 mph).	309
Figure G. 22: West Truck Load Placement 8-16 km/h (5-10 mph).	310
Figure G. 23: West Truck Load Placement 105-121 km/h (65-75 mph).	311
Figure G. 24: West Truck Load Placement 105-121 km/h (65-75 mph).	312
Figure G. 25: West Truck Load Placement 105-121 km/h (65-75 mph).	313
Figure G. 26: West Truck Load Placement 105-121 km/h (65-75 mph).	314
Figure G. 27: Center Truck Load Placement 8-16 km/h (5-10 mph).	315
Figure G. 28: Center Truck Load Placement 8-16 km/h (5-10 mph).	316
Figure G. 29: Center Truck Load Placement 8-16 km/h (5-10 mph).	317
Figure G. 30: Center Truck Load Placement 8-16 km/h (5-10 mph).	318
Figure G. 31: Center Truck Load Placement 105-121 km/h (65-75 mph).	319
Figure G. 32: Center Truck Load Placement 105-121 km/h (65-75 mph).	320
Figure G. 33: Center Truck Load Placement 105-121 km/h (65-75 mph).	321
Figure G. 34: Center Truck Load Placement 105-121 km/h (65-75 mph).	322
Figure G. 35: East Truck Load Placement 8-16 km/h (5-10 mph).	323
Figure G. 36: East Truck Load Placement 8-16 km/h (5-10 mph).	324
Figure G. 37: East Truck Load Placement 8-16 km/h (5-10 mph).	325
Figure G. 38: East Truck Load Placement 8-16 km/h (5-10 mph).	326
Figure G. 39: East Truck Load Placement 105-121 km/h (65-75 mph).	327
Figure G. 40: East Truck Load Placement 105-121 km/h (65-75 mph).	328
Figure G. 41: East Truck Load Placement 105-121 km/h (65-75 mph).	329

Figure G. 42: East Truck Load Placement 105-121 km/h (65-75 mph).	330
---	-----

Appendix H: Field Test and Finite Element Analyses Results

Figure H. 1: West Truck Load Placement Maximum Principal Web Gap Stresses Before and After Retrofit.....	331
Figure H. 2: West Truck Load Placement Directional Web Gap Stresses Before and After Retrofit.	332
Figure H. 3: West Truck Load Placement Directional Web Gap Stresses Before and After Retrofit.	333
Figure H. 4: Center Truck Load Placement Maximum Principal Web Gap Stresses Before and After Retrofit.....	334
Figure H. 5: Center Truck Load Placement Directional Web Gap Stresses Before and After Retrofit.	335
Figure H. 6: Center Truck Load Placement Directional Web Gap Stresses Before and After Retrofit.	336
Figure H. 7: East Truck Load Placement Maximum Principal Web Gap Stresses Before and After Retrofit.....	337
Figure H. 8: East Truck Load Placement Directional Web Gap Stresses Before and After Retrofit.	338
Figure H. 9: East Truck Load Placement Directional Web Gap Stresses Before and After Retrofit.	339
Figure H. 10: Maximum Principal Stresses at Top Web Gap for West Load Truck Placement with Connection Plate-To-Web and Flange-To-Web Weld Cracks Present.	340
Figure H. 11: Maximum Principal Stresses at Top Web Gap for Center Load Truck Placement with Connection Plate-To-Web and Flange-To-Web Weld Cracks Present.	341
Figure H. 12: Maximum Principal Stresses at Top Web Gap for East Load Truck Placement with Connection Plate-To-Web and Flange-To-Web Weld Cracks Present.....	342
Figure H. 13: Maximum Principal Stresses at Top Web Gap for All Load Truck Placements with Only Connection Plate-To-Web Weld Crack Present.	343

List of Tables

Part I: Introduction

N/A

Part II: Experimental Investigation of Distortion-Induced Fatigue Repair in 9.1 m [30 ft.] Test System

Table 1: Test 1 Specimen trials for North (N) and South (S) girders with load range	19
Table 2: Test 2 Specimen trials for North (N) and South (S) girders with load range	19
Table 3: Test 1 Specimen trials with load range and bottom flange stresses	20
Table 4: Test 2 Specimen trials with load range and bottom flange stresses	21
Table 5: Cracking at end of Trial 1.6 (6,011,097 Cycles)	26
Table 6: Cracking at End of Trial 2.7 (4,016,092 Cycles).....	28

Part III: Field and Analytical Testing of Angles-With-Plate Retrofit for Distortion-Induced Fatigue in Kansas Bridge 135-87 (043/044)

N/A

Appendix A: Test Specimen Specifications

Table A. 1: Labeling Definition for Data Acquisition	113
--	-----

Appendix B: Calibration Constants

Table B. 1: Calibration Constants for Strain Transducers	115
Table B. 2: Calibration Constants for LVDTs	115
Table B. 3: Calibration Constants for String Potentiometers	116
Table B. 4: Calibration Constants for Load Cells.....	116

Appendix C: Loading Protocol

N/A

Appendix D: Finite Element Study

Table 1: Finite Element Modeling Matrix for Cracks around Stiffener-Web-Weld	126
Table 2: Cross Frame Element Stresses with 25 mm [1 in.] Horseshoe Crack (MPa [ksi]).....	136
Table 3: Maximum Principal Hot Spot Stresses with 25 mm [1 in.] Horseshoe Crack (MPa [ksi])	139
Table 4: Maximum Principal Hot Spot Stresses for Experimental Trials With Bolt Failure	142

Appendix E: Experimental Data

Table E. 1: Concrete Compressive Strengths in psi.....	149
Table E. 2: North Girder – Test 1 Crack Figures.....	150
Table E. 3: South Girder – Test 1 Crack Figures.....	153
Table E. 4: North Girder – Test 2 Crack Figures.....	156
Table E. 5: South Girder – Test 2 Crack Figures.....	158
Table E. 6: Load Distribution from Load Cells – Test 1	161
Table E. 7: Load Distribution from Load Cells – Test 2	161
Table E. 8: Legend for Strain Plots.....	162

Appendix F: Kansas Bridge 135-087 (043/044) Plans

N/A

Appendix G: Filtered Field Test Data

N/A

Appendix H: Field Test and Finite Element Analyses Results

N/A

Part I: Introduction

Distortion Induced-Fatigue in Steel Bridges

Prior to the mid-1980s, steel girder bridges in the United States were constructed without a positive connection between the cross frame connection stiffeners and the girder flanges. This lack of connection created a flexible region between the web, flange, and connection stiffener known as a “web gap.” Due to differential deflection between adjacent girders caused by loading under traffic, these web gap regions experienced large out-of-plane rotations at the cross frame connections. These repeated out-of-plane rotations caused distortion-induced fatigue and led to severe cracking in the web gap.

Although the 1983 American Association of State Highway and Transportation Officials (AASHTO) Bridge Design Specification addressed the issue of distortion-induced fatigue cracking in new steel bridge designs, bridges designed before 1983 that are still in service today have these flexible web gap regions. Many of the web gap regions in these bridges have experienced distortion-induced fatigue cracking, which could lead to severe structural damage if allowed to propagate further into the girder webs. Thus, repairs must be installed to mitigate the growth of distortion-induced fatigue cracks in these steel bridges.

Angles-with-Plate Retrofit

Performance and installation issues encountered when using currently available methods to repair distortion-induced fatigue cracking led to the research and development of a new retrofitting technique at the University of Kansas. This technique, termed the “angles-with-plate” retrofit, has been the focus of numerous physical and analytical investigations. In addition to ensuring that the angles-with-plate retrofit would be an effective repair strategy, investigators at the University of Kansas also wanted it to be a retrofit measure that could simplify installation and have the ability to be installed under traffic.

One of the most common current techniques used to repair distortion-induced fatigue cracking involves bolting back-to-back angles to the connection stiffener and girder flange. While this technique has proven to be effective, it is often difficult to implement. Since attachment to the girder flange must occur, installation in the top web gap requires bridge deck removal, a costly process that can majorly disrupt traffic. Additionally, in bridges where cross

frame members extend into the vertical plane of the girder flange, cross frame members must be removed before installing the back-to-back angles to girder flange retrofit, which can complicate installation of the retrofit in both the top and bottom web gap regions.

The angles-with-plate retrofit technique addresses these installation issues by eliminating connection to the girder flange. Instead, positive connection is provided between the connection stiffener and the girder web. The angles-with-plate retrofit is made up of a pair of angles and a backing plate that are applied on opposite sides of the girder web. One leg of each angle is bolted to the connection plate while the other leg of each angle is bolted through the girder web to the backing plate. Since no connection to the girder flange is required, installation of the angles-with-plate retrofit does not require removal of the bridge deck when installed in the top web gap. Additionally, the angles-with-plate retrofit is unlikely to necessitate cross frame removal, since installation can often take place without the need to go through an outstanding leg of a cross frame member. By eliminating the need to remove vital structural members during installation, the angles-with-plate technique provides a repair for distortion-induced fatigue cracking that is simpler to install and requires less need for traffic interruption.

Physical and analytical studies on a 2.8 m (9.3 ft.) steel girder and cross frame subassembly at the University of Kansas focused on evaluating the performance of the angles-with-plate retrofit under only out-of-plane bending effects. The successful performance of the angles-with-plate retrofit in these studies led to larger, more extensive investigations. The angles-with-plate retrofit was assessed in physical and analytical studies on a 9.1 m (30 ft.) long three-girder test bridge and in a full-scale analytical study of an active bridge system located near Park City, KS (Kansas Bridge 135-87(043/044)), all of which considered not only out-of-plane but also in-plane bending effects. Results from the 2.8 m (9.3ft.) girder subassembly and 9.1 m (30 ft.) test bridge physical investigations showed that application of the angles-with-plate retrofit effectively reduced out-of-plane rotations in the web gap region and mitigated distortion-induced crack propagation. Additionally, finite element analyses of the 2.8 m (9.3ft.) girder subassembly, 9.1 m (30 ft.) test bridge, and an active bridge system showed that the angles-with-plate retrofit reduced stress demands in the web gap regions.

Effective performance of the angles-with-plate retrofit led investigators at the University of Kansas to recommend the use of the retrofit to the Kansas Department of Transportation (KDOT) on Kansas Bridge 135-87(043/044), the active bridge system studied in the full-scale

analytical investigation mentioned previously. Kansas Bridge 135-87(043/044) is a steel girder twin bridge structure that has experienced extensive distortion-induced fatigue cracking in its web gap regions. Upon acceptance of the recommendation, KDOT installed the angles-with-plate retrofit on the twin bridge structure. To assess the performance of the retrofit in an active bridge, investigators at the University of Kansas monitored Kansas Bridge 135-87(043/044) both before and after installation of the angles-with-plate retrofit under live truck loads.

Part II of this dissertation details the physical tests performed on the 9.1 m (30 ft.) three-girder test bridge and presents findings on the performance of both the angles-with-plate retrofit and a stiffened version of the angles-with-plate retrofit in mitigating distortion-induced fatigue cracking. Part III of this dissertation expounds on the history of distortion-induced fatigue cracking in Kansas Bridge 135-87(043/044) and the findings that led to recommendation of the angles-with-plate retrofit for its repair. Details of the field tests performed on Kansas Bridge 135-87(043/044) both before and after installation of the angles-with-plate retrofit are provided, along with comparisons of the field test results to complementary finite element analyses of the bridge. In addition, Part III also provides results from a supplementary finite element analysis that investigated the behavior of the top web gap under application of the angles-with-plate retrofit.

Part II: Experimental Investigation of Distortion-Induced Fatigue Repair in 9.1 m [30 ft.] Test System

Kathleen S. McElrath¹

Amanda S. Hartman²

Caroline R. Bennett³

Adolfo B. Matamoros⁴

Stanley T. Rolfe⁵

Abstract

With infrastructure in the United States deteriorating at an alarming rate, repair of existing roadway bridges is critical for state highway agencies to responsibly allocate scarce resources. For steel bridges that were constructed prior to the mid-1980s, distortion-induced fatigue cracking can be a serious problem. Retrofit or repair techniques currently used in the field may not completely halt crack growth and/or can be expensive to implement. A distortion-induced fatigue repair technique that is commonly implemented in the field is to provide positive connection between the transverse connection plate and girder flange. However, this technique often requires partial removal of the concrete deck to access the top of the flange to make the connection.

To address these concerns, an innovative retrofit technique developed at the University of Kansas was analyzed to determine its effectiveness as a distortion-induced fatigue repair and its suitability for field implementation. The approach taken by the authors was to use a retrofit termed “angles-with-plate” that utilized two angle segments and a backing plate to connect the girder connection plate and the web.

To investigate the performance of this retrofit, a 9.1-m [30-ft] long three-girder test bridge was constructed and tested under fatigue loading to develop, and subsequently repair, distortion-induced fatigue cracking. A total of 28 test trials were performed with varying load

¹ Kathleen S. McElrath, Graduate Research Assistant, University of Kansas, 1530 W. 15th St., Lawrence, KS 66045

² Amanda S. Hartman, Graduate Research Assistant, University of Kansas, 1530 W. 15th St., Lawrence, KS 66045

³ Caroline R. Bennett, PhD, PE, Associate Professor, University of Kansas, 1530 W. 15th St., Lawrence, KS 66045

⁴ Adolfo B. Matamoros, PhD, Peter T. Flawn Distinguished Professor, University of Texas at San Antonio, One UTSA Cir., San Antonio, TX 78249

⁵ Stanley T. Rolfe, PhD, PE, A.P. Learned Distinguished Professor, University of Kansas, 1530 W. 15th St., Lawrence, KS 66045

ranges to assess the effectiveness and applicability of the angles-with-plate retrofit. In addition to assessing retrofit performance, crack growth as well as girder deflections and strains were monitored. It was found that retrofit application reduced web gap rotation, while the diagonal cross frame angle framing into the top web gap experienced an increase in tensile strain. When implemented with crack-arrest holes, the angles-with-plate retrofit performed well at mitigating distortion-induced fatigue cracking in steel girders.

Introduction

During and prior to the 1970s, many steel bridges were constructed without much knowledge of structural fatigue. Several structural failures occurred in Europe in the 1930s that involved bridges in which cross frame or diaphragm connection plates were welded directly to tension flanges (Fisher and Keating 1989); therefore, common practice until 1985 was to not weld connection plates to the tension flange. Although the intention of this detailing practice was to prevent failures similar to those in European steel bridges from occurring, the intentional lack of connection tended to result in details characterized by an area of very high stresses, leading to prevalent fatigue cracking in bridges with this detailing. Many steel bridge structures designed and constructed during this time period have exhibited extensive fatigue cracking due to distortion-induced fatigue, presenting bridge engineers and management staff with a challenging and expensive situation.

Distortion-induced fatigue commonly occurs at connections of transverse structural members (Roddis and Zhao 2001). Web gaps that exist between connection plates and girder top flanges are the most common location for fatigue cracking. As a bridge experiences traffic loading, adjacent steel girders undergo different levels of deflection. This results in cross frame members inducing secondary, out-of-plane forces on the adjacent girders that are deforming differently. Since the top flange of the girder is restrained from rotation by the concrete deck and the bottom flange is free to rotate, distortion of the web gap region occurs as shown in Figure 1. While secondary forces carried by the cross frames may be low in magnitude, they often translate into high stresses in a girder's web due to the high flexibility of the web gap. With the presence of a multitude of stress concentrations in the congested geometry of the web gap region, fatigue cracking can be expected to occur.

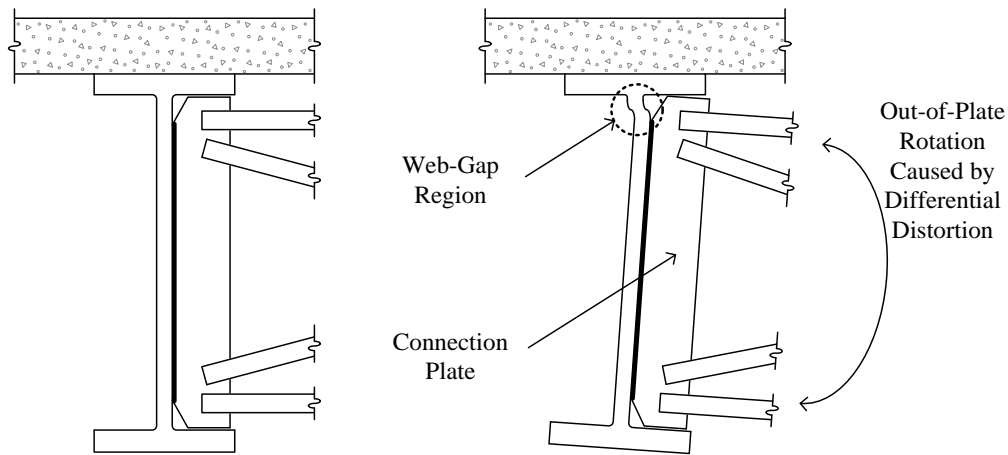


Figure 1: Out-of-plane rotation causing distortion-induced fatigue.

Background

In addition to being a common occurrence in steel bridges, distortion-induced fatigue is also a problem that is both difficult and expensive to repair. There are a number of techniques that can be used to retrofit bridges for distortion-induced fatigue, including drilled crack-arrest holes, cross frame removal, slotting the connection plate, utilizing a back-up stiffener, and connecting the connection plate to the girder's top flange. Each of these techniques has associated advantages and disadvantages, and it is useful to bridge engineers and owners to have multiple options from which to choose.

Crack-arrest holes are often drilled at the tips of sharp cracks to halt crack growth as a first line of defense against fatigue crack propagation; however, “hole drilling alone is not effective at stopping fatigue cracks when the cracks are initiated from out-of-plane distortions” (Grondin et al. 2002; Liu 2015). Although crack-arrest holes may temporarily slow or stop crack growth, they are not a permanent fix for cracking due to distortion-induced fatigue. Instead, crack-arrest holes are often used in conjunction with other retrofit techniques such as providing an alternate load path via a structural repair.

Cross frame removal is another retrofit option that has been examined for distortion-induced fatigue (Tedesco et al. 1995; Roddis and Zhao 2001). The concept of this technique is to remove secondary members between adjacent girders, which eliminates the out-of-plane forces induced by them, thus eliminating distortion-induced fatigue. However, when cross frames are removed from an existing bridge system, consideration should be given to: (1)

effectiveness of the bridge system to laterally-distribute live loads; (2) effectiveness of the system to carry wind loading; and (3) future needs regarding deck replacement. Cross frames provide restraint to prevent lateral-torsional buckling while a bridge is under construction and in negative bending regions post-construction. Due to lateral-torsional buckling considerations, cross frames or other bracing is a necessity during deck replacement and cross frames generally cannot be removed from negative bending moment regions. Additionally, Tedesco et al (1995) indicated that cross frame removal increases individual girder moment demand by approximately 8-14%, due to lower amounts of live load distribution.

Back-up stiffeners are a retrofit scheme that function by stiffening the web gap region, reducing distortion-induced fatigue effects. Placed on the opposite side of the web from a cross frame connection plate, back-up stiffeners are simply transverse stiffeners that strengthen the web gap and reduce out-of-plane rotation of the web gap region. Although Hassel et al. (2010) concluded that back-up stiffeners can be effective in skewed bridge applications with staggered cross frame layouts, the authors found that these stiffeners are less effective in non-staggered bridges applications where the only potential retrofit locations are on the fascia side of the exterior girders.

Positive connection to the girder flange can be accomplished using several methods. Commonly, angles are used to provide connection between the flange and connection plate by bolting one leg to the flange and attaching the other to the connection plate through either a bolted or welded connection (Roddiss and Zhao 2003, Fisher et al. 1990). This method was found to be effective at halting fatigue crack initiation and propagation; however, applications of this technique are not without challenges. For example, bolting to the flange is preferred over welding due to the greater fatigue sensitivity at welded details - if the web gap being repaired is at the top flange of the girder, application of this technique usually requires removal of at least portions of the concrete deck, bringing about inconvenient traffic disruption and expense.

An alternative retrofit technique to the traditional means of positive connection is the “angles-with-plate” retrofit, which has been the subject of a number of investigative efforts at the University of Kansas (Alemdar et al. 2013a; Alemdar et al. 2013b; Przywara 2013). The retrofit described in Alemdar et al. (2013a; 2013b) consisted of two angles which attached the connection plate to the girder web. The angles were used in conjunction with a back plate on the opposite side of the girder web to distribute out-of-plane forces over a large area of the web.

Since this retrofit did not require any attachment to the flange, it eliminated any need for deck removal and can be installed under traffic. This technique was evaluated through a series of tests performed on 2.8-m [9.3-ft] long girder-cross frame subassemblies loaded under a demanding distortion-induced fatigue loading protocol. An analytical investigation was performed in parallel to the physical simulations.

The test set-up used in Alemdar et al. (2013a; 2013b) was such that the girder-cross frame subassembly was tested upside-down, with the girder's top flange rotationally restrained to the laboratory strong floor. Cyclic loads were applied through a servo-controlled hydraulic actuator attached to the free end of the cross frame elements. This test set-up eliminated in-plane bending effects on the test girders and presented a demanding out-of-plane fatigue test. The test set-up used by Alemdar et al. is shown in Figure 2.

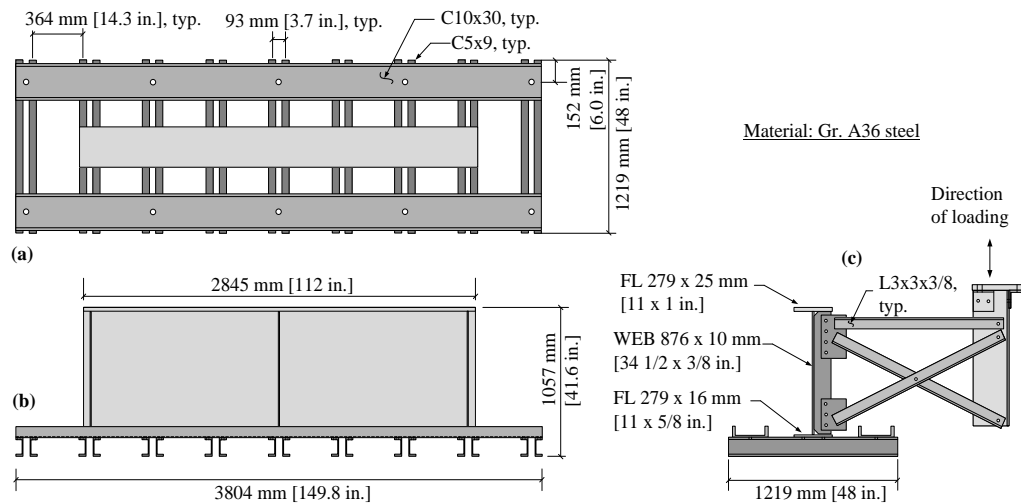


Figure 2: Test set-up for 2.8 m [9.3 ft.] girder sub-assembly testing (Alemdar et al. 2013a; 2013b).

The test set-up and computational models were used to generate an initial set of data for the angles-with-plate retrofit. This showed that the technique was effective under pure out-of-plane fatigue loading, reducing web gap stresses and propensity of crack propagation under distortion-induced fatigue.

Objective and Scope

The objective of this study was to investigate the effectiveness of the angles-with-plate retrofit technique initially studied by Alemdar et al. (2013a; 2013b) in reducing distortion-induced fatigue crack propensity in a more realistic test set-up, wherein both out-of-plane and in-plane effects are considered.

The scope of this study included performing 28 test trials on a three-girder test bridge that was 9.1-m [30-ft] long and included a composite concrete deck. The first 14 of these test trials were performed as a part of one test, denoted Test 1, while the next 14 were performed as a part of a second test, denoted Test 2. Results from a parallel analytical investigation can be found in Part 4 of Hartman (2010). Results of these studies are currently limited to straight, non-skewed bridge girders.

Experimental Program

Since the goal of this investigation was to evaluate the effectiveness of the angles-with-plate retrofit in a test that captured both in-plane bending effects and secondary stresses from distortion-induced fatigue, a set-up was constructed that included three 9.1-m [30-ft] long girders connected with X-type cross frames at the two simple support locations and at midspan. A concrete bridge deck was cast in sections and was connected to the girders such that it would act compositely. All loads were applied through a 1470 kN [330-kip] servo-controlled hydraulic actuator. The loading end of the actuator was situated over a steel bearing plate centered on the bridge deck. Details regarding the test set-up have been provided in the following sections.

Test 1 and Test 2 were identical in set-up and instrumentation. However, Test 2 was performed to further investigate the effectiveness of a stiffened version of the angles-with-plate retrofit on a “new” bridge specimen. Each girder in the test bridge includes two splices, allowing for replacement of the center segment of each girder. Therefore, the middle segments of all three girders were replaced for Test 2. At the completion of Test 1, all instrumentation and the concrete deck were removed and the sections of girders located at the center of the test bridge were replaced with new girder sections. The cross frames that were at the center of the bridge were switched out with cross frames that had been located at the bridge ends during Test 1. This was done so that cross frames that had seen the least severe loading could be used during Test 2.

Once the steel members were replaced, the concrete deck panels were re-installed and the test bridge was instrumented in matching locations to Test 1.

Test trials are referred to by a combination of the Test number (1 or 2) and the Trial number (1 through 14). For example, Trial 14 of Test 1 is referred to as Trial 1.14, and Trial 5 of Test 2 is referred to as Trial 2.5.

Girder Specifications

Test specimen dimensions were based on laboratory space constraints and a sample bridge from American Iron and Steel Institute (AISI) Example 1: Simple-Span Composite I Girder (AISI 1997). Approximately half scale of the AISI sample bridge (in cross-section), the 9.1 m [30 ft.] long girders were comprised of a 16 x 279 mm [5/8 x 11 in.] top flange, 6 x 876 mm [1/4 x 2 ft.-10 1/2 in.] web, and 25 x 279 mm [1 x 11 in.] bottom flange. All girders were supported on rollers to minimize axial forces with a center-to-center span length of 8.7 m [28 ft.-6 in.] between supports. Test section dimensions and girder span with load placement are shown in Figure 3. In the laboratory, the longitudinal axis of the bridge system was oriented east-west which defined the exterior girders as being the north and south girders. At the section shown in Figure 3(a), looking west, the exterior girder shown on the right is the north girder and the left is the south girder.

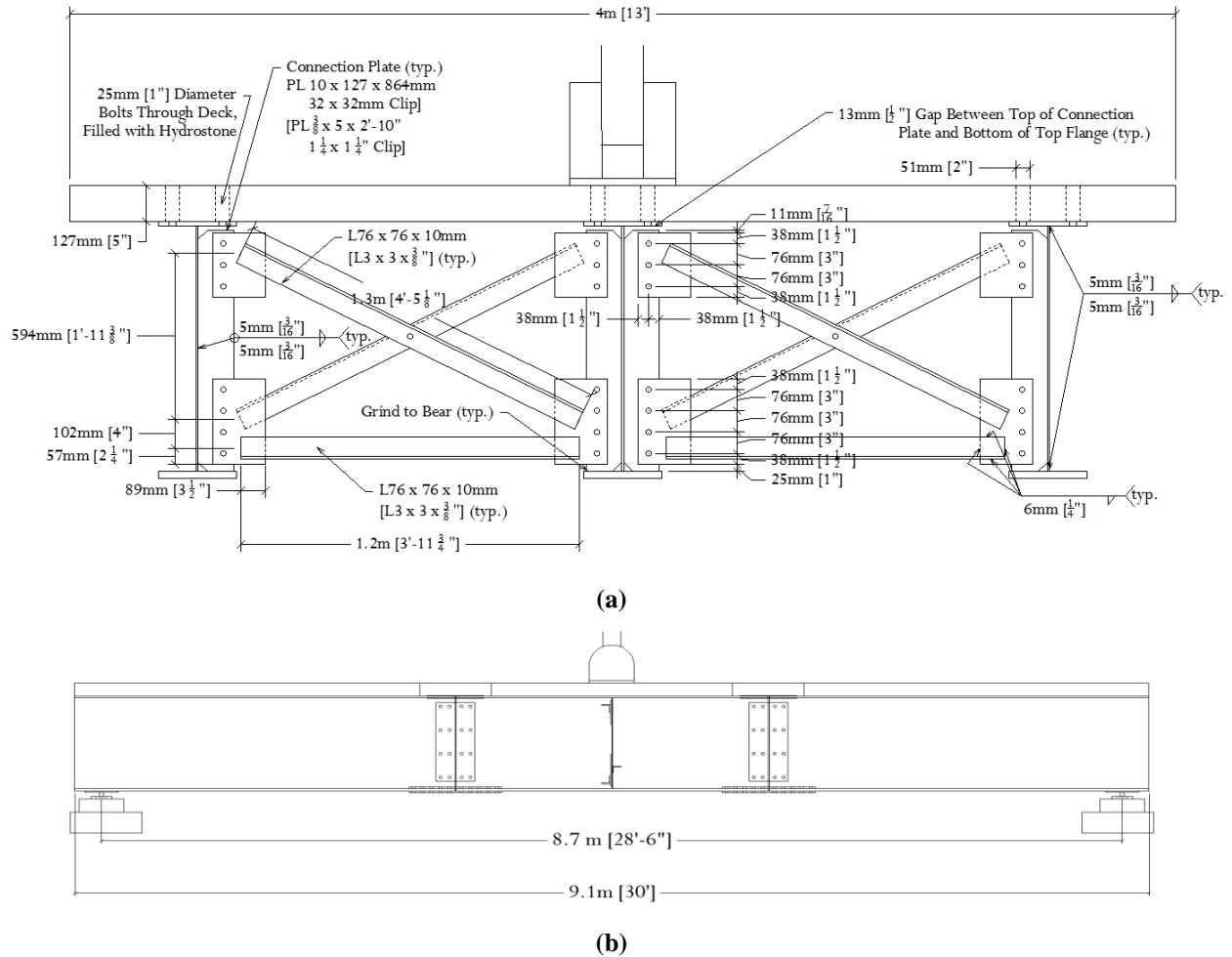


Figure 3: (a) Dimensions and schematic of test region cross frames. (b) Girder span and load application.

The concrete deck was cast in five sections; 51-mm [2-in.] diameter circular voids were created during the casting procedure, spaced to provide one bolt through the girder flange on either side of the web at a maximum spacing of 432 mm [1 ft.-5 in.]. Complete casting layout has been provided in Appendix A. Each portion of deck was cast using formwork on the laboratory floor and then lifted into place after they had been cured. The voids cast into the concrete deck elements matched a hole layout shop-drilled into the top flanges of the girders, providing a location for high-strength structural bolts to be placed through. After the bolts were installed, the remaining void area was filled with Hydrostone. In this manner, horizontal shear transfer was achieved between the steel girders and the concrete deck elements. The compressive strength of the concrete used in the deck was found to range from 267 MPa [3900 psi] to 33 MPa [4800 psi] when tested at 28-days.

Loading

During each test trial, cyclic loading was delivered by a MTS 201.70 actuator (1470 kN [330 kips] capacity in compression) powered by a MTS 505.90 90 GPM pump and controlled with a MTS FlexTest II CTC Controller. A 25-mm [1.0-in.] thick steel plate used to distribute the concentrated compressive force delivered by the actuator was centered on the bridge deck and grouted in place under the footprint of the actuator. Loading was applied at midspan over the interior girder, as shown in the schematic in Figure 3. Cyclic loading was applied at rates varying between 1.0 – 2.0 Hz depending on the load range being applied. The load range was varied throughout the test series, from 27-267 kN (6-60 kips) to 53-534 kN (12-120 kips), as explained further in sections describing the test sequence.

Instrumentation

The test bridge was instrumented such that strain, vertical deflections, and lateral deflections could be measured through the test sequence. Additionally, load and displacement data were recorded from the actuator using the same data acquisition system as was used for all other sensors. Sensors included the following: load cells, linear variable differential transformers (LVDTs), string potentiometers, Bridge Diagnostics Inc. (BDI) strain transducers, and strain gages. Global bridge response was monitored using load cells, LVDTs, string potentiometers, and strain transducers. Six load cells, one at each girder end, were used to monitor load distribution between girders. Load cells were calibrated using a 6.55V power supply.

LVDTs and string potentiometers were powered using a 15V power supply. Initially, in Trial 1.1, LVDTs were used to monitor vertical girder deflections at midspan as well as lateral displacements for each exterior girder at three different locations along the height of each girder (Figure 4(a)). Since exterior girder deflections included both vertical and lateral displacements, it was found that the LVDT core could not extend and retract freely which resulted in inaccurate deflection measurements. Due to this, four string potentiometers (Figure 4(b)) replaced the original three LVDTs monitoring lateral girder displacements for the remaining trials in Test 1, and all of the trials in Test 2.

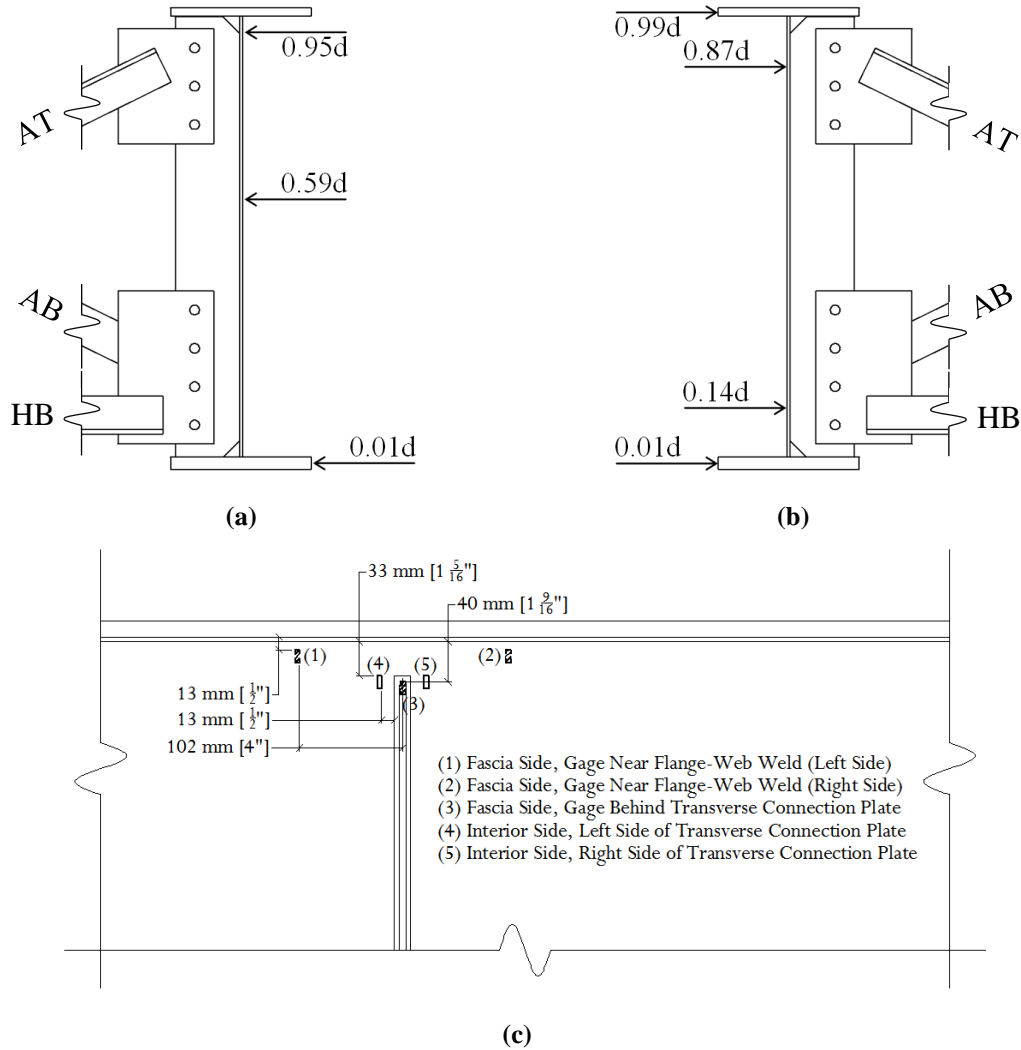


Figure 4: Instrumentation placements for (a) LVDTs, (b) string potentiometers, and (c) strain gages.

Six Bridge Diagnostics, Inc. (BDI) strain transducers were used in the test set-up. Each girder was instrumented with two strain transducers near midspan, one placed at top and bottom of each girder web to monitor in-plane bending strains in the three girders. BDI strain transducers were powered with 5V. To avoid local concentrations due to geometry, these were placed 50.8 mm [2 in.] below or above the flanges, and were located a longitudinal distance 654 mm [25 3/4 in.] from the connection plates at midspan.

Bondable strain gages were included in the bridge instrumentation plan to monitor strains in the web gap region. Bondable strain gages were powered directly through the data acquisition system in a quarter bridge configuration with excitation voltages of 2.5V or 3.3V. Strain gages used with the NI-9219 DAQ module were powered by 2.5V and strain gages used with the NI-

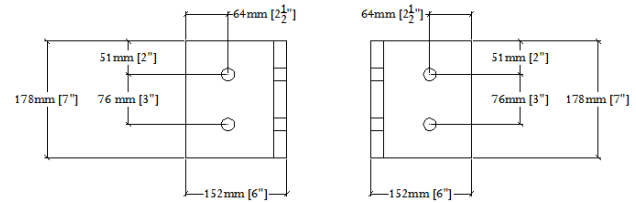
9236 DAQ module were powered by 3.3V. In total, 20 Micro-Measurements WK-06-250BG-350 gages were placed in web gap regions as shown in Figure 4(c). Additionally, bondable strain gages were placed on each cross frame angle at midspan of the girders oriented along the axis of the cross frame member. On the horizontal member of the cross frame (“HB” in Figure 4), the gage was placed mid-span. For the diagonal members (“AT” and “AB” in Figure 4) which were bolted at mid-span, the gages were placed at the quarter-point of the span nearest the exterior girder.

Due to the scale of the project and large sensor array, synchronizing the data was a critical step. All data was recorded using a single data acquisition system manufactured by National Instruments (NI cDAQ 9188 chassis with NI 9205, NI 9212, NI 9236, and NI 9239 modules). A protocol was written in Labview 2011 to read, compress, and record data in a text file. The quantity of data required an extremely large sampling rate to sufficiently increase the buffer size within the NI cDAQ 9188 chassis. Sampled data were post-compressed to produce an effective sampling rate of approximately 20 samples/second. All appropriate calibration factors were applied within the Labview protocol, such that data written to the measurement file contained appropriate units.

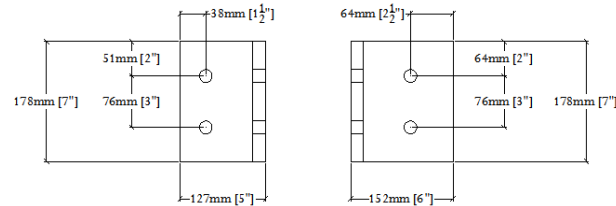
Prior to retrofit application, data was recorded under static load application every 15,000 cycles for both Tests 1 and 2. In other words, the test was paused every 15,000 cycles and the system was loaded monotonically so that changes in the bridge’s static response could be examined over time – this is referred to throughout this paper as a “static test.” Throughout test trials performed on the bridge in the retrofitted state, such data was recorded at the beginning and end of each trial (which usually had a duration of 1.2 million cycles). During each static test, loading was manually controlled, progressing from 0 kN [0 kip] to 356 kN [80 kip] while data was recorded continuously. Raw data was then imported into Microsoft Excel and post-processed to examine data at 11 kN [2.5 kip] load increments. As the load range applied to the test bridge was different in various test trials, the maximum load to which data was recorded was increased to 445 kN [100 kip] and then to 534 kN [120 kip], and the corresponding data increment was increased to 22 kN [5 kip].

Retrofit Specifications

The retrofit investigated in Trials 1.2-1.6 contained two angles providing attachment between the connection plate and girder web with a backing plate on the opposing face of the web. Two L152x152x19 mm [L6x6x3/4 in] angles were bolted to the connection plate and girder web while a 457x457x19 mm [18x8x3/4 in] back plate was used to distribute out-of-plane forces over a large web area, as shown in the schematic in Figure 5.

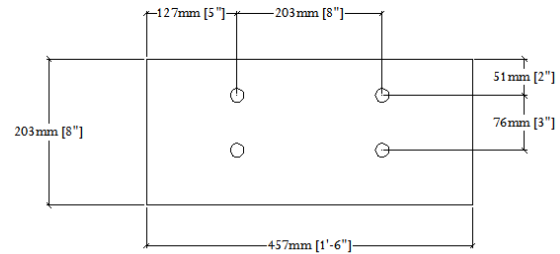


L152x152x19mm
[L6x6x3/4"]



L127x152x19mm
[L5x6x3/4"]

(a)



L457x203x19mm
[18x8x3/4"]

(b)

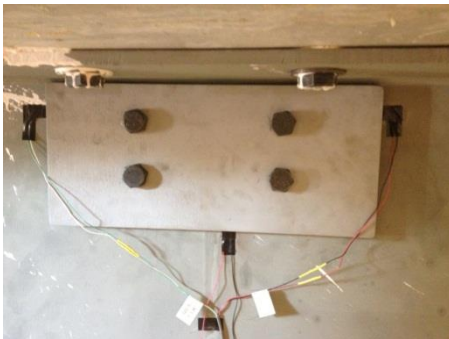


Figure 5: Retrofit as applied to top web gap in test specimen.

Due to fit interferences with the cross frame angles, it was necessary that two retrofit angles each have one leg shortened by 25 mm [1 in.]. Shim plates were also utilized to avoid weld interference. The bolt layout consisted of a total of six fully-tightened 19-mm [3/4-in.]

diameter Gr. A325 bolts for each retrofit application. The bolts were installed using an impact wrench and Squirter Direct Tension Indicator (DTI) washers. Squirter DTIs have flexible silicone embedded in the depressions that squirt out of the side of the washer when the correct tension is achieved in the bolt. The bolt array was snug-tightened on the first pass. After this, the bolts were tightened with the impact wrench until the orange silicone appeared from the squirt locations. The bolts through the angle legs and cross frame stiffener were tightened first, followed by the bolts through the angle legs, girder web, and backing plate.

The retrofit applied in Trial 1.7 and 2.2-2.7 was identical to that used in Trials 1.2-1.6, except that stiffening elements were added to the angle elements of the retrofit, as shown in Figure 6. This version of the retrofit is referred to as the “stiffened angles-with-plate” retrofit.



Figure 6: Stiffened angles-with-plate retrofit applied to exterior girders in Trials 1.7 and 2.2-2.7.

Cracking and Inspection

Crack inspection was performed at regular intervals while the bridge was subjected to cyclic loading. Inspection techniques included photographic and visual inspection as well as evaluation of strain measurement data. Zyglo Penetrant (ZL-27A) by Magnaflux and an ultraviolet flashlight were used to visually identify crack openings and tips. When dye penetrant was sprayed on the region of interest during cyclic loading, surface cracks could be seen pulsing under the ultraviolet light. At each inspection, photographs were taken using a Cannon Rebel

XTi DSLR with an 18-55mm lens. Early photographic images contained a small scale taped to the girder web used for determining crack length. Later, photographs were scaled to the previous images to verify crack measurements obtained visually and to monitor crack growth.

Test 1

In addition to visual and photographic inspection, strain gages were monitored through static data collection at 15,000 cycles, 20,000 cycles, and 30,000 cycles, and then every 15,000 cycles until retrofitting at 150,000. Strain readings from gages placed on the fascia side directly behind the connection plate (shown in Figure 4(c)) were compared throughout testing of the bridge in the unretrofitted condition. These gages measured the largest strains and were found to be highly sensitive to cracking in the connection plate-web weld.

As discussed further in the following sections of this paper, it was found that girder cracking first initiated and propagated around the connection plate-web weld in the top web gaps of the south and north girders. These cracks were closely monitored and classified by three different categories: (1) cracks growing down the weld (termed “vertical cracks”), (2) cracks growing out from the weld in the longitudinal direction of the girders (termed “spider cracks”), and (3) cracks extending through the web thickness (termed “through cracks”). Each of these three crack patterns is shown in Figure 7. Additionally, cracking was found near the flange-web weld; these were termed “longitudinal cracks.”

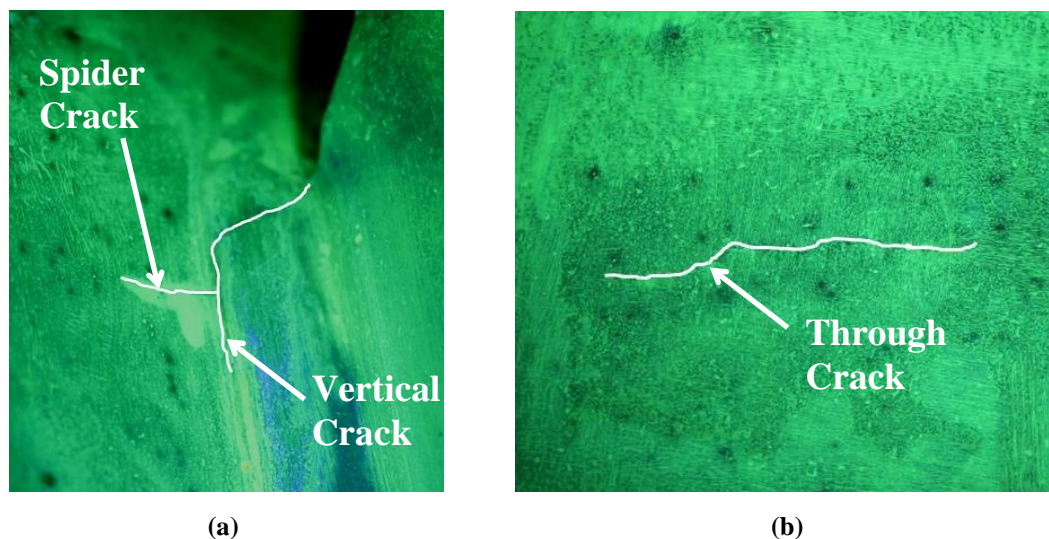


Figure 7: Crack definition for (a) interior side of girder web at cross frame connection plate and (b) exterior or fascia side of girder web.

Test 2

Visual and photographic inspection was performed every 5,000 cycles in Test 2.1, and strain gages were monitored through static data collection every 15,000 cycles until retrofitting at 50,000 cycles. Similar to Test 1, cracks were closely monitored and classified as “vertical cracks,” “spider cracks,” “through cracks,” or “longitudinal cracks.” Contrary to Test 1, however, cracking first initiated near the flange-web weld before appearing around the connection plate-web weld in the top web gap of the south girder. In the north girder, crack initiation and propagation followed the same pattern as that seen in Test 1.

Test Trials

Twenty-eight test trials were performed on the test bridge in total, as summarized in Tables 1 and 2. For each loading protocol on the bridge system, the two exterior girders (the north girder and the south girder) underwent a test trial. For example, in Test 1, Trial 2, there is reported a Trial 1.2N (north girder) and Trial 1.2S (south girder). The center girder was not listed as undergoing a test trial since the center girder web did not experience any cracking throughout the test sequences. Trials 1.1 and 2.1 consisted of unretrofitted specimens in which cracking was allowed to initiate and propagate until crack lengths of 24 mm [1 in.] and 38 mm [1.5 in.] were achieved, respectively. Trials 1.2-1.7 and 2.2-2.7 were indicative of the bridge with the exterior girders in the retrofitted condition (sometimes with the addition of crack-arrest holes), with each trial having a duration of 1.2 million cycles, with the exception of Trials 1.4, 2.4, 2.5, 2.6, and 2.7. Trials 1.4 and 2.4-2.7 did not reach 1.2 million cycles, for reasons discussed further in the following sections.

Table 1: Test 1 Specimen trials for North (N) and South (S) girders with load range

Trial	Specimen Description	Target Load Range
1.1N	Bare specimen	27-267 kN
1.1S		[6-60 kip]
1.2N	“Angles-with-plate” retrofit applied in top web gap	27-267 kN
1.2S		[6-60 kip]
1.3N	Same as Trials 1.2N and 1.2S: “Angles-with-plate” retrofit applied in top web gap	36-356 kN
1.3S		[8-80 kip]
1.4N	Small drilled holes with “angles-with-plate” applied in top web gap	44-445 kN
1.4S		[10-100 kip]
1.5N	Larger drilled hole with “angles-with-plate” retrofit applied in top web gap	44-445 kN
1.5S		[10-100 kip]
1.6N	Same as Trials 5N and 5S: Larger drilled hole with “angles-with-plate” retrofit applied in top web gap	53-534 kN
1.6S		[12-120 kip]
1.7N	Stiffened version of the “angles-with-plate” retrofit was installed in the top web gap	53-534 kN
1.7S		[12-120 kip]

Table 2: Test 2 Specimen trials for North (N) and South (S) girders with load range

Trial	Specimen Description	Target Load Range
2.1N	Bare specimen	27-267 kN
2.1S		[6-60 kip]
2.2N	Drilled holes with stiffened version of the “angles-with-plate” retrofit applied in top web gap	27-267 kN
2.2S		[6-60 kip]
2.3N	Drilled holes with stiffened version of the “angles-with-plate” retrofit applied in top web gap	36-356 kN
2.3S		[8-80 kip]
2.4N	Drilled holes with stiffened version of the “angles-with-plate” retrofit applied in top web gap	36-356 kN
2.4S		[8-80 kip]
2.5N	Drilled holes with stiffened version of the “angles-with-plate” retrofit applied in top web gap	36-356 kN
2.5S		[8-80 kip]
2.6N	Same as Trials 2.5N and 2.5S in top web gap; four-angle retrofit applied in bottom web gap of center girder	44-445 kN
2.6S		[10-100 kip]
2.7N	Same as Trials 2.5N and 2.5S in top web gap with four-angle retrofit applied in bottom web gap of center girder; cross frame replaced between center and south girders	44-445 kN
2.7S		[10-100 kip]

The load range applied to the test bridge was varied over the course of the testing sequences to create a demanding evaluation of the angles-with-plate retrofit effectiveness at reducing distortion-induced fatigue crack propensity. The load range applied to the bridge in

Trials 1.1S, 1.1N, 1.2S, and 1.2N was 27-267 kN [6-60 kip] which corresponded to a maximum normal bending stress of 29.6 MPa [4.3 ksi] in the bottom flange of the center girder. For those trials, this load range was found to produce vertical strains of approximately 250 $\mu\epsilon$ – 850 $\mu\epsilon$ in the top web gap regions of the south and north girders, and to produce a maximum vertical deflection at midspan of 2.0 mm [0.077 in.]. Details regarding the strain and deflection measurements under the various load ranges for both Tests 1 and 2 have been provided in Tables 3 and 4.

Table 3: Test 1 Specimen trials with load range and bottom flange stresses

Trial	Sample Load kN [kip]	Girder Max. Deflection mm [in.]	Girder Maximum Bottom Flange Stress MPa [ksi]	Uncracked Top Web Gap Strain Gages (3)/(4 & 5) ($\mu\epsilon$)	Cracked Top Web Gap Strain Gages (3)/(4 & 5) ($\mu\epsilon$)
1.1N	267 [60]	0.8 [0.033]	9.7 [1.4]	-705/285-352	-818/252-333
<i>Center</i>		2.0 [0.077]	29.6 [4.3]	N/A	N/A
1.1S		0.8 [0.032]	8.3 [1.2]	-839/522-556	-854/521-556
1.2N	267 [60]	0.9 [0.034]	9.7 [1.4]	-705/285-352	
<i>Center</i>		1.9 [0.075]	29.6 [4.3]	N/A	
1.2S		0.8 [0.032]	8.3 [1.2]	-839/522-556	
1.3N	356 [80]	1.1 [0.044]	13.1 [1.9]	-963/377-468	
<i>Center</i>		2.3 [0.091]	40.0 [5.8]	N/A	
1.3S		1.1 [0.042]	11.0 [1.6]	-1120/694-742	
1.4N	445 [100]	1.3 [0.051]	16.5 [2.4]		
<i>Center</i>		3.4 [0.134]	48.3 [7.0]		
1.4S		1.4 [0.055]	14.5 [2.1]		
1.5N	445 [100]	1.4 [0.056]	15.9 [2.3]		
<i>Center</i>		3.7 [0.145]	--		
1.5S		1.3 [0.052]	12.4 [1.8]		
1.6N	534 [120]	1.6 [0.062]	17.9 [2.6]		
<i>Center</i>		4.5 [0.178]	--		
1.6S		1.5 [0.059]	15.9 [2.3]		
1.7N	534 [120]	1.4 [0.054]	15.2 [2.2]		
<i>Center</i>		4.9 [0.193]	--		
1.7S		1.3 [0.053]	13.1 [1.9]		

Table 4: Test 2 Specimen trials with load range and bottom flange stresses

Trial	Sample Load kN [kip]	Girder Max. Deflection mm [in.]	Girder Maximum Bottom Flange Stress MPa [ksi]	Uncracked Top Web Gap Strain Gages (3)/(4 & 5) ($\mu\epsilon$)	Cracked Top Web Gap Strain Gages (3)/(4 & 5) ($\mu\epsilon$)
2.1N	267 [60]	0.8 [0.031]	8.3 [1.2]	-924/784-843	-914/815-843
<i>Center</i>		2.1 [0.082]	--	N/A	N/A
2.1S		0.8 [0.033]	9.0 [1.3]	-950/789-1011	-919/832-1100
2.2N	267 [60]	0.7 [0.029]	7.6 [1.1]	-924/784-843	
<i>Center</i>		2.2 [0.087]	--	N/A	
2.2S		0.8 [0.030]	8.3 [1.2]	-950/789-1011	
2.3N	356 [80]	1.0 [0.038]	10.3 [1.5]	-1252/1099-1175	
<i>Center</i>		3.0 [0.117]	--	N/A	
2.3S		1.0 [0.041]	11.0 [1.6]	-1308/1101-1421	
2.4N	356 [80]	1.1 [0.043]	11.7 [1.7]	-1252/1099-1175	
<i>Center</i>		2.7 [0.107]	--	N/A	
2.4S		1.2 [0.046]	12.4 [1.8]	-1308/1101-1421	
2.5N	356 [80]	0.9 [0.035]	9.7 [1.4]	-1252/1099-1175	
<i>Center</i>		3.1 [0.122]	--	N/A	
2.5S		1.0 [0.038]	11.0 [1.6]	-1308/1101-1421	
2.6N	445 [100]	1.4 [0.057]	13.8 [2.0]		
<i>Center</i>		3.5 [0.137]	--		
2.6S		1.4 [0.054]	15.9 [2.3]		
2.7N	445 [100]	1.1 [0.045]	11.0 [1.6]		
<i>Center</i>		3.9 [0.154]	--		
2.7S		1.1 [0.043]	11.0 [1.6]		

All values in Tables 3 and 4, with the exception of uncracked strains, were recorded at the end of the reported trial. Strains in the uncracked north and south girders were only recorded up to a load of 356 kN [80 kip]. Strains in cracked north and south girders were only recorded for Trials 1.1N, 1.1S, 2.1N, and 2.1S since retrofit application caused gages in the top web gap to fail. Maximum girder deflection at midspan was measured directly using an LVDT under each girder. Strain transducer data was used to determine maximum bottom flange bending stress. For each girder, the two strain transducers were used to develop a strain profile. These were placed in the web; however, bending strains were extrapolated to the bottom flange (the extreme fiber). Additionally, these strains were not located at midspan so they were modified to represent midspan strains using a linear variation between support and midspan due to single point loading at midspan. Since large amounts of data were collected, each strain reading is an average of four consecutive data points. All data was averaged in a similar fashion and data for the given maximum load was extracted which resulted in a single set of data for each load.

Three other load ranges were applied in various test trials: 36-356 kN [8-80 kip] (Trials 1.3S, 1.3N, 2.3S, 2.3N, 2.4S, 2.4N, 2.5S, and 2.5N); 44-445 kN [10-100 kip] (Trials 1.4S, 1.4N, 1.5S, 1.5N, 2.6S, 2.6N, 2.7S, and 2.7N); and 53-534 kN [12-120 kip] (Trials 1.6S, 1.6N, 1.7S, and 1.7N). The largest load range used in the test sequence, 53-534 kN [12-120 kip], produced a maximum vertical deflection at midspan under the 53-534 kN [12-120 kip] load range of 4.9 mm [0.193 in.] in Trial 1.7. An issue with the bottom strain transducer resulted in nonlinear data for bending stresses in the bottom flange of the center girder under the 53-534 kN [12-120 kip] load range. Extrapolating from previous loading data for the 53-534 kN [12-120 kip] loading, an approximate maximum normal bending stress in the bottom flange of the center was determined to be 57.9 MPa [8.4 ksi].

The load ranges were chosen to be quite large and were higher than what was expected for typical fatigue loadings in an actual bridge structure. Choosing large variation in load range was intended to assess retrofit performance over a full range of load demand. The authors did not wish to approach the test design by using loadings that would ensure no crack initiation or propagation under the retrofit. Therefore, it was expected that cracking would propagate under the high load demands, even while retrofitted. Changes in crack propagation rates between unretrofitted and retrofitted conditions were therefore of key interest to the investigators.

Results and Discussion

Throughout testing, data was recorded through the instrumentation plan discussed and crack growth was monitored and charted. By examining crack length against the number of applied cycles, the rate of crack propagation was compared between the various unretrofitted and retrofitted test cycles. Changes in bridge behavior and crack propagation rates were used to evaluate the retrofit effectiveness. Cross frame strains and girder lateral deflections helped to establish changes in bridge behavior while crack inspections were used to track crack propagation.

Changes in overall bridge response were observed by comparing cross frame strains when girders were in an uncracked condition with cross frame strains when girders were in a cracked condition. Similarly, this observation was made for the cross frames with girders in the unretrofitted versus the retrofitted conditions after cracking in the girders had occurred. Lateral deflections of the north and south girder profiles were also monitored throughout testing. In

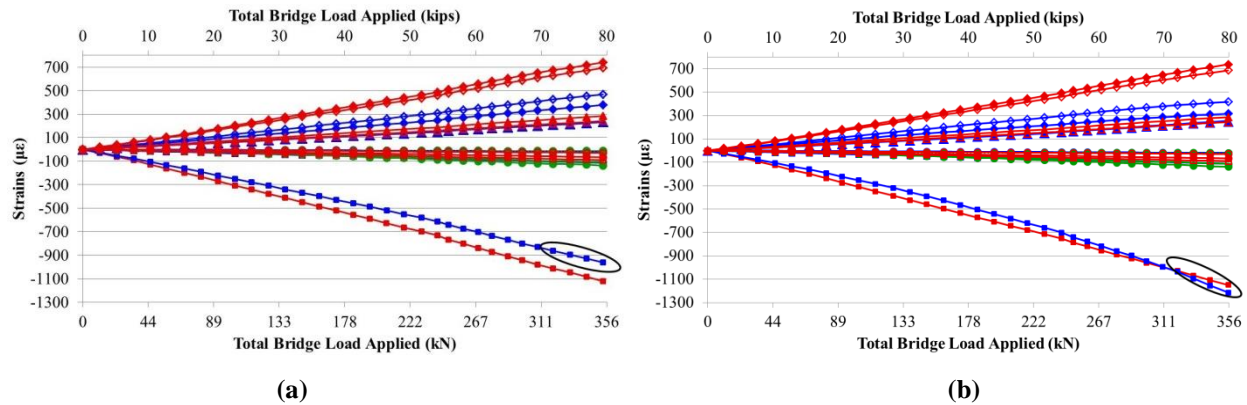
addition to these global bridge responses, crack initiation was established through strain gage data while crack propagation was monitored through visual and photographic inspection.

Crack Initiation and Propagation

Crack propagation was of particular importance to the investigators since the primary method for establishing retrofit effectiveness is the ability of the retrofit to slow or halt crack growth. Initially, measurements from bondable strain gages in the top web gaps on the north and south girders were used to identify possible crack initiation. After crack initiation was visually confirmed using dye penetrant, crack propagation was monitored and charted while the girder was in the unretrofitted condition. Crack lengths were also monitored before and after retrofit applications, providing information regarding crack propagation while retrofits were in place. Changes in crack propagation rate were of particular interest. In the following sections crack initiation and propagation behavior for the north and south girders in Test 1 and Test 2 have been explained in detail.

Crack Initiation – Test 1

At the beginning of the test sequence (Trials 1.1S and 1.1N), the uncracked, unretrofitted test bridge was cycled between 27-267 kN [6-60 kip] at a frequency of 1 Hz. Visual inspections of the web gap regions were performed every 5,000 cycles while static data from all instrumentation was recorded every 15,000 cycles. Strain gages placed on the fascia side of the north girder (gage 3 in Figure 4(b)) indicated potential cracking at 15,000 cycles. Figure 8 displays the *increase* in strain from -950 $\mu\epsilon$ to -1225 $\mu\epsilon$ experienced by the gage of interest.



North Girder				Middle Girder				South Girder			
North Face (Fascia)		Stiffener Side (Stiffener)		North Face		South Face		North Face (Stiffener)		South Face (Fascia)	
—○— B(3)	—△— T(2)	—◇— T(5)	—□— B(5)	—○— B(4)	—◇— B(5)	—◇— B(5)	—◇— B(4)	—◇— T(4)	—◇— B(4)	—◇— B(3)	—△— T(1)
—●— T(3)	—▲— T(1)	—◆— T(4)	—◆— B(4)					—◇— T(5)	—◇— B(5)	—◇— T(3)	—△— T(2)

Figure 8: Strains in top web gaps at (a) 0 cycles and (b) 15,000 cycles. Top web gap denoted by T in legend and bottom web gap denoted by B. Number denotes gage location from Figure 4(c).

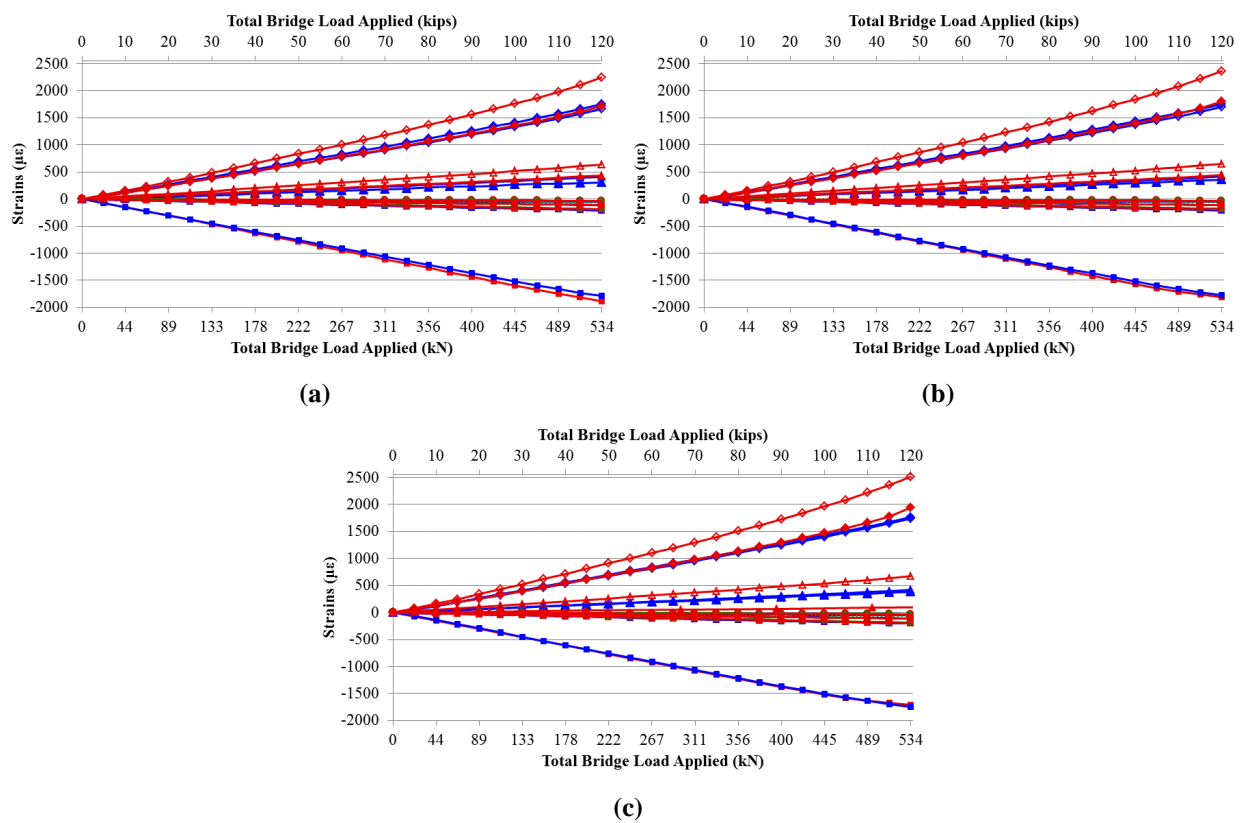
Although strain gages indicated potential cracking on the north girder, a visual inspection performed using dye penetrant was unable to identify visible cracking at that point; however, at 20,000 cycles (just 5,000 additional cycles) cracking was visually identified at the connection plate-web weld in the north girder. This indicated excellent agreement between the two crack indication / inspection techniques.

Crack Initiation – Test 2

Trial 2.1 was similar in sequence to Trial 1.1. The bridge was cycled between 27-267 kN [6-60 kip] at a frequency of 1 Hz, and static data from all instrumentation was recorded after every 15,000 cycles. Based on crack initiation observations from Test 1, the first visual inspection was performed at 15,000 cycles. During this inspection, a crack was detected in the top web gap of the south girder at the flange-web weld. No major change in strain was measured by the top strain gages between 0 and 15,000 cycles; gages near the top flange were likely spaced too far from the connection stiffener to detect this crack. Additionally, this crack was not expected to be the initial crack in the girder, as the connection plate-web weld crack had appeared first in Test 1, as well as in other investigations (Alemdar et al. 2013a; 2013b).

After the initial 15,000 cycles, visual inspections were performed every 5,000 cycles for the remainder of Trial 2.1. Initiation of the connection plate-web weld crack occurred between 30,000 and 45,000 cycles in the top web gap of the south girder. Figure 9 displays changes in

strain measurements between 15,000, 30,000, and 45,000 cycles. At 30,000 cycles, no connection plate-web weld crack was apparent upon physical inspection; however, the top strain gages near the connection plate were indicating increases in strain magnitude, indicating that a crack was likely to appear in the near future. The connection plate-web weld crack became visible in the top web gap of the south girder at 45,000 cycles, at which point the strain gage on the fascia side of the south girder (gage 3 in Figure 4(b)) indicated an increase in strain of 170 $\mu\epsilon$. Additionally, the two top strain gages on the stiffener side indicated increases in strain between 220 $\mu\epsilon$ and 265 $\mu\epsilon$.



North Girder				Middle Girder				South Girder			
North Face (Fascia)		Stiffener Side (Stiffener)		North Face		South Face		North Face (Stiffener)		South Face (Fascia)	
—○— B(3)	—△— T(2)	—◇— T(5)	—□— B(5)	—○— B(4)	—◇— B(5)	—◇— B(5)	—◇— B(4)	—◇— T(4)	—◇— B(4)	—◇— B(3)	—△— T(1)
—◇— T(3)	—△— T(1)	—◇— T(4)	—◇— B(4)					—◇— T(5)	—◇— B(5)	—◇— T(3)	—△— T(2)

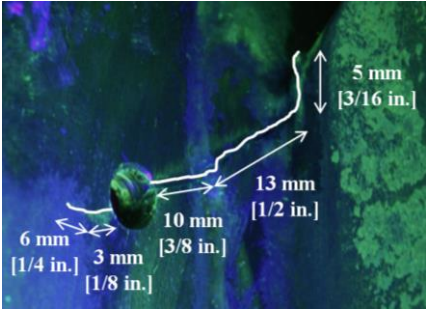
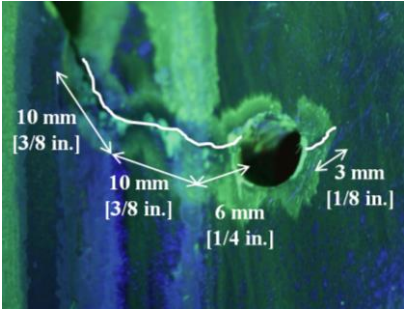
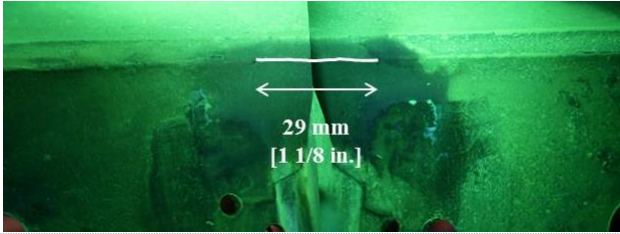
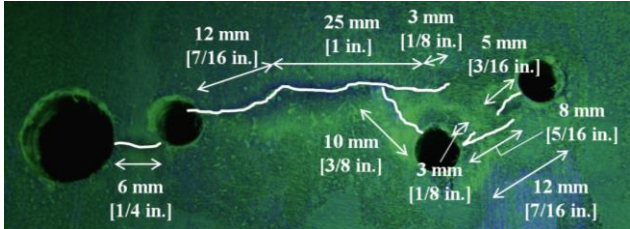
Figure 9: Strains in top web gaps at (a) 15,000 cycles, (b) 30,000 cycles, and (c) 45,000 cycles. Top web gap denoted by T in legend and bottom web gap denoted by B. Number denotes gage location from Figure 4(c).

Crack Propagation Pattern – Test 1

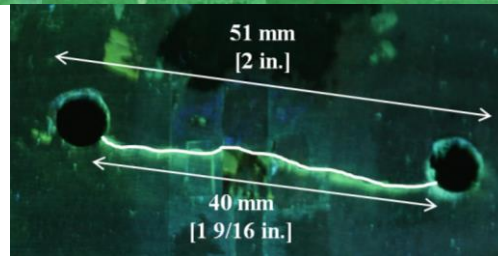
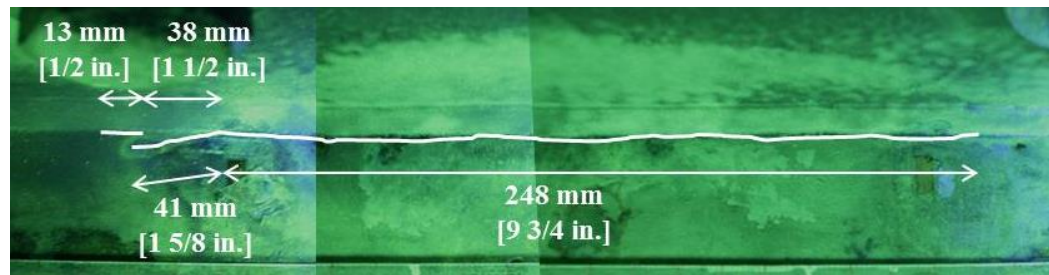
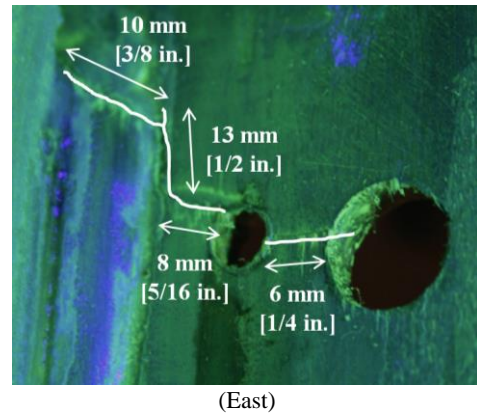
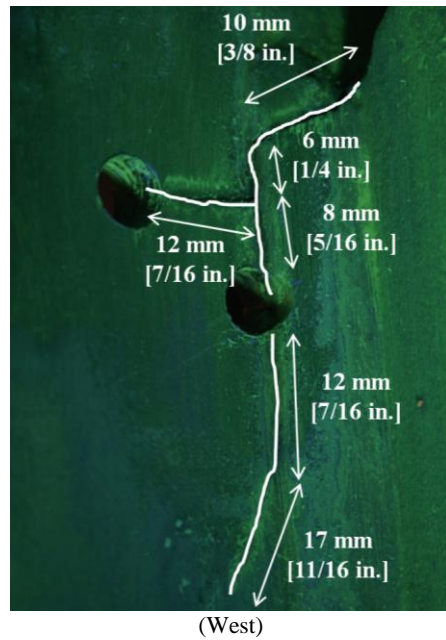
In Trials 1.1S and 1.1N, cracking initiated at the weld near the clip in the transverse connection plate. Cracking progressed diagonally down through the weld until reaching the girder web.

During Trial 1.1S, cracking progressed down the weld toe in the south girder until branching out into a spider crack. These spider cracks propagated outward away from the transverse connection plate. On the left side of the transverse connection plate, cracking also progressed down the web at the weld toe. Cracking in the north girder progressed slightly differently, in that cracks did not propagate into the web until Trial 1.2N and did not follow the weld toe. Longitudinal cracks at the flange-web weld were found in Trials 1.6N and 1.6S. The point of initiation was unclear for the longitudinal cracking, since the north girder longitudinal cracks were quite large when discovered at the end of Trial 1.6N. Table 5 shows the cracking patterns at the end of Trials 1.6S and 1.6N.

Table 5: Cracking at end of Trial 1.6 (6,011,097 Cycles)

	Left Side of Connection Plate	Right Side of Connection Plate
South Girder	 <p>(East)</p>	 <p>(West)</p>
		
		

North Girder



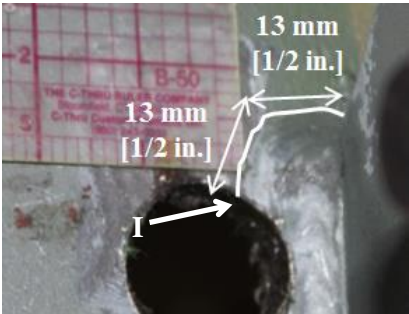
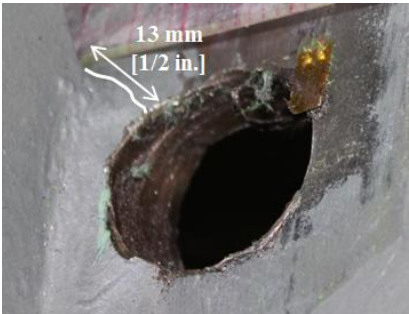
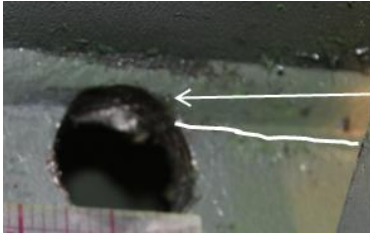
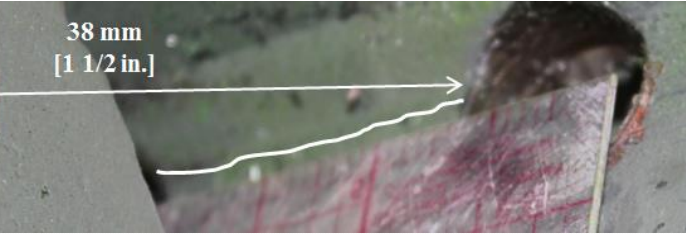
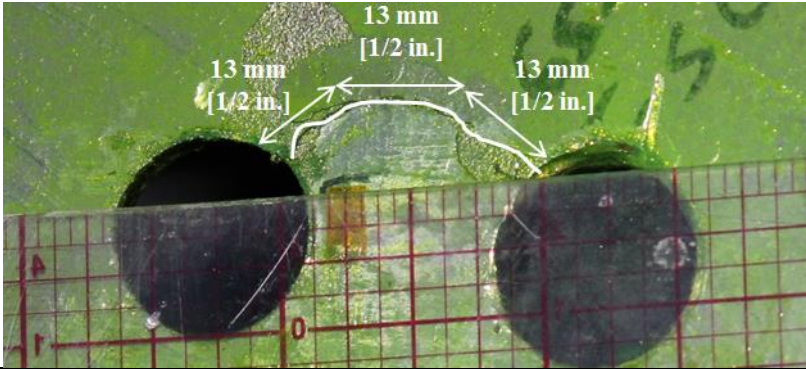
Crack Propagation Pattern – Test 2

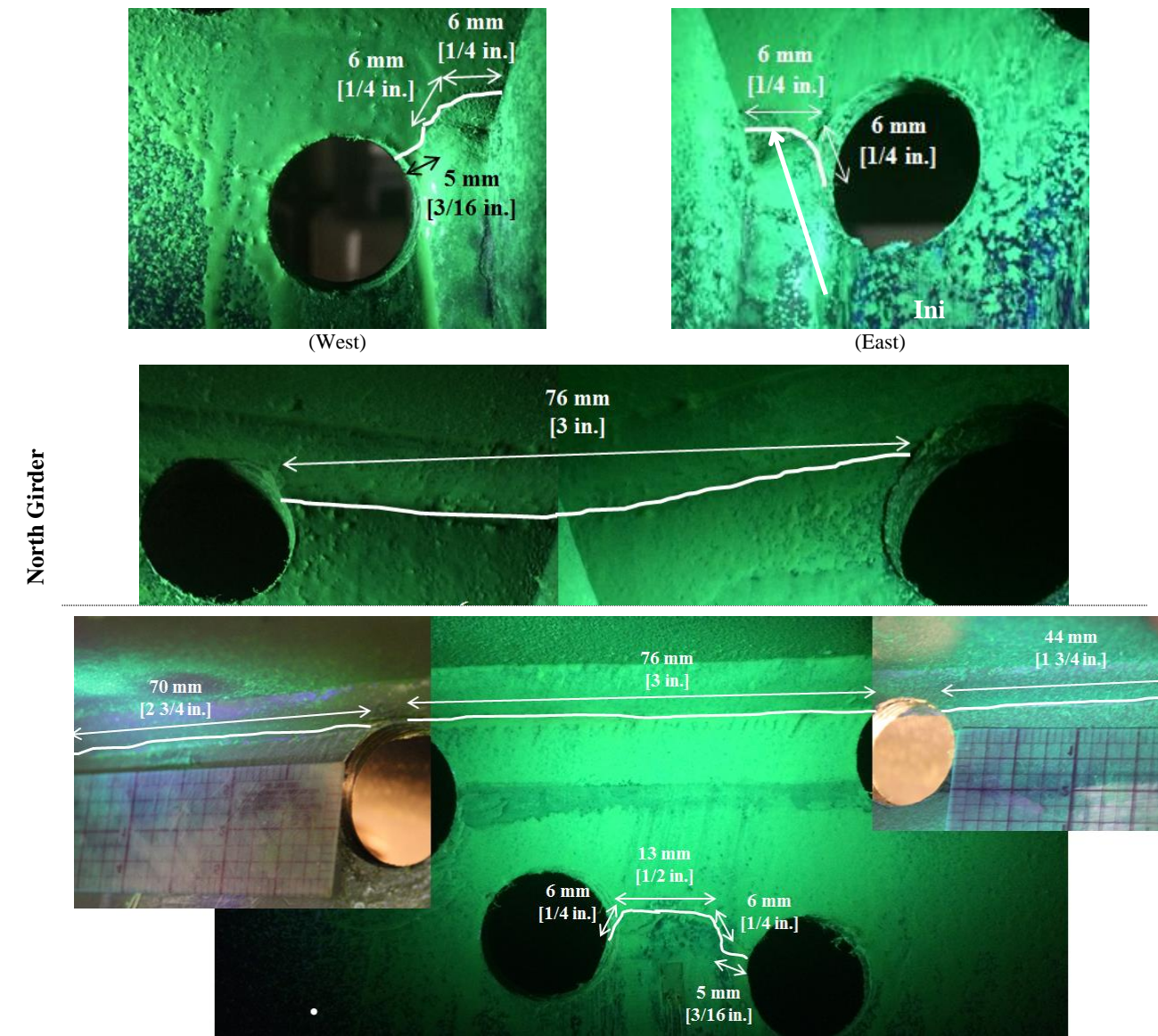
During Trial 2.1S, a longitudinal crack at the flange-web weld was found in the top web gap of the south girder, directly above the connection plate. This crack did not propagate until initiation of the crack near the clip in the transverse connection plate, also in Trial 2.1S. The longitudinal crack propagated along the flange-web weld, while the connection plate-web weld progressed around and down each side of the weld toe. The connection plate-web weld cracks in

the south girder never branched into spider cracks. Table 6 shows the cracking patterns at the end of Trials 2.7S.

The north girder behaved differently in that cracking first initiated at the weld near the clip in the transverse connection plate during Trial 2.1N and no progression in this crack was physically detected until Trial 2.3N. The crack propagated around the weld toe before branching into a spider crack on the west side of the connection plate. Propagation around the east side of the weld toe was not seen until Trial 2.4N. A longitudinal crack at the flange-web weld was also found in Trial 2.3N, directly above the connection plate, which progressed along the flange-web weld. Table 6 shows the cracking patterns at the end of Trials 2.7N.

Table 6: Cracking at End of Trial 2.7 (4,016,092 Cycles)

	Left Side of Connection Plate	Right Side of Connection Plate
	 <p>(East)</p>	 <p>(West)</p>
South Girder		
		



Trials 1.1N-1.7N Crack Growth (North Girder Test 1 Trials)

Crack length is plotted against the number of fatigue cycles in Figure 10, for cracks around the connection plate. Cracks were categorized as vertical cracks, spider cracks, through cracks, or longitudinal cracks. When holes were drilled at crack tips, an instantaneous jump was recorded in the graph that is not connected by a line. For locations where a crack grew into an existing crack-arrest hole, only the crack propagation was plotted. As shown in Figure 10, an instantaneous jump at the end of that test trial is shown with a solid line to denote the difference between drilling a crack-arrest hole and propagating into a pre-existing hole. The crack

propagation plot in Figure 10 is also labeled with other notable test events, including cross frame failures that occurred during Trial 1.4N and Trial 1.7N.

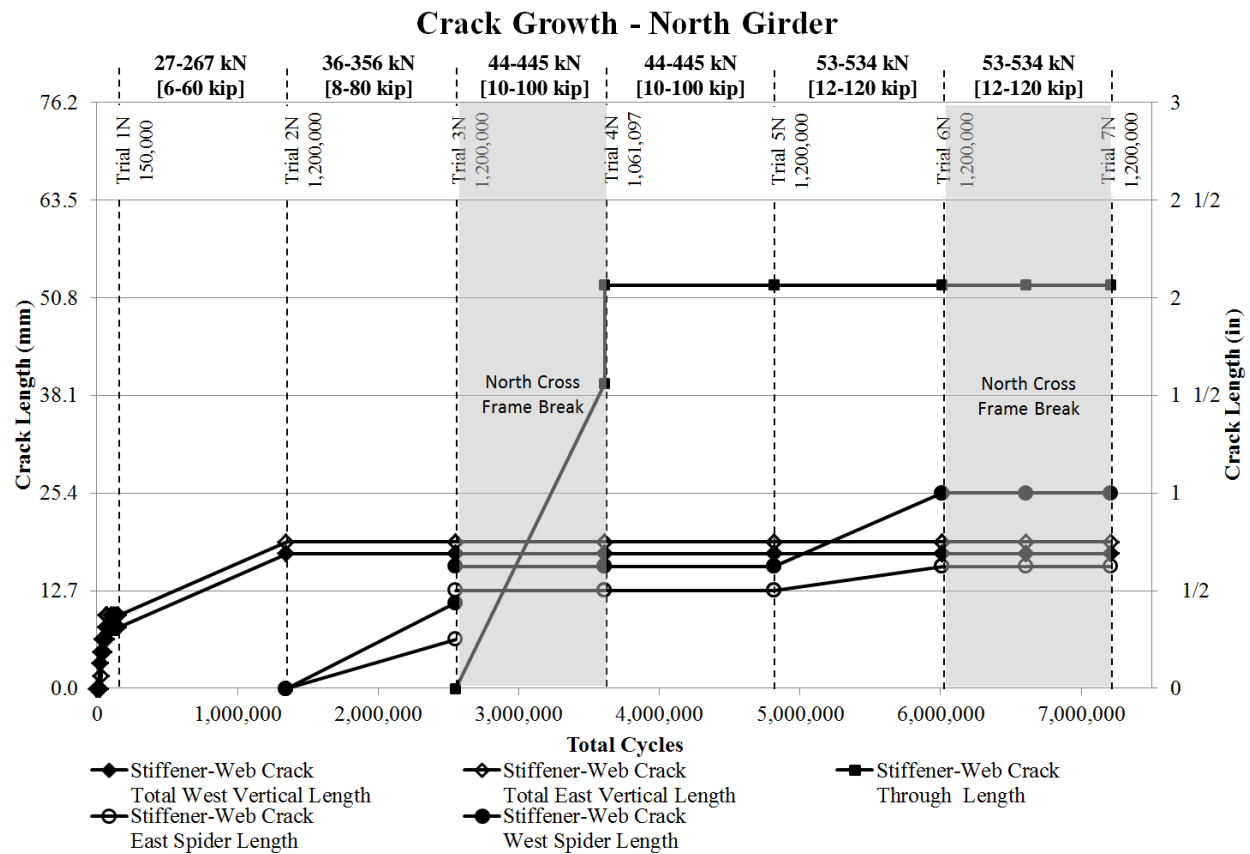


Figure 10: North girder crack growth around transverse connection plate in Test 1.

Cracking initiated in the north girder at approximately 20,000 cycles during Trial 1.1N. During Trial 1.1N, cracking in the north girder reached a length of 8 mm [5/16 in.] on the left side (west) and 10 mm [3/8 in.] on the right side (east) of the transverse connection plate. Both cracks propagated diagonally downward through the weld throat, but did not propagate outwards into the web. Cracking in the north girder stabilized around 65,000 cycles with no further growth during Trial 1.1N, which was 150,000 cycles in total.

With the angles-with-plate retrofit in place during Trial 1.2N, north girder cracking lengthened under the retrofit application. Based on previous research (Alemdar et al. 2013a; 2013b) and a detailed finite element study of the 9.1 m [30 ft.] test bridge by Hartman (2010), it is postulated that in this extreme situation where the stress demands are high for a small crack, small amounts of propagation may occur under the retrofit; however, as cracking propagates, this

high stress decreases and cracking will slow. Additionally, the load range utilized during testing of the model bridge is greater than would normally be withstood in field applications. A comparison of crack propagation rates between Trials 1.1N and 1.2N show that the average crack propagation rate was decreased from $1.2\text{E-}04$ mm/cycle [$4.6\text{E-}06$ in./cycle] in Trial 1.1N to $1.6\text{E-}05$ mm/cycle [$6.3\text{E-}07$ in./cycle] in Trial 1.2N.

During Trial 1.3N, cracks again propagated into the web of the north girder in the form of spider cracks. Spider crack length out into the web was measured to be 11 mm [$7/16$ in.] on the west side of the connection plate and 6 mm [$1/4$ in.] on the east side of the connection plate. Spider crack dimensions provided are in addition to the cracking that occurred through the weld, which is 18-mm [$11/16$ -in.] long on the west side of the connection plate and 19-mm [$3/4$ -in.] long on the east side of the connection plate.

Small crack-arrest holes with a 6-mm [$1/4$ -in.] diameter were drilled at the crack tips before the start of Trial 1.4N, the angles-with-plate retrofit was reapplied, and the load range was increased to 44-445 kN [10-100 kip]. Approximately 650,000 cycles into Trial 1.4N, a faint clicking noise was observed originating from the connection plate in the north girder. After inspection of strain data, no notable change in bridge response was noticed. However, when the bridge was visually inspected 1.06 million cycles into Trial 1.4N, the cross frame between the north and middle girders was found to be cracked completely through at the tab plate, as shown in Figure 11.



Figure 11: North cross frame failure during Trial 4N.

During inspection, there was no evidence of fretting due to the angles-with-plate retrofit. Measured strains in the cross frame element prior to fracture were approximately $375\text{ }\mu\epsilon$, which, based on modulus of elasticity for steel of 200 GPa [29,000 ksi], correlated with an approximate stress of 75 MPa [11 ksi]. It is estimated that the crack started at the bottom corner of the weld toe where the cross frame diagonal member (AT) framed into the tab plate.

Due to the cross frame member failure (member AT) during Trial 1.4N, the angles-with-plate retrofit was removed and a detailed inspection was performed for the entire bridge. After inspection, it was noticed that the north girder through-crack developed between the two 6-mm [1/4-in.] diameter crack-arrest holes. However, the spider cracking had not progressed through the crack-arrest holes.

Due to the cross frame failure experienced in Trial 1.4N, Trial 1.5N was performed as a repeat of Trial 1.4N. No crack propagation was experienced during Trial 1.5N; however, at the end of Trial 1.6N in which the load was increased to 53-534 kN [12-120 kip], a 298 mm [11 3/4 in.] longitudinal crack was discovered at the top flange-web weld. Prior to Trial 1.6N inspection, the last inspection was performed at the end of Trial 1.5N. At this time, no longitudinal crack was reported; however, ridges at the weld toe and extremely small crack opening displacements impeded crack detection. It should be noted that the loading applied during Trial 1.6N was expected to be much larger than typical fatigue bridge loading. Due to this, the final trials are believed to have pushed this specimen well beyond most practical applications.

Prior to the start of Trial 1.7N, 19 mm (3/4 in.) crack-arrest holes were drilled at the crack tips of the 298 mm (11 3/4 in.) longitudinal crack at the top flange-web weld and a stiffened version of the angles-with-plate retrofit was applied. Approximately 150,000 cycles into Trial 1.7N, the longitudinal crack grew past the crack-arrest hole on the west side of the retrofit. An additional 19 mm (3/4 in.) crack-arrest hole was drilled at the tip of the crack. As testing continued, the crack again grew past the additional crack-arrest hole. It was decided that the crack was in a state of unstable propagation and crack-arrest holes would not contain the longitudinal crack growth at this level of loading. Instead of continuing to drill crack-arrest holes, the longitudinal crack at the top flange-web weld was welded 300,000 cycles into Test Trial 1.7N. It was recognized that this invalidated any further results from Trial 1.7N, and it should be emphasized that the welding of the flange-web weld crack was only performed so that

testing on the south girder could continue for short duration, and is *not* a recommended fatigue repair.

Approximately 1.19 million cycles into Trial 1.7N, a clicking noise was noticed originating from the center girder. It was discovered that the cross frame between the north and middle girders cracked completely through the bottom horizontal angle. The crack occurred on the end of the angle nearest to the middle girder.

Trials 1.1S-1.7S Crack Growth (South Girder Test 1 Trials)

Cracking experienced around the transverse connection plate in the south girder in Test 1 is shown in Figure 12. The same crack definitions were applied as those used in the north girder as described in the previous section. Drilled holes are denoted by an instantaneous jump with no line, and cracks that propagated into an existing hole were denoted by an instantaneous jump with a connecting solid line.

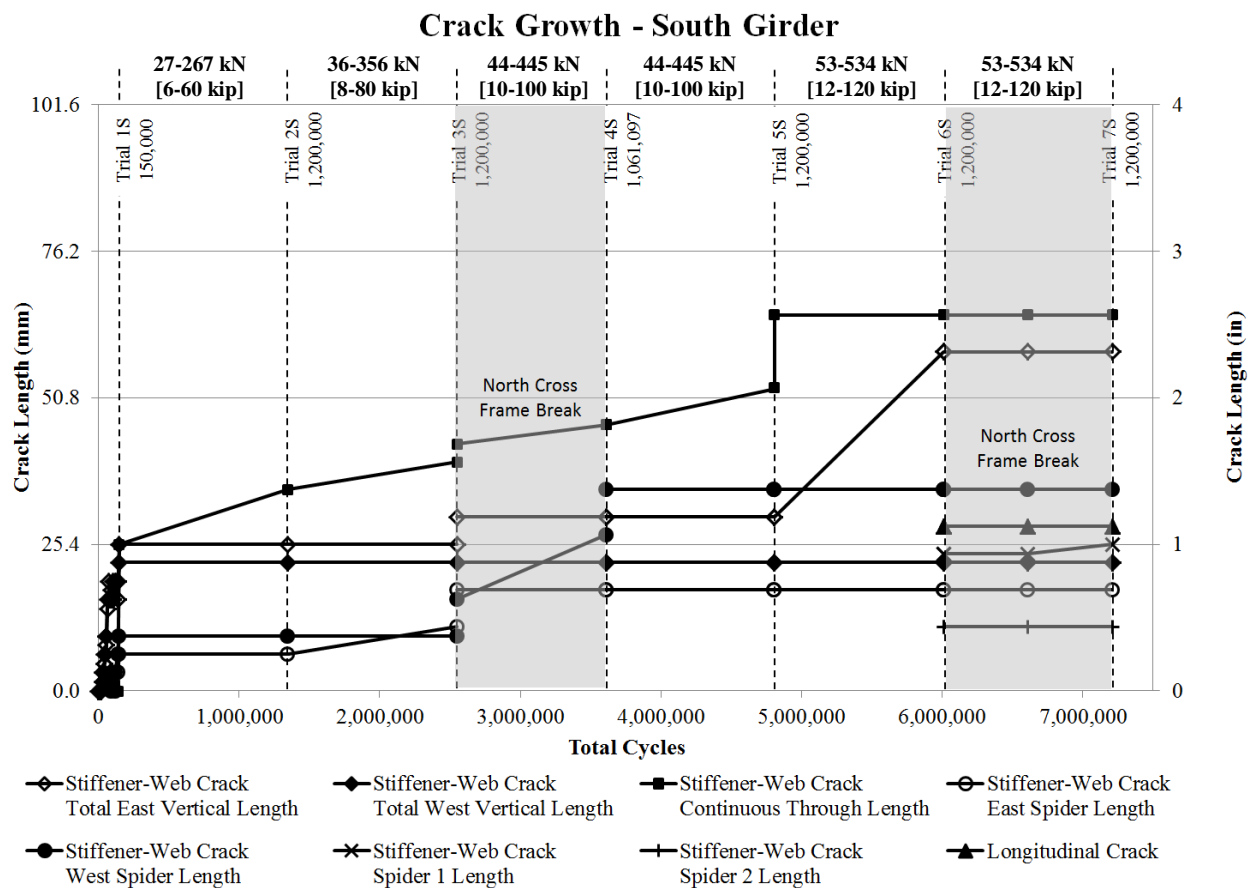


Figure 12: South girder crack growth around transverse connection plate in Test 1.

Cracking in the south girder initiated during Trial 1.1S at 30,000 cycles in the unretrofitted condition, approximately 10,000 cycles after north girder cracking initiated. South girder cracking propagated through the connection plate weld and into the web at a steady rate until about 75,000 cycles. At this time, vertical cracking along the weld toe slowed. The first evidence of spider cracking began at 105,000 cycles. Between 105,000 and 120,000 cycles, the spider cracking propagated through the web, debonding the strain gage (3) (Figure 4(c)) on the fascia side of the south girder. This crack initiation was hidden behind the bonded gage and was first detected at 150,000 cycles. During Trial 1.1S, a maximum crack length of 25 mm [1 in.] was reached by the vertical cracking on the left side of the connection plate that also propagated through the web to produce a “through-crack” length.

During Trial 1.2S, under application of the angles-with-plate retrofit, cracking on the interior face of the girder did not change; however, fascia cracking increased by a length 6 mm [1/4 in.]. This crack was formed as a through-thickness crack from the spider cracking seen on the interior side of the girder. The total length of the crack seen on the fascia side was 35 mm [1 3/8 in.] which correlated with the total projected crack length on the interior side of the girder including the spider crack length (9.5 mm + 6 mm [3/8 in. + 1/4 in.]), connection plate width (9.5 mm [3/8 in.]), and weld width (9.5 mm [3/8 in.]). It is believed that the change in the fascia girder crack length can be attributed to the existing interior crack propagating through the thickness of the girder.

Trial 1.3S resulted in crack propagation. Spider cracking reached 11 mm [7/16 in.] on the east side of the connection plate and 10 mm [3/8 in.] on the west side of the connection plate. Vertical cracking on the east side of the connection plate did not propagate during Trial 1.3S. Through-crack length increased by 5 mm [3/16 in.]. At the end of Trial 1.3S, 6-mm [1/4-in.] diameter crack-arrest holes were drilled at the crack tips of the spider cracks and the vertical crack in the south girder.

Trial 1.4S was halted due to north cross frame failure as discussed previously. At the end of Trial 1.4S, minimal crack growth was seen in the through-web crack on the south girder, while the spider crack on the right side (west side) of the south girder grew through the 6-mm [1/4-in.] diameter crack-arrest hole. At the tip of this extended crack, a 13-mm [1/2-in.] diameter hole was drilled for the start of Trial 1.5S.

Similar to behavior observed in the north girder, cracking did not propagate under the angles-with-plate retrofit during Trial 1.5S. Increasing the load during Trial 1.6S resulted in some crack growth. Along the connection plate-web weld, cracking grew down vertically through the 6-mm [1/4-in.] crack-arrest hole as seen in Table 5. Careful inspection of the flange-web weld resulted in confirmation of a longitudinal crack detected with 29 mm [1 1/8 in.] length on the connection plate side of the web. As with the north girder, loading during this test cycle was larger than expected fatigue loading.

Prior to the start of Trial 1.7S, 19 mm (3/4 in.) crack-arrest holes were drilled as close as possible to the crack tips of the 29 mm (1 1/8 in.) longitudinal crack at the top flange-web weld and the stiffened version of the angles-with-plate retrofit was applied. Due to the size of the crack and its location above the connection plate in the top web gap, it was not possible to drill the crack-arrest holes exactly at the crack tips. It was assumed that if the crack grew, it would grow to the crack-arrest holes. Upon completion of Trial 1.7S, no growth was detected in the longitudinal crack at the top flange-web weld. Minimal crack growth occurred in one of the stiffener-web spider cracks between crack-arrest holes on the fascia side of the south girder.

Trials 2.1N-2.7N Crack Growth (North Girder Test 2 Trials)

Cracking in the top web gap of the north girder during Test 2 trials is shown in Figures 13 and 14. Figure 13 shows crack growth around the transverse connection plate, while Figure 14 shows longitudinal crack growth along the flange-web weld. The cracks were each categorized using the same definitions from Test 1, as vertical cracks, spider cracks, through cracks, or longitudinal cracks. An instantaneous jump in crack length not connected by a solid line indicates where crack-arrest holes were drilled at crack tips. If a crack grew into an existing crack-arrest hole, the crack propagation was depicted by connecting the instantaneous jump with a solid line.

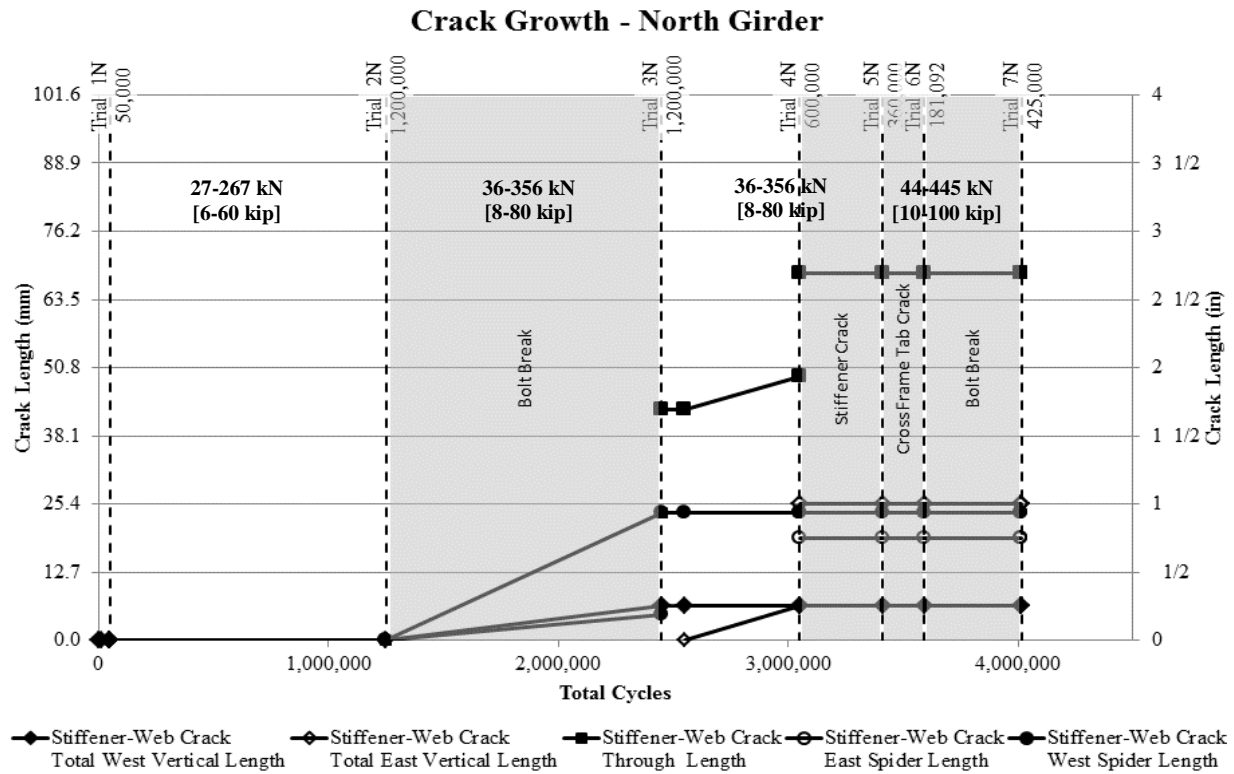


Figure 13: North girder crack growth along transverse connection plate in Test 2.

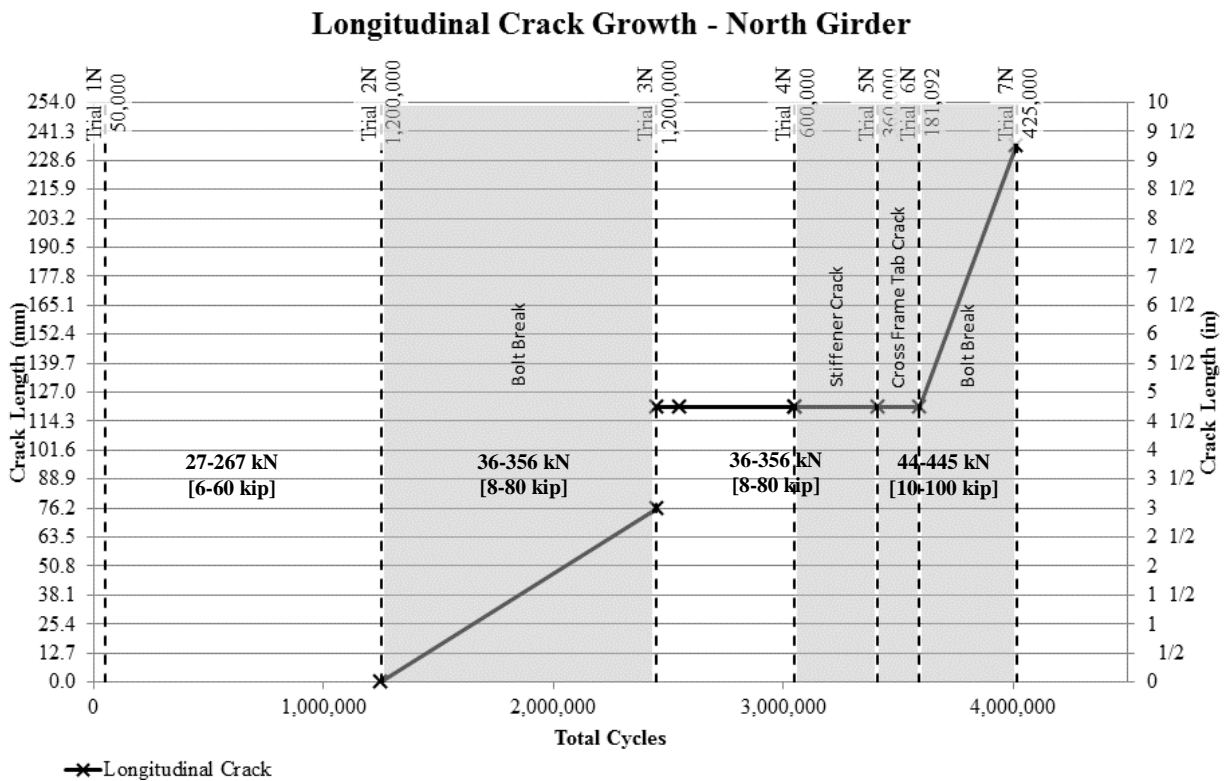


Figure 14: North girder crack growth along flange-web weld in Test 2.

Cracking initiated in the north girder at approximately 50,000 cycles during Trial 2.1N. Since crack lengths recorded in Trial 2.1S warranted application of the retrofit at 50,000 cycles, no further growth was seen in the north girder cracking in Trial 2.1N. The longitudinal crack in the south girder had reached what was considered a critical length of 38 mm [1.5 in.]; therefore, it was decided that retrofits would be applied to the bridge after 50,000 cycles despite the fact that little crack activity had been noted in the north girder.

The stiffened version of the angles-with-plate retrofit was applied at the beginning of Trial 2.2N. Trial 2.2N reached 1.2 million cycles, after which no crack propagation was visually detected in the north girder. Trial 2.3N also reached 1.2 million cycles. However, upon removal of the retrofit at the end of Trial 2.3N, it was found that the top bolt connecting the east angle to the backing plate had failed in tension, as seen in Figure 15. Upon inspection, the crack at the connection plate-web weld had propagated 6 mm [1/4 in.] down the left (west) side of the weld and out into the web in the form of a spider crack 5 mm [3/16 in.]. The connection plate-web weld crack and spider crack were also visible on the fascia side of the girder. A 76 mm [3 in.] longitudinal crack was also found at the flange-web weld on the fascia side of the north girder's web at the end of Trial 2.3N.

A finite element study of the 9.1 m [30 ft.] test bridge was performed to study the effect that the failed bolt may have had on crack growth. Findings from this study can be found in Appendix D. Based on comparisons of stress demand in models that represented the bridge with an intact retrofit and another with the version of the retrofit with a failed bolt, development of the flange-web weld longitudinal crack and propagation of the connection plate-web weld crack under the retrofit were likely due to loss of stiffness from the failed bolt.



Figure 15: Broken bolt at the end of Trial 2.3N.

Crack-arrest holes with a 19 mm [3/4 in.] diameter were drilled at the crack tips at the start of Trial 2.4N. Due to the crack growth that occurred during Trial 2.3N, the retrofit was removed and the north girder was inspected 100,000 cycles into Trial 2.4N. No crack growth was detected and the trial was continued an additional 500,000 cycles. At this point, the retrofit was removed and the north girder was inspected again. The crack at the connection plate-web weld had propagated 6 mm [1/4 in.] down the right (east) side of the weld and was visible on both sides of the web. A 19 mm [3/4 in.] diameter crack-arrest hole was drilled at the crack tip and cyclic loading continued. Due to factors explained in the following paragraph, this was marked as the end of the trial. Therefore, Trial 2.4N reached a total of 600,000 cycles.

360,000 cycles into Trial 2.5N, a loud “thunking” sound was heard when removing load at the end of a testing cycle. Upon inspection, a large crack was found in the cross frame connection plate at the south face of the center girder, as shown in Figure 16. It appeared that the crack initiated at the weld toe where the connection plate framed into the center girder web and then propagated through the connection plate. No crack in the connection plate had been detected at the end of Trial 2.4N. Due to this, the 360,000 cycles that ran after the end of Trial 2.4N and before detection of the connection plate crack was deemed Trial 2.5N. The stiffened version of the angles-with-plate retrofit was removed and the north girder was inspected. No visible crack progression was seen past the crack-arrest holes in the top web gap, but the longitudinal flange-web weld crack did propagate through the web on the stiffener side of the girder.



Figure 16: Crack found in cross frame connection plate at the south face of the center girder.

The connection plate failure was repaired using four 25 mm [1 in.] thick angles. Two angles were placed back-to-back on both sides of the connection plate and bolted through the center girder web to another pair of back-to-back angles. The four-angle repair is shown in Figure 17.

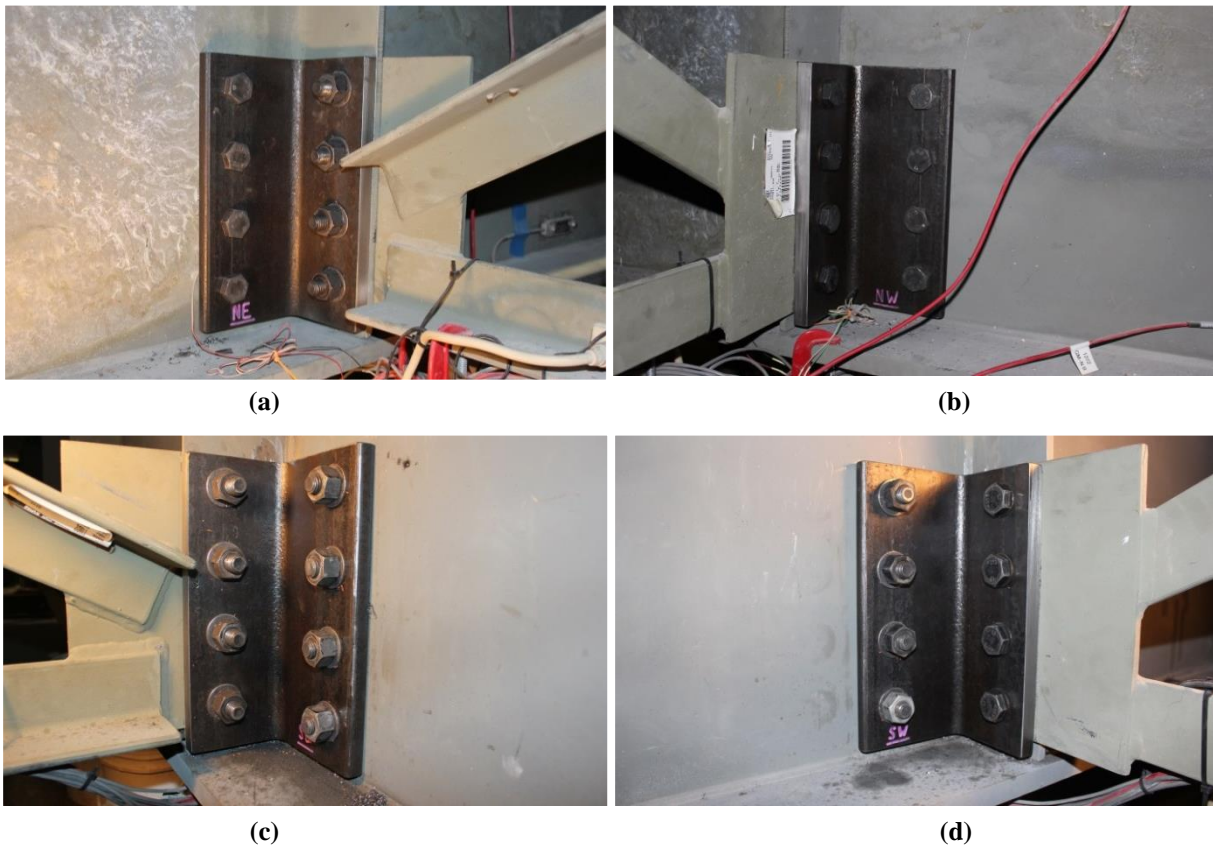


Figure 17: South cross frame connection plate four-angle repair from (a) northeast, (b) northwest, (c) southeast and (d) southwest face of center girder.

After the connection plate on the center girder was repaired, Trial 2.6N was performed. This trial reached only 181,092 cycles due to another failure at the cross frame connection, which occurred just outside the repaired failure from the previous trial. This failure, as shown in Figure 18, occurred in the tab plate where the bottom cross frame member (HB) framed into the tab plate near the south face of the center girder. It is estimated that the four-angle repair stiffened the weakened area, and thus moved the failure just outside the stiffened area to a more flexible region. After this failure occurred, the stiffened version of the angles-with-plate retrofit was removed and the north girder was inspected. No visible crack progression was detected.



Figure 18: South cross frame tab plate failure from (a) east and (b) west side of cross frame.

The cracked cross frame was repaired and replaced with a cross frame from the bridge support region, which had seen less demanding loading throughout its service life, and Trial 2.7N was performed. After each set of cyclic loading, visual inspections were performed to check for cracking in the cross frames and to inspect the bolts in the retrofit. After 425,000 cycles, it was found that the top bolt connecting the east angle to the backing plate had failed in tension in a very similar manner to that shown in Figure 15.

Upon inspection of the north girder after retrofit removal, no crack progression was seen past the crack-arrest holes in the connection plate-web weld crack. However, there was crack progression in the longitudinal flange-web weld crack. The longitudinal crack progressed 70 mm [2 3/4 in.] past the east crack-arrest hole and 44 mm [1 3/4 in.] past the west crack-arrest hole. Stress demands were again compared from a finite element study of the 9.1 m [30 ft.] test bridge performed to study the effect that the failed bolt may have had on crack growth. Based on

results from the study, propagation of the flange-web weld longitudinal crack was likely due to loss of stiffness from the bolt failure.

Trials 2.1S-2.7S Crack Growth (South Girder Test 2 Trials)

Cracking experienced around the transverse connection plate and along the flange-web weld in the south girder is shown in Figure 19. Crack definitions were the same as those used in the north girder and described in the previous sections. Application of crack-arrest holes is indicated by an instantaneous jump in the graph with no connecting line. Cracks that propagated to an existing crack-arrest hole are indicated by an instantaneous jump connected by a solid line.

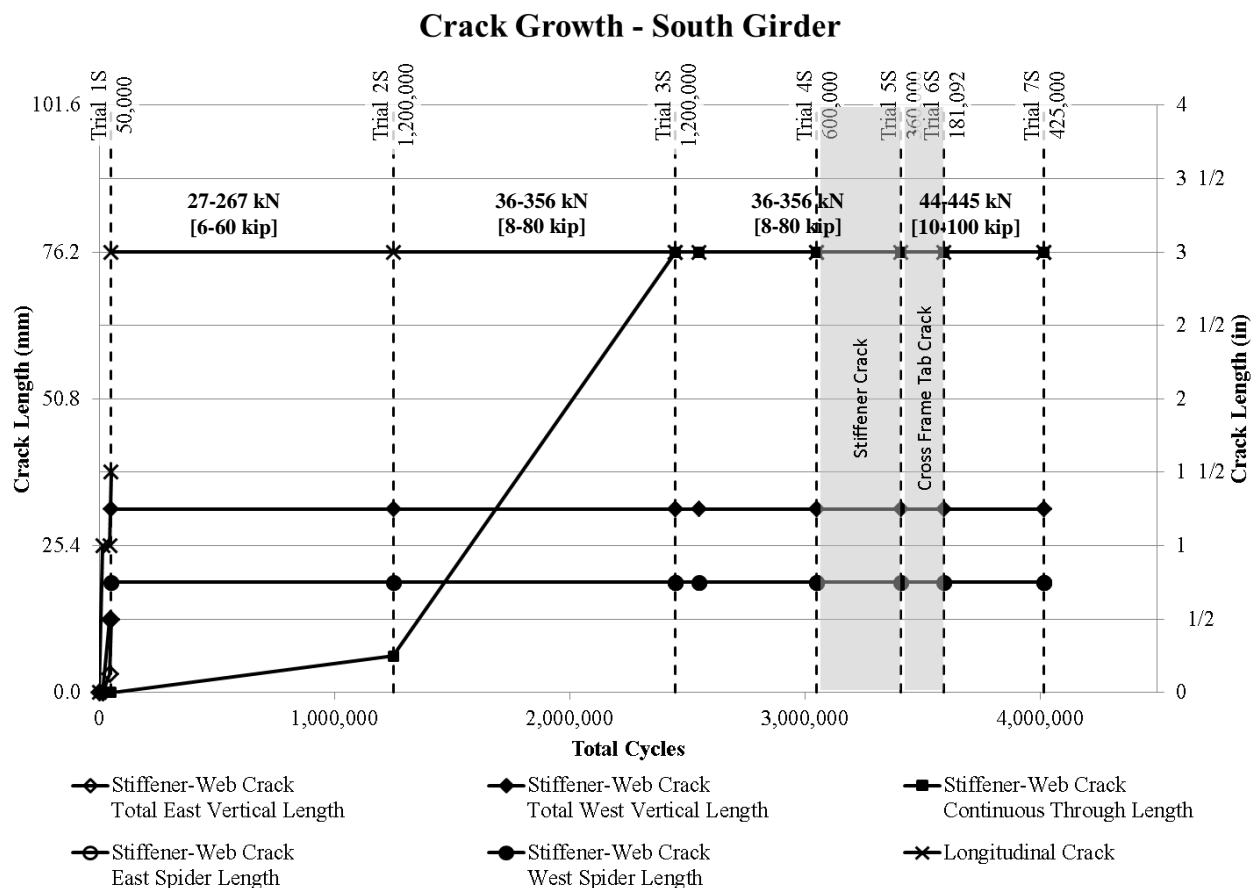


Figure 19: South girder crack growth around transverse connection plate and flange-web weld in Test 2.

Cracking in the south girder initiated during Trial 2.1S between 0 and 15,000 cycles in the flange-web weld. Upon first visual detection, the longitudinal crack was 25 mm [1 in.]. Additional crack growth was not detected until 45,000 cycles, when the connection plate-web weld crack initiated. After 50,000 cycles, the longitudinal flange-web weld crack had

propagated to 38 mm [1.5 in.] and the connection plate-web weld crack had propagated down both the east and west side of the weld to a length of 13 mm [1/2 in.] each. The investigators did not want the longitudinal crack to progress further before retrofitting, so Trial 2.1S was concluded at 50,000 cycles.

Crack-arrest holes 19 mm [3/4 in.] in diameter were drilled at the crack tips in the south girder at the start of Trial 2.2S. Under application of the stiffened version of the angles-with-plate retrofit, no crack progression was seen past the crack-arrest holes, but the connection plate-web weld crack did propagate through-thickness to the fascia side at a length of 6 mm [1/4 in.]. Trial 2.3S was performed and after reaching 1.2 million cycles, the only change in cracking that was detected was the connection plate-web weld crack propagating through the web on the fascia side of the girder. No crack progression was seen past the crack-arrest holes after completion of Trial 2.3S.

Trial 2.4S, 2.5S, 2.6S, and 2.7S were halted at 600,000 cycles, 360,000 cycles, 181,092 cycles, and 425,000 cycles respectively due to south cross frame connection failures and a broken bolt in the north girder retrofit as discussed in the previous section. Upon removal of the stiffened version of the angles-with-plate retrofit and inspection of the south girder at the end of each of these trials, no crack progression was detected in the top web gap of the south girder.

Girder Cross Frame Strains

Strain measurements on individual cross frame members at mid-span were monitored to establish the amount of out-of-plane force acting on the web gap as well as to determine the distribution of forces through the cross frame elements. Cross frame labeling notation is shown in Figure 4(a) and (b) where angle top (AT) and angle bottom (AB) indicates the inclined cross frame angles framing into the top and bottom web gaps, respectively. The horizontal angle in the cross frame is labeled horizontal bottom, (HB).

Test 1

Figure 20(a) and (b) show the effects of crack initiation on cross frame strain measurements. Prior to cracking, cross frame members AT and HB for the north and south girders experienced approximately the same strain in tension while AB experienced a similar strain magnitude in compression. Once cracking occurred in the connection plate-web weld of

each girder, member AT experienced a reduction in strain of approximately $75 \mu\epsilon$ while HB and AB experienced increases in strain of approximately $50 \mu\epsilon$. Due to cracking in the top web gap, less force was transferred into the cross frame member framing into top web gap, while the remaining members picked up additional load. As crack length increased, cross frame member strain distributions were seen to remain similar, as can be seen through a comparison of Figure 20(b) and (c).

Figure 20(c) and (d) show the change in strains between unretrofitted and retrofitted conditions after 1.35 million cycles. With the angles-with-plate retrofit applied in the top web gap, inclined cross frame angles framing into the top web gap (AT) experienced an increase in tensile strain of more than 50%. Since the inclined cross frame member framing into the top web gap experienced an increase in strain, both cross frame members framing into the bottom web gap experienced decreases in strain. Inclined cross frame members framing into exterior girder bottom web gaps (AB) experienced a decrease in compressive strains while horizontal members framing into the bottom web gaps (HB) experienced a decrease in tensile strains. Strain increases in elements framing into the top web gap do not directly provide any information about propensity for crack growth. It does, however, show that the retrofit allowed for more force transfer into the web since the cross frame strains were larger when retrofitted as compared with the unretrofitted condition.

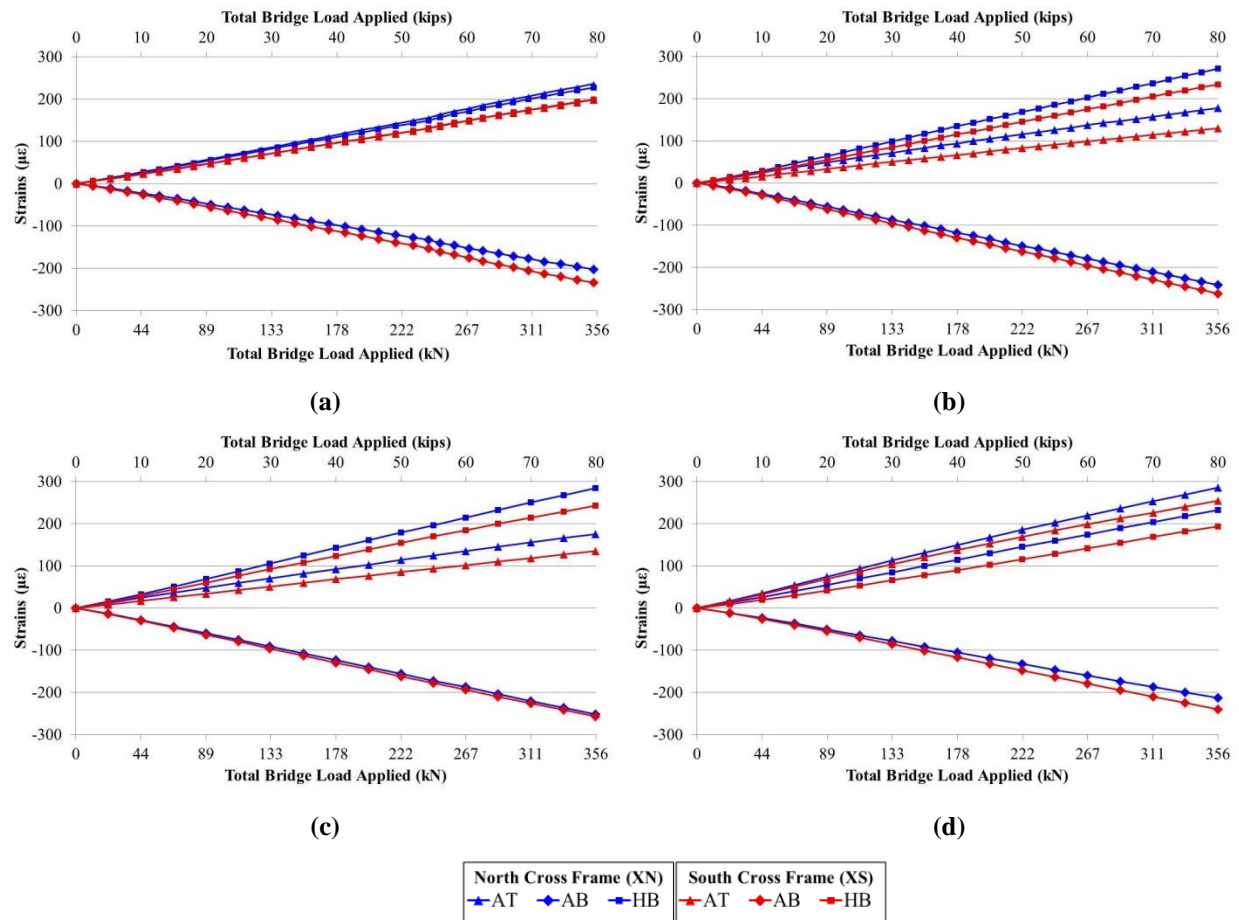


Figure 20: Cross frame strains for (a) uncracked, unretrofitted at 0 cycles, (b) cracked at 150,000 cycles, (c) cracked, unretrofitted at 1.35 million cycles, and (d) cracked, retrofitted at 1.35 million cycles.

Test 2

Figure 21(a) and (b) show the effect of crack initiation for Test 2 on strains recorded in the cross frame members. As in Test 1, approximately the same strain magnitudes were recorded for cross frame members AT and HB in tension and for cross frame member AB in compression before cracking occurred. After cracking occurred in the top web gap for the north and south girders, member AT experienced a reduction in strain of approximately 100 µε, while members HB and AB experienced increases in strain of approximately 50 µε. Similar to Test 1, strain distributions remained similar after crack initiation in the unretrofitted top web gap state. In comparing Figure 21(b) and (c), strain distribution at 1.25 million cycles was similar to that at 2.45 million cycles.

Figure 21(c) and (d) show that the relationship between the cross frame strains in the unretrofitted and retrofitted conditions after 2.45 million cycles. This relationship is similar to that seen in Test 1. Tensile strains in cross frame member AT increased by approximately 50%, and strain magnitudes in cross frame members HB and AB decreased, with HB experiencing lower tensile strains and AB experiencing lower compressive strains. As in Test 1, this relationship does not speak to propensity for crack growth, but does show that application of the stiffened version of the angles-with-plate retrofit in the top web gap allowed for more force transfer into the web through the cross frame member framing into the top web gap. The values of strain in these members were comparable between Tests 1 and 2, indicating that the stiffened angles-with-plate retrofit transferred similar levels of forces into the web as the non-stiffened version in Test 1.

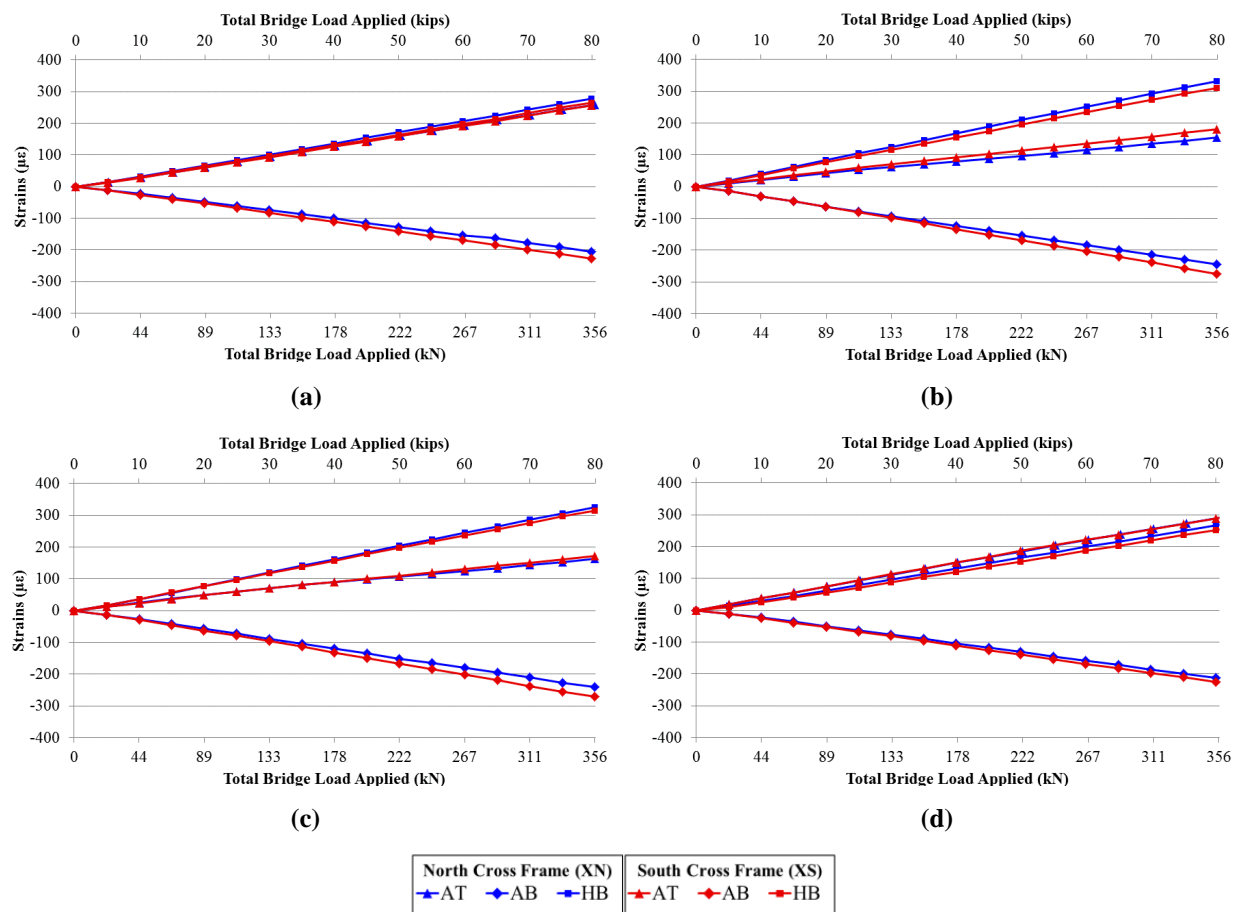


Figure 21: Cross frame strains for (a) uncracked, unretrofitted at 0 cycles, (b) cracked, unretrofitted at 1.25 million cycles, (c) cracked, unretrofitted at 2.45 million cycles, and (d) cracked, retrofitted at 2.45 million cycles.

As was discussed in previous sections, the cross frame between the center and south girders experienced two failures during Test 2. These failures occurred nearest to the center girder, in the region of the connection between the bottom cross frame members, AB and HB, and the transverse connection plate. Figure 22(a) and (b) show a comparison of cross frame strains before and after the first failure occurred. Change in tensile strains in cross frame member AT was small compared to changes in the HB and AB members. Cross frame member HB and AB strain magnitudes reduced by approximately 60%, with HB experiencing lower tensile strains and AB experiencing lower compressive strains. Figure 23(a) and (b) show a comparison of cross frame strains before and after the second failure occurred. This failure had much less impact on the cross frame strains, with each cross frame member experiencing less than 1% change in strain magnitudes. Of the members, however, the one that saw the largest change was south cross frame member HB, which makes sense based on where the second failure occurred. These results indicate that the first failure had a larger impact on the cross frame strains than the second failure. In the first failure, the cross frames became less effective at transferring force to the exterior girders.

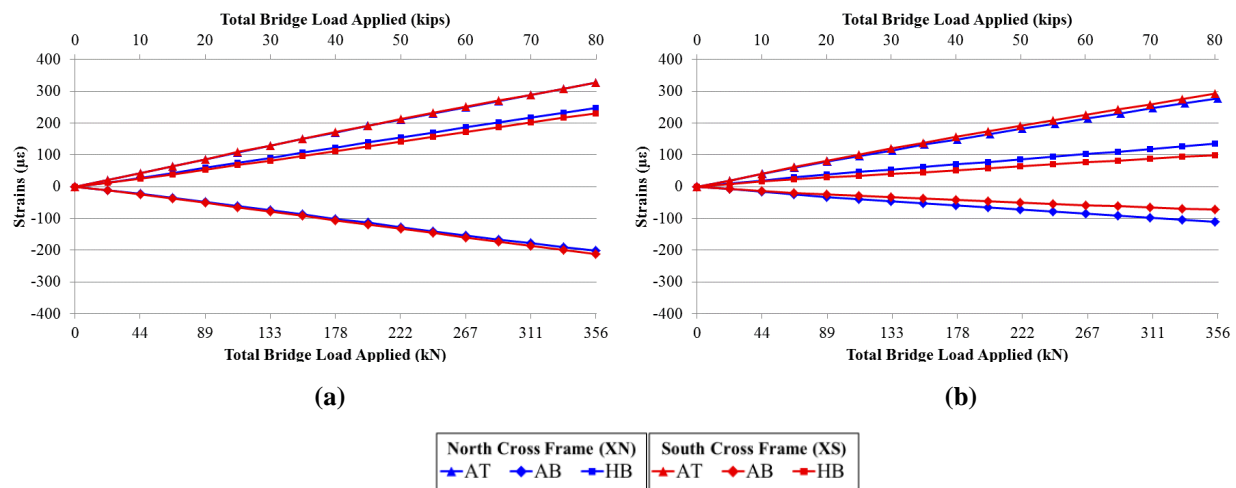


Figure 22: Cross frame strains for (a) cracked, retrofitted at 3.05 million cycles, (b) cracked connection plate at 3.41 million cycles.

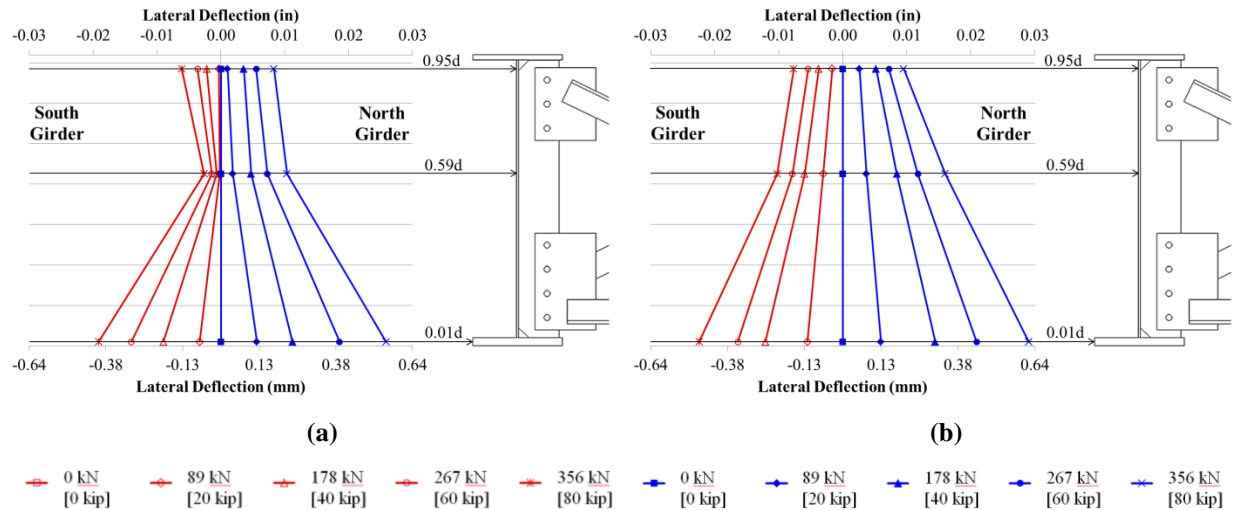


Figure 24: Girder lateral displacements at 150,000 cycles (end of Trials 1S and 1N) for (a) unretrofitted and (b) retrofitted conditions.

Lateral girder deflections of the north girder were found to be similar in shape to those obtained from tests of the 2.8 m [9.3 ft.] girder sub-assemblies (Alemdar et al. 2013a; 2013b). South girder deflections were found to behave a little differently than those from the north girder and the girder sub-assemblies tested by Alemdar et al. (2013a; 2013b). Between the top and middle LVDTs, the south girder hinged inward (less displacement) at mid-height while the north girder and component girders experienced increases in lateral displacement. The larger differential displacement between LVDTs placed at the top and mid-height of the south girder may have contributed to more crack growth as seen experimentally.

With the initial LVDT placements, little information could be inferred about the top web gap displacements; however, girder deflection was found to be nearly linear when the retrofit was applied (Figure 24(b)). To gain greater information regarding web gap rotations, four string potentiometers replaced the existing three LVDTs. After 1.35 million cycles (end of Trials 1.2S and 1.2N), both pre- and post-retrofit girder lateral displacements can be seen in Figure 25.

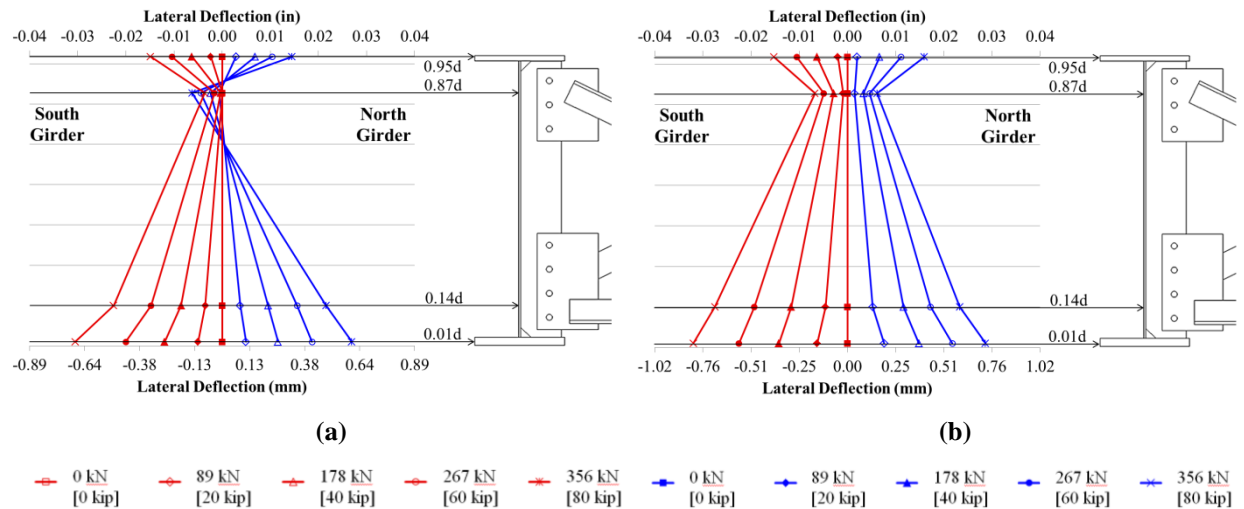


Figure 25: Girder lateral displacements at 1.35 million cycles for (a) unretrofitted and (b) retrofitted conditions.

Revised instrumentation locations provided an improved description of girder deflections. Without retrofit, displacement reversal was found to occur in the top web gap (Figure 25(a)) of the north and south girders. Once the retrofit was applied, this reversal was reduced while lateral displacements of girder flanges remained nearly constant. Since web gap rotation is considered to be a driving factor (Jajich and Schultz 2003) in distortion-induced fatigue cracking, reducing web gap rotation was anticipated to reduce fatigue susceptibility.

Test 2

Figure 26 shows similar behavior of top web gap displacement in Test 2 as seen in Test 1. Displacement reversal of the top web gap occurred before application of the retrofit. This displacement reversal was reduced upon installation of the retrofit. Applying the stiffened version of the angles-with-plate retrofit appeared to offer a similar level of web gap rotation restraint as the non-stiffened version used in Test 1.

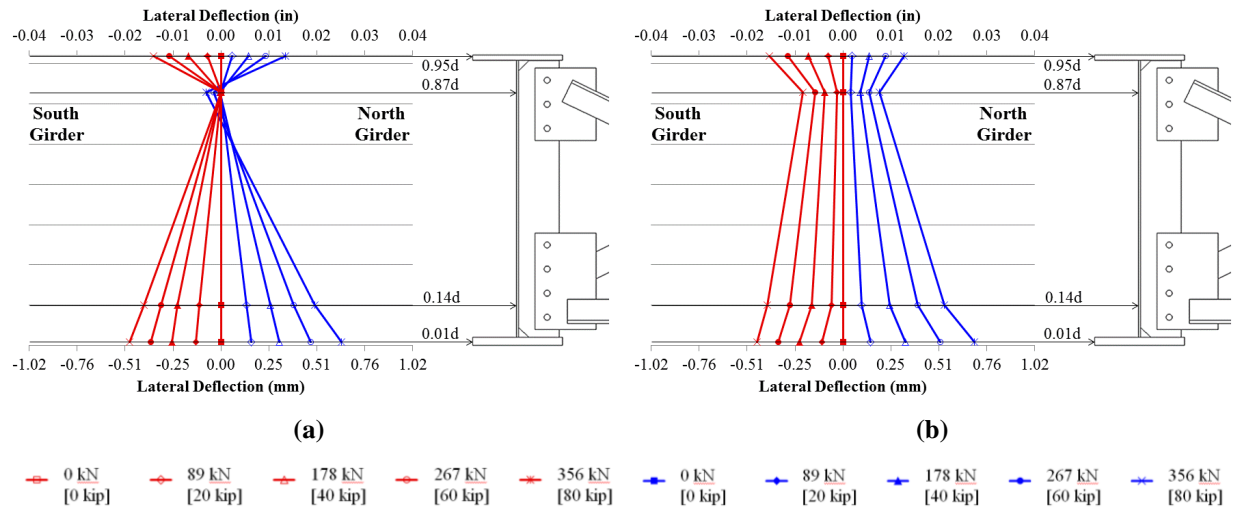


Figure 26: Girder lateral displacements at 50,000 cycles for (a) unretrofitted and (b) retrofitted conditions.

Conclusions

The objective of this study was to determine the effectiveness of the angles-with-plate retrofit and the stiffened version of the angles-with-plate retrofit for reducing distortion-induced fatigue propensity when applied to a steel test bridge that included in-plane bending effects as well as out-of-plane effects. The research team's conclusions are as follows:

- Cross frame members framing into the top web gap experienced an increase in tensile strain of more than 50% when the angles-with-backing plate retrofit was applied to a cracked specimen as compared with an unretrofitted cracked specimen. Application of the angles-with-plate retrofit allows more force to be transferred into the web as compared with an unretrofitted condition. Since crack growth was slowed when retrofitted, the angles-with-plate retrofit combats distortion-induced fatigue cracking even though additional force is being transferred into the web.
- Strain gages placed on the opposing web face at the web gap location were found to be good tools with which to detect crack initiation in the web gap region. Changes in strain were noticeable just prior to visibly-detectable cracking in the web gap region.
- Measurements taken with LVDTs and string potentiometers showed that out-of-plane web gap rotations were decreased after top web gaps were retrofitted using the angles-with-plates technique, indicating a lower distortion-induced fatigue demand on the web

gap region. No major advantage was seen in this relationship when the stiffened version of the angles-with-plate retrofit was tested.

- In Test 1, when the angles-with-plate retrofit was applied over top web gap regions with existing sharp cracks, crack growth was slowed. Maximum unretrofitted growth was 25 mm [1 in.] over 150,000 cycles at 27-267 kN [6-60 kip] load while maximum retrofitted growth was 11 mm [7/16 in.] over 1,200,000 cycles at 36-356 kN [8-80 kip] load.
- In Test 1, when the angles-with-plate retrofit was applied over top web gap regions with cracks that had been modified with small crack-arrest holes drilled at the crack tips, crack growth was halted under 44-445 kN [10-100 kip] loading with a maximum longitudinal bending stress due to fatigue of 48.3 MPa [7.0 ksi].
- In Test 2, when the stiffened version of the angles-with-plate retrofit was applied in the south girder over the top web gap region with cracks that had been modified with crack-arrest holes, crack growth was halted under 36-356 kN [8-80 kip] loading and 44-445 kN [10-100 kip] loading.
- In Test 2, when the stiffened version of the angles-with-plate retrofit was applied in the north girder over the top web gap region, crack growth occurred under 36-356 kN [8-80 kip] and 44-445 kN [10-100 kip] loading when bolt failure occurred in the retrofit. When bolt failure did not occur and the stiffened version of the angles-with-plate retrofit was applied in the north girder over the top web gap region with cracks that had been modified with crack-arrest holes, crack growth was not detected under 36-356 kN [8-80 kip] loading and 44-445 kN [10-100 kip] loading.
- Trials 4 and 7 of Test 1 and Trials 4, 5, and 6 of Test 2 indicate that the angles-with-plate retrofit is shifting the distortion-induced fatigue problem from the sensitive fatigue detail in the web gap region to the less sensitive fatigue detail in the cross frame. Loading during these test cycles was larger than would be expected for fatigue loading in an actual bridge structure, indicating that cross frames would not be seeing such high demands in real world applications.

Given the widespread nature of distortion-induced fatigue in existing steel bridge infrastructure, identification of effective, practical, and inexpensive retrofit techniques are in great demand. The angles-with-plate retrofit tested in a large-scale bridge test set-up under

demanding cyclic loads successfully retarded fatigue cracks. The angle-with-plate retrofit is an important development in this area, as it does not require deck removal or flange attachment. Development of this retrofit technique has the potential to greatly streamline the process of repairing steel bridges susceptible to distortion-induced fatigue in a manner that is effective, economical, and easily implementable.

References

- Alemдар, F., Overman, T., Matamoros, A., Bennett, C., and Rolfe, S. (2013a). "Repairing Distortion-Induced Fatigue Cracks in Steel Bridge Girders using Angles-with-Plate Retrofit Technique, Part I: Physical Simulations." *Journal of Structural Engineering*, ASCE, In Press
- Alemдар, F., Nagati, D., Matamoros, A., Bennett, C., and Rolfe, S. (2013b). "Repairing Distortion-Induced Fatigue Cracks in Steel Bridge Girders using Angles-with-Plate Retrofit Technique, Part II: Computer Simulations." *Journal of Structural Engineering*, ASCE, In Press.
- American Iron and Steel Institute (AISI) Example 1: Simple-Span Composite I Girder (1997). *American Iron and Steel Institute*.
- Connor, R. and Fisher, J. (2006). "Identifying Effective and Ineffective Retrofits for Distortion Fatigue Cracking in Steel Bridges Using Field Instrumentation." *Journal of Bridge Engineering*, 11(6), 745-752.
- Fisher, J. W., Jian, J., Wagner, D. C., and Yen, B. T. (1990). "Distortion-Induced Fatigue Cracking in Steel Bridges." *National Cooperative Highway Research Program Report #336*, Transportation Research Board, National Research Council, Washington, D. C.
- Fisher, J.W. and Keating, P.B. (1989). "Distortion-Induced Fatigue Cracking of Bridge Details with Web-gaps." *Journal of Constructional Steel Research*, 12(3-4), 215-228.
- Grondin, G.Y., Fraser, R., and D'Andrea, M. (2002). "Testing and Evaluating of Fatigue Damaged Girders." *4th Structural Specialty Conference of the Canadian Society for Civil Engineering*.
- Hartman, A. (2013). "Analytical and Experimental Investigation for Distortion-Induced Fatigue in Steel Bridges." Doctor of Philosophy Dissertation, University of Kansas.
- Hassel, H., Hartman, A., Bennett, C., Matamoros, A., and Rolfe, S. (2010). "Distortion-Induced Fatigue in Steel Bridges: Causes, Parameters, and Fixes." *2010 ASCE/SEI Structures Congress Proceedings*. 471-483.

- Jajich, D. and Schultz, A.E. (2003). "Measurement and Analysis of Distortion-Induced Fatigue in Multigirder Steel Bridges." *Journal of Bridge Engineering*, 8(2), 84-91.
- Liu, H. "A Finite-Element-Based Approach to Modeling Cracking & Repairs for Distortion-Induced Fatigue in Steel Bridges." PhD Thesis, University of Kansas, 2015.
- Nagati, D. (2012). "Repair of Steel Bridge Girders Damaged by Distortion-Induced Fatigue." Master's Thesis, University of Kansas.
- Overman, T. (2012). "Analytical Investigation of Repair Methods for Fatigue Cracks in Steel Bridges." Master's Thesis, University of Kansas.
- Przywara, J. (2013). "Applications of the Extended Finite Element Method (XFEM) for the Analysis of Distortion-Induced Fatigue Cracking in Highway Bridge Girders." Master's Thesis, University of Kansas.
- Roddis, W.M.K. and Zhao, Y. (2001). "Out-of-Plane Fatigue Cracking in Welded Steel Bridges: Why It Happened and How It Can Be Repaired." *Welding Innovation*, 27(2), 2-7.
- Roddis, K.W.M. and Zhao, Y. (2003). "Finite-Element Analysis of Steel Bridge Distortion-Induced Fatigue." *Journal of Bridge Engineering*, 8(5), 259-266.
- Tedesco, J.W.; Stallings, J. M.; and Tow, D.R. (1995). "Finite Element Method Analysis of Bridge Girder-Diaphragm Interaction." *Computers and Structures*, 56(2-3), 461-473.

Part III: Field and Analytical Testing of Angles-With-Plate Retrofit for Distortion-Induced Fatigue in Kansas Bridge 135-87 (043/044)

Kathleen S. McElrath¹

Caroline R. Bennett²

Adolfo B. Matamoros³

Jian Li⁴

Stanley T. Rolfe⁵

Abstract

A steel girder twin bridge structure located near Park City, Kansas has experienced extensive distortion-induced fatigue cracking in its web gap regions. Due to the bridge's skewed, staggered configuration, the majority of these cracks have occurred in the bottom web gap region. The bridge was previously the subject of a series of detailed finite element analyses that investigated the effectiveness of several types of retrofits in repairing its distortion-induced fatigue cracks. One of these retrofits, the "angles-with-plate" retrofit, was developed and tested at the University of Kansas as a new retrofitting technique aimed at providing a more economical and easy-to-install distortion-induced fatigue cracking repair. The retrofit is made up of a pair of angles and a backing plate that connect the cross frame connection plate and girder web in order to stiffen the web gap region. Results from the finite element analyses determined that the angles-with-plate retrofit was the most effective and economical choice for repairs in the bridge, and plans were made for its installation.

To investigate the performance of the angles-with-plate retrofit, two field tests were performed that monitored behavior of the bridge both before and after the retrofit was installed. Results from these field tests were compared with results from complementary finite element analyses to determine the overall effectiveness of the retrofit. In the bottom web gap region, where cracking is most prevalent in the bridge, the angles-with-plate retrofit was successful at

¹ Kathleen S. McElrath, Graduate Research Assistant, University of Kansas, 1530 W. 15th St., Lawrence, KS 66045

² Caroline R. Bennett, PhD, PE, Associate Professor, University of Kansas, 1530 W. 15th St., Lawrence, KS 66045

³ Adolfo B. Matamoros, PhD, Peter T. Flawn Distinguished Professor, University of Texas at San Antonio, One UTSA Cir., San Antonio, TX 78249

⁴ Jian Li, PhD, Assistant Professor, University of Kansas, 1530 W. 15th St., Lawrence, KS 66045

⁵ Stanley T. Rolfe, PhD, PE, A.P. Learned Distinguished Professor, University of Kansas, 1530 W. 15th St., Lawrence, KS 66045

lowering stress demands that would lead to crack propagation. The same conclusion could not clearly be made for all cases in the bridge's less problematic top web gap region, so a secondary set of finite element analyses was performed to gain a better understanding of what was happening in that region. Further analyses of the two common types of distortion-induced fatigue cracking determined that, while not always large, the angles-with-plate retrofit was successful in reducing stress demands in the top web gap region.

Therefore, it was concluded that the angles-with-plate retrofit was an effective repair for the problematic bottom web gap regions of the bridge, and if needed, can be used effectively in the less demanding top web gap region.

Introduction

Before implementation of the 1983 American Association of State Highway and Transportation Officials (AASHTO) Bridge Specifications, steel bridge girders in the United States were often designed leaving a small gap between the connection plate of the cross frames and the girder flanges. This detail, often referred to as a “web gap,” was used to avoid a fatigue-vulnerable location that would be caused by welding transverse connection plates to girder flanges. To prevent this type of damage, the connection plates were often cut short and left unattached to the girder flanges (Grondin, Fraser and D'Andrea 2002). Since no connection was provided between the elements, the web gap region located between the transverse connection plate and the girder flange was left unstiffened. The unforeseen effect of this detail was that out-of-plane cross frame forces induced large localized strains in the web gap region and that made it highly susceptible to distortion-induced fatigue cracking. This unstiffened web gap region has since been found to be the culprit for extensive fatigue cracking in steel bridges in the United States.

In order to repair distortion-induced fatigue cracking in bridges, retrofit measures that reduce the stress demands in the web gap regions must be installed. Current retrofit measures in use today have either performance or constructability issues. Recent research at the University of Kansas has focused on the development of a retrofit measure that simplifies the installation process and effectively stiffens the web gap region. This retrofit measure, termed the “angles-with-plate” retrofit, has been the subject of numerous analytical and experimental studies at the University of Kansas (Alemdar et al. 2013a, 2013b; Richardson 2012; Hartman 2013). Based on

successful performance of the retrofit measure in those investigations, the angles-with-plate retrofit was recommended to the Kansas Department of Transportation as a means to repair distortion-induced fatigue damage in a steel girder bridge located near Park City, Kansas. This bridge was designated by KDOT as Kansas Bridge 135-87(043/044). Investigators at the University of Kansas monitored Kansas Bridge 135-87(043/044) under live loading both before and after the angles-with-plate retrofit was installed to gage the effectiveness of the retrofit measure in relieving stress demands in the web gap regions of a bridge that is in service.

Background

Out-of-plane distortion of the web gap occurs when adjacent girders experience differential deflections under live loads. The differential deflection causes the cross frames to rotate and impose out-of-plane forces on the transverse connection plates. The girders to which the connection plates are welded can experience high out-of-plane stresses in the flexible web gap region, made more severe by the presence of stress concentrations due to geometric discontinuities. The combination of high-magnitude stresses and the small number of cycles needed to induce distortion-induced fatigue cracking have led to large numbers of cracks appearing in the web gaps of steel girder bridges constructed before the mid-1980s (Fisher 1984).

Depending on bridge layout, fatigue cracking can occur in either the top or bottom web gap regions. The literature shows that the majority of distortion-induced fatigue cracking occurs in top web gap regions. The top girder flange is restrained by the concrete deck, which inhibits its lateral displacement. The bottom flange of the girder has more freedom to deform laterally. Therefore, distortion tends to occur in the restrained, relatively flexible top web gap region. An exception to this case is the case of skewed bridges with staggered cross frames, where stress demands likely to produce fatigue cracking have been shown to be more prevalent in the bottom web gap (Hartman, Hassel, et al. 2010). Staggered cross frames in skewed bridges are placed at different stations along the girder, which tends to increase differential displacements (Grondin, Fraser and D'Andrea 2002). In addition to this, Hartman et al. (2010) found that staggered cross frame layouts caused the bottom girder flange to laterally displace in reverse curvature, while the top girder flange was restrained from doing so by the concrete deck. Thus, it was hypothesized that the increased differential deflections and reverse curvature response of the bottom girder

flange led to maximum stress demands and the potential for fatigue cracking being higher in the bottom web gaps of skewed bridges with staggered cross frames.

Detailing changes have been implemented since the 1983 AASHTO specification, which was the first AASHTO bridge design specification to mandate a positive connection between a connection plate and the adjacent flange. This change in the code provisions addressed the issue of out-of-plane displacements at web gap regions in new designs, but many steel bridges designed prior to 1983 and still in service are susceptible to distortion-induced fatigue and have experienced cracking due to this problem. To prevent distortion-induced fatigue cracks from propagating further into the girder web, which could cause severe structural damage, the cracks need to be properly repaired. Two commonly-used techniques to address distortion-induced fatigue damage include drilling holes at crack tips to arrest crack growth and using angles at the connection plate to stiffen the web gap region.

Crack-arrest holes are drilled at the tip of the crack and may be effective in stopping crack propagation in low stress regions, but cracking is likely to recur depending upon the crack type and location of occurrence or if the stress range increases (Liu 2015). They are also only effective in arresting existing cracks and not in preventing new cracks. However, crack-arrest holes are easy to install and are generally considered useful when used in conjunction with other retrofitting techniques. Bolting back-to-back angles to each side of the connection plate and to the girder flange is a widely-used method for stiffening the web gap region. While this technique is effective, it is inconvenient and costly when applied to the top web gap because the concrete deck has to be disturbed for the bolts to be installed in the steel girder flange (Roddis and Zhao 2001).

Development of the Angles-With-Plate Retrofit

Recent research performed at the University of Kansas has investigated a new retrofit technique, which is referred to as the angles-with-plate retrofit. The retrofit consists of a pair of angles and a backing plate applied on opposite sides of the girder web at the web gap regions. One leg of each angle is bolted back-to-back through the transverse connection plate, while the other leg of each angle is bolted to the backing plate through the girder web. Application of the angles-with-plate retrofit provides an alternate load path that redistributes the concentrated force in the web gap region to a larger area of the girder web. The retrofit does not require deck

removal when applied in the top web gap, since there is no attachment to the girder flange. This simplifies retrofit application and allows for the retrofit to be installed without removing traffic lanes, providing a more cost effective solution for mitigating distortion-induced fatigue cracks in steel bridge girders.

Alemdar et al. (2013a) performed physical tests to investigate the effectiveness of the angle-with-plate retrofit. The investigations were performed using 2.8 m (9.3 ft.) girder-cross frame subassemblies. The set-up used for these tests can be seen in Figure 1. In a steel girder bridge, the top flange of a girder is laterally restrained by the bridge deck. In order to replicate this in the laboratory, the girder-cross frame subassemblies were tested upside down to restrain the top flange of the girder using the laboratory strong floor. This set-up eliminated in-plane bending stresses that would occur in bridges due to dead and live gravity loads and left only out-of-plane stress demands on the girder. The out-of-plane stress demands were implemented by applying cyclic loads at the free end of the cross frame. Initiation and propagation of fatigue cracks were monitored through eight test trials to determine the effectiveness of the angles-with-plate retrofit.

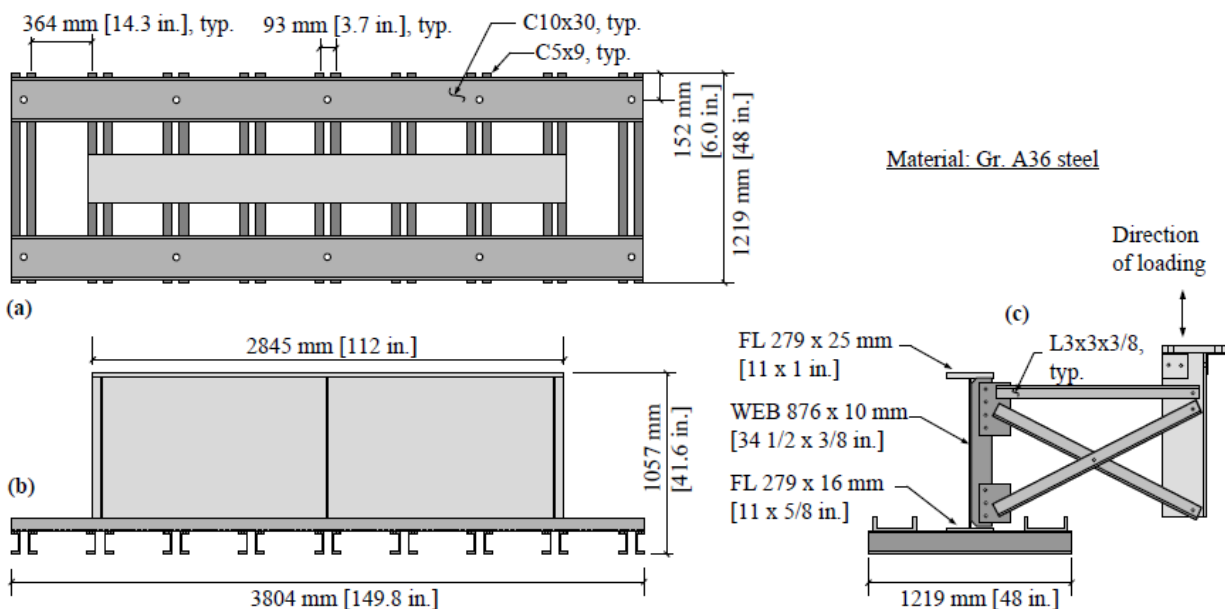


Figure 1: Test set-up for 2.8 m (9.3 ft.) girder subassembly test (Alemdar, Overman, et al. 2013a).

An analytical study of the behavior of this retrofit measure is presented in the study by Alemdar et al. (2013b). Computer simulations of the girder-cross frame subassemblies were created to verify that the stress field in the web gap of the laboratory specimens was similar to that computed in the web gap of girders in a bridge system subjected to truck loads. Results from the analytical investigation showed that the stress fields in the web gap and points of fatigue crack initiation in the 2.8 m (9.3 ft.) subassembly were similar to those found in bridge system simulations performed by Hassel et al. (Hassel, et al. 2013).

Results from the physical and parallel analytical tests by Alemdar et al. (2013a, 2013b) showed that the two primary types of cracks that occur in the web gap region are horseshoe-shaped cracks that propagate along the toe of the transverse connection plate-to-girder web weld (referred to hereafter as connection plate-to-web weld cracks), and longitudinal cracks that propagate along the girder flange-to-web (referred to hereafter as flange-to-web weld cracks). The tests showed that the angles-with-plate retrofit measure was successful in mitigating propagation of these two types of cracks. In comparison with unretrofitted specimens, web gap stresses were reduced and crack growth was negligible in the retrofitted specimens. Thus, under pure out-of-plane fatigue loading, the angles-with-plate retrofit proved to be effective.

A physical test that captured both in-plane and out-of-plane effects (Hartman 2013) investigated the angles-with-plate retrofit using a 9.1 m (30 ft.) three-girder test bridge with a composite concrete deck (Figure 2). X-type cross frames were located at mid-span and at the two end support locations. Regularly-spaced high strength bolts were used to attach the concrete deck to the top flanges of the girders to achieve composite action. The bolts were grouted in place after they were installed.

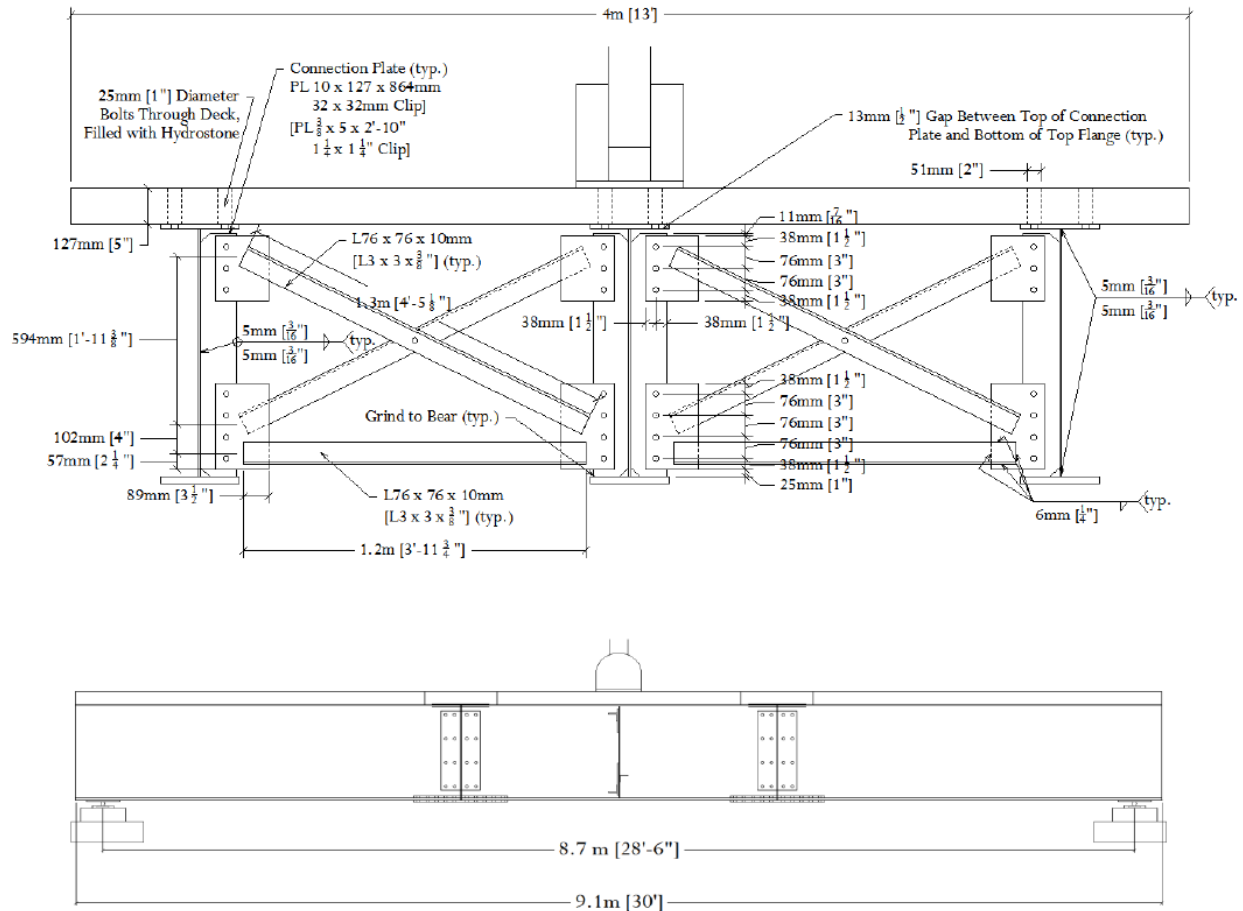


Figure 2: Test set-up for 9.1 m (30 ft.) three girder test bridge (Hartman 2013).

Twelve fatigue test trials were performed at varying load ranges, applied at the center of the bridge deck using a servo-controlled hydraulic actuator. This fatigue loading resulted in distortion-induced fatigue cracks in the top web gap regions of the two exterior girders, which were subsequently repaired using the angles-with-plate retrofit. After the angles-with-plate retrofit was applied, crack growth, girder deflections, cross frame strains, and web gap region strains were monitored throughout the test trials to determine the effectiveness of the angles-with-plate retrofit.

Physical test results reported by Hartman (2013) showed that application of the angles-with-plate retrofit lowered crack propagation rates for distortion-induced fatigue cracks in the web gap region, and that web gap distortion was reduced. Growth of existing sharp-tip cracks was shown to slow after application of the angles-with-plate retrofit. When applied over web

gap regions with crack tips that were modified by small-diameter crack-arrest holes, crack growth was halted under realistic fatigue bridge loadings.

Hartman (2013) also performed an analytical investigation of the 9.1 m (30 ft.) test bridge. The objective of this investigation was to complement the physical laboratory tests, to examine the influence of crack type and crack length, and to compare the angles-with-plate retrofit with other existing retrofit techniques. Varying lengths of connection plate-to-web weld cracks and flange-to-web weld cracks were modeled in unretrofitted and retrofitted versions of computational models to determine the effectiveness of different types of retrofits in mitigating distortion-induced fatigue crack growth. In addition to the angles-with-plate technique, two other retrofit measures were modeled. One of these was the existing retrofit technique in which two angles are placed back-to-back and bolted to the connection stiffener and girder flange. The other retrofit measure simulated involved the use of a back-up stiffener. In this technique a full-depth secondary stiffener is placed on the opposite side of the girder web at the connection plate in an effort to stiffen the web gap region.

Stress demands in the web gap region were reduced under all retrofit techniques in the simulations performed by Hartman (2013). The full-depth back-up stiffener technique was the least effective because it provided a very small reduction in stress demand. The angles-with-plate retrofit measure provided the greatest reduction in stress demand at the connection plate-to-web weld cracks, while the angles-to-top girder flange retrofit measure provided the greatest reduction in stress demand at the flange-to-web weld cracks. Although it was not the most effective, the angles-with-plate retrofit measure still provided a notable reduction in stress demand at the flange-to-web weld crack.

Overall, the tests and simulations performed using the 2.8 m (9.3 ft.) girder cross frame subassembly and 9.1 m (30 ft.) test bridge showed that the angles-with-plate retrofit measure can be an effective method for repairing distortion-induced fatigue web gap region cracks. Although the simulation results indicated that the angles-with-plate technique did not perform better than the existing retrofit technique of bolting back-to-back angles to the connection plate and top flange in all instances, the angles-with-plate retrofit measure still showed good performance in mitigating fatigue crack growth and reducing web gap region stress demand in these cases. When ease of construction is considered, the angles-with-plate retrofit measure provides major benefits over the angles-to-top flange retrofit measure. Because it does not require attachment to

the top flange, there is no need for deck removal. This aspect greatly reduces the cost of retrofit installation and reduces traffic disruption, providing an effective and more economical retrofit technique (Alemdar, Overman, et al. 2013a, 2013b, Hartman 2013).

History of Kansas Bridge 135-87(043/044)

Kansas Bridge 135-87(043/044) is an in-service twin bridge structure located near Park City, KS in Sedgwick County over Chisolm Creek. The bridge system has an average daily traffic of 14,400, which is comprised 16% by trucks. Each welded steel plate girder bridge carries two lanes of traffic, with Bridge 043 carrying traffic in the southbound direction and Bridge 044 carrying traffic in the northbound direction. The bridge system was designed in 1964 and constructed in 1970, and it has unstiffened web gap regions that are prone to distortion-induced fatigue cracking. Prevalent cracking has been reported in the bridge system, with the majority of cracking appearing in the bottom web gaps. However, some cracking was also reported in top web gap regions.

The bridges each have two 23 m (76 ft.) end spans and a 29 m (95 ft.) middle span, and are skewed at an angle of 21°. Both bridges are comprised of five composite steel girders spaced at 2.7 m (9 ft.) with 1220x8 mm (48x5/16 in.) webs and 305x29 mm (12x1-1/8 in.) flanges that taper to a width of 457 mm (18 in.) over the center supports. These girders are labeled A through E, with A being the west girder. The 191 mm (7-1/2 in.) thick reinforced concrete deck was resurfaced in 2004 and provides a roadway width of 12 m (40 ft.). Lateral support is provided by cross frames that are placed in a staggered configuration oriented perpendicular to the girders in all locations except at the interior bolster supports, where they are placed back-to-back and parallel to the skew. Half sections of the bridge, which show views at the cross frame locations near mid-span and at the interior supports, are shown in Figure 3. Additional plans and details can be referenced in the original structural drawings of the bridge found in Appendix F.

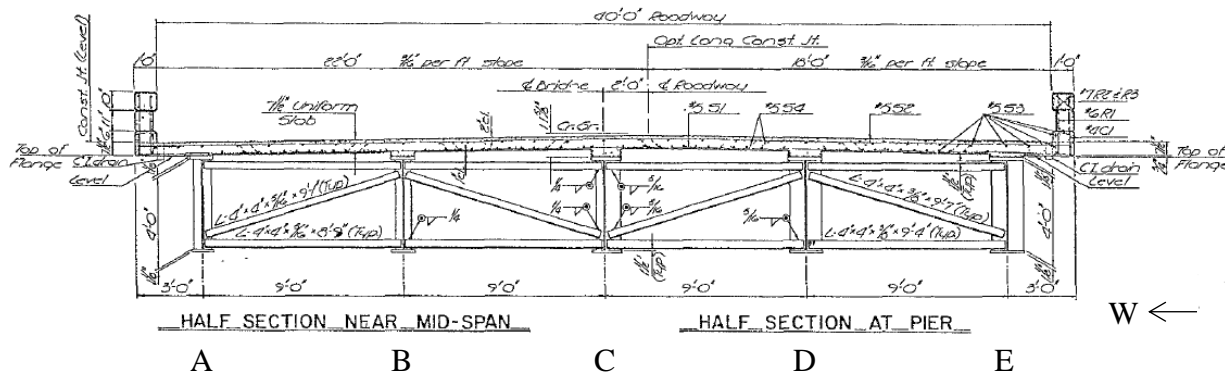


Figure 3: Cross-section of Kansas Bridge 135-87(043/044).

As previously mentioned, studies have shown that skewed bridges with staggered cross frames are more likely to have distortion-induced fatigue cracks in the bottom web gaps due to high differential deflections and reverse curvature deformations of the bottom girder flange (Hartman, Hassel, et al. 2010). This is the case with Kansas Bridge 135-87(043/044), which has a 21° skew and staggered cross frames. According to a 2010 routine snoop inspection, the majority of fatigue cracks are located in the bottom web gaps. Figure 4 shows a plan of the bridge with locations of cracking indicated.

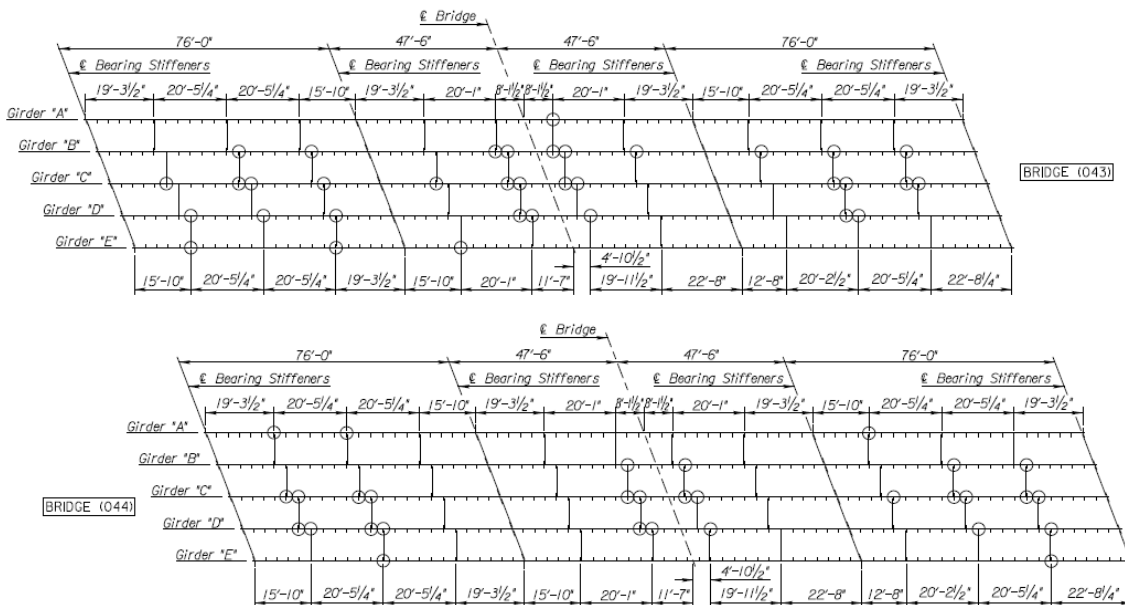


Figure 4: Plan of Kansas Bridge 135-87(043/044); circled areas indicate locations where cracks have been reported.

Crack types A, B, C, and D (Figure 5) have all been reported on Kansas Bridge 135-87(043/044). Type A cracks occur horizontally at the connection plate-to-web weld. Type B cracks occur vertically along the connection plate-to-web weld. Type C cracks propagate away from the connection plate-to-web weld into the base metal of the girder web, and Type D cracks occur along the flange-to-web weld. Drilled crack-arrest holes were implemented in past repairs, but no additional retrofit measures had been applied to the bridge prior to 2013.

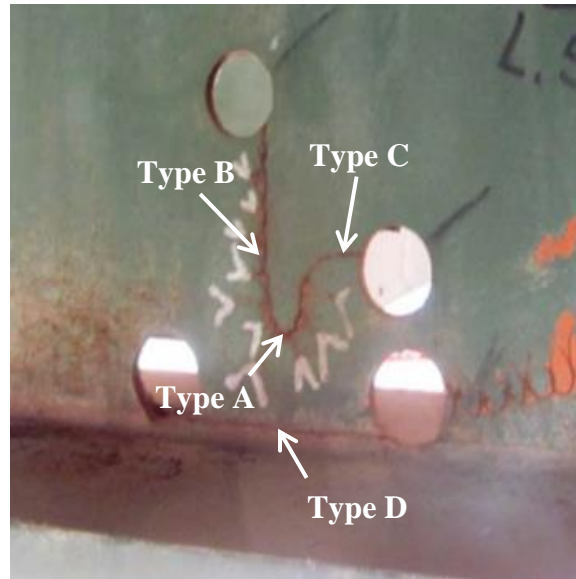


Figure 5: Types of cracks occurring in Kansas Bridge 135-87(043/044).

Retrofit Recommendation for Kansas Bridge 135-87(043/044)

As part of an investigation performed for the Kansas Department of Transportation (KDOT), a series of finite element analyses of Kansas Bridge 135-87(043/044) were completed. As previously mentioned, the bridge has a history of distortion-induced fatigue cracks in its web gap regions. The purpose of the finite element analysis was to recommend a retrofit scheme to prevent further initiation and propagation of the cracks based on reduction of web gap stresses and ease of retrofit application. Different variations of the angles-with-plate retrofit were evaluated in the study, as well as three other retrofit techniques. The second retrofit measure was similar to the angles-with-plate retrofit, except that the backing plate was replaced by a backing angle that was bolted to the flange. The other two retrofit techniques included the commonly-used retrofit technique of connecting back-to-back angles between the girder flange and transverse connection plate, and a KDOT-proposed retrofit measure. In the KDOT-proposed

retrofit measure, angles were placed at each corner of the cross frame as a means to stiffen all web gap regions. In each retrofit location, 19 mm ($\frac{3}{4}$ in.) diameter tensioned bolts were modeled (Richardson 2012).

A detailed three-dimensional finite element (FE) model of Kansas Bridge 135-87 (043/044) was built and loaded with its self-weight. A 9.3 kN/m (0.64 k/ft.) lane load was applied along the full length of the bridge over the top flange width of Girder C. Cracks were modeled at the top and bottom web gaps of the third cross frame of span two in Girder C. These cracks included a 25 mm (1 in.) connection plate-to-web weld crack and a 51 mm (2 in.) flange-to-web weld crack. Models of the bridge both with and without retrofit measures were assessed to determine the percentage of stress reduction provided by each type of retrofit (Richardson 2012).

The angles-with-plate retrofit was studied parametrically in the FE models to determine which combination of angle/plate thicknesses and lengths was most effective. It was found that varying the thickness of the backing plate had a greater effect on the performance of the retrofit measure than varying the thickness of the angles. The retrofit measure with a 25 mm (1 in.) backing plate and 13 mm (0.5 in.) angles resulted in a decrease in stress demand almost as large as when both the angles and backing plate had equal thicknesses of larger values. Length of the angles was shown to have little effect on stress reduction in the web gap regions (Richardson 2012).

The angles-with-plate retrofit was applied in both the bottom and top web gap regions. In the bottom web gap region, the angles-with-plate retrofit was shown to reduce the connection plate-to-web weld crack stress demand by 80% and the flange-to-web weld crack stress demand by 82%. In the top web gap region, the angles-with-plate retrofit was shown to reduce these stresses by 34% and 28%, respectively. While this was less than the bottom web gap stress reductions, it should be noted that stresses in the top web gap region were small in comparison to those found in the bottom web gap region, which is expected in a bridge with skewed, staggered geometry (Richardson 2012).

The other three retrofit measures were only modeled in the bottom web gaps. The angles-with-backing plate retrofit performed better in this region than all others with the exception of the retrofit measure that replaced the backing plate with a backing angle attached to the girder flange. However, the difference in performance was only 1-2%. The extra labor and

material required to apply the backing angle to the girder flange would not be warranted with only this slight difference in stress reduction. Additionally, connection of the backing angle to the top flange would require bridge deck removal (Richardson 2012).

While the remaining two retrofit techniques studied were also successful in reducing stress demand in the bottom web gap region, they were not as effective as the angles-with-backing plate technique. They also presented installation obstacles. As mentioned previously, the existing retrofit technique of bolting back-to-back angles to the connection plate and girder flange requires bridge deck removal when applied at the top flange.

Also, Kansas Bridge 135-87 (043/044) has cross frames with two horizontal cross frame members framing directly into the connection stiffener at the top and bottom web gaps, as shown in Figure 6.

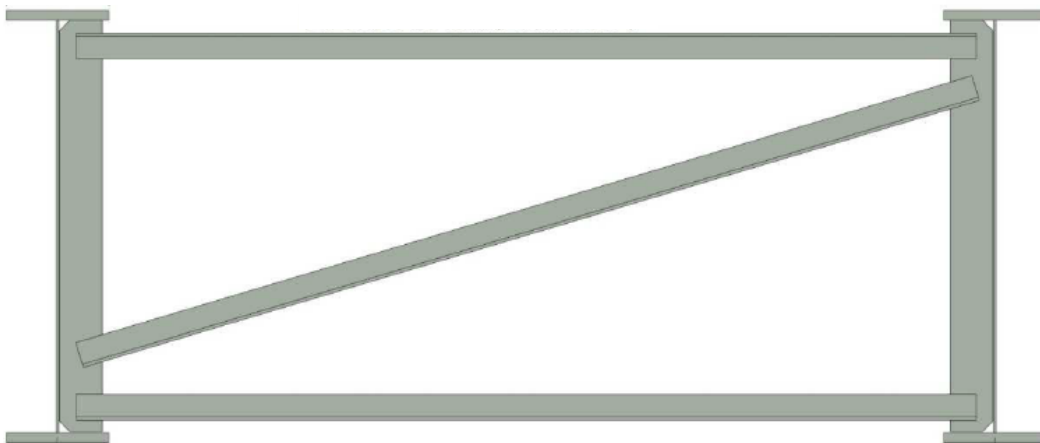


Figure 6: Cross frame geometry of Kansas Bridge 135-87(043/044) (Richardson 2012).

In bridges with cross frame geometry such as this, application of the retrofit measure attaching the cross frame to the girder flange would first require removal of at least the horizontal cross frame members. Similarly, the KDOT-proposed retrofit technique of applying angles at each corner of the cross frame would also require cross frame members to be removed before application (Richardson 2012).

Richardson (2012) concluded that the angles-with-plate retrofit was effective in reducing stresses in the web gap regions and would be the most cost effective and convenient repair

technique. Because this retrofit technique does not require attachment to the girder flange, field implementation would be simplified in both web gap regions. In the top web gap, bridge deck removal would not be required. In both web gap regions, cross frame removal would be unnecessary, because the angles-with-plate retrofit could be bolted through the horizontal cross frame members while avoiding their outstanding legs. These benefits would reduce labor costs and avoid disruptions to daily traffic. Therefore, it was recommended to KDOT that they use the angles-with-plate retrofit on Kansas Bridge 135-87(043/044) to repair distortion-induced fatigue cracking in the susceptible web gap regions. Based on the parametric results of the angles-with-plate retrofit, recommended dimensions for the angles and backing plate were L152x152x25 mm (L6x6x1 in.) and L457x145x25 mm (PL18x5-11/16x1 in.), as shown in Figure 7.

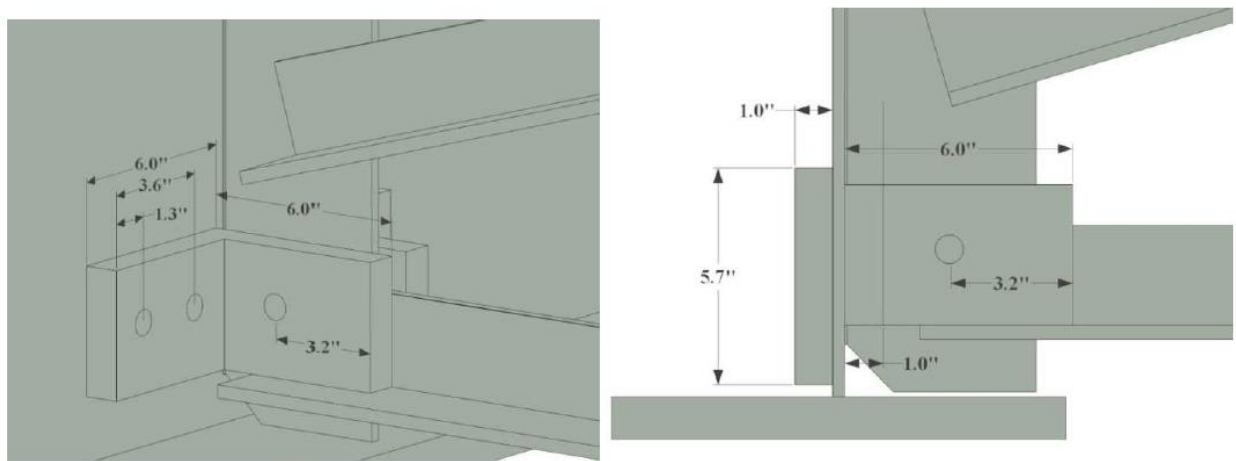


Figure 7: Angles-with-plate retrofit recommended to KDOT for repair of Kansas Bridge 135-87(043/044) (Richardson 2012).

Objective

In the spring of 2013, KDOT installed the angles-with-plate retrofit on Kansas Bridge 135-87(043/044). The objective of this study was to assess the performance of the angles-with-plate retrofit in its field application and determine its effects on the stress demand in the web gap regions of the bridge. This was done by performing field testing on the bridge both before and after the retrofit was installed and comparing the results of those tests to a refined finite element analysis of the bridge.

Field Tests

The first field test was performed at the bridge site in March 2013 before KDOT installed the angles-with-plate retrofit. After KDOT installed the retrofit, the second field test was performed in July 2013. In both tests, KDOT provided a test truck of known weight, approximately 222 kN (50 kips), that was driven over the bridge with no other traffic on the structure. Data was recorded six separate times for each field test, as the test truck traveled at 8-16 km/h (5-10 mph) and 105-121 km/h (65-75 mph) down the east lane, the west lane, and the center of the bridge.

Field testing was performed on the northbound bridge, Bridge 044. This bridge was selected for testing because KDOT installed the angles-with-plate retrofit measure in both its top and bottom web gaps, as opposed to only in the bottom web gap for the southbound bridge (Bridge 043). KDOT chose to do this so that the cracking behavior in the southbound bridge could be compared with that in the northbound bridge in the future to examine the effectiveness of the repair. Figure 8 shows details of the retrofit measure that was installed. Member sizes and bolt-hole spacings were slightly different from those recommended by the University of Kansas due to member availability, edge distance requirements, and installation clearances.

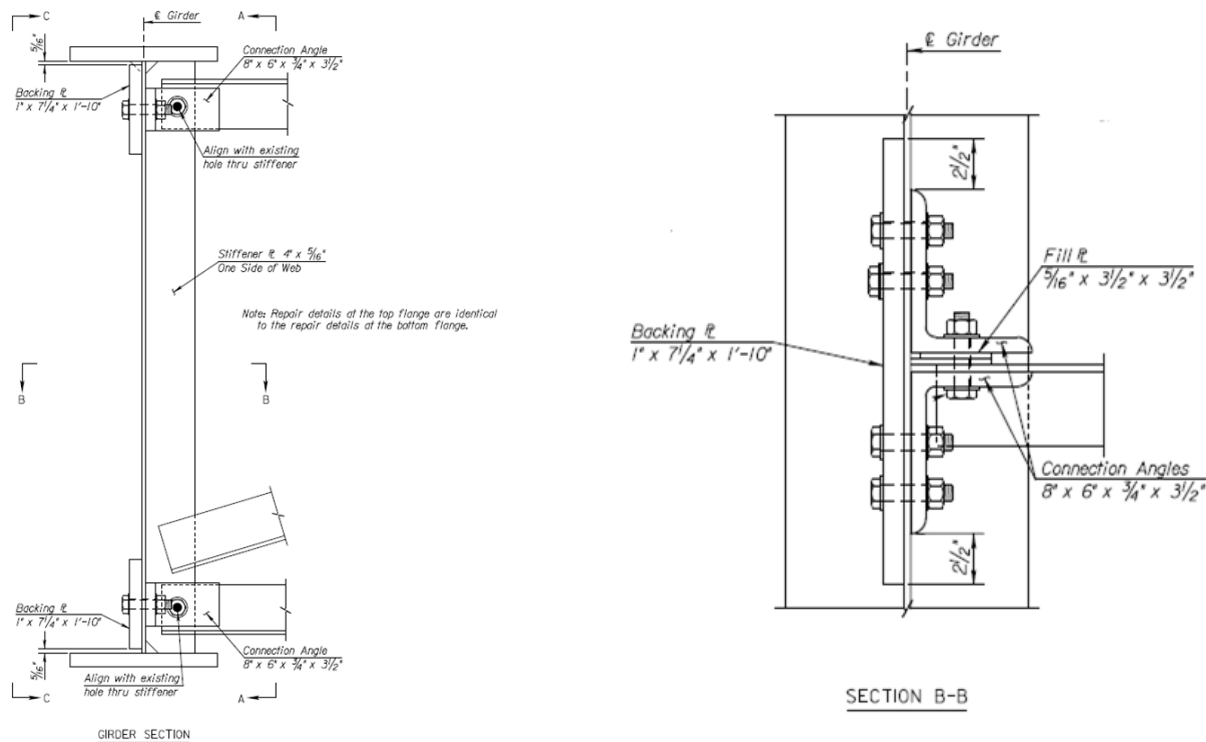


Figure 8: Details of retrofit applied to the bridges.

Instrumentation

The selected location for testing on the bridge was chosen based on the types of fatigue cracks reported in the web gaps and ease of access for placing instrumentation. The selected location for instrumentation was Girder C of the northbound bridge at cross frame 1-2, which was the second cross frame from the south end of the bridge. This location had Types A, B, C, and D cracks. Types B, C, and D cracks were located in the bottom web gap region and crack-arrest holes had been previously drilled. The top web gap had one 19 mm (3/4 in.) Type A crack that had not been previously repaired. Figure 9 shows a photograph of the bottom web gap at the location where the majority of the instrumentation was placed.

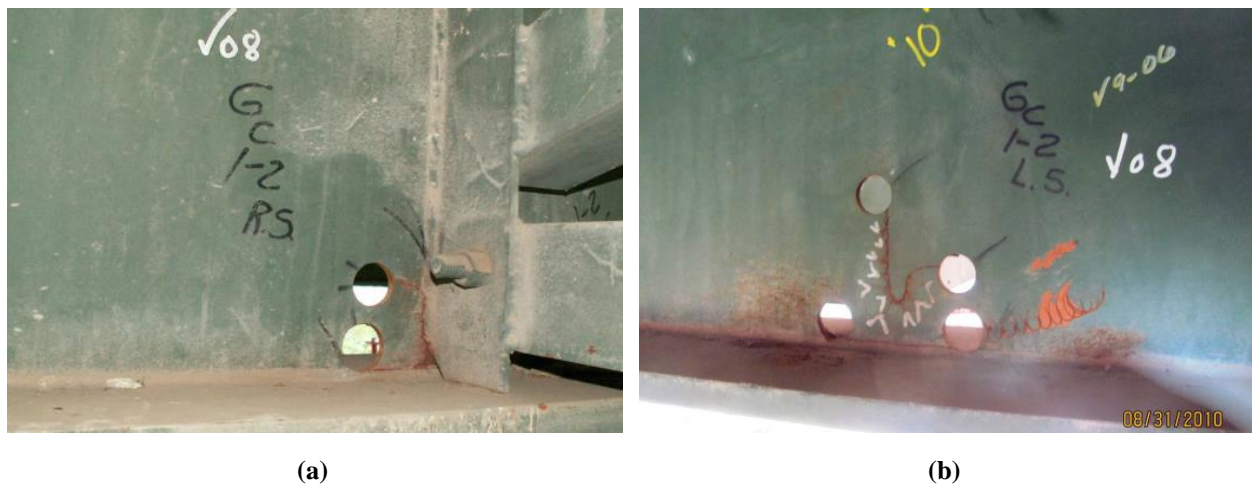


Figure 9: Cracking at the instrumentation location on the (a) stiffener side (b) non-stiffener side.

Instrumentation used for the field tests included 16 bondable strain gages, 11 Bridge Diagnostics Inc. (BDI) strain transducers, one string potentiometer, two inclinometers, and one linear variable differential transformer (LVDT). The bondable strain gages were used to record strain readings at the web gap regions to quantify stress demand in the web gap areas. The BDI strain transducers were used to record strains for the girder flanges and for the cross frame members between Girders C and D. The string potentiometer was used to measure deflection of Girder C at the transverse connection plate, and the inclinometers and LVDT were used to record out-of-plane rotation and displacement of the top web gap relative to the top girder flange.

The bondable strain gages were Micro-Measurements WK-06-250BG-350 gages and were powered directly through a NI-9236 module in a quarter bridge configuration using an

excitation voltage of 3.3V. The strain gages were placed on the girder web near both the bottom and top flanges, and were placed on both sides of the girder web. The side on which the cross frame was attached to the connection plate is referred to as the *stiffener side*, while the opposing side is referred to as the *non-stiffener side*. The strain gages were placed at the same locations in the top and bottom web gaps. The goal was to keep the strain gages in the same locations for the first test and the second test. In some cases, strain gages were moved or not applied in the second test because the footprint of the retrofit covered the strain gage locations from the first test. Figure 10 shows the strain gage locations for both tests for the stiffener and non-stiffener sides of the girder web. Strain gages were purposely located far away from crack tips so that they would not be placed in regions of severe strain gradient. This was done so that a less placement-sensitive strain could be read by the gage, resulting in more accurate comparisons for the pre-retrofit and post-retrofit field tests. Additionally, application of the retrofit would have covered any strain gages in the immediate region of the web gap, making a comparison of results between tests impossible.

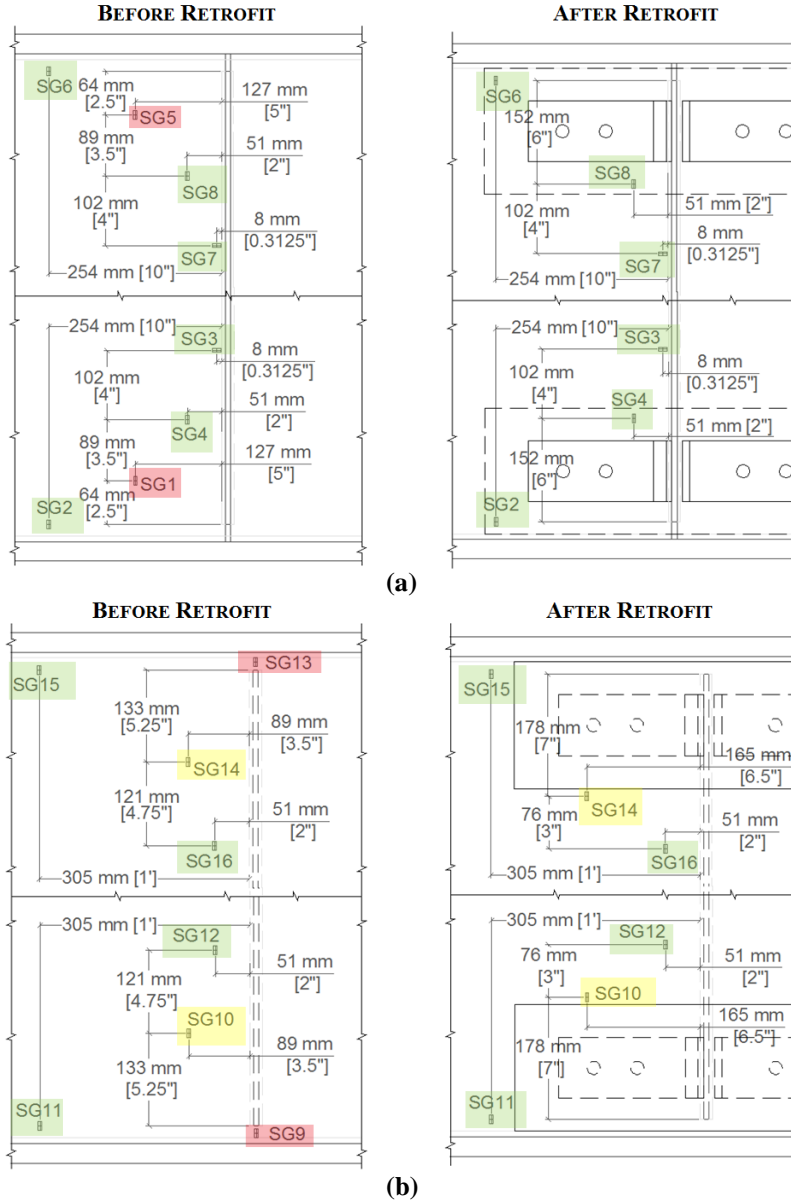


Figure 10: Strain gage locations for both tests on the (a) stiffener side (b) non-stiffener side. Green highlighting indicates that the strain gage was placed in the same location for the second test, yellow highlighting indicates that the strain gage was moved for the second test, and red highlighting indicates that the strain gage was not applied for the second test.

The BDI strain transducers were powered with 5V and connected to a NI-9205 module for data recording. The BDI strain transducers were placed on the bottom flange of each girder, on the top flange of Girder C, and on the cross frame members between Girders C and D. The BDIs on Girder C were placed five feet to the north of the cross frame, while the BDI strain

transducers on the remaining girders were placed so that they followed the skew of the bridge. Figure 11 shows the locations of the BDIs in both section and plan view.

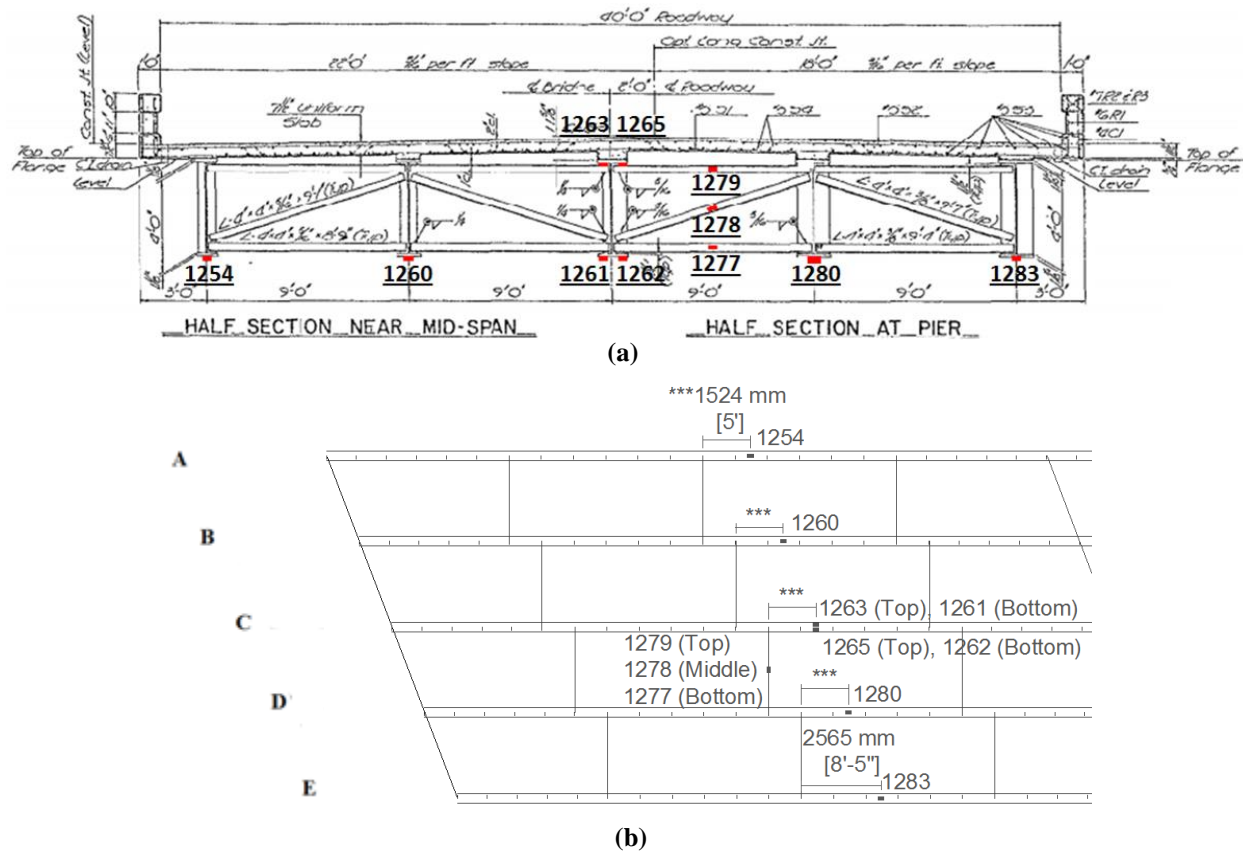


Figure 11: BDI strain transducer locations for both tests in (a) section view (b) plan view.

The string potentiometer was placed under Girder C. It was attached to the middle of the bottom flange, directly under where the connection plate connected to the girder web. Inclinoimeters were placed at the connection plate on Girder C. One inclinometer was placed at the vertical midpoint of the connection plate while the other was attached to the bottom flange of Girder C. The LVDT was attached to the underside of the top flange of Girder C and positioned near the top of the connection plate, similar to the setup shown in Figure 12. The string potentiometer and LVDT were powered using 15V and were connected to a NI-9223 module for data recording, while the inclinometers were powered using 5V and were connected to a NI-9205 module for data recording.

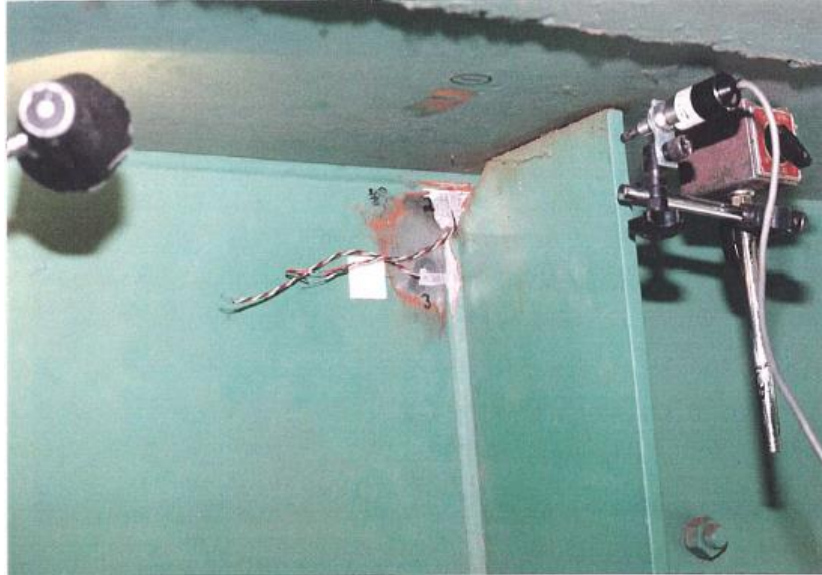


Figure 12: Photograph of LVDT placement similar to that used in the first and second field test.

All data was recorded using a National Instruments data acquisition system. This system was comprised of a single NI cDAQ 9188 chassis that housed each of the NI modules. The NI software, Labview (2011), was used to write an application that read and recorded the data into a text file. The data was recorded using a sampling rate of approximately 800 samples per second. Calibration factors were applied in the Labview software so that data was recorded into the text file with proper units.

Unforeseen electrical noise and connection grounding issues were encountered during the first field test. This resulted in very noisy data and also prevented viable readings from the BDI strain transducers. Measures were taken during the second field test to overcome these challenges. A PS Power Plant Premier was used to regulate the line voltage from the generator, which provided cleaner power for the instrumentation and reduced electrical noise. A 2.4 m (8 ft.) copper-bonded grounding rod was installed in the ground and connected to the generator with 14 gauge wire. Additionally, the NI-9205 module that read data from the BDIs was changed to a differential measurement configuration. These measures reduced the electrical noise and adequately solved the connection grounding issues, resulting in cleaner data and viable results for the BDI strain transducers during the second field test.

Loading

The loaded weight of the truck for the first test was 217 kN (48.8 kip) while for the second test, the loaded weight was 250 kN (56.3 kip). KDOT enforced traffic control, allowing the loaded test truck to pass over the bridge alone over the east lane, west lane, and center of the bridge. Each of these runs was completed twice at 8-16 km/h (5-10 mph) and 105-121 km/h (65-75 mph), for a total of six truck tests, each for the pre-retrofit and post-retrofit field tests. Data was recorded separately via the data acquisition system for each truck test. Because the loads were different, data from the second test was normalized to the loading of the first test to make clear comparisons between the first and second field tests.

Finite Element Models

To accurately reflect field testing conditions, a second series of full-scale finite element models of Kansas Bridge 135-87(043/044) were created using Abaqus version 6.12-3. In these models, focus was shifted from the third cross frame of span two of Girder C to the second cross frame of span one of Girder C, because this was the location where measurements were recorded during field tests. Additionally, crack conditions at the testing location, truck loadings, and the as-installed retrofit measure were modeled as faithfully as possible to coincide with field conditions. Models were analyzed with cracks in both the unretrofitted and retrofitted conditions. Screenshots from the FE models are shown in Figure 13.

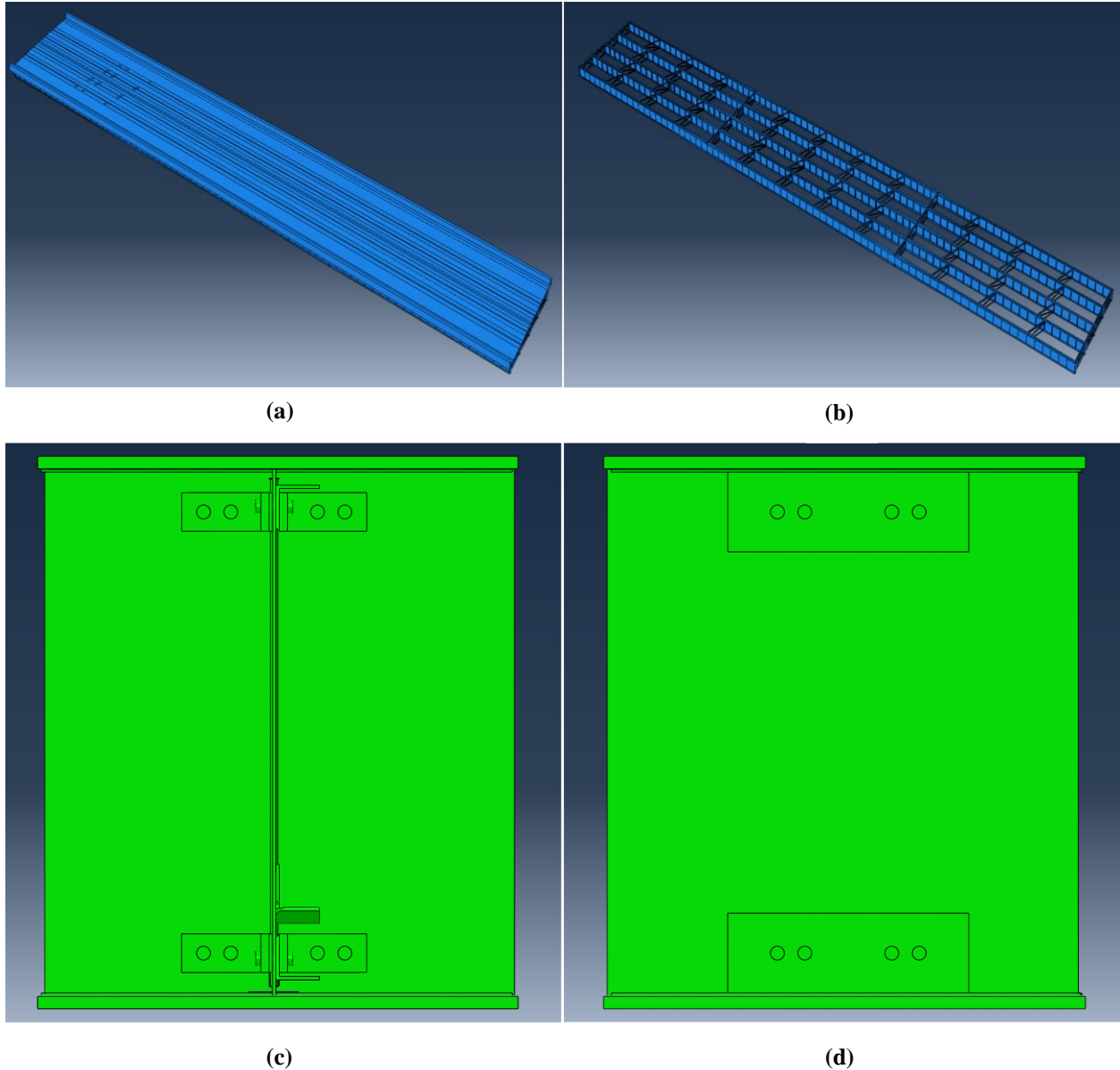


Figure 13: (a) Full scale model with concrete deck (b) Full scale model without concrete deck (c) stiffener side of Girder C with angles-with-plate retrofit (d) non-stiffener side of Girder C with angles-with-plate retrofit.

All materials were modeled as linear elastic. Concrete was modeled with a modulus of elasticity of 25,000 MPa (3,605 ksi) and a Poisson's ratio of 0.2, while steel was modeled with a modulus of elasticity of 200,000 MPa (29,000 ksi) and a Poisson's ratio of 0.3. All structural elements were modeled and assembled in Abaqus version 6.12-3 using three-dimensional solid elements to match as closely as possible the original and repair structural plans, which are

included in Appendix F. The end supports of the bridge are rockers, while the two interior supports are bolsters. These support conditions were modeled as rollers and pins, respectively.

The concrete deck was sloped as in the structural plans and modeled as one part with the two side barriers. The concrete haunches were created in five parts, each being sized and sloped according to their position to the bottom of the bridge deck on each girder. The concrete deck, barriers, and haunches were meshed using structured hexahedral elements (C3D8R) with a mesh size of 127 mm (5 in.). The deck was attached to the haunches and the haunches to the top flanges of the steel girders using tie constraints.

The steel girders were modeled in three parts: the web, top flange, and bottom flange. The top flange and bottom flange were connected to the web using 8 mm (5/16 in.) fillet welds. The fillet welds were modeled as right triangles and connected to the flanges and girders using tie constraints. Intermediate stiffeners were modeled and attached directly to the girder webs with tie constraints. Stiffeners serving as cross frame connection plates were modeled and connected to the girder webs with 4.8 mm (3/16 in.) fillet welds using tie constraints. With the exception of the Girder C web, these steel elements were meshed using structured hexahedral elements (C3D8R) with a mesh size of 25mm (1 in.). A dense mesh was applied to the web gap regions at the second cross frame of span one in Girder C (the focus area of the analyses). At these locations, structured hexahedral elements (C3D8R) with a mesh size of 2.5 mm (0.1 in.) were used over an area that measured 305x1016 mm (12x40 in.) symmetrically about the connection stiffener in the top and bottom web gap regions. Transition regions were modeled using swept hexahedral elements (C3D8R).

The retrofit measure was modeled to match the dimensions of that installed in the field, which included two angles, a backing plate, and a fill plate between the angle and connection plate on the side without a cross frame element. Retrofit elements were modeled with structured and swept hexahedral elements (C3D8R) and a mesh size of 6 mm (0.25 in.). Bolts and bolt holes were modeled with 19 mm (3/4 in.) diameters to match those used by KDOT. Bolt heads and nuts were connected directly to the elements they were in contact with using tie constraints. The angles, backing plates, and fill plates were modeled with hard contact interactions with a friction coefficient of 0.35. Bolts were modeled with a tension bolt load of 125 kN (28 kip), which was applied to each bolt shank using the bolt load function in Abaqus. A bolt load step was created in the model to activate the bolt loads prior to application of the remaining loads.

Cracks were modeled using the Extended Finite Element Method (XFEM) implementation in Abaqus, which allows cracks to be modeled at any location in an element. Cracks were modeled as three-dimensional extruded shell elements and given depths equal to the girder web thickness. The lengths of the cracks were modeled as closely as possible to those observed in the field at the testing location, as shown in Figure 14. The crack pattern in the bottom web gap included a 116 mm (4-9/16 in.) Type D crack, a 117 mm (4-5/8 in.) Type B crack on the north side of the connection plate, and a 51 mm (2 in.) Type B crack that propagated out into a 33 mm (1-5/16 in.) Type C crack on the south side of the connection plate. The crack pattern in the top web gap included a 19 mm ($\frac{3}{4}$ in.) Type A crack.

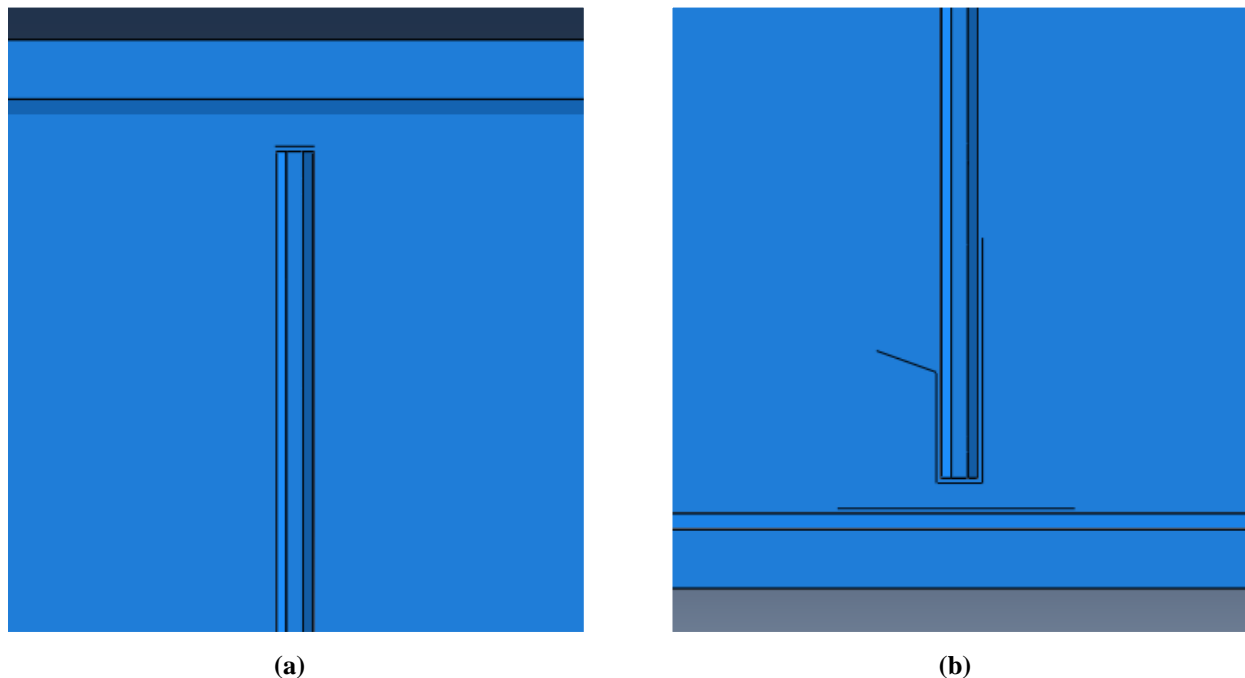


Figure 14: Crack patterns modeled at (a) top web gap (b) bottom web gap.

Because the goal of the field testing was to determine the change in stresses under the action of live loads due to the application of the retrofit, no dead loads were applied. In the field, stresses from the dead loads were already essentially applied to the bridge, so instrumentation only measured what took place in response to traffic live loads. Thus, only the loading from the truck was applied in the finite element models. The loads from the truck were modeled as tire contact areas on the concrete deck. The tire contact areas were modeled with widths of 508 mm (20 in.) and lengths of 254 mm (10 in.). These dimensions were taken from AASHTO LRFD

Bridge Design Specifications Section 3.6.1.2.5 for wheels consisting of one or two tires. The lengths between tire contact areas were kept the same as the axle distances measured on the trucks used in the field tests, which were 4 m (13.2 ft.) between the first and second axle, and 1.3 m (4.4 ft.) between the second and third axle. The width between tire contact areas was kept the same as the axle width measured on the trucks used in the field tests, which was 1.8 m (6.1 ft.). A sketch of the truck tire contact area dimensions is shown in Figure 15.

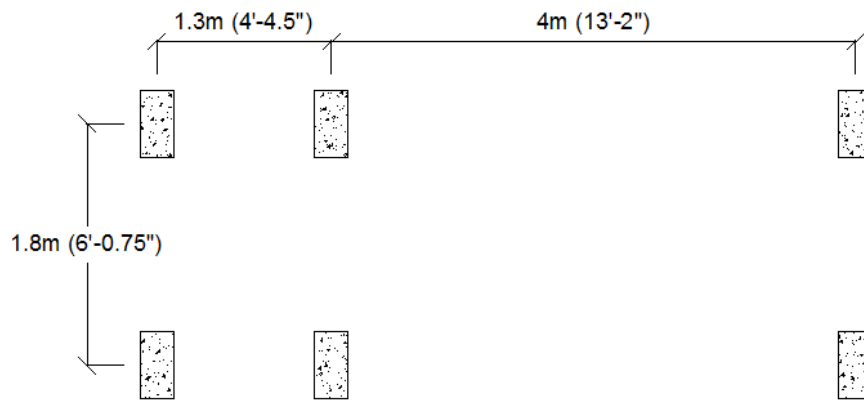


Figure 15: Truck tire contact area dimensions and placements, as measured in the field.

The truck load from the first test, 217 kN (48.8 kip), was used in the models, because the field test results were normalized to this load. Distribution of the truck load was based on the Design Truck in the AASHTO Code, which has a front axle load of 36 kN (8 kip) and two rear axle loads of 142 kN (32 kip) each. This correlated to a front axle load in the model of 24 kN (5.4 kip) and rear axle loads of 96 kN (21.7 kip). Each of these axle loads were halved and applied over their respective tire contact areas as pressure loads, which resulted in front tire contact area loads of 93 kPa (13.5 psi) and rear tire contact area loads of 374 MPa (54.25 ksi). The truck load was modeled in the west and east lanes and over the center of the bridge. Screenshots of these model loads are shown in Figure 16.

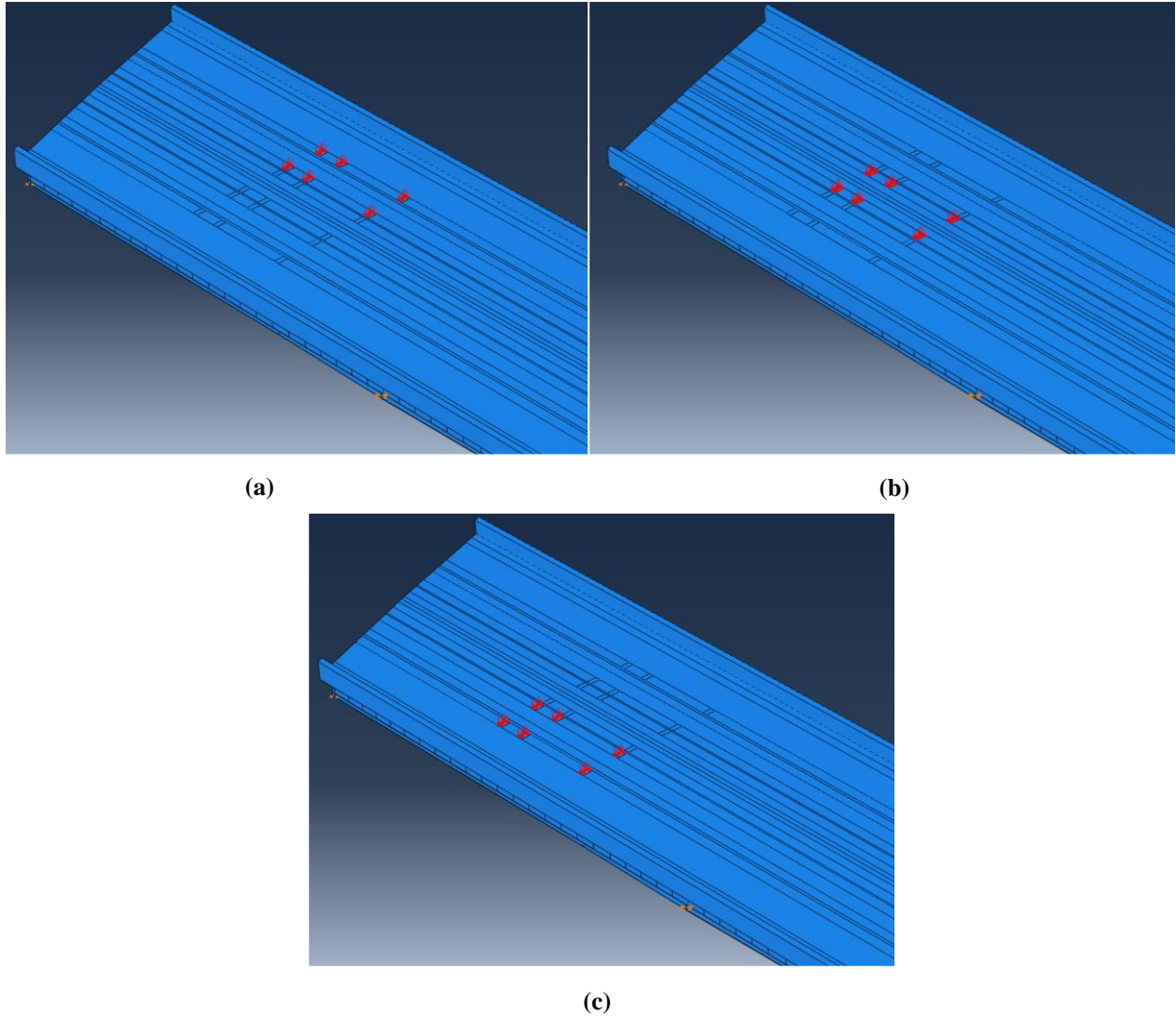


Figure 16: Truck load modeled in (a) west lane (b) bridge center (c) east lane.

To compare results of the finite element model with field test results, the truck location that produced the maximum stress demands was determined. This was accomplished by executing a suite of models in the unretrofitted state in which the truck was “moved” along the bridge in 610 mm (24 in.) increments. A total of seventy-five models, twenty-five for each truck lane position, were analyzed. Stresses were extracted from locations that corresponded to the bondable strain gage locations from the field tests, and then results from each model were compiled into stress curves. The highest stresses from the curves were found to correlate to a truck located a distance of 13.7 m (45 ft.) from the southwest corner of the bridge to the furthest rear axle of the truck. After this truck position was established, six models were analyzed with

this loading and results from these models were compared with the two field test results. Three models were analyzed in the unretrofitted condition with the truck load in the east lane, west lane, and bridge center, and three models were analyzed in the retrofitted condition with the truck load in the east lane, west lane, and bridge center.

Top Web Gap Comparison

Separate finite element analyses that evaluated different crack patterns in the top web gap region were also performed. In these analyses, the cracking pattern in the top web gap was changed to determine what effect this had on stresses in the top web gap region. Crack patterns in the bottom web gap remained the same as those modeled from the field test conditions. The top web gap was modeled with both a 25 mm (1 in.) crack at the connection plate-to-web weld and a 51 mm (2 in.) crack at the flange-to-web weld. Models were also created that included each of these cracks occurring separately in the top web gap. Models of the bridge with these crack conditions were analyzed in both the unretrofitted and retrofitted conditions under the established east lane, west lane, and bridge center truck load positions detailed in the previous section, which led to a total of nine finite element models.

The Hot Spot Stress (HSS) technique was used to compare stresses in the top web gap region between the unretrofitted and retrofitted conditions. Using this technique, maximum principal stresses were taken from nodes along a path located half the thickness of the girder web away from the cracks. Previous studies by Richardson (2012) and Hartman (2013) have shown that distortion-induced fatigue crack growth closely follows maximum principal stress paths. The HSS paths in this study were taken along the length and around the tips of the connection plate-to-web weld and flange-to-web weld cracks to capture the high stresses present in these regions. Figure 17 shows these stress paths for each crack type. HSS 1 refers to the path taken around the connection plate-to-web weld crack, while HSS 2 refers to the path taken around the flange-to-web weld crack.

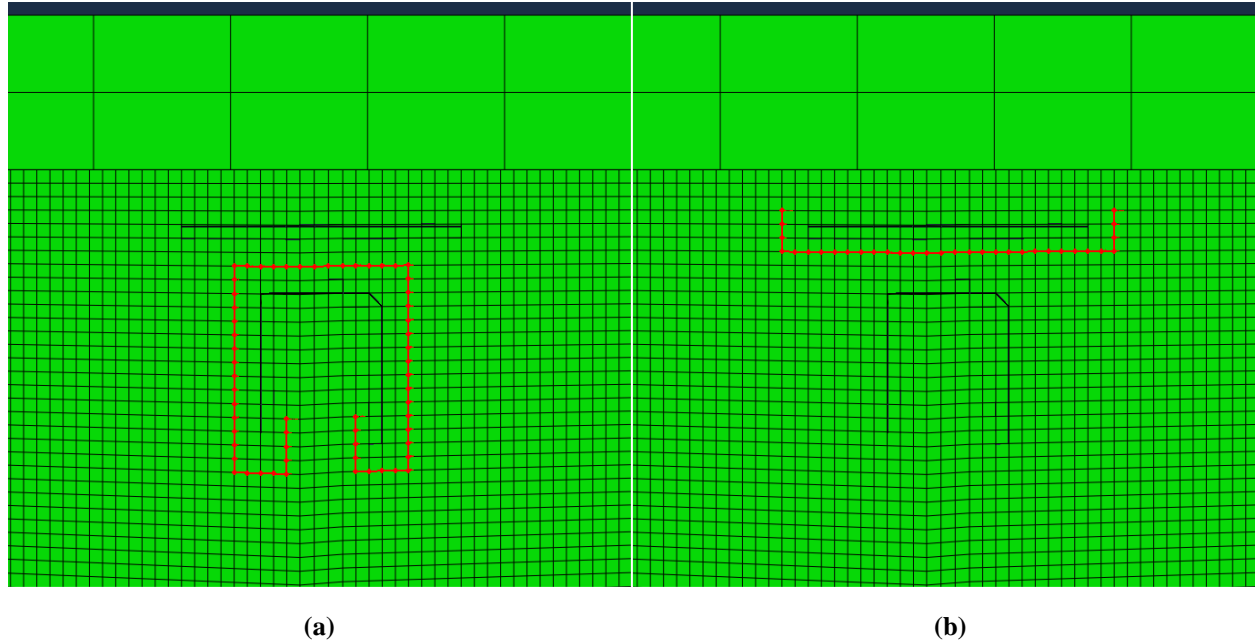


Figure 17: Maximum principal stress paths (a) HSS 1 (b) HSS 2.

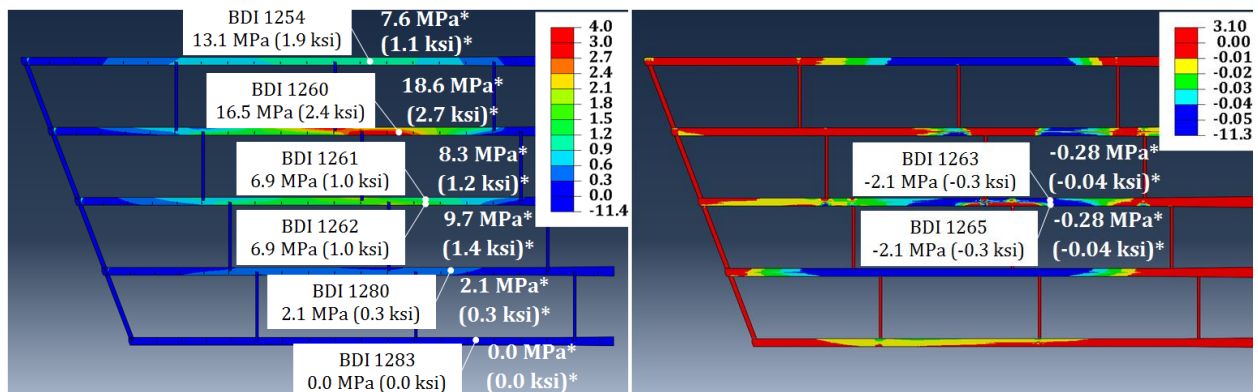
Results and Discussion

To reduce noise in the field test data, a low-pass filter was created and applied in Matlab to create a smoothing effect on the data. The data output from each instrument was passed through the filter, which had a passband frequency of 10 Hz and a stopband frequency of 50 Hz. Data curves from each instrument for each field test trial can be found in Appendix G. Strain readings were converted into stresses and compared with results from finite element analyses of the bridge. Peak strain values were taken from the field test data curves, converted into stresses, and compared with values from the FEM analyses of the bridge.

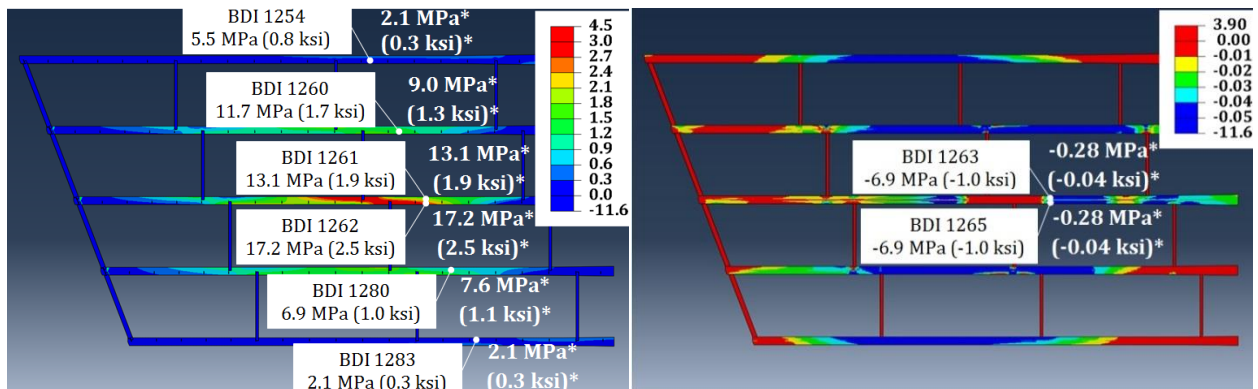
Global Behavior – Field and FEM Investigations

Figures 18 and 19 show the maximum stresses for the BDI strain transducers for the west lane, east lane, and center truck loadings for the second field test. As previously mentioned, electrical noise and connection grounding issues prevented the BDI strain transducers from producing viable data during the first field test. In these figures, the field test data overlays the FE analyses results; field test values are presented with callout boxes to indicate instrument location. The stress values shown in Figures 18 and 19 show that maximum stresses in the girders and cross frames coincided with the respective truck position. For instance, as the truck

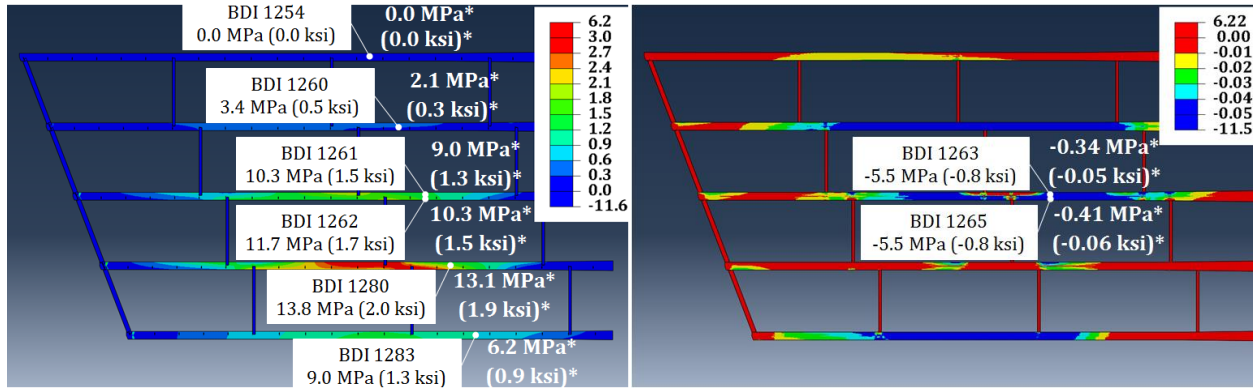
traveled over the west lane, the highest stress was recorded for the BDI strain transducers located on the girders under that lane. This was the same relationship for each truck loading location and corresponding girder BDI. The BDI strain transducers placed on the cross frame show that the bridge center and east lane loadings had the most effect on the cross frame members. Center loading produced the highest tensile stress in the diagonal cross frame member, while the east lane loading produced the highest tensile stresses in the top and bottom horizontal cross frame members. The BDI instrument results followed expected trends intuitively and corresponded to the expected global behavior of the bridge girders. Additionally, the values from the field test correlated well with those from the FE analyses, indicating that the FE models provided a good representation of the behavior of the bridge.



(a)



(b)



(c)

Figure 18: Girder flange BDI results from field tests and FE analyses for (a) west truck load placement (b) center truck load placement (c) east truck load placement. Bottom flange BDIs are shown on the left side of the figure, while top flange BDIs are shown on the right. Legend stresses are in ksi. *FE analyses values.

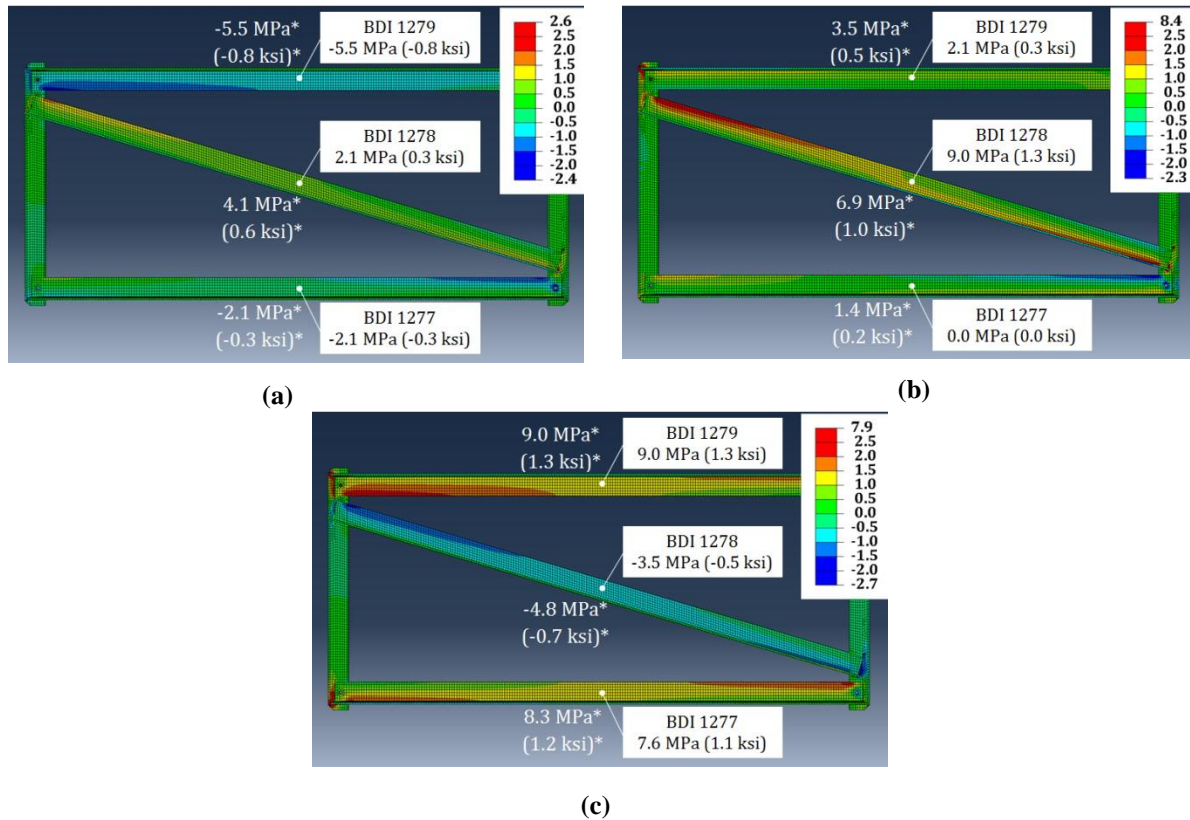


Figure 19: Cross frame BDI results from field tests and FE analyses for (a) west truck load placement (b) center truck load placement (c) east truck load placement. Legend stresses are in ksi. *FE analyses values.

The string potentiometer results for west lane, east lane, and bridge center truck loadings are shown in Figure 20. Maximum vertical deflection of girder C at the connection plate occurred when the truck traveled over the center of the bridge. There was no change in deflection between the first test and the second test, indicating that application of the retrofit did not have an impact on vertical deflection, which was the expected result. As with the BDI results, the values from the field test corresponded to those of the FE analyses, indicating that the FE models provided a good representation of the behavior of the bridge.

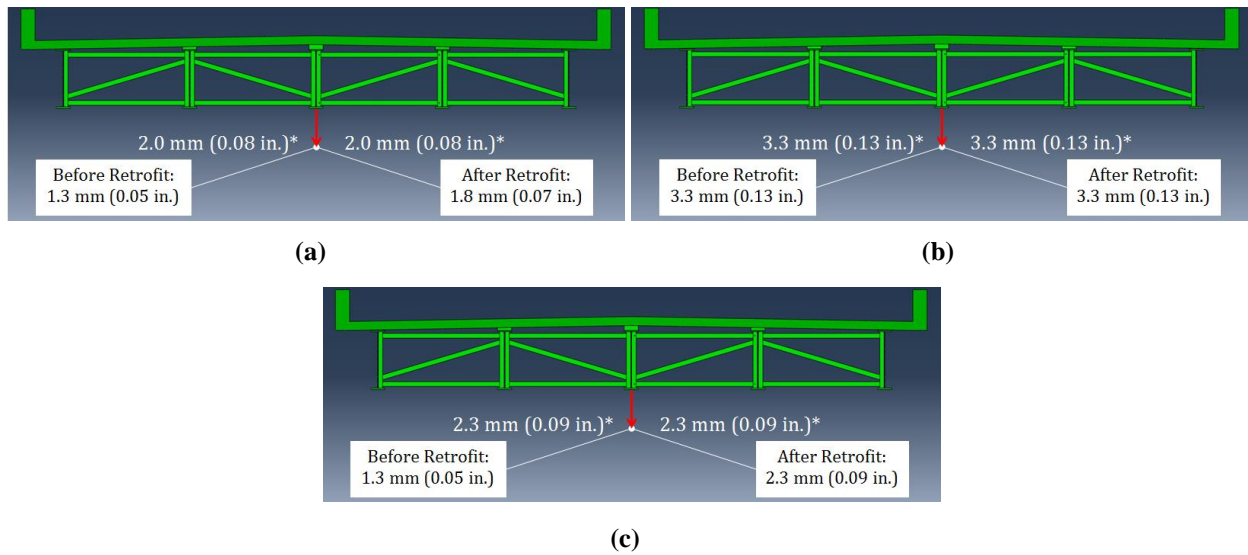


Figure 20: String potentiometer results from field tests and FE analyses for (a) west truck load placement (b) center truck load placement (c) east truck load placement. *FE analyses values.

Local Behavior - Field and FEM Investigations

Bondable strain gages were used to measure local stress demands at the top and bottom girder web gap regions. The strain gages were placed in the same locations for the top and bottom web gaps. Strain gage readings are presented herein for the field tests, and computed results from identical locations in the finite element analyses are also reported. Results are shown in terms of both maximum principal stresses and directional stresses. Directional stresses are used to make a direct comparison between field test strain gage readings and FE analyses results. Strain gages in the field were placed either vertically or horizontally, and are compared accordingly with the appropriate directional stresses from the finite element models. Maximum principal stresses, while not comparable directly with what was measured in the field, capture both in-plane and out-of-plane stresses and are shown to illustrate the overall behavior of the web gap regions before and after the retrofit was applied. All results are shown for the stiffener and non-stiffener sides of Girder C, both before and after retrofit application.

Figures 21, 22, 23, and 24 show results and comparisons of strain gage readings between the unretrofitted and retrofitted states. Corresponding strain gage measurements and FE results generally show that the stress demand at the bottom web gap was at least 20% higher than that of the top web gap for tests before the retrofit was applied. Because the majority of fatigue cracks

found on the bridge have occurred in the bottom web gap, this was expected. It also supports the findings from previous research that in skewed bridges with staggered cross frame configurations the maximum stress demands and fatigue cracking are expected to occur in the bottom web gaps.

For all loading scenarios, field test and FE results show that peak stresses in the bottom web gap were reduced after application of the angles-with-plate retrofit. Reduction of stresses in this area is very favorable because, as previously mentioned, the bottom web gap is the region of Kansas Bridge 135-87(043/044) in which the highest web gap out-of-plane stress demands are experienced. Therefore, the reduction of stresses in the bottom web gap region shows that the angles-with-plate retrofit should be successful in slowing or halting crack propagation for the most problematic areas on the bridge.

For stresses nearest the top flange, peak stresses showed favorable reduction and behavior after application of the angles-with-plate retrofit for the center truck loading test. For the east and west lane truck loadings, small reductions in stress demand, and in a few cases, stress increases, were observed in the top web gap region. Although the top web gap region was found to experience lower stress demands before the retrofit than the bottom web gap, this is still a result that warranted further investigation. For this reason, an additional analytical investigation was performed that focused on the top web gap region of the bridge.

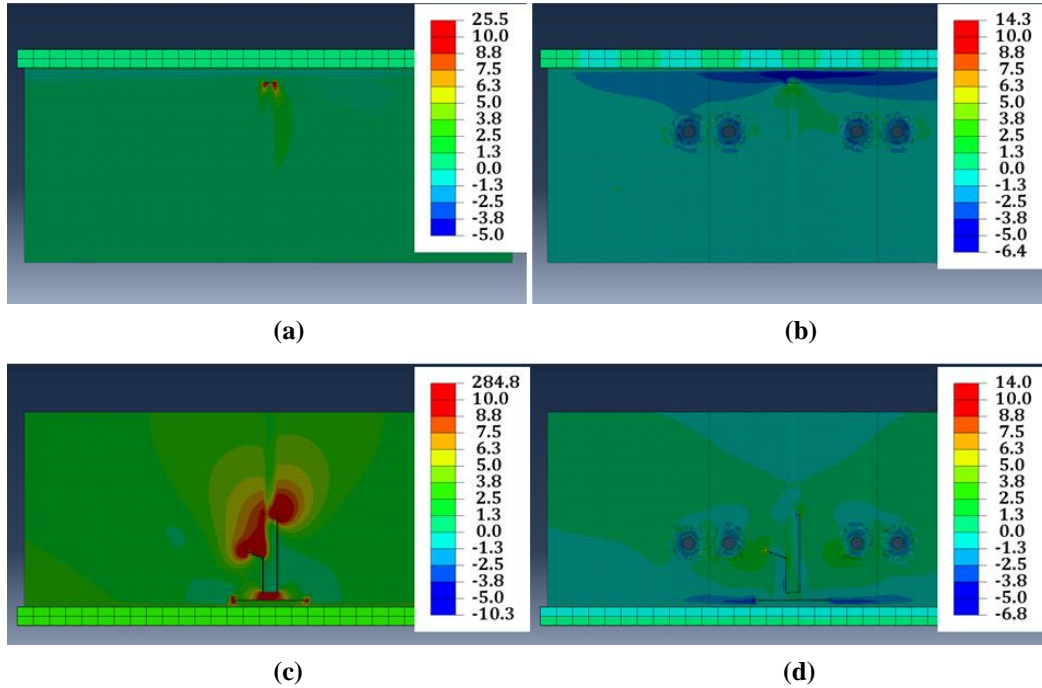


Figure 21: Maximum principal stresses for center load truck placement at (a) top web gap, before retrofit (b) top web gap, after retrofit (c) bottom web gap, before retrofit (d) bottom web gap, after retrofit. Legend stresses are in ksi.

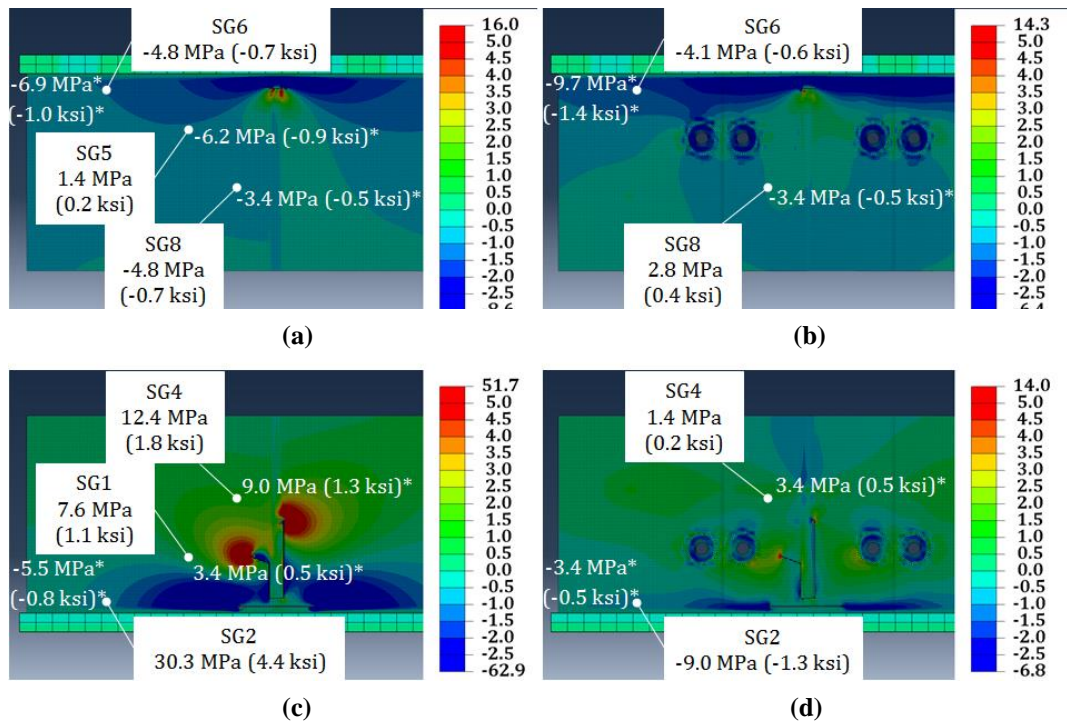


Figure 22: Directional stresses for center load truck placement at (a) top web gap, before retrofit (b) top web gap, after retrofit (c) bottom web gap, before retrofit (d) bottom web gap, after retrofit. Legend stresses are in ksi. *FE analyses values.

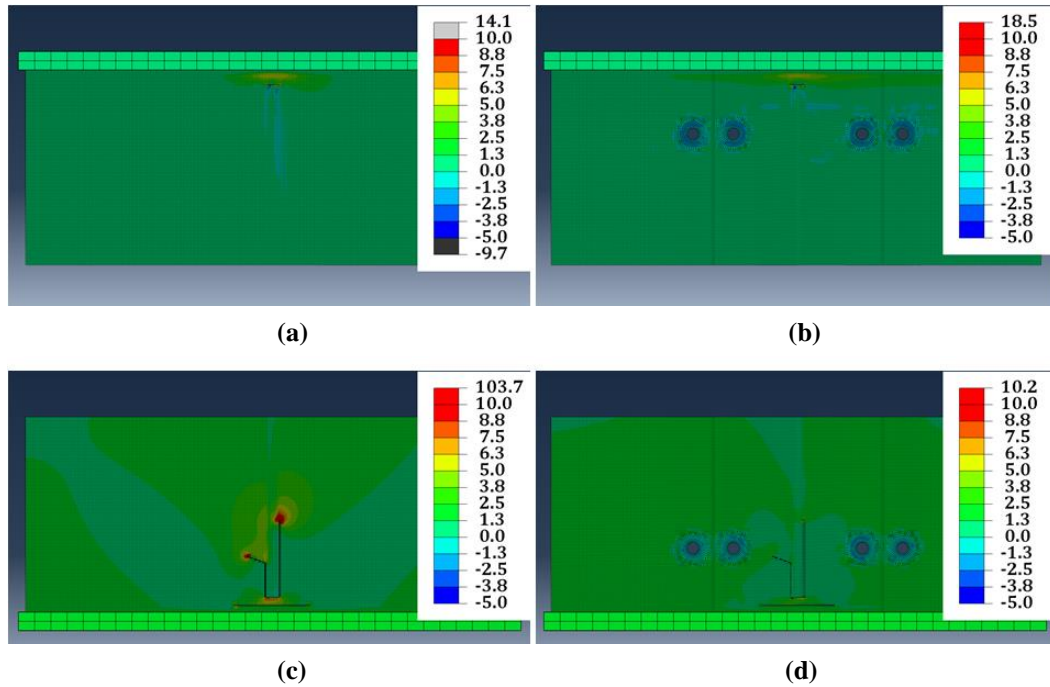


Figure 23: Maximum principal stresses for west load truck placement at (a) top web gap, before retrofit (b) top web gap, after retrofit (c) bottom web gap, before retrofit (d) bottom web gap, after retrofit. Legend stresses are in ksi.

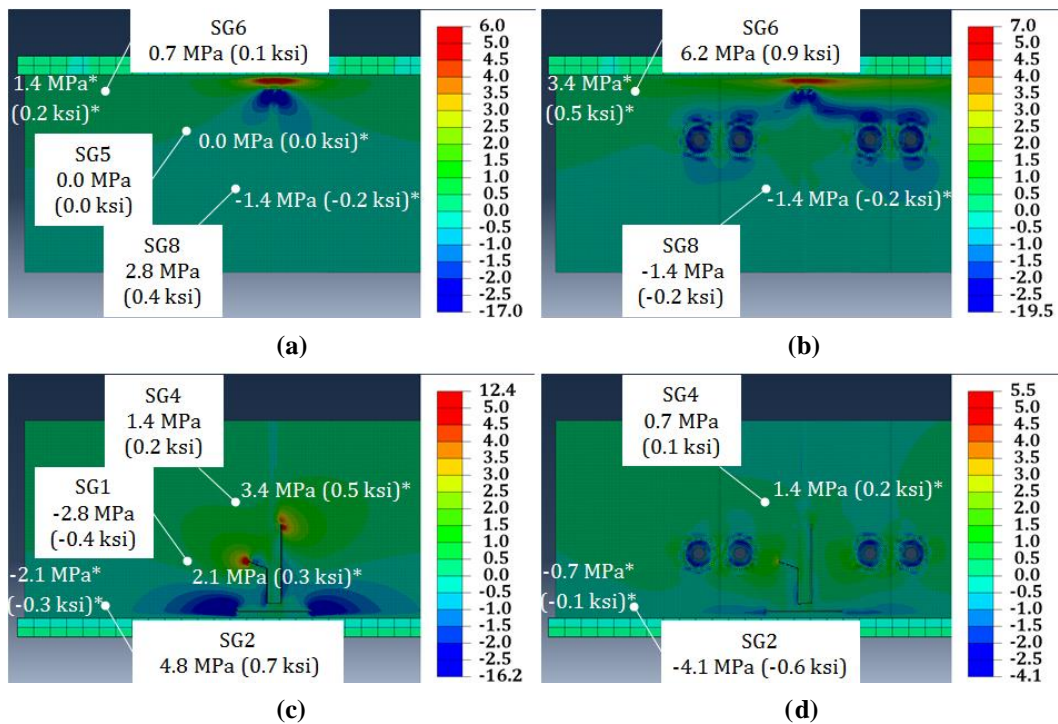


Figure 24: Directional stresses for west load truck placement at (a) top web gap, before retrofit (b) top web gap, after retrofit (c) bottom web gap, before retrofit (d) bottom web gap, after retrofit. Legend stresses are in ksi. *FE analyses values.

Top Web Gap Behavior - FEM Investigation

Hartman's (2013) study of a non-skewed, 9.1 m (30 ft.) test bridge showed that stress demand in the top web gap region decreased as crack length increased. This phenomenon is most apparent when cracks are at their smallest lengths. It should be noted again that the crack in the top web gap at the testing location of Kansas Bridge 135-87(043/044) was a 19 mm (3/4 in.) crack at the connection plate-to-web weld. Typical behavior of this type of crack upon growth is propagation around the toe of the connection plate weld.

Based on the findings by Hartman (2013), it was hypothesized in this study that if the 19 mm (3/4 in.) top web gap crack in the FE model of Kansas Bridge 135-87(043/044) was lengthened into a 25 mm (1 in.) horseshoe-shaped crack, unretrofitted stress demands would decrease and the retrofit would essentially become more effective in the top web gap of Kansas Bridge 135-87(043/044). Investigators in this study also wanted to investigate behavior of the top web gap if a longitudinal top flange-to-web weld crack was introduced in the FE model of Kansas Bridge 135-87(043/044). From KDOT inspection reports, the most severe crack of this type was 51 mm (2 in.), so this was the longitudinal crack length selected for the FE analyses. The inspection reports also indicated that the connection plate-to-web weld cracks and flange-to-web weld cracks occurred both separately and together in the top web gap region, so all three scenarios were investigated in the finite element models.

Using the HSS technique, stress demands around both cracks were compared using the stress paths previously shown in Figure 17. HSS 1 stresses were higher on the stiffener side for both the bridge center and east lane truck loadings, while for the west lane truck loading HSS 1 stresses were higher on the non-stiffener side. The opposite was true for the HSS 2 stress path. Stresses along this path were highest on the non-stiffener side for both the bridge center and east lane truck loadings and on the stiffener side for the west lane truck loading.

Figures 25, 26, and 27 show maximum principal stresses when both the connection plate-to-web weld and flange-to-web weld cracks were present for all three truck location loadings, both before and after retrofit application. Under bridge center truck loading, the retrofit reduced HSS 1 and HSS 2 stress demands by 66% and 35%, respectively. Under west lane truck loading, HSS 1 stress was reduced by 27% and HSS 2 stress was reduced by 26%. Under east lane truck loading, HSS1 and HSS 2 stresses were reduced by 53% and 23%, respectively.

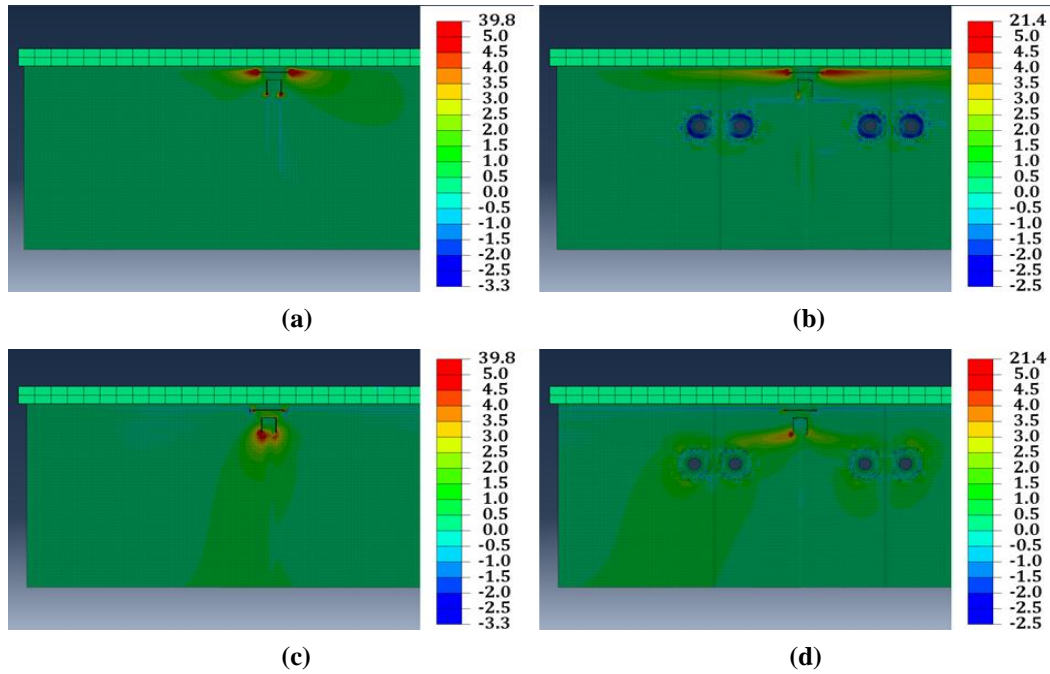


Figure 25: Maximum principal stresses at top web gap for west load truck placement when both the connection plate-to-web and flange-to-web weld cracks are present for (a) stiffener side, before retrofit (b) stiffener side, after retrofit (c) non-stiffener side, before retrofit (d) non-stiffener side, after retrofit. Legend stresses are in ksi.

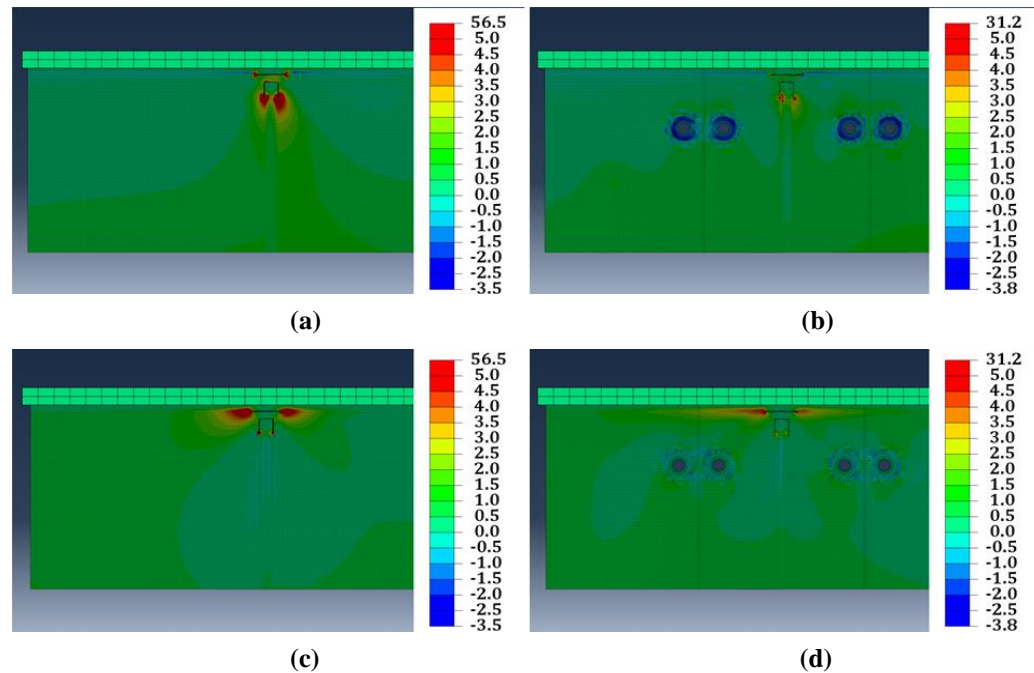


Figure 26: Maximum principal stresses at top web gap for center load truck placement when both the connection plate-to-web and flange-to-web weld cracks are present for (a) stiffener side, before retrofit (b) stiffener side, after retrofit (c) non-stiffener side, before retrofit (d) non-stiffener side, after retrofit. Legend stresses are in ksi.

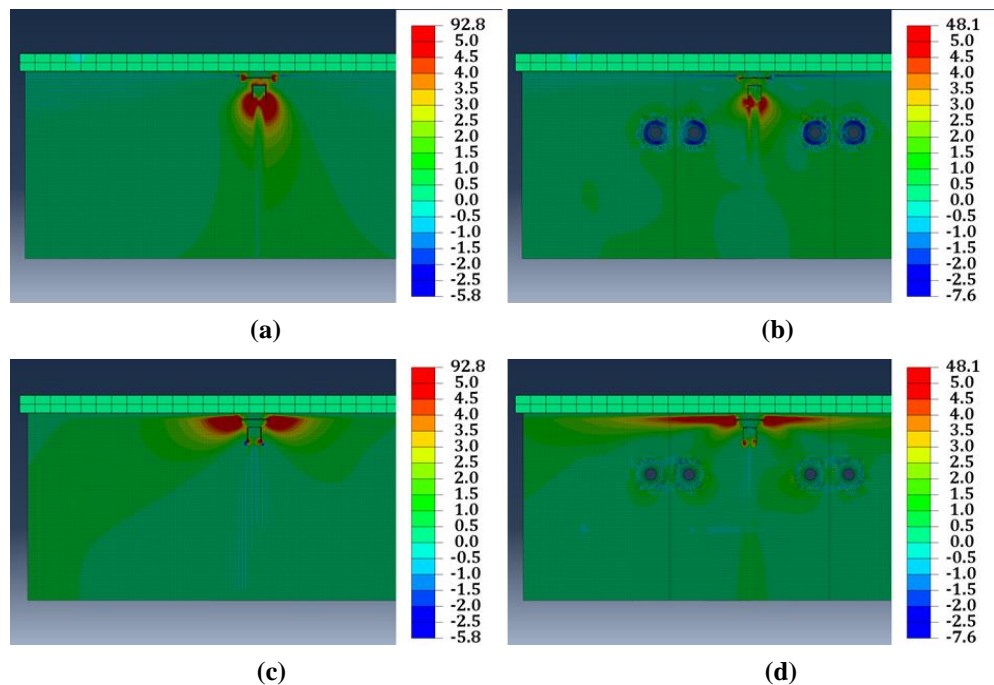


Figure 27: Maximum principal stresses at top web gap for east load truck placement when both the connection plate-to-web and flange-to-web weld cracks are present for (a) stiffener side, before retrofit (b) stiffener side, after retrofit (c) non-stiffener side, before retrofit (d) non-stiffener side, after retrofit. Legend stresses are in ksi.

Figure 28 shows maximum principal stresses from all three truck location loadings, both before and after retrofit application, for the top web gap when only the connection plate-to-web weld crack was present. After application of the retrofit, HSS 1 stress was reduced under the bridge center, west lane, and east lane truck loadings by 63%, 26%, and 50%, respectively. Figure 29 shows maximum principal stresses, both before and after retrofit application, for the top web gap when only the flange-to-web weld crack was present. Application of the retrofit reduced HSS 2 stress demand under the bridge center, west lane, and east lane truck loadings by 23%, 14%, and 2%, respectively. Overall, HSS 1 and HSS 2 stresses were highest under the east lane truck loading, thus stress reductions under this loading were more critical than those under the west lane and bridge center truck loadings.

HSS 1 stresses were reduced only slightly more for the case where both connection plate-to-web weld and flange-to-web weld cracks were present than in the case where only the connection plate-to-web weld crack was present. HSS 2 stresses were reduced less in the case where only the flange-to-web weld crack was present compared with the case where both cracks were present. These results indicate that the flange-to-web weld crack stresses are affected more

by the appearance of connection plate-to-web weld crack, and that the appearance of the flange-to-web weld crack has little effect on the connection plate-to-web weld crack.

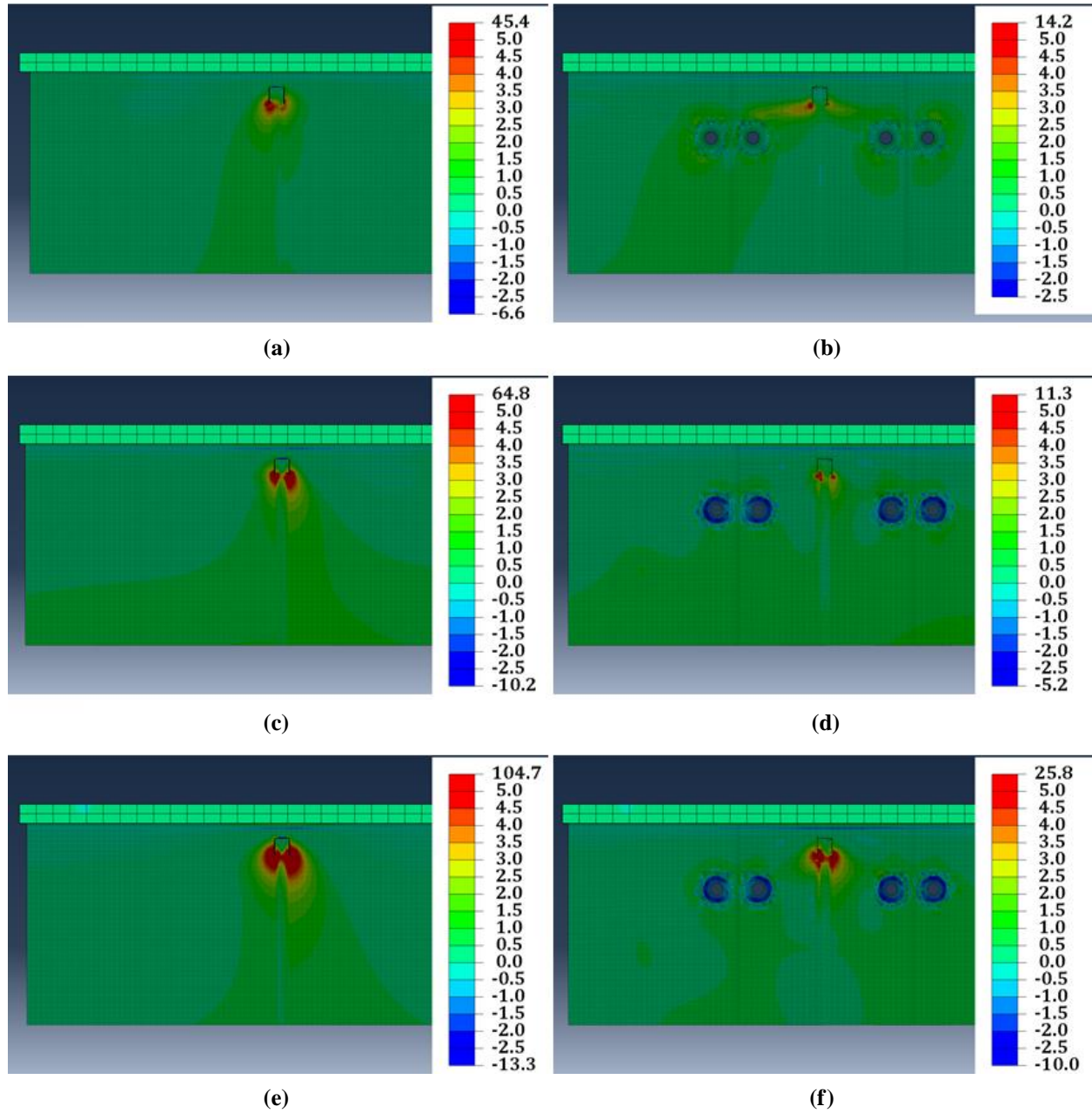


Figure 28: Maximum principal stresses at top web gap when only connection plate-to-web weld crack is present for (a) west load truck placement, before retrofit (b) west load truck placement, after retrofit (c) center load truck placement, before retrofit (d) center load truck placement, after retrofit (e) east load truck placement, before retrofit (f) east load truck placement, after retrofit. Legend stresses are in ksi.

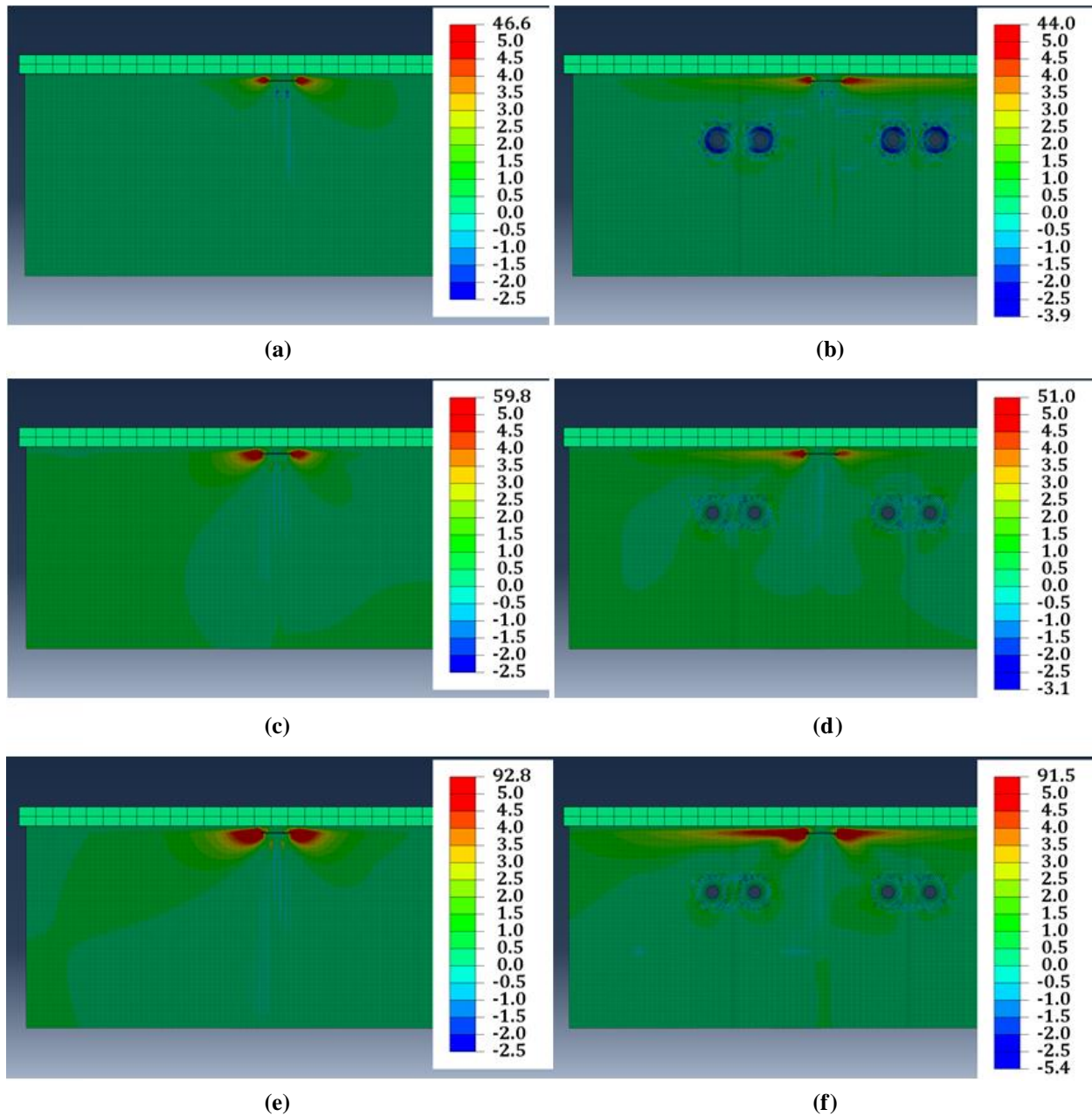


Figure 29: Maximum principal stresses at top web gap when only flange-to-web weld crack is present for (a) west load truck placement, before retrofit (b) west load truck placement, after retrofit (c) center load truck placement, before retrofit (d) center load truck placement, after retrofit (e) east load truck placement, before retrofit (f) east load truck placement, after retrofit. Legend stresses are in ksi.

In all cases, stress demands were reduced in the top web gap region by application of the angles-with-plate retrofit measure. Although stresses were reduced less when just the flange-to-web weld crack was present, the stress patterns shown in Figure 29 indicate that when the flange-to-web weld crack is present, the stresses in the connection plate-to-web weld crack region are

also high and are likely to produce the connection plate-to-web weld crack. The same is true for the case with just the connection plate-to-web weld crack with respect to the stress patterns in the flange-to-web weld crack region, as shown in Figure 28. These are favorable results in that the appearance of both the connection plate-to-web weld and flange-to-web weld cracks showed improvement in the performance of the angles-with-plate retrofit.

Further investigation of the top web gap region due to concerning results from the field test and corresponding FE analyses led to supportive results for application of the angles-with-plate retrofit. By extending the 19 mm (3/4 in) Type A crack around the connection plate-to-web weld, retrofit performance improved. Because this is the typical propagation for this type of crack, this would be the expected crack pattern if any growth of the Type A crack was to take place in top web gap of Kansas Bridge 135-87(043/044). The results from the additional set of FE analyses show that performance of the retrofit would improve if this were to take place, and further growth of the crack would be unlikely. Even upon addition of a flange-to-web weld crack in the FE models, top web gap stresses were reduced after application of the retrofit. Although stresses in the top web gap region are much smaller in comparison with the bottom web gap region in Kansas Bridge 135-87(043/044), and most fatigue cracking has been reported in the bottom web gap region, these results show that the angles-with-plate retrofit should also be effective in the top web gap region.

It is important to emphasize that the field tests and analytical models focused solely on the top web gap at the second cross frame of span one of Girder C. Due to the findings in this investigation, it is recommended that further investigations be made into other cross frame locations on adjacent girders of Kansas Bridge 135-87(043/044) to gain additional insight into top web gap behavior of the bridge. As stated previously, Type A and D cracks were present both separately and together in top web gap regions of the bridge. Figure 30 indicates top web gap crack locations and the types of cracks present at each location. Additional studies of web gap stresses and retrofit behavior at those locations would provide a better and more comprehensive understanding of top web gap behavior, as the cracks occur in interior and exterior girders in both positive and negative moment regions. It is also recommended that full-scale analytical models of additional skewed bridges with staggered cross frame layouts be developed and studied to further investigate top web gap fatigue cracking behavior and performance of the angles-with-plate retrofit in the top web gap of bridges with such geometry.

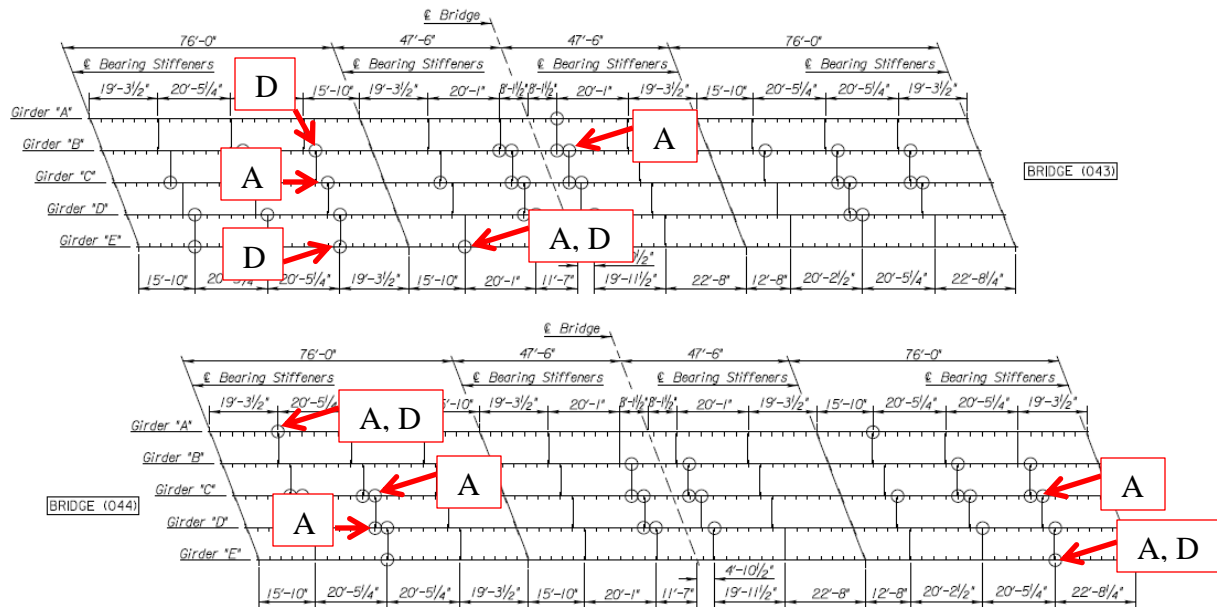


Figure 30: Top web gap crack locations in Kansas Bridge 135-87(043/044) with crack types indicated.

Conclusions

Kansas Bridge 135-87(043/044) has a history of fatigue cracks, the majority of which are located in the bottom web gap. Field testing was performed on the bridge both before and after the angles-with-plate retrofit was installed at all cross frame locations. Complementary FE analyses were performed to provide context to the field test results and to obtain an improved overall view of what is occurring in the web gap regions of the bridge and the effect that the angles-with-plate retrofit had on reducing stress demands in those regions. Results for the top web gap region under the east and west lane truck loading scenarios led to the execution of an additional set of FE analyses to develop a better understanding of the top web gap behavior. Based on results from these investigations, it can be concluded that:

- Readings from the BDI strain transducers and string potentiometer produced the expected global behavior trends of the bridge. Stress and deflection values corresponded intuitively to the respective east lane, west lane, and bridge center truck loadings and correlated well with FE results.
- Comparisons between stresses in the top and bottom web gaps for the tests performed before the retrofit was applied showed that stress demands were at least 20% higher in the bottom web gap than in the top web gap. This supports previous research which

found that skewed bridges with staggered cross frames are more susceptible to fatigue cracking in the bottom web gap regions than the top. It also explains why more fatigue cracks have been reported in the bottom web gap regions than in the top web gap regions in Kansas Bridge 135-87(043/044).

- Stress demands decreased after installation of the retrofit in the bottom web gap for each load placement. Since the bottom web gaps are where fatigue cracking has been most critical in Kansas Bridge 135-87(043/044), this indicates that the angles-with-plate retrofit is an effective retrofit for the most problematic areas of the bridge.
- Stress demands decreased in the top web gap region for the center truck load placement, but increased or stayed nearly the same for the east and west truck load placements for the crack pattern seen in the field tests and FE analyses. Upon further investigation of the top web gap region in an additional suite of FE analyses, retrofit performance was found to improve as the Type A crack was allowed to propagate into its typical horseshoe-shaped pattern around the connection plate-to-web weld. HSS 1 stresses decreased for west and east truck load placements by 26% and 50%, respectively. Upon addition of a separate flange-to-web weld crack, HSS 2 stresses decreased in the top web gap region for west and east truck lane loadings by 14% and 2%, respectively.
- Analyses of the connection plate-to-web weld crack alone indicated stress patterns that would lead to a flange-to-web weld crack, and vice versa. In FE analyses where both the connection plate-to-web weld and flange-to-web weld cracks were modeled simultaneously, HSS 1 and HSS 2 stresses reduced by 27% and 26%, respectively, for the west truck load placement. For the east truck load placement, HSS 1 and HSS 2 stresses reduced by 53% and 23%, respectively.

Field tests and finite element simulations performed for Kansas Bridge 135-87(043/044) show that the angles-with-plate retrofit is an effective solution for mitigating fatigue cracks in problematic bottom web gap regions of staggered, skewed bridges. In the less demanding top web gap regions of such bridges, the retrofit also shows that it should be effective. However, results from the top web gap behavior study do warrant further investigation. This behavior of top web gap stresses and performance of the angles-with-plate retrofit in mitigating those stresses should be further studied in other girders in the analytical model of Kansas Bridge 135-87(043/044) and in additional full-scale models of bridges with skewed, staggered geometry.

The geometry of the cross frame members and their connection directly to the transverse connection plates in Kansas Bridge 135-87(043/044) shows that the angles-with-plate retrofit is a more cost effective and simpler retrofit to install in bridges with similar cross frame construction. Since attachment to the girder flanges is unnecessary, cross frame members do not have to be removed for installation of the angles. The angles can be applied over the cross frame members in both the bottom and top web gap regions. Additionally, if applied in the top web gap region, bridge deck removal is unnecessary, which lowers costs and allows for less traffic interruptions. Thus, in addition to being effective, the angles-with-plate retrofit is a simpler and more cost effective technique that can be used to repair distortion-induced fatigue cracking in steel girder bridges.

References

- Alemдар, F., T. Overman, A. Matamoros, C. Bennett, and S. Rolfe. "Repairing Distortion-Induced Fatigue Cracks in Steel Bridge Girders using Angles-with-Plate Retrofit Technique, Part I: Physical Simulations." *Journal of Structural Engineering* (ASCE), 2013a.
- Alemдар, F., T. Overman, A. Matamoros, C. Bennett, and S. Rolfe. "Repairing Distortion-Induced Fatigue Cracks in Steel Bridge Girders using Angles-with-Plate Retrofit Technique, Part II: Computer Simulations." *Journal of Structural Engineering* (ASCE), 2013b.
- Connor, R.J. and Fisher, J.W. "Identifying Effective and Ineffective Retrofits for Distortion Induced Fatigue Cracking in Steel Bridges Using Field Instrumentation." *Journal of Bridge Engineering* 11, no. 6 (2006): 745-752.
- Fisher, J.W. and Mertz, D.R. "Fatigue and Fracture in Steel Bridges." *The Conference on Bridges*, 1984: 10-21.
- Grondin, G.Y., R. Fraser, and M. D'Andrea. "Testing and Evaluation of Fatigue Damaged Girders." *4th Structural Specialty Conference of the Canadian Society for Civil Engineering*, 2002.
- Hartman, A. "Analytical and Experimental Investigation for Distortion-Induced Fatigue in Steel Bridges." PhD Thesis, University of Kansas, 2013.
- Hartman, A., H. Hassel, C. Adams, C. Bennett, A. Matamoros, and S. and Rolfe. "Effects of Cross-Frame Placement and Skew on Distortion-Induced Fatigue in Steel Bridges." *TRB: Journal of Transportation Research Board* 2200, no. 1 (2010): 62-68.

- Hassel, H., C. Bennett, A. Matamoros, and S. and Rolfe. "Parametric Analysis of Cross-Frame Layout on Distortion-Induced fatigue in Skewed Steel Bridges." *Journal of Bridge Engineering* (ASCE) 18, no. 7 (2013): 601-611.
- Jones, J., C. Bennett, A. Matamoros, S. Rolfe, and K. and Roddis. "Fighting Fatigue in Steel Bridges." *TR News, Transportation Research Board (TRB)*, no. 259 (Nov/Dec 2008).
- Liu, H. "A Finite-Element-Based Approach to Modeling Cracking & Repairs for Distortion-Induced Fatigue in Steel Bridges." PhD Thesis, University of Kansas, 2015.
- Richardson, T. "Analytical Investigation of Repair Methods for Fatigue Cracks in Steel Bridges." MS Thesis, University of Kansas, 2012.
- Roddis, W.M.K, and Y. Zhao. "Out-of-Plane Fatigue Cracking in Welded Steel Bridges." *Welding Innovation* 27, no. 2 (2001): 2-7.
- Zhao, Y., and W.M.K. Roddis. "Fatigue Behavior and Retrofit Investigation of Distortion-Induced Web Gap Cracking." *Journal of Bridge Engineering* 12, no. 6 (2007): 737-745.

Girders

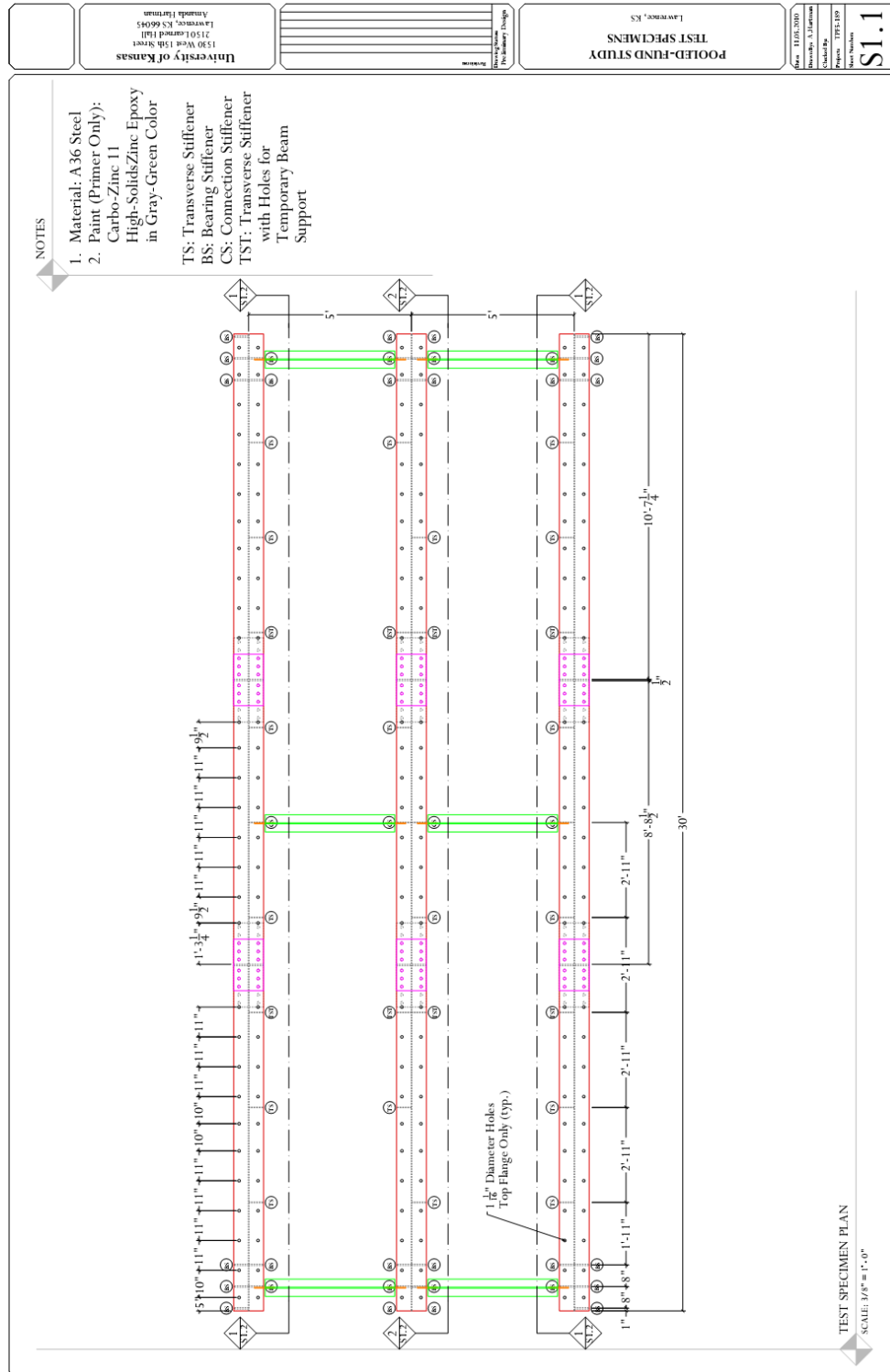


Figure A. 1: Specimen plan.

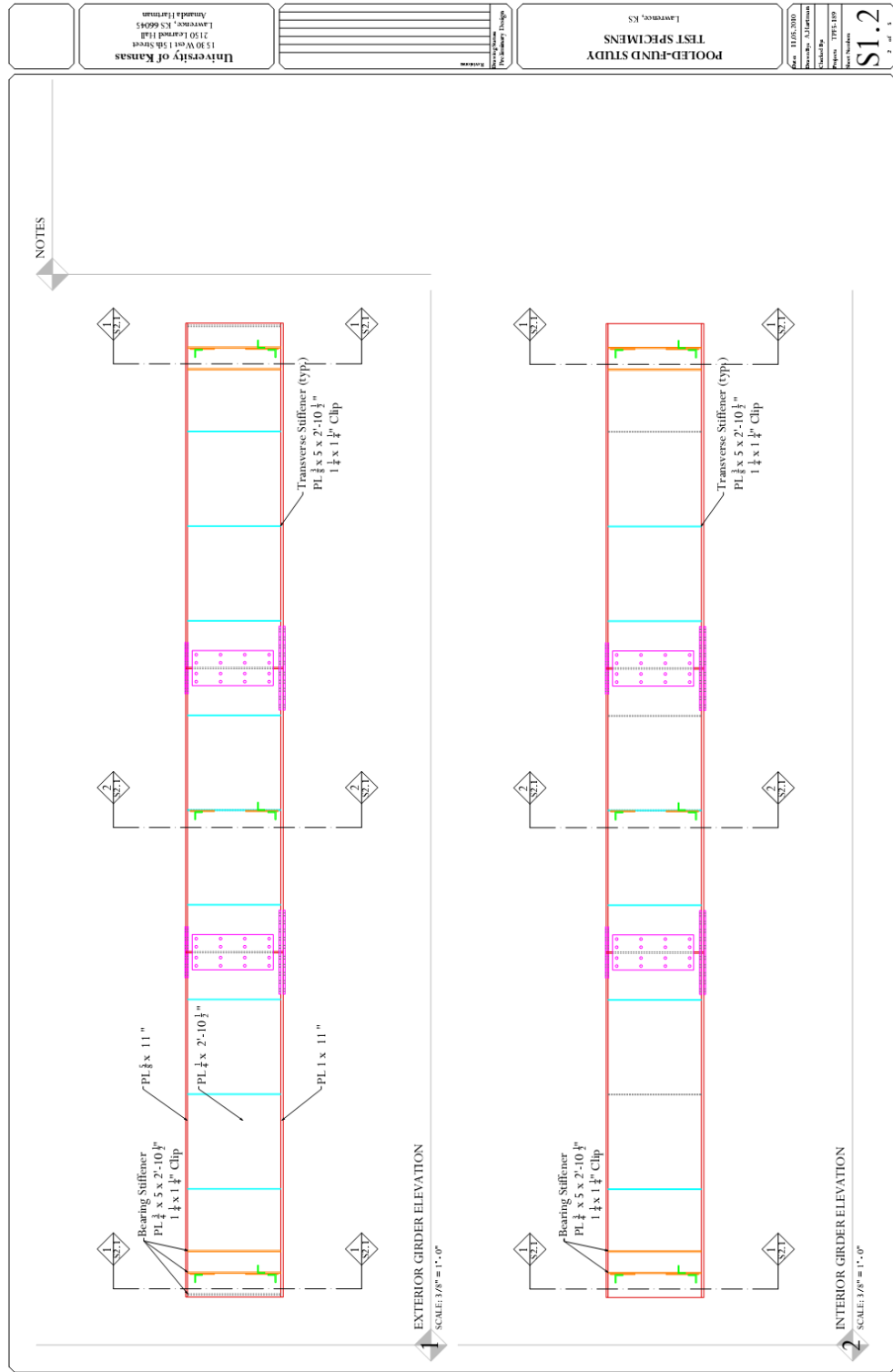


Figure A. 2: Specimen girder elevations.

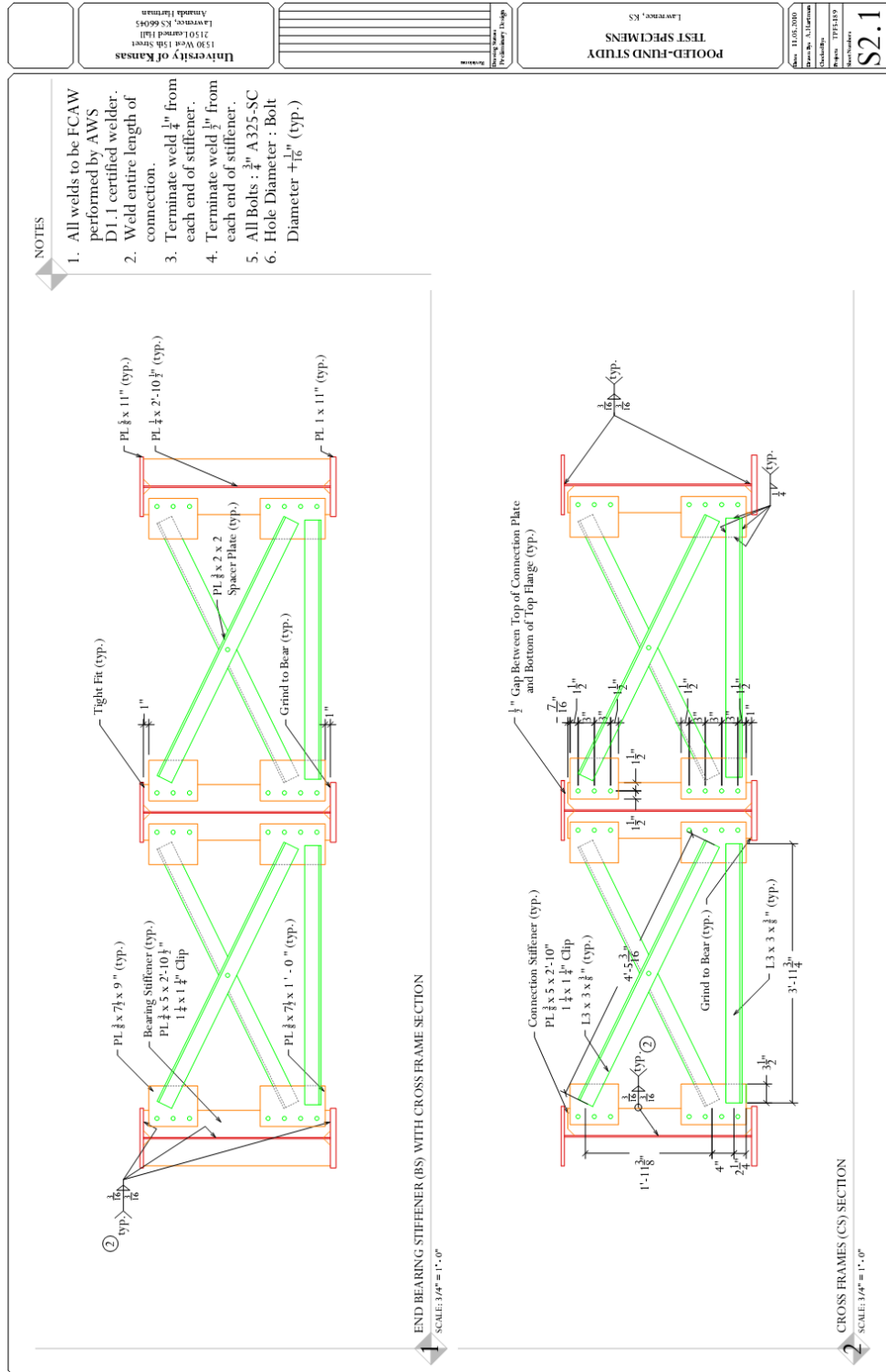
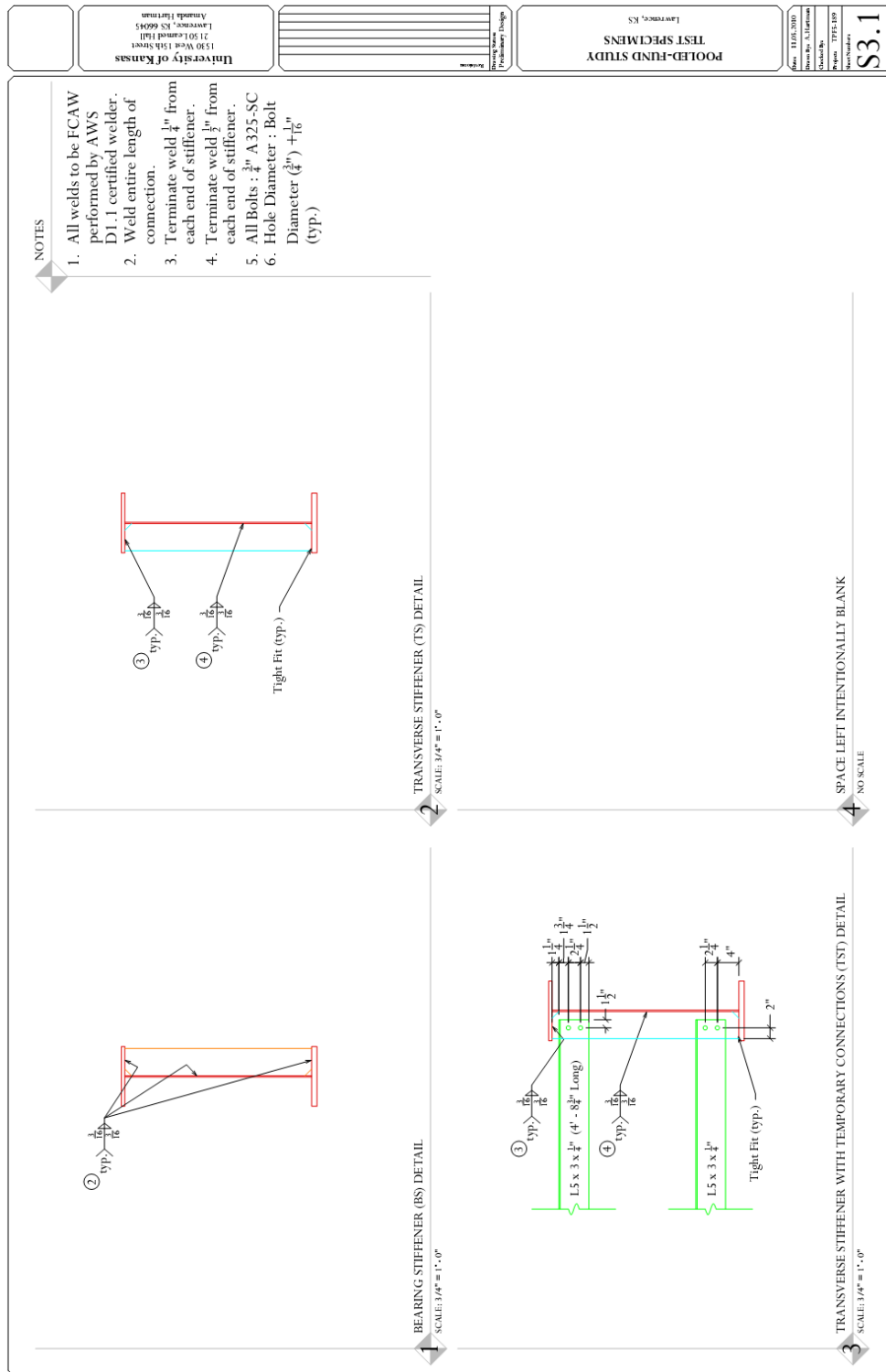


Figure A. 3: Specimen cross frame elevations.





Retrofit

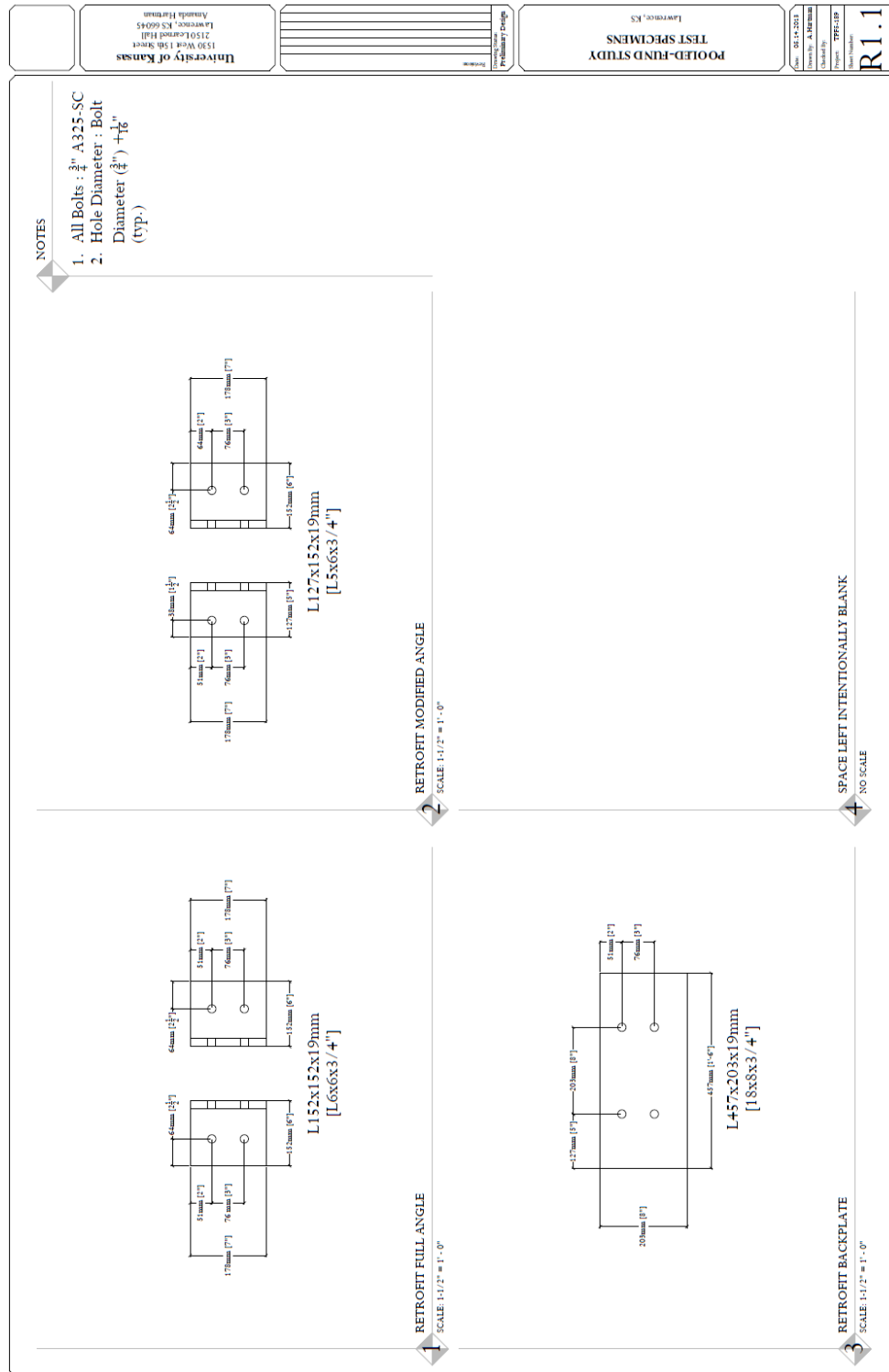
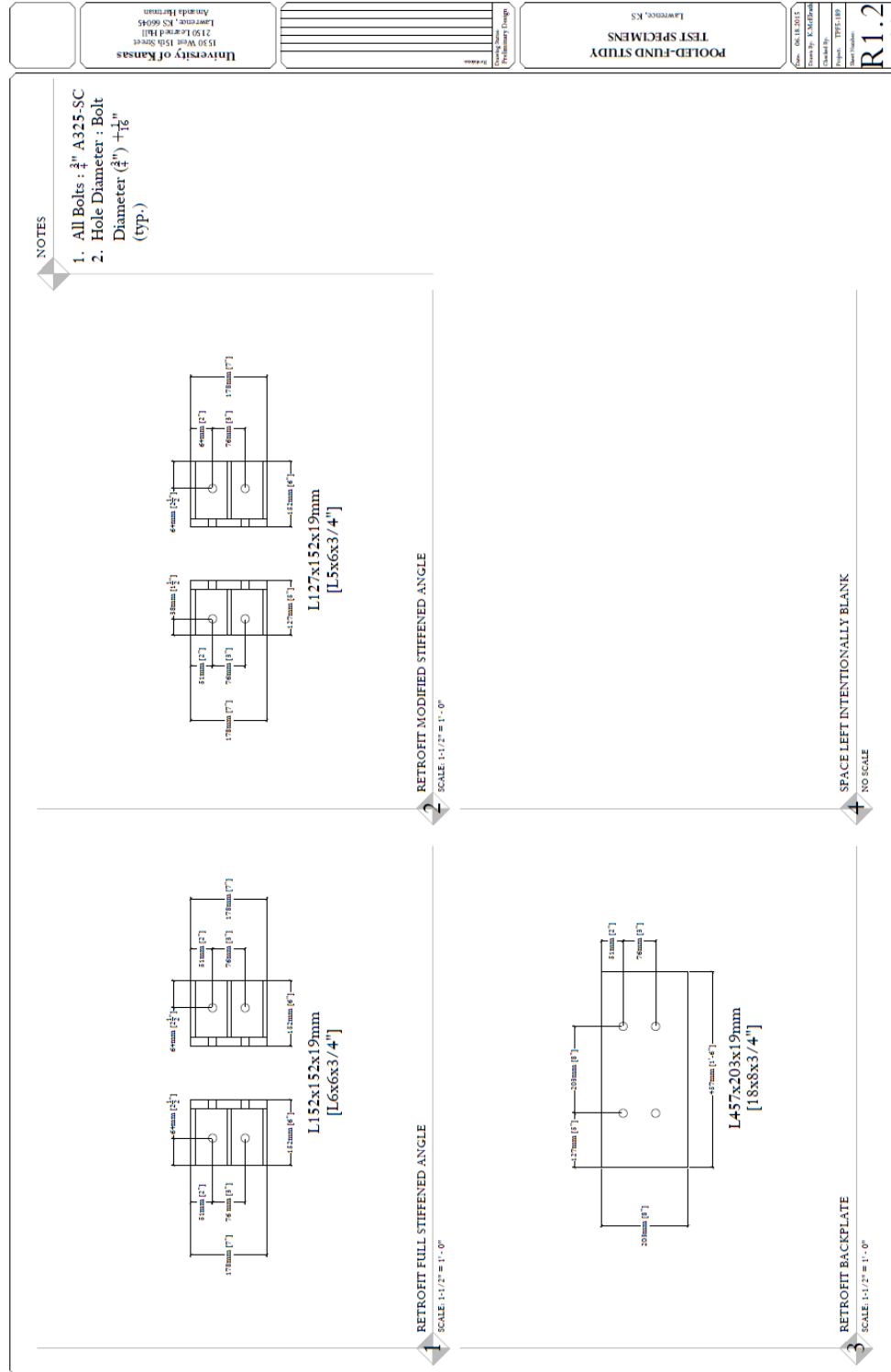


Figure A. 6: ¾ in. Retrofit Dimensions.



Load Cells

Load cells were designed by Daniel Nagati. All information on load cells can be found in his master's thesis (Nagati 2012).

Concrete Deck

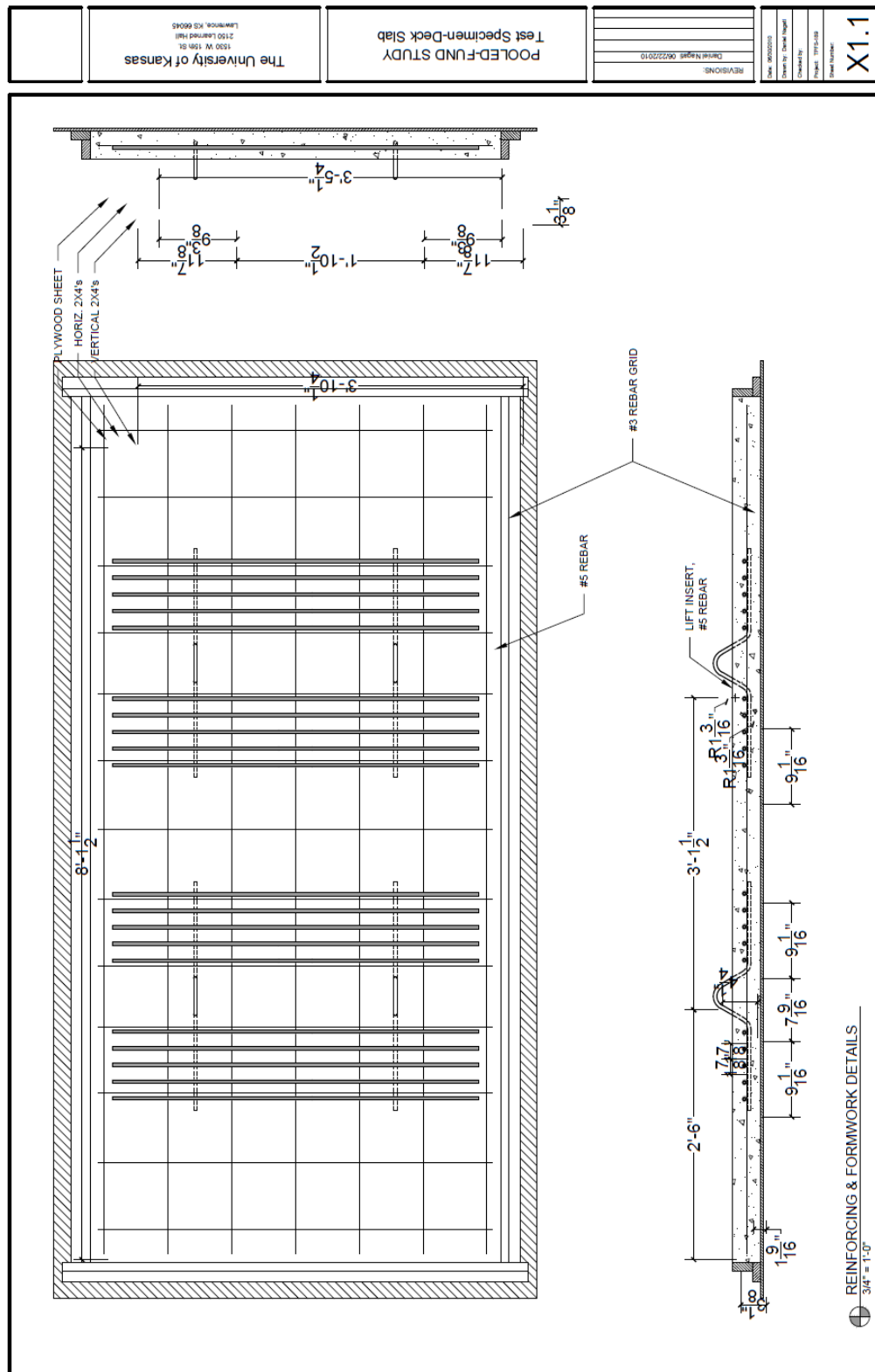
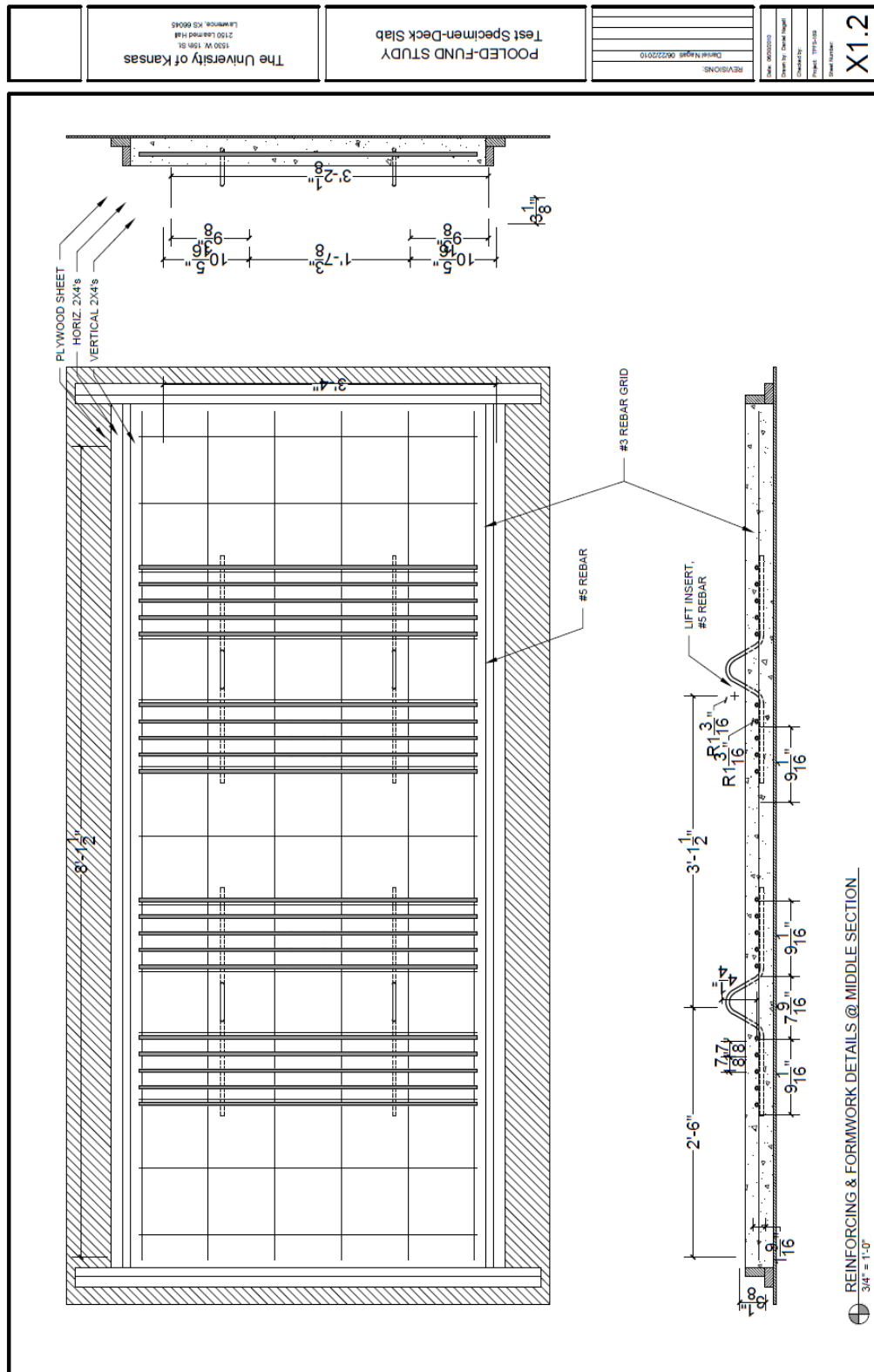


Figure A. 8: Deck reinforcement.



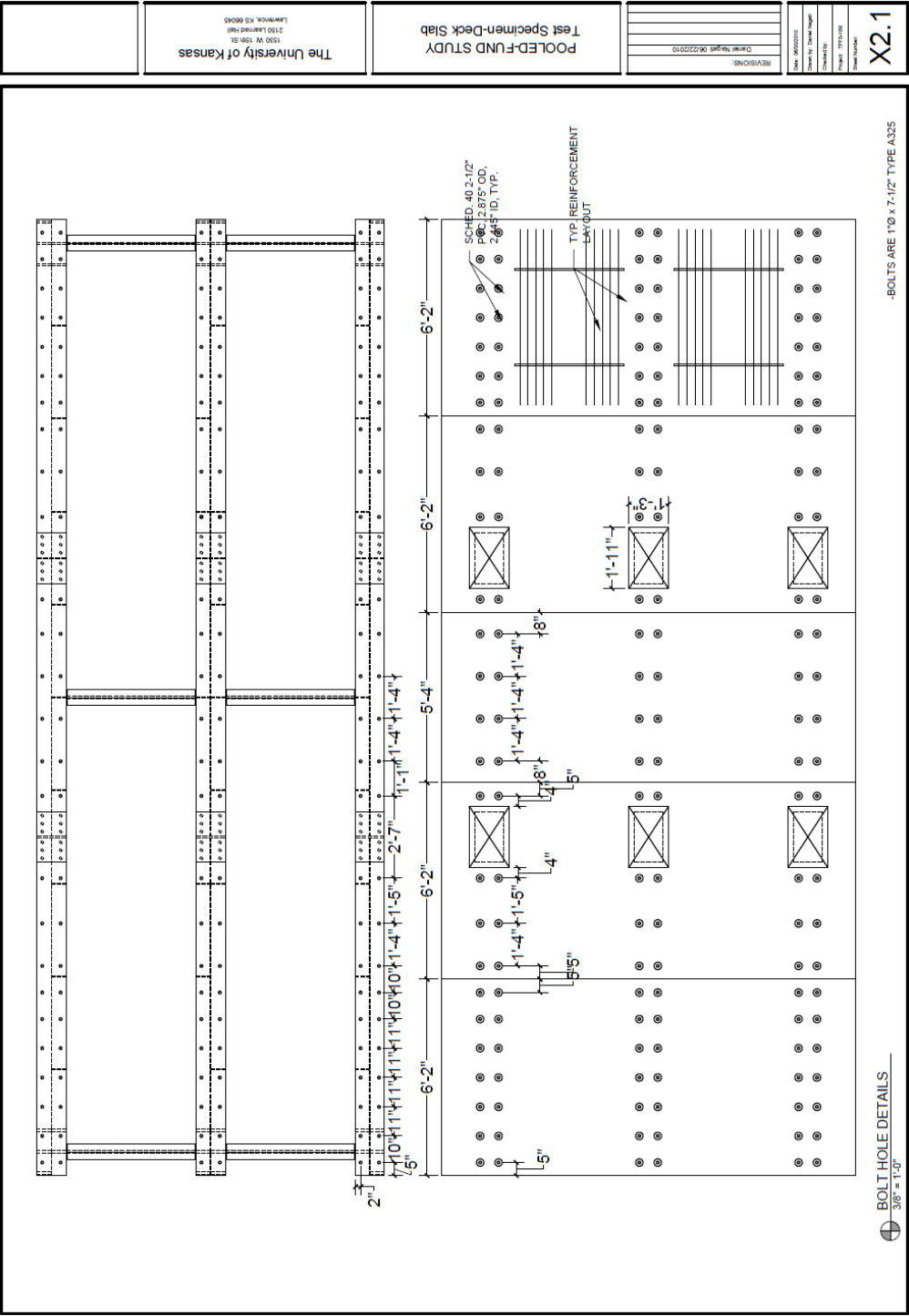
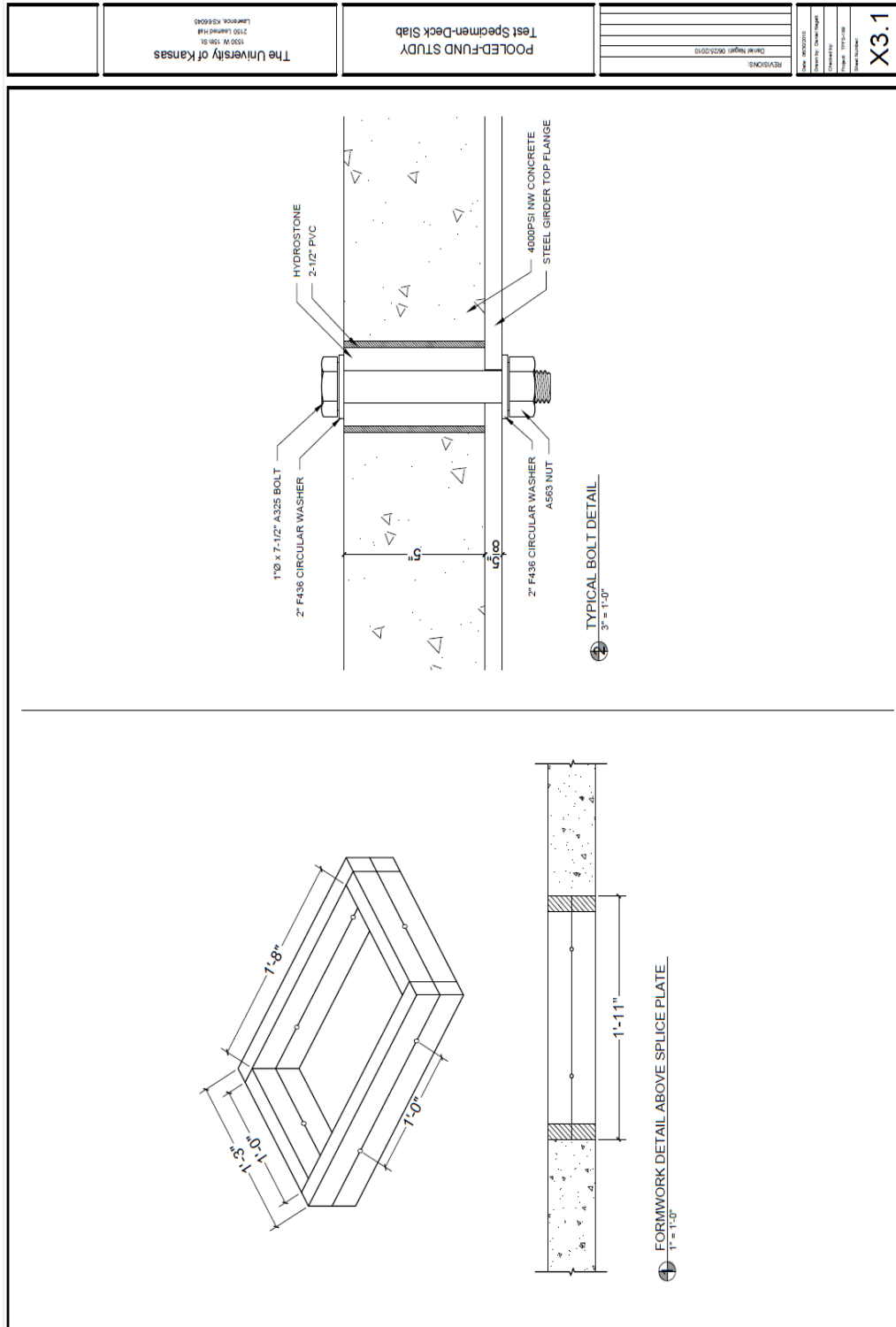


Figure A. 10: Deck panel and hole layout.



Gage Placement

Data was recorded under static load application at a number of points during the test program. Due to the large number of gages and length of testing, continuous data was not recorded. During collection of data during static loading, load was slowly increased on the bridge to capture gage data at defined loading increments. At the beginning of testing, a 2.5 kip load increment was used for loads up to 80 kip. Once bridge loading exceeded 80 kip, a larger increment of 5 kip was used up to a load of 100 kip. Once loading exceeded 100 kip, static data was recorded up to 120 kip.

Lateral Girder Deflections – LVDTs or String Potentiometers

Initially LVDTs were placed at three heights along the girder as shown in Figure A. 12(a). Initial gage locations matched closely with previous 9 ft. girder testing at the University of Kansas (Nagati 2012). At 1.35 million cycles when LVDTs were not reliable under loading, the switch was made to string potentiometers. Additionally, data collection locations were changed to isolate displacements occurring in the web gaps as shown in Figure A. 12(b).

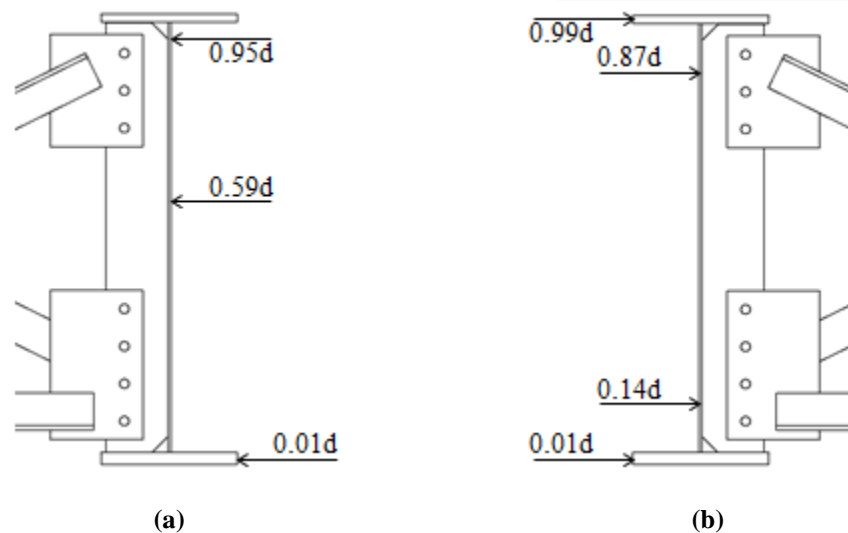


Figure A. 12: Lateral deflection monitoring for (a) LVDT placement and (b) String Potentiometer placement.

Vertical Girder Deflections – LVDTs

LVDTs were placed at the center of each girder on the bottom flange to measure maximum girder deflection.

Strain Gages

Strain gages were placed in web gaps of all girders. Placements can be seen in Figure A. 13.

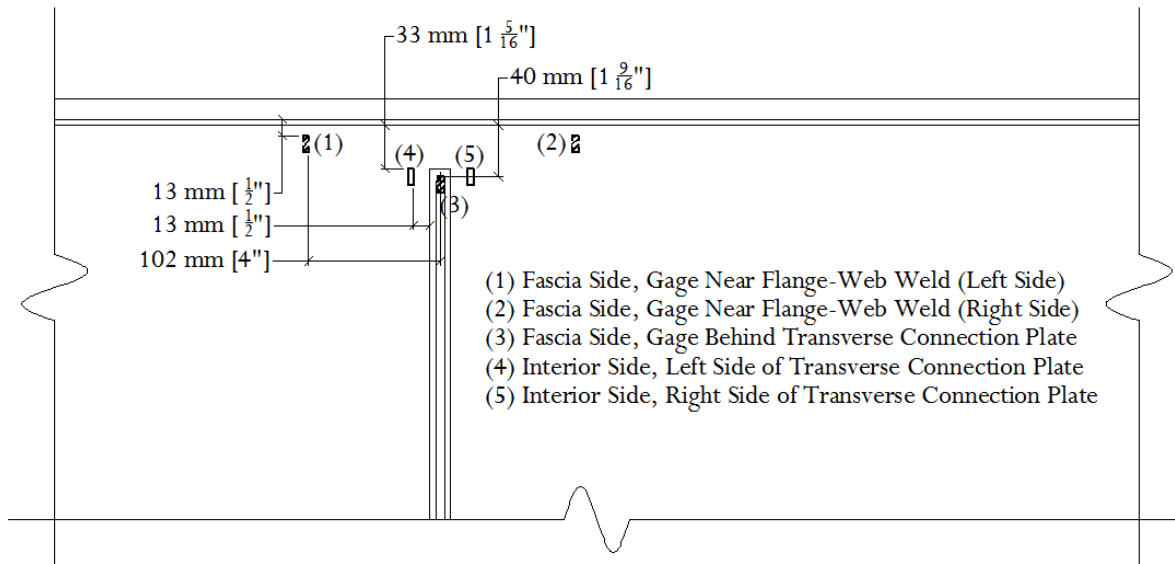


Figure A. 13: Web gap strain gage placements.

On the fascia side of exterior girders, in the top web gap only, gages (1) and (2) were placed. These gages were intended to capture high stresses near the flange-web weld. Gage (3) is placed on the fascia side of exterior girders in both the top and bottom web gaps. Since gage (3) was placed directly behind the connection plate, it was an indicator of initial cracking. All top and bottom web gaps of each girder were instrumented with gages (4) and (5). These gages are intended to capture high stresses around the connection plate-web weld. After the first retrofit application, all gages in the top web gaps of the exterior girders were destroyed and no longer recorded data.

Strain gages were placed on all cross frame element located in the test region. Each gage was oriented along the axis of the element. On the horizontal angle of the cross frame, the gage was placed mid-span. For the diagonal members which were bolted at mid-span, the gages were placed at the quarter-point of the span nearest the exterior girder.

Strain Transducers

Bridge Diagnostics Inc. (BDI) strain transducers were placed on each girder to monitor bending. One BDI was placed 2 in. down from the top flange and one was placed 2 in. up from the bottom flange. These BDIs were placed away from the connection plate to minimize localized effects. This separation distance was 2'-1 3/4" as shown in Figure A. 14.

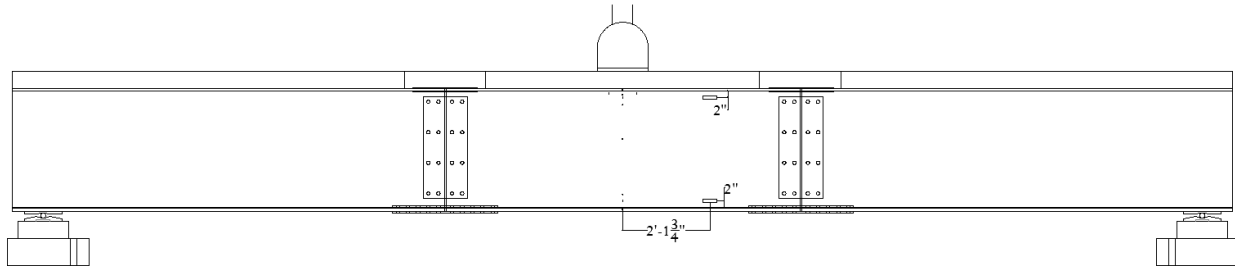


Figure A. 14: BDI placements.

Gage Labeling

All gages were labeled in a consistent pattern. Table A. 1 defined the gage labeling used for data collection.

Table A. 1: Labeling Definition for Data Acquisition

Gage Label	Description
Girder Labeling Scheme	
GN-N	North Girder, North Face of Web
GN-S	North Girder, South Face of Web
GM-N	Middle Girder, North Face of Web
GM-S	Middle Girder, South Face of Web
GS-N	South Girder, North Face of Web
GS-S	South Girder, South Face of Web
Cross Frame Labeling Scheme	
XN AT	Inclined Cross Frame Angle Framing into North Girder Top Web Gap
XN AB	Inclined Cross Frame Angle Framing into North Girder Bottom Web Gap
XN HB	Horizontal Cross Frame Angle Framing into North Girder Bottom Web Gap
XS AT	Inclined Cross Frame Angle Framing into South Girder Top Web Gap
XS AB	Inclined Cross Frame Angle Framing into South Girder Bottom Web Gap
XS HB	Horizontal Cross Frame Angle Framing into South Girder Bottom Web Gap
Strain Gage Labeling Scheme	
B-SC	Bottom Web Gap, Gage (3) – Behind Stiffener
T-SC	Top Web Gap, Gage (3) – Behind Stiffener
T-LE	Top Web Gap, Gage (1/2) – Longitudinal East of Stiffener
T-LW	Top Web Gap, Gage (1/2) – Longitudinal West of Stiffener

B-UE	Bottom Web Gap, Gage (4/5) – Horseshoe East of Stiffener
B-UW	Bottom Web Gap, Gage (4/5) – Horseshoe West of Stiffener
T-UE	Top Web Gap, Gage (4/5) – Horseshoe East of Stiffener
T-UW	Top Web Gap, Gage (4/5) – Horseshoe West of Stiffener
BDI Labeling Scheme	
GN-N T	North Face of North Girder near Top Flange
GN-N B	North Face of North Girder near Bottom Flange
GM-N T	North Face of Middle Girder near Top Flange
GM-N B	North Face of Middle Girder near Bottom Flange
GS-S T	South Face of South Girder near Top Flange
GS-S B	South Face of South Girder near Bottom Flange
Load Cell Labeling Scheme	
WN LCA	Load Cell under West Support of North Girder
WM LCB	Load Cell under West Support of Middle Girder
WS LCC	Load Cell under West Support of South Girder
EN LCD	Load Cell under East Support of North Girder
EM LCE	Load Cell under East Support of Middle Girder
ES LCF	Load Cell under East Support of South Girder
LVDT Labeling Scheme	
GS-S T LVDT1	South Face of South Girder near Top Web Gap
GS-S M LVDT2	South Face of South Girder near Mid-Height
GS-S B LVDT3	South Face of South Girder at Bottom Flange
GN-N T LVDT4	North Face of North Girder near Top Web Gap
GN-N M LVDT5	North Face of North Girder near Mid-Height
GN-N B LVDT6	North Face of North Girder at Bottom Flange
GS LVDT7	South Girder Vertical Deflection at Mid-Span
GM LVDT8	Middle Girder Vertical Deflection at Mid-Span
GN LVDT9	North Girder Vertical Deflection at Mid-Span
String Potentiometer Labeling Scheme	
GS-S T SP1	South Face of South Girder at Top Flange
GS-S M SP2	South Face of South Girder below Top Web Gap
GS-S B SP3	South Face of South Girder above Bottom Web Gap
SPA	South Face of South Girder at Bottom Flange
GN-N T SP4	North Face of North Girder at Top Flange
GN-N M SP5	North Face of North Girder below Top Web Gap
GN-N B SP6	North Face of North Girder above Bottom Web Gap
SPB	North Face of North Girder at Bottom Flange

Appendix B: Calibration Constants

Strain Transducers from Bridge Diagnostics Inc. (BDI)

Calibrations are provided by Bridge Diagnostics Inc. but must be modified based on supplied voltage. A supply voltage of 5 V was applied to each strain transducer.

$$\text{Calibration Constant} = \frac{\text{General Factor } \mu\epsilon/mV/V \cdot 1000mV/V}{\text{Input Voltage } V}$$

These modified constants for the strain transducers can be found in Table B. 1.

Table B. 1: Calibration Constants for Strain Transducers

Strain Transducer Label	General Factor	Calibration Constant (5V)
BDI 1269	503.9 $\mu\epsilon/mV/V$	100,780 $\mu\epsilon/V$
BDI 1270	497.0 $\mu\epsilon/mV/V$	99,400 $\mu\epsilon/V$
BDI 1271	503.5 $\mu\epsilon/mV/V$	100,700 $\mu\epsilon/V$
BDI 1272	496.7 $\mu\epsilon/mV/V$	99,340 $\mu\epsilon/V$
BDI 1273	493.6 $\mu\epsilon/mV/V$	98,720 $\mu\epsilon/V$
BDI 1274	502.4 $\mu\epsilon/mV/V$	100,480 $\mu\epsilon/V$

Linear Variable Differential Transformer (LVDT)

Linear variable differential transformers were calibrated using a Pratt & Whitney Machine. LVDTs were supplied with a 15 V power source from Micro Measurements. Calibration constants for LVDTs can be found in Table B. 2.

Table B. 2: Calibration Constants for LVDTs

LVDT Label	Calibration Constant
LVDT 1	0.099386 in./V
LVDT 2	0.100298 in./V
LVDT 3	0.100361 in./V
LVDT 4	0.099289 in./V
LVDT 5	0.099631 in./V
LVDT 6	0.101083 in./V
LVDT 7	0.393128 in./V
LVDT 8	0.399862 in./V
LVDT 9	0.400382 in./V

All LVDTs were from Measurement Specialties—LVDT 1-6 were model number 500 DC-SE with 0.5 in. range and LVDT 7-9 were model number 2000 DC-SE with 2.0 in range. LVDT 1-6 (measuring lateral displacement of North and South girders) were replaced with string potentiometers.

String Potentiometers

All string potentiometers were P510-5 with 004 option ordered from UniMeasure, Inc. String potentiometers were calibrated using the Baldwin. String potentiometers were supplied with the same 15 V power supply for LVDTs. Table B. 3 displays the calibration constants for string potentiometers used for testing.

Table B. 3: Calibration Constants for String Potentiometers

String Potentiometer Label	Calibration Constant
SP 1	0.500994 in./V
SP 2	0.497380 in./V
SP 3	0.498466 in./V
SP 4	0.498820 in./V
SP 5	0.497397 in./V
SP 6	0.496723 in./V
SP A	0.502021 in./V
SP B	0.499675 in./V

Load Cells

Load cells were calibrated using a 6.55V power supply. Table B. 4 contains calibration constants for load cells.

Table B. 4: Calibration Constants for Load Cells

Load Cell Label	Calibration Constant
LC A	10237.4 kip/V
LC B	10052.8 kip/V
LC C	10713.9 kip/V
LC D	10280.4 kip/V
LC E	10111.9 kip/V
LC F	10155.1 kip/V

Appendix C: Loading Procedure

Pump Protocol

Turning the Pump On for 90 GPM Pump

1. On the touch screen control panel, press the lower middle of the screen to access options. Once pressed, the screen should light up.
2. Before turning on any pumps, check the number of hours each pump has ran. To do this, select HPU. Number of hours for each pump will be displayed. Note which two pumps have the fewest hours. For testing using the 330 kip actuator, two pumps must be active.
3. Return to the main menu. Push and hold the enabled button for one of the pumps having the least number of hours. It will take a few seconds to activate.
4. To turn on the first pump, press and hold low pressure. This will turn the pump on to low pressure. Monitor the pressure readout on the screen.
5. Once the pressure reads around 300 psi, press and hold high pressure.
6. Once the pressure stabilizes around 3000 psi, the other pump can be enabled. To do this, press and hold the enable button for the pump containing the second-least number of hours.
7. If all three pumps are needed, repeat step 6 with the final pump.

Turning the Pump Off for 90 GPM Pump

1. If the touch screen is not active, press the lower middle of the screen to access options.
2. At least two pumps should be on high pressure. Turn the first pump off by pressing and holding the disable button for that pump. Wait a few seconds before proceeding.
3. If all three pumps were on, press and hold the disable button for the second pump. This will leave only one pump remaining.
4. With only one pump running, press and hold high pressure. This will turn high pressure off. Monitor the pressure readout and wait to proceed until the pressure drops to around 300 psi.
5. Once pressure drops to 300 psi, press and hold low pressure turning off the remaining pump. The final pump will automatically return to disabled.

Actuator Warm-Up

1. Activate the Function Generator in Station Manager.
2. On the Manual Command, check the box to Enable Manual Command. At this point, set the offsets; however, offsets will need re-zeroed (re-offset) for load before running a program.
3. Turn on the hydraulic fluid.
4. Change the Control Mode to Displacement and force the actuator to 15 kips.
5. Change the Control Mode to Force.
6. In the Function Generator, the Target Setpoint should be 15 kips and the Amplitude should be 5 kips.
7. On the Manual Command, uncheck the Enable Manual Command box.
8. Push Play in the Function Generator.
9. Display the Scope box to monitor the amplitude.

Tuning

1. In the Function Generator, change the dropdown menu to Tuning.
2. When prompted, enter the password, "Tuning."
3. Go to Station Setup.
4. Under Channels, adjust Force and Displacement using the Tuning Fork button.

New Program

1. Open Applications dropdown menu. Select Multipurpose Testware (Edit Only). Click OK when default warning pops up.
2. Open an existing procedure and save as a new procedure.
3. Ramp to absolute end level load (mean of stress range)
4. Set Absolute End Level 1 to low end of stress range
5. Set Absolute End Level 2 to high end of stress range
6. Save before closing.

Testing

1. Once the system is warmed up testing can begin. On the Manual Command, check the box to Enable Manual Command. Check interlock controls.
2. Change the Control Mode to Displacement and take the actuator to the desired load (mean of stress range).
3. Activate MPT.
4. Open the new procedure.
5. Create new specimen and change the name in the dropdown menu.
6. Turn on 'Scope' to see command and output.
7. On the Manual Command, uncheck the Enable Manual Command box.
8. Push play.
9. Be prepared to hit pause or stop in case something goes wrong.

Appendix D: Finite Element Study

PARAMETRIC RETROFIT ANALYSIS FOR DISTORTION-INDUCED FATIGUE IN A 9.1 M (30 FT.) TEST BRIDGE

Amanda S. Hartman¹

Caroline R. Bennett²

Adolfo B. Matamoros³

Stanley T. Rolfe⁴

Kathleen S. McElrath⁵

ABSTRACT

Developing and testing retrofit techniques to halt distortion-induced fatigue cracking of steel bridge structures can be time consuming and expensive. Finite element modeling is a tool that can be used to reduce the expenses associated with testing such retrofits. In this study, the effectiveness of several existing retrofit techniques was examined for the 9.1 m [30 ft.] test bridge to form a series of baseline values against which to evaluate several variations of the “angles-with-plate” retrofit technique under investigation at the University of Kansas.

Existing techniques investigated included a full depth back-up stiffener as well as bolted angles providing positive attachment from the connection plate to the girder flange. The research team developed “angles-with-plate” technique uses two angles and a backing plate attached to the girder web (called angles-with-backing plate retrofit). Through finite element modeling, three variations of the angles-with-backing plate retrofit were investigated in which the thickness was adjusted and stiffeners were added to the angles.

During investigation, two crack patterns were studied with several crack lengths ranging from 25 mm [1 in.] to 203 mm [8 in.]. Cracking studied included a horseshoe crack around the connection plate-web weld and a longitudinal crack at the flange-web weld. For the connection plate-web weld, the stiffened angles-with-backing plate provided the largest stress reduction;

¹ Amanda S. Hartman, Graduate Research Assistant, University of Kansas, 1530 W. 15th St., Lawrence, KS 66045

² Caroline R. Bennett, PhD, PE, Associate Professor, University of Kansas, 1530 W. 15th St., Lawrence, KS 66045

³ Adolfo B. Matamoros, PhD, Professor, University of Kansas, 1530 W. 15th St., Lawrence, KS 66045

⁴ Stanley T. Rolfe, PhD, PE, A.P. Learned Distinguished Professor, University of Kansas, 1530 W. 15th St., Lawrence, KS 66045

⁵ Kathleen S. McElrath, Graduate Research Assistant, University of Kansas, 1530 W. 15th St., Lawrence, KS 66045

however, for the flange-web weld, angles providing positive attachment to the girder flange reduced the stress the most. Based on the analytical results of the investigation, further experimental tests at the University of Kansas explored the stiffened angles-with-backing plate retrofit.

INTRODUCTION AND BACKGROUND

Many steel bridges built prior to 1985 have experienced distortion-induced fatigue caused by lack of positive connection between connection stiffeners and girder flanges. As differential deflection occurs between adjacent bridge girders, the weak web gap region experiences repeated out-of-plane rotation which causes fatigue. Several methods have been used to mitigate distortion-induced fatigue cracking including: crack-arrest holes, cross frame removal, back-up stiffeners, positive attachment between transverse connection stiffeners and flanges, and slotting the transverse connection stiffener (Hassel et al. 2010).

In addition to repair techniques currently in practice, the University of Kansas has developed a new retrofit technique which provides additional positive attachment between the transverse connection stiffener and girder web. This technique is termed “angles-with-plate” retrofit. This retrofit has been shown in previous studies to mitigate crack propagation in a 2.8 m [9 ft.] girder sub-assembly (Alemdar et al. 2013a; 2013b). However, the physical and computational simulations conducted in Alemdar et al. (2013a; 2013b) were representative of a test set-up in which the girder was only subjected to out-of-plane bending effects.

Extensive finite element analyses of these retrofit techniques (of both the more traditional techniques and the newly-developed “angles-with-plate” technique) have been conducted at the University of Kansas. Hassel et al. (2010) used Abaqus v.6.8-2 in which full-scale non-skewed and skewed bridges were evaluated with the following techniques: cross frame removal, back-up stiffeners, positive attachment between connection plates and flanges (using two angles), and slotting the connection plate. When the retrofits were applied at every cross-frame location (excluding cross-frame removal), positive attachment between connection plates and flanges were found to provide the largest reduction in stress around the connection plate-to-web weld. However, this study failed to consider hot spot stresses at the flange-to-web weld. Additionally, the newly-developed angles-with-plate retrofit technique was not analyzed in the bridge models studied by Hassel et al. (2010).

In a separate investigation, a series of computational and physical studies were performed by Alemdar et al. (2013a; 2013b) aimed at evaluating the performance of the angles-with-plate retrofit when applied on a 2.8-m [9-ft.] long steel girder sub-assembly. This assembly was comprised of a girder segment oriented upside-down with the top flange attached to the concrete strong floor. An upward force was applied to the cross frame to imitate an adjacent girder deflecting downward in a real bridge. At the ends of the 2.8 m [9.3 ft.] girder segment, small angles were attached to the flange that was not connected to the laboratory floor at one end, and at the load frame at the other end. This was intended to simulate, in an admittedly rudimentary fashion, the out-of-plane restraint provided by longitudinal girder continuity in a real bridge system as shown in Figure 1.

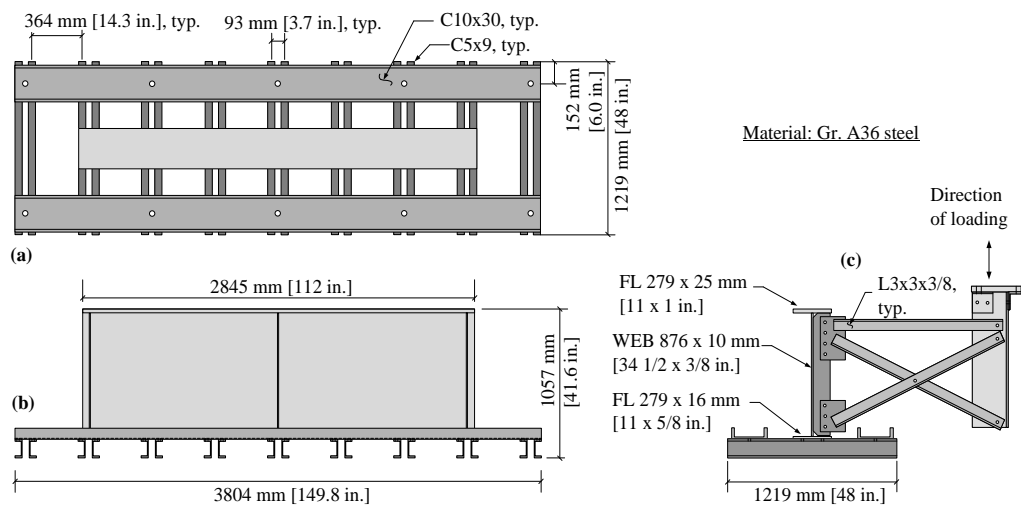
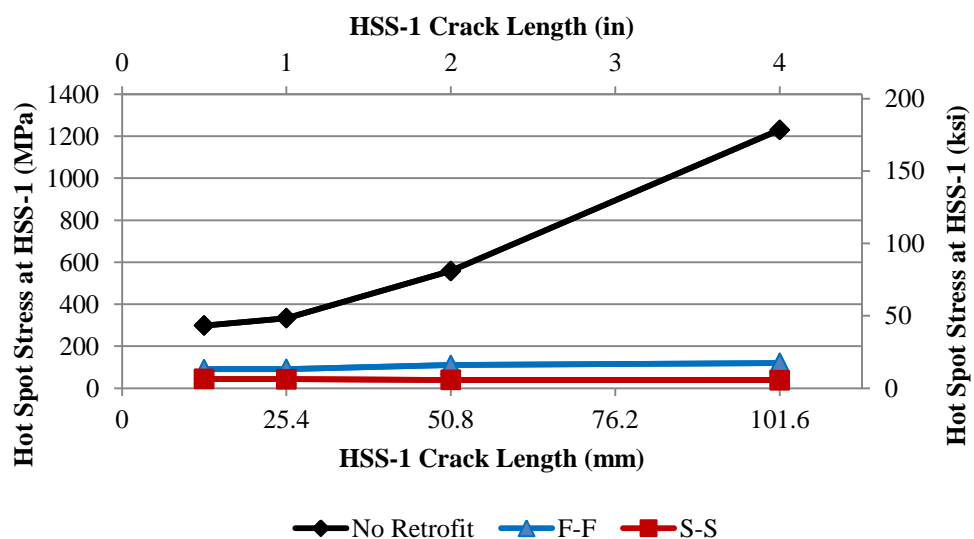


Figure 1: Girder sub-assembly set-up for 2.8 m [9 ft.] testing and finite element modeling (Alemdar et al. 2013a; 2013b).

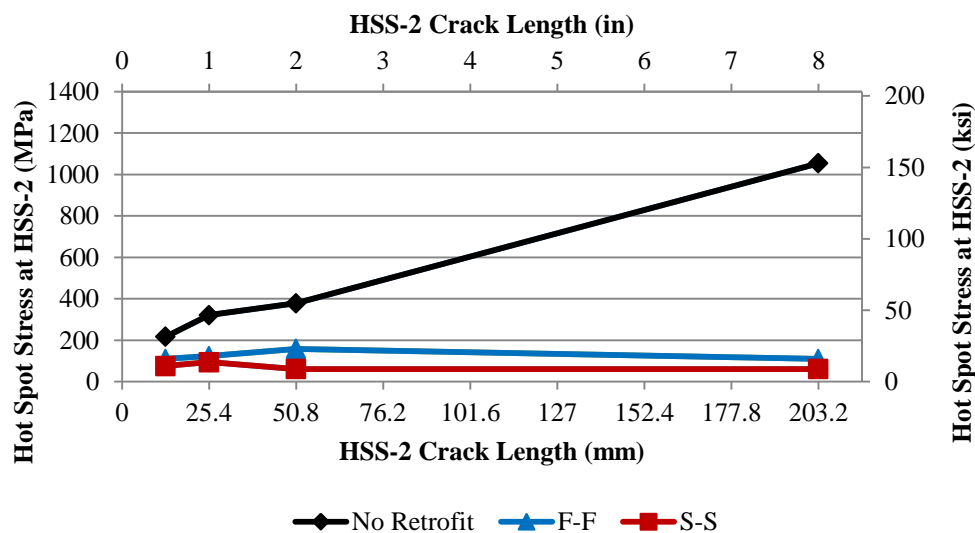
In the test set-up, the girder flange connected to the concrete floor was intended to represent the top flange in a real bridge that exhibits no flange rotation (e.g. an extremely stiff concrete deck). Finite element modeling followed the actual sub-girder assembly closely, including the flange restraint mechanism.

In a computational parametric study provided in Przywara (2013), the angles-with-plate retrofit and set-up used in Alemdar et al. (2013a; 2013b) was studied extensively by varying angle and plate thicknesses. Thickness variations considered for the angle and plate elements included: 6 mm [1/4 in.], 13 mm [1/2 in.], and 25 mm [1 in.]. With a web thickness of 9.5 mm [3/8 in.], retrofit-to-web thickness ratios of 0.7, 1.3, and 2.7 were examined (Alemdar et al.

2013a; Przywara 2013). For both the flange-to-web weld (hot spot stress path 2, HSS-2) and the connection plate-to-web weld (hot spot stress path 1, HSS-1), stresses were found to increase at fatigue-susceptible locations as crack length increased, as shown in Figure 2. Retrofit results are shown for stiff (S-S) angles-with-plate (25-mm [1-in.] thick) and flexible (F-F) angles-with-plate (6-mm [1/4-in.] thick) combinations.



(a)



(b)

Figure 2: Hot spot stress at (a) HSS-1 crack and (b) HSS-2 crack for no retrofit, F-F retrofit, and S-S retrofit (Przywara 2013).

For large crack lengths, Przywara (2013) showed that both stiff and flexible angles-with-plate retrofit configurations provided reduction in hot spot stresses in both hot spot locations (at the connection plate-to-web weld and at the flange-to-web weld). Retrofitting small cracks did not result in a similar reduction in stress. Additionally, it was found that increasing the retrofit thickness/stiffness caused a slightly larger reduction in hot spot stress; however, this difference was not found to be significant.

Based on the analyses and physical testing outlined in Alemdar et al. (2013), it was found that “the angles-with-plate measure was effective in preventing distortion of the web-gap region, reducing stress demands calculated at the critical points by an order of magnitude.” Additionally, experimental testing “showed that there was negligible crack growth when the angles-with-plate retrofit measure was implemented” (Alemdar et al. 2013).

OBJECTIVE AND SCOPE

The primary objective of this study was to analytically evaluate the effectiveness of the new “angles-with-plate” retrofit technique on a 9.1 m [30 ft.] bridge system subjected to both in-plane and out-of-plane bending effects as compared with existing retrofit techniques. The effects of crack length on the effectiveness of the angles-with-plate retrofit was investigated, as was the effect of reduced deck stiffness.

The computational simulations presented in this paper corresponded to an experimental test set-up in which a three-girder, 9.1-m [30-ft] long test bridge was tested under fatigue loading. Details regarding the physical tests of the test bridge have been presented in a companion paper.

FINITE ELEMENT MODELING METHODOLOGY

The test bridge geometry described in the companion paper was modeled as faithfully as possible using the commercially-available software Abaqus v.6.10. Screenshots from the bridge model are shown in Figure 3.

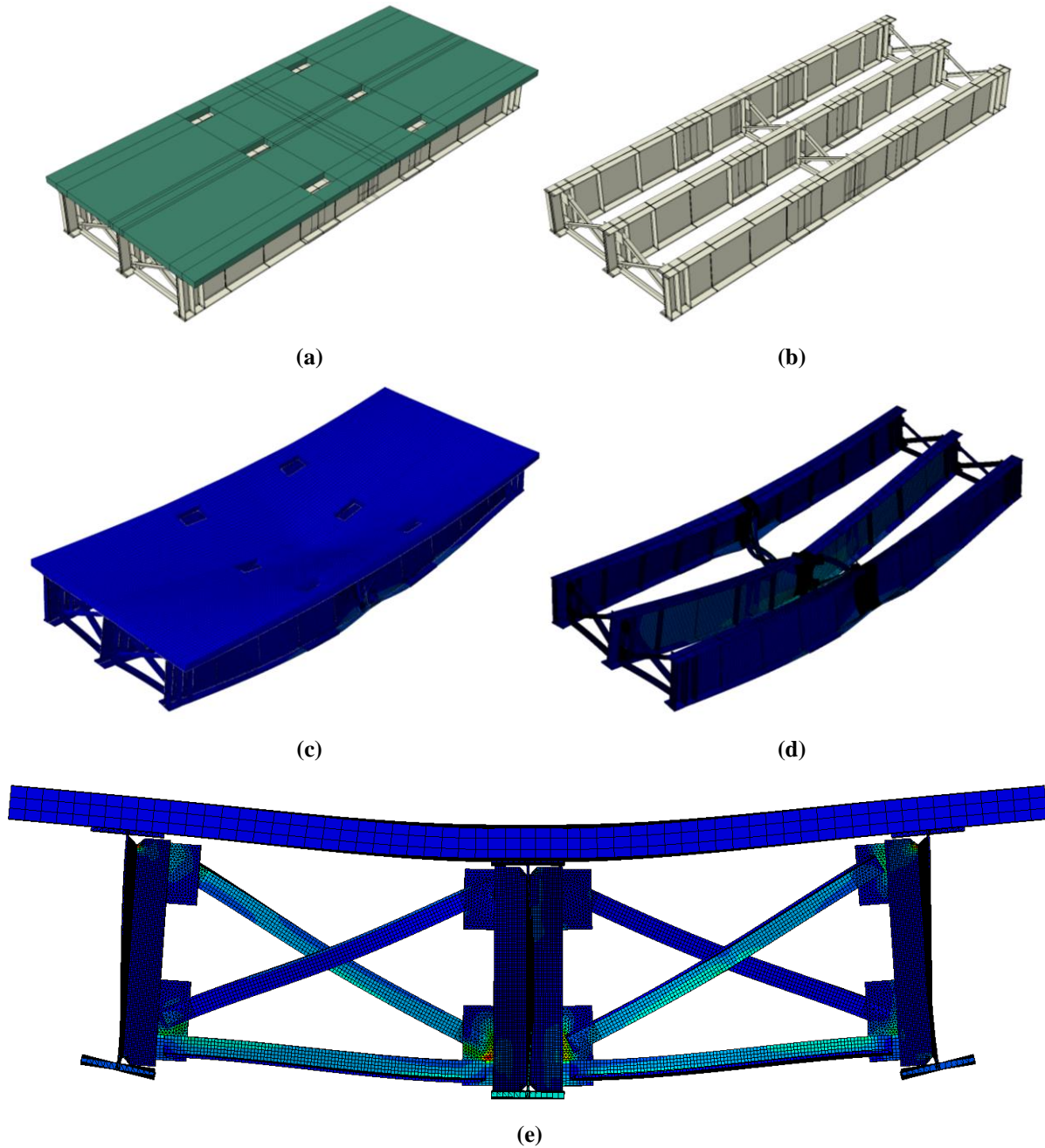


Figure 3: (a) Overall model with concrete deck, (b) overall model without concrete deck, (c) deflected model with concrete deck, deflection scale=425, (d) deflected model without concrete deck, deflection scale=425, and (e) deflected section cut at mid-span, deflection scale=100.

Forty-five finite element models were constructed and analyzed as variations of the baseline test bridge geometry. Models included cracked and uncracked conditions in the top web

gap of the exterior (north and south) girders. Cracked models included either a horseshoe-shaped crack or a longitudinal crack. A modeling test matrix is shown in Table 1.

Table 1: Finite Element Modeling Matrix for Cracks around Stiffener-Web-Weld

Model Description / Crack Length		No Crack	25 mm [1 in.]	38 mm [1-1/2 in.]	51 mm [2 in.]	64 mm [2-1/2 in.]	76 mm [3 in.]	101 mm [4 in.]	203 mm [8 in.]
Connection Plate-to-Web Cracks	Unretrofitted condition	X	X	X	X	X	X	X	X
	Reduced deck stiffness with unretrofitted condition				X				
	Broken Cross Frame		X						
	Angles-with-plate repair with 19-mm [3/4-in.] thicknesses		X	X	X	X	X		
	Stiffened angles-with-plate repair with 19-mm [3/4-in.] thicknesses		X	X	X	X	X		
	Angles-with-plate repair with 13-mm [1/2-in.] thicknesses		X	X	X	X	X		
	Traditional angles repair connected to flange with 19-mm [3/4-in.] thickness		X	X	X	X	X		
	Back-up stiffener repair placed on fascia side		X	X	X	X	X		
Flange-to-Web Cracks	Unretrofitted Condition		X		X		X	X	X
	Angles-with-backing plate repair with 19-mm [3/4-in.] thicknesses		X		X		X	X	X

Horseshoe-shaped (U-shaped) cracks were modeled around the connection plate weld toe having leg lengths from 25.4-76.2 mm [1.0-3.0 in.] and the leg length of the crack was varied in 12.7-mm [0.5-in.] increments. Additionally, two cracks with leg lengths of 101 mm and 203 mm [4.0 in. and 8.0 in.] were also considered. Crack lengths correlated with the vertical length of each leg of the crack. In separate analyses, longitudinal cracks were placed near the flange-to-

web weld. Three longitudinal crack lengths were studied which included: 25mm [1 in.], 51 mm [2 in.], and 76 mm [3 in.].

All bridge components were constructed in Abaqus v.6.10 using three dimensional elements including mostly hexahedral elements (C3D8R) and some tetrahedral elements (C3D4) for transition regions. Each model contained approximately 3 million elements and 10 million degrees of freedom. A dense mesh was applied to the web gap region while other locations within the bridge contained a coarser mesh as shown in Figure 4(a). Based on a convergence study performed on the dense mesh region around the connection plate-web weld, the optimal mesh size of the web gap was determined to be 2.5 mm [0.1 in.] (Figure 4(b)).

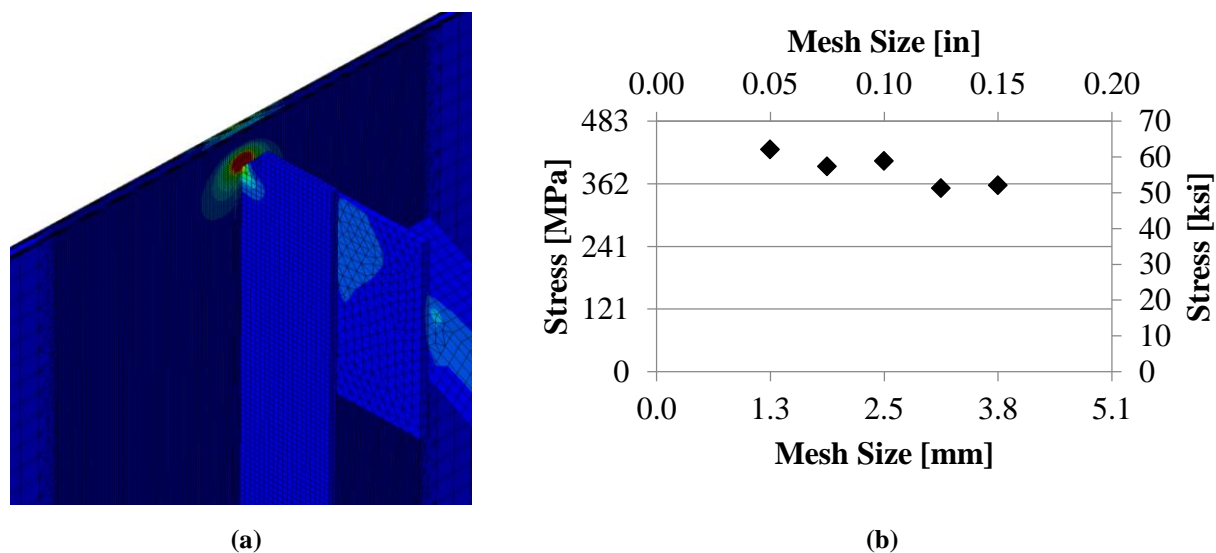


Figure 4: (a) Dense mesh (2.54 mm [0.1 in.]) in web gap region transitions to coarse mesh (25.4 mm [1.0 in.]) and (b) mesh sensitivity study for changing dense region mesh.

Steel and concrete were modeled as linear-elastic materials where the moduli of elasticity for each were taken as 200,000 MPa [29,000 ksi] and 25,000 MPa [3,605 ksi], respectively. Poisson's ratio for steel and concrete were assumed to be 0.3 and 0.2, respectively. For the reduced deck stiffness model, the concrete modulus of elasticity was halved. The entire 9.1 m [30 ft.] test bridge was modeled and assembled in Abaqus v.6.10 using 3D solid elements, including welds, cross frames, stiffeners, and deck.

Since modeling bolts and bolt tension are computationally expensive endeavors, the base model of the test bridge contained surface-to-surface ties at girder splice locations and cross

frame connections. Welds were modeled using surface-to-surface ties and when appropriate, hard contacts were used to prevent parts from moving through one another during loading.

Retrofitted models required further refinement with regard to bolting. To improve computational efficiency, modeled bolt heads and nuts were tied directly to the surfaces in which they were in contact. All other surfaces contained hard contact interactions with a frictional coefficient of 0.35. All bolts were modeled as 19-mm [3/4-in.] diameter which was consistent with those used in the physical tests. For models that included application of retrofits, behavior was desired that would replicate the slip-critical bolt conditions implemented in the physical tests. For the slip-critical connection, an initial bolt pretension step was created in the models that induced a bolt load of 125 kN [28 kip] on each bolt using the bolt load function in Abaqus v.6.10.

Static loading applied in the models correlated with the upper bound load of 267 kN [60 kip] from the first test trial in the physical test sequence (Test Trials 1S and 1N). In the models, this load was spread over two areas of 400x114 mm [15-3/4 x 4-1/2 in.] to represent the application of the load through the two “feet” of the actuator’s swivel end. Loading was applied at midspan of the center girder as was done in the physical tests. Due to this load placement, primary regions of interest were found to occur in the top web gaps of the exterior girders. This region of interest was consistent with previous research results obtained for an unstaggered bridge condition in which highest stresses were found to occur in top web gaps for exterior girders (Hartman et. al 2010).

Cracks were modeled using the Extended Finite Element Method (XFEM) in Abaqus v.6.10. Using XFEM, cracks of various shapes could be easily modeled without affecting the mesh in the region of interest. Additionally, cracks could be placed anywhere within elements, not just located at element boundaries. U-shaped cracks (wrapping around the connection plate weld) and longitudinal cracks (along the flange-to-web weld) were modeled using three-dimensional planar elements with a depth larger than the girder web thickness of 6.35 mm [1/4 in.].

An identified limitation to using XFEM is that only two crack tips can exist for one crack. In experimental testing, cracks were found to often branch out into multiple “spider” cracks. This branching cannot be modeled using XFEM; however, even though branched cracks were found to exist experimentally, generally the vertical portion of the crack was observed to

progress down the weld while the branch crack (spider crack) growth slowed (Nagati 2012). In the companion paper in Part 3, only the east side of the south girder connection stiffener has following this pattern; however, cracking in the test bridge is relatively small (less than 51 mm [2 in.] in the horseshoe crack). Due to this, spider cracks were not modeled as they were observed to only temporarily grow until stress concentrations at the weld became larger than the stress concentrations at the spider crack tip. The vertical crack that wrapped around the connection plate-to-web weld was referred to as a horseshoe-shaped crack. In addition to horseshoe-shaped cracking, a separate longitudinal crack was modeled near the flange-to-web weld.

COMPUTING CRACK PROPENSITY: HOT SPOT STRESS ANALYSIS

Traditionally, in-plane fatigue is classified using nominal stresses; however, the three-dimensional stress state in the web gap region cannot accurately be captured using only nominal bending stress. To capture both normal and out-of-plane stresses, maximum principle stresses were extracted from the models. Richardson (2012) and Nagati (2012) found that crack growth closely followed maximum principal hot spot as shown in Figure 5. White lines superimposed on the stress contours in Figure 5 denote crack growth seen experimentally.

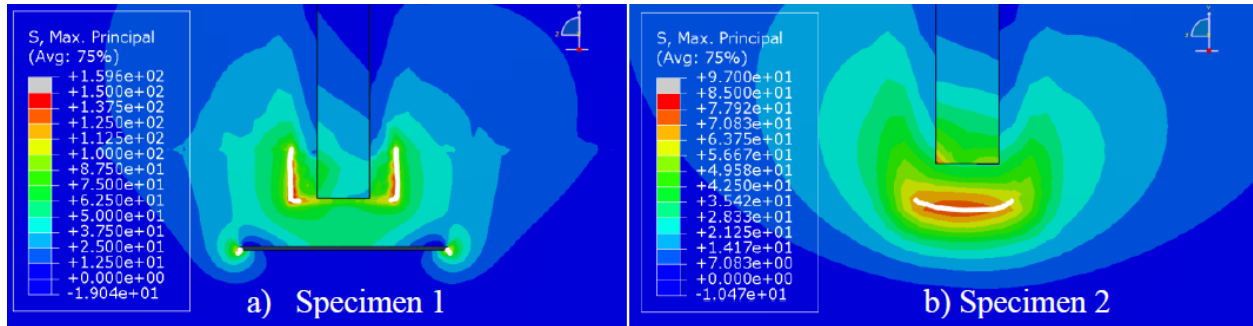


Figure 5: Cracking and maximum principal hot spot stresses (Nagati 2012).

Complicated geometry and stresses in the web gap region made accurate comparisons between models a difficult task. A one-point hot spot stress (HSS) procedure was used as the basis for this comparison in which stresses were extracted at a set distance (half the web thickness, 3 mm [1/8 in.]) from the discontinuity, either a weld or crack. This procedure has

been found to be less sensitive to mesh density than extracting maximum stress from the models (Adams 2009). Two hot spot stress paths were chosen for consideration as shown in Figure 6.

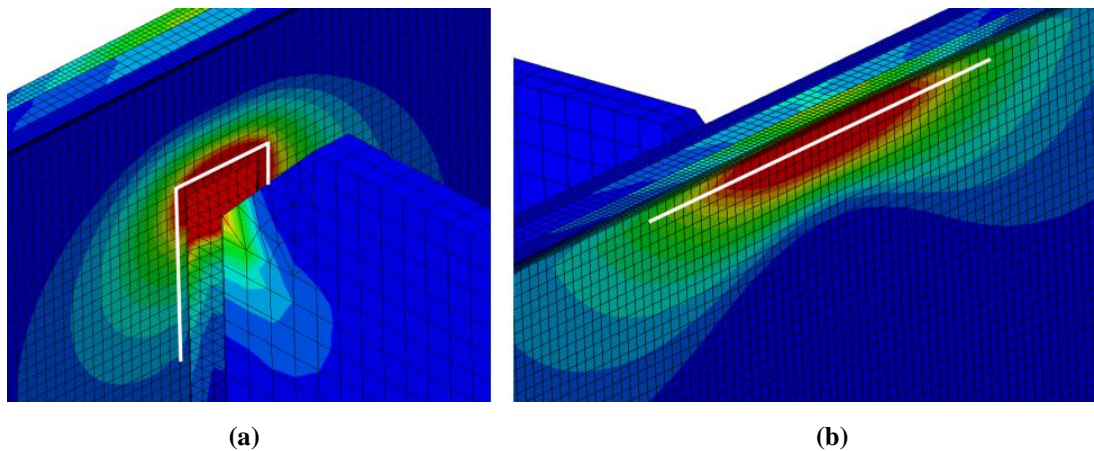


Figure 6: Hot Spot Stress Paths for (a) interior connection plate side or connection plate-web weld, (b) exterior fascia side or flange-web weld.

DESCRIPTION OF RETROFITS

Three retrofit configurations were investigated in the computational simulations. First, an existing retrofit technique was explored in which positive attachment was provided between the connection plate and top flange using two angles oriented back-to-back. Next, a back-up stiffener technique was studied in which the web gap was stiffened by a secondary stiffener placed on the opposing web face. This retrofit can be applied using either a partial depth or full depth transverse stiffener; however, only a full depth stiffener was studied as it was expected to produce the best result, based upon findings from previous studies (Hassel et. al 2010). Back-up stiffeners were modeled using transverse stiffener dimensions and placed on the girder fascia side. Third, a retrofit in which attachment was provided between the connection plate and web through two angles and a back plate was explored. This last retrofit has been extensively investigated at the University of Kansas and has been termed the “angles-with-plate” technique (Alemdar et al. 2013a; 2013b). Several variations of the angles-with-backing plate retrofit were explored, in which the thickness of the angle and plate elements were varied (with retrofit-to-web ratios of 2 and 3), and one case in which the angles were modified to include internal stiffeners. Schematics of the retrofits studied are shown in Figure 7.

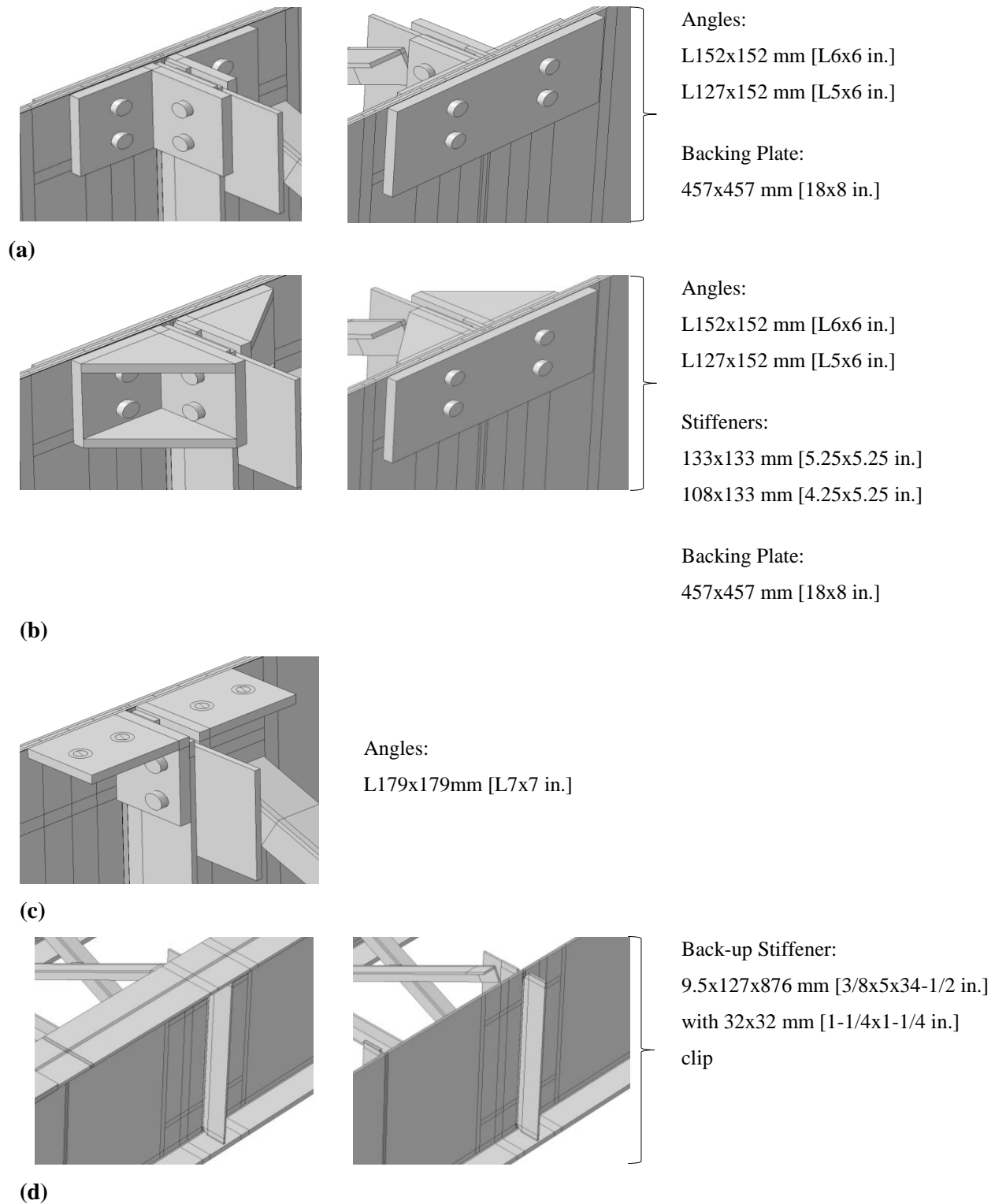


Figure 7: Views of various retrofits examined in finite element models: (a) angles-with- plate retrofit; (b) stiffened angles-with-plate retrofit; (c) positive attachment between transverse connection stiffener and top flange retrofit; and (d) full depth back-up stiffener bearing on top and bottom flanges.

RESULTS

All cracked and/or retrofitted models were normalized based on stress demands computed in the uncracked, unretrofitted finite element model. Although 45 models were analyzed, representative results have been presented in this paper. For the two hot spot stress paths considered, stresses at the connection plate-to-web weld and at the flange-to-web weld were found to be within 3% of one another in the uncracked, unretrofitted bridge model. Since all stresses presented have been normalized to hot spot stress demands from the uncracked, unretrofitted models, new stresses due to cracking and/or retrofitting have been approximately normalized to the same initial hot spot stress value due to this circumstance.

STRESS VS. CRACK LENGTH

For all horseshoe-shaped crack lengths studied, hot spot stress decreased or remained nearly constant as crack length increased for both retrofitted and unretrofitted conditions. The percentage of uncracked hot spot stress due to change in length of the horseshoe-shaped crack has been presented in Figure 8.

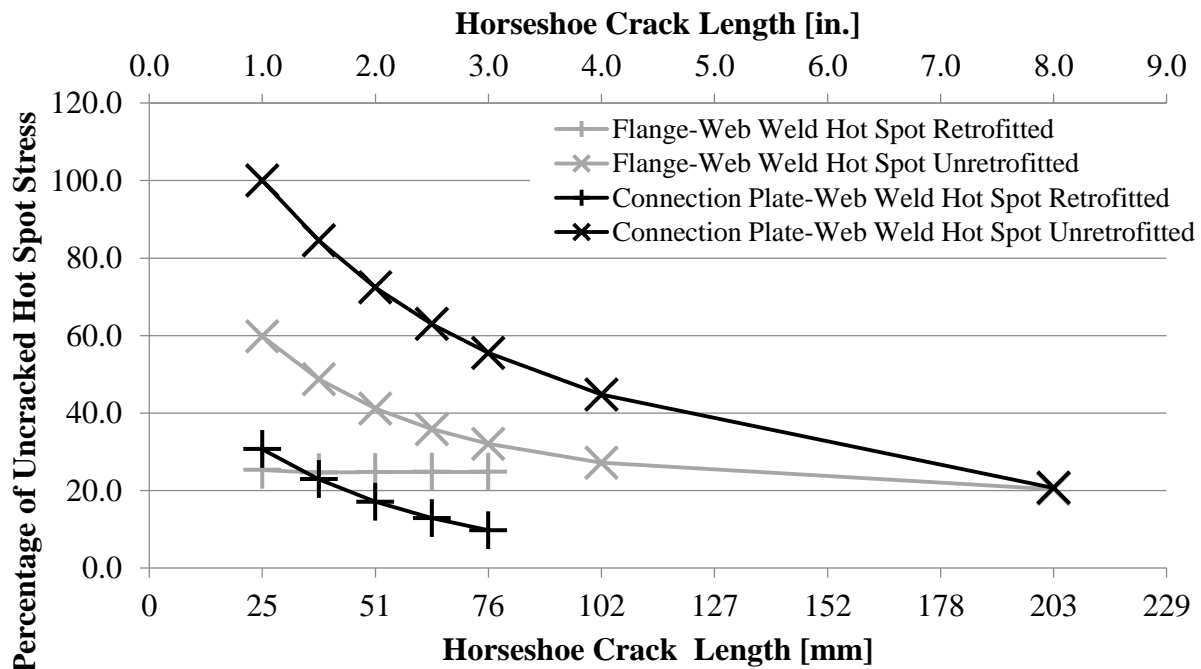


Figure 8: Percentage of uncracked hot spot stresses with change in horseshoe crack length for connection plate-web weld and flange-web weld.

Cracks were physically located at the connection plate-to-web weld toe on the web. For both the unretrofitted and retrofitted conditions, hot spot stress at the connection plate-to-web weld decreased as crack length was increased. At the flange-to-web weld in an unretrofitted state, the hot spot stress decreased as the horseshoe-shaped crack length was increased; however, for the retrofitted condition, hot spot stress remained nearly constant.

For the longitudinal flange-to-web crack lengths studied, hot spot stress behavior was found to be similar to that for the horseshoe-shaped cracks. As longitudinal crack length was increased, hot spot stresses for both the flange-to-web weld and connection plate-to-web weld decreased as shown in Figure 9. Initiation of a 25 mm [1 in.] longitudinal crack provided little reduction in flange-to-web hot spot stress demand, and increased stress demand at the connection plate-to-web weld by approximately 14%. Since both stresses were normalized to similar uncracked hot spot stresses (within 3% of each other), Figure 9 indicates that once a longitudinal crack initiated, a horseshoe-shaped crack is highly likely to initiate due to increased stresses at the connection plate-to-web weld.

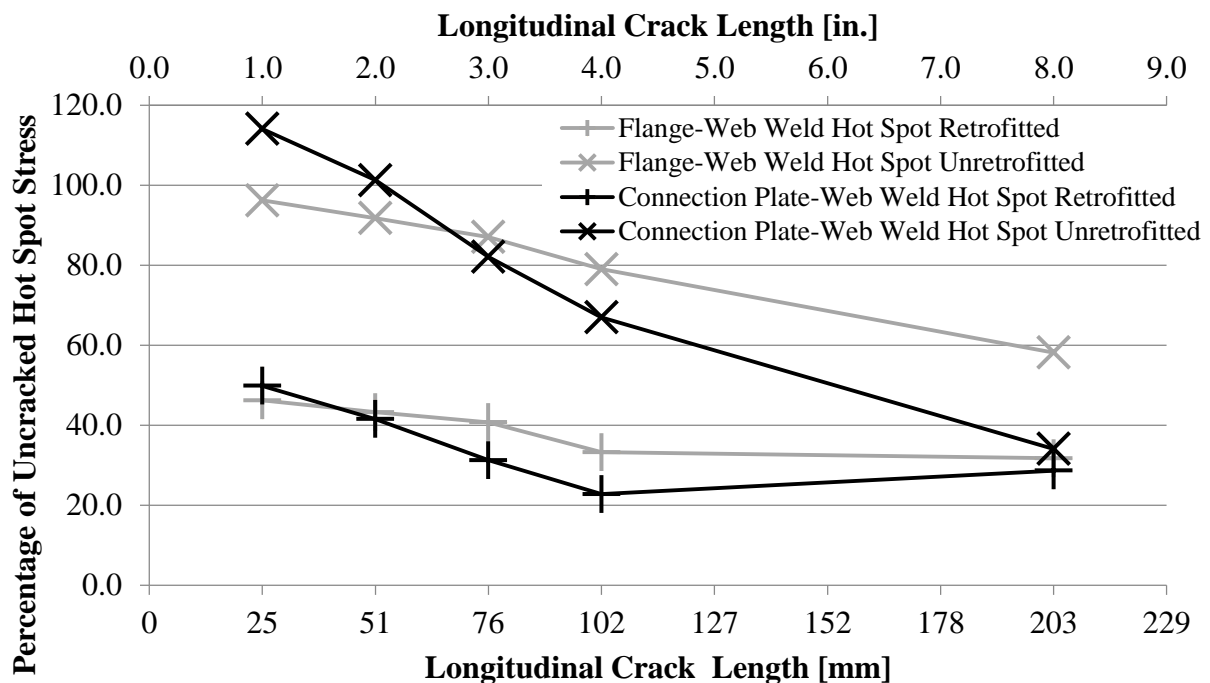


Figure 9: Percentage of uncracked hot spot stresses with change in longitudinal crack length for connection plate-web weld and flange-web weld.

Retrofit effectiveness in the presence of only a longitudinal crack was found to decrease for the connection plate-to-web weld as crack length increased. The reduction in stress from cracked, unretrofitted to cracked, retrofitted for the connection plate-to-web weld was approximately 5% for a 203-mm [8-in.] longitudinal crack and 64% for a 25-mm [1-in.] crack. For the flange-to-web weld location, stress reduction due to retrofitting did not vary greatly with increasing crack length.

The reduction in hot spot stresses as crack length increased contradicts the findings inform the girder sub-assembly (2.8 m [9.3 ft.]) finite element modeling presented in Przywara (2013) and Alemdar et al. (2013a). For the models of the girder sub-assemblies, crack growth propensity increased as crack length increased. As explained in the introduction section, the girder sub-assemblies contained a flange (representing a top flange in a bridge) fixed to a concrete floor. This fixity with a corresponding lack of flange rotation, as well as the complete lack of longitudinal bending within the girder, is hypothesized to be the primary cause of the differences in girder performance between the girder sub-assembly tests and the scaled bridge tests reported herein.

EFFECT OF REDUCED DECK STIFFNESS

Since cracking should be expected to occur in a concrete deck, reduced deck stiffness was applied to the model to determine the effect of deck stiffness on stress demand in the web gap region. For this condition, only a horseshoe-shaped crack was considered. In both hot spot locations in the top web gap, halving the concrete deck stiffness was found to increase stresses in the web gap region. This increase was approximately 20% of the hot spot stresses computed in a model with full deck stiffness with a horseshoe-shaped crack around the connection plate-to-web weld. Effect of reduced deck stiffness on south girder top web-gap stresses can be seen in Figure 10.

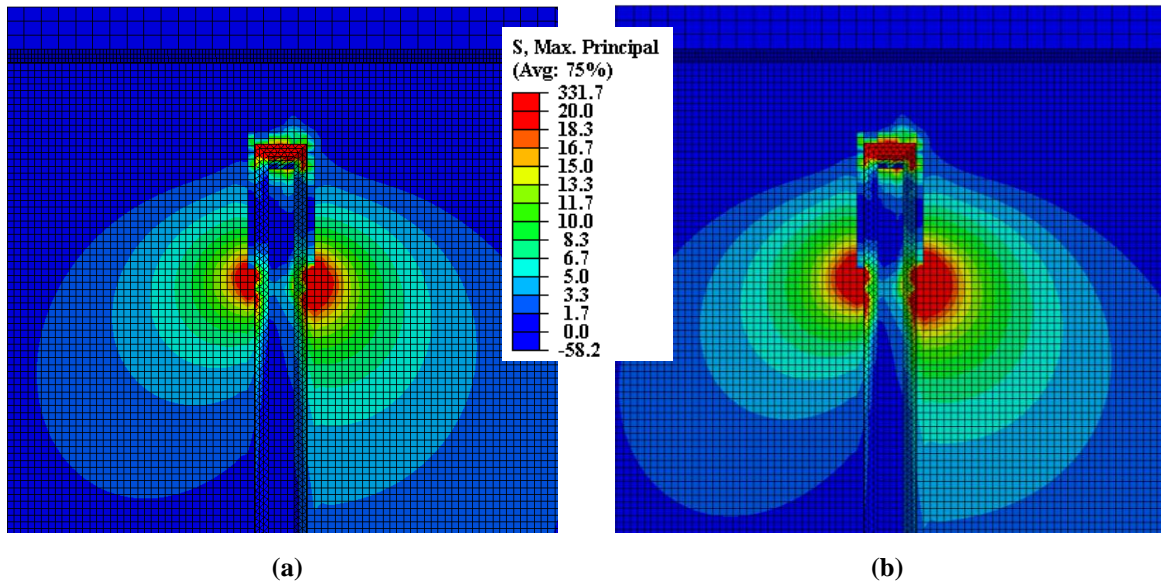


Figure 10: Maximum principal stresses with scale from 0 MPa to 138 MPa [0 ksi to 20 ksi] for (a) unretrofitted model with normal deck stiffness and (b) unretrofitted model with reduced deck stiffness and a 51 mm [2 in.] crack. Legend stresses are in ksi.

EFFECT OF BROKEN CROSS FRAME

During experimental testing as outlined in the companion paper (Part 2), the north cross frame at mid-span experienced a fracture through the diagonal member framing into the top web-gap of the north girder. The effect of this failure on the bridge system was analyzed in a model of the bridge with a 25-mm [1-in.] horseshoe-shaped crack. In this finite element model, which directly modeled the severed cross frame member where it should have framed into the north girder top web-gap, hot spot stresses where the cross frame element previously framed into the girder decreased. This reduction in stresses in the top web-gap of the north girder was approximately 77%. At the bottom web-gap of the same girder, hot spot stresses more than doubled. This correlated well with the computed maximum principal stress magnitudes in the cross frame members framing into the north girder, which saw a decrease in the broken member and an increase in the horizontal element framing into the bottom web-gap. In the south girder, away from the broken cross frame, maximum principal stresses in all cross frame elements decreased. Cross frame stresses can be seen in Table 2.

Table 2: Cross Frame Element Stresses with 25 mm [1 in.] Horseshoe Crack (MPa [ksi])

	Angles-and-Plate 19 mm [3/4 in.]			Angles-and-Plate 19 mm [3/4 in.] with Broken Cross Frame Element		
	Maximum Principal	Horizontal	Vertical	Maximum Principal	Horizontal	Vertical
Inclined Cross Frame Element Framing into North Girder Top Web- Gap	39 [5.7]	28 [4.1]	8 [1.1]	0 [0.0]	0 [0.0]	0 [0.0]
Inclined Cross Frame Element Framing into North Girder Bottom Web-Gap	0 [0.0]	-19 [-2.8]	-6 [-0.9]	0 [0.0]	-23 [-3.4]	-11 [-1.6]
Horizontal Cross Frame Element Framing into North Girder Bottom Web-Gap	29 [4.2]	30 [4.3]	0 [0.0]	41 [6.0]	38 [5.5]	0 [0.0]
Inclined Cross Frame Element Framing into South Girder Top Web- Gap	37 [5.3]	28 [4.1]	7 [1.0]	24 [3.5]	19 [2.7]	5.5 [0.8]
Inclined Cross Frame Element Framing into South Girder Bottom Web-Gap	0 [0.0]	-23 [-3.3]	-6 [-0.9]	0 [0.0]	-19 [-2.8]	-5.5 [-0.8]
Horizontal Cross Frame Element Framing into South Girder Bottom Web-Gap	29 [3.9]	29 [4.2]	0 [0.0]	24 [3.5]	24 [3.5]	0 [0.0]

Girder lateral deflections can be seen in Figure 11. Deflections show as if looking at the girder deflection profiles. The north girder bottom flange moves out toward the right (positive deflection in the plot) and the south girder bottom flange moves out toward the left (negative deflection in plot). The response of the north and south girders in the cracked, unretrofitted condition (25 mm [1 in.] horseshoe-shaped crack) and the response of the girders with the same crack geometry under the angles-with-plate retrofit were found to be symmetric. For the north girder (where the cross frame element was broken), lateral girder deflections were decreased after the cross-frame member was severed, resulting in decreased girder rotation between top and bottom flanges. Additionally, top web-gap differential deflection was found to be nearly zero. Different behavior was found to define the south girder after the cross-frame was severed. In the

south girder, top web-gap differential deflection was still decreased, but bottom flange deflection increased, resulting in larger girder rotation between top and bottom flanges.

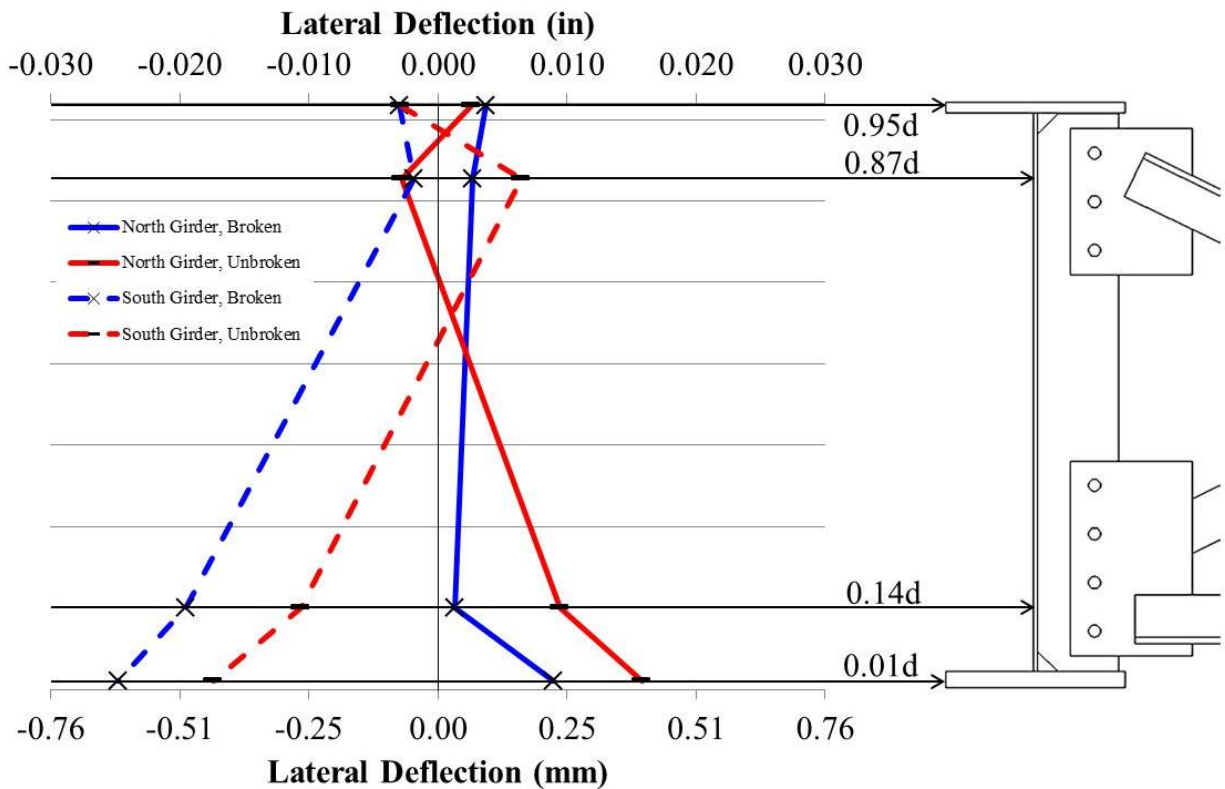


Figure 11: Girder lateral deflections with unbroken cross frame elements and broken cross frame element framing into the north girder top web-gap.

Cross section deflected shapes have been shown in Figure 12. These figures provide images for the results outlined in Figure 11. A localized stress concentration (hot spot) can be seen at the on the tab plate near the end of the inclined cross frame angle as shown in Figure 12(a). Once the cross frame element is broken, little force exists in the tab plate and therefore little out-of-plane forces are transferred into the north girder top web-gap as seen in Figure 12(b). Symmetric bending was found to occur while both cross frames were fully attached; however, deflections were asymmetric under the broken cross frame condition. For the north girder, slightly more flange rotation and less web rotation as shown in Figure 12.

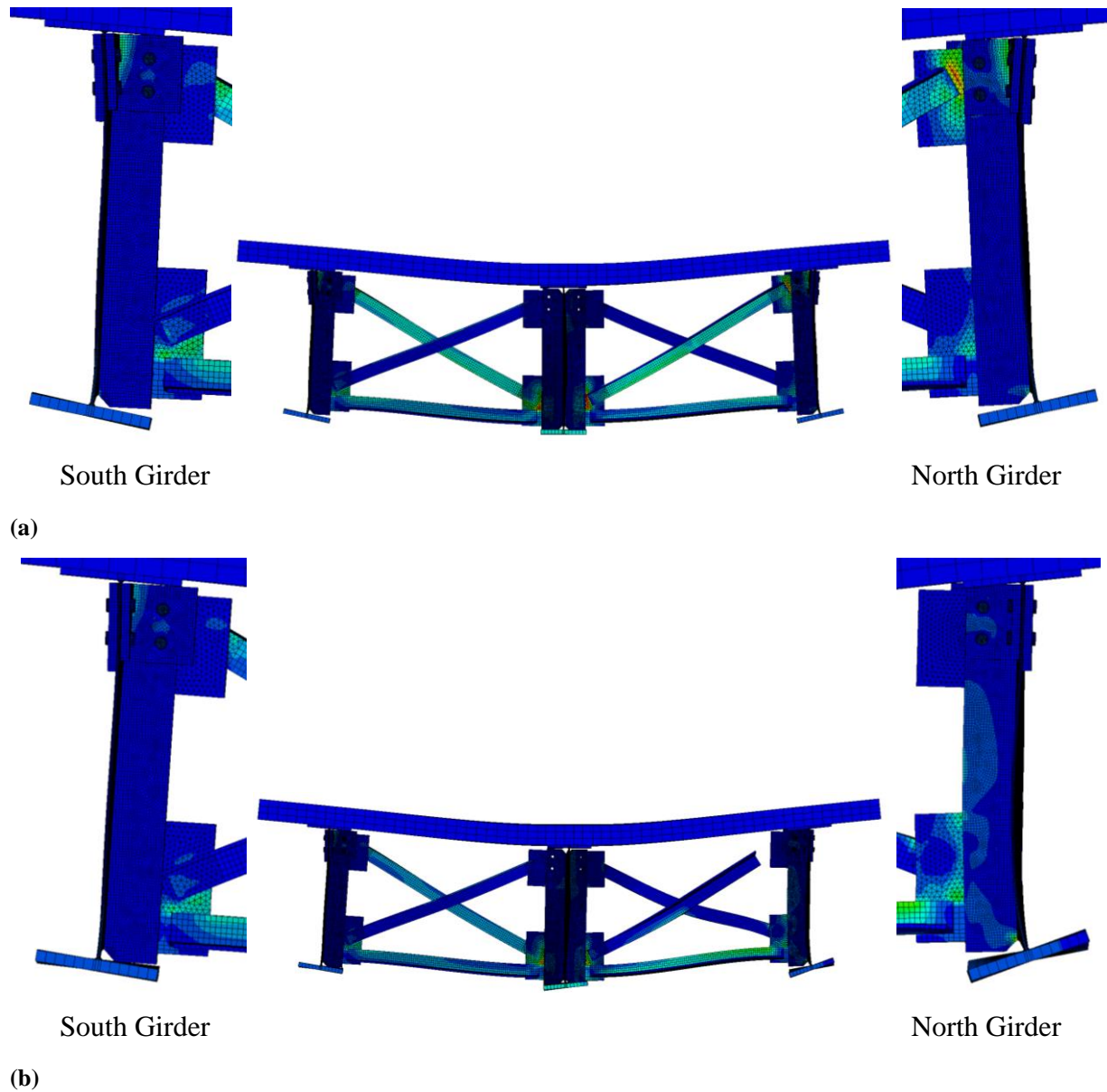


Figure 12: Girder deflection profiles for (a) 25 mm [1 in.] cracked and retrofitted model and (b) 25 mm [1 in.] cracked and retrofitted model with broken north cross frame element.

Hot spot stresses were influenced by the broken north cross frame element framing into the top web-gap. Stresses extracted from finite element models have been presented in Table 3. When the north girder cross frame element framing into the north girder top web-gap was severed, the hot spot stress at the north girder connection plate-to-web weld decreased by more than 50%. In the north girder bottom web-gap, connection plate-to-web weld stress more than doubled. South girder stresses were only slightly affected by the broken north cross frame.

Table 3: Maximum Principal Hot Spot Stresses with 25 mm [1 in.] Horseshoe Crack (MPa [ksi])

	Angles-and-Plate 19 mm [3/4 in.]	Angles-and-Plate 19 mm [3/4 in.] with Broken Cross Frame Element
North Girder Top Web-Gap Connection Plate-Web Weld	71 [10.3]	29 [4.2]
North Girder Top Web-Gap Flange-Web Weld	101 [14.6]	37 [5.4]
North Girder Bottom Web-Gap Connection Plate-Web Weld	92 [13.4]	191 [27.7]
North Girder Bottom Web-Gap Flange-Web Weld	38 [5.5]	77 [11.1]
South Girder Top Web-Gap Connection Plate-Web Weld	52 [7.6]	60 [8.7]
South Girder Top Web-Gap Flange-Web Weld	102 [14.8]	66 [9.6]
South Girder Bottom Web-Gap Connection Plate-Web Weld	97 [14.1]	56 [8.1]
South Girder Bottom Web-Gap Flange-Web Weld	41 [5.9]	25 [3.6]

EFFECT OF RETROFIT BOLT FAILURE

During the corresponding experimental testing on the 9.1-m [30-ft] long test bridge under the stiffened angles-with-plate repair, a bolt in the retrofit on the north girder failed in tension on two occasions. The bolt, located at the top of the retrofit on the east side of the stiffener, connected the leg of the angle to the backing plate through the girder web. The bolt failed in tension during Trials 2.3N and 2.7N, when the test bridge was cycling between loading ranges of 36-356 kN [8-80 kip] and 44-445 kN [10-100 kip], respectively. Before the first occurrence of the bolt failure in Trial 2.3N, minimal cracking was detected in the north girder. Upon inspection after the bolt failure was discovered, additional cracking was found at both the connection plate-to-web weld and the flange-to-web weld. Cracking in the north girder did not grow until the next bolt failure occurred during Trial 2.7N. After the second bolt failure occurred, the flange-to-web weld crack was found to have grown even more.

To determine the effect that the bolt failure had on the web-gap stresses, the finite element model with the stiffened angles-with-plate repair was modified to replicate as closely as possible the cracking conditions of the experimental tests before the failures occurred. For Trial

2.3N, cracking conditions were modeled as small crack at the top of the connection plate-to-web weld that had not yet propagated around the toe of the weld. For Trial 2.7N, cracking conditions were modeled as a 25-mm [1-in] horseshoe-shaped crack around the connection plate-to-web weld and 121-mm [4-3/4-in.] longitudinal crack near the flange-to-web weld. Two models for each bolt failure were analyzed, one with a functioning bolt and one without a functioning bolt at the top east corner of the retrofit. The hot spot stresses were compared between the two models to determine if the bolt failure was a major factor in the crack growth seen in the north girder during the corresponding experimental testing of the 9.1-m [30-ft] long test bridge. Results from the models replicating Trials 2.3N and 2.7N are shown in Figure 13 and Figure 14, respectively.

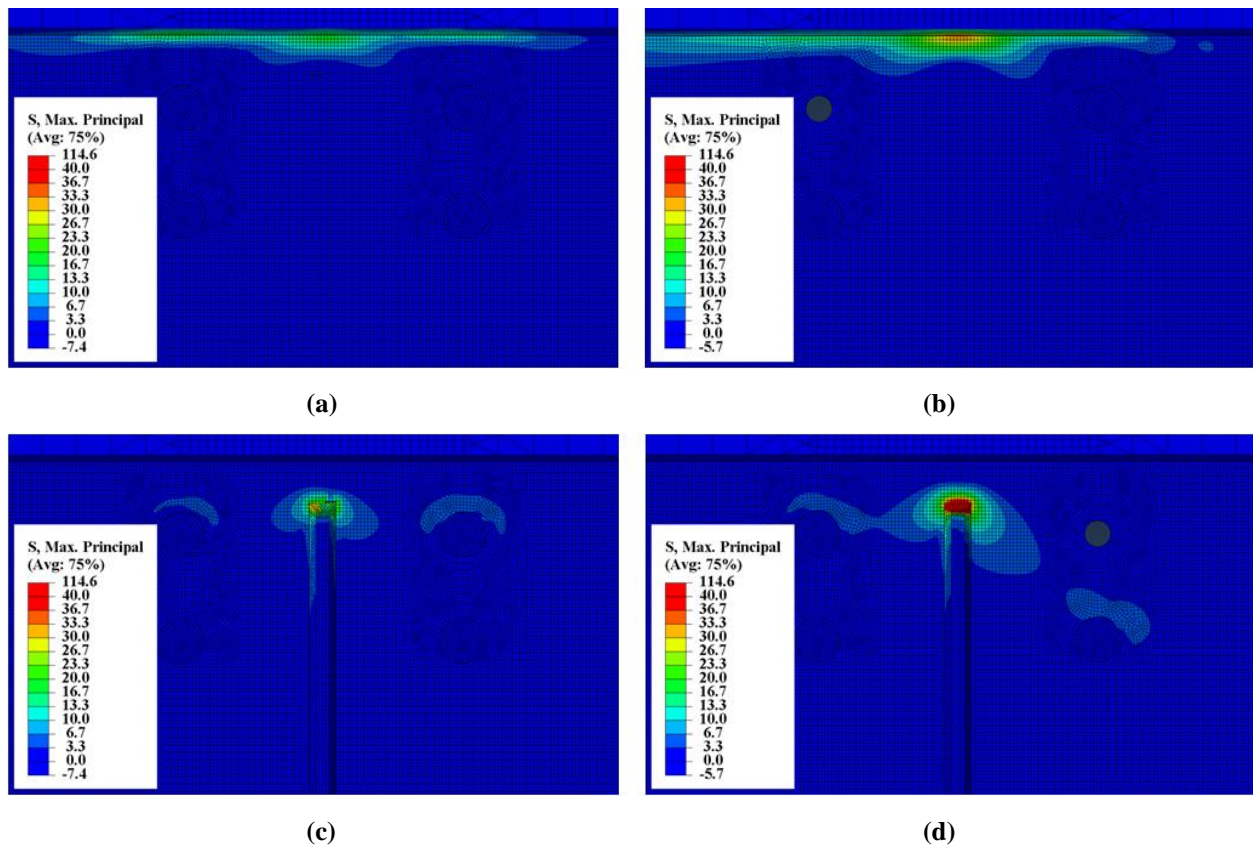


Figure 13: Maximum principal stresses for model replicating Trial 2.3N under the stiffened angles-with-plate repair with (a) functioning bolt, shown from fascia side, (b) missing bolt, shown from fascia side, (c) functioning bolt, shown from stiffener side, and (d) missing bolt, shown from stiffener side. Legend stresses are in ksi.

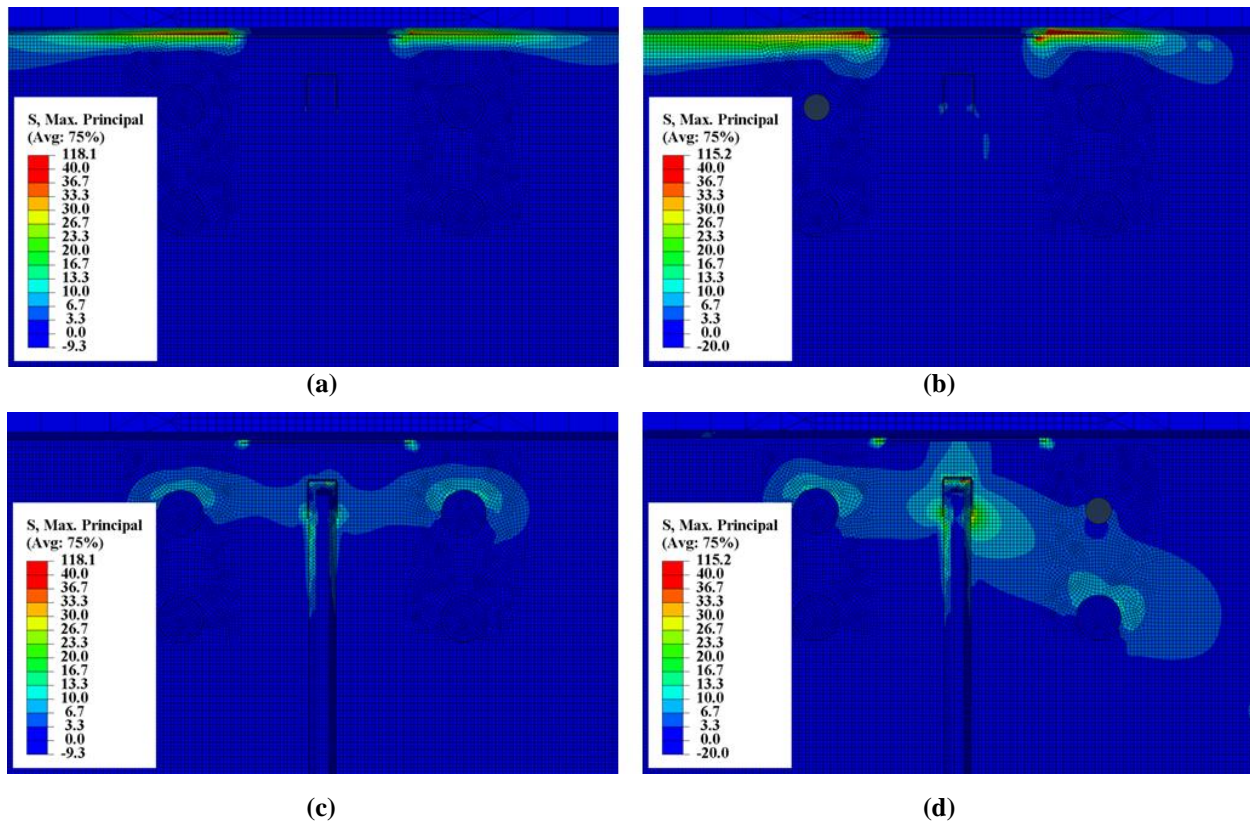


Figure 14: Maximum principal stresses for model replicating Trial 2.7N under the stiffened angles-with-plate repair with (a) functioning bolt, shown from fascia side, (b) missing bolt, shown from fascia side, (c) functioning bolt, shown from stiffener side, and (d) missing bolt, shown from stiffener side. Legend stresses are in ksi.

Hot spot stresses taken around the connection plate-to-web weld and the flange-to-web weld resulted in the maximum principal stresses shown in

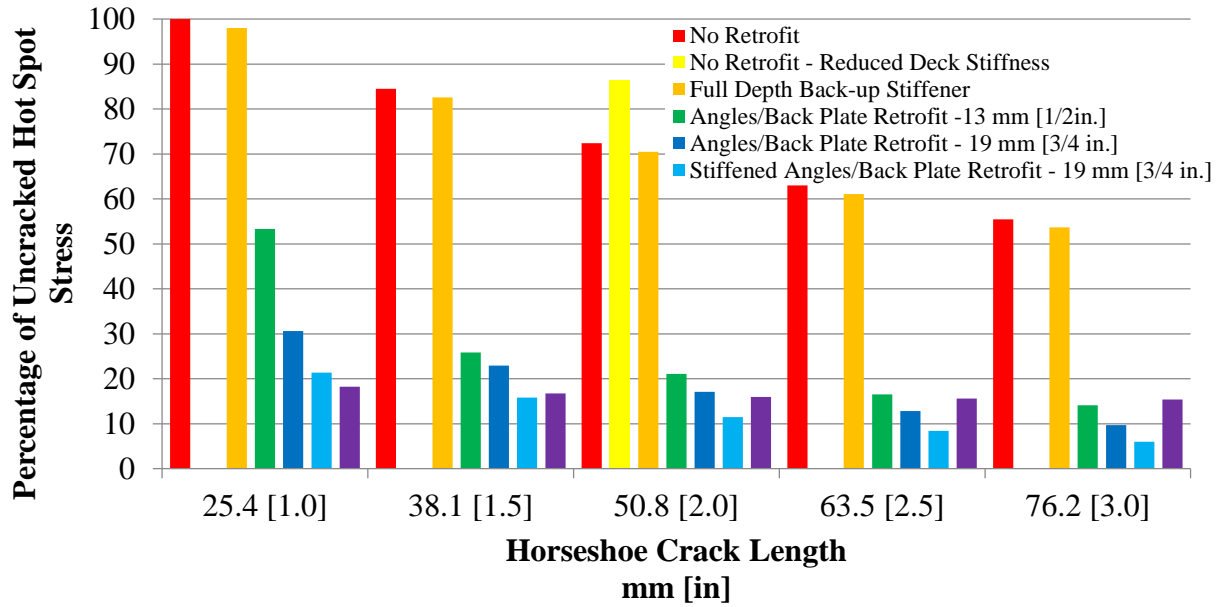
Table 4. Stresses at the connection plate-to-web weld and the flange-to-web weld increased by 76% and 78%, respectively, after the bolt was removed in the finite element model that replicated Trial 2.3N. Stresses at the flange-to-web weld increased by 54% after the bolt was removed in the finite element model that replicated Trial 2.7N. These increases in stress demands offer a probable explanation as to why large crack growth was recorded in the top web-gap of the north girder under application of the stiffened version of the angles-with-plate retrofit during experimental testing. Loss of stiffness in the retrofit caused by the bolt failure likely led to increases in web-gap stress, thus causing crack growth at the connection plate-to-web weld and flange-to-web weld in Trial 2.3N and at the flange-to-web weld in Trial 2.7N.

Table 4: Maximum Principal Hot Spot Stresses for Experimental Trials With Bolt Failure

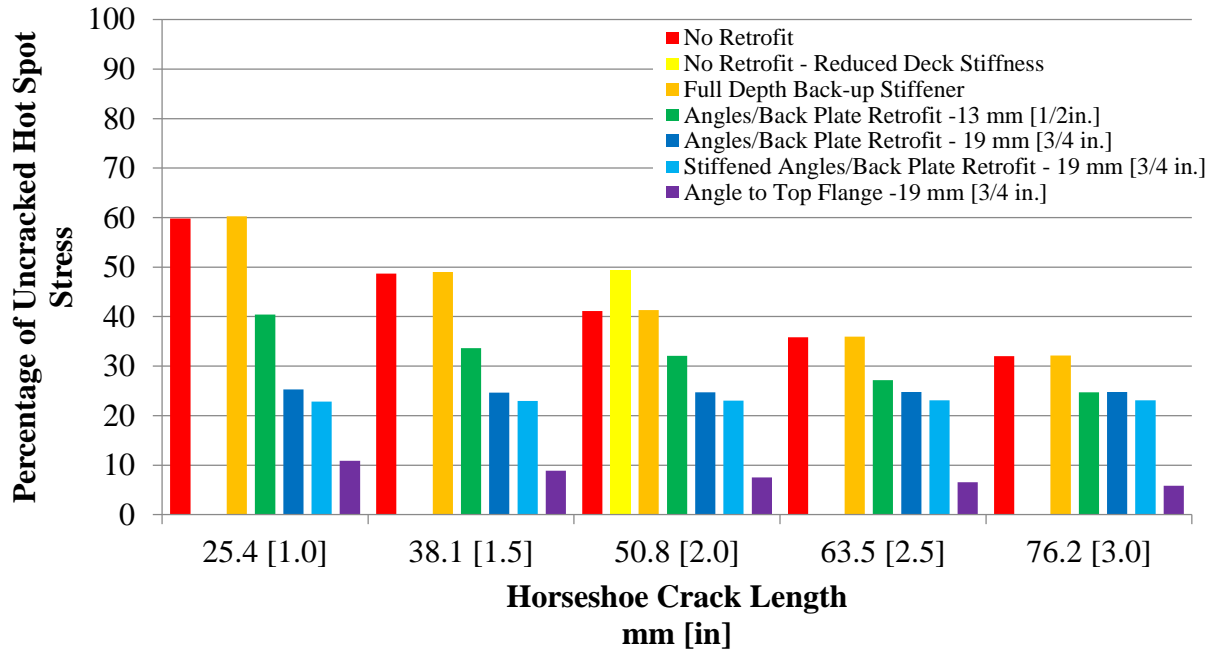
Experimental Test Trial	North Girder Top Web-gap Location	Stiffened Angles-with-Plate With Functioning Bolt	Stiffened Angles-with-Plate Without Bolt
Trial 2.3N	Connection Plate-Web Weld	155 [22.5]	272 [39.5]
	Flange-Web Weld	127 [18.4]	226 [32.8]
Trial 2.7N	Connection Plate-Web Weld	85 [12.3]	204 [29.6]
	Flange-Web Weld	163 [23.6]	250 [36.3]

RETROFIT COMPARISON

The relative effectiveness of the various retrofits investigated have been presented by showing the stress demands in the web gap region in the retrofitted condition as percentage of the stress demands from the uncracked, unretrofitted condition. All retrofits were analyzed and applied over a horseshoe-shaped crack only. The angles-with-plate retrofit was also analyzed with longitudinal cracks. The percent of uncracked stress in connection plate-to-web weld and flange-to-web weld for changing horseshoe-shaped crack lengths are shown in Figure 15(a) and 13(b), respectively. For all retrofits considered, the pattern of stress reduction was similar for all crack lengths studied. As crack length increased from 25 mm [1 in.] to 76 mm [3 in.], the percent reduction in hot spot stress decreased for both the connection plate-to-web weld and flange-to-web weld locations. As crack length increases, hot spot stresses decrease as shown in Figure 8 and Figure 9. As the retrofit was applied to larger cracks with lower initial stresses, the reduction in stress decreased. Additionally, at a crack length of 76 mm [3 in.], all retrofits provide a reduction in stress of more than 80%. Continuing to improve on this stress (which is already low) becomes inefficient.



(a)



(b)

Figure 15: Percent of uncracked stress at (a) connection plate-web weld and (b) flange-web weld for various retrofit techniques and crack lengths.

Since similar patterns were found for each of the crack lengths investigated, results for a horseshoe-shaped crack length of 51 mm [2 in.] are shown in Figure 16.

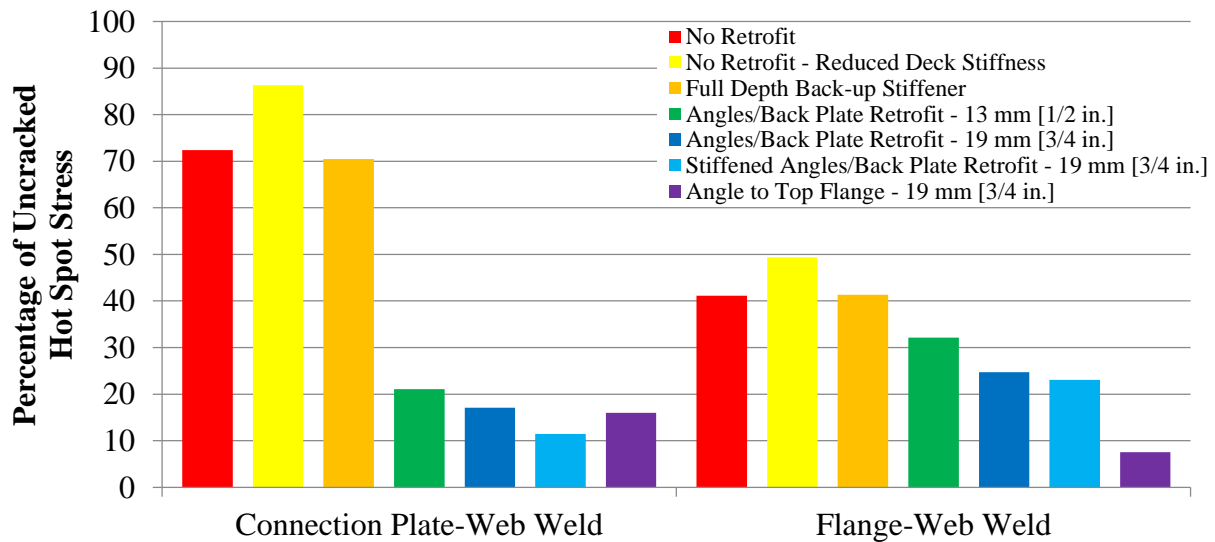


Figure 16: Percentage of uncracked hot spot stresses for connection plate-web weld and flange-web weld with various retrofit conditions and a 51 mm [2 in.] horseshoe crack.

As shown, an initial horseshoe-shaped crack length of 51 mm [2 in.] resulted in a connection plate-web weld hot spot stress of approximately 72% of the uncracked state while flange-web weld hot spot stress was approximately 41% of the uncracked state. Retrofit performance was based on additional reduction from the cracked state. As stated previously, initial uncracked hot spot stresses for each location were within 3% of each other. Therefore, all retrofitted hot spot stresses were normalized against a similar value and can be compared directly. In other words, because of this coincidence, a reduction of 10% in the connection plate-web weld is approximately the same as a 10% reduction in the flange-web weld.

Full depth back-up stiffeners provided minimal relief in hot spot stress for both welds of interest. Since the bridge studied was a non-skewed bridge with cross frames placed back-to-back, this corroborates previous findings (Hartman et. al 2010). Excluding back-up stiffeners, all other retrofits resulted in a reduction of stress demand.

Based on all models studied, the best retrofit for reduction of hot spot stress around the connection plate-web weld was found to be the stiffened angles-with-backing plate. For a 51

mm [2 in.] crack, stiffening the angles resulted in an additional reduction of over 5% when compared with the performance of the unstiffened retrofit; however, adding stiffeners did not greatly improve the stress reduction for the flange-to-web weld. In this location, the additional reduction due to added stiffness was less than 2%.

For the angles-with-plate retrofit, changes in thickness impacted the hot spot stress demand at the two fatigue-susceptible welds. At the connection plate-to-web weld for a 51 mm [2 in.] horseshoe-shaped crack, a retrofit thickness of 13 mm [1/2 in.] provided a stress reduction of approximately 51%. Increasing the retrofit thickness to 19 mm [3/4 in.] provided an additional stress reduction of 4%. Similarly for the flange-to-web weld, a thickness of 13 mm [1/2 in.] decreased stresses by 9% while a thickness of 19 mm [3/4 in.] decreased stresses an additional 7%. Based on this data, it is estimated that increasing the angles and plate thicknesses would not continue to provide much additional reduction in stress—there would be a point in which increasing thickness provides little or no additional benefit.

For the flange-to-web weld, it was found the best performing retrofit was the angles connected with the girder top flange. This retrofit minimized the differential rotation between the girder flange and web, forcing the elements to rotate together rather than separately. This retrofit was also found to perform slightly better than the 19-mm [3/4-in.] thick angles-with-backing plate retrofit for the connection plate-to-web weld. Although this traditional retrofit indicated good performance, these findings must be balanced against the required additional welding and/or deck removal with traffic disruption for field implementation.

CONCLUSIONS

Since many steel bridges built prior to 1985 are in need of repair, it is critical to develop effective retrofit techniques for many different bridge configurations. Finite element simulations can be used to evaluate retrofit effectiveness and can also provide meaningful insight into appropriate retrofit thickness and performance to complement laboratory and/or field implementation. In this study, several retrofits were considered including: full depth back-up stiffeners, angles-with-backing plate (several variations), and angles connected to the top flange. Additionally, the effect of a broken cross frame element, retrofit bolt failures, and reduced deck stiffness due to cracking were analyzed. The following conclusions were found:

- Hot spot stresses at connection plate-to-web welds and flange-to-web welds decreased or remained constant as horseshoe-shaped crack length was increased in both unretrofitted models and angles-with-plate (19 mm [3/4 in.] thickness) retrofitted models.
- Hot spot stresses at connection plate-to-web welds and flange-to-web welds decreased as longitudinal crack length was increased in both unretrofitted models and angles-with-plate (19 mm [3/4 in.] thickness) retrofitted models. Initiation of a longitudinal crack increased hot spot stresses at the connection plate-to-web weld; therefore, horseshoe-shaped cracking would likely initiate soon after the formation of a longitudinal crack.
- When deck stiffness was halved, hot spot stresses in both the connection plate-to-web weld and flange-to-web weld increased 20%.
- Although the analysis of the cross frame failure did not provide any significant conclusions, changes in bridge response were evident. With the broken north cross frame, the south cross frame and girder did *not* pick up much more load in terms of web-gap stresses. In fact, web-gap stresses actually decreased in the top web-gap flange-web weld and the bottom web-gap flange-web weld and connection plate-web weld. In terms of stresses, the only location within the bridge that gathered more load was the north girder bottom web-gap and horizontal cross frame member in the north cross frame.
- Due to the cross frame failure, slight increases in flange rotation and decreases in web rotation were experienced by the north girder. South girder lateral deflections increased due to north cross frame failure while north girder lateral deflection decreased.
- Due to retrofit bolt failure, increases in hot spot stresses at the connection plate-to-web weld and flange-to-web weld were experienced by the north girder. Loss of stiffness caused by the bolt failure would likely lead to crack growth.
- For all crack lengths studied, the order of retrofit effectiveness remained constant. As crack lengths increased, initial hot spot stresses decreased, resulting in less stress reduction due to retrofitting.
- Both hot spot stresses experienced reduction due to retrofitting. Full depth back-up stiffeners provided minimal stress relief in the system due to bridge configuration.
- Retrofit performance listed in order from most reduction to least reduction was found to be as follows for the connection plate-to-web weld: stiffened angles-with-backing plate

19 mm [3/4 in.], angles to top flange 19 mm [3/4 in.], angles-with-backing plate 19 mm [3/4 in.], angles-with-backing plate 13 mm [1/2 in.], and full depth back-up stiffener.

- Retrofit performance listed in order from most reduction to least reduction was found to be as follows for the flange-web weld: angles to top flange 19 mm [3/4 in.], stiffened angles-with-backing plate 19 mm [3/4 in.], angles-with-backing plate 19 mm [3/4 in.], angles-with-backing plate 13 mm [1/2 in.], and full depth back-up stiffener.
- To improve angles-with-backing plate performance, addition of stiffeners to the angles may be a viable option. This may allow for reduction in thickness of angles and backing plate for field implementation.

Although numerous modeling efforts have been performed at the University of Kansas in the past, the models and associated physical tests were aimed at girder sub-assemblies. These sub-assemblies only included out-of-plane effects and did not capture longitudinal bending effects.

In the analyses described in this study, a significant effort was placed in determining an appropriate retrofit technique for a 9.1 m [30 ft.] laboratory test bridge. These models were also used to explain bridge and retrofit behavior.

Based on this investigation, effective retrofits (primarily considering angles-with-plate variations) can be chosen for application on the test bridge. As such, the next retrofit selected for test bridge implementation is stiffened angles-with-plate. With laboratory test data to validate results, efforts will then be placed toward field implementation in which the angles-with-plate retrofit will provide an effective and inexpensive technique requiring little-to-no traffic closure.

REFERENCES

Adams, C. (2009). "Finite Element Study on Bridge Details Susceptible to Distortion-Induced Fatigue." Master's Thesis, University of Kansas.

Alemдар, F., Overman, T., Matamoros, A., Bennett, C., and Rolfe, S. (2013a). "Repairing Distortion-Induced Fatigue Cracks in Steel Bridge Girders using Angles-with-Plate Retrofit Technique, Part I: Physical Simulations." *Journal of Structural Engineering*, ASCE, In Press.

Alemдар, F., Nagati, D., Matamoros, A., Bennett, C., and Rolfe, S. (2013b). "Repairing Distortion-Induced Fatigue Cracks in Steel Bridge Girders using Angles-with-Plate Retrofit Technique, Part II: Computer Simulations." *Journal of Structural Engineering*, ASCE, In Press.

Hartman, A., Hassel, H., Adams, C., Bennett, C., Matamoros, A., and Rolfe, S. (2010). "Effects of Cross-Frame Placement and Skew on Distortion-Induced Fatigue in Steel Bridges." TRB: Journal of the Transportation Research Board. 2200 (1). 62-68.

Hassel, H., Hartman, A., Bennett, C., Matamoros, A., and Rolfe, S. (2010). "Distortion-Induced Fatigue in Steel Bridges: Causes, Parameters, and Fixes." *2010 ASCE/SEI Structures Congress Proceedings*. 471-483.

Nagati, D. (2012). "Repair of Steel Bridge Girders Damaged by Distortion-Induced Fatigue." Master's Thesis, University of Kansas.

Przywara, J. (2013). "Applications of the Extended Finite Element Method (XFEM) for the Analysis of Distortion-Induced Fatigue Cracking in Highway Bridge Girders." Master's Thesis, University of Kansas.

Richardson, T. (2012). "Analytical Investigation of Repair Methods for Fatigue Cracks in Steel Bridges." Master's Thesis, University of Kansas.

Appendix E: Experimental Data

Concrete Material Properties

Table E. 1: Concrete Compressive Strengths in psi

Slab	Pour	7-day	Strength	14-day	Strength	21-day	Strength	28-day	Strength	56-day	Strength
#1	7/9/2010	7/16/2010	3270	7/23/2010	4030			8/6/2010	4014	9/3/2010	4916
#2 MCM	7/28/2010							8/25/2010	4173	9/22/2010	4244
#2 KU	7/28/2010									9/22/2010	5712
#3	8/20/2010	8/27/2010	3714	9/3/2010	4686			9/17/2010	4863	10/15/2010	5270
#4	9/10/2010	9/17/2010	3484	9/24/2010	4209			10/8/2010	3979	11/5/2010	4668
#5	10/1/2010	10/8/2010	3395	10/15/2010	4244			10/29/2010	4757	11/26/2010	
Base Block	2/15/2011					3/8/2011	7445	3/15/2011	8842		

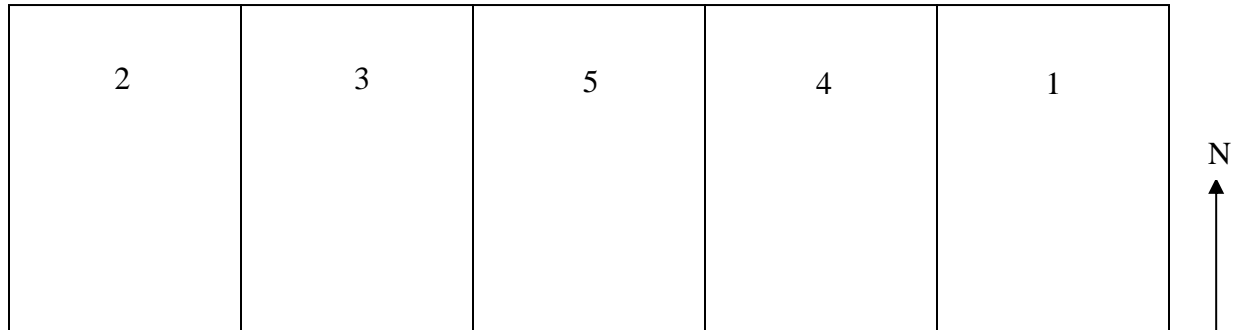


Figure E. 1: Deck Layout and Labeling

Crack Growth

North Girder – Test 1

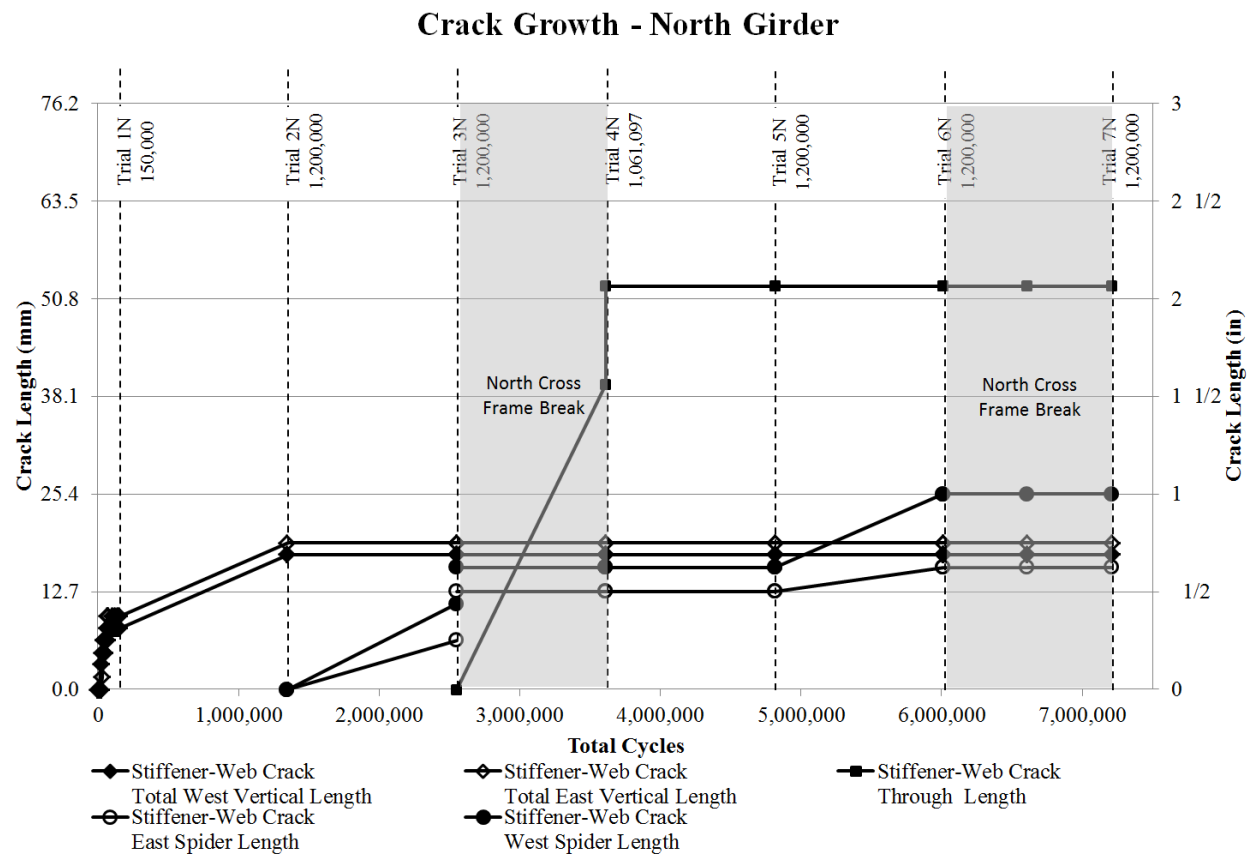
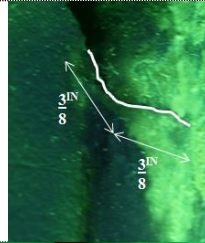


Figure E. 2: North girder crack growth

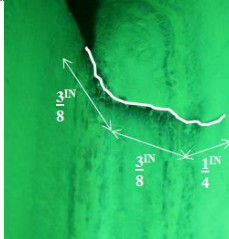
Table E. 2: North Girder – Test 1 Crack Figures

Trial	West of Stiffener	East of Stiffener	Fascia
1.1			

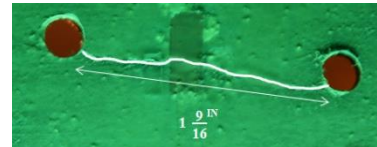
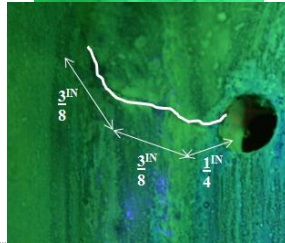
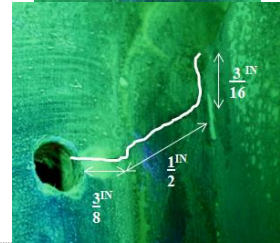
1.2



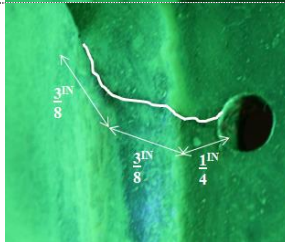
1.3



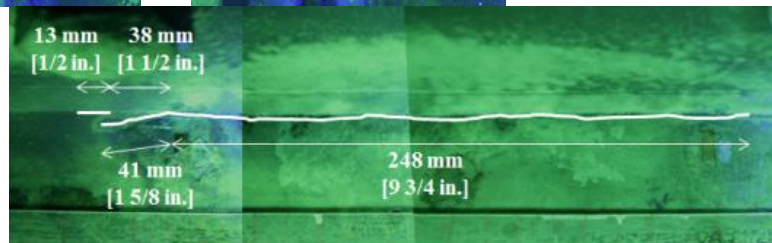
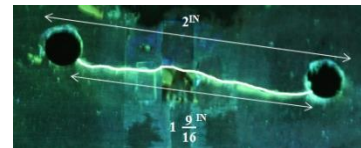
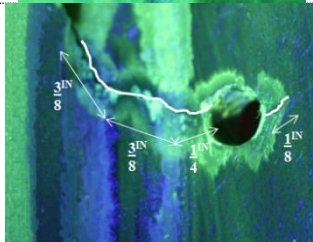
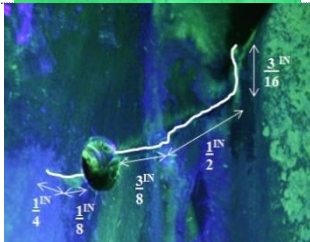
1.4



1.5



1.6



1.7



South Girder – Test 1

Crack Growth - South Girder

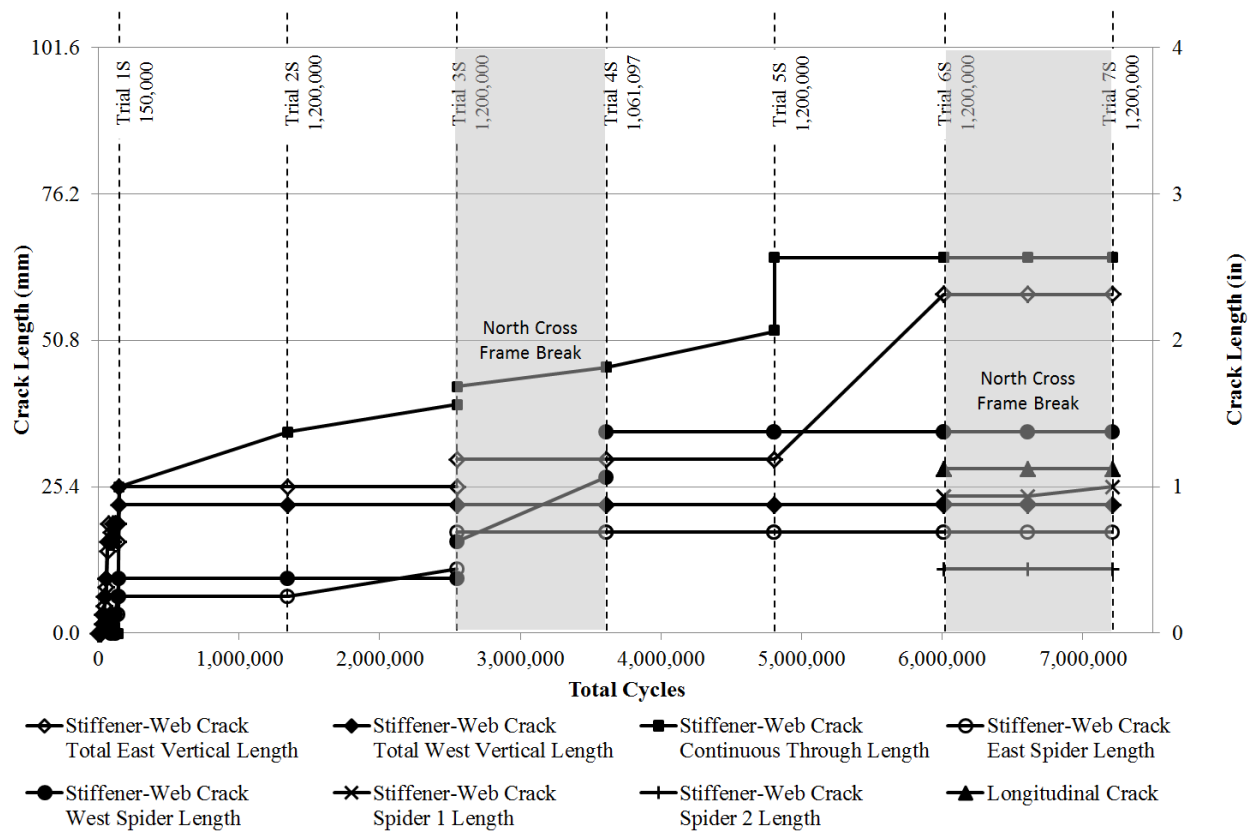

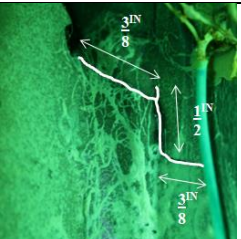

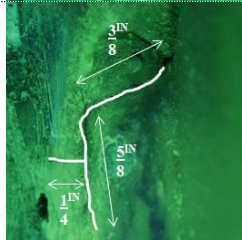
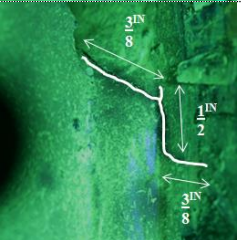
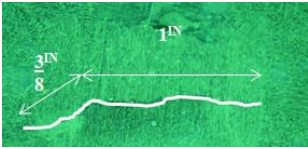
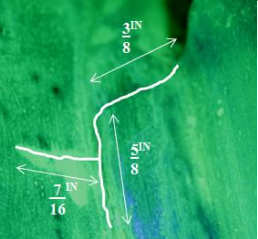
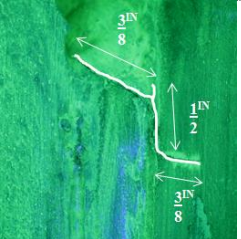
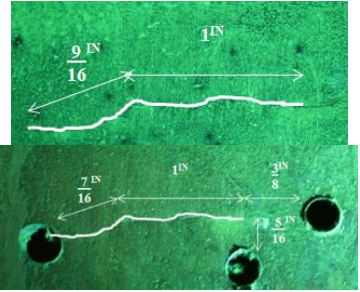
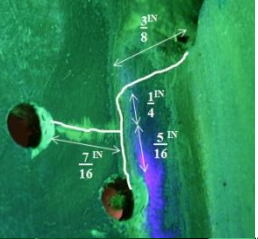

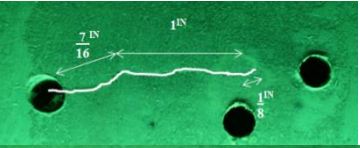
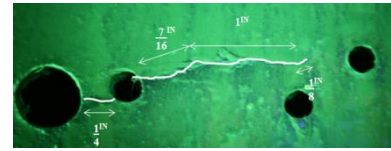
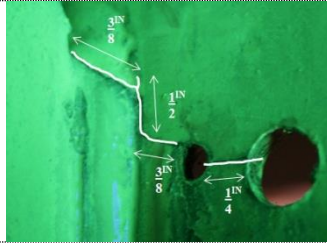
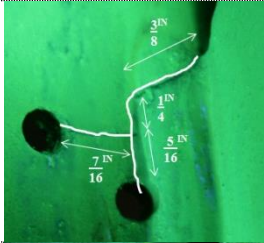


Figure E. 3: South girder crack growth

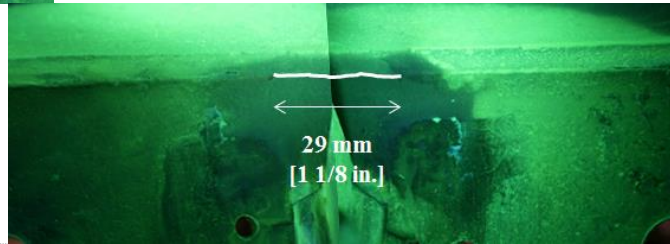
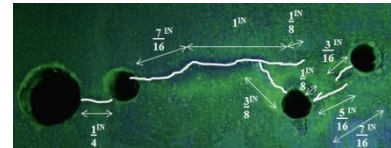
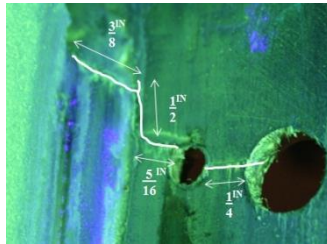
Table E. 3: South Girder – Test 1 Crack Figures

Trial	East of Stiffener	West of Stiffener	Fascia
1.1			
1.2			
1.3			
1.4			

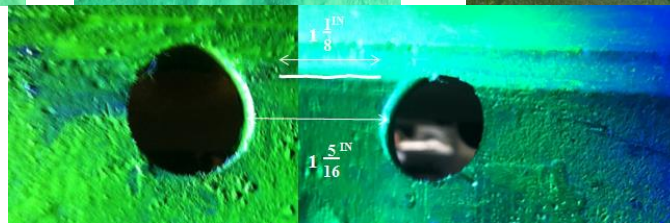
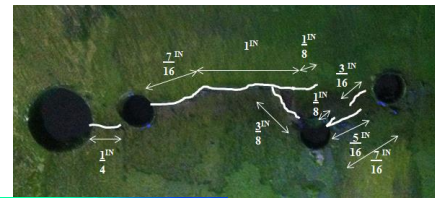
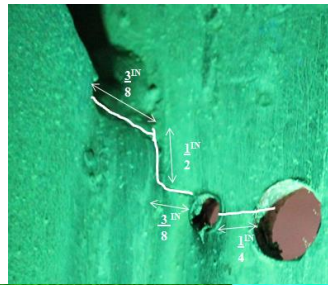
1.5



1.6



1.7



North Girder – Test 2

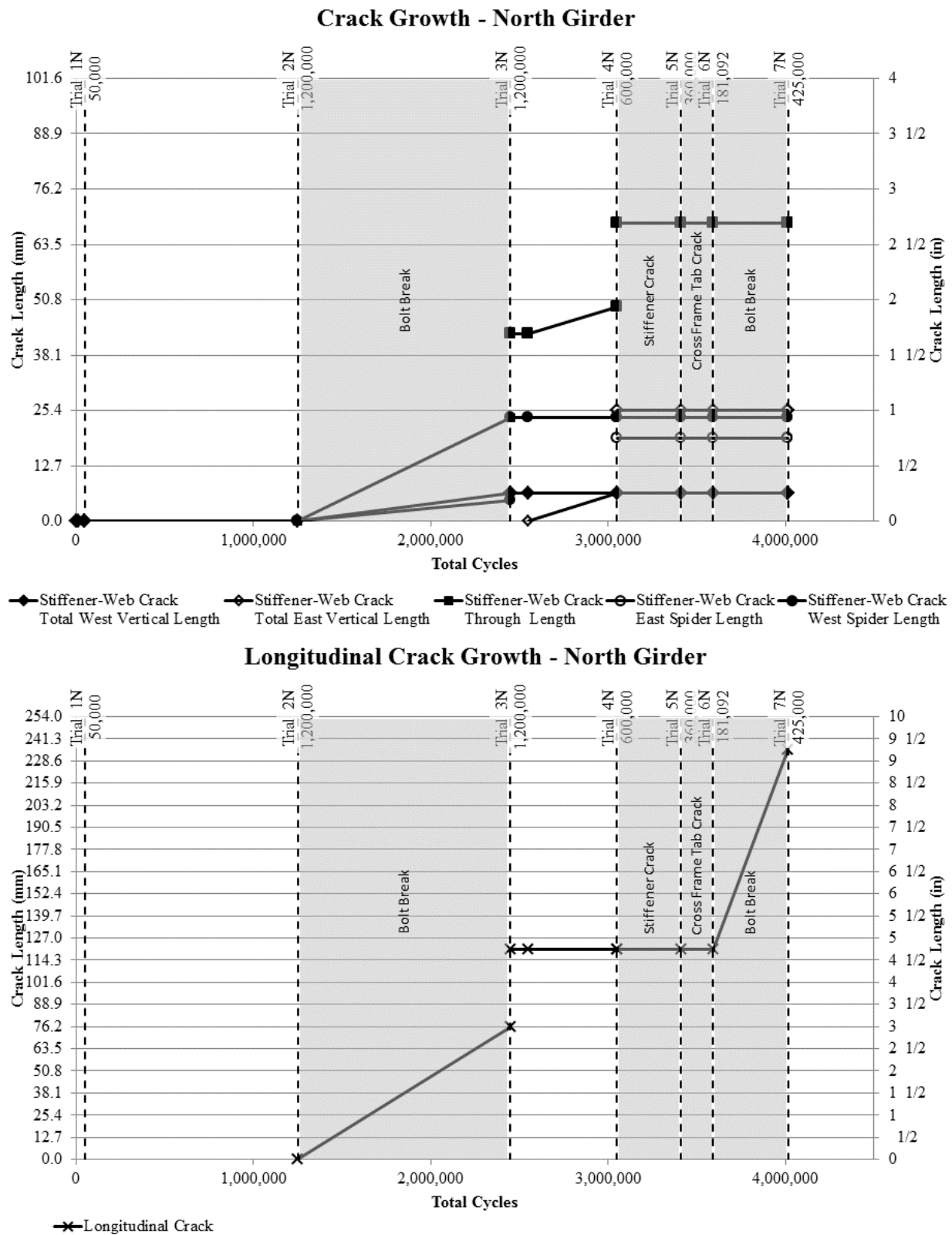
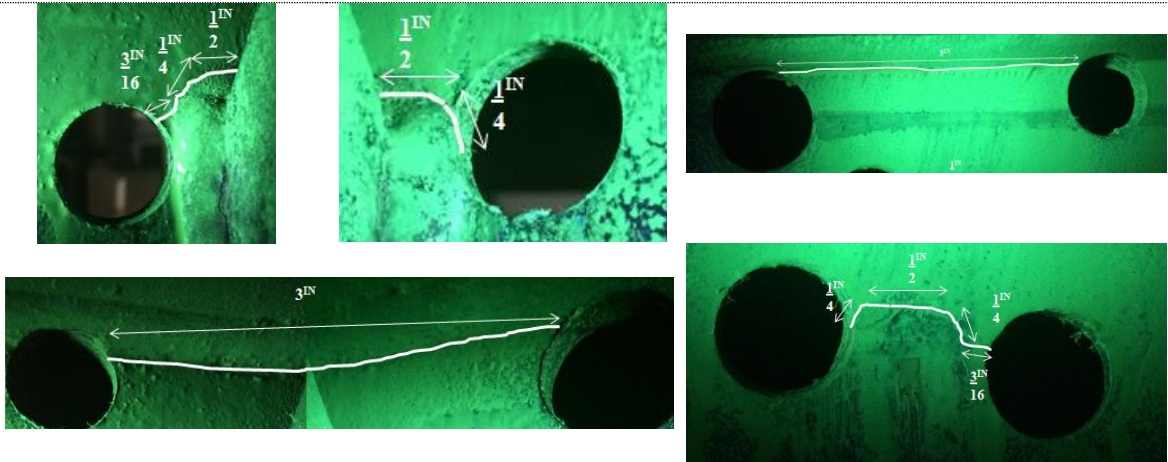


Figure E. 4: North girder crack growth

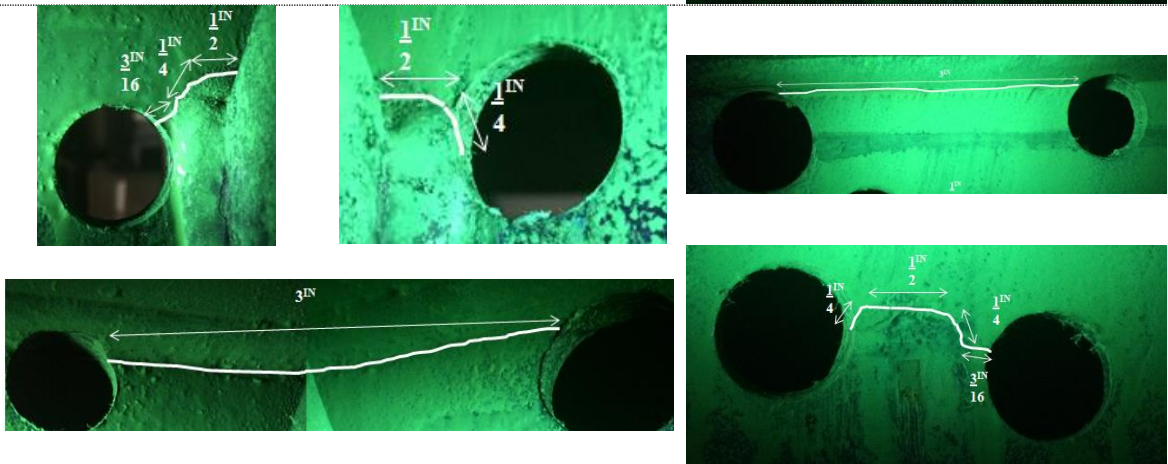
Table E. 4: North Girder – Test 2 Crack Figures

Trial	West of Stiffener	East of Stiffener	Fascia
2.1			
2.2			
2.3			
			
2.4			
			

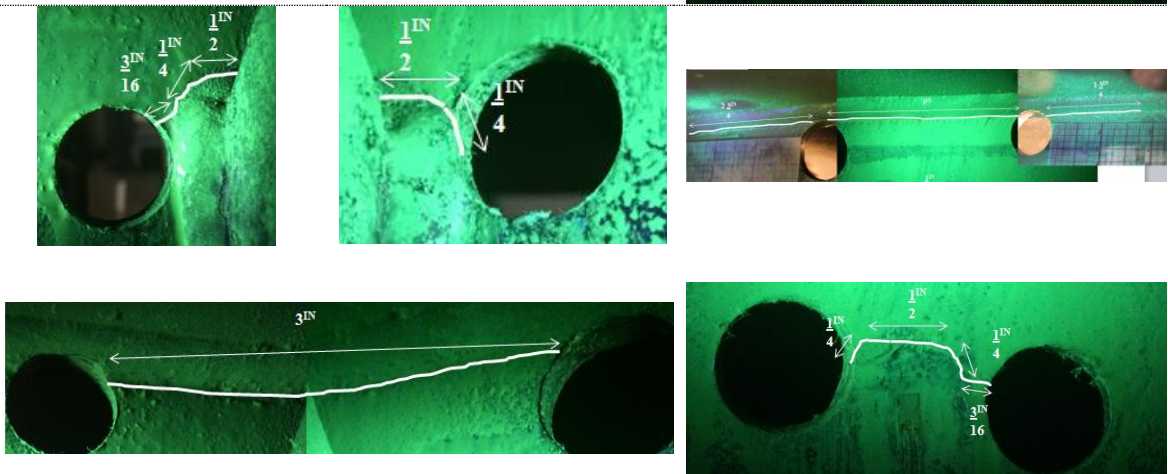
2.5



2.6



2.7



South Girder – Test 2

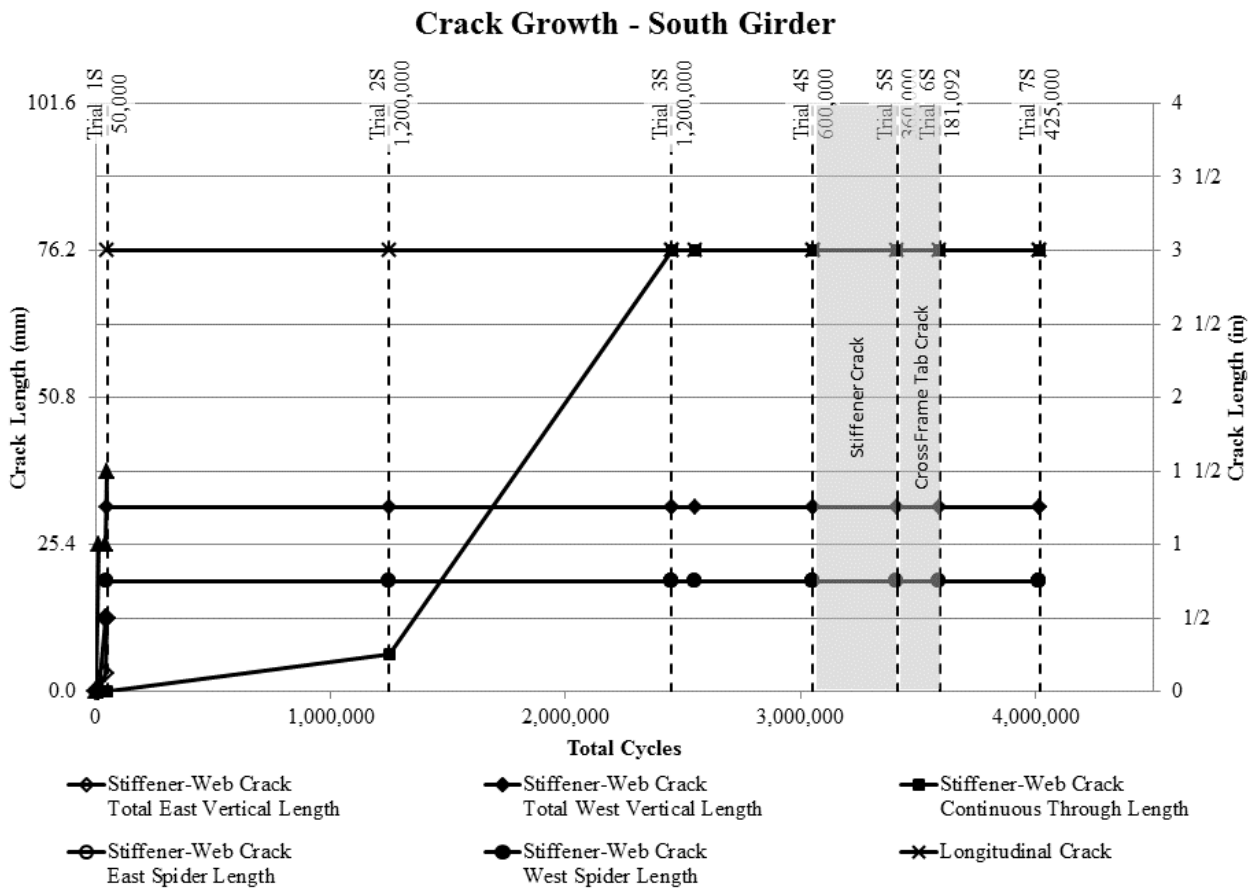
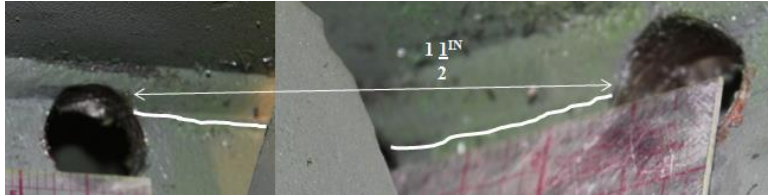
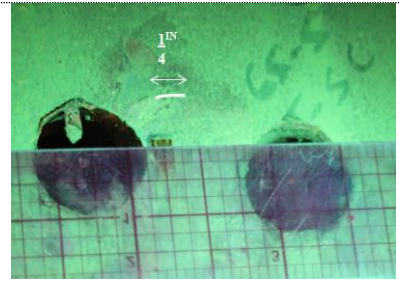
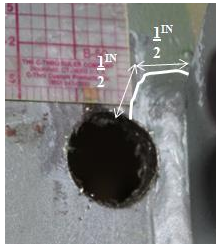


Figure E. 5: South girder crack growth

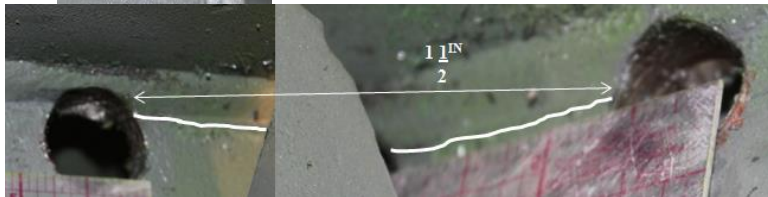
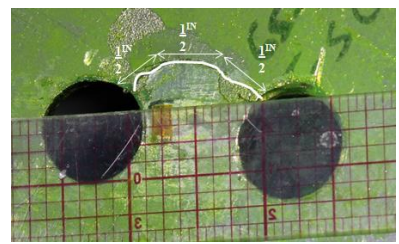
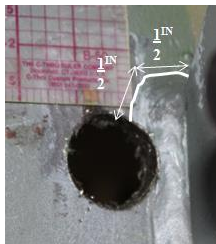
Table E. 5: South Girder – Test 2 Crack Figures

Trial	East of Stiffener	West of Stiffener	Fascia
2.1			

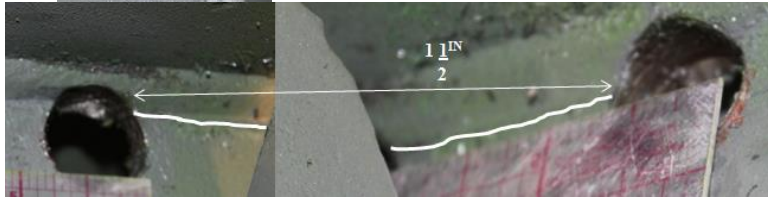
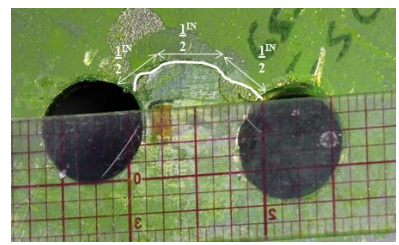
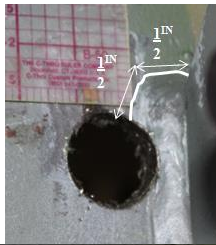
2.2



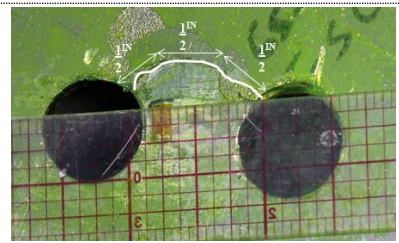
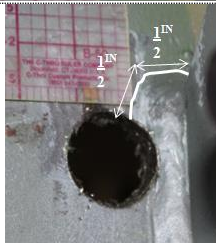
2.3



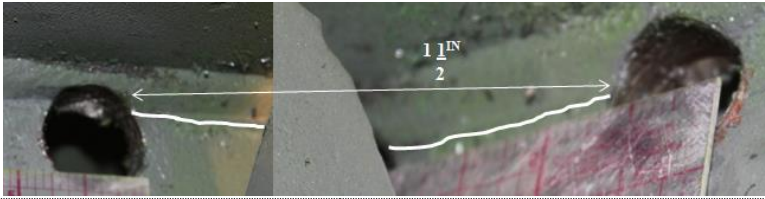
2.4



2.5



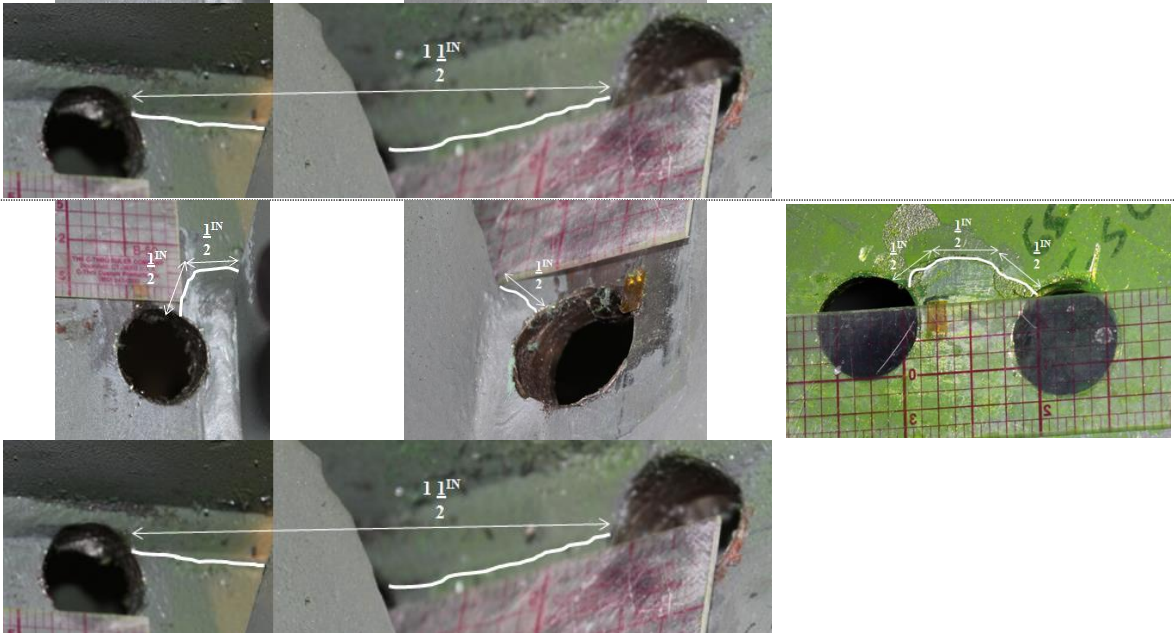
2.5



2.6



2.7



Load Distribution

Near the beginning of testing, load cells monitored load at each girder end. From this data, load distribution can be determined. For each set of static data, the average percentage of total load for each girder end was determined.

Test 1

Table E. 6 shows these results for 0 cycles and 150,000 cycles both without and with the angles-and-plate retrofit.

Table E. 6: Load Distribution from Load Cells – Test 1

Load Cell\Cycles	0	150,000 w/o Retrofit	150,000 w/ Retrofit
WN LCA	10%	11%	11%
WM LCB	28%	No Data	No Data
WS LCC	11%	11%	12%
EN LCD	12%	12%	13%
EM LCE	28%	30%	28%
ES LCF	11%	10%	11%

In general, exterior girders (north and south) take approximately 21-24% of the total load on the bridge. The interior girder supports the remaining load (52-58%). As cracking occurs between 0 and 150,000 cycles, minimal changes in load distribution can be seen. Retrofitting the system slightly increases load supported by exterior girders when compared with the unretrofitted state at 150,000 cycles. Retrofitting results in similar load distribution to an uncracked specimen at 0 cycles.

Test 2

Table E. 67 shows these results for 0 cycles and 50,000 cycles both without and with the angles-and-plate retrofit.





















Table E. 7: Load Distribution from Load Cells – Test 2

Load Cell\Cycles	0	50,000 w/o Retrofit	50,000 w/ Retrofit
WN LCA	9%	10%	9%
WM LCB	25%	23%	24%
WS LCC	13%	15%	15%
EN LCD	15%	15%	14%
EM LCE	25%	24%	26%
ES LCF	13%	13%	12%

In general, exterior girders (north and south) take approximately 22-28% of the total load on the bridge. The interior girder supports the remaining load (47-50%). As cracking occurs between 0 and 50,000 cycles, minimal changes in load distribution can be seen. Retrofitting the system slightly decreases load supported by exterior girders when compared with the unretrofitted state at 50,000 cycles. Retrofitting results in similar load distribution to an uncracked specimen at 0 cycles.

Experimental Data Plots

Table E. 8: Legend for Strain Plots

North Girder				Middle Girder				South Girder			
North Face (Fascia)		Stiffener Side (Stiffener)		North Face		South Face		North Face (Stiffener)		South Face (Fascia)	
 B(3)	 T(2)	 T(5)	 B(5)	 B(4)	 B(5)	 B(5)	 B(4)	 T(4)	 B(4)	 B(3)	 T(1)
 T(3)	 T(1)	 T(4)	 B(4)					 T(5)	 B(5)	 T(3)	 T(2)

Test 1

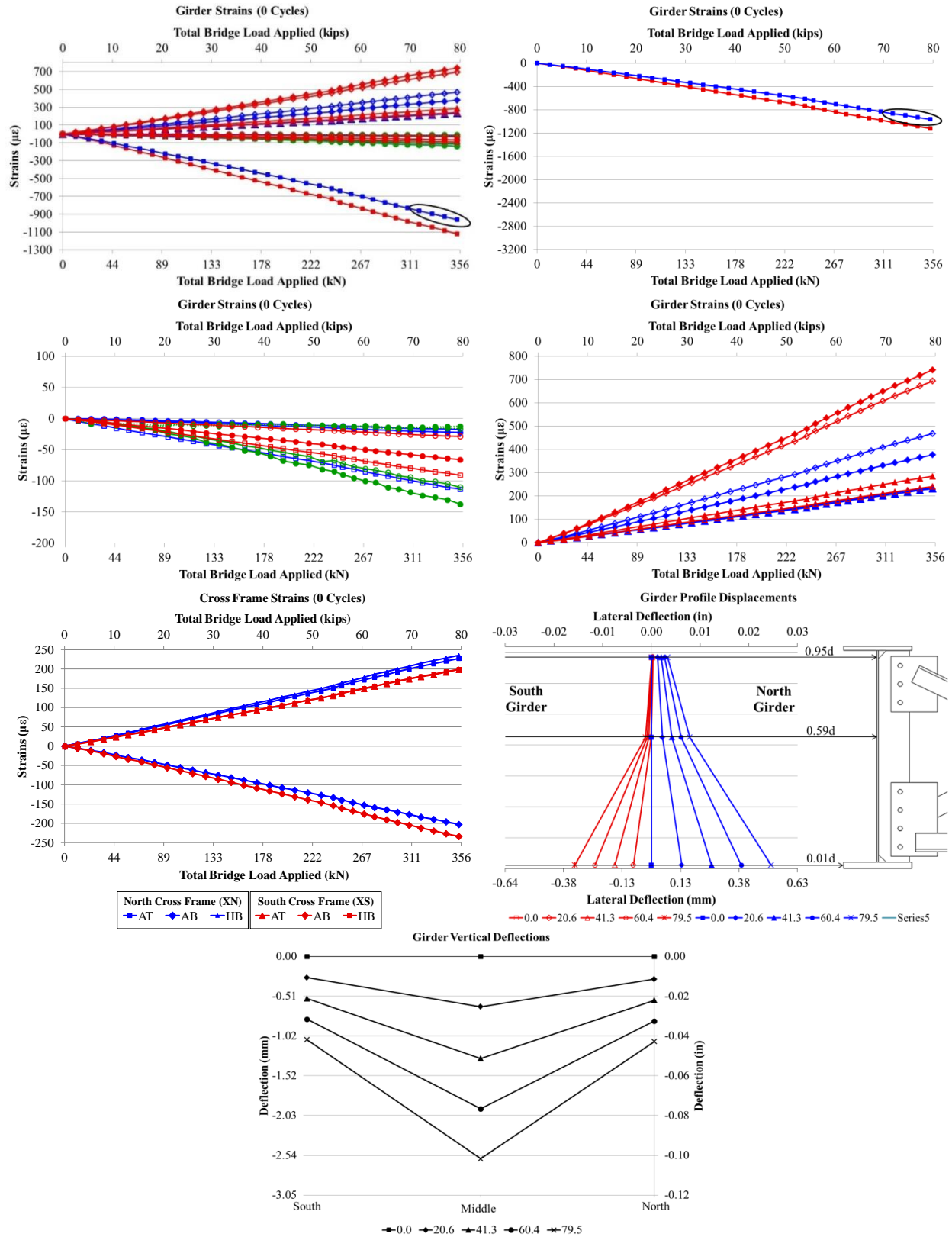


Figure E. 6: Static (0 Cycles) 5.24.2012

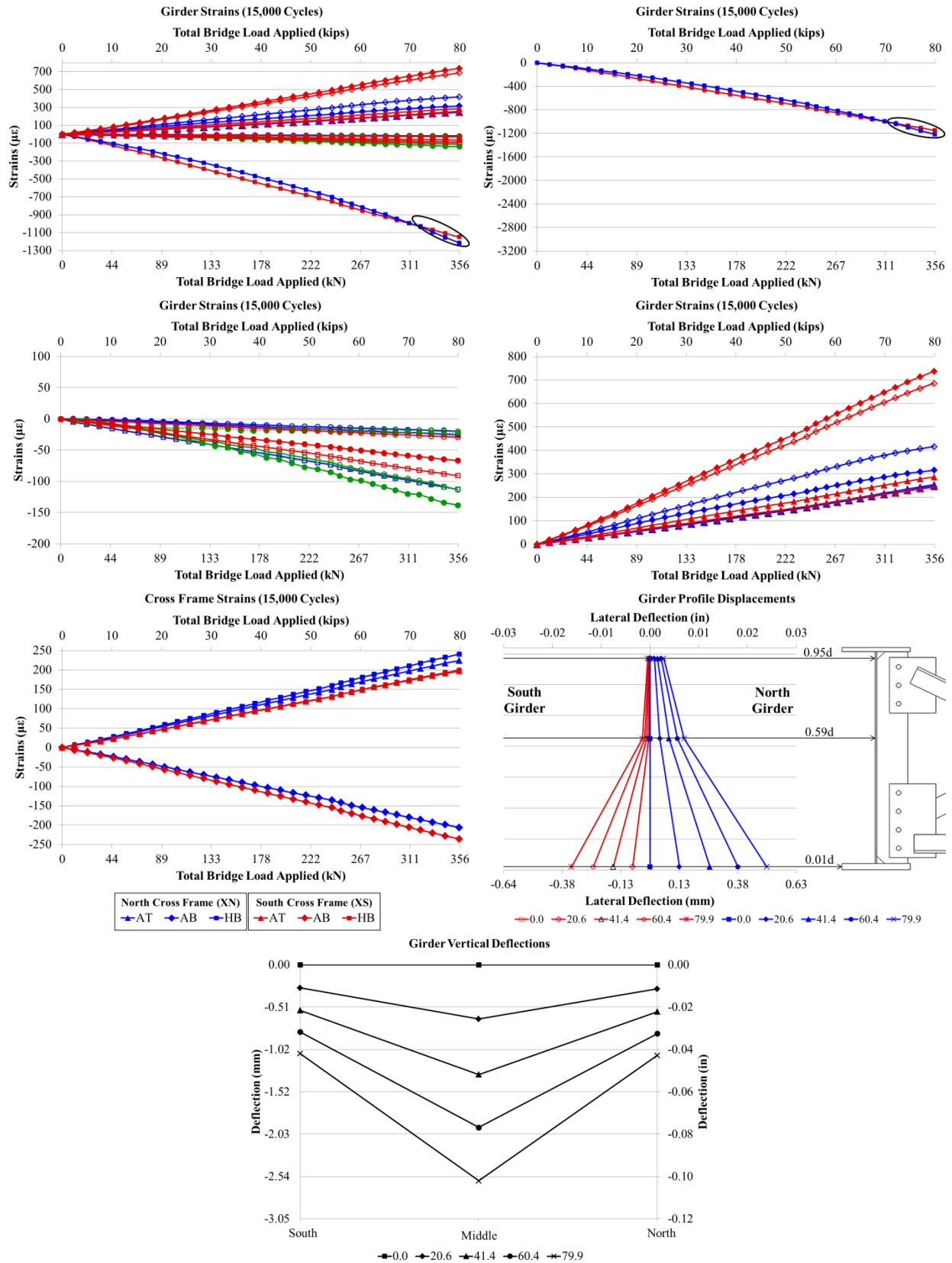


Figure E. 7: Static (15000 Cycles) 5.24.2012

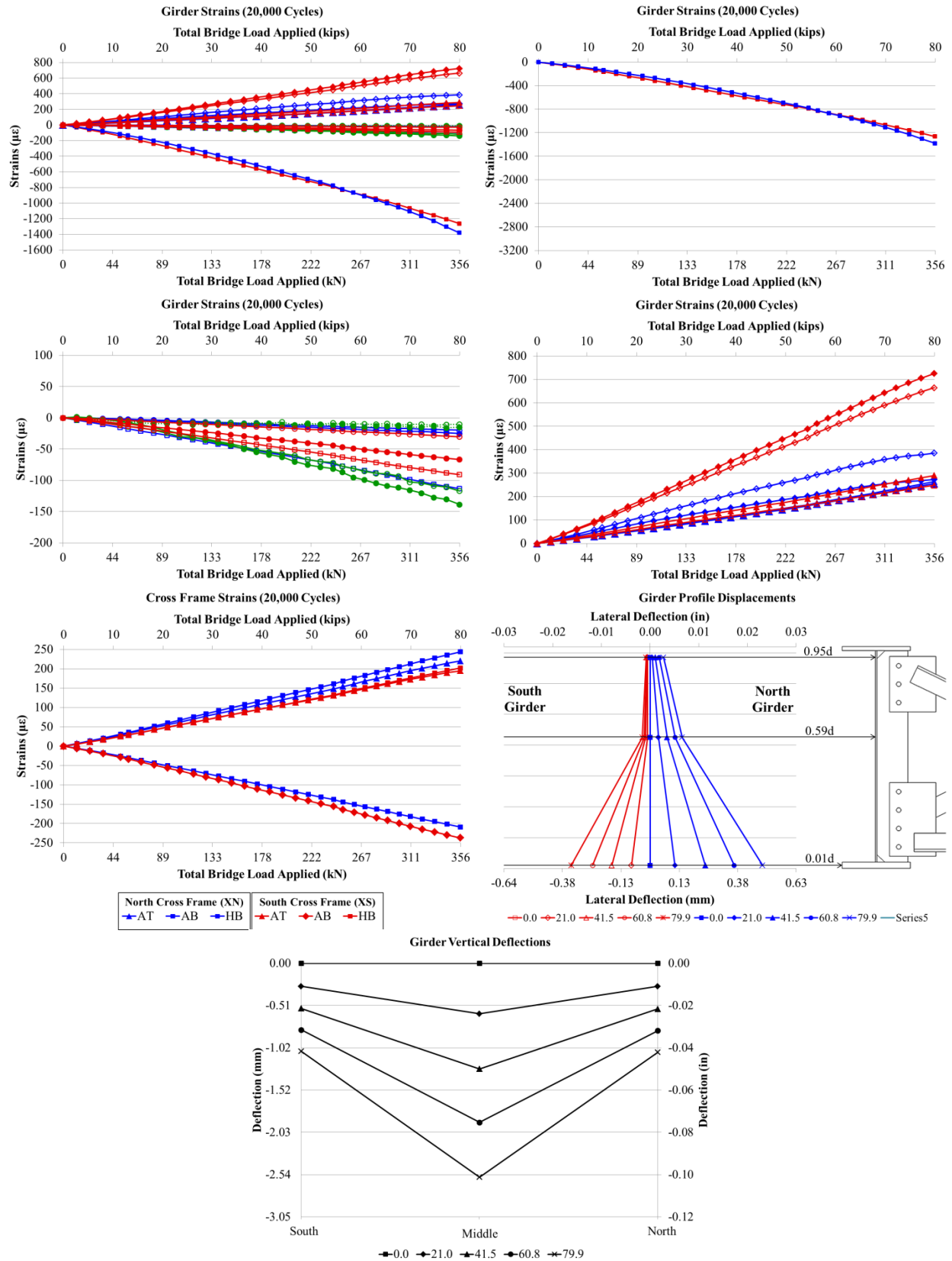


Figure E. 8: Static (20000 Cycles) 5.25.2012

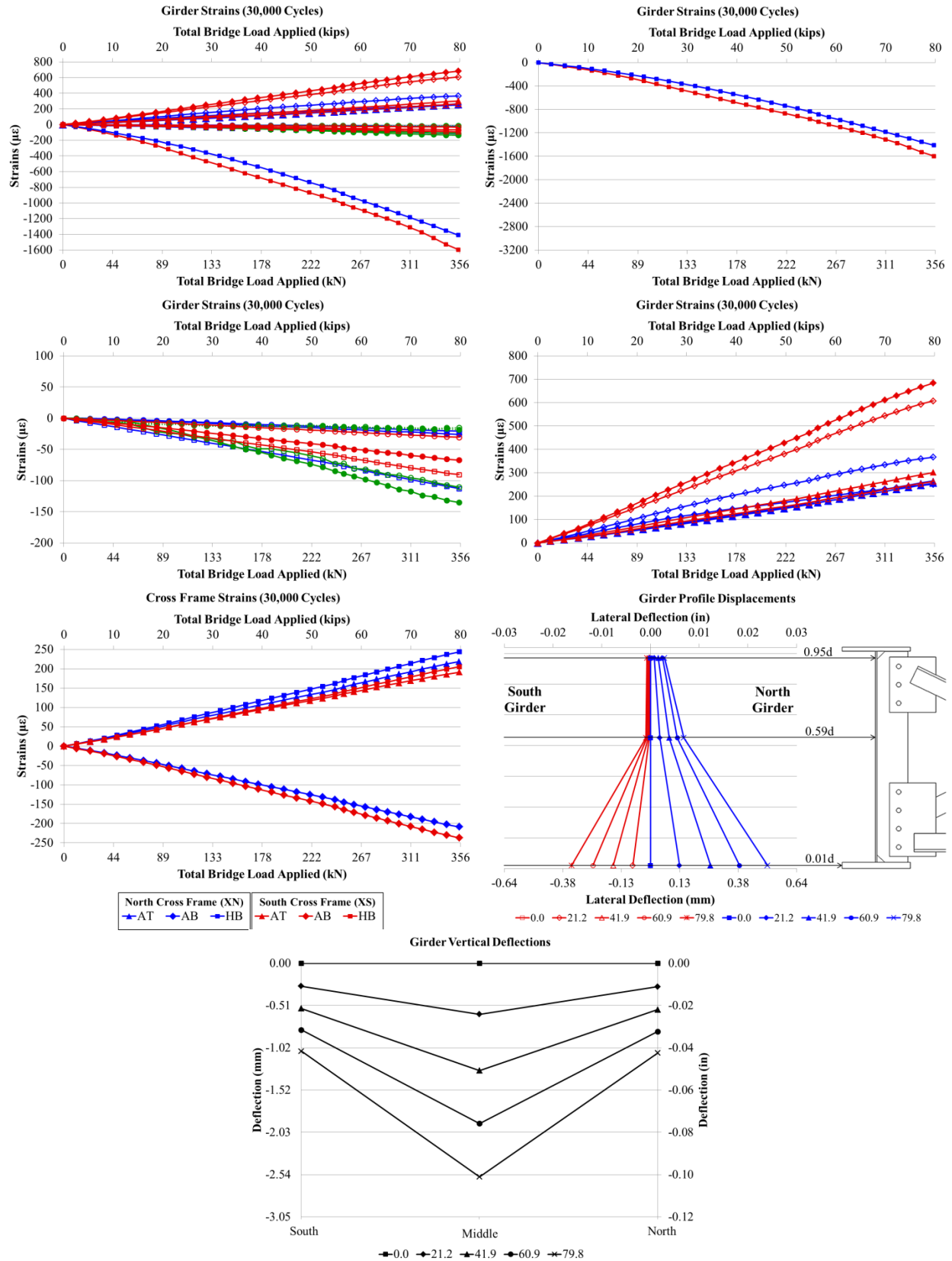


Figure E. 9: Static (30000 Cycles) 5.29.2012

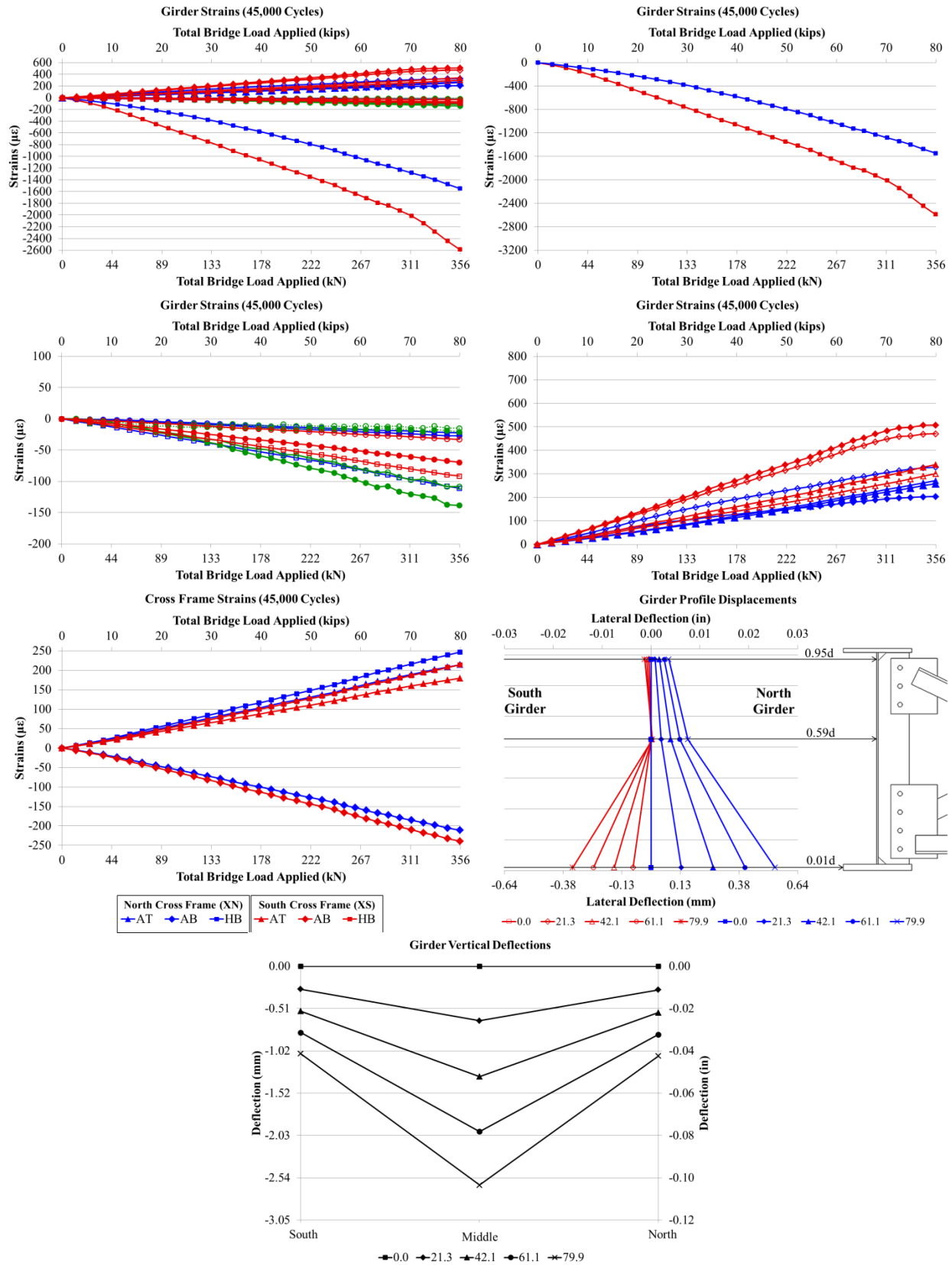


Figure E. 10: Static (45000 Cycles) 5.31.2012

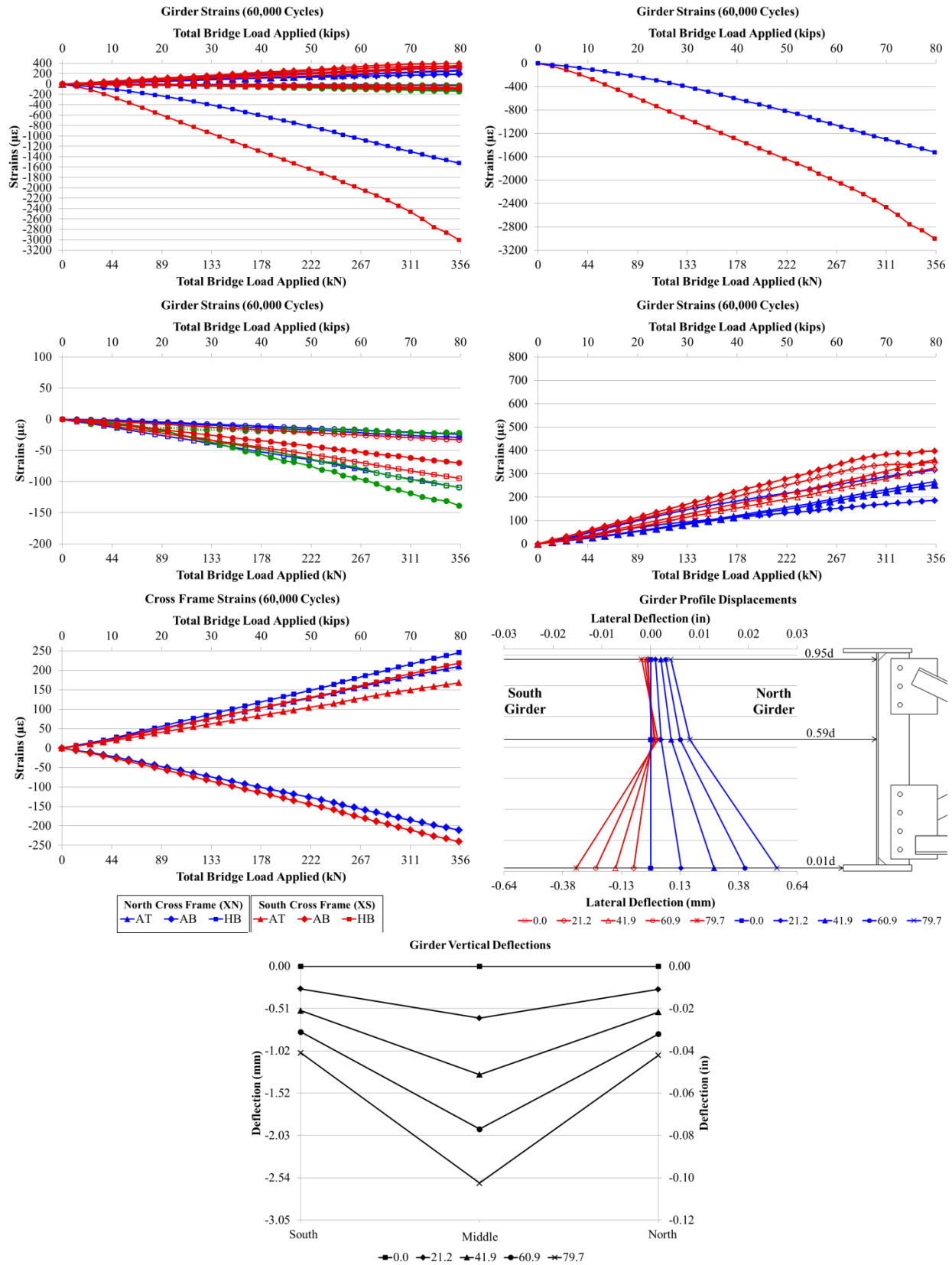


Figure E. 11: Static (60000 Cycles) 5.31.2012

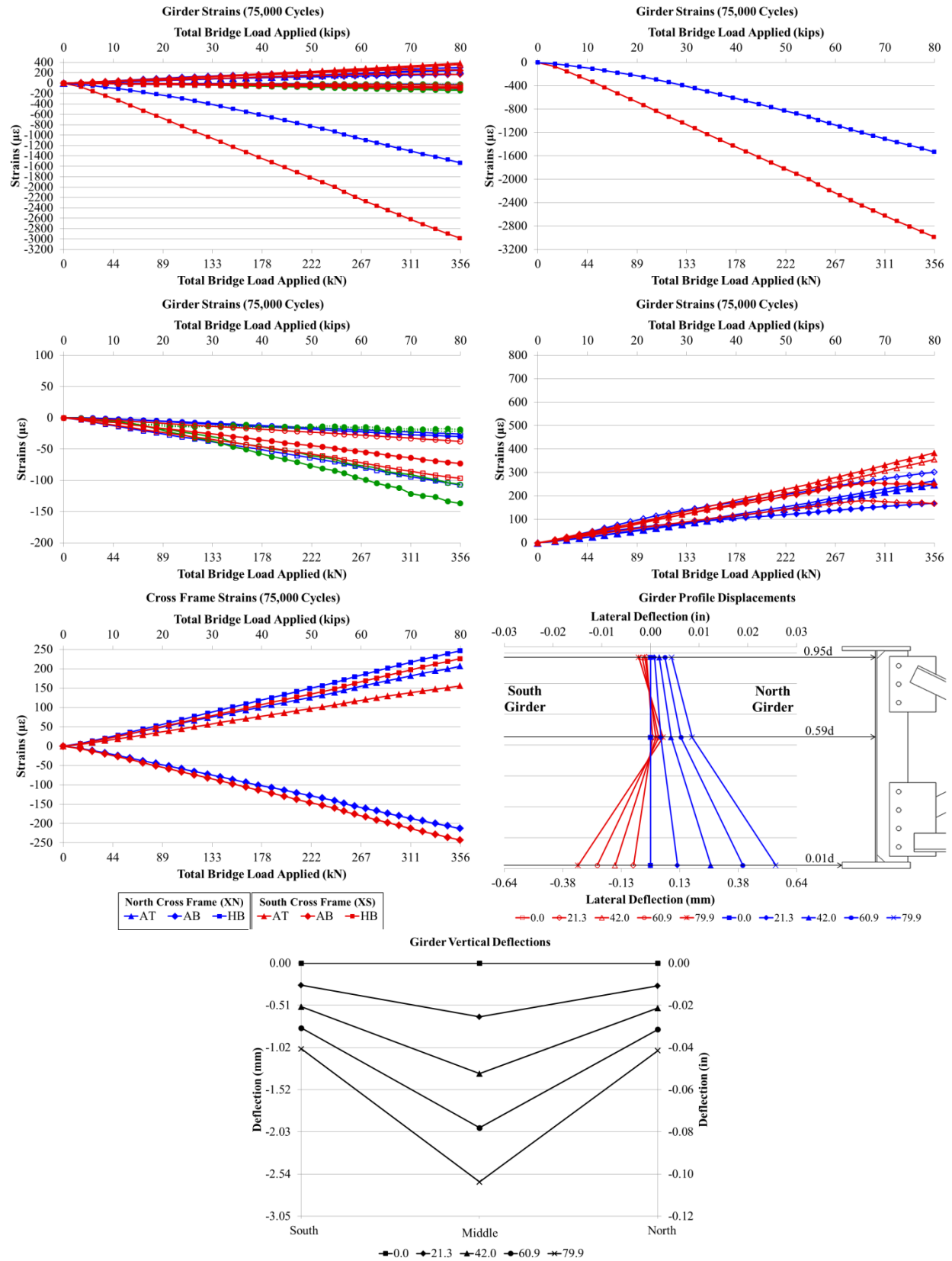


Figure E. 12: Static (75000 Cycles) 6.01.2012

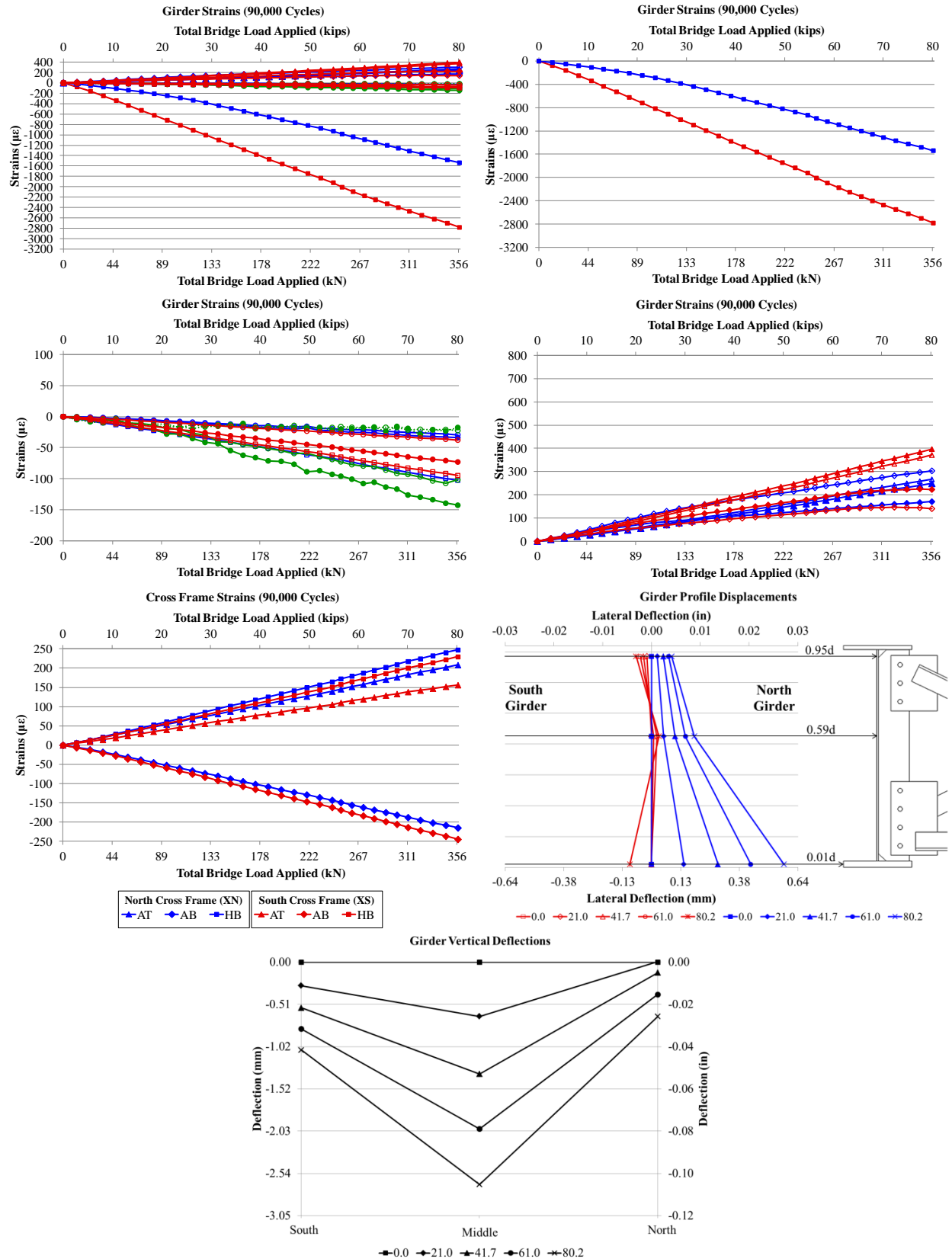


Figure E. 13: Static (90000 Cycles) 6.04.2012

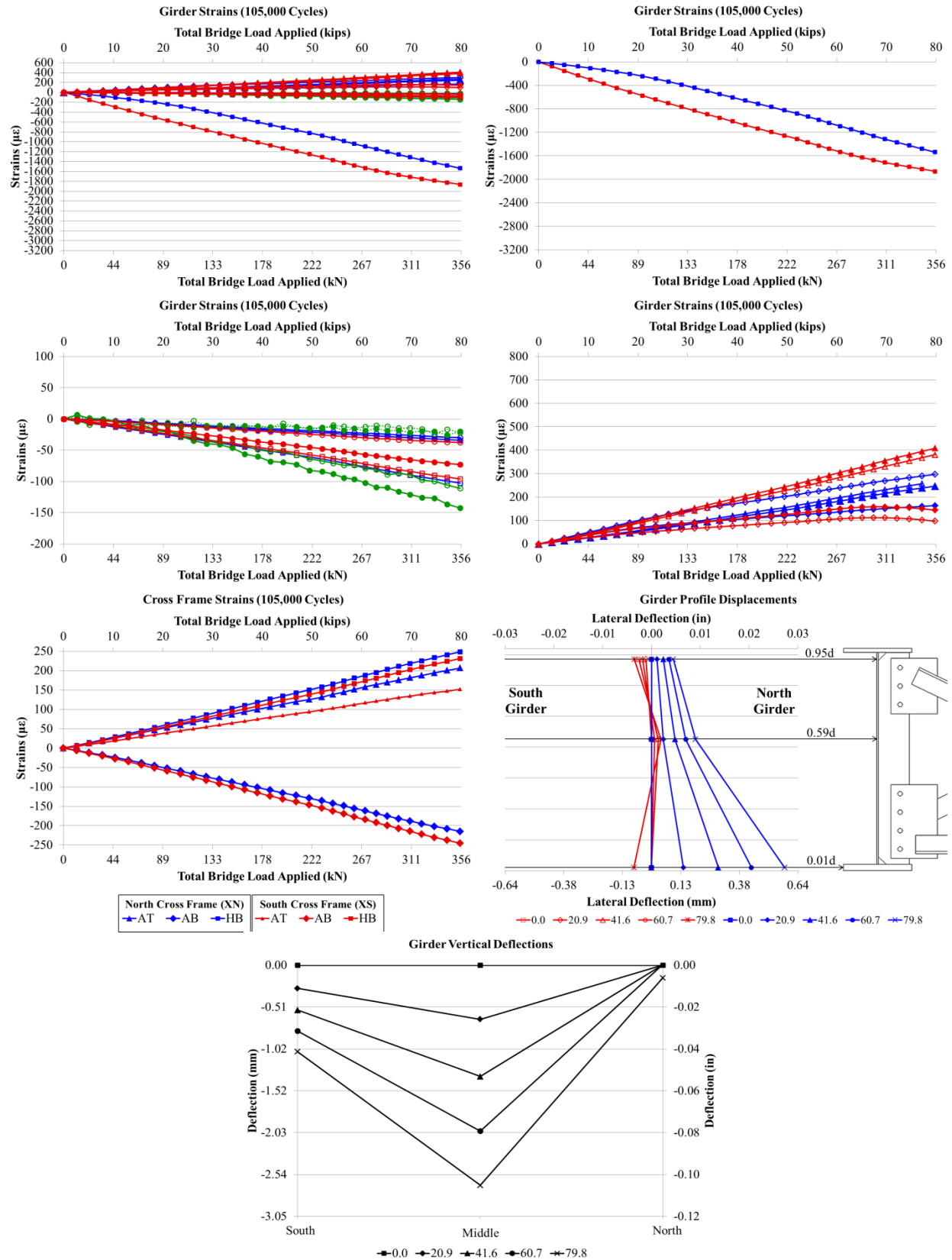


Figure E. 14: Static (105000 Cycles) 6.05.2012

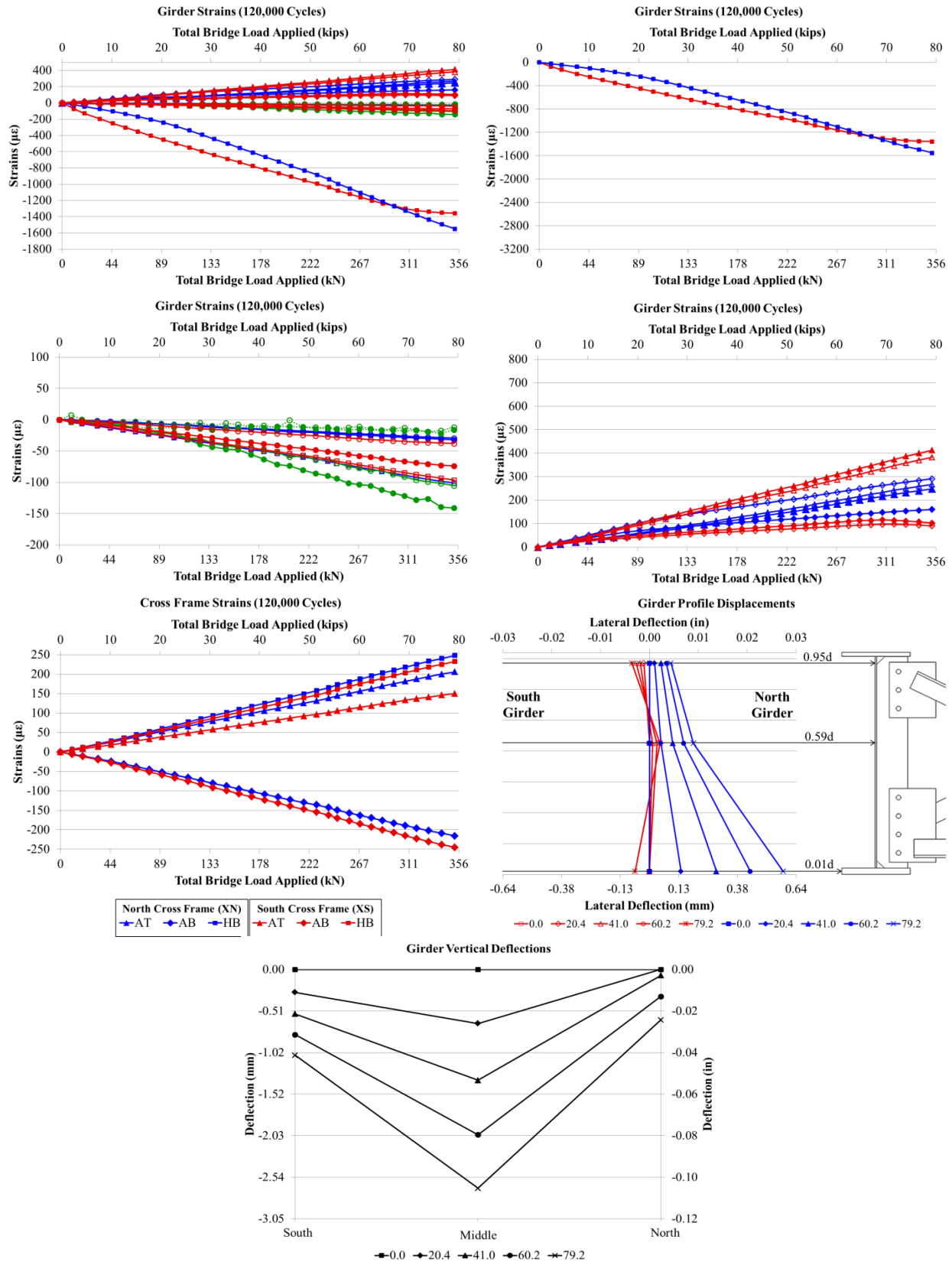


Figure E. 15: Static (120000 Cycles) 6.06.2012

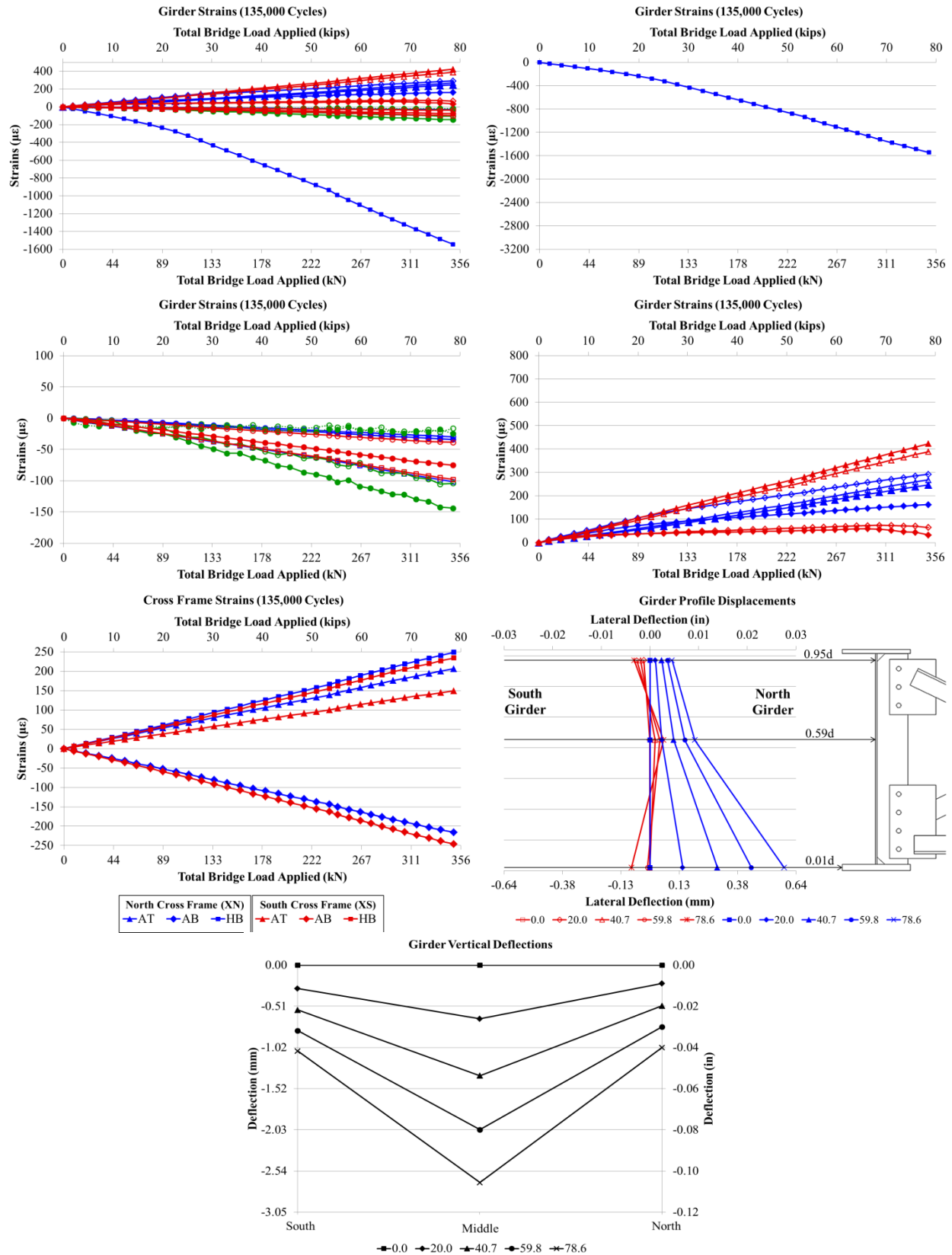


Figure E. 16: Static (135000 Cycles) 6.06.2012

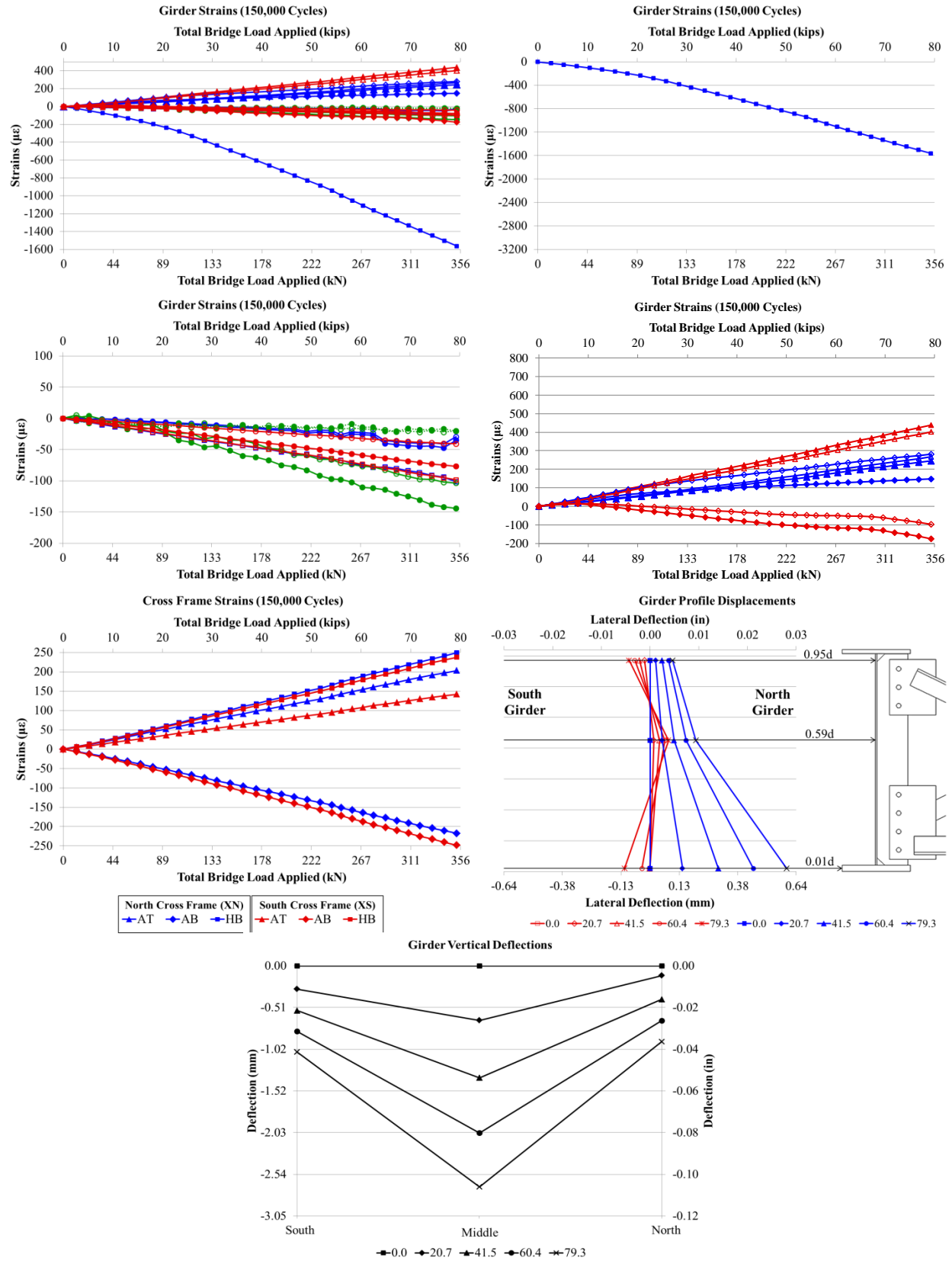


Figure E. 17: Static (150000 Cycles) 6.07.2012

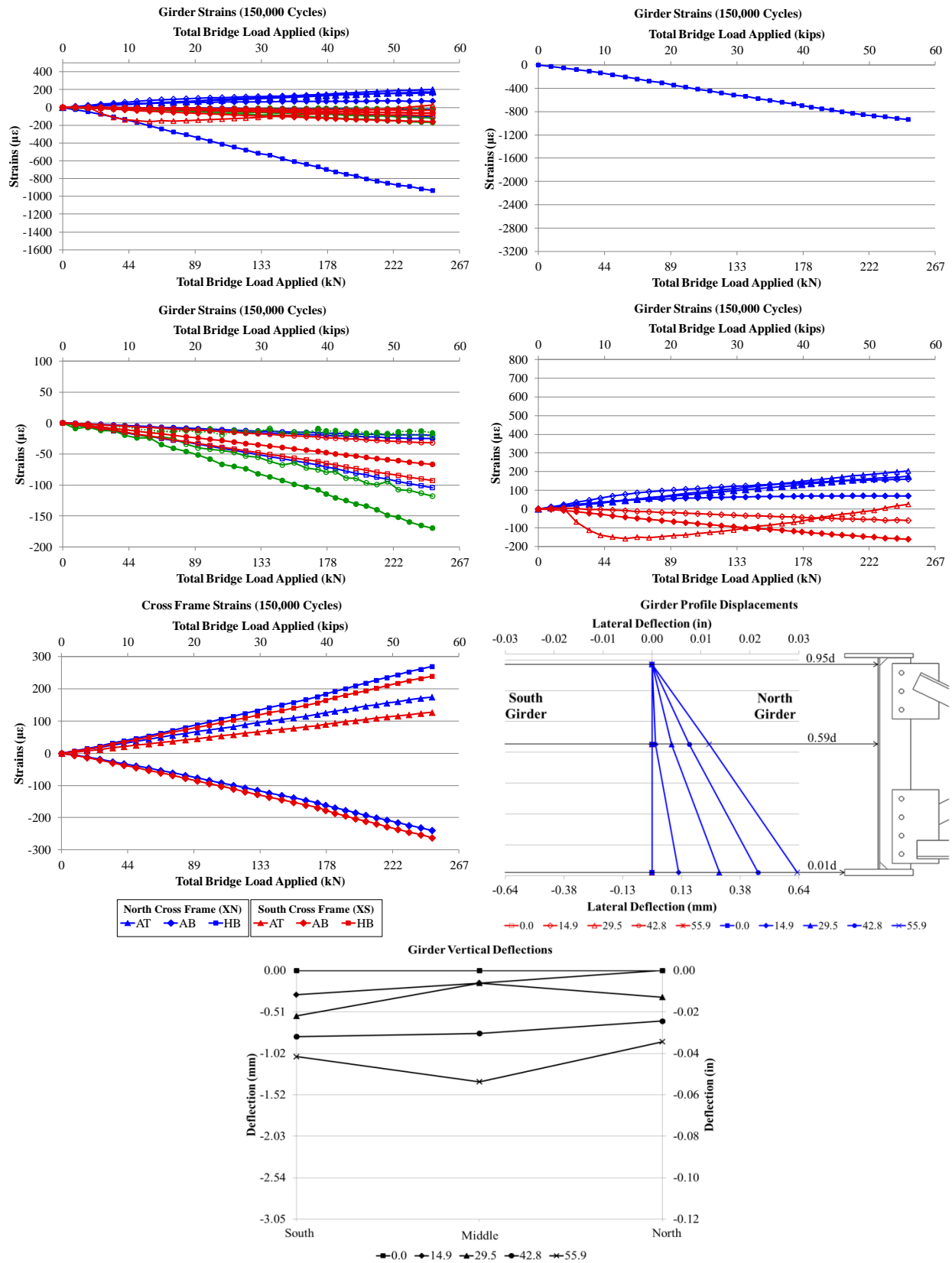


Figure E. 18: Static (150000 Cycles) 7.24.2012

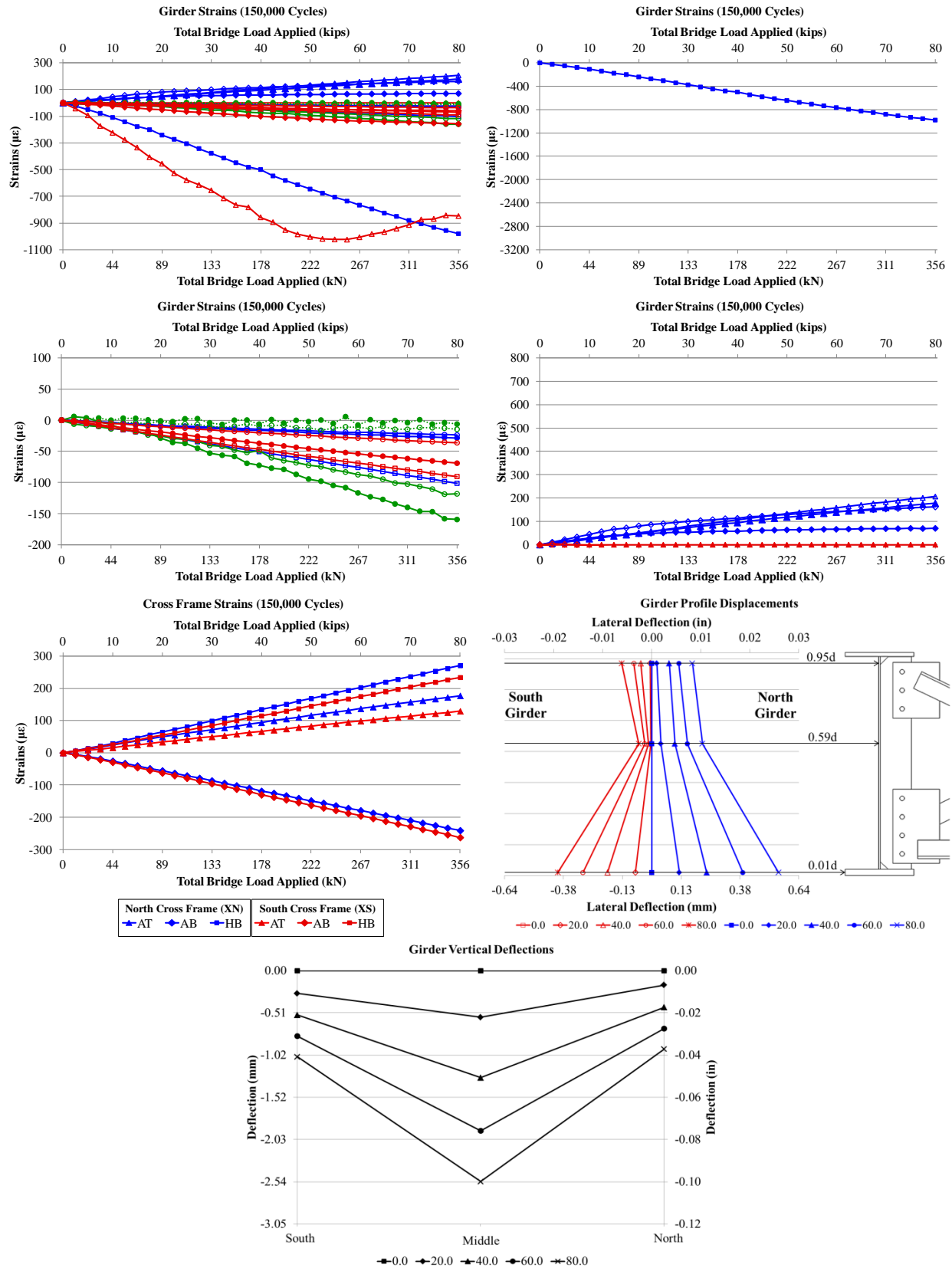


Figure E. 19: Static (150000 Cycles) 09.18.2012 - Without Retrofit

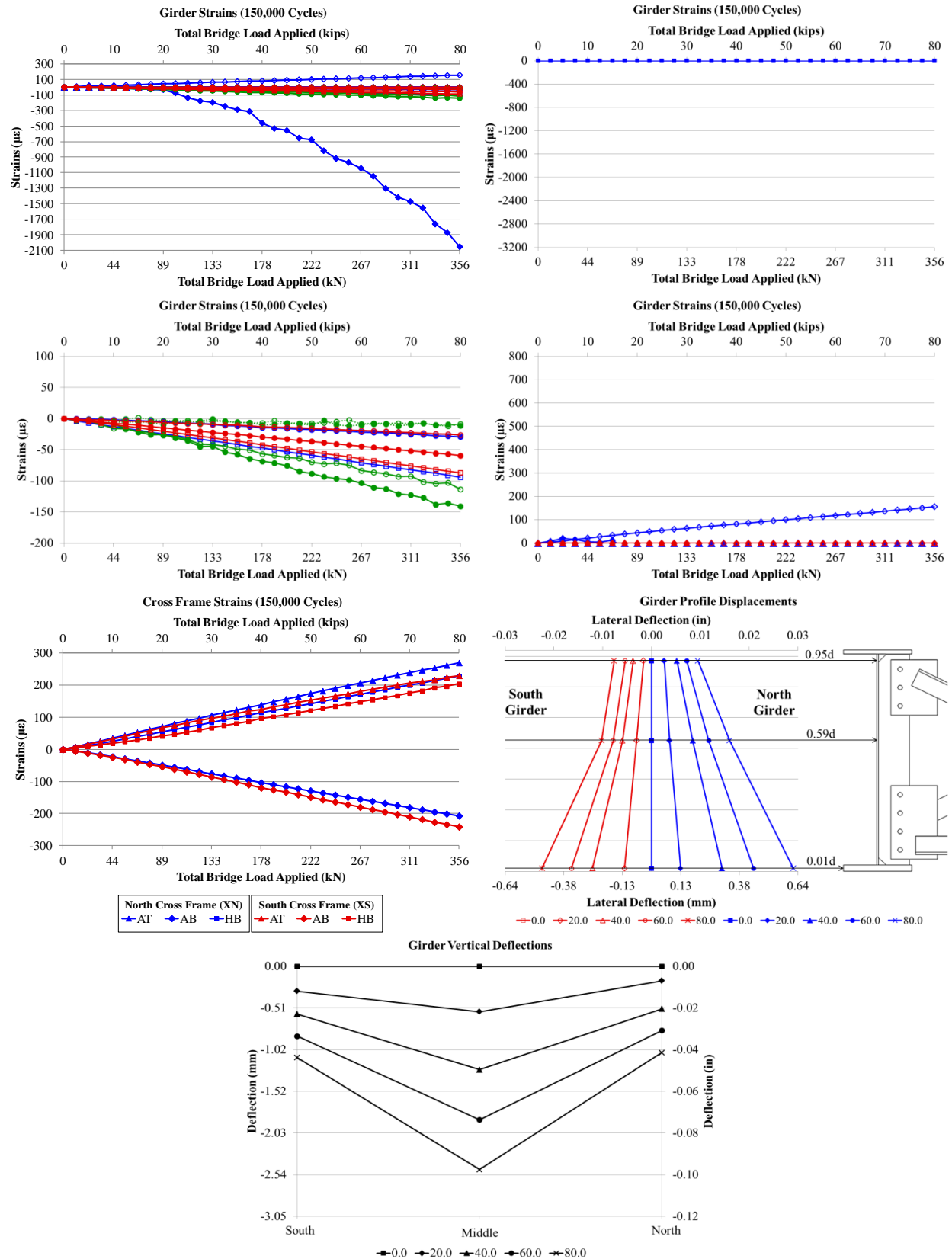


Figure E. 20: Static (150000 Cycles) 9.27.2012 – With Retrofit

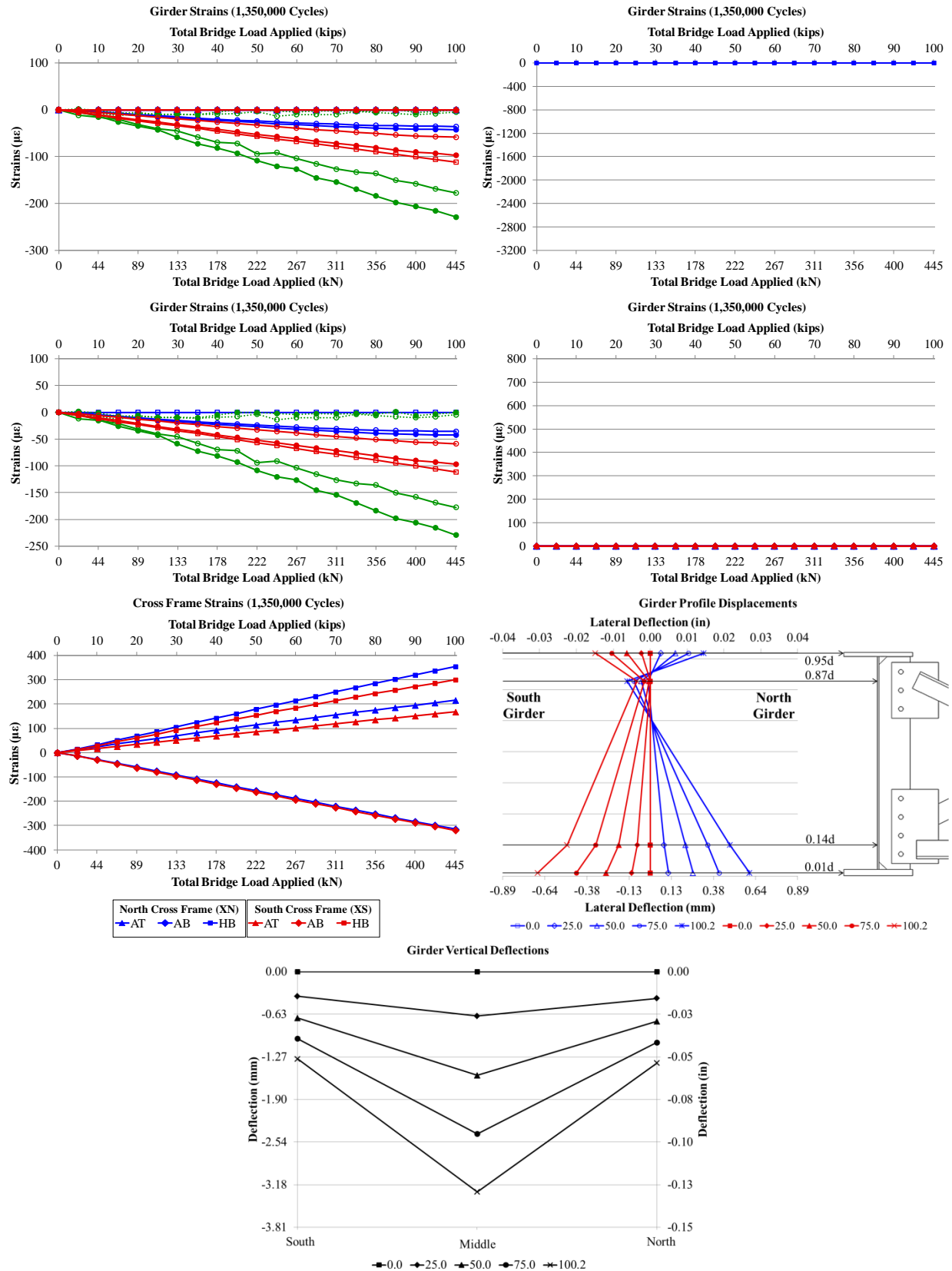


Figure E. 21: Static (1350000 Cycles) 12.07.2012– Without Retrofit

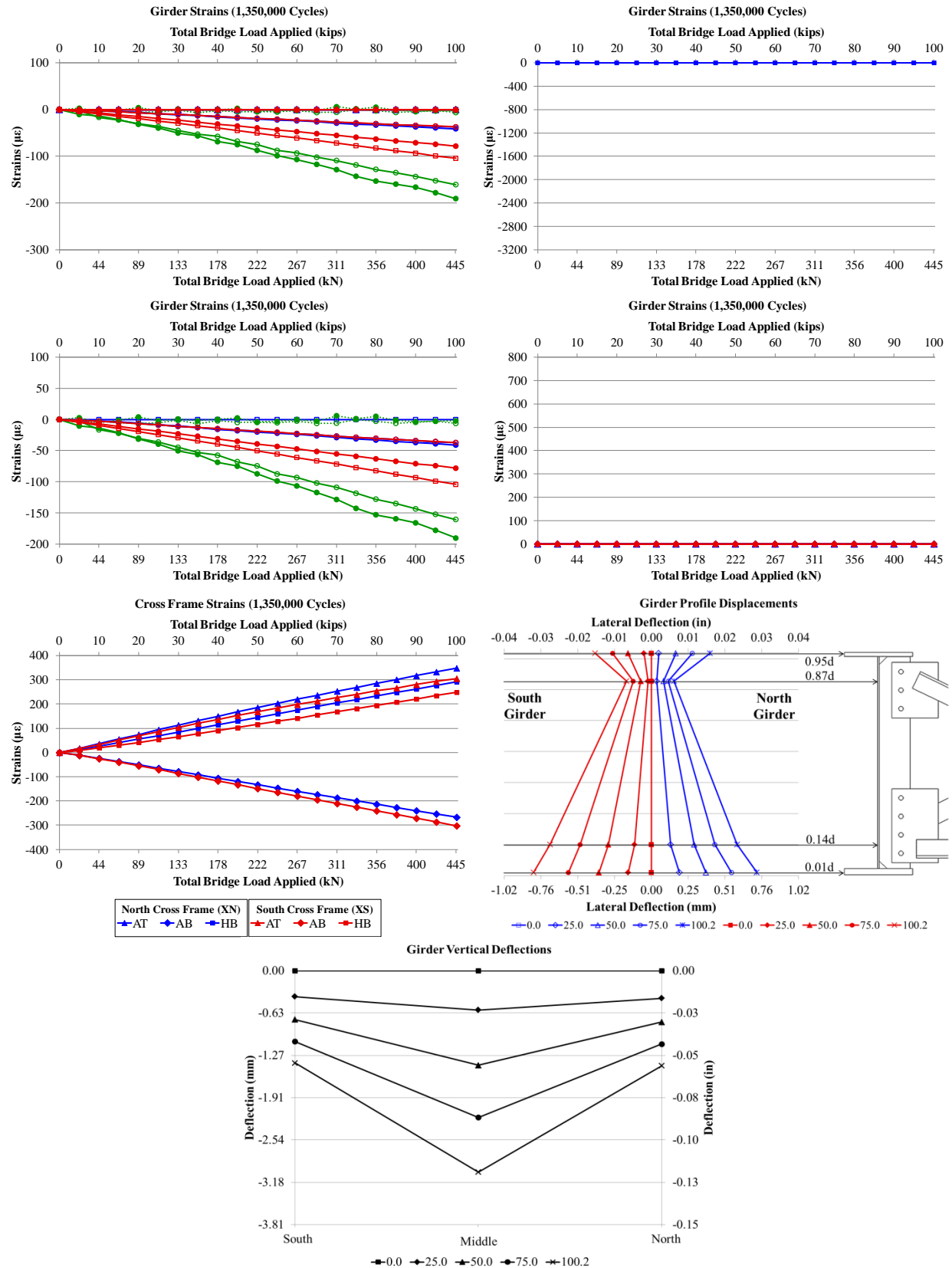


Figure E. 22: Static (1350000 Cycles) 12.07.2012 – With Retrofit

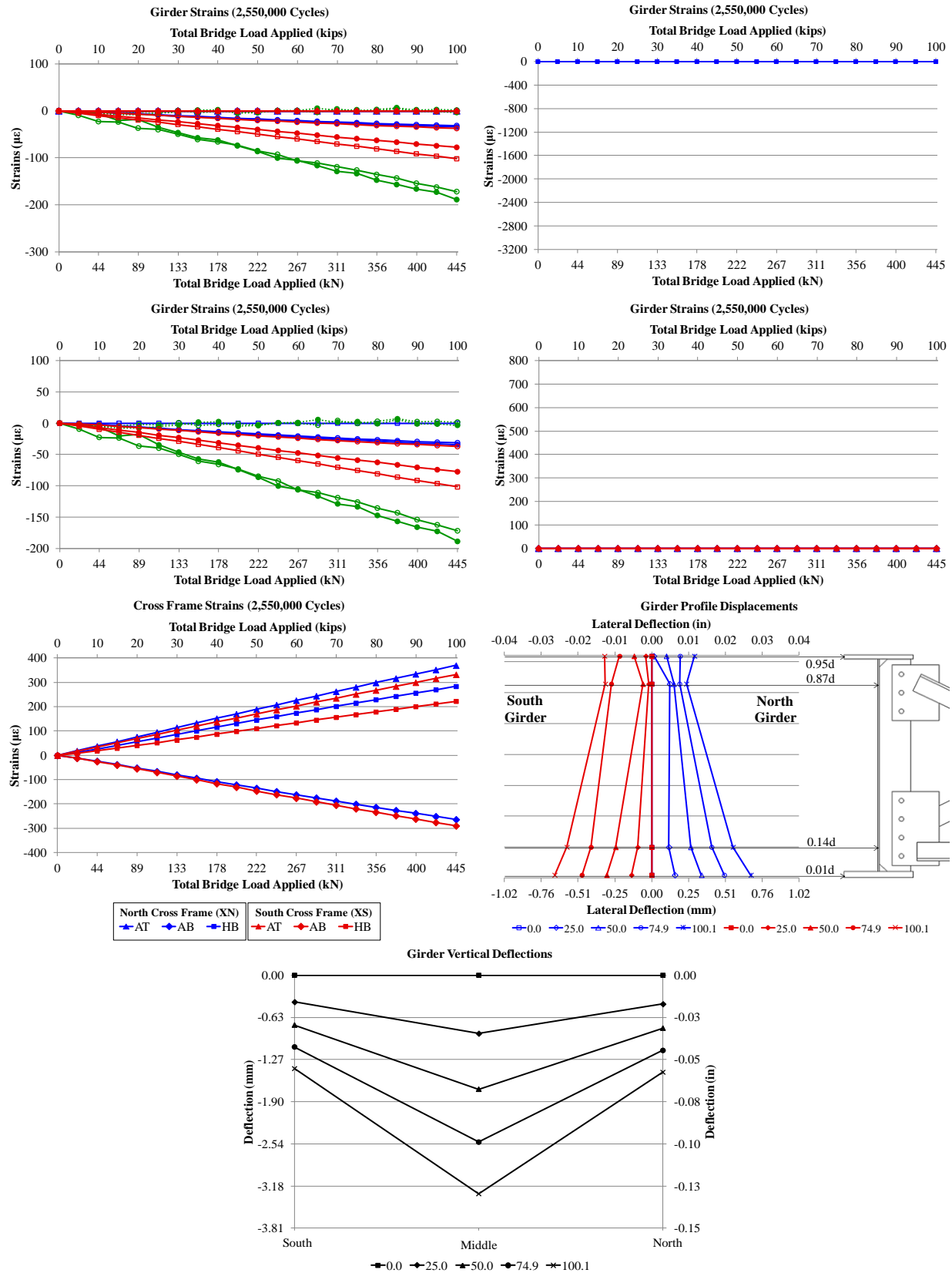


Figure E. 23: Static (2550000 Cycles) 12.21.2012 – With Retrofit

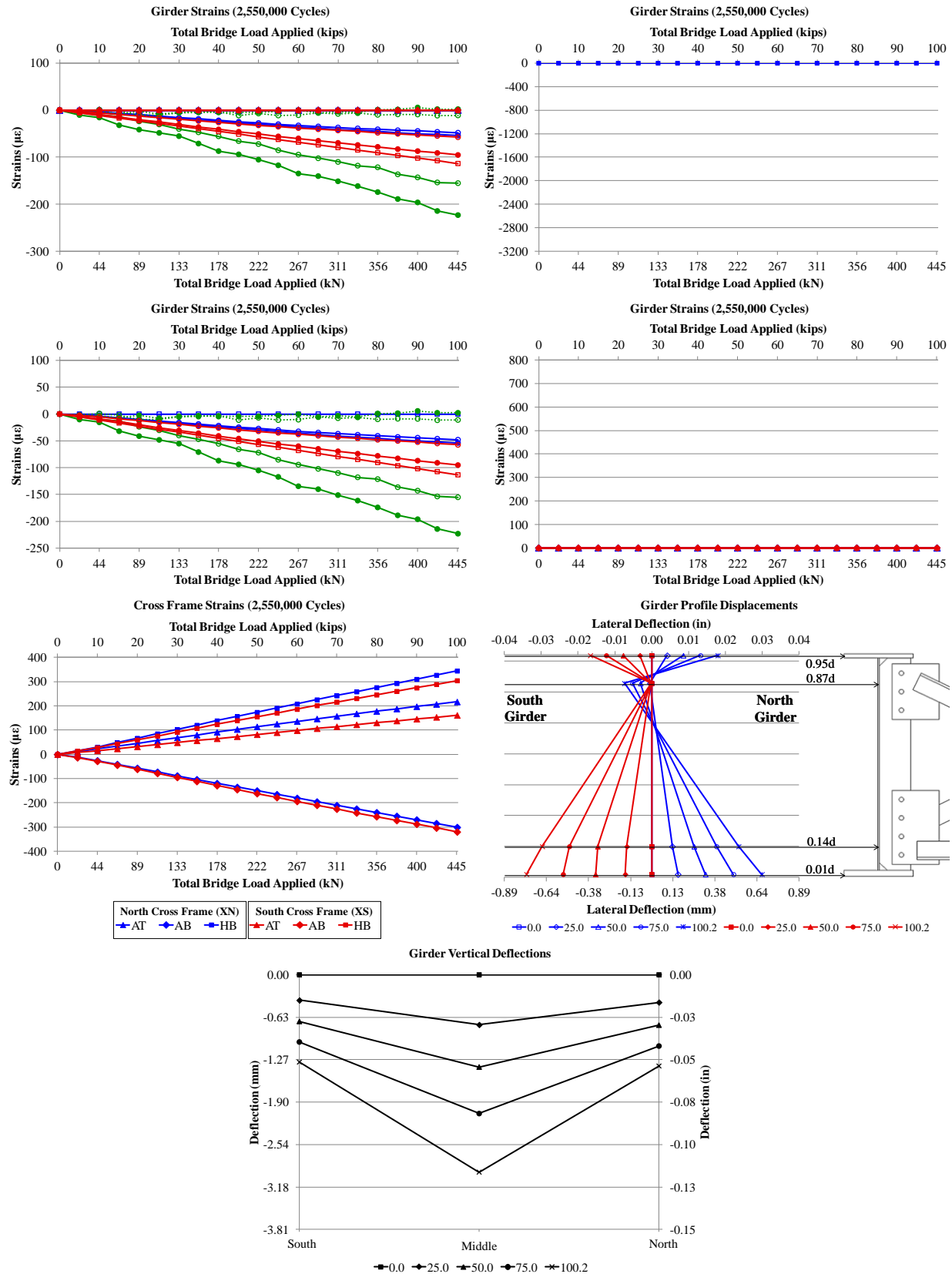


Figure E. 24: Static (2550000 Cycles) 12.21.2012 – Without Retrofit

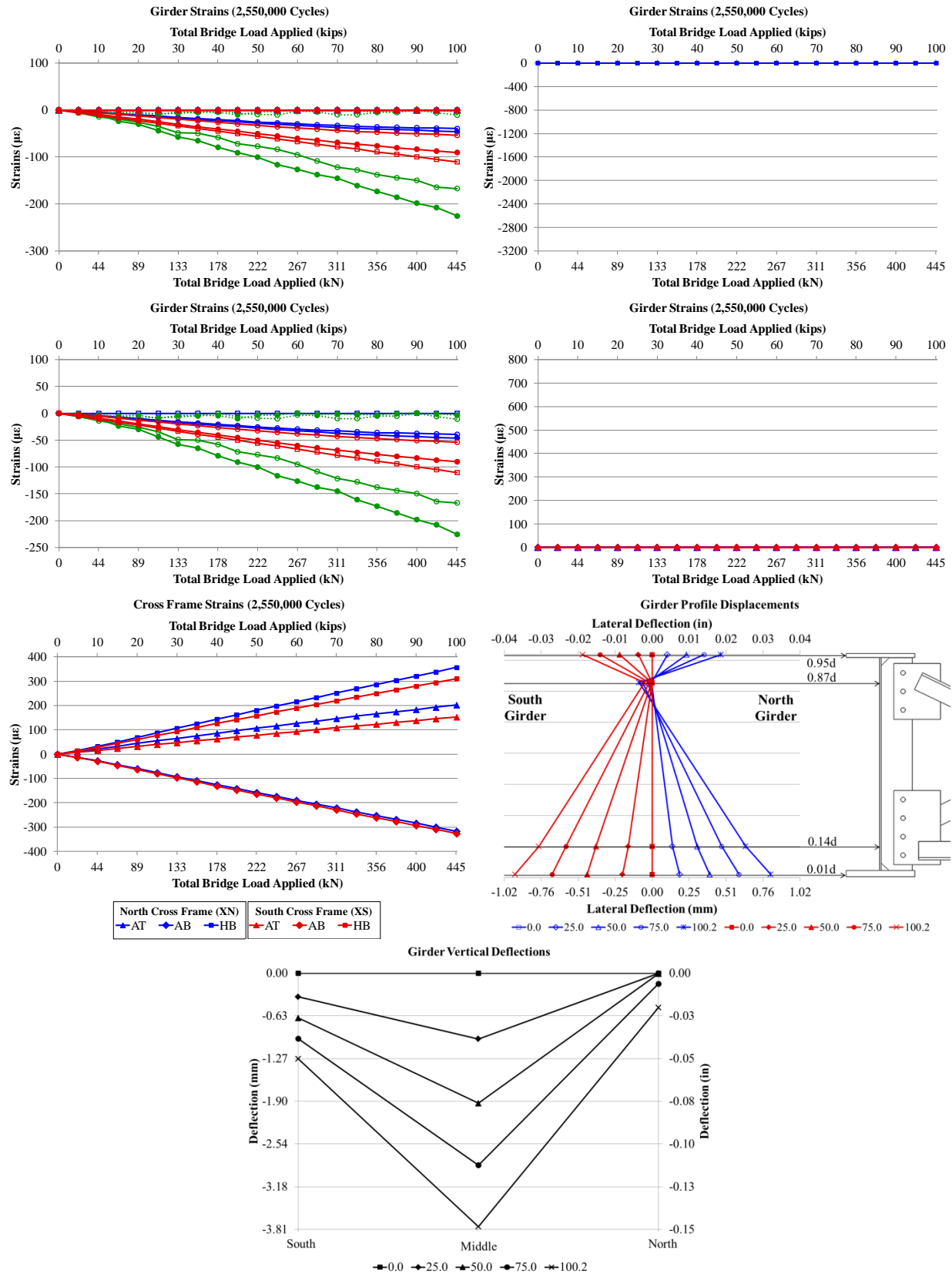


Figure E. 25: Static (2550000 Cycles) 01.03.2013 - Without Retrofit Drilled Holes

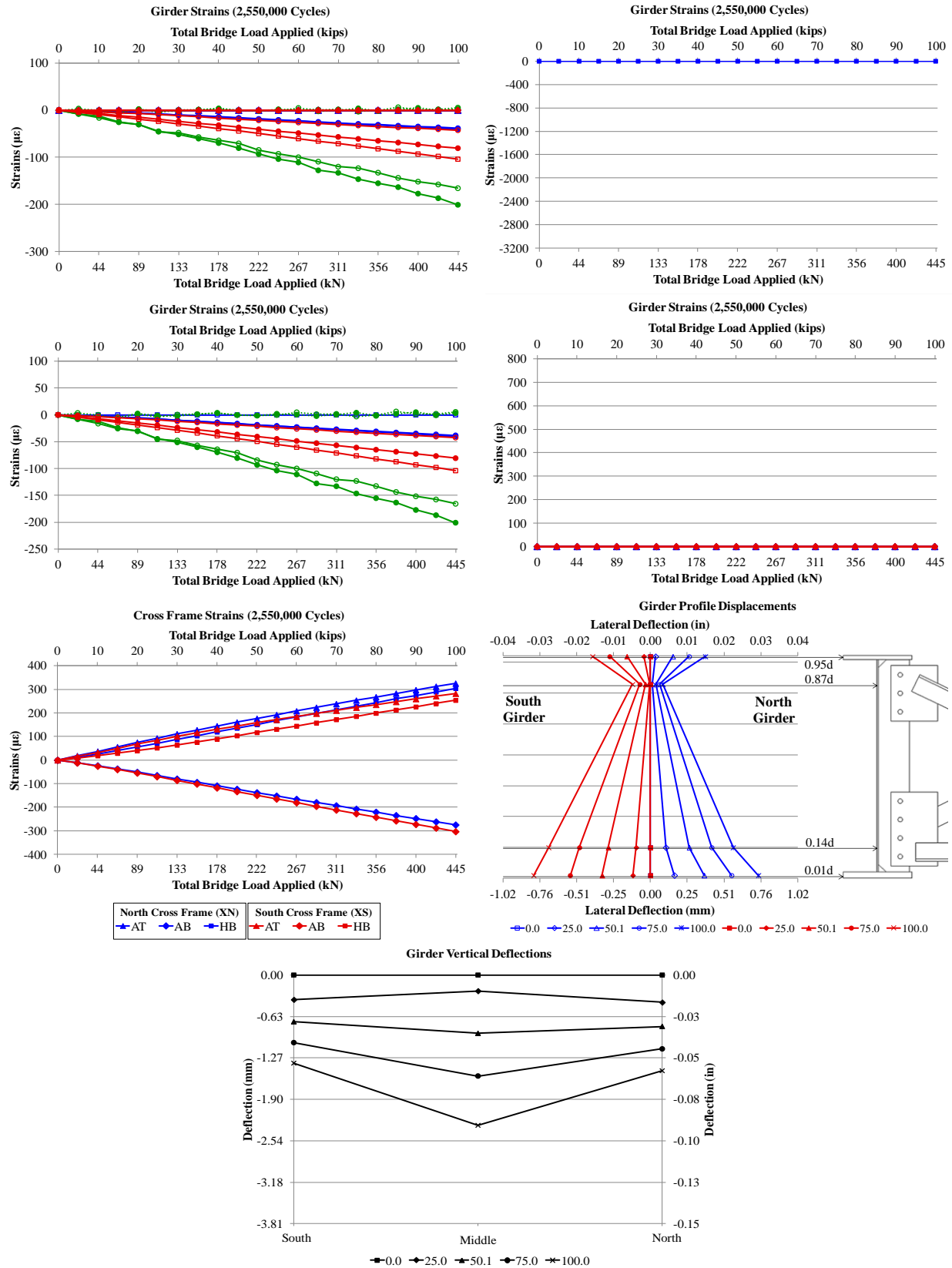


Figure E. 26: Static (2550000 Cycles) 01.04.2013 - With Retrofit Drilled Holes

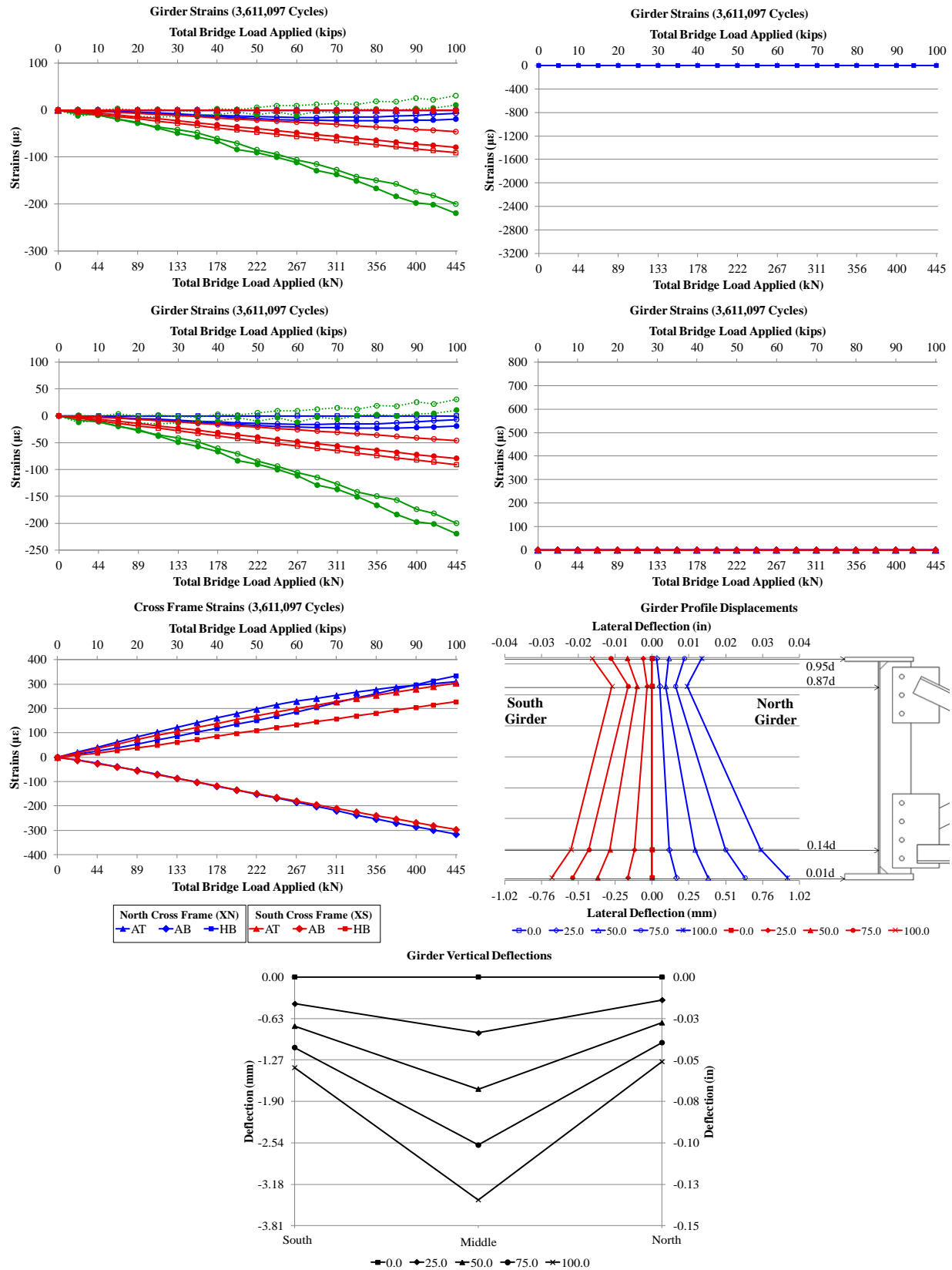


Figure E. 27: Static (3611097 Cycles) 01.17.2013 - With Retrofit Cracked Cross Frame Drilled Holes

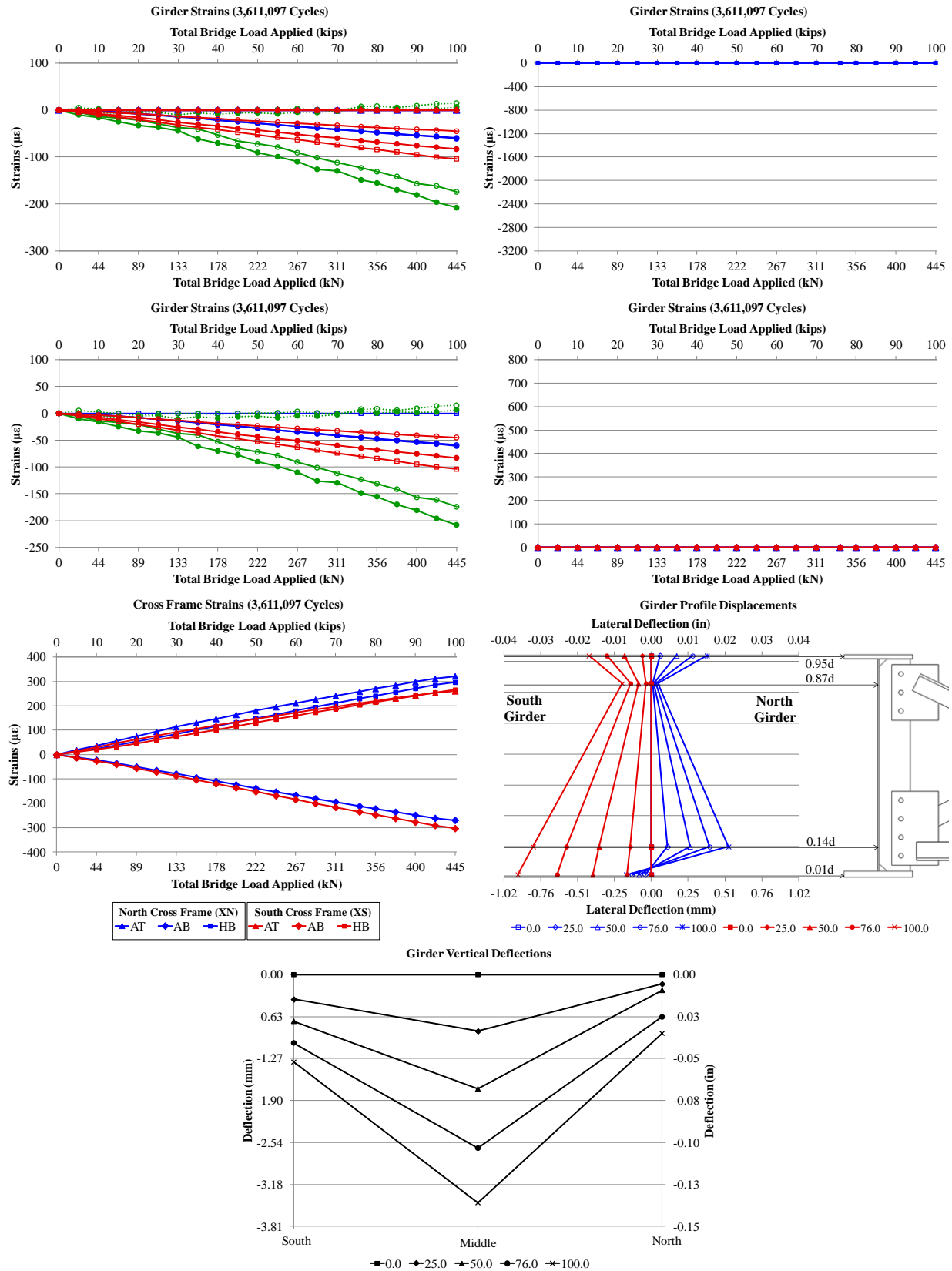


Figure E. 28: Static (3611097 Cycles) 01.22.2013- With Retrofit New Crossframe 0.5in Hole

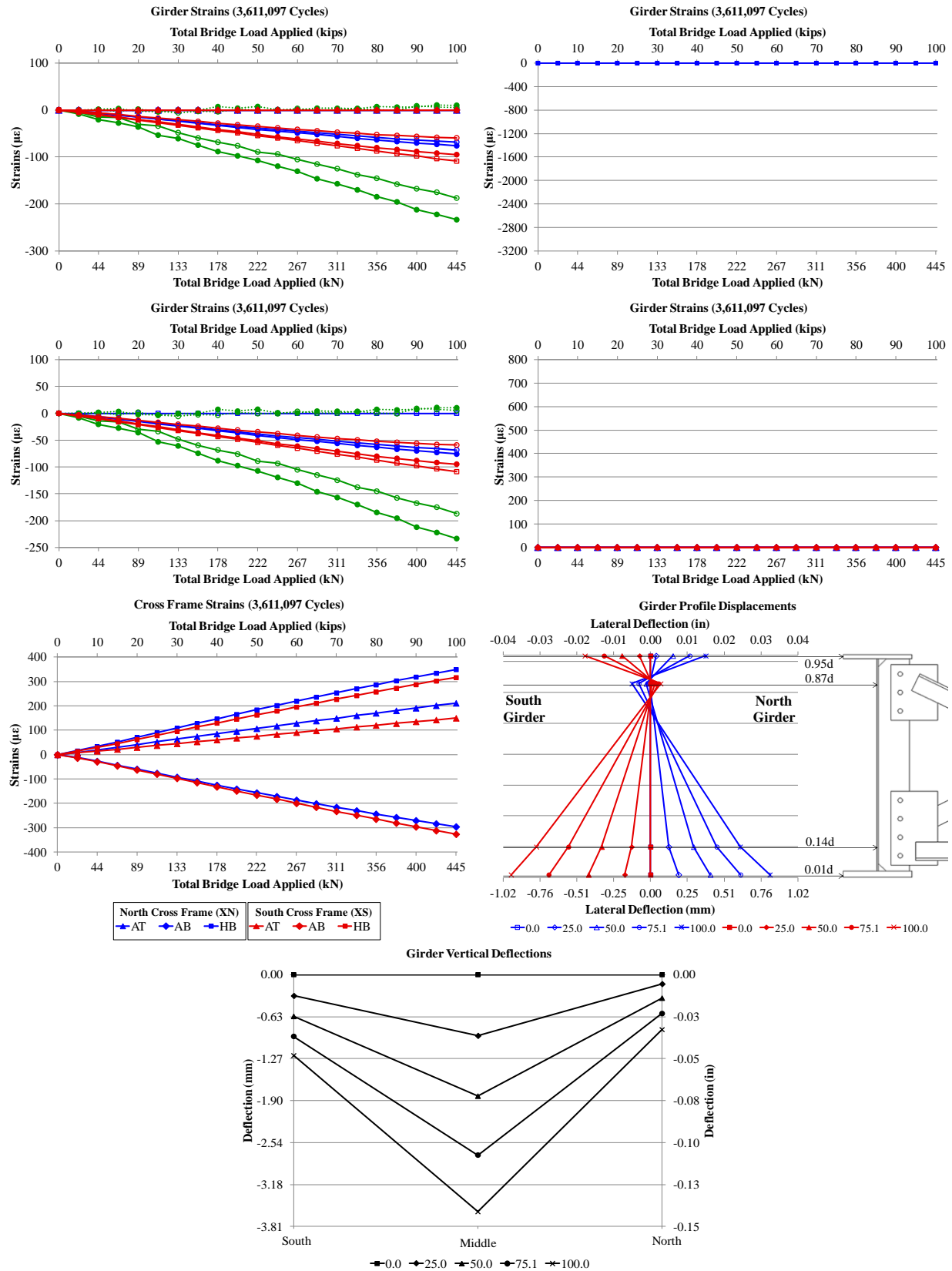


Figure E. 29: Static (3611097 Cycles) 01.22.2013 - Without Retrofit New Crossframe 0.5in Hole

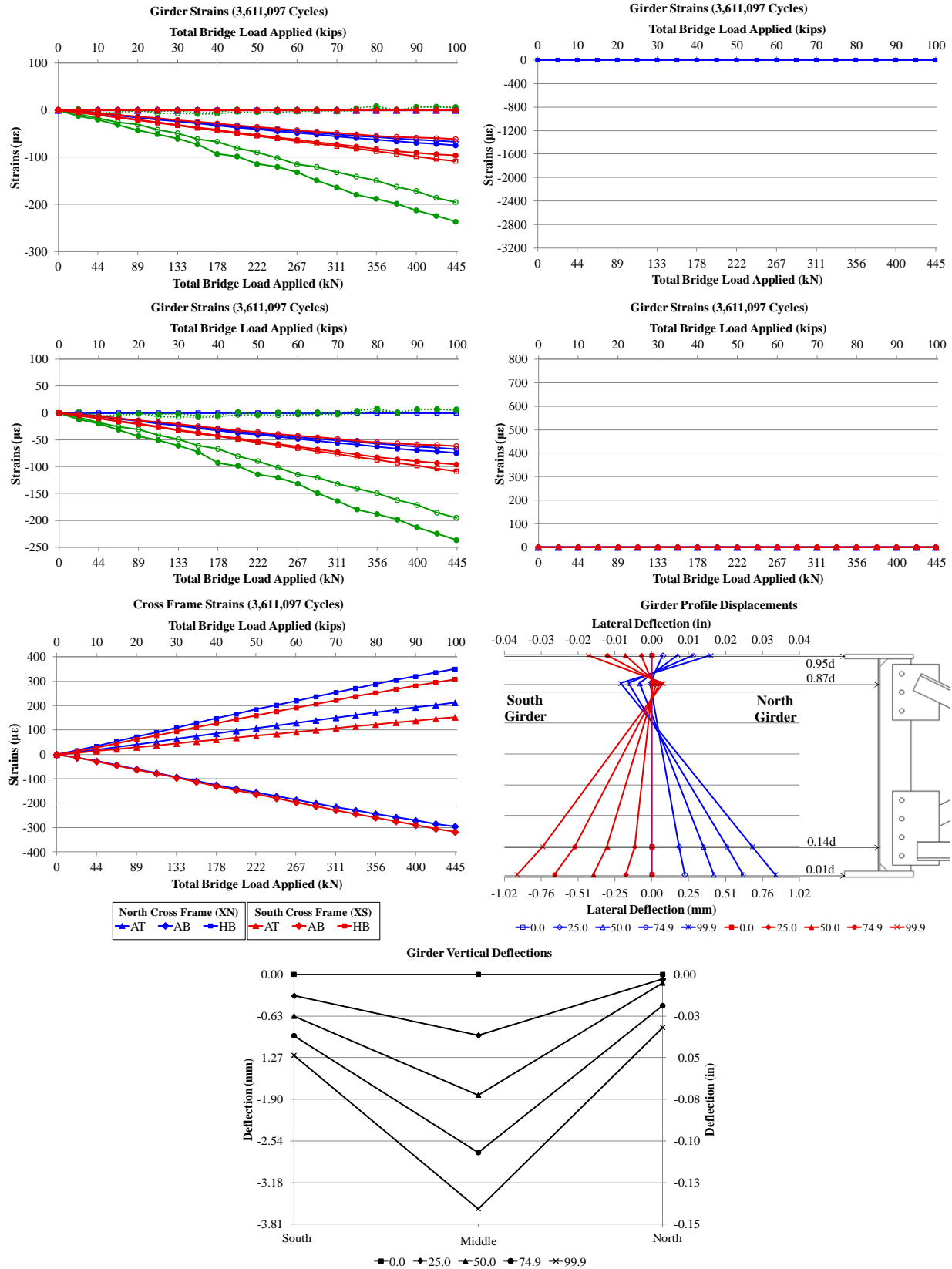


Figure E. 30: Static (3611097 Cycles) 01.22.2013 - Without Retrofit New Crossframe

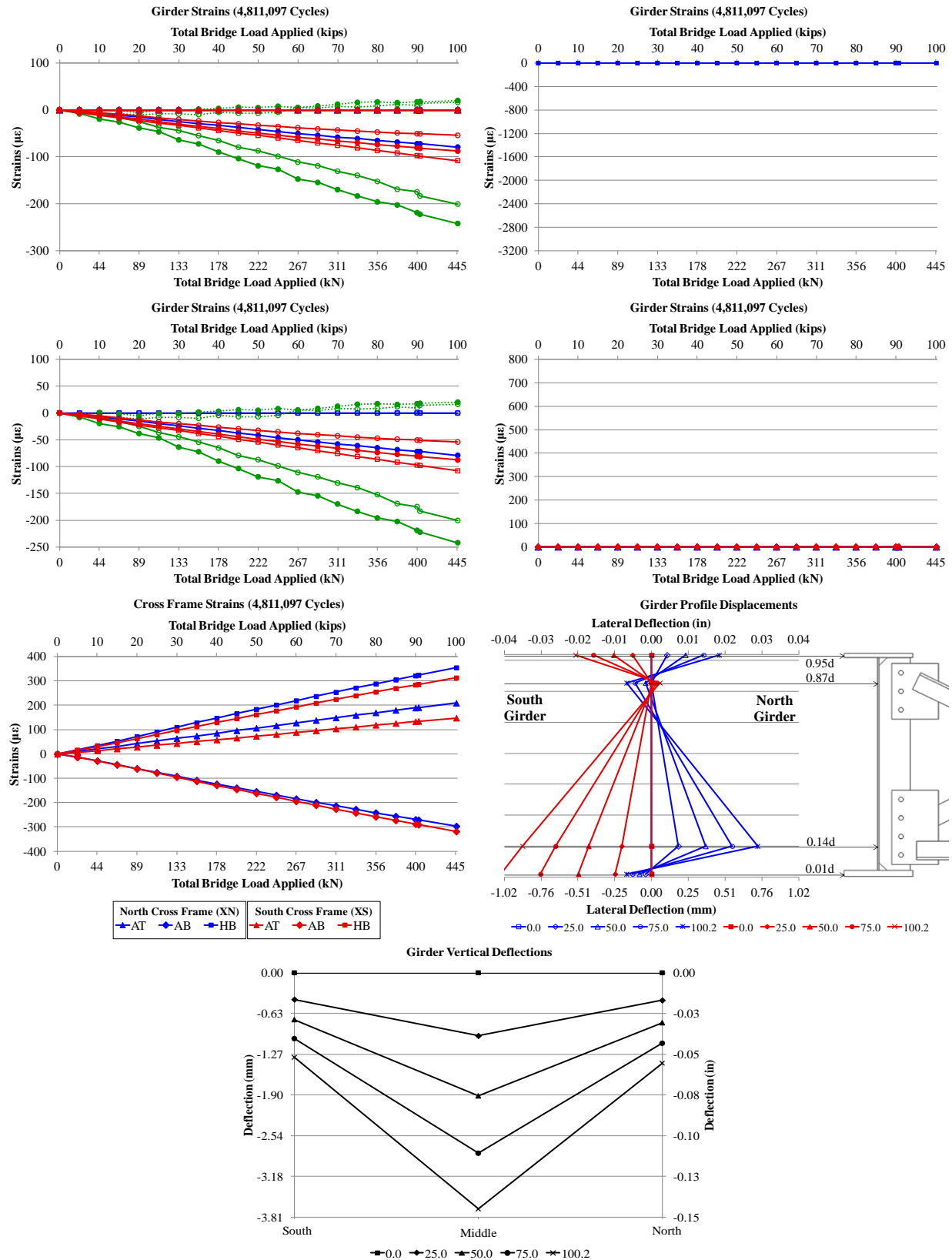


Figure E. 31: Static (4811097 Cycles) 02.15.2013 - Without Retrofit

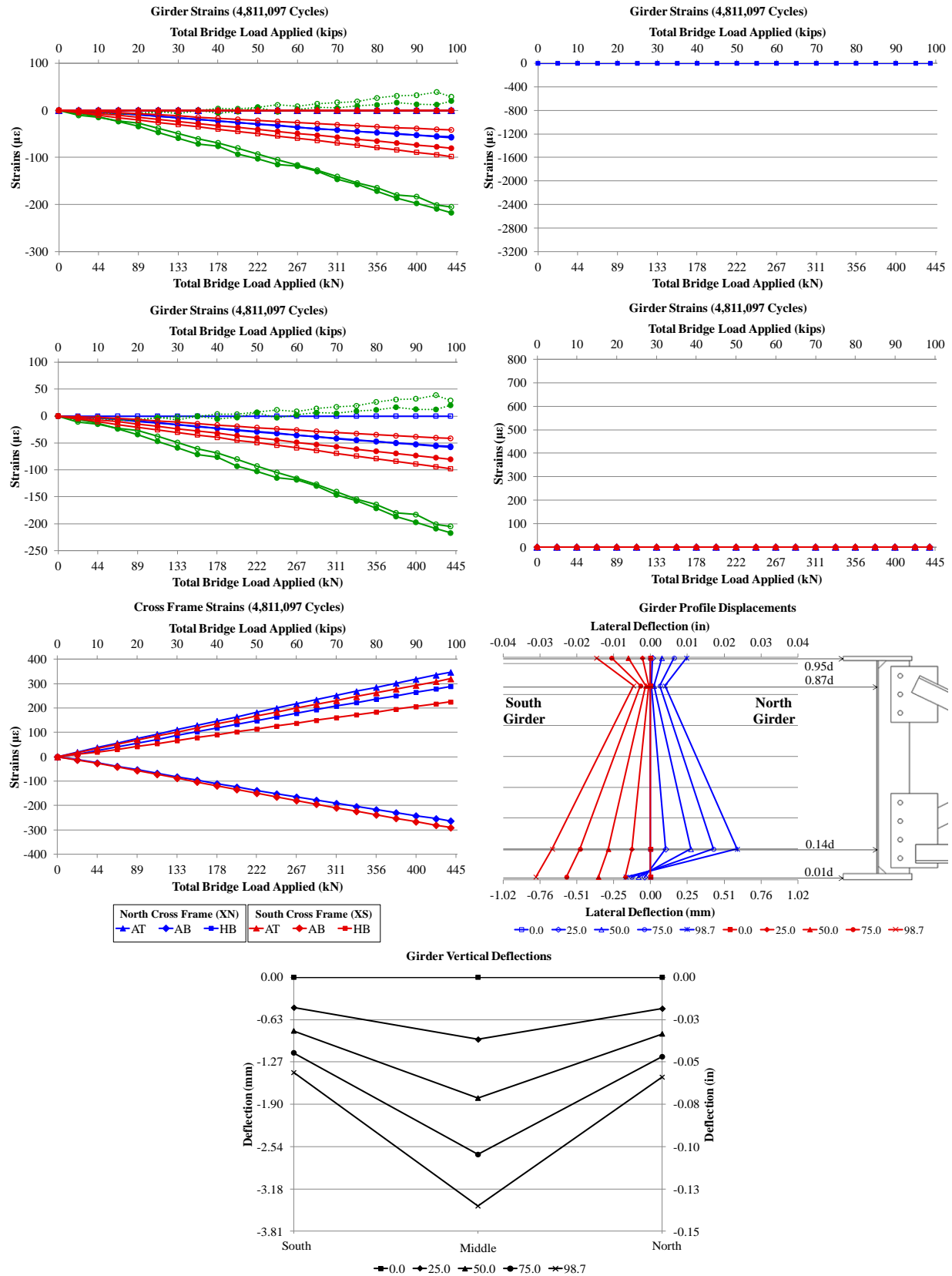


Figure E. 32: Static (4811097 Cycles) 02.15.2013 - With Retrofit

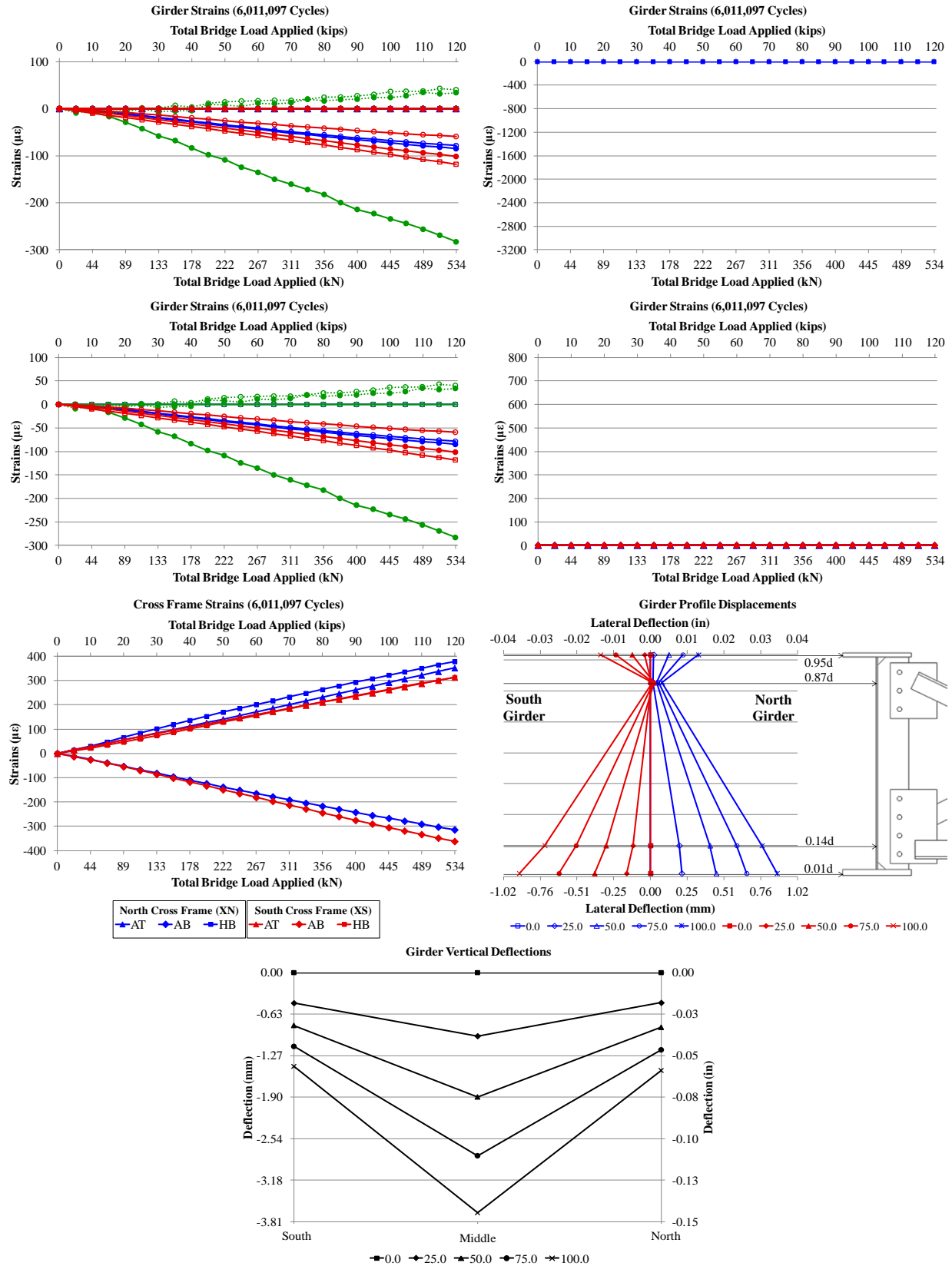


Figure E. 33: Static (6011097 Cycles) 04.16.2013 - With Retrofit

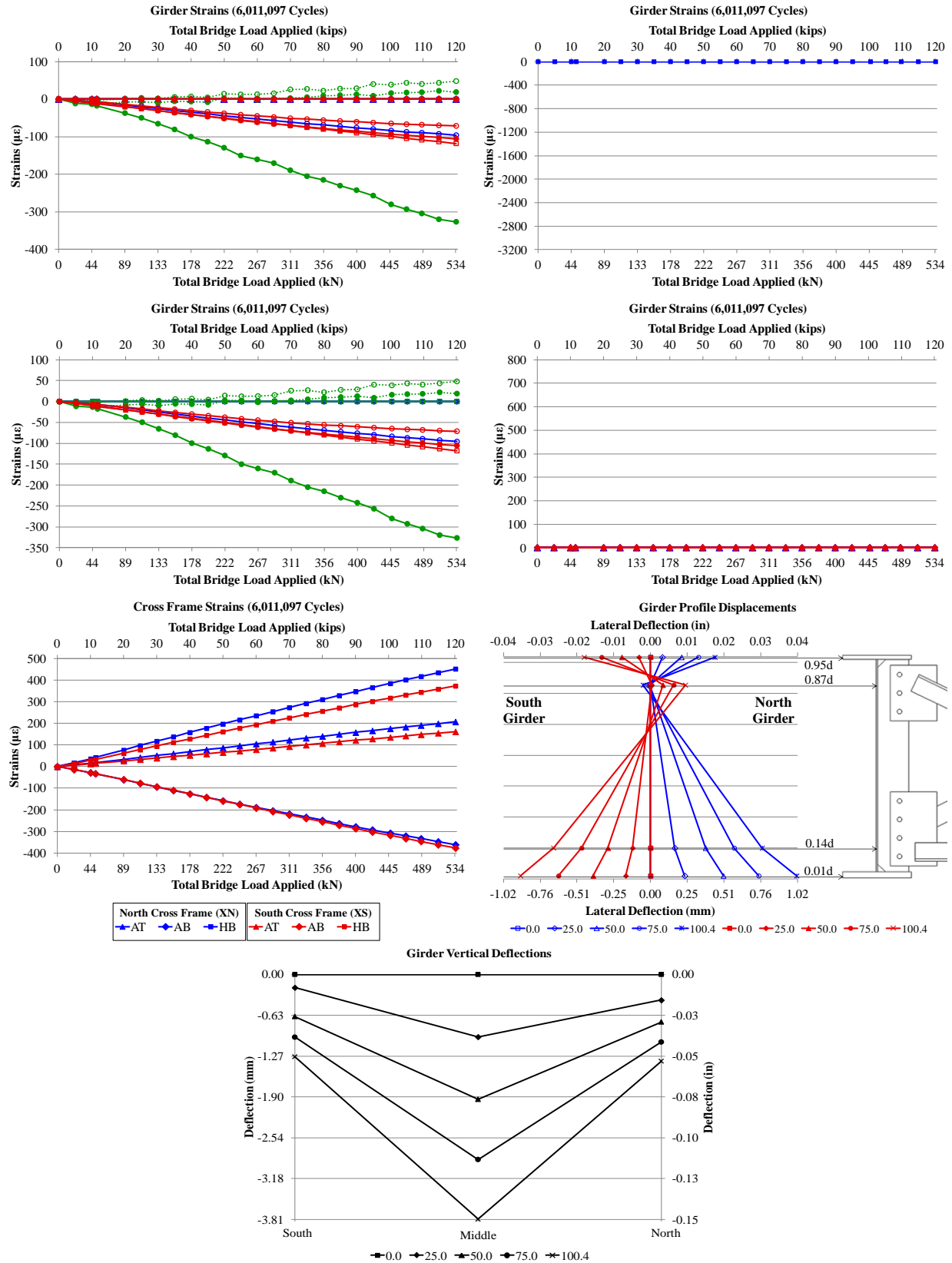


Figure E. 34: Static (6011097 Cycles) 05.20.2013 - Without Retrofit

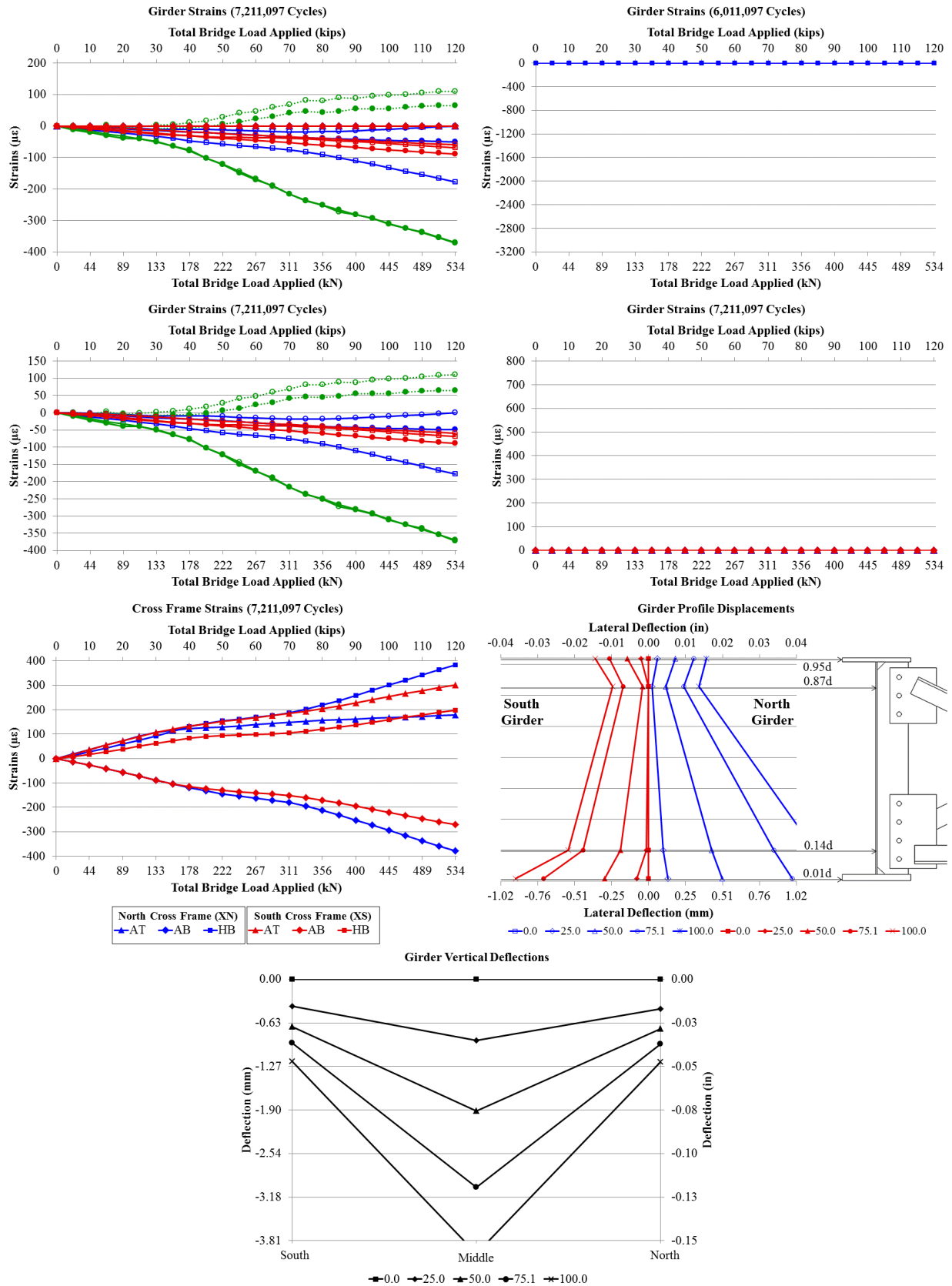


Figure E. 35: Static (7211097 Cycles) 07.11.2013 - With Retrofit North Girder Weld Cracked Cross Frame

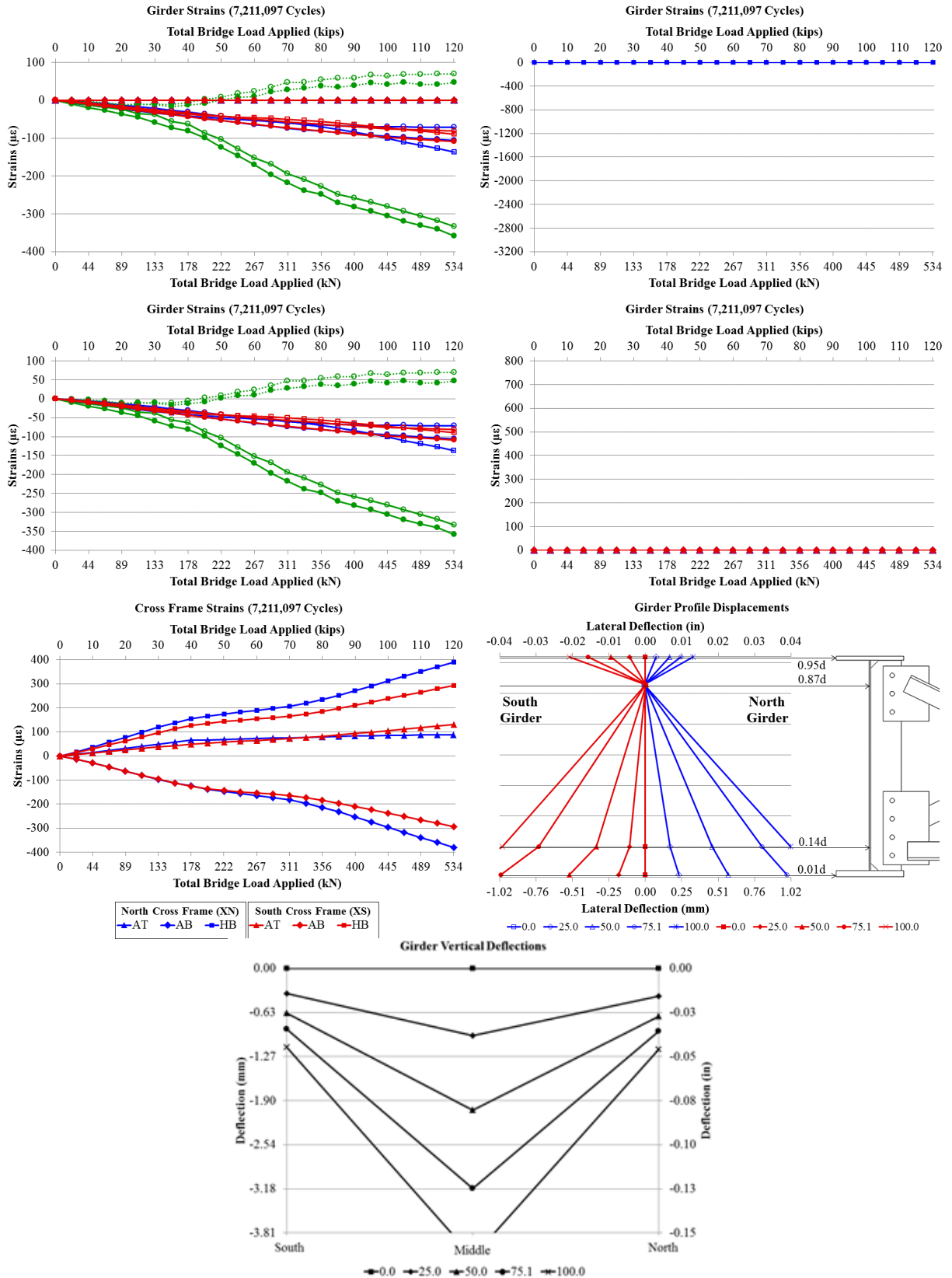


Figure E. 36: Static (7211097 Cycles) 07.11.2013 - Without Retrofit North Girder Weld Cracked Cross Frame

Test 2

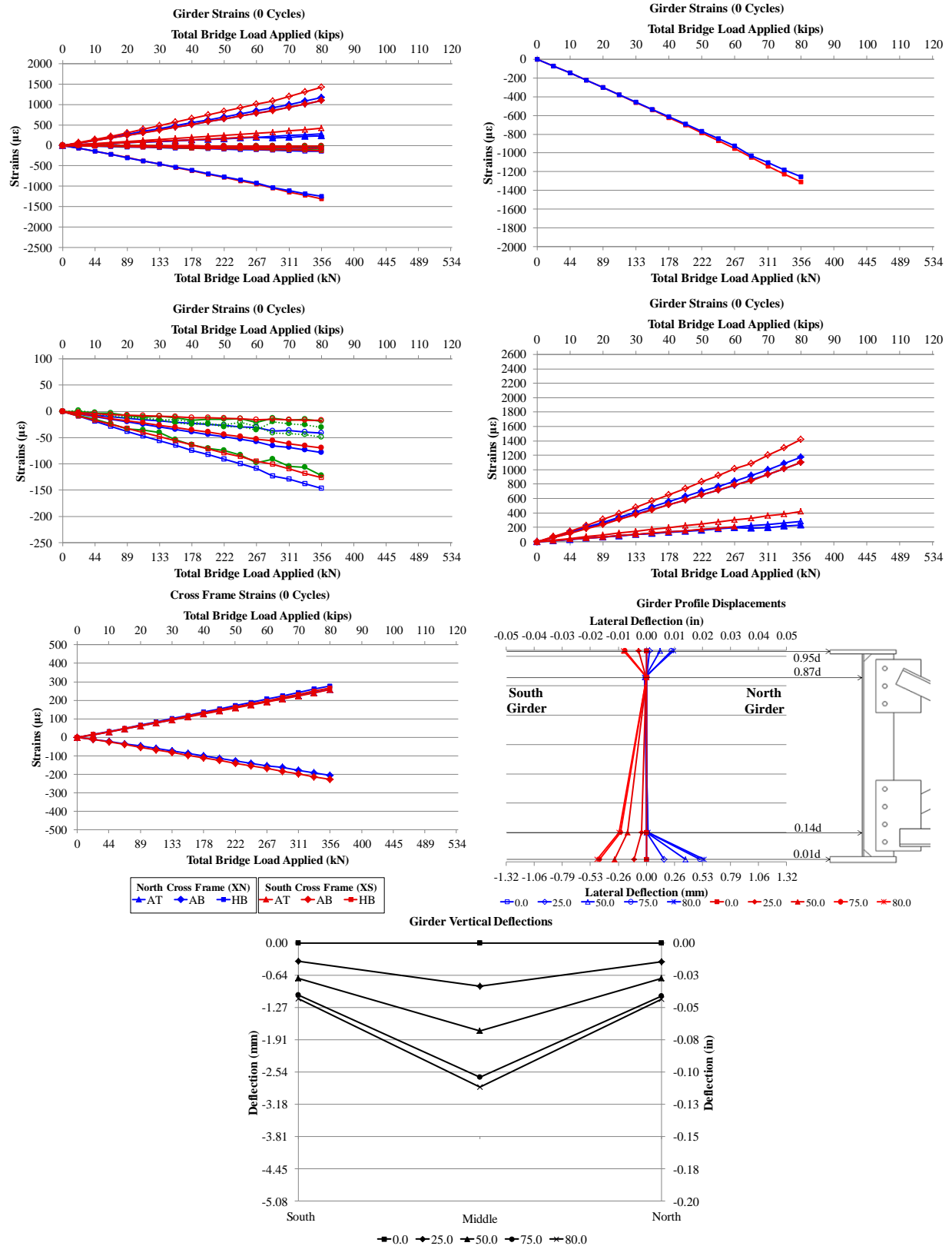


Figure E. 37: Static (0 Cycles) 07.15.2014

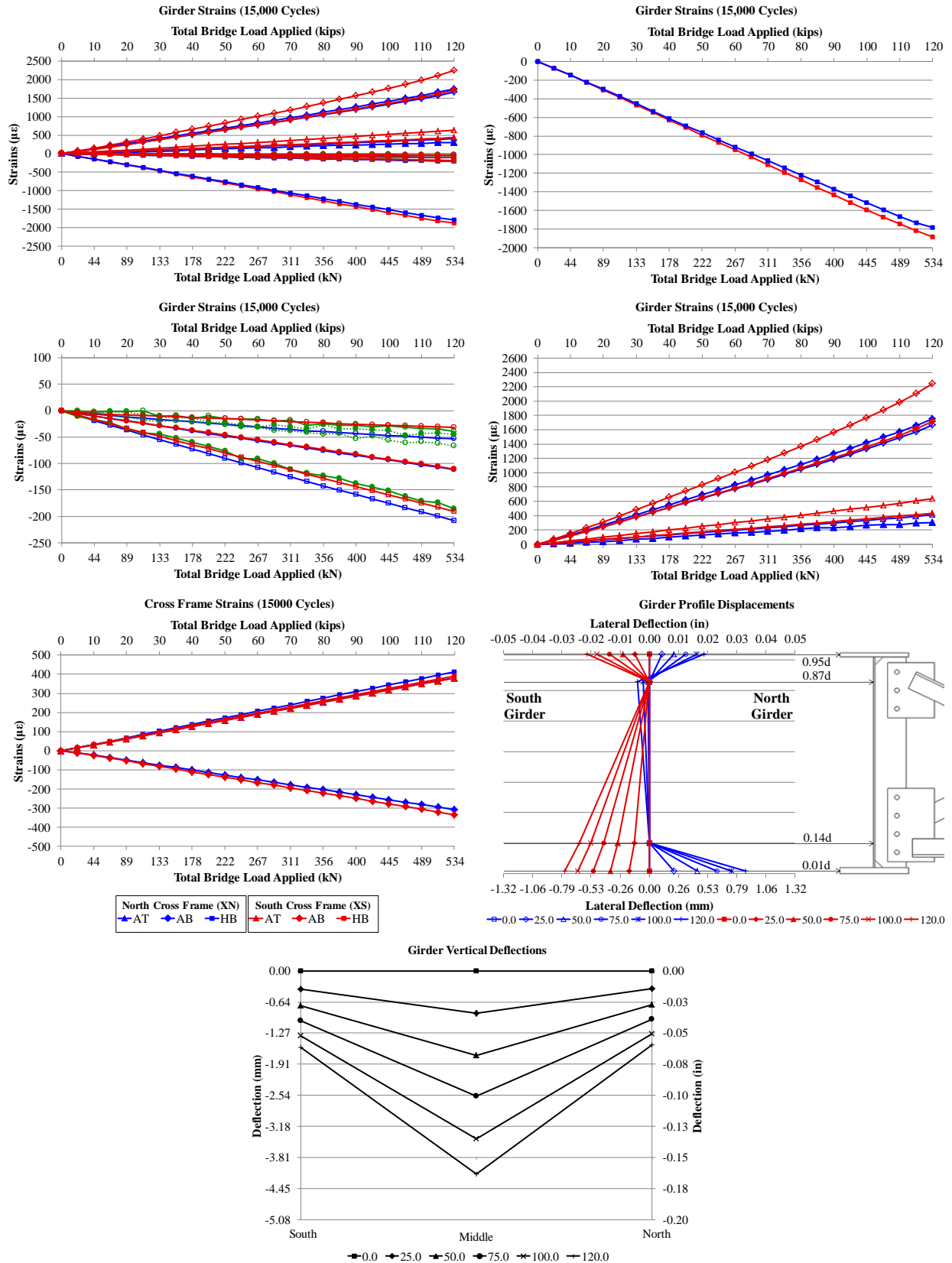


Figure E. 38: Static (15000 Cycles) 07.16.2014

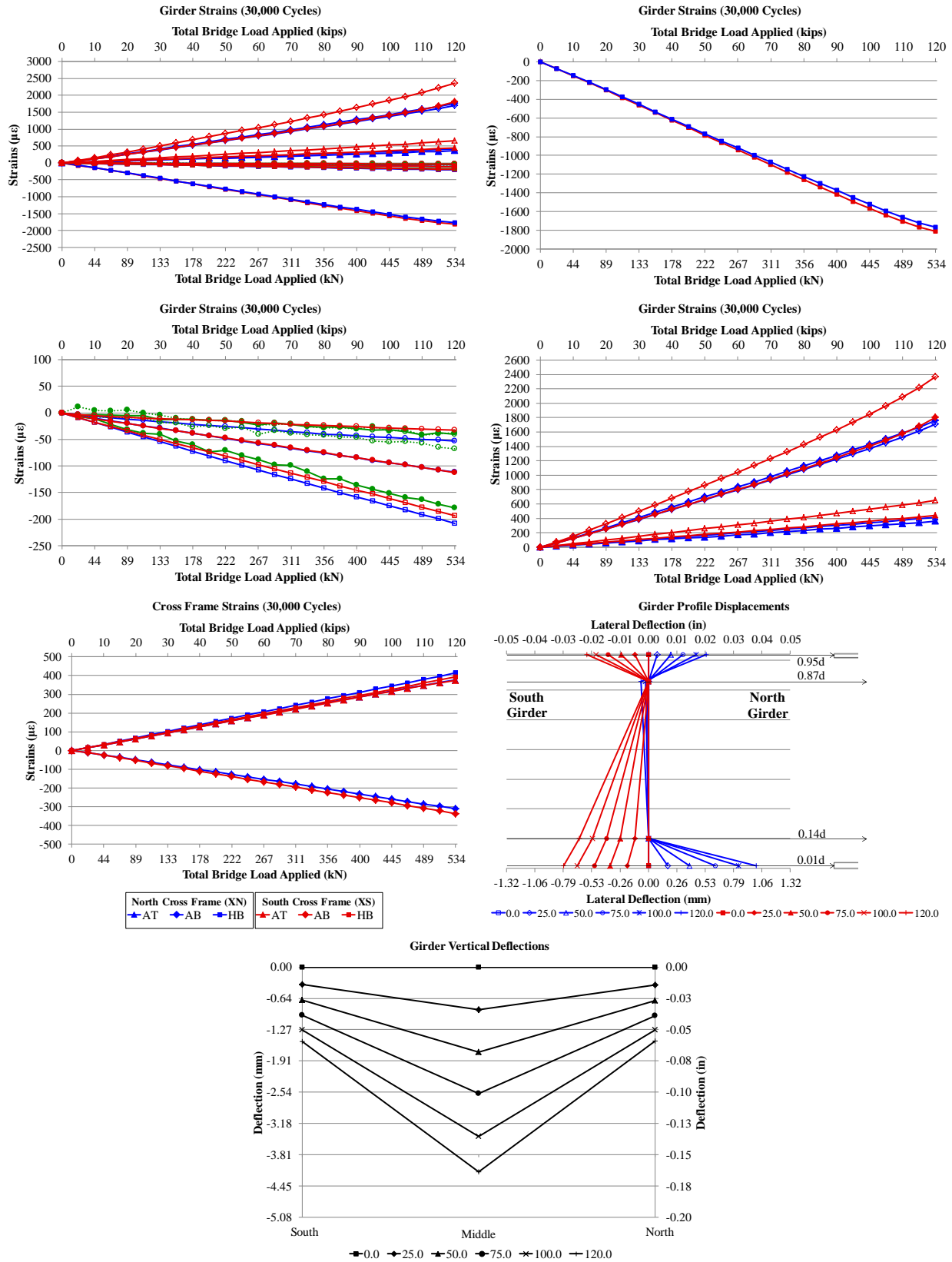


Figure E. 39: Static (30000 Cycles) 07.17.2014

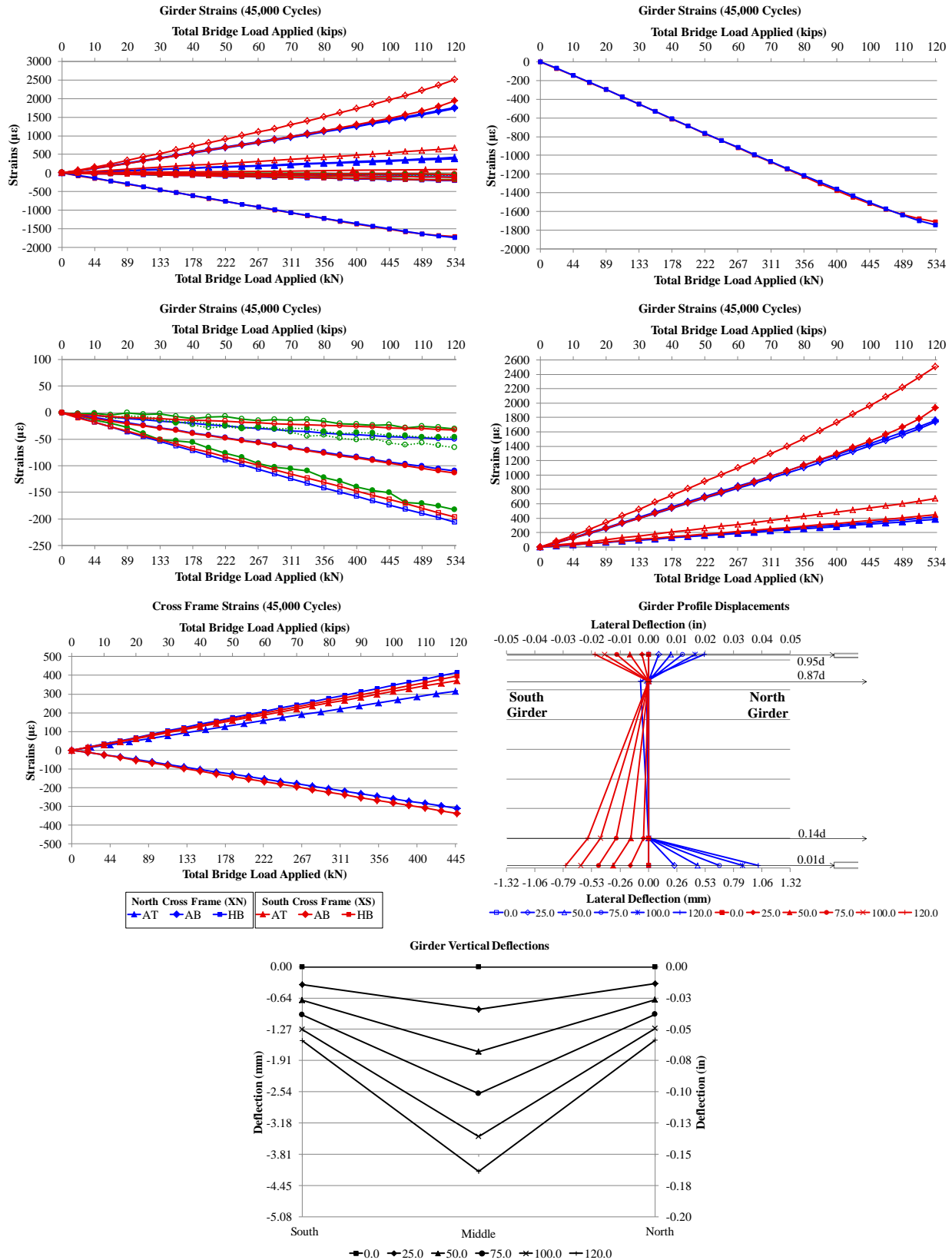


Figure E. 40: Static (45000 Cycles) 07.21.2014

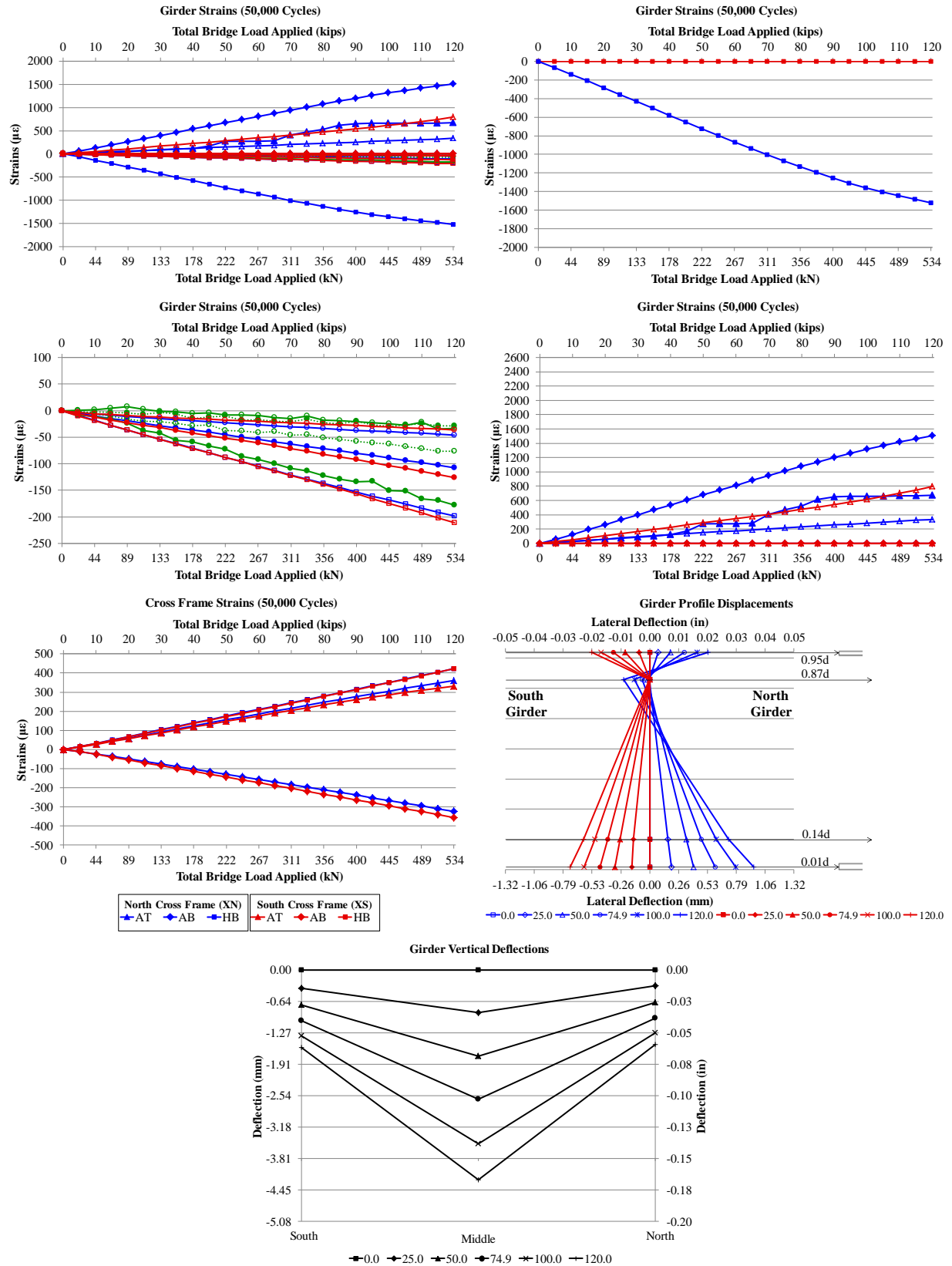


Figure E. 41: Static (50000 Cycles) 07.28.2014 Without Retrofit Drilled Holes

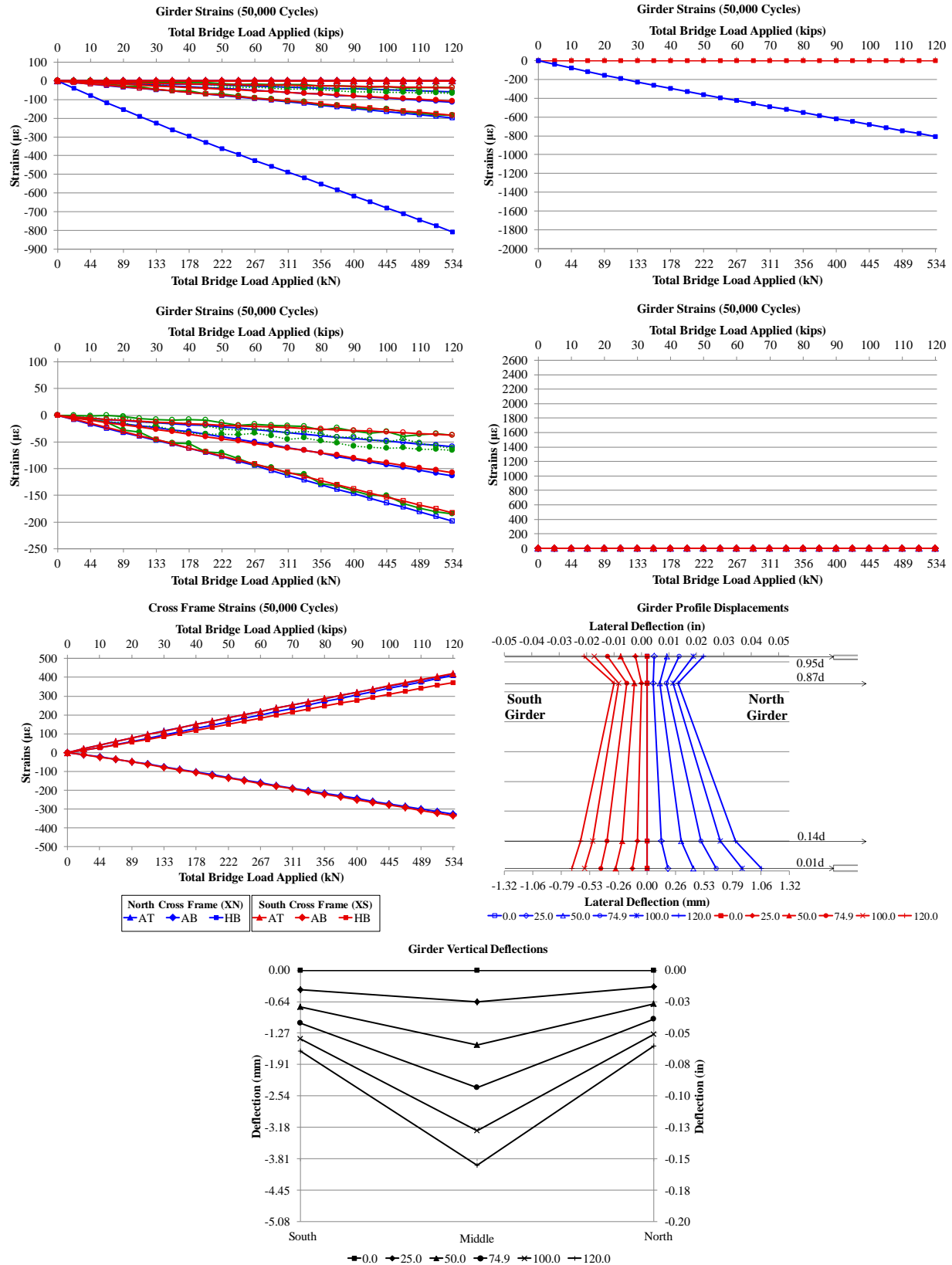


Figure E. 42: Static (50000 Cycles) 07.28.2014 With Retrofit Drilled Holes

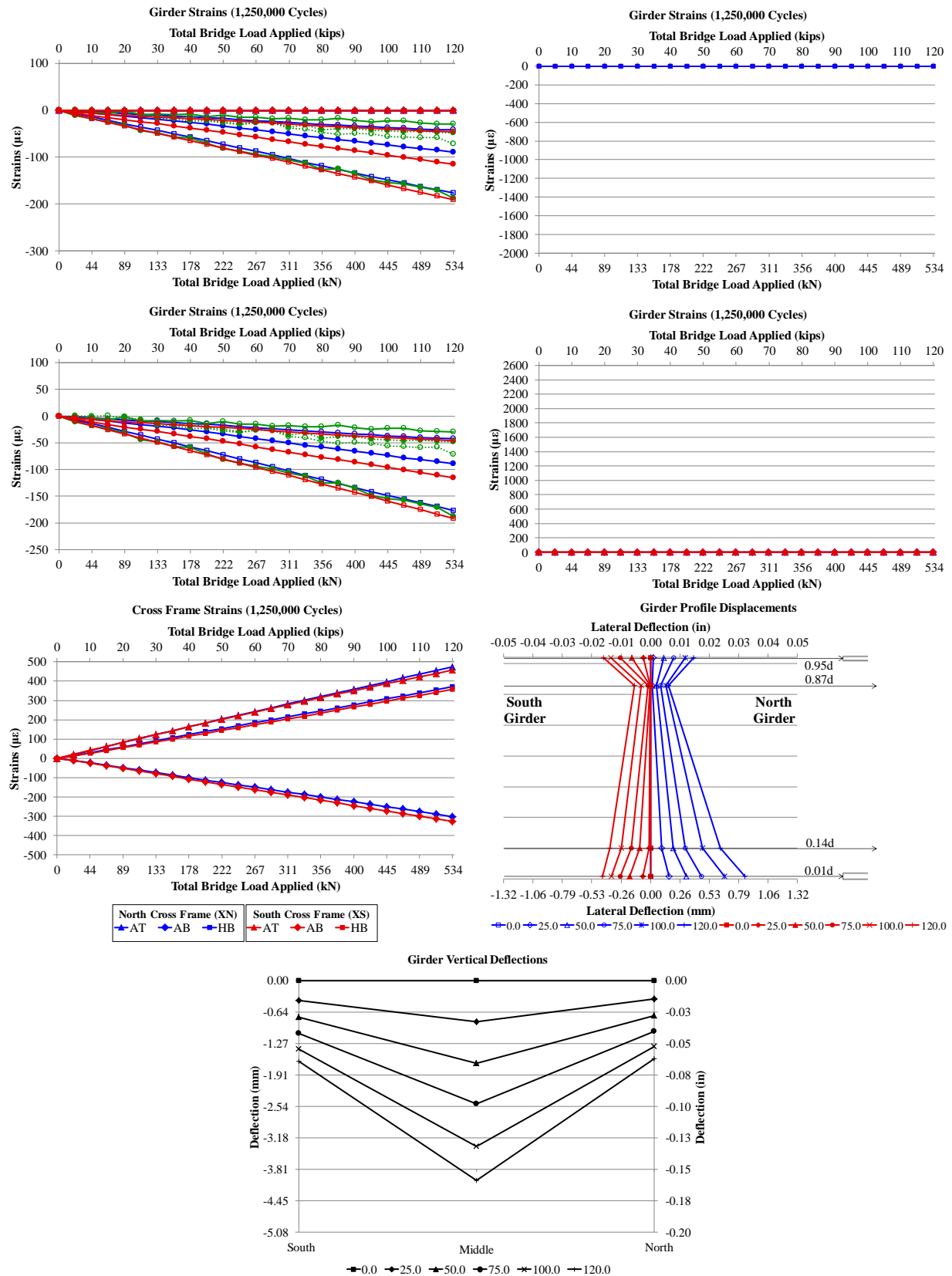


Figure E. 43: Static (1250000 Cycles) 08.29.2014 With Retrofit

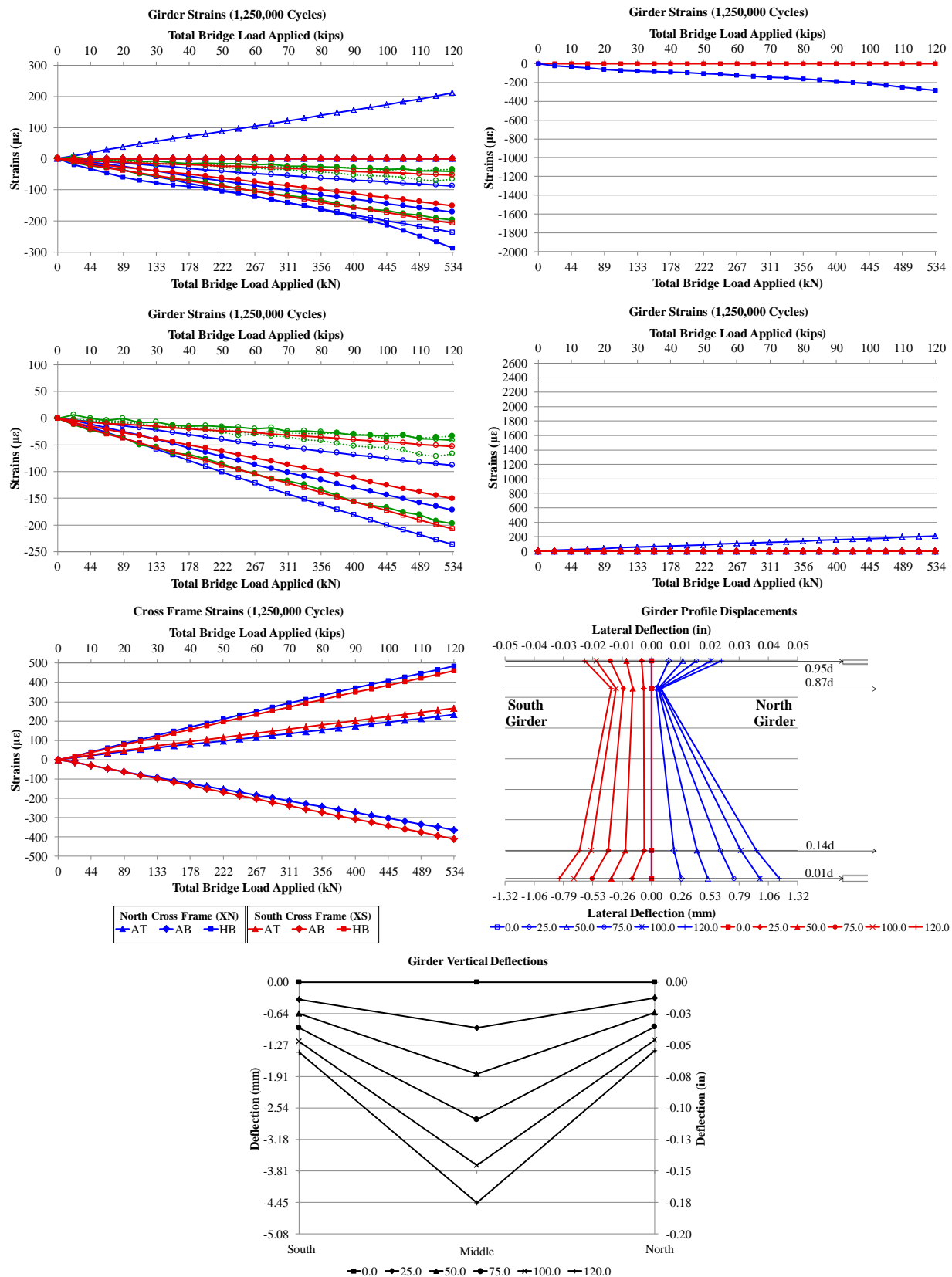


Figure E. 44: Static (1250000 Cycles) 08.29.2014 Without Retrofit

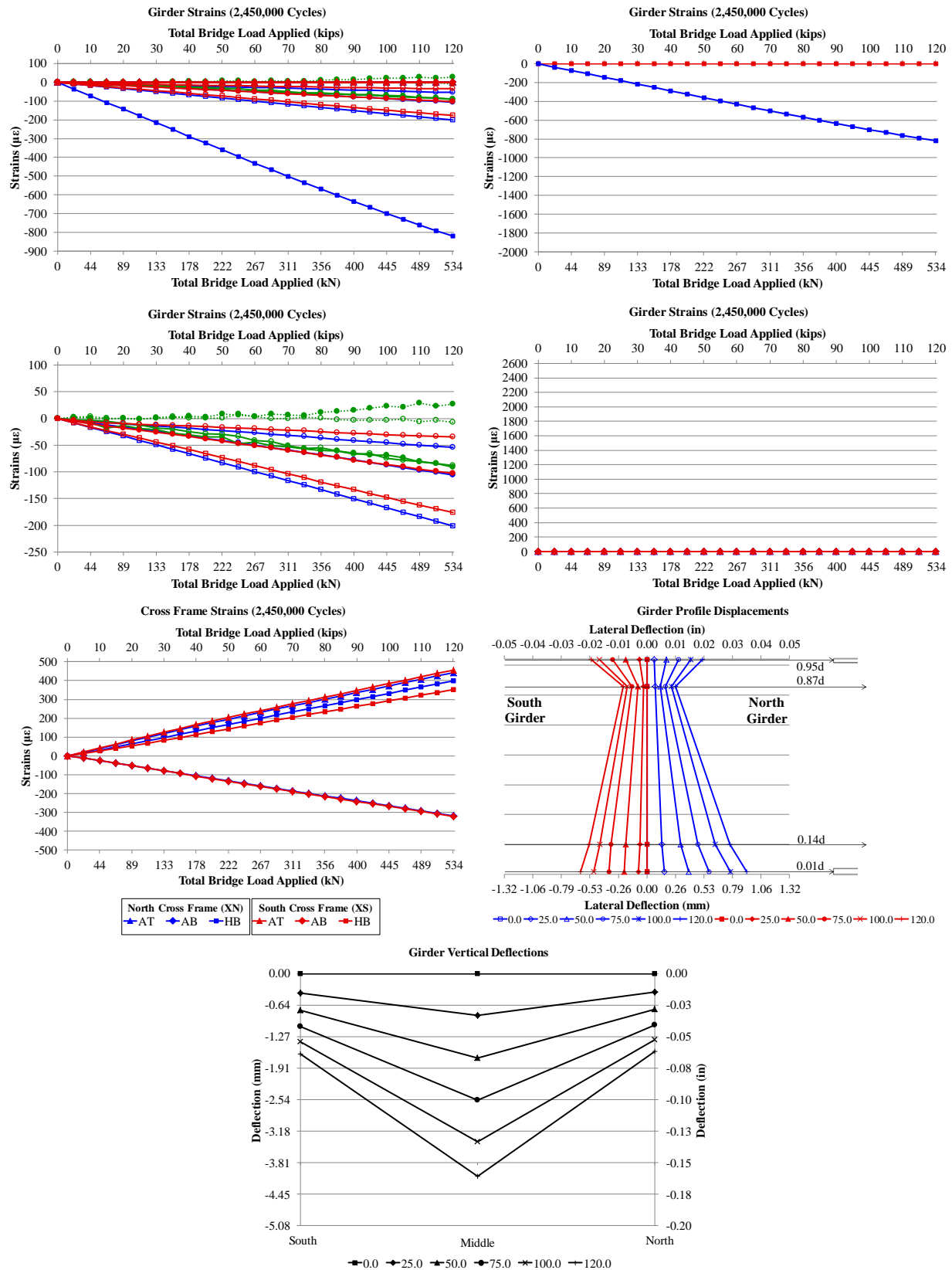


Figure E. 45: Static (2450000 Cycles) 09.30.2014 With Retrofit

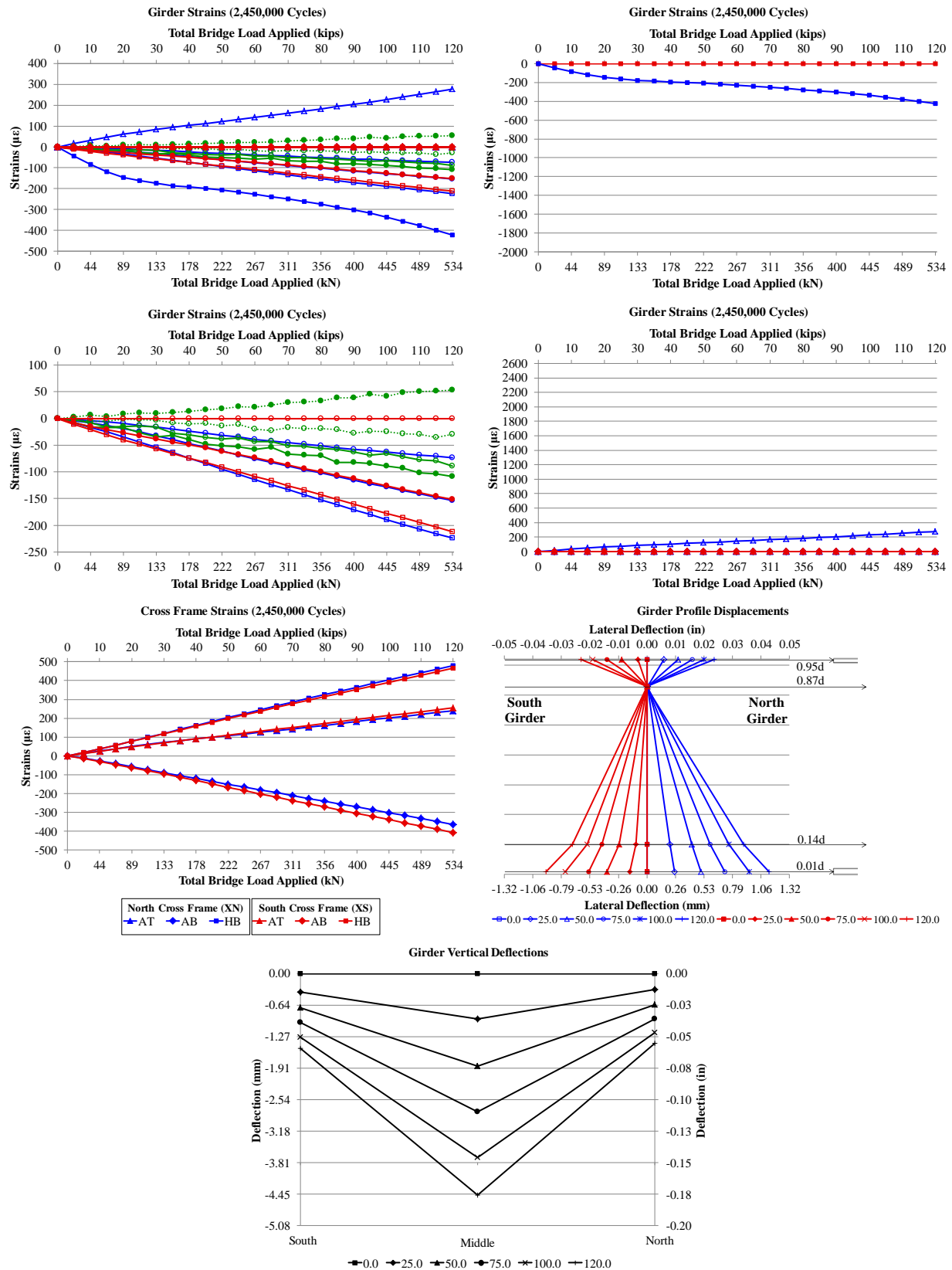


Figure E. 46: Static (2450000 Cycles) 10.02.2014 Without Retrofit

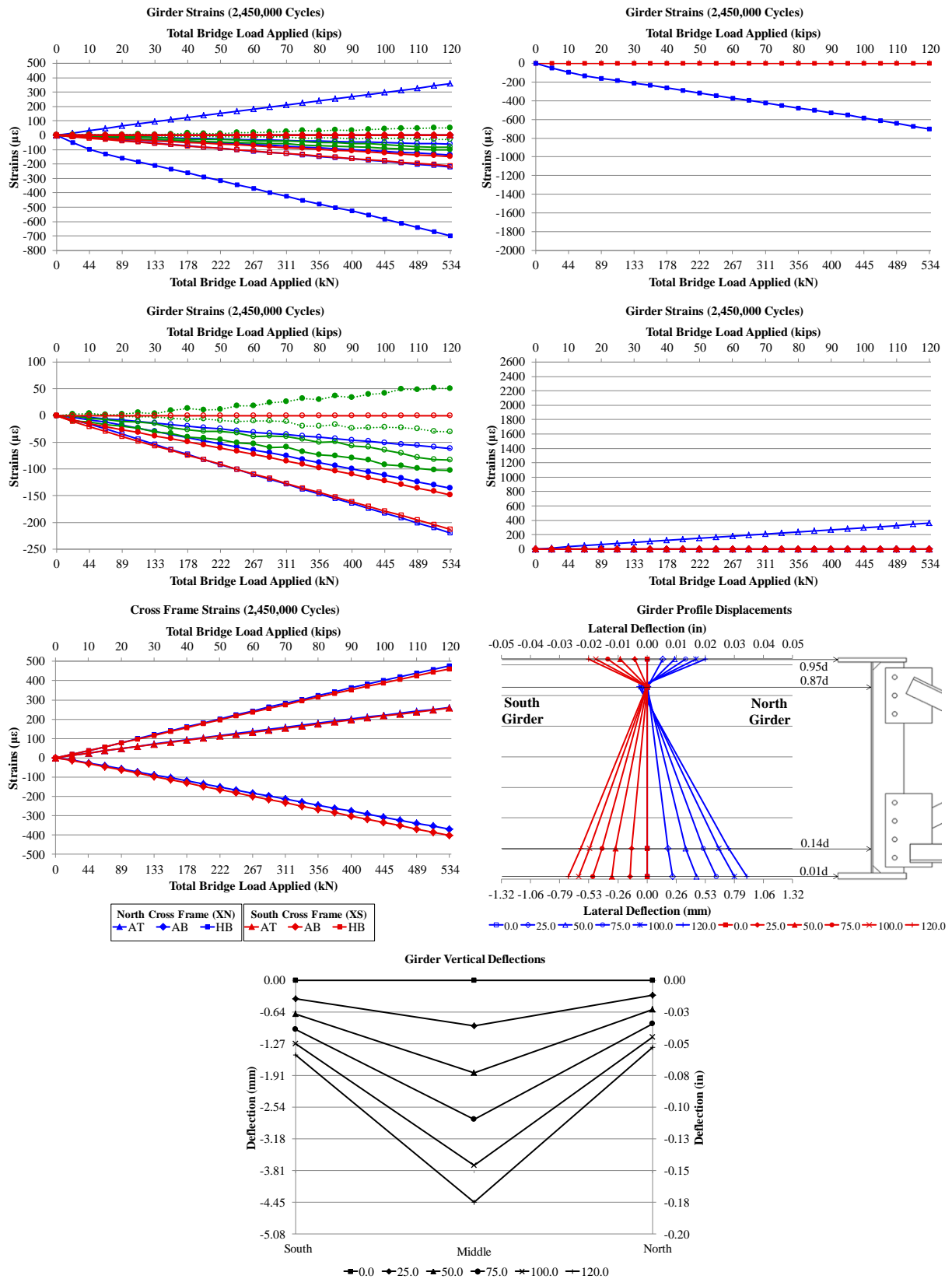


Figure E. 47: Static (2450000 Cycles) 10.02.2014 Without Retrofit Drilled Holes in North Girder

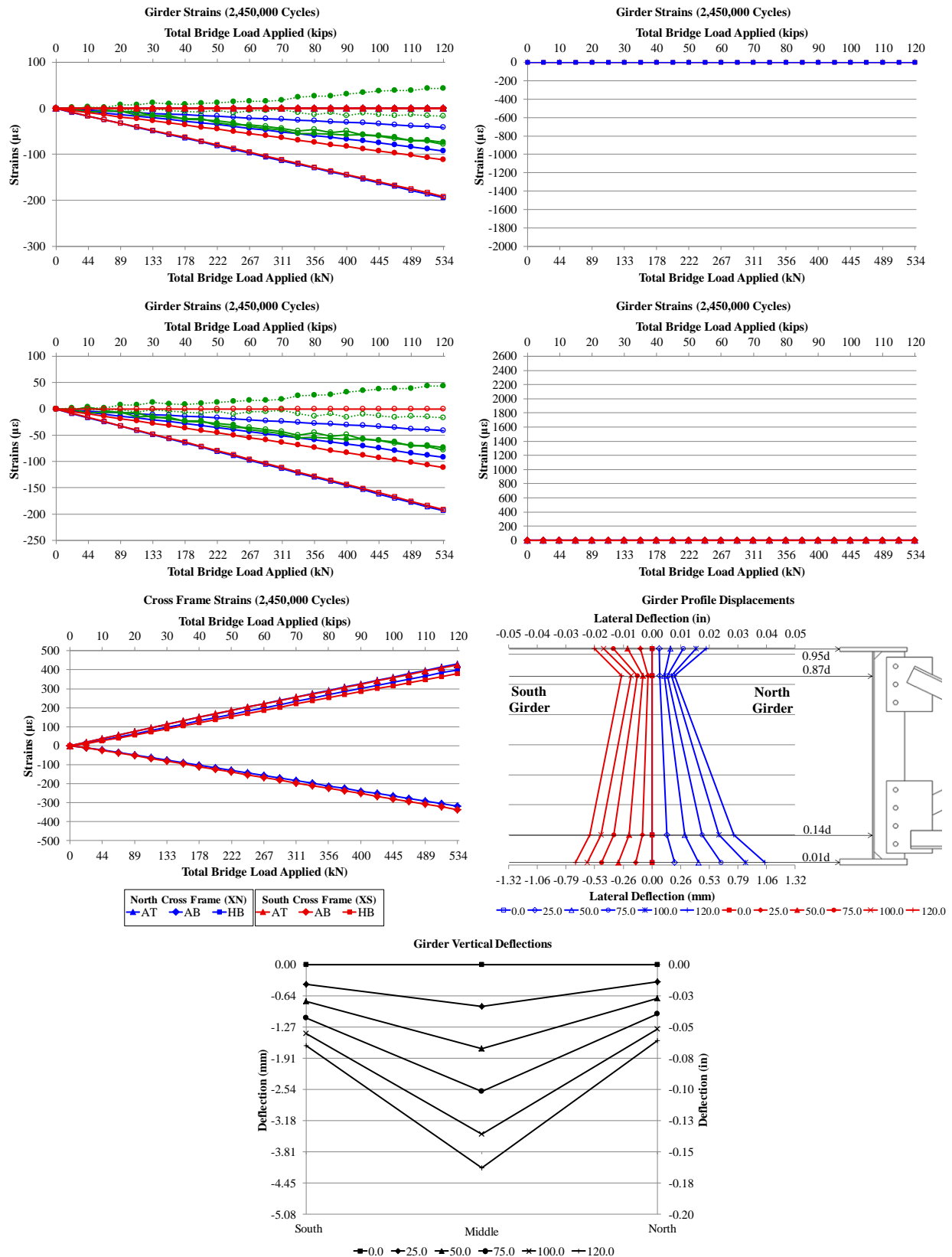


Figure E. 48: Static (2450000 Cycles) 10.02.2014 With Retrofit Drilled Holes in North Girder

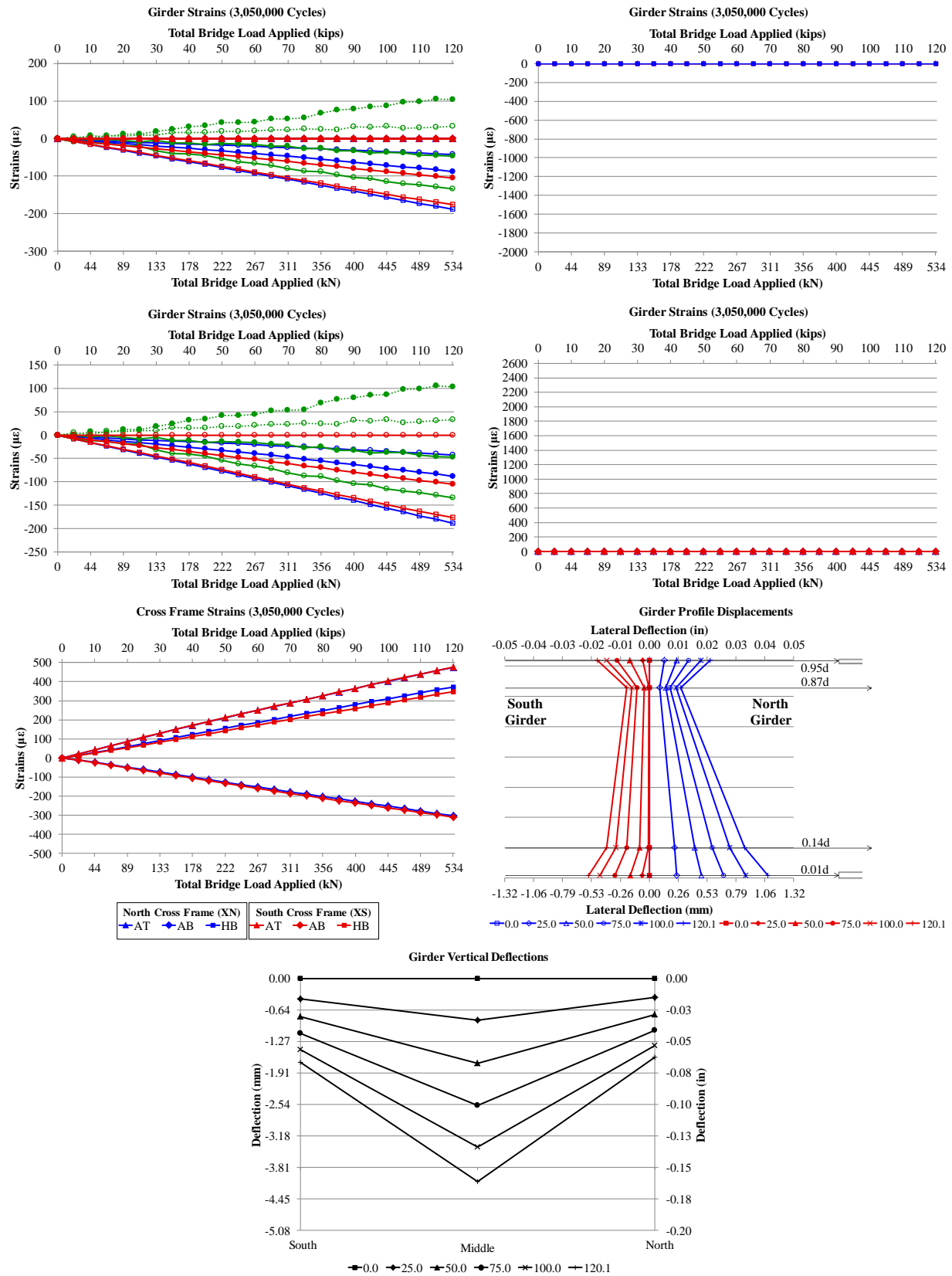


Figure E. 49: Static (3050000 Cycles) 10.23.2014 With Retrofit

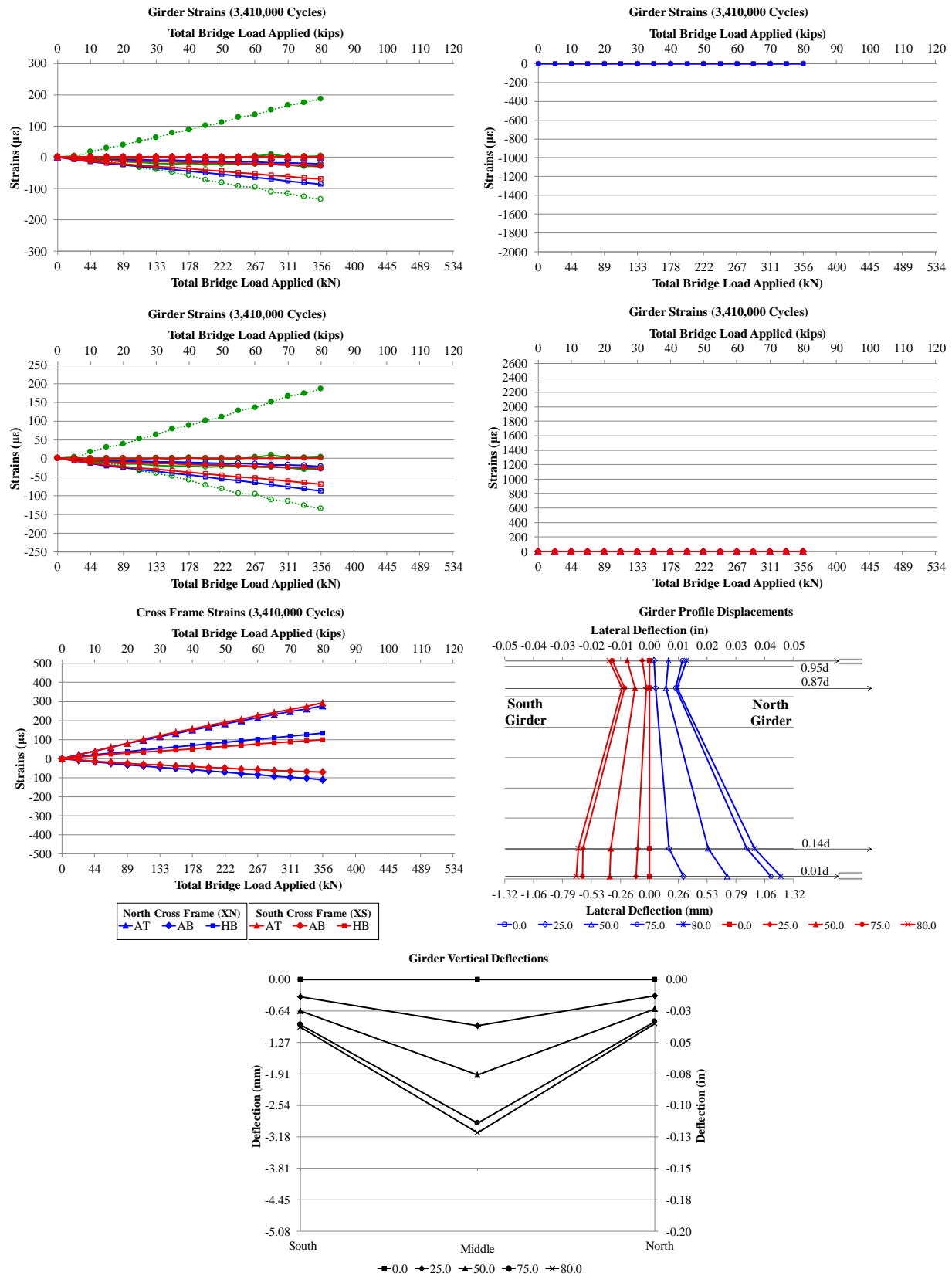


Figure E. 50: Static (3410000 Cycles) 11.14.2014 With Retrofit Cracked Connection Stiffener

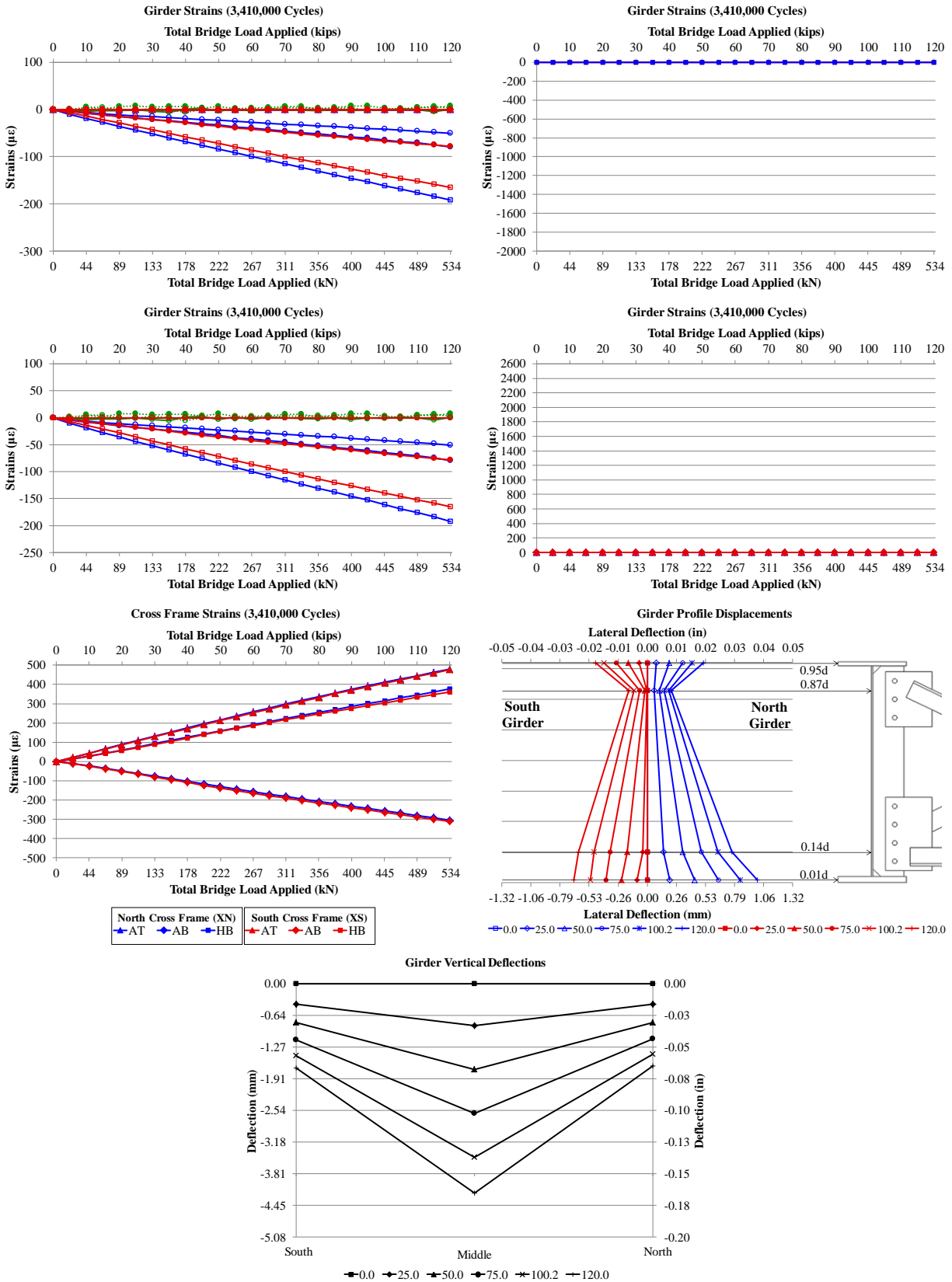


Figure E. 51: Static (3410000 Cycles) 01.12.2015 With Retrofit Cracked Connection Stiffener Repair

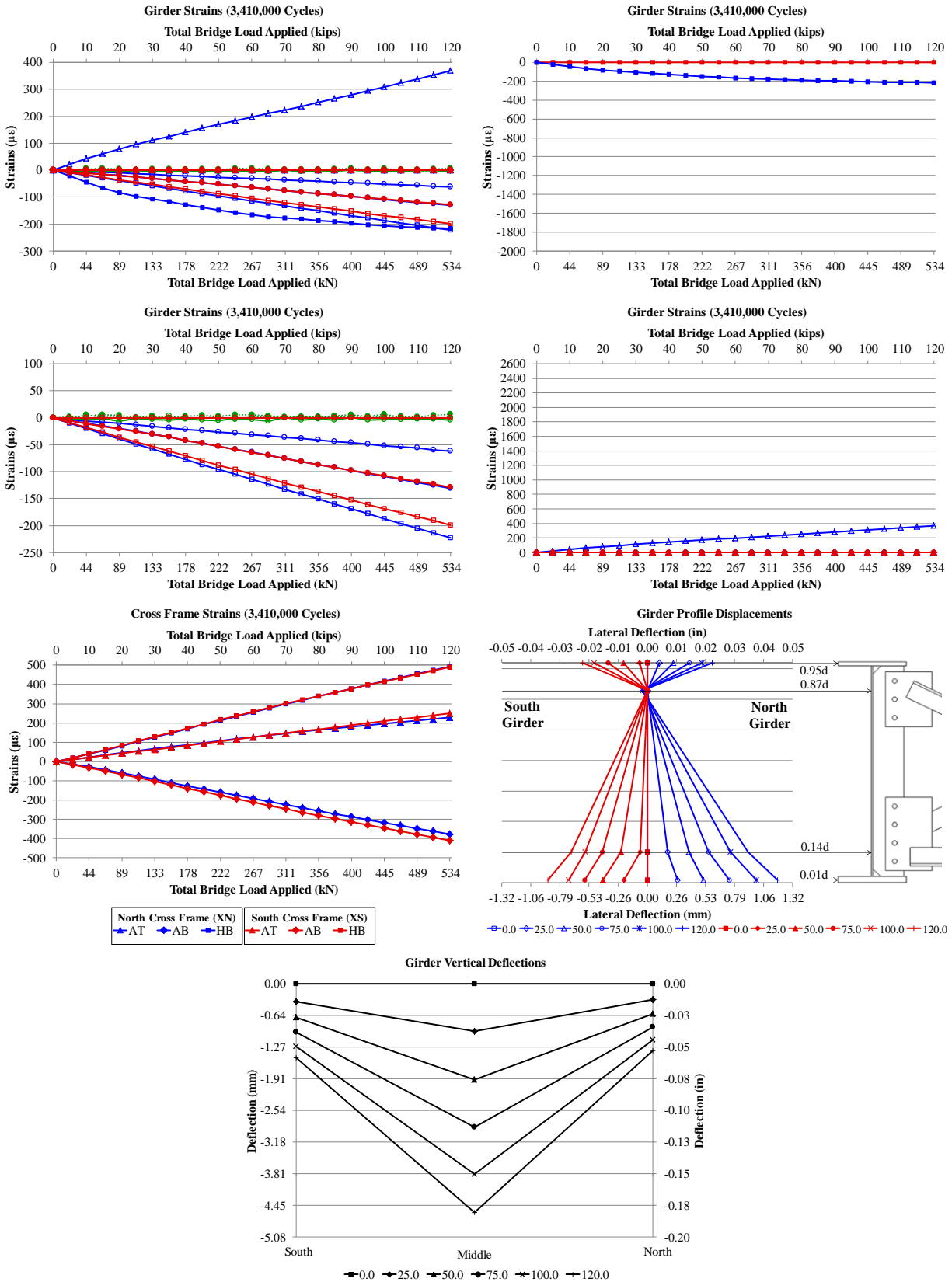


Figure E. 52: Static (3410000 Cycles) 01.12.2015 Without Retrofit Cracked Connection Stiffener Repair

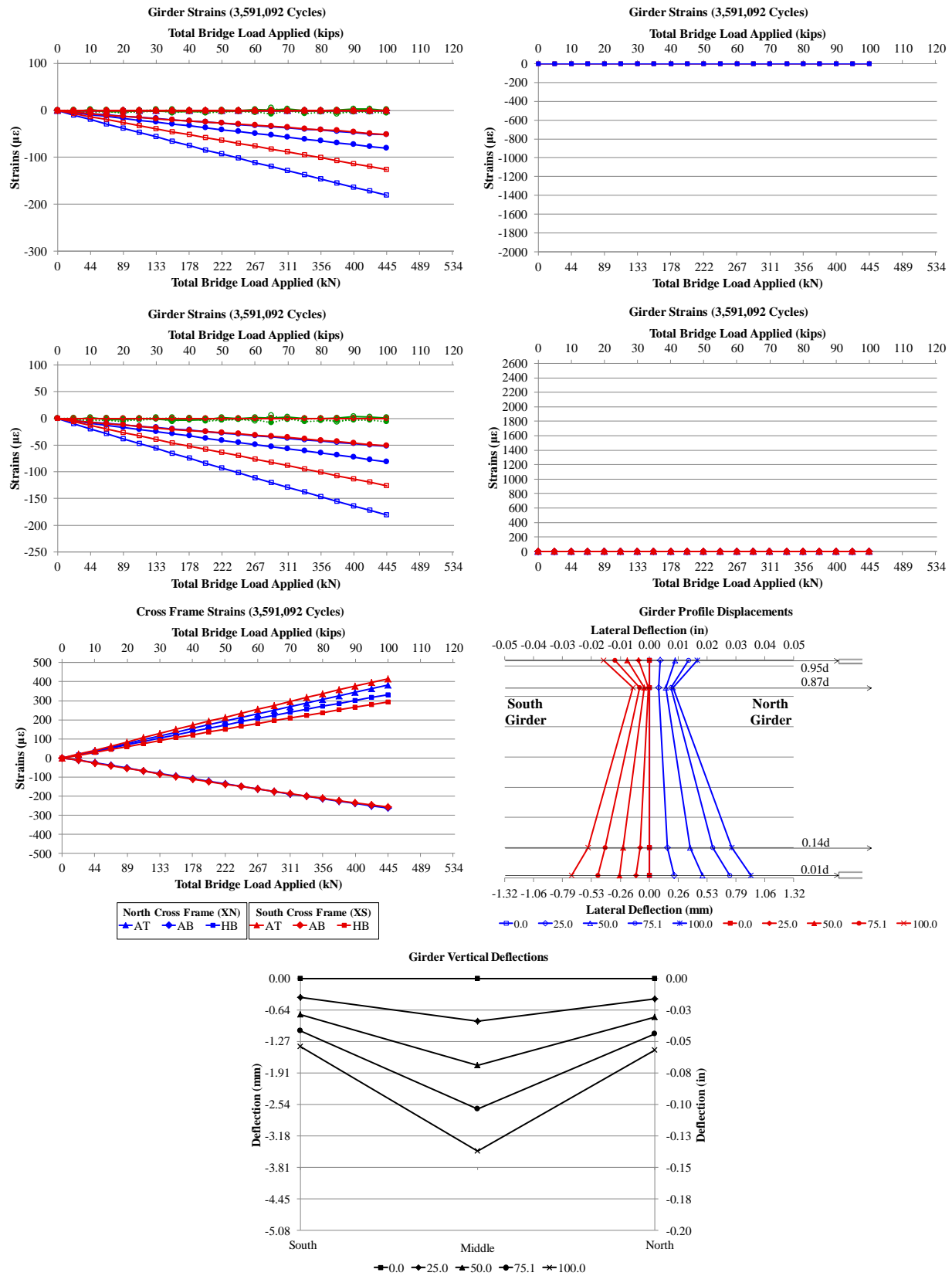


Figure E. 53: Static (3591092 Cycles) 01.27.2015 With Retrofit Cracked Cross Frame Tab

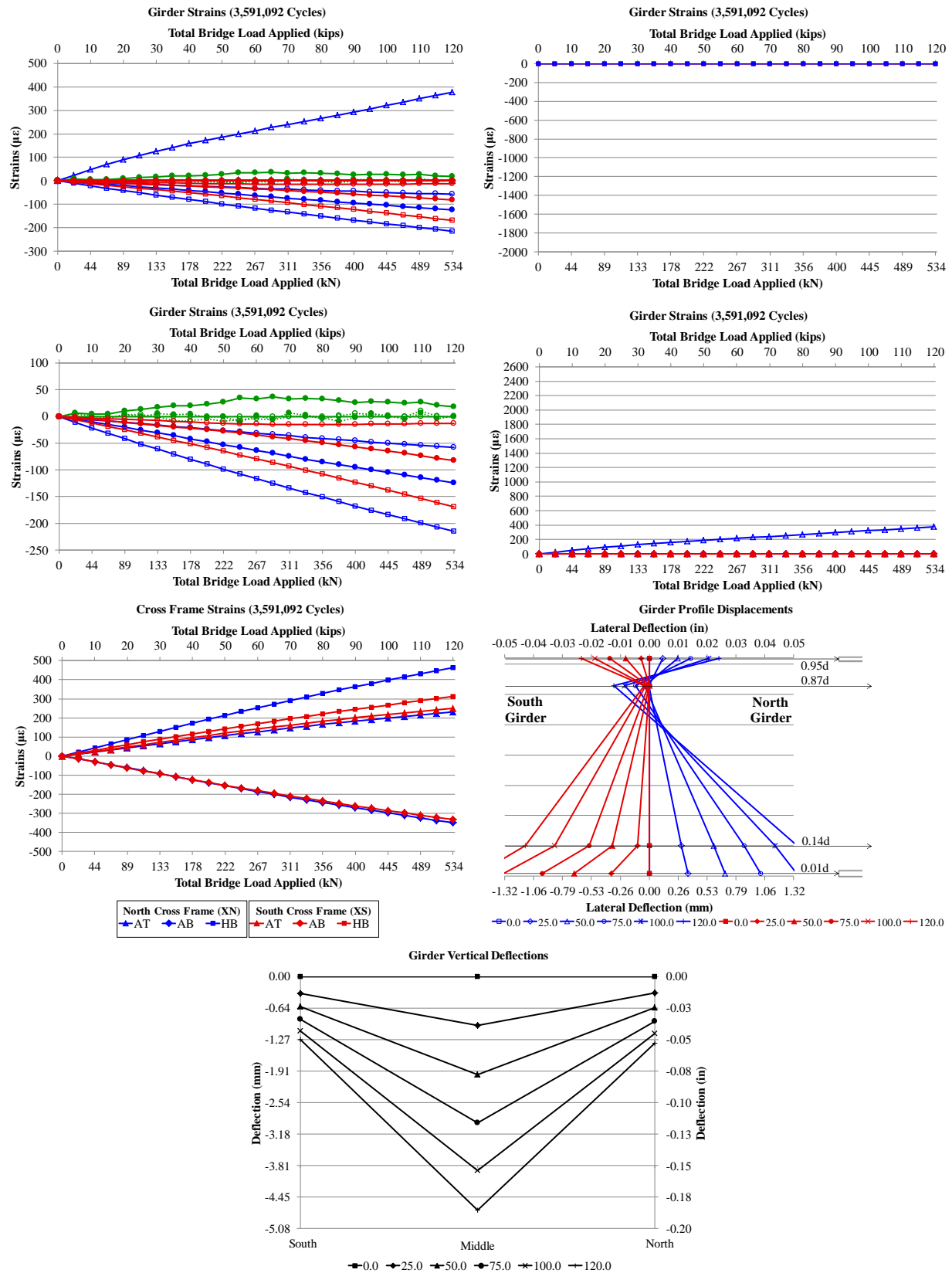


Figure E. 54: Static (3591092 Cycles) 02.18.2015 Without Retrofit New Cross Frame

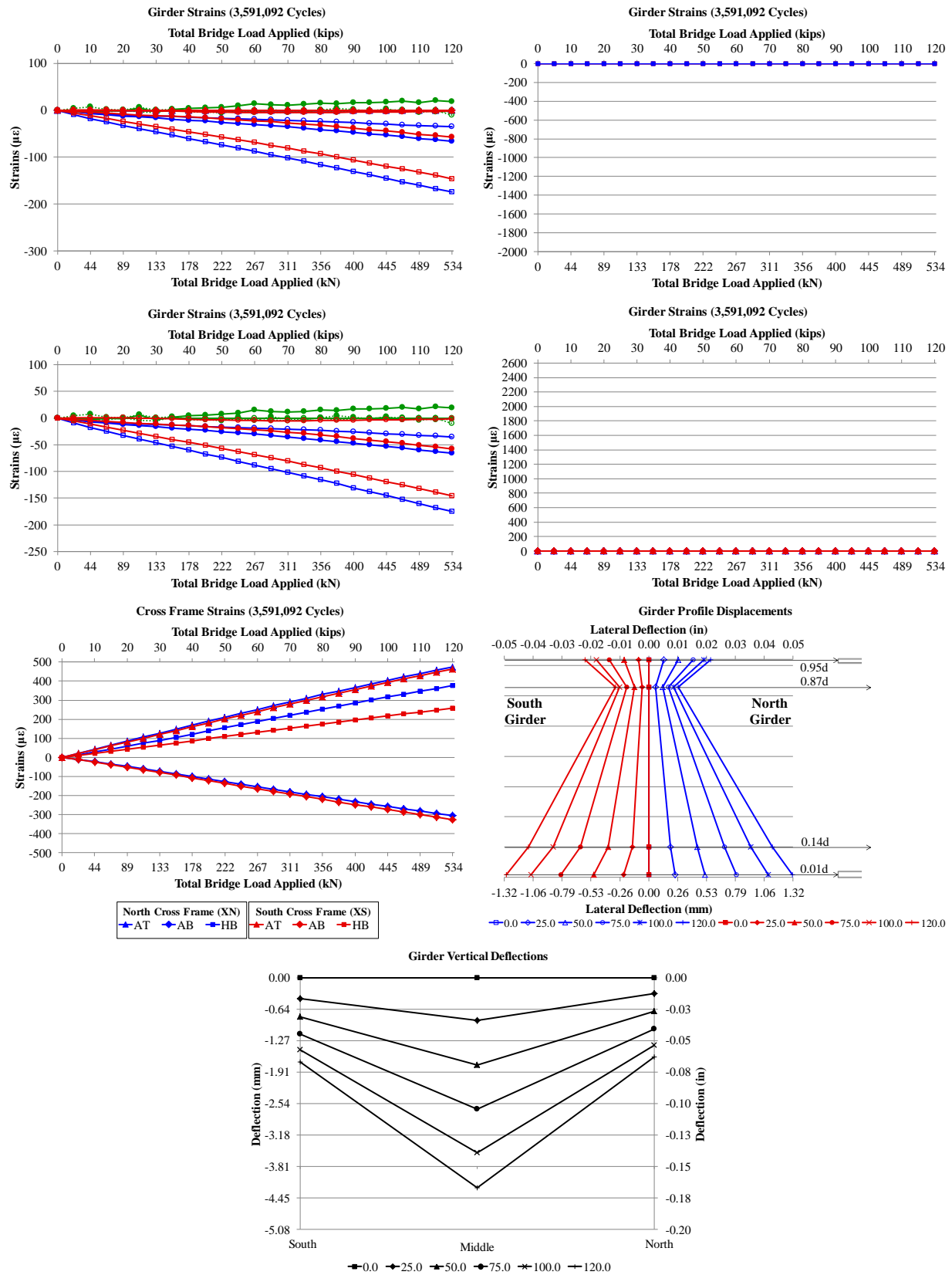
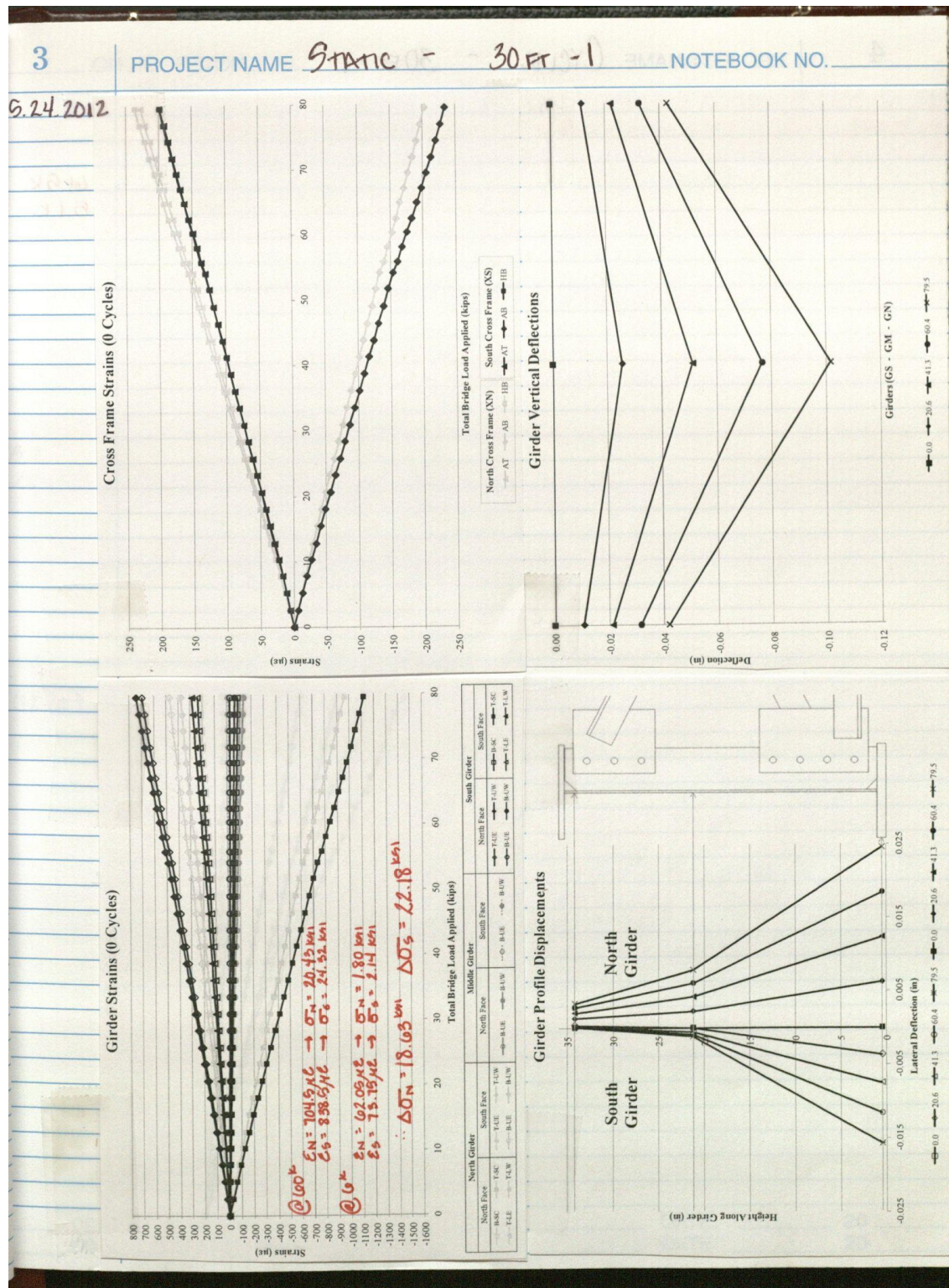


Figure E. 55: Static (3591092 Cycles) 02.24.2015 With Retrofit New Cross Frame

Test 1



4

PROJECT NAME CYCLIC - 30FT-1

NOTEBOOK NO.

5

05.24.2012
(10:54)

15000 CYCLES, 1 Hz (TOTAL 15000)

DISPLACEMENT

MAX 0.127 IN \rightarrow 0.145 IN

MIN 0.013 IN

FORCE

MEAN 33.4 K

MAX 60.8 K \rightarrow 61.6 K

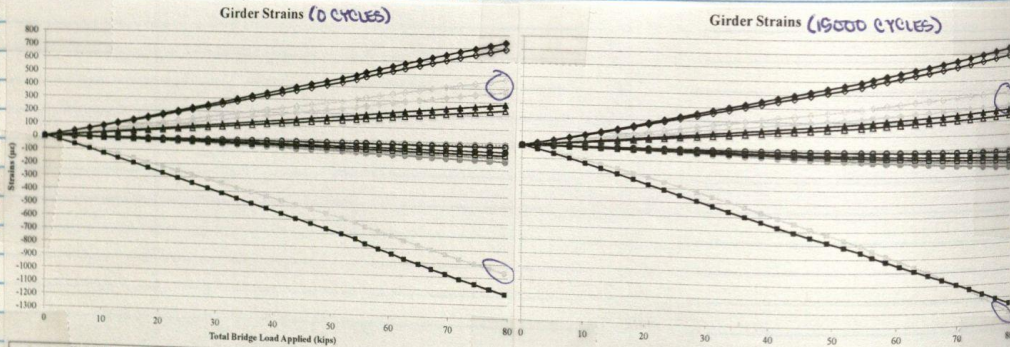
AMPL. 27.3 K

MIN 6.0 K \rightarrow 5.1 K

DATA: * MTS SPECIMEN 10:54 \rightarrow 30FT-1 CYCLIC (15000) 05.24.2012
 STATIC BEGIN 9:53 \rightarrow 30FT-1 STATIC BEGIN 05.24.2012
 CYCLIC BEGIN 10:52 \rightarrow 30FT-1 CYCLIC BEGIN 05.24.2012
 CYCLIC END 10:01 \rightarrow 30FT-1 CYCLIC END 05.24.2012
 STATIC END 10:18 \rightarrow 30FT-1 STATIC END 05.24.2012

* ACTUAL TIME SHOWS... FILE TIME IS 10:37

NO CRACK DETECTED VISUALLY



North Girder		Middle Girder		South Girder	
North Face	South Face	North Face	South Face	North Face	South Face
8-4E	8-4W	8-4E	8-4W	8-4E	8-4W
8-4E	8-4W	8-4E	8-4W	8-4E	8-4W

05.29.2012
(10:32)

5000 CYCLES, 1 Hz (TOTAL 20000)

DISP

MAX 0.126 IN \rightarrow 0.133 IN

MIN 0.010 IN

FORCE

MEAN 33.7 K

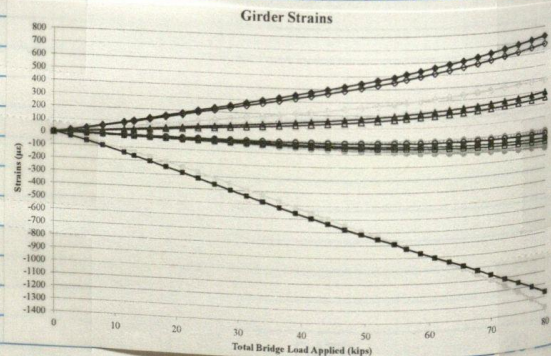
MAX 63.1 K

AMPL. 27.9 K \rightarrow 27.9 K

MIN 4.8 K

DATA: * MTS SPECIMEN 10:32 \rightarrow 30FT-1 CYCLIC (5000) 05.29.2012
 CYCLIC END 11:50 \rightarrow 30FT-1 CYCLIC END 05.29.2012
 STATIC END 12:10 \rightarrow 30FT-1 STATIC END 05.29.2012

* FILE TIME = 10:15

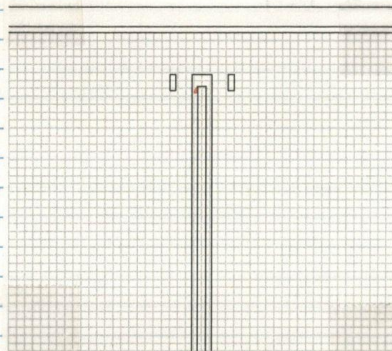
SIGNATURE
READ AND UNDERSTOOD

DATE

20

05.29.2012
(10:31)

(12:10)



$\frac{1}{8}$ " CRACK IN NORTH GIRDER,
SOUTH FACE, WEST OF
STIFFENER

CRACK IN WELD AT JUNCTURE
BETWEEN WELD AND STIFFENER
PROPAGATING DIAGONAL FROM
CORNER AS SHOWN
CRACK ON OPPOSITE SIDE OF ANGLE
FRAMING IN

05.29.2012
(10:31)

5000 CYCLES, 1 Hz (TOTAL 25,000)

DISP

MAX 0.128 IN \rightarrow 0.130 IN

MIN 0.010 IN

FORCE

MEAN 32.8 k \rightarrow 33.4 k MAX 61.6 k \rightarrow 62.4 k

AMPL 21.7 k

MIN 4.6 k \rightarrow 4.4 k

DATA: * MTS SPECIMEN $\xrightarrow{10:31}$ 30FT-1 CYCLIC (a5000) 05.29.2012
CYCLIC END $\xrightarrow{12:18}$ 30FT-1 CYCLIC-a END 05.29.2012

* FILE TIME = 10:13

PREVIOUS CRACK NOT SEEN USING PENETRANT

(12:16)

5000 CYCLES, 1 Hz (TOTAL 30,000)

DISP

MAX 0.134 IN

MIN 0.014 IN

FORCE

MEAN 33.9 k

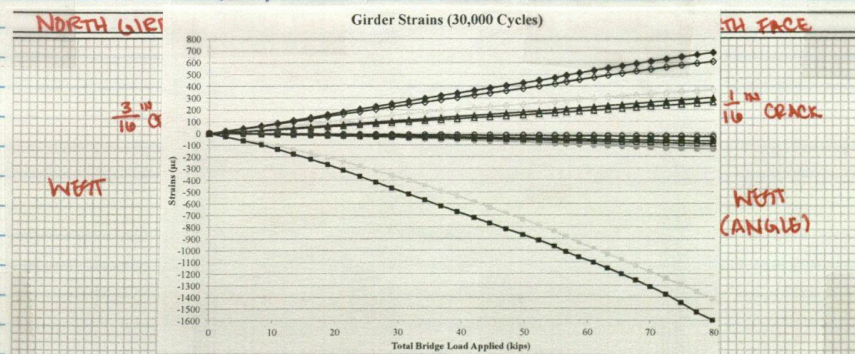
MAX 63.3 k

AMPL 28.0 k

MIN 9.4 k \rightarrow 5.2 k

DATA: * MTS SPECIMEN $\xrightarrow{12:16}$ 30FT-1 CYCLIC (b5000) 05.29.2012
CYCLIC END $\xrightarrow{13:41}$ 30FT-1 CYCLIC-b END 05.29.2012
STATIC END $\xrightarrow{13:53}$ 30FT-1 STATIC-b END 05.29.2012

* FILE TIME = 11:59



SIGNATURE _____
READ AND UNDERSTOOD _____

DATE _____ 20
DATE _____ 20

(14:00)

5000 CYCLES, 1 HZ (TOTAL 39,000)

DISP

MAX 0.134 IN \rightarrow 0.135 INMIN 0.019 IN \rightarrow 0.016 IN

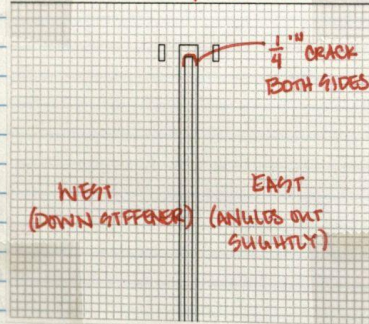
FORCE

MEAN 33.3 K \rightarrow 33.9 K MAX 61.8 KAMPL. 27.8 K \rightarrow 27.7 K MIN 5.9 K \rightarrow 4.8 K

DATA: * MTS SPECIMEN ^{14:00} 30FT-1 CYCLIC (C5000) 09.29.2012
 CYCLIC END ^{15:24} 30FT-1 CYCLIC-C END 09.29.2012

* FILE TIME: 13.42

NORTH GIRDER, SOUTH FACE

NO CHANGE IN SOUTH
GIRDER CRACKS09.31.2012
(10:49)09.30.2012
(11:54)

10000 CYCLES, 1 HZ (TOTAL 49,000)

DISP

MAX 0.128 IN \rightarrow 0.141 INMIN 0.007 IN \rightarrow -0.003 IN

FORCE

MEAN 34.0 K \rightarrow 34.0 K MAX 63.4 K \rightarrow 68.7 KAMPL. 29.3 K \rightarrow 31.7 K MIN 3.2 K \rightarrow 1.2 K

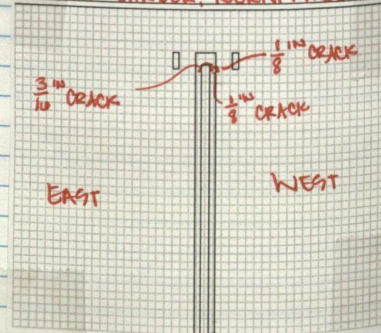
DATA: * MTS SPECIMEN ^{11:34} 30FT-1 CYCLIC (A10000) 09.30.2012
 CYCLIC END ^{13:45} 30FT-1 CYCLIC-A END 09.30.2012
 STATIC END \rightarrow 30FT-1 STATIC-A END 09.30.2012

* FILE TIME: 11:37

5000 CYCLES

NO CHANGE IN NORTH
GIRDER CRACKS

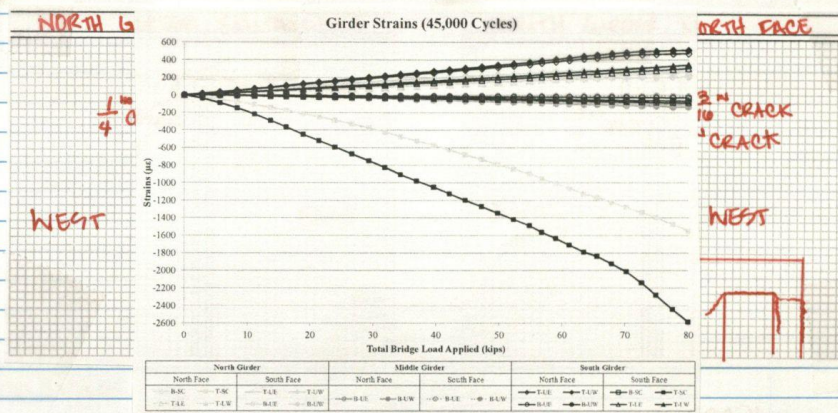
SOUTH GIRDER, NORTH FACE

SIGNATURE _____
READ AND UNDERSTOOD _____DATE _____
DATE _____20
20

10,000 CYCLES

.8 k
 9 k → 4.8 k
 9.29.2012
 12.29.2012

SOUTH
 6



05.31.2012
 (10:49)

15,000 CYCLES, 1 HZ (TOTAL 60,000)

DSP

MAX 0.126 IN → 0.121 IN

MIN 0.001 IN → 0.014 IN

FORCE

MEAN 34.4 k → 33.7 k MAX 62.0 k → 59.7 k

AMPL 26.9 k → 29.1 k MIN 6.9 k → 8.2 k

DATA: * HIS SPECIMEN 10:45 30FT-1 CYCLIC (15,000) 05.31.2012
 STATIC BEGIN 10:12 30FT-1 STATIC-a BEGIN 05.31.2012
 CYCLIC END 15:13 30FT-1 CYCLIC-a END 05.31.2012
 STATIC END 15:30 30FT-1 STATIC-a END 05.31.2012

* FILE TIME: 10:28

ADJUSTED TUNING

ORIGINAL FORCE

P: 0.07

NEW FORCE

P: 0.03 → 0.04

I: 0.006

I: 0.006

D: 0.0002

D: 0.0001

F: 0.0

F: 0.0003

512 HZ

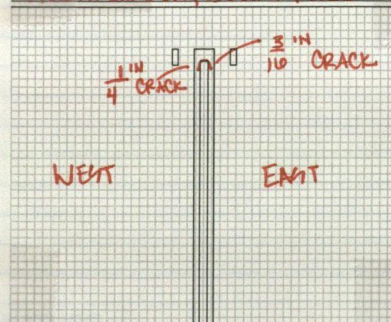
512 HZ

ORIGINAL DISP.

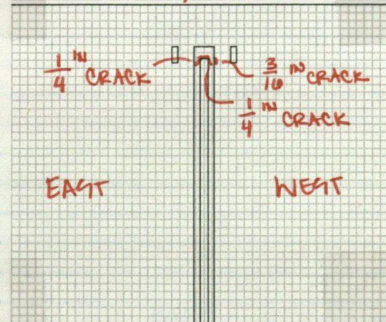
P: 12; I: 0.005; D: 0.0001, 512 HZ

5000 CYCLES

NORTH GIRDER, SOUTH FACE



SOUTH GIRDER, NORTH FACE

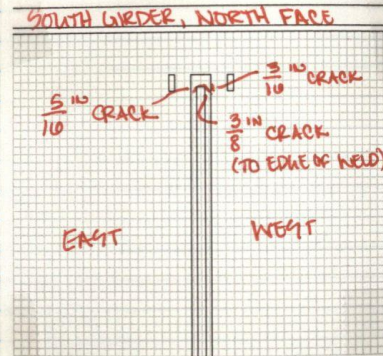
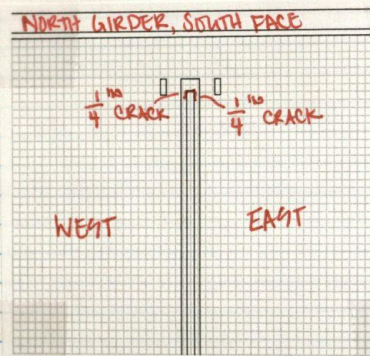


SIG.
 READ AND UNDERSTOOD

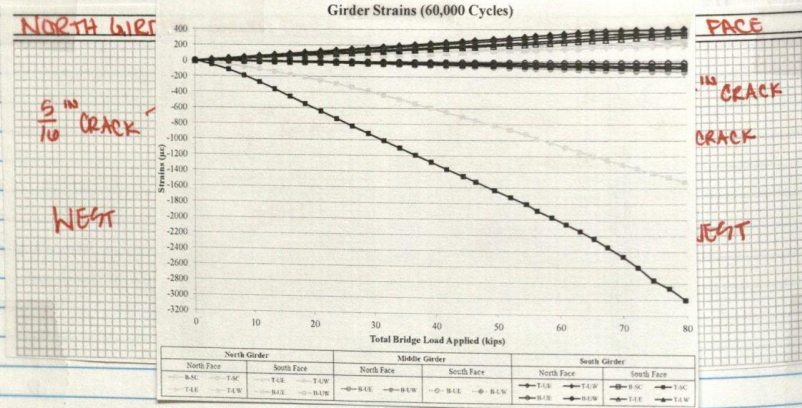
DATE

20

10,000 CYCLES



15,000 CYCLES

06.01.2012
(11:29)

15,000 CYCLES, 1 Hz (TOTAL 75,000)

DISP.

MAX 0.123 IN → 0.119 IN

MIN 0.007 IN → 0.004 IN

FORCE

MEAN 33.7 K → 33.4 K MAX 61.3 K → 61.2 K

AMPL. 27.7 K → 27.5 K MIN 3.7 K → 5.4 K

DATA: * HIS SPECIMEN 11:29 30FT-1 CYCLIC (15,000) 06.01.2012
 CYCLIC END 15:30 30FT-1 CYCLIC-a END 06.01.2012
 STATIC END 15:45 30FT-1 STATIC-a END 06.01.2012
 * FILE TIME: 11:07

SIGNATURE _____
READ AND UNDERSTOOD _____DATE _____
DATE _____20
20

5000 CYCLES

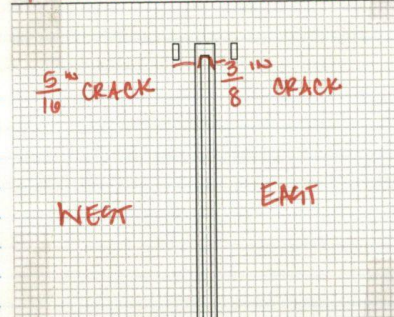
ACE

CRACK

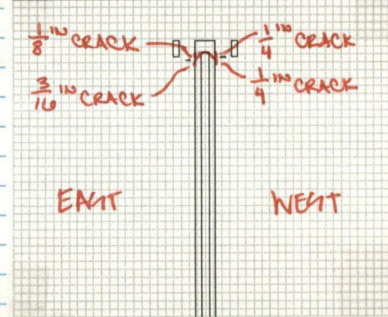
CRACK
(E OF WELD)

IT

NORTH GIRDER, SOUTH FACE



SOUTH GIRDER, NORTH FACE



10000 CYCLES

FACE

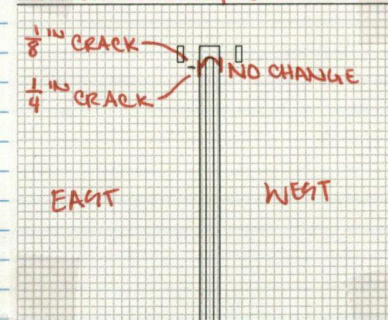
CRACK

CRACK

GIT

NO CHANGE IN NORTH
GIRDER CRACKS

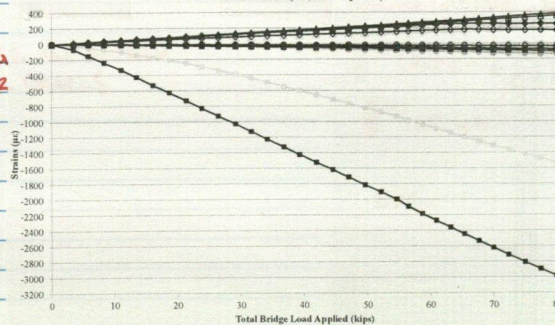
SOUTH GIRDER, NORTH FACE



15000 CYCLES

NO CHANG
GIRDER

Girder Strains (75,000 Cycles)



NORTH FACE

NO CHANGE

WEST

61.2K

5.4K

2.01.2012

01.2012

01.2012

North Girder				Middle Girder				South Girder			
North Face	South Face	North Face	South Face	North Face	South Face	North Face	South Face	North Face	South Face	North Face	South Face
→ BSC	→ TSC	→ TSC	→ TSC	→ TSC	→ TSC	→ TSC	→ TSC	→ TSC	→ TSC	→ TSC	→ TSC
→ TSC	→ TSC	→ TSC	→ TSC	→ TSC	→ TSC	→ TSC	→ TSC	→ TSC	→ TSC	→ TSC	→ TSC

SIGNATURE
READ AND UNDERSTOODDATE
DATE20
20

06.04.2012
(11:19)

15000 CYCLES, 1Hz (TOTAL 90,000)

DSP

MAX 0.122IN \rightarrow 0.129INMIN 0.011IN \rightarrow 0.009IN

FORCE

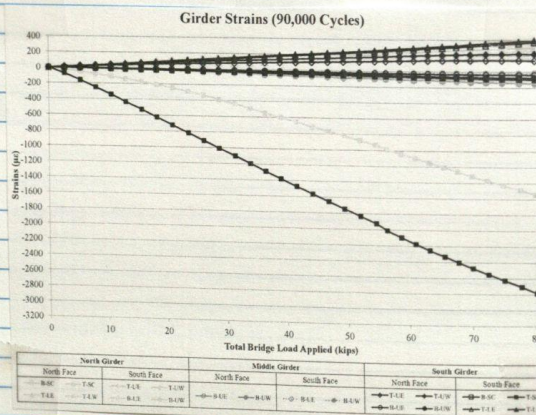
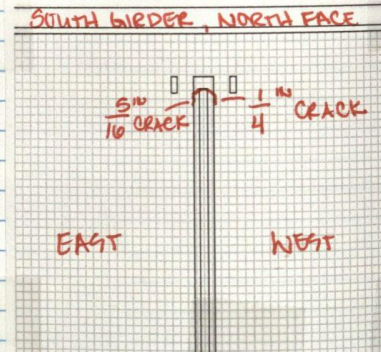
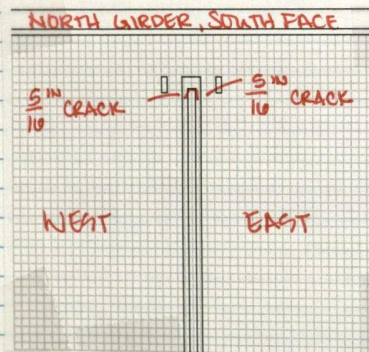
MEAN 33.2 K

MAX 60.3 K \rightarrow 61.7 KAMPL 26.3 K \rightarrow 26.8 KMIN 6.8 K \rightarrow 4.9 K

ADJUSTED FORCE P-GAIN TO 0.05

DATA: * HTS SPECIMEN \rightarrow 30FT-1 CYCLE (15000) 06.04.2012CYCLIC END \rightarrow 30FT-1 CYCLE-a END 06.04.2012STATIC END \rightarrow 30FT-1 STATIC-a END 06.04.2012

* FILE TIME: 10:58

06.09.2012
(10:10)SIGNATURE _____
READ AND UNDERSTOOD _____DATE _____
DATE _____20
20

OK NO.

11

PROJECT NAME

NOTEBOOK NO.

06.09.2012
(10:10)

15000 CYCLES, 1 HE (TOTAL 109,000)

DSP

MAX 0.129 IN

MIN 0.011 IN

FORCE

MEAN 33.2 K

MAX 60.4 K

AMPL 26.0 K

MIN 5.8 K

DATA: * MTS SPECIMEN 10:10 30FT-1 CYCLIC (a15000) 06.09.2012
 CYCLIC END 14:22 30FT-1 CYCLIC-a END 06.09.2012
 STATIC END 14:34 30FT-1 STATIC-a END 06.09.2012

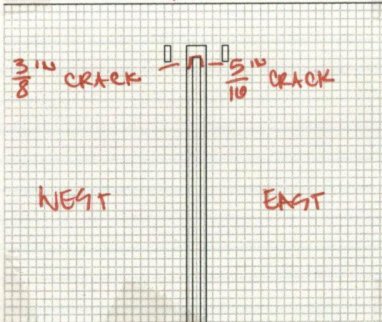
* FILE TIME: 9:54

N FACE

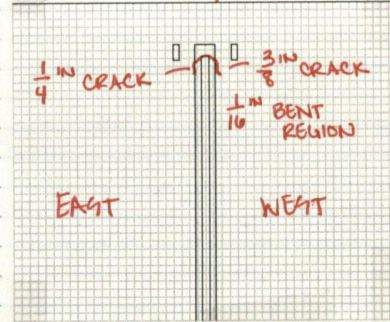
CRACK

WEST

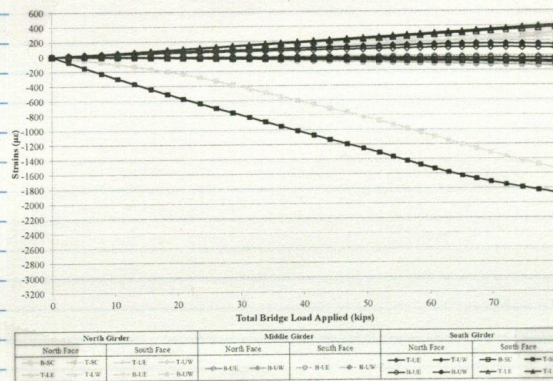
NORTH GIRDER, SOUTH FACE



SOUTH GIRDER, NORTH FACE



Girder Strains (105,000 Cycles)

SIGNATURE
READ AND UNDERSTOODDATE
DATE 20

(14:35)

10000 CYCLES, 1HZ (TOTAL 115,000)

(12:49)

DISP MAX 0.133IN

MIN 0.017IN \rightarrow 0.019IN

FORCE

MEAN 33.4K \rightarrow 32.9K MAX 62.5KAMPL 26.9K \rightarrow 26.4K MIN 6.1K \rightarrow 5.9KDATA: * MTS SPECIMEN $\xrightarrow{14:35}$ 30Pr-1 CYCLIC (b10000) 06.05.2012

* FILE TIME: 14:18

06.06.2012 5000 CYCLES, 1HZ (TOTAL 120,000)

(11:10)

DISP

MAX 0.124IN \rightarrow 0.133INMIN 0.009IN \rightarrow 0.007IN

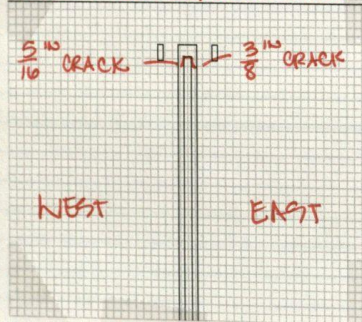
FORCE

MEAN 33.8K

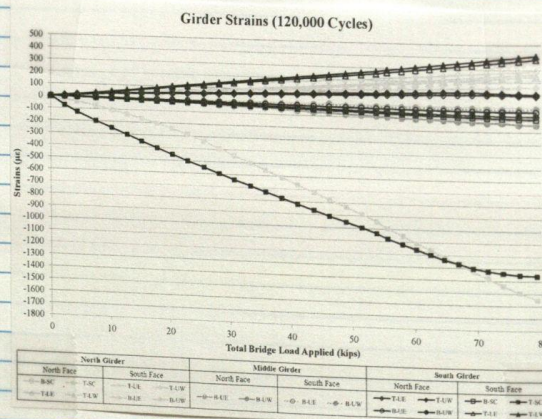
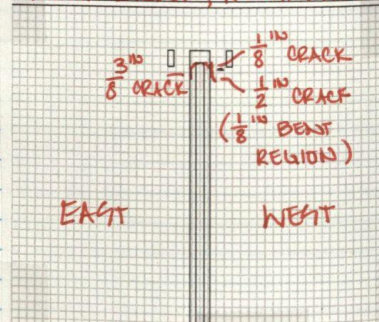
MAX 60.1K \rightarrow 69.9KAMPL 26.2K \rightarrow 28.1KMIN 5.5K \rightarrow 4.4KDATA: * MTS SPECIMEN $\xrightarrow{11:10}$ 30Pr-1 CYCLIC (a5000) 06.06.2012CYCLIC END $\xrightarrow{12:35}$ 30Pr-1 CYCLIC-a END 06.06.2012STATIC END $\xrightarrow{12:46}$ 30Pr-1 STATIC-a END 06.06.2012

* FILE TIME: 10:53

NORTH GIRDER, SOUTH FACE



SOUTH GIRDER, NORTH FACE

SIGNATURE _____
READ AND UNDERSTOOD _____DATE _____
DATE _____20
20

BOOK NO.

13

PROJECT NAME

NOTEBOOK NO.

(12:49) 15000 CYCLES, 1HZ (TOTAL 135,000)

DISP MAX 0.138 IN \rightarrow 0.139 INMIN 0.011 IN \rightarrow 0.003 INFORCE MEAN 338 K \rightarrow 330 KMAX 62.2 K \rightarrow 66.3 KAMPL 28.9 K \rightarrow 30.9 KMIN 5.0 K \rightarrow 1.3 K \rightarrow 5.9 K

05.2012

DATA:

* MTS SPECIMEN

30 FT-1 CYCLIC (615000) 06.06.2012

CYCLIC END

30 FT-1 CYCLIC - b END 06.06.2012

STATIC END

30 FT-1 STATIC - b END 06.06.2012

* FILE TIME:

AT 5700 CYCLES \rightarrow ADJUSTED P-GAIN TO 0.04

FORCE MAX 67.8 K

MIN 1.8 K

 \rightarrow 69.9 K \rightarrow 4.4 K

06.06.2012

06.06.2012

06.06.2012

TH FACE

NO CRACK

NO CRACK

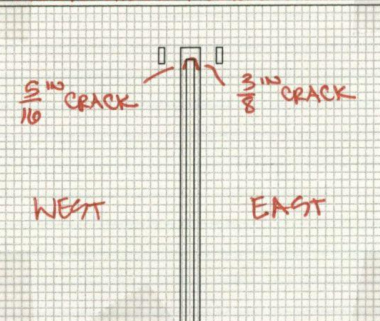
BENT

ELONG)

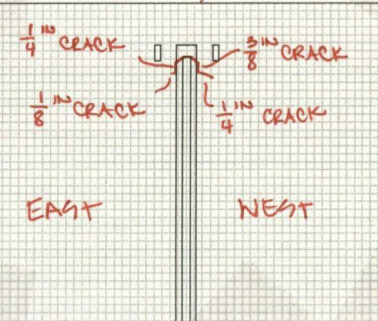
WEST

WEST

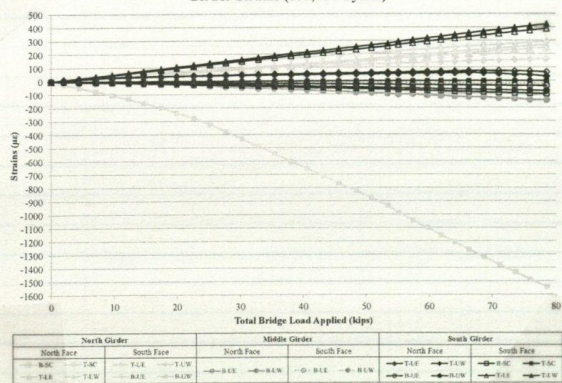
NORTH GIRDER, SOUTH FACE



SOUTH GIRDER, NORTH FACE



Girder Strains (135,000 Cycles)

LO4T: 69-S T-9C (POSSIBLE START OF CRACK ON BACK SIDE \rightarrow THROUGH CRACK)SIGNATURE
READ AND UNDERSTOODDATE 20
DATE 20

06.07.2012
(9:44)

15000 CYCLES, 1 HZ (TOTAL 150,000)

DSP

MAX 0.1301W → 0.1391W

MIN 0.0091W

FORCE

MEAN 32.9 K → 33.6 K MAX 63.6 K → 65.1 K

AMPL 27.8 K → 28.9 K MIN 3.8 K → 3.3 K

DATA: * MTS SPECIMEN → 30FT-1 CYCLIC (15000) 06.07.2012

CYCLIC END → 30FT-1 CYCLIC - A END 06.07.2012

STATIC END → 30FT-1 STATIC - A END 06.07.2012

* FILE TIME: 9:26

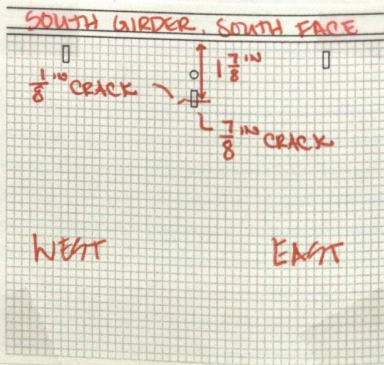
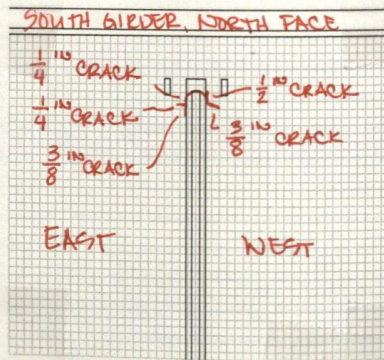
AT 4900 CYCLES → ADJUSTED P-GAIN TO 0.03

FORCE MAX 80.6 K

MIN -0.2 K

→ DISPLACEMENT P-GAIN TO 6

NO CHANGE IN NORTH
GIRDER CRACKS



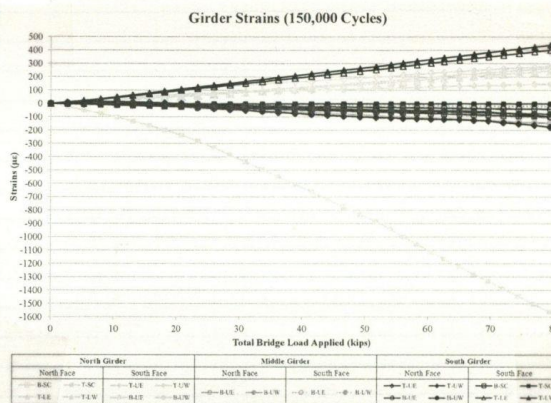
09.27.2012

SIGNATURE _____
READ AND UNDERSTOOD _____

DATE _____
DATE _____

20
20

1K → 45.1k
 1K → 33k
 07.2012
 7.2012
 7.2012



GAGE CHANGES: G9-S T-9C MOVED 1" EAST AND 1" DOWN
 → G9-S T-9E

G9-S T-9E REPLACED

G9-N T-9E REPLACED

STRING POT 1-6 REPLACED LVDTs 1-6

DATA: STATIC → 30FF-1 STATIC 09.18.2012

RETROFIT APPLIED → TOP WEB GMP, N & S

- ANGLES

- BACKPLATE

60-600k

09.27.2012 5000 CYCLES, 2 Hz (RETROFIT 5000, TOTAL 155,000)

DISP MAX 0.119 in

MIN 0.010 in

FORCE MEAN 33.3 k

HAX 60.9 k

AMPL 25.6 k

MIN 6.8 k

DATA: * H18 SPECIMEN → 30FF-1 CYCLE (5000) 09.27.2012

STATIC BEGIN → 30FF-1 STATIC 09.27.2012

* FILE TIME: 13:39

ADJUSTED FORCE P-GAIN TO 0.07

SIGNATURE
 READ AND UNDERSTOOD

DATE 20
 DATE 20

Date	Cycles	Time	File Time	Specimen Name / Notes	Displacement		Force	
					Max	Min	Max	Min
09.27.2012	6000	13:03	13:05	30Fr-1 Cyclic (5000) 09.27.2012 Force P→0.07	0.119	0.010	29.6	60.9
09.28.2012	10000	9:28	9:12	30Fr-1 Cyclic (15000) 09.28.2012	0.118	0.008	29.2	60.9
10.01.2012	185000	10:12	9:57	30Fr-1 Cyclic (15000) 10.01.2012	0.125	0.013	29.4	60.4
	200000	12:21	12:05	30Fr-1 Cyclic (15000) 10.01.2012	0.120	0.008	29.5	60.0
	219000	14:34	14:18	30Fr-1 Cyclic (15000) 10.01.2012	0.122	0.008	29.0	60.4
	230000	16:42	16:26	30Fr-1 Cyclic (15000) 10.01.2012	0.122	0.010	29.1	60.9
10.02.2012	249000	11:10	10:55	30Fr-1 Cyclic (15000) 10.02.2012	0.121	0.008	29.8	60.1
	269000	13:26	13:11	30Fr-1 Cyclic (15000) 10.02.2012	0.121	0.007	29.9	60.4
	289000	15:40	15:25	30Fr-1 Cyclic (15000) 10.02.2012	0.122	0.010	29.7	60.9
10.03.2012	309000	8:44	8:29	30Fr-1 Cyclic (15000) 10.03.2012	0.122	0.013	29.4	60.1
	329000	11:04	10:48	30Fr-1 Cyclic (15000) 10.03.2012	0.121	0.008	29.5	60.2
	349000	13:19	13:03	30Fr-1 Cyclic (15000) 10.03.2012	0.121	0.006	29.6	60.5
	369000	15:24	15:08	30Fr-1 Cyclic (15000) 10.03.2012 Force P→0.08 I→0.007	0.121	0.011	29.6	60.2
	389000	17:39	17:19	30Fr-1 Cyclic (15000) 10.03.2012	0.124	0.010	29.0	60.9
10.04.2012	409000	8:28	8:12	30Fr-1 Cyclic (15000) 10.04.2012	0.124	0.010	29.0	60.7
	429000	10:32	10:16	30Fr-1 Cyclic (15000) 10.04.2012	0.123	0.008	29.4	60.4
	449000	12:46	12:30	30Fr-1 Cyclic (15000) 10.04.2012	0.122	0.010	29.9	60.2
	469000	14:50	14:34	30Fr-1 Cyclic (15000) 10.04.2012	0.118	0.008	29.1	60.9
	489000	17:14	16:58	30Fr-1 Cyclic (15000) 10.04.2012	0.110	0.006	29.0	60.2
10.05.2012	509000	7:53	7:38	30Fr-1 Cyclic (15000) 10.05.2012	0.126	0.008	29.2	60.9
	529000	10:08	9:52	30Fr-1 Cyclic (15000) 10.05.2012	0.125	0.008	29.3	60.4
	549000	12:26	12:10	30Fr-1 Cyclic (15000) 10.05.2012	0.118	0.007	29.7	60.9
10.06.2012	569000	13:10	12:54	30Fr-1 Cyclic (15000) 10.06.2012	0.124	0.008	29.6	60.2
	589000	15:19	15:03	30Fr-1 Cyclic (15000) 10.06.2012	0.124	0.009	29.7	60.4
10.07.2012	609000	17:10	16:54	30Fr-1 Cyclic (15000) 10.07.2012	0.124	0.008	29.7	60.9
	629000	19:24	19:08	30Fr-1 Cyclic (15000) 10.07.2012	0.124	0.008	29.7	60.9
10.08.2012	649000	21:38	21:22	30Fr-1 Cyclic (15000) 10.08.2012	0.124	0.008	29.7	60.9
	669000	23:52	23:36	30Fr-1 Cyclic (15000) 10.08.2012	0.124	0.008	29.7	60.9
10.09.2012	689000	26:06	25:50	30Fr-1 Cyclic (15000) 10.09.2012	0.124	0.008	29.7	60.9
	709000	28:20	28:04	30Fr-1 Cyclic (15000) 10.09.2012	0.124	0.008	29.7	60.9
10.10.2012	729000	30:34	30:18	30Fr-1 Cyclic (15000) 10.10.2012	0.124	0.008	29.7	60.9
	749000	32:48	32:32	30Fr-1 Cyclic (15000) 10.10.2012	0.124	0.008	29.7	60.9
10.11.2012	769000	34:52	34:36	30Fr-1 Cyclic (15000) 10.11.2012	0.124	0.008	29.7	60.9
	789000	37:06	36:50	30Fr-1 Cyclic (15000) 10.11.2012	0.124	0.008	29.7	60.9
10.12.2012	809000	39:20	39:04	30Fr-1 Cyclic (15000) 10.12.2012	0.124	0.008	29.7	60.9
	829000	41:34	41:18	30Fr-1 Cyclic (15000) 10.12.2012	0.124	0.008	29.7	60.9
10.13.2012	849000	43:48	43:32	30Fr-1 Cyclic (15000) 10.13.2012	0.124	0.008	29.7	60.9
	869000	46:02	45:46	30Fr-1 Cyclic (15000) 10.13.2012	0.124	0.008	29.7	60.9
10.14.2012	889000	48:16	48:00	30Fr-1 Cyclic (15000) 10.14.2012	0.124	0.008	29.7	60.9
	909000	50:30	50:14	30Fr-1 Cyclic (15000) 10.14.2012	0.124	0.008	29.7	60.9
10.15.2012	929000	52:44	52:28	30Fr-1 Cyclic (15000) 10.15.2012	0.124	0.008	29.7	60.9
	949000	54:58	54:42	30Fr-1 Cyclic (15000) 10.15.2012	0.124	0.008	29.7	60.9
10.16.2012	969000	57:12	56:56	30Fr-1 Cyclic (15000) 10.16.2012	0.124	0.008	29.7	60.9
	989000	59:26	59:10	30Fr-1 Cyclic (15000) 10.16.2012	0.124	0.008	29.7	60.9
10.17.2012	1009000	61:40	61:24	30Fr-1 Cyclic (15000) 10.17.2012	0.124	0.008	29.7	60.9
	1029000	63:54	63:38	30Fr-1 Cyclic (15000) 10.17.2012	0.124	0.008	29.7	60.9
10.18.2012	1049000	66:08	65:52	30Fr-1 Cyclic (15000) 10.18.2012	0.124	0.008	29.7	60.9
	1069000	68:22	68:06	30Fr-1 Cyclic (15000) 10.18.2012	0.124	0.008	29.7	60.9
10.19.2012	1089000	70:36	70:20	30Fr-1 Cyclic (15000) 10.19.2012	0.124	0.008	29.7	60.9
	1109000	72:50	72:34	30Fr-1 Cyclic (15000) 10.19.2012	0.124	0.008	29.7	60.9
10.20.2012	1129000	75:04	74:48	30Fr-1 Cyclic (15000) 10.20.2012	0.124	0.008	29.7	60.9
	1149000	77:18	77:02	30Fr-1 Cyclic (15000) 10.20.2012	0.124	0.008	29.7	60.9
10.21.2012	1169000	79:32	79:16	30Fr-1 Cyclic (15000) 10.21.2012	0.124	0.008	29.7	60.9
	1189000	81:46	81:30	30Fr-1 Cyclic (15000) 10.21.2012	0.124	0.008	29.7	60.9
10.22.2012	1209000	83:50	83:34	30Fr-1 Cyclic (15000) 10.22.2012	0.124	0.008	29.7	60.9
	1229000	86:04	85:48	30Fr-1 Cyclic (15000) 10.22.2012	0.124	0.008	29.7	60.9
10.23.2012	1249000	88:18	88:02	30Fr-1 Cyclic (15000) 10.23.2012	0.124	0.008	29.7	60.9
	1269000	90:32	90:16	30Fr-1 Cyclic (15000) 10.23.2012	0.124	0.008	29.7	60.9
10.24.2012	1289000	92:46	92:30	30Fr-1 Cyclic (15000) 10.24.2012	0.124	0.008	29.7	60.9
	1309000	94:50	94:34	30Fr-1 Cyclic (15000) 10.24.2012	0.124	0.008	29.7	60.9
10.25.2012	1329000	97:04	96:48	30Fr-1 Cyclic (15000) 10.25.2012	0.124	0.008	29.7	60.9
	1349000	99:18	99:02	30Fr-1 Cyclic (15000) 10.25.2012	0.124	0.008	29.7	60.9
10.26.2012	1369000	101:32	101:16	30Fr-1 Cyclic (15000) 10.26.2012	0.124	0.008	29.7	60.9
	1389000	103:46	103:30	30Fr-1 Cyclic (15000) 10.26.2012	0.124	0.008	29.7	60.9
10.27.2012	1409000	105:50	105:34	30Fr-1 Cyclic (15000) 10.27.2012	0.124	0.008	29.7	60.9
	1429000	108:04	107:48	30Fr-1 Cyclic (15000) 10.27.2012	0.124	0.008	29.7	60.9
10.28.2012	1449000	110:18	110:02	30Fr-1 Cyclic (15000) 10.28.2012	0.124	0.008	29.7	60.9
	1469000	112:32	112:16	30Fr-1 Cyclic (15000) 10.28.2012	0.124	0.008	29.7	60.9
10.29.2012	1489000	114:46	114:30	30Fr-1 Cyclic (15000) 10.29.2012	0.124	0.008	29.7	60.9
	1509000	116:50	116:34	30Fr-1 Cyclic (15000) 10.29.2012	0.124	0.008	29.7	60.9
10.30.2012	1529000	119:04	118:48	30Fr-1 Cyclic (15000) 10.30.2012	0.124	0.008	29.7	60.9
	1549000	121:18	121:02	30Fr-1 Cyclic (15000) 10.30.2012	0.124	0.008	29.7	60.9
10.31.2012	1569000	123:32	123:16	30Fr-1 Cyclic (15000) 10.31.2012	0.124	0.008	29.7	60.9
	1589000	125:46	125:30	30Fr-1 Cyclic (15000) 10.31.2012	0.124	0.008	29.7	60.9
11.01.2012	1609000	127:50	127:34	30Fr-1 Cyclic (15000) 11.01.2012	0.124	0.008	29.7	60.9
	1629000	129:54	129:38	30Fr-1 Cyclic (15000) 11.01.2012	0.124	0.008	29.7	60.9
11.02.2012	1649000	132:08	131:52	30Fr-1 Cyclic (15000) 11.02.2012	0.124	0.008	29.7	60.9
	1669000	134:22	134:06	30Fr-1 Cyclic (15000) 11.02.2012	0.124	0.008	29.7	60.9
11.03.2012	1689000	136:36	136:20	30Fr-1 Cyclic (15000) 11.03.2012	0.124	0.008	29.7	60.9
	1709000	138:50	138:34	30Fr-1 Cyclic (15000) 11.03.2012	0.124	0.008	29.7	60.9
11.04.2012	1729000	140:54	140:38	30Fr-1 Cyclic (15000) 11.04.2012	0.124	0.008	29.7	60.9
	1749000	143:08	142:52	30Fr-1 Cyclic (15000) 11.04.2012	0.124	0.008	29.7	60.9
11.05.2012	1769000	145:12	144:56	30Fr-1 Cyclic (15000) 11.05.2012	0.124	0.008	29.7	60.9
	1789000	147:26	147:10	30Fr-1 Cyclic (15000) 11.05.2012	0.124	0.008	29.7	60.9
11.06.2012	1809000	149:30	149:14	30Fr-1 Cyclic (15000) 11.06.2012	0.124	0.008	29.7	60.9
	1829000	151:44	151:28	30Fr-1 Cyclic (15000) 11.06.2012	0.124	0.008	29.7	60.9
11.07.2012	1849000	153:58	153:42	30Fr-1 Cyclic (15000) 11.07.2012	0.124	0.008	29.7	60.9
	1869000	156:02	155:46	30Fr-1 Cyclic (15000) 11.07.2012	0.124	0.008	29.7	60.9
11.08.2012	1889000	158:16	158:00	30Fr-1 Cyclic (15000) 11.08.2012	0.124	0.008	29.7	60.9
	1909000	160:30	160:14	30Fr-1 Cyclic (15000) 11.08.2012	0.124	0.008	29.7	60.9
11.09.2012	1929000	162:44	162:28	30Fr-1 Cyclic (15000) 11.09.2012	0.124	0.008	29.7	60.9
	1949000	164:58	164:42	30Fr-1 Cyclic (15000) 11.09.2012	0.124	0.008	29.7	60.9
11.10.2012	1969000	167:02	166:46	30Fr-1 Cyclic (15000) 11.10.2012	0.124	0.008	29.7	60.9
	1989000	169:16	169:00	30Fr-1 Cyclic (15000) 11.10.2012	0.124	0.008	29.7	60.9
11.11.2012	2009000	171:30	171:14	30Fr-1 Cyclic (15000) 11.11.2012	0.124	0.008	29.7	60.9
	2029000	173:44	173:28	30Fr-1 Cyclic (15000) 11.11.2012	0.124	0.008	29.7	60.9
11.12.2012	2049000	175:58	175:42	30Fr-1 Cyclic (15000) 11.12.2012	0.124	0.008	29.7	60.9
	2069000	178:02	177:46	30Fr-1 Cyclic (15000) 11.12.2012	0.124	0.008	29.7	60.9
11.13.2012	2089000	180:16	180:00	30Fr-1 Cyclic (15000) 11.13.2012	0.124	0.008	29.7	60.9
	2109000	182:30	182:14	30Fr-1 Cyclic (15000) 11.13.2012	0.124	0.008	29.7	60.9
11.14.2012	2129000	184:44	184:28	30Fr-1 Cyclic (15000) 11.14.2012	0.124	0.008	29.7	60.9
	2149000	186:58	186:42	30Fr-1 Cyclic (15000) 11.14.2012	0.124	0.008	29.7	60.9
11.15.2012	2169000	189:02	188:46	30Fr-1 Cyclic (15000) 11.15.2012	0.124	0.008	29.7	60.9
	2189000	191:16	191:00	30Fr-1 Cyclic (15000) 11.15.2012	0.124	0.008	29.7	

Date	Cycles		Time	File Time	Specimen Name / Notes	Displacement		Force	
	Trial	Total				Max	Min	Ampl	Max
10.11.2012	3040000	545000	9:07	8:51	30FT-1 CYCLIC (Δ15000) 10.11.2012	0.127	0.007	33.2	62.0
						0.125	0.009	33.4	61.4
	410000	500000	12:04	11:48	30FT-1 CYCLIC (Δ15000) 10.11.2012	0.123	0.013	33.0	62.1
						0.125	0.008	33.4	61.2
	425000	575000	15:29	15:13	30FT-1 CYCLIC (Δ15000) 10.11.2012	0.125	0.014	33.7	61.3
						0.124	0.011	33.5	61.0
	440000	590000	18:08	17:52	30FT-1 CYCLIC (Δ15000) 10.11.2012	0.126	0.014	34.0	62.7
						0.126	0.010	33.6	61.2
	455000	605000	20:34	20:17	30FT-1 CYCLIC (Δ15000) 10.11.2012	0.124	0.012	34.1	62.6
						0.124	0.009	33.6	62.6
10.12.2012	470000	620000	23:53	23:36	30FT-1 CYCLIC (Δ15000) 10.11.2012	0.126	0.012	33.7	63.3
						0.122	0.008	33.4	61.9
	485000	635000	10:01	9:45	30FT-1 CYCLIC (Δ15000) 10.12.2012	0.128	0.007	33.7	62.5
						0.126	0.007	33.9	62.2
	500000	650000	12:22	12:06	30FT-1 CYCLIC (Δ15000) 10.12.2012	0.126	0.012	34.2	63.5
						0.184	0.009	33.9	62.3
	515000	665000	14:37	14:21	30FT-1 CYCLIC (Δ15000) 10.12.2012	0.129	0.012	34.3	64.9
						0.125	0.007	33.8	61.8
	530000	680000	9:57	9:42	30FT-1 CYCLIC (Δ15000) 10.12.2012	0.115	0.007	33.5	59.4
					Force P → 0.09	0.120	0.008	33.3	61.5
10.13.2012	545000	695000	13:05	12:50	30FT-1 CYCLIC (Δ15000) 10.13.2012	0.123	0.008	33.4	62.9
						0.124	0.005	33.4	62.1
	560000	710000	11:08	10:53	30FT-1 CYCLIC (Δ15000) 10.13.2012	0.128	0.013	33.5	64.4
						0.127	0.010	33.3	61.1
	575000	725000	13:16	13:00	30FT-1 CYCLIC (Δ15000) 10.13.2012	0.128	0.014	33.8	62.4
10.17.2012	590000	740000	15:33	15:17	30FT-1 CYCLIC (Δ15000) 10.16.2012	0.130	0.016	33.5	62.6
						0.130	0.014	33.3	61.4
	605000	755000	10:53	10:38	30FT-1 CYCLIC (Δ15000) 10.17.2012	0.119	0.007	33.0	60.6
						0.123	0.006	33.1	61.6
	620000	770000	13:22	13:06	30FT-1 CYCLIC (Δ15000) 10.17.2012	0.125	0.011	33.4	62.5
						0.124	0.008	33.3	60.6
	635000	785000	15:46	15:31	30FT-1 CYCLIC (Δ15000) 10.17.2012	0.125	0.011	33.5	62.2
						0.124	0.007	33.4	61.2
	650000	800000	8:21	8:06	30FT-1 CYCLIC (Δ15000) 10.18.2012	0.126	0.014	33.4	60.4
						0.127	0.011	33.2	62.1
10.18.2012	665000	815000	10:38	10:22	30FT-1 CYCLIC (Δ15000) 10.18.2012	0.127	0.014	33.4	62.1
						0.125	0.008	33.2	60.8
	680000	830000	12:45	12:29	30FT-1 CYCLIC (Δ15000) 10.18.2012	0.128	0.014	33.6	62.5
						0.124	0.008	33.4	60.6
	695000	845000	14:53	14:38	30FT-1 CYCLIC (Δ15000) 10.18.2012	0.123	0.012	33.7	62.5
						0.121	0.004	33.5	61.0
	710000	860000				0.125	0.004	33.5	61.1
						0.121	0.006	33.5	61.0
	725000	875000	11:46	11:31	30FT-1 CYCLIC (Δ15000) 10.19.2012	0.117	0.003	34.1	62.9
						0.115	-0.002	33.5	61.2
10.19.2012	740000	890000	13:54	13:38	30FT-1 CYCLIC (Δ15000) 10.19.2012	0.113	0.003	33.7	62.1
						0.116	-0.002	33.5	61.0
						0.126	0.001	33.5	61.4

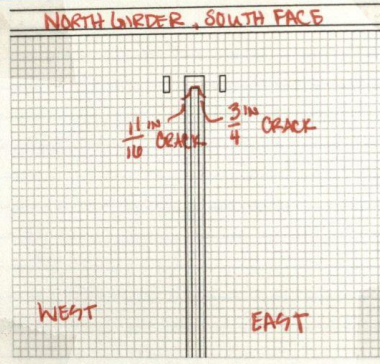
READ AND UNDERSTOOD

DATE

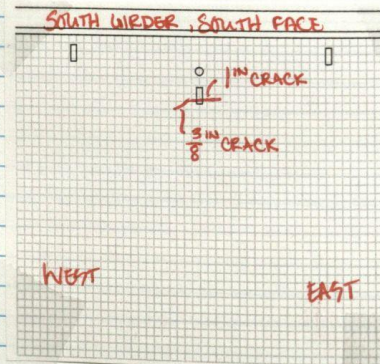
20

Date	Cycles	Time	File Time	Specimen Name / Notes	Displacement		Force	
					Max	Min	Ampl	Max
10.22.2012	1,010,000	10:01	9:45	306r-1 CREVIC (A15000) 10.22.2012 FORCE P → 0.10	0.130	0.016	32.9	61.3
	1,029,000	12:50	12:34	306r-1 CREVIC (B15000) 10.22.2012	0.129	0.014	33.2	61.0
	1,175,000	14:57	14:42	306r-1 CREVIC (A15000) 10.22.2012	0.129	0.014	33.1	62.1
					0.128	0.011	33.3	62.2
					0.128	0.008	33.4	61.2
					0.125	0.004	33.4	61.2
10.24.2012	1,190,000	11:20	11:04	306r-1 CREVIC (A15000) 10.24.2012 FORCE P → 0.09 I → 0.009	0.129	0.015	33.6	61.3
	1,200,000	13:43	13:27	306r-1 CREVIC (B10000) 10.24.2012 FORCE P → 0.08 I → 0.010	0.130	0.011	33.6	62.6
					0.130	0.014	33.7	62.4
					0.133	0.014	33.8	62.5

RETROFIT REMOVED



SOUTH GIRDER, NORTH FACE → NO CHANGE



RE UNDERSTOOD

DATE
DATE20
20

RETROFIT APPLIED
TOP WEB-GAP, N&S

- ANGLES
- BACKPLATE

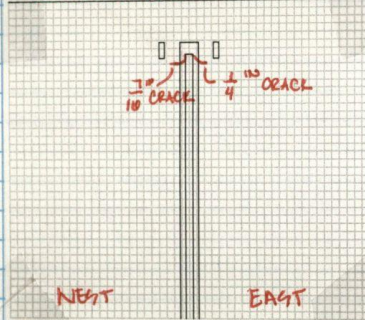
8-80^K

Date	Cycles	Time	File Time	Specimen Name / Notes	Displacement		Force	
					Max	Min	Mean	Ampl
12.11.2012	150,000	12:02	11:46	30Fr-1 CYCLIC (150000) 12.11.2012	0.174	0.003	49.1	31.0
	1,500,000				0.168	0.017	49.6	36.5
					0.168	0.014	44.9	36.5
					0.163	0.008	44.9	36.4
12.12.2012	300,000	9:41	9:26	30Fr-1 CYCLIC (150000) 12.12.2012	0.167	0.015	49.9	36.4
	1,650,000				0.165	0.012	44.8	36.1
					0.166	0.015	45.0	36.2
					0.167	0.011	45.0	36.4
12.13.2012	400,000	9:34	9:18	30Fr-1 CYCLIC (150000) 12.13.2012	0.172	0.020	45.6	36.8
	1,800,000				0.169	0.017	49.1	36.1
					0.169	0.013	49.0	36.1
12.14.2012	600,000	9:34	9:18	30Fr-1 CYCLIC (150000) 12.14.2012	0.172	0.032	49.0	36.6
	1,900,000				0.172	0.017	49.0	36.7
					0.171	0.015	44.9	36.7
					0.171	0.014	45.0	36.6
12.17.2012	700,000	11:41	11:24	30Fr-1 CYCLIC (150000) 12.17.2012	0.170	0.023	44.6	36.0
	2,100,000				0.170	0.023	44.6	36.9
					0.170	0.011	44.7	36.6
					0.169	0.012	44.8	35.9
12.18.2012	900,000	11:05	10:49	30Fr-1 CYCLIC (150000) 12.18.2012	0.173	0.023	45.0	36.0
	2,150,000				0.169	0.020	44.8	36.5
					0.169	0.014	44.8	35.9
12.19.2012	1,050,000	10:40	10:23	30Fr-1 CYCLIC (150000) 12.19.2012	0.169	0.021	49.1	36.0
	2,400,000				0.169	0.009	44.8	35.5
					0.169	0.014	44.8	35.6
12.20.2012	1,200,000	12:52	12:36	30Fr-1 CYCLIC (150000) 12.20.2012	0.178	0.028	49.4	36.0
	2,550,000				0.175	0.016	44.8	35.5
					0.167	0.013	44.8	35.5
					0.162	0.014	44.8	35.6

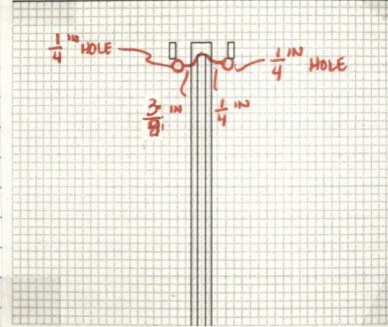
SIGNATURE _____
READ AND UNDERSTOOD

RETOFIT REMOVEDEDGE OF CRACK AT
EDGE OF CSH

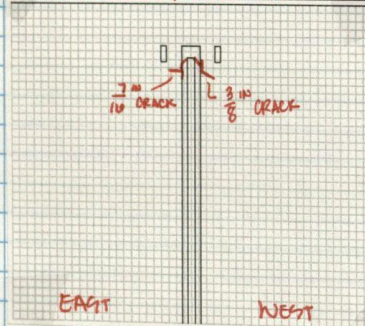
NORTH GIRDER, SOUTH FACE



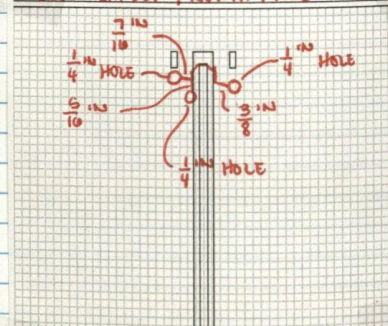
NORTH GIRDER, SOUTH FACE



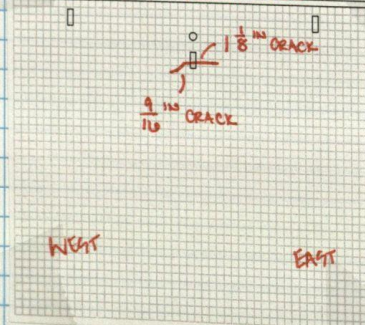
SOUTH GIRDER, NORTH FACE



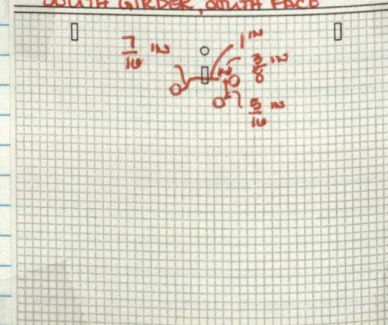
SOUTH GIRDER, NORTH FACE



SOUTH GIRDER, SOUTH FACE



SOUTH GIRDER, SOUTH FACE

SIGNATURE _____
READ AND UNDERSTOOD _____DATE _____
DATE _____20
20

RETROFIT APPLIED

TOP WEB GAP N & S

- ANGLES

- BACK PLATE

- $\frac{1}{4}$ " CRACK STOP HOLES

10-100K

01.10.2013 : NOTICED FAINT CLICKING SOUND AT NORTH GIRDER
CROSS FRAME (~ 650,000 CYCLES)

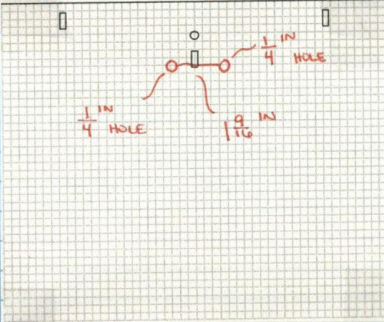
01.17.2013 : NORTH CROSS FRAME BROKEN (1,061,097 CYCLES)

SIGNATURE _____
READ AND UNDERSTOOD _____DATE _____ 20
DATE _____ 20

Date	Cycles	Total	Time	File Time	Specimen Name / Notes	Displacement		Force	
						Max	Min	Mean	Ampl
01.04.2013	190,000	2,700,000	12:21	12:04	30Fr-1 CYCLIC (150000) 01.04.2013 FORCE P→0.05	0.230	0.016	56.6	46.5
						0.230	0.016	57.2	49.2
						0.209	0.018	56.6	46.9
						0.221	0.009	57.0	46.0
01.09.2013	300,000	2,850,000	14:43	19:27	30Fr-1 CYCLIC (150000) 01.05.2013	0.215	0.034	57.4	44.3
						0.211	0.025	56.7	44.3
						0.216	0.018	56.6	49.6
						0.215	0.011	56.7	46.5
01.07.2013	450,000	3,800,000	4:58	9:42	30Fr-1 CYCLIC (150000) 01.07.2013	0.222	0.035	56.7	45.4
						0.218	0.025	56.7	45.7
						0.210	0.024	56.7	45.6
						0.213	0.015	56.9	44.4
						0.209	0.027	56.9	44.4
						0.218	0.017	56.9	44.1
01.08.2013	600,000	3,150,000	14:21	14:04	30Fr-1 CYCLIC (150000) 01.08.2013	0.219	0.035	57.0	44.1
						0.212	0.023	56.8	44.4
						0.213	0.025	56.8	44.4
						0.212	0.027	56.7	44.1
						0.225	0.032	56.8	44.3
01.10.2013	750,000	3,300,000	9:04	8:48	30Fr-1 CYCLIC (150000) 01.10.2013	0.225	0.044	57.0	44.3
						0.222	0.032	56.7	43.7
						0.219	0.023	56.6	43.8
						0.223	0.033	56.6	43.5
01.14.2013	900,000	3,450,000	12:42	12:25	30Fr-1 CYCLIC (150000) 01.14.2013	0.222	0.036	56.8	44.8
						0.225	0.029	56.9	44.2
						0.226	0.013	56.5	43.1
						0.208	0.022	56.3	43.2
						0.218	0.020	56.6	46.7
01.15.2013	1,050,000	3,600,000	16:49	16:32	30Fr-1 CYCLIC (150000) 01.15.2013	0.216	0.025	56.8	46.6
						0.226	0.015	56.8	46.9
						0.214	0.012	56.8	47.2
						0.220	0.006	56.5	46.5
						0.225	0.027	56.6	46.8
01.17.2013	1,450,000 1,061,097	3,750,000 3,611,097	7:40	7:24	30Fr-1 CYCLIC (150000) 01.17.2013	0.234	0.031	56.9	46.9
						0.228	0.029	56.10	46.7
									44.2

RETROFIT REMOVED

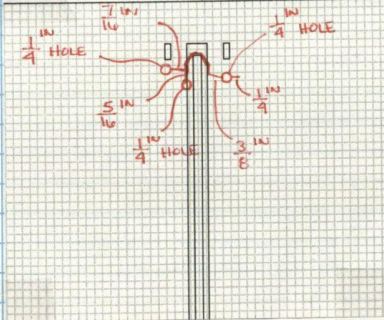
NORTH GIRDER, NORTH FACE



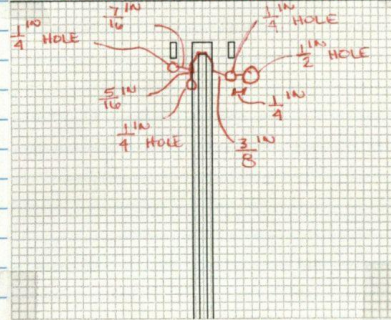
NORTH GIRDER, SOUTH FACE

→ NO CHANGE

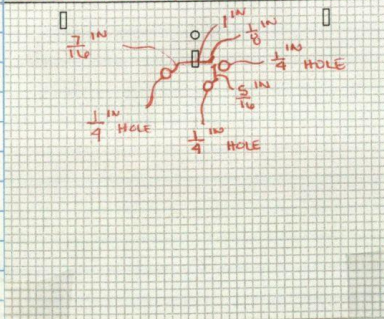
SOUTH GIRDER, NORTH FACE



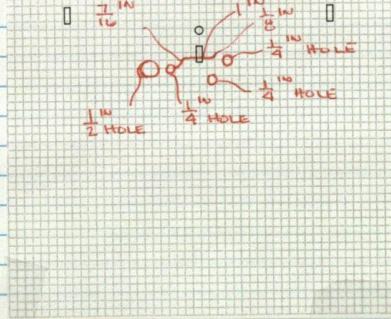
SOUTH GIRDER, NORTH FACE



SOUTH GIRDER, SOUTH FACE



SOUTH GIRDER, SOUTH FACE

SIGNATURE _____
READ AND UNDERSTOOD _____DATE _____ 20
DATE _____ 20

RETROFIT APPLIED

TOP WEB W/ N & S

- ANGLES

- BACKPLATE

- $\frac{1}{4}$ " HOLES W/ 1 - $\frac{1}{2}$ " HOLE ON SOUTH W/ RIB, WEST OF STIFFENER

10 - 100K

SIGNATURE _____
READ AND UNDERSTOOD _____DATE _____ 20____
DATE _____ 20____

TIL: 3/6/11, 097

TTL: 3611,097

Date	Trial	Cycles	Time	File Time	Specimen Name / Notes	Displacement		Force			Data Time
						Max	Min	Mean	Ampl	Max	Min
01.23.2013	1500000	3761097	0951	0934	30 FT-1 CYCLIC (150000) 01.23.2013	0.214	-0.007	56.1	45.6	102.5	10.0
					PAUSED	0.212	0.022	57.2	46.9	104.1	10.0
					01/24	0.215	0.019	57.3	47.0	103.4	9.8
					PAUSED	0.214	0.022	56.4	47.2	104.6	9.1
					01/25	0.216	0.017	57.3	47.1	105.7	9.0
					PAUSED	0.215	0.021	57.5	47.7	105.5	8.5
					01/25	0.215	0.021	57.2	47.6	105.0	9.6
					PAUSED	0.217	0.018	57.4	47.7	104.8	9.6
					01/24	0.211	0.033	56.4	47.2	105.1	9.3
					01/24	0.220	0.021	57.1	47.0	105.4	8.3
01.29.2013	3000000	3911097	1447	1430	30 FT-1 CYCLIC (150000) 01.29.2013	0.220	0.024	57.2	47.0	105.7	9.3
					01/30	0.216	0.025	56.9	46.7	103.8	10.0
					01/30	0.219	0.023	57.1	46.8	104.8	9.5
					01/30	0.216	0.023	57.1	46.9	104.0	10.2
					01/30	0.217	0.021	57.0	46.6	104.2	9.9
					01/30	0.217	0.019	56.9	46.6	102.6	10.0
					01/30	0.227	0.019	57.0	46.8	105.6	9.9
					01/30	0.227	0.035	56.9	44.4	104.9	10.7
					01/30	0.216	0.026	56.6	46.6	103.3	10.0
					02/01	0.220	0.025	57.4	46.0	104.1	9.3
					02/01	0.215	0.021	57.2	46.0	103.6	10.8
					02/01	0.216	0.020	57.2	46.2	105.3	10.4
02.05.2013	1000000	4211097	1042	1026	30 FT-1 CYCLIC (150000) 02.05.2013	0.226	0.037	56.3	44.4	104.5	10.2
					02/06	0.227	0.032	56.9	45.6	104.9	9.5
					02/06	0.216	0.028	56.6	44.9	102.8	11.0
					02/06	0.218	0.031	56.6	45.1	101.7	11.4
					02/06	0.218	0.035	56.4	44.7	101.1	11.6
					02/06	0.220	0.034	56.4	44.5	101.3	11.6
					02/06	0.222	0.035	56.8	44.8	102.8	11.7
					02/06	0.221	0.037	56.4	44.7	101.2	11.7
					02/07	0.223	0.032	56.8	44.1	102.1	10.4
					02/07	0.224	0.027	57.0	44.0	104.4	8.4
					02/07	0.228	0.034	56.7	43.9	103.5	12.5
02.11.2013	900000	4511097	0821	0805	30 FT-1 CYCLIC (150000) 02.11.2013	0.225	0.038	55.8	43.2	100.9	10.2
					02/11	0.221	0.036	56.5	45.0	101.5	11.5
					02/11	0.223	0.020	56.7	45.9	103.0	9.0
					02/11	0.225	0.030	56.7	45.0	103.7	9.7
					02/11	0.224	0.031	56.7	45.1	104.2	11.0
02.12.2013	1050000	4611097	1307	1250	30 FT-1 CYCLIC (150000) 02.12.2013	0.223	0.032	56.8	44.9	102.3	9.7
					02/12	0.221	0.036	56.7	45.2	101.8	11.6
					02/12	0.222	0.037	56.8	45.1	101.9	11.5
					02/12	0.224	0.031	56.6	44.9	102.2	11.2
					02/12	0.223	0.033	56.5	45.0	101.9	11.2
					02/12	0.227	0.036	56.5	44.7	102.7	11.5

*123194 - FANT CLIPPING ON INT. GARDER
** - LOAD " " SOUTH GARDER

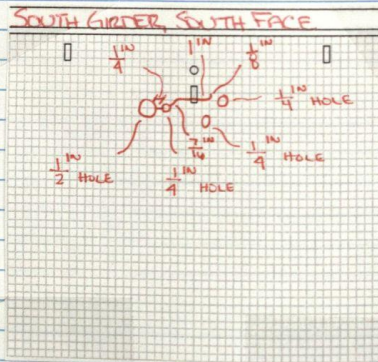
Date	Cycles	Time	File Time	Specimen Name / Notes	Displacement		Force		Data Time
					Max	Min	Ampl	Mean	
02.14.2013	1200000	4811047	0738	0721 30 FT-1 CYCLE (150X20)	0.229	0.038	45.3	50.4	10.7
					0.228	0.032	44.7	50.5	9.1
					0.225	0.034	44.9	50.3	10.9
				02/15	0.222	0.029	45.1	50.4	10.9
					0.218	0.028	45.2	50.5	11.0
					0.202	0.028	45.8	50.7	10.6

RETROFIT REMOVED

NORTH GIRDER, NORTH FACE → NO CHANGE

NORTH GIRDER, SOUTH FACE → NO CHANGE

SOUTH GIRDER, NORTH FACE → NO CHANGE

SIGNATURE _____
READ AND UNDERSTOOD _____DATE _____
DATE _____20____
20____

BOOK NO. 27

PROJECT NAME

NOTEBOOK NO.

RETROFIT APPLIED

TOP WEB GAP N & S

12 - 120^K

- ANGLES

- BACKPLATE

- $\frac{1}{4}$ " HOLES W/ 1 - $\frac{1}{2}$ " HOLE ON SOUTH GIRDER, WEST OF STIFFENER

SIGNATURE
READ AND UNDERSTOOD

DATE
DATE

20
20

[illegible]

RETROFIT APPLIED

TOP WEB GAP NPS

12-120*

- STIFFENED ANGLES

- BACKPLATE

- $\frac{1}{4}$ " HOLES W/ $1\frac{1}{2}$ " HOLE ON SOUTH GIRDER, WEST OF STIFFENER- 4- $\frac{3}{4}$ " HOLES; 2 ON N GIRDER AT TOP FLANGE TO WEB WELD,
2 ON S GIRDER AT TOP FLANGE TO WEB WELD

07.08.2013: CLICKING SOUND N GIRDER

07.09.2013: CRACK AT TOP FLANGE TO WEB WELD IN N6 GREN
PAST CRACK ARREST HOLE ON WEST SIDE OF STIFFENER.
NEW $\frac{3}{4}$ " CRACK ARREST HOLE DRILLED AT
CRACK TIP07.12.2013: CRACK AT TOP FLANGE TO WEB WELD IN N6 GREN
TO, RAPIDLY ON WEST SIDE OF STIFFENER. THE
CRACK WAS WELDED AFTER 300,000 CYCLES
WELD: GRIND A V GROOVE IN CENTER OF CRACK.
WELDED TWO PASSES WITH 7014 WELDING ROD.
MACHINE SET AT 180 DC + REVERSE POLARITY
WELDING ROD + E-7014

07.31.2013: CLICKING IN MIDDLE GIRDER, EAST OF BEAM SPLICE.

08.02.2013: NORTH GIRDER CRISS FRAME BROKEN (1,200,000 CYCLES)

SIGNATURE _____
READ AND UNDERSTOOD _____DATE _____ 20
DATE _____ 20

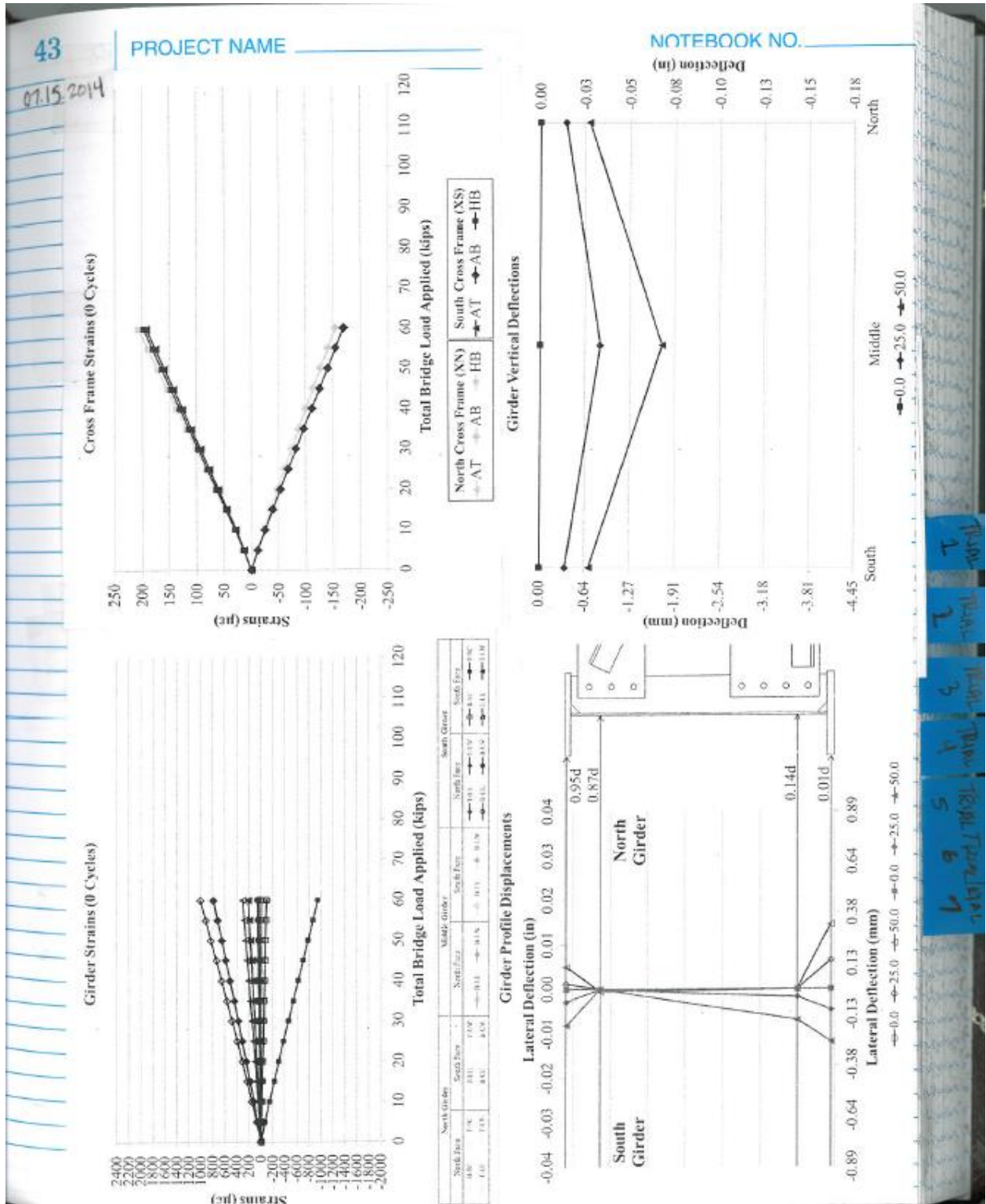
[illegible]

SIGNATURE _____
READ AND UNDERSTOOD

DATE
DATE20
20

30FT-2

Year	Team	Trials	Trials	Trials	Trials	Trials
1	Team 1	1	1	1	1	1
2	Team 2	2	2	2	2	2
3	Team 3	3	3	3	3	3
4	Team 4	4	4	4	4	4
5	Team 5	5	5	5	5	5
6	Team 6	6	6	6	6	6
7	Team 7	7	7	7	7	7



07.16.2014
(10:00)15000 CYCLES, 1 HZ (TOTAL 15000)
DISPLACEMENT

MAX: 0.105 IN

MIN: -0.012 IN

FORCE

MEAN 33.0 K

MAX 61.3 K

AMPL. 27.2 K

MIN 5.7 K

DATA: * MTS SPECIMEN 10:40

30 FT-2 CYCLIC (15000) 07.16.2014

STATIC BEGIN → 30 FT-2 STATIC BEGIN 07.17.2014

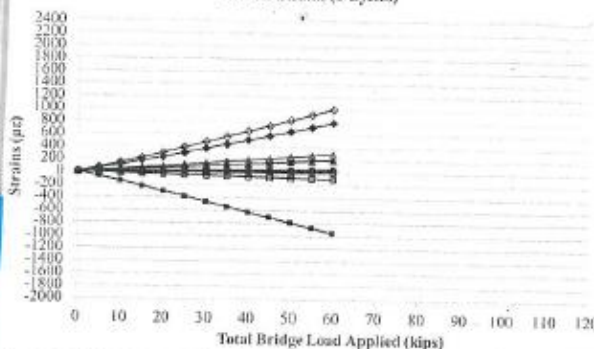
STATIC BEGIN → 30 FT-2 STATIC BEGIN 07.15.2014

STATIC END → 30 FT-2 STATIC (15000) 07.16.2014

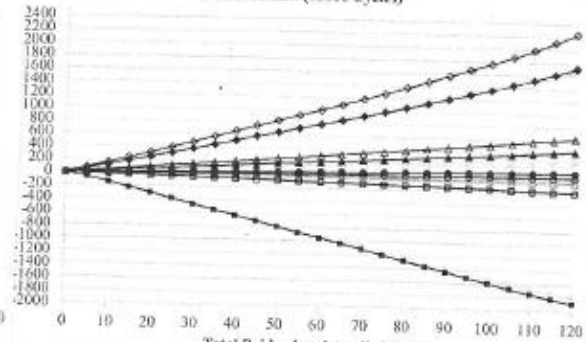
* ACTUAL TIME SHOWN... FILE TIME IS 9:48

CRACK DETECTED SOUTH GIRDER, NORTH FACE AT FLANGE TO WEB WELD

Girder Strains (0 Cycles)



Girder Strains (15000 Cycles)



South Girder				Middle Girder				North Girder			
South Face	North Face	Web	Flange	South Face	North Face	Web	Flange	South Face	North Face	Web	Flange
0.00	0.00	0.00	0.00	0.00	0.00	0.00	0.00	0.00	0.00	0.00	0.00
0.00	0.00	0.00	0.00	0.00	0.00	0.00	0.00	0.00	0.00	0.00	0.00

07.17.2014
(8:41)5000 CYCLES, 1 HZ (TOTAL 20,000)
DISPLACEMENT

MAX 0.109 IN

MIN -0.018 IN

FORCE

MEAN 33.2 K

MAX 62.4 K

AMPL. 21.98 K

MIN 5.6 K

DATA: * MTS SPECIMEN 8:46

* FILE TIME = 8:30

30 FT-2 CYCLIC (5000) 07.17.2014

NO CHANGE IN SOUTH GIRDER
CRACK07.17.2014
(10:46)5000 CYCLES, 1 HZ (TOTAL 25,000)
DISPLACEMENT

MAX 0.109 IN

MIN -0.008 IN

FORCE

MEAN 33.7 K

MAX 61.6 K

AMPL. 21.5 K

MIN 5.3 K

DATA: * MTS SPECIMEN 10:46

* FILE TIME = 10:35

30 FT-2 CYCLIC (5000) 07.17.2014

NO CHANGE IN SOUTH GIRDER
CRACK

SIGNATURE _____

READ AND UNDERSTOOD _____

DATE _____

20

DATE _____

20

47

PROJECT NAME _____

NOTEBOOK NO. _____

07.17.2014
(12:48)

5000 CYCLES, 1 HZ (TOTAL 30,000)

DISPLACEMENT

MAX ~~0.109~~ 0.112 INMIN ~~-0.008~~ -0.005 IN

FORCE

MEAN 33.6 k

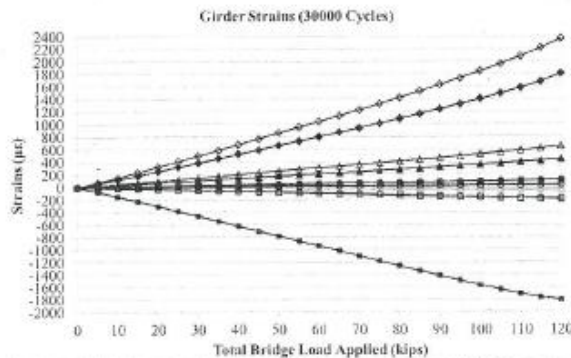
MAX 61.5 k

AMPL. 27.4 k

MIN 6.1 k

DATA: * MTS SPECIMEN ^{12:48} → 30 FT-2 CYCLIC (5000) 07.17.2014 3
STATIC END → 30 FT-2 STATIC (30000) 07.17.2014

* FILE TIME = 12:31

IF IN SOUTH
CRACK07.18.2014
(9:41)

5000 CYCLES, 1 HZ (TOTAL 35,000)

DISPLACEMENT

MAX 0.109 IN

MIN -0.008 IN

FORCE

MEAN 33.8 k

MAX 61.5 k

AMPL. 27.2 k

MIN 6.4 k

DATA: * MTS SPECIMEN ^{9:41} → 30 FT-2 CYCLIC (5000) 07.18.2014

* FILE TIME = 9:43

NO CHANGE IN SOUTH
GIRDER CRACK07.18.2014
(11:52)

5000 CYCLES, 1 HZ (TOTAL 40,000)

DISPLACEMENT

MAX 0.110 IN

MIN -0.006 IN

FORCE

MEAN 33.4 k

MAX 61.1 k

AMPL. 26.9 k

MIN 6.2 k

DATA: * MTS SPECIMEN ^{11:52} → 30 FT-2 CYCLIC (5000) 07.18.2014 2

* FILE TIME = 11:41

NO CHANGE IN SOUTH
GIRDER CRACKSIGNATURE _____
READ AND UNDERSTOOD _____DATE _____ 20
DATE _____ 20

07.21.2014
(9:01)

5000 CYCLES, 1 HZ (TOTAL 45000)

DISPLACEMENT

MAX 0.112 IN

MIN -0.002 IN

FORCE

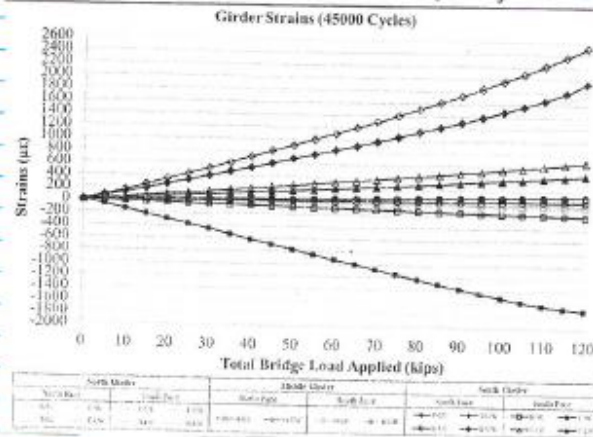
MEAN 33.5 K MAX 61.2 K

AMPL. 26.9 K MIN 6.6 K

DATA: * MTS SPECIMEN 9:25 30 FT-2 CYCLE (5000) 07.21.2014

* FILE TIME: 8:50

STATIC END → 30 FT-2 STATIC (45000) 07.21.2014

07.21.2014
(11:46)

5000 CYCLES, 1 HZ (TOTAL 50000)

DISPLACEMENT

MAX 0.117 IN

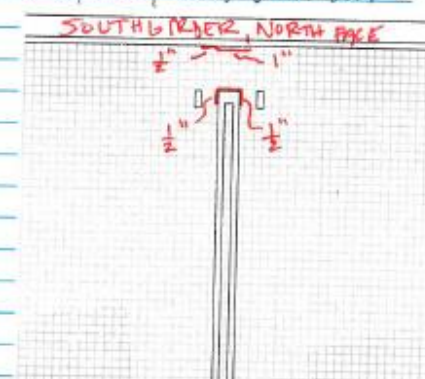
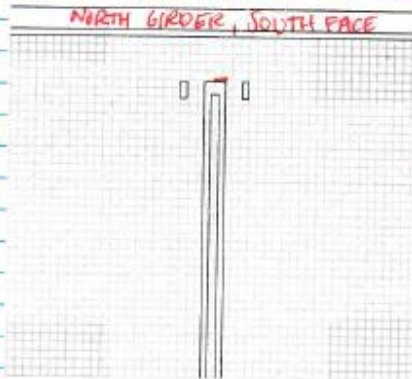
MIN -0.002 IN

FORCE

MEAN 33.7 K MAX 61.2 K

AMPL. 26.9 K MIN 6.6 K

DATA: * MTS SPECIMEN 11:45 30 FT-2 CYCLE (5000) 07.21.2014 2

SIGNATURE _____
READ AND UNDERSTOOD _____DATE _____ 20
DATE _____ 20

RETROFIT APPLIED

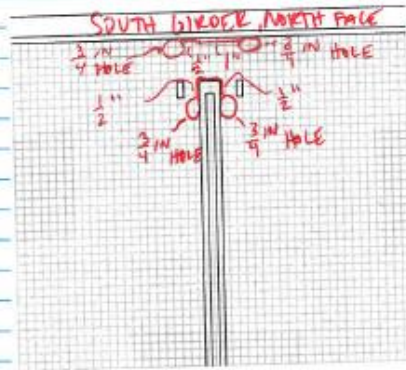
TOP WEBB GAP N & S

- STIFFENED ANGLES

- BACK PLATE

- 3/4 IN HOLES ON SOUTH GIRDER AT EACH CRACK END

6-60 K

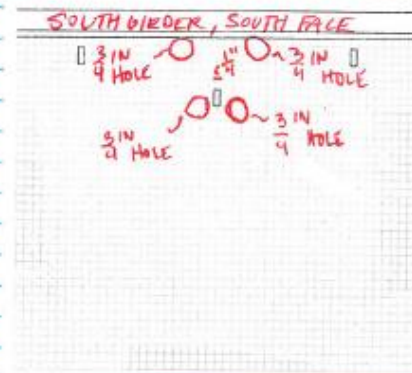
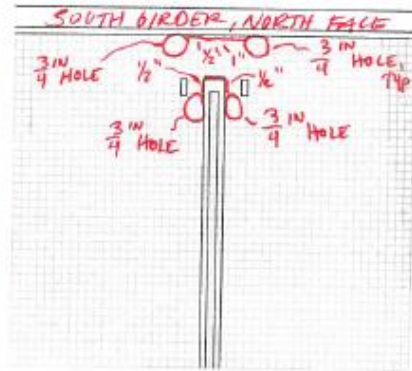
SIGNATURE _____
READ AND UNDERSTOOD _____DATE _____ 20
DATE _____ 20

Strains (µg)

Date	Cycles	Total	Time	File Name	Specimen Name / Notes	Displacement	Max	Min	Ampl	Force	Min	Max	Date/Time
08.12.2014	50000	600000	9:35	9:24	30 Fr-2 (4000)(5000) 08.12.2014	0.148 0.150	0.034 0.036	0.032 0.031	26.8 26.7	58.9 59.9	5.9 6.0	14.05 14.10	
08.13.2014	50000	650000	9:15	9:03	30 Fr-2 (4000)(5000) 08.13.2014	0.144 0.146	0.031 0.032	0.032 0.031	26.5 26.5	58.6 58.7	5.6 5.6	14.32 14.35	
08.14.2014	50000	700000	10:09	9:58	30 Fr-2 (4000)(5000) 08.14.2014	0.151 0.152	0.035 0.037	0.035 0.036	27.1 27.1	60.1 60.1	6.0 6.0	14.59 14.59	
08.15.2014	50000	750000	9:16	9:28	30 Fr-2 (4000)(5000) 08.15.2014	0.127 0.125	0.015 0.013	0.015 0.013	26.1 26.0	58.1 58.2	5.8 5.8	14.56 14.56	
08.16.2014	50000	800000	9:10	9:29	30 Fr-2 (4000)(5000) 08.16.2014	0.126 0.123	0.013 0.013	0.013 0.013	26.0 26.0	58.0 58.0	5.8 5.8	14.54 14.54	
08.18.2014	75000	875000	8:06	7:57	30 Fr-2 (4000)(5000) 08.18.2014	0.126 0.126	0.013 0.013	0.013 0.013	26.0 26.0	58.0 58.0	5.8 5.8	14.54 14.54	
08.19.2014	75000	950000	7:41	7:35	30 Fr-2 (4000)(5000) 08.19.2014	0.109 0.105	0.006 0.006	0.006 0.006	26.3 26.3	58.3 58.3	5.8 5.8	14.54 14.54	
08.20.2014	50000	1000000	7:17	7:06	30 Fr-2 (4000)(5000) 08.20.2014	0.102 0.102	0.002 0.002	0.002 0.002	26.3 26.3	58.3 58.3	5.8 5.8	14.54 14.54	

Date	Cycles	Total	Time	File Time	Specimen Name / Notes	Displacement		Strain (%)	Force		Min	Max	Data Time
						Max	Min		Angle	Mean			
08.21.2014	50000	1050000	7:26	7:15	30 Fr-2 Cyclic (5000) 08.21.2014	0.104	-0.007	32.4	27.1	32.4	5.6	60.2	9:16
						0.108	-0.007	32.4	27.1	32.4	5.6	60.2	9:16
						0.110	-0.006	32.4	27.1	32.4	5.6	60.2	9:16
						0.112	-0.004	32.4	27.1	32.4	5.6	60.2	9:16
						0.110	-0.002	32.4	27.1	32.4	5.6	60.2	9:16
						0.111	-0.002	32.4	27.1	32.4	5.6	60.2	9:16
						0.110	-0.002	32.4	27.1	32.4	5.6	60.2	9:16
						0.113	-0.003	32.4	27.1	32.4	5.6	60.2	9:16
						0.114	-0.001	32.4	27.1	32.4	5.6	60.2	9:16
						0.114	-0.001	32.4	27.1	32.4	5.6	60.2	9:16
						0.116	-0.001	32.4	27.1	32.4	5.6	60.2	9:16
						0.109	-0.006	32.4	27.1	32.4	5.6	60.2	9:16
						0.113	-0.005	32.4	27.1	32.4	5.6	60.2	9:16
						0.110	-0.004	32.4	27.1	32.4	5.6	60.2	9:16
						0.113	-0.002	32.4	27.1	32.4	5.6	60.2	9:16
						0.114	-0.001	32.4	27.1	32.4	5.6	60.2	9:16
						0.108	-0.003	32.4	27.1	32.4	5.6	60.2	9:16
						0.109	-0.006	32.4	27.1	32.4	5.6	60.2	9:16
						0.113	-0.003	32.4	27.1	32.4	5.6	60.2	9:16
						0.114	-0.003	32.4	27.1	32.4	5.6	60.2	9:16
						0.113	-0.001	32.4	27.1	32.4	5.6	60.2	9:16
						0.113	-0.001	32.4	27.1	32.4	5.6	60.2	9:16
						0.113	-0.001	32.4	27.1	32.4	5.6	60.2	9:16
						0.114	-0.000	32.4	27.1	32.4	5.6	60.2	9:16
						0.113	-0.001	32.4	27.1	32.4	5.6	60.2	9:16
						0.113	-0.001	32.4	27.1	32.4	5.6	60.2	9:16
						0.114	-0.000	32.4	27.1	32.4	5.6	60.2	9:16

RETROFIT REMOVED



DATE 20
DATE 20

RETROFIT APPLIED

TOP WEB GAP N.E.S

- STIFFENED ANGLES

- BACKPLATE

- 3/4 IN HOLES ON SOUTH WEBBER AT EACH CRACK END

8-80 K

SIGNATURE _____

READ AND UNDERSTOOD _____

DATE _____

20

DATE _____

20

3
4
5
6
7
8
9
10
11
12
13
14
15
16
17
18
19
20
21
22
23
24
25
26
27
28
29
30
31
32
33
34
35
36
37
38
39
40
41
42
43
44
45
46
47
48
49
50
51
52
53
54
55
56
57
58
59
60
61
62
63
64
65
66
67
68
69
70
71
72
73
74
75
76
77
78
79
80
81
82
83
84
85
86
87
88
89
90
91
92
93
94
95
96
97
98
99
100

Date	Cycles		Time	File Name / Notes	Displacement		Force		Data Time
	Total	Test			Max	Min	Appl	Max	
09.03.2014	50000	1300000	16:47 10:35	30 Hz 2 Cyclic (50000) 09.13.2014	0.116	-0.006	35.7	80.3	12:29
					0.141	-0.013	35.5	80.2	13:39
					0.143	-0.005	35.4	80.1	14:46
					0.145	-0.004	35.4	80.1	15:46
					0.146	-0.002	35.6	80.2	17:33
09.04.2014	50000	1350000	10:01	30 Hz 2 Cyclic (50000) 09.04.2014	0.147	-0.001	35.9	79.9	12:43
					0.146	-0.002	36.1	80.1	13:52
					0.147	-0.001	35.8	80.0	14:52
					0.149	-0.000	35.8	80.1	15:35
					0.151	-0.002	35.9	80.9	16:52
09.05.2014	50000	1400000	7:09	30 Hz 2 Cyclic (50000) 09.05.2014	0.146	0.000	35.8	79.8	10:21
					0.149	-0.001	35.4	80.4	11:42
					0.142	-0.006	36.2	80.5	14:56
					0.141	-0.011	36.2	80.5	14:56
					0.140	-0.006	35.6	80.6	14:17
					0.142	-0.007	35.6	80.3	17:37
					0.144	-0.005	35.8	80.3	
09.07.2014	50000	1500000	9:51	30 Hz 2 Cyclic (50000) 09.07.2014	0.148	0.000	36.1	80.6	11:34
					0.146	-0.003	35.7	80.3	13:31
					0.145	-0.003	35.7	80.3	16:44
					0.147	-0.002	35.6	80.5	
					0.143	-0.005	36.1	80.5	
					0.143	-0.010	35.9	80.6	12:58
					0.138	-0.011	35.9	80.4	15:15
					0.137	-0.012	35.9	80.4	16:49
					0.138	-0.012	35.9	80.4	
09.11.2014	50000	1600000	10:11	30 Hz 2 Cyclic (50000) 09.11.2014	0.130	-0.022	37.1	81.5	10:01
					0.130	-0.021	35.9	81.3	11:06
					0.124	-0.025	35.3	80.1	13:26
					0.121	-0.028	35.7	80.1	14:50
					0.120	-0.027	35.9	80.8	16:54
					0.130	-0.028	35.9	80.2	
					0.142	-0.004	35.7	80.0	14:07
					0.142	-0.010	36.0	80.4	16:46
					0.128	-0.012	36.1	80.4	
					0.137	-0.012	35.9	80.4	10:13
					0.134	-0.010	35.8	80.4	13:25
					0.136	-0.011	36.1	80.4	17:47
					0.135	-0.014	36.0	80.2	19:38
					0.136	-0.015	35.9	80.2	
09.16.2014	75000	1800000	8:46	30 Hz 2 Cyclic (75000) 09.16.2014	0.138	-0.008	35.6	80.3	10:31
					0.138	-0.011	35.4	80.3	13:14
					0.135	-0.012	35.7	80.6	16:05
					0.136	-0.012	35.9	80.3	18:56
					0.137	-0.011	35.9	80.2	19:01
					0.138	-0.011	35.9	80.2	

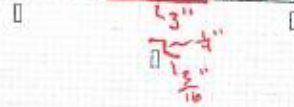
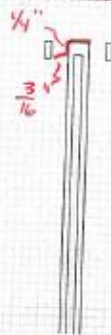
Date	Time	File Time	Specimen Name / Notes	Displacement	Force	Max	Date/Time
09.17.2014	7:31	7:19	30 Fr-2 CYCLIC (75000) 09.17.2014	Min 0.144 Max 0.172	Ampl 30.2 35.6	88.5 80.2	9.14 9.10 16:29 17:45
09.18.2014	9:31	9:19	30 Fr-2 CYCLIC (75000) 09.18.2014	Min 0.144 Max 0.172	Ampl 30.2 35.6	88.5 80.2	9.14 9.10 16:29 17:45
09.19.2014	7:09	6:57	30 Fr-2 CYCLIC (75000) 09.19.2014	Min 0.144 Max 0.172	Ampl 30.2 35.6	88.5 80.2	9.14 9.10 16:29 17:45
09.20.2014	7:53	7:41	30 Fr-2 CYCLIC (75000) 09.20.2014	Min 0.144 Max 0.172	Ampl 30.2 35.6	88.5 80.2	9.14 9.10 16:29 17:45
09.21.2014	8:16	8:04	30 Fr-2 CYCLIC (75000) 09.21.2014	Min 0.144 Max 0.172	Ampl 30.2 35.6	88.5 80.2	9.14 9.10 16:29 17:45
09.22.2014	7:32	7:20	30 Fr-2 CYCLIC (75000) 09.22.2014	Min 0.144 Max 0.172	Ampl 30.2 35.6	88.5 80.2	9.14 9.10 16:29 17:45
09.23.2014	9:15	9:03	30 Fr-2 CYCLIC (75000) 09.23.2014	Min 0.144 Max 0.172	Ampl 30.2 35.6	88.5 80.2	9.14 9.10 16:29 17:45
09.24.2014	7:26	7:14	30 Fr-2 CYCLIC (75000) 09.24.2014	Min 0.144 Max 0.172	Ampl 30.2 35.6	88.5 80.2	9.14 9.10 16:29 17:45
09.25.2014	9:32	9:20	30 Fr-2 CYCLIC (75000) 09.25.2014	Min 0.144 Max 0.172	Ampl 30.2 35.6	88.5 80.2	9.14 9.10 16:29 17:45
09.26.2014	8:16	8:04	30 Fr-2 CYCLIC (75000) 09.26.2014	Min 0.144 Max 0.172	Ampl 30.2 35.6	88.5 80.2	9.14 9.10 16:29 17:45
09.29.2014	7:53	7:41	30 Fr-2 CYCLIC (75000) 09.29.2014	Min 0.144 Max 0.172	Ampl 30.2 35.6	88.5 80.2	9.14 9.10 16:29 17:45

Bolt broken on N6.

Bolt broken on N/G.

TRAIL - TRAIL TIME

a b c d e f g h i j k l m n o p q r s t u v w x y z

RETROFIT REMOVEDNORTH GIRDER, NORTH FACENORTH GIRDER, SOUTH FACESOUTH GIRDER, SOUTH FACE

DATE _____ 20
 DATE _____ 20

RETROFIT APPLIED

TOP WEB GAP N'S

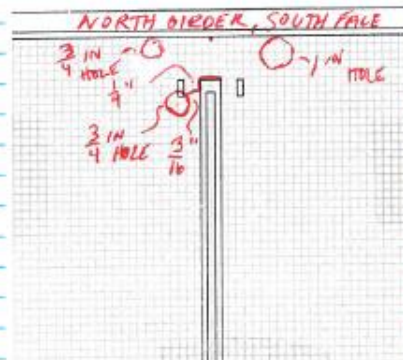
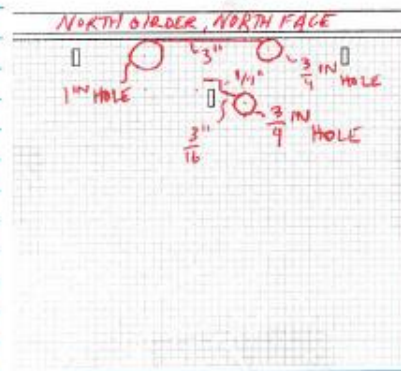
8-80K

• STIFFENED ANGLES

• BACK PLATE

• $\frac{3}{4}$ IN HOLES ON SOUTH GIRDER AT EACH CRACK END• $\frac{3}{4}$ IN HOLES ON NORTH GIRDER AT FLANGE TO WEB WELD (CRACK END), WEST OF STIFFENER.• $\frac{3}{4}$ IN HOLE ON NORTH GIRDER STIFFENER NEAR CRACK END, WEST OF STIFFENER

• 1 IN HOLE ON NORTH GIRDER AT FLANGE TO WEB WELD (CRACK END), EAST OF STIFFENER

SIGNATURE _____
READ AND UNDERSTOOD _____DATE _____ 20
DATE _____ 20

Date	Cycles		Time	File Time	Specimen Name / Notes	Displacement		Force			Data Time
	Total	Total				Max	Min	Ampl	Max	Min	
10-03-2014	51000	250000	6:21	6:19	70 FT-2 (44116 (50000))	0.144	-0.003	85.9	80.2	8.2	7:44
						0.144	-0.008	85.9	80.3	8.8	7:44
						0.141	-0.025	85.9	80.3	8.8	7:44
						0.139	-0.019	85.8	80.5	8.2	7:44
10-04-2014	30000	2550000	10:16	9:55	70 FT-2 (44116 (50000))	0.148	-0.002	85.9	80.2	8.3	13:08
					REMOVED RETROFIT ON NG AND INSPECTED. NO CRACK GROWTH	0.147	-0.006	85.7	81.3	7.9	14:07
						0.142	-0.010	85.4	80.3	6.1	16:53

RETROFIT REMOVED

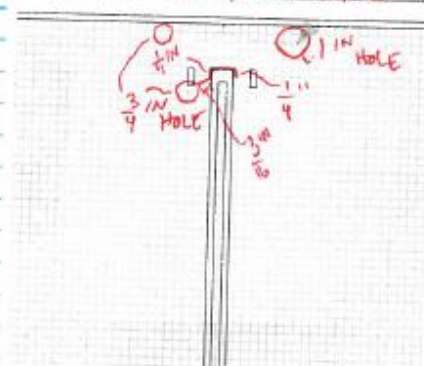
- NG ONLY

- INSPECTED NG, NO CRACK GROWTH

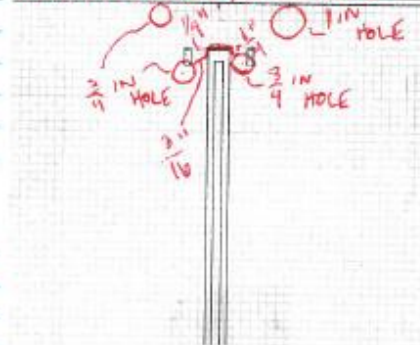
RETROFIT REMOVED

- N6 & SC

- GROWTH IN CRACK AT STIFFENER ON SOUTH FACE OF N6 ON EAST SIDE

NORTH GIRDER, SOUTH FACE

- 3/4 IN HOLE DRILLED AT END OF CRACK ON SOUTH FACE OF N6 ON EAST SIDE OF STIFFENER

NORTH GIRDER, SOUTH FACE

* RETROFIT HOLES IN STIFFENER AND WEB ON NORTH GIRDER INCREASED BY 1/16 IN. HOLE SIZE IN STIFFENER ANGLES AND BACK PLATE NOT CHANGED.

SIGNATURE _____
READ AND UNDERSTOOD _____DATE _____ 20
DATE _____ 20

8-80K **RETROFIT APPLIED**
 TOP WEB GAP NPS
 - STIFFENER ANGLES
 - BACK PLATE
 - 3/4 IN HOLES IN SOUTH GIRDER AT EACH CRACK END
 - 3/4 IN HOLES ON NORTH GIRDER STIFFENER WELD CRACK ENDS, WEST & EAST OF STIFFENER
 - 3/4 IN HOLE ON NORTH GIRDER AT FLANGE TO WEB WELD CRACK END, WEST OF STIFFENER
 - 1 IN HOLE ON NORTH GIRDER AT FLANGE TO WEB WELD CRACK END, EAST OF STIFFENER

11.03.2014: NOTED LOUD THUNKING SOUND WHEN REMOVING LOAD AT END OF TESTING CYCLE. Upon inspection, A LARGE CRACK WAS FOUND IN STIFFENER ON SOUTH FACE OF MIDDLE GIRDER AT THE BOTTOM OF CROSS FRAME.

STATIC TEST RUN TO 80 K WITH CRACK NOT REPAIRED.

CRACK WELDED

ANGLES APPLIED ON EAST AND WEST SIDES OF STIFFENER, BOTH NORTH AND SOUTH FACE OF MIDDLE GIRDER

Date	Trial	Cycles	Total	Time	File Time	Specimen Name / Notes	Displacement			Force			Time
							Max	Min	Mean	Avg	Max	Min	
10-27-2014	60000	311000	311000	8:34	8:22	30 F-2 CYCLIC (60000) 10.27.2014	0.147	-0.004	40.5	36.2	80.6	7.8	11:20
10-28-2014	60000	317000	317000	8:47	8:35	30 F-2 CYCLIC (60000) 10.28.2014	0.142	-0.009	44.3	35.8	80.1	7.4	11:22
10-29-2014	60000	323000	323000	9:16	9:04	30 F-2 CYCLIC (60000) 10.29.2014	0.140	-0.010	44.3	35.4	80.4	8.2	11:56
10-30-2014	60000	329000	329000	8:50	8:43	30 F-2 CYCLIC (60000) 10.30.2014	0.146	-0.007	44.5	36.2	81.0	8.1	12:16
10-31-2014	60000	335000	335000	8:25	8:13	30 F-2 CYCLIC (60000) 10.31.2014	0.143	-0.007	44.2	36.0	80.4	8.0	12:16
11-03-2014	60000	341000	341000	9:21	9:09	30 F-2 CYCLIC (60000) 11.03.2014	0.151	-0.005	44.3	36.0	80.7	7.9	11:23
						CRACK FOUND IN MIDDLE GIRDER STIFFENER, BOTTOM SOUTH SIDE. CRACK WELDED AND RETROFIT APPLIED ON EACH SIDE OF STIFFENER ON NORTH AND SOUTH FACE OF MIDDLE GIRDER	0.159	-0.006	44.2	35.9	80.9	8.0	11:33

SIGNATURE _____
 READ AND UNDERSTOOD _____

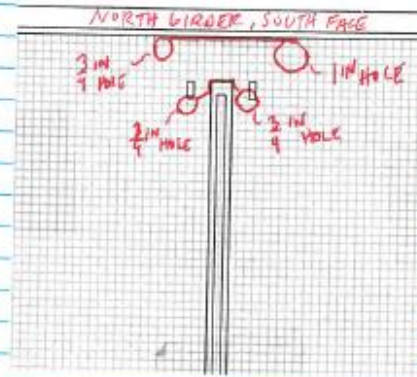
DATE _____

20

RETROFIT REMOVED

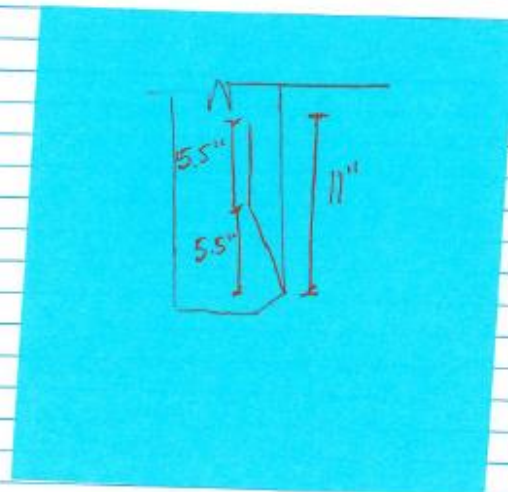
- N6

- CRACK IN TOP FLANGE TO WEB WELD BETWEEN CRACK ARREST HOLES GREW THROUGH ON SOUTH SIDE. NO VISIBLE CRACK GROWTH PAST CRACK ARREST HOLES ON SOUTH OR NORTH FACES



- S6

- NO VISIBLE CRACK GROWTH

SIGNATURE _____
READ AND UNDERSTOOD _____DATE _____ 20____
DATE _____ 20____

RETROFIT APPLIED

TOP WEB GAP N/S

10-100K

- STIFFENER ANGLES

- BACK PLATE

- $\frac{3}{4}$ IN HOLES ON SOUTH GIRDER AT EACH CRACK END- $\frac{3}{4}$ IN HOLES ON NORTH GIRDER STIFFENER WELD CRACK ENDS,
WEST & EAST OF STIFFENER- $\frac{3}{4}$ IN HOLE ON NORTH GIRDER AT FLANGE TO WEB WELD CRACK
END, WEST OF STIFFENER- 1 IN HOLE ON NORTH GIRDER AT FLANGE TO WEB WELD CRACK
END, EAST OF STIFFENER

BOT WEB GAP MIDDLE GIRDER

- 4 ANGLES

01.20.2015: CRACK FOUND IN STIFFENER PLATE ON SOUTH SIDE OF
MIDDLE GIRDER AT CROSS FRAME TO CROSS FRAME TAB WELD
OUTSIDE OF 4 ANGLE RETROFIT APPLIED AT BOT WEB GAP
OF MIDDLE GIRDER, BOTTOM ANGLE.

SIGNATURE _____
READ AND UNDERSTOOD _____DATE _____ 20
DATE _____ 20

Date	Cycles		Time	File Time	Specimen Name / Notes	Displacement		Force		Min	Max	Data Time
	Trail	Total				Max	Min	Ampl	Mean			
01.13.2015	50000	346000	8:52	8:39	30 FT-2 CYCLIC (50000) 01.13.2015	0.173 0.185	-0.0135 -0.0055	48.9 46.3	55.4 56.0	102.1 102.5	9.97 9.57	9:15
01.16.2015	50000	351000	8:41	8:34	30 FT-2 CYCLIC (50000) 01.16.2015	0.178 0.194	-0.0075 -0.0017	49.5 48.3	55.6 55.4	104.4 101.9	9.6 9.8	10:24 10:26
01.19.2015	50000	352000	8:11	7:18	30 FT-2 CYCLIC (50000) 01.19.2015	0.190 0.197	0.004 0.003	46.4 45.2	55.1 55.6	103.5 103.5	9.8 9.6	17:51
01.20.2015	50000 31042	346000 3591042	8:13	8:00	30 FT-2 CYCLIC (50000) 01.20.2015	0.191 0.193	0.003 0.006	44.7 44.7	55.0 55.7	102.7 100.7	10.1 10.4	11:42 17:15

CRACK IN CROSS FRAME ON
SOUTH SIDE OF MIDDLE
BORDER - AT CROSS FR
TO STIFFENER WELD

RETROFIT REMOVED
- NB + SB INSPECTED
- NO VISIBLE CRACK
GROWTH



- CROSS FRAME BETWEEN
MIDDLE AND SOUTH
BORDERS REMOVED AND
REPLACED WITH END
CROSS FRAME BETWEEN
NORTH BORDER AND
MIDDLE BORDER. NOT
PREVIOUSLY USED IN
MIDDLE, BUT USED
THROUGHOUT 30 FT-1
AND 30 FT-2 AT END

SIC
READ AND UNDERSTOOD

DATE 20
DATE 20

RETROFIT APPLIED

TOP WEB GAP NPS

- STEEFENER ANGLES

10-100K

- BACK PLATE

- 3/4 IN HOLES ON SOUTH GIRDER AT EACH CRACK END

- 3/4 IN HOLES IN NORTH GIRDER STIFFENER WELD CRACK ENDS,
WEST & EAST OF STIFFENER- 3/4 IN HOLE ON NORTH GIRDER AT FLANGE TO WEB WELD
CRACK END, WEST OF STIFFENER- 1 IN HOLE ON NORTH GIRDER AT FLANGE TO WEB WELD CRACK
END, EAST OF STIFFENER

BOT WEB GAP MINNIE GIRDER

- 4 ANGLES

SIGNATURE _____

READ AND UNDERSTOOD _____

DATE _____

DATE _____

20

20

Date	Cycles		Time	File Name	Specimen Name / Notes	Displacement		Force		Date Time
	Trail	Total				Max	Min	Ampl	Max	
02/21/2015	25000	3616092	10:23	10:10	30 FT-2 CYCLIC (25000) 02.27.2015	0.183	-0.011	56.0	103.2	7.74
						0.182	-0.010	44.7	103.7	6.2
						0.175	-0.0093	47.4	102.8	10.6
03/02/2015	25000	3641092	9:56	9:43	30 FT-2 CYCLIC (25000) 03.02.2015	0.188	-0.015	57.9	102.0	7.9
						0.188	-0.034	44.3	103.9	9.1
						0.181	-0.008	44.8	100.1	10.7
03/03/2015	50000	3691092	9:36	9:24	30 FT-2 CYCLIC (50000) 03.03.2015	0.184	-0.018	55.6	101.2	7.2
						0.187	-0.0071	45.0	103.2	7.8
						0.183	-0.0034	45.2	101.3	10.4
03/04/2015	50000	3741092	9:44	9:30	30 FT-2 CYCLIC (50000) 03.04.2015	0.184	-0.0038	55.8	101.3	10.5
						0.184	-0.0071	45.2	103.2	7.8
						0.187	-0.0095	45.1	105.0	7.0
03/05/2015	50000	3791092	9:45	8:51	30 FT-2 CYCLIC (50000) 03.05.2015	0.179	-0.0035	55.8	101.2	7.7
						0.179	-0.0021	45.2	101.2	7.7
						0.183	-0.0021	45.2	101.2	7.7
						0.182	-0.0076	45.2	102.3	9.3
						0.182	-0.0106	44.9	101.3	10.1
03/06/2015	25000	3816092	10:28	10:15	30 FT-2 CYCLIC (25000) 03.06.2015	0.192	-0.0052	56.5	103.4	7.4
						0.180	-0.006	44.9	102.7	10.8
						0.184	-0.0015	44.9	101.3	10.7
03/09/2015	25000	3841092	10:24	10:11	30 FT-2 CYCLIC (25000) 03.09.2015	0.195	-0.0019	56.3	102.9	7.1
						0.192	-0.0029	46.2	102.1	9.1
						0.182	-0.000	45.5	103.3	9.2
03/10/2015	50000	3891092	11:00	9:49	30 FT-2 CYCLIC (50000) 03.10.2015	0.191	-0.0047	55.8	101.8	10.1
						0.191	-0.0023	47.8	104.9	8.6
						0.181	-0.0087	45.9	101.9	9.9
03/11/2015	50000	3941092	8:17	8:04	30 FT-2 CYCLIC (50000) 03.11.2015	0.197	-0.0067	55.8	102.0	8.8
						0.196	-0.0006	46.0	102.8	9.8
						0.202	-0.0057	47.6	104.2	8.6
						0.196	-0.0044	46.2	102.7	9.7
						0.197	-0.0054	46.6	103.0	9.0
						0.197	-0.0087	45.4	102.0	10.2
03/12/2015	50000	3991092	9:41	9:28	30 FT-2 CYCLIC (50000) 03.12.2015	0.198	-0.008	56.3	102.5	10.4
						0.202	-0.0132	45.9	101.9	7.6
						0.196	-0.011	45.9	100.9	10.9
						0.197	-0.0044	44.8	101.2	10.4
						0.196	-0.0103	44.8	101.1	10.4
						0.199	-0.0116	44.8	101.4	10.9
03/21/2015	25000	4016092	11:30	11:17	30 FT-2 CYCLIC (25000) 03.21.2015	0.193	-0.0074	56.2	102.4	9.9
						0.193	-0.0013	44.5	102.3	9.9
						0.201	-0.0046	44.8	101.0	10.0
										15:55
					Boat broken on N6 cracks found. 1" crack stop holes drilled at crack ends.					

READ AND UNDERSTOOD

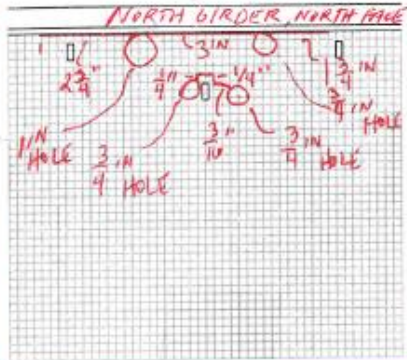
DATE

20

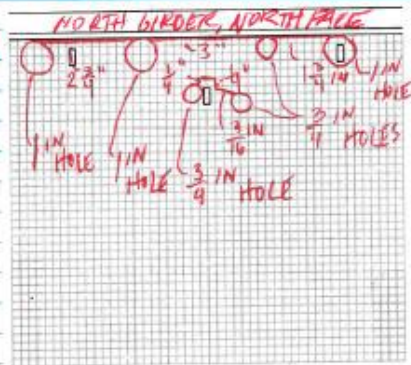
RETROFIT REMOVED

- N6

- CRACK IN TOP FLANGE TO WEB WELD GREW PAST CRACK
ARREST HOLES



- 1 IN HOLES DRILLED AT END OF CRACKS ON NORTH
GIRDER



SIGNATURE _____
READ AND UNDERSTOOD _____

DATE _____ 20_____
DATE _____ 20_____

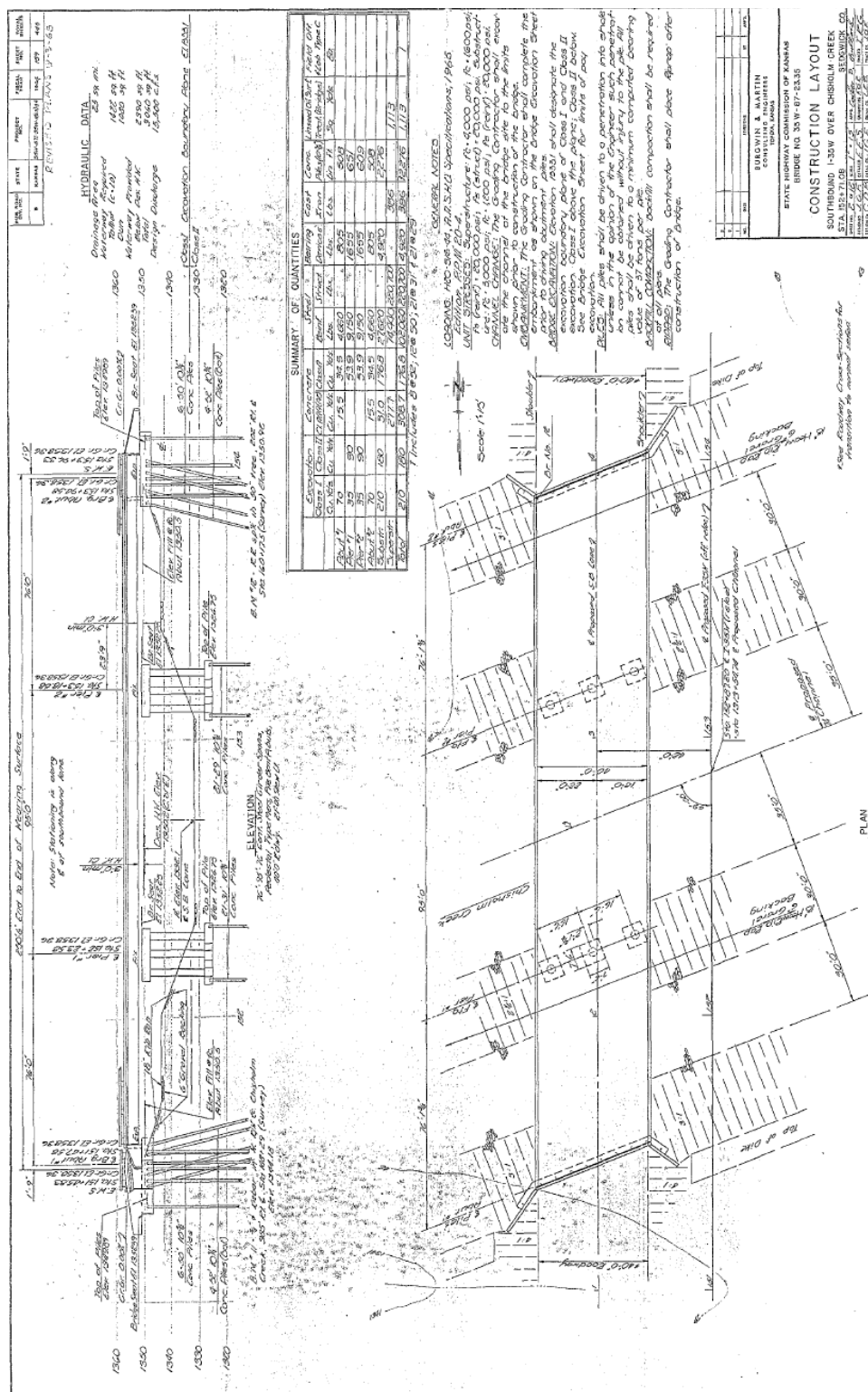


Figure F. 2: Construction layout of southbound bridge.

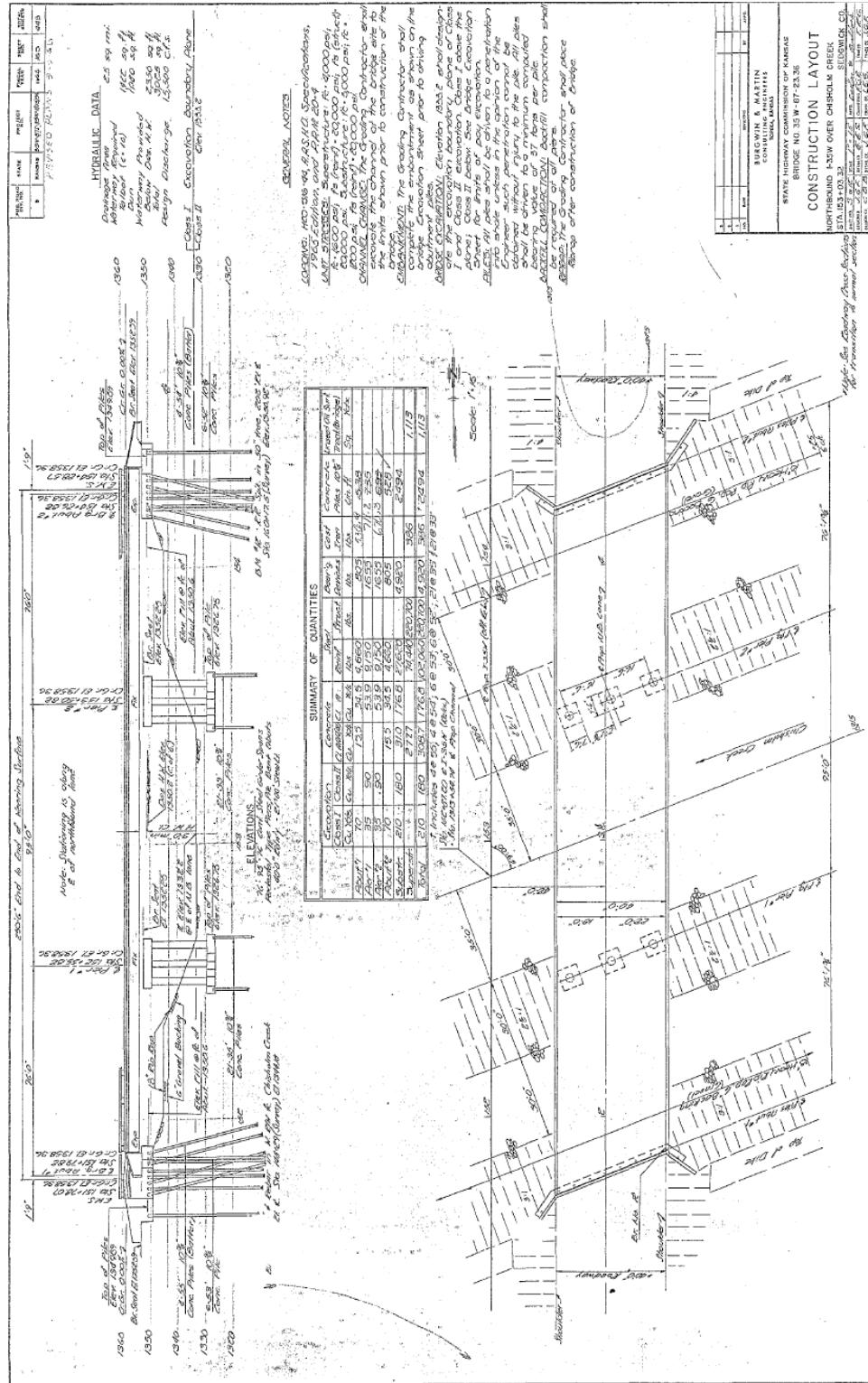
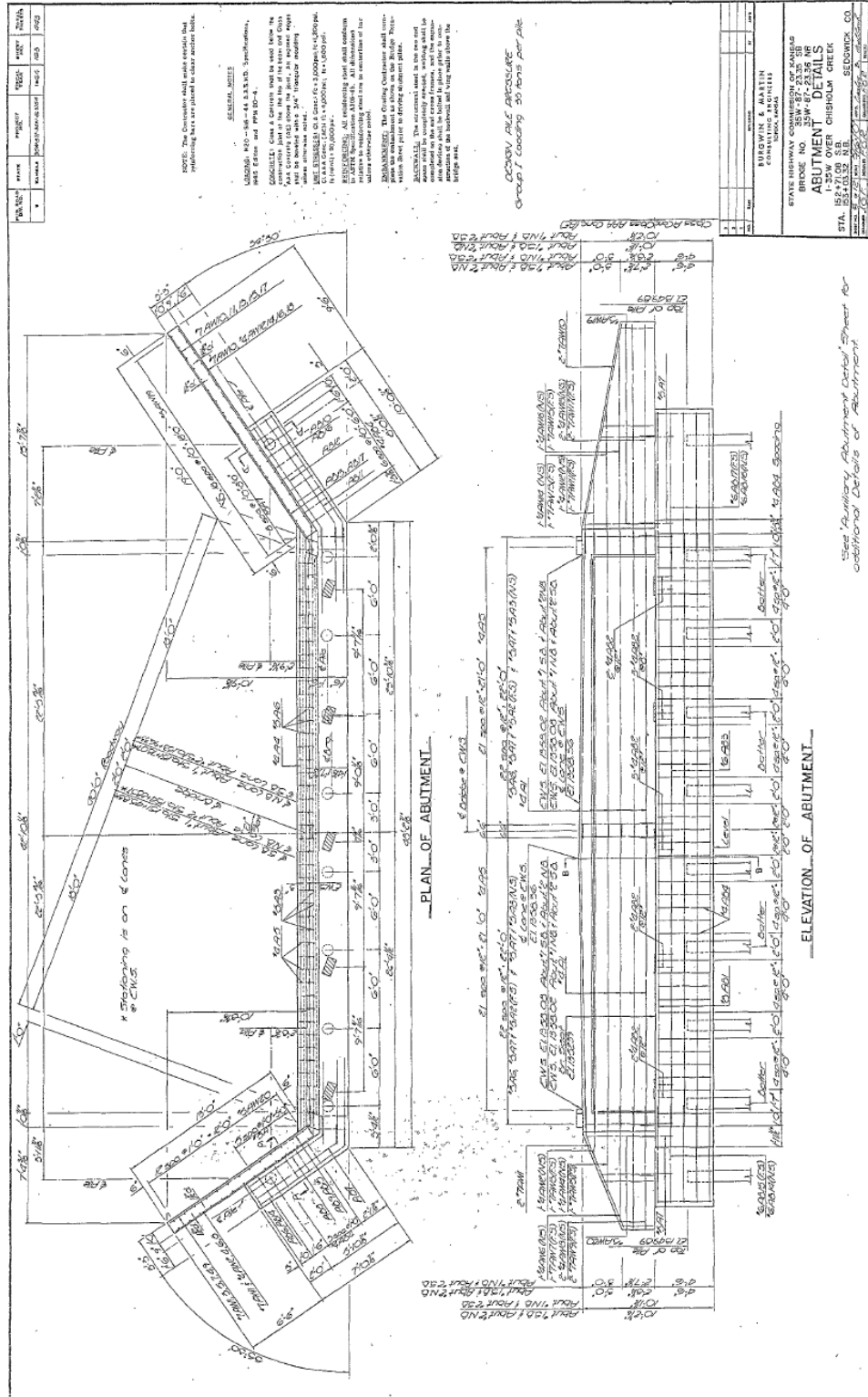
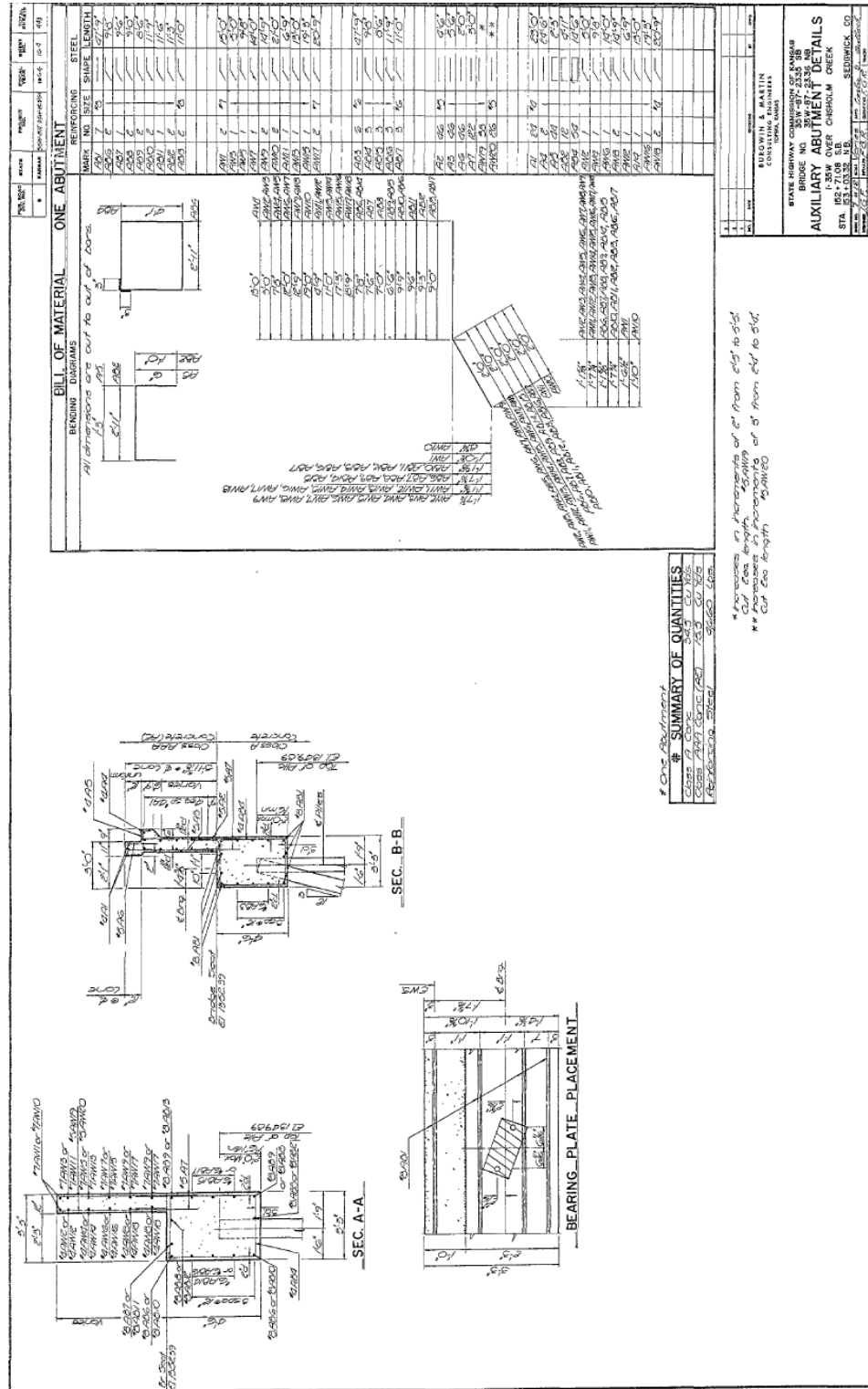
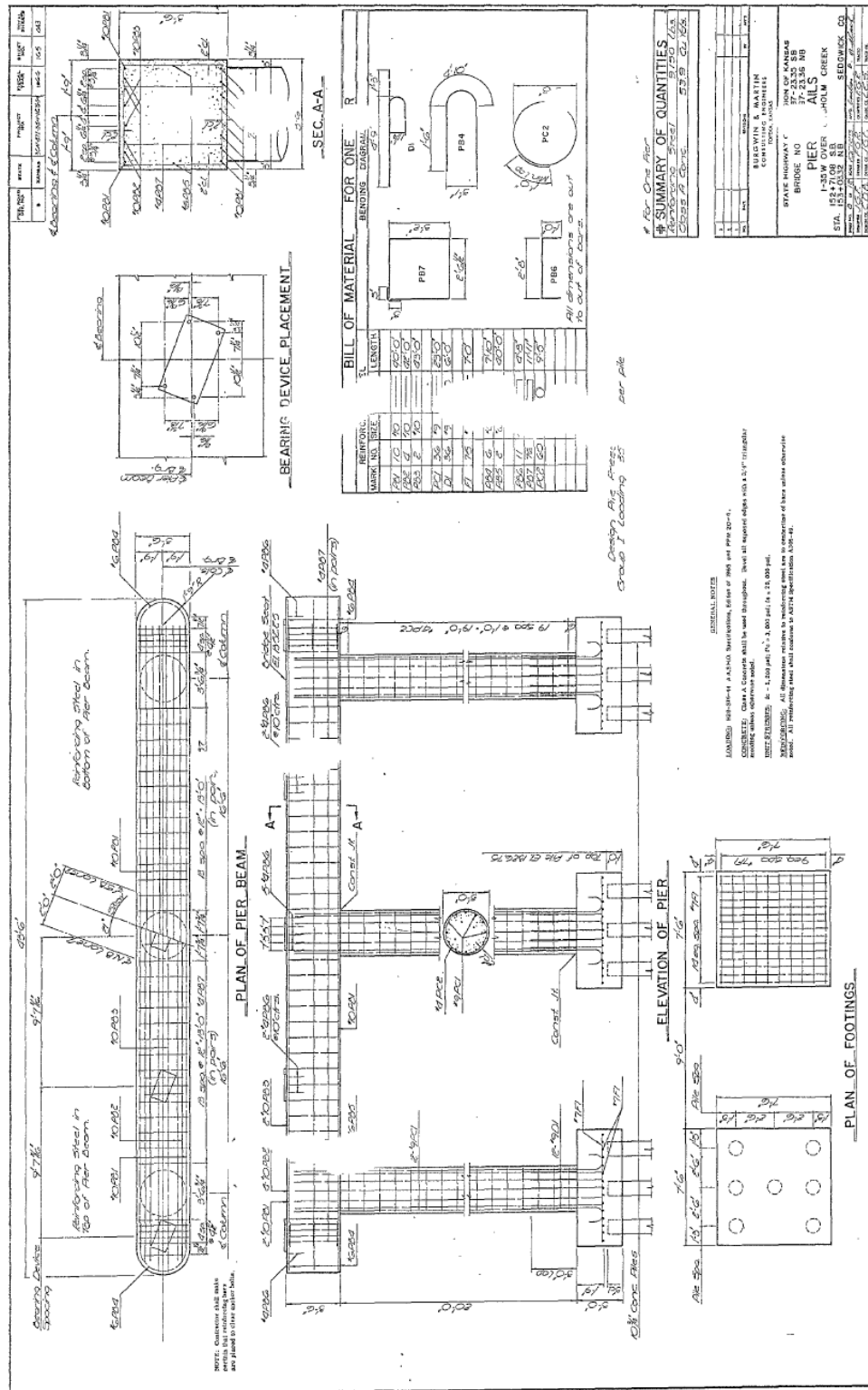


Figure F. 3: Construction layout of northbound bridge.













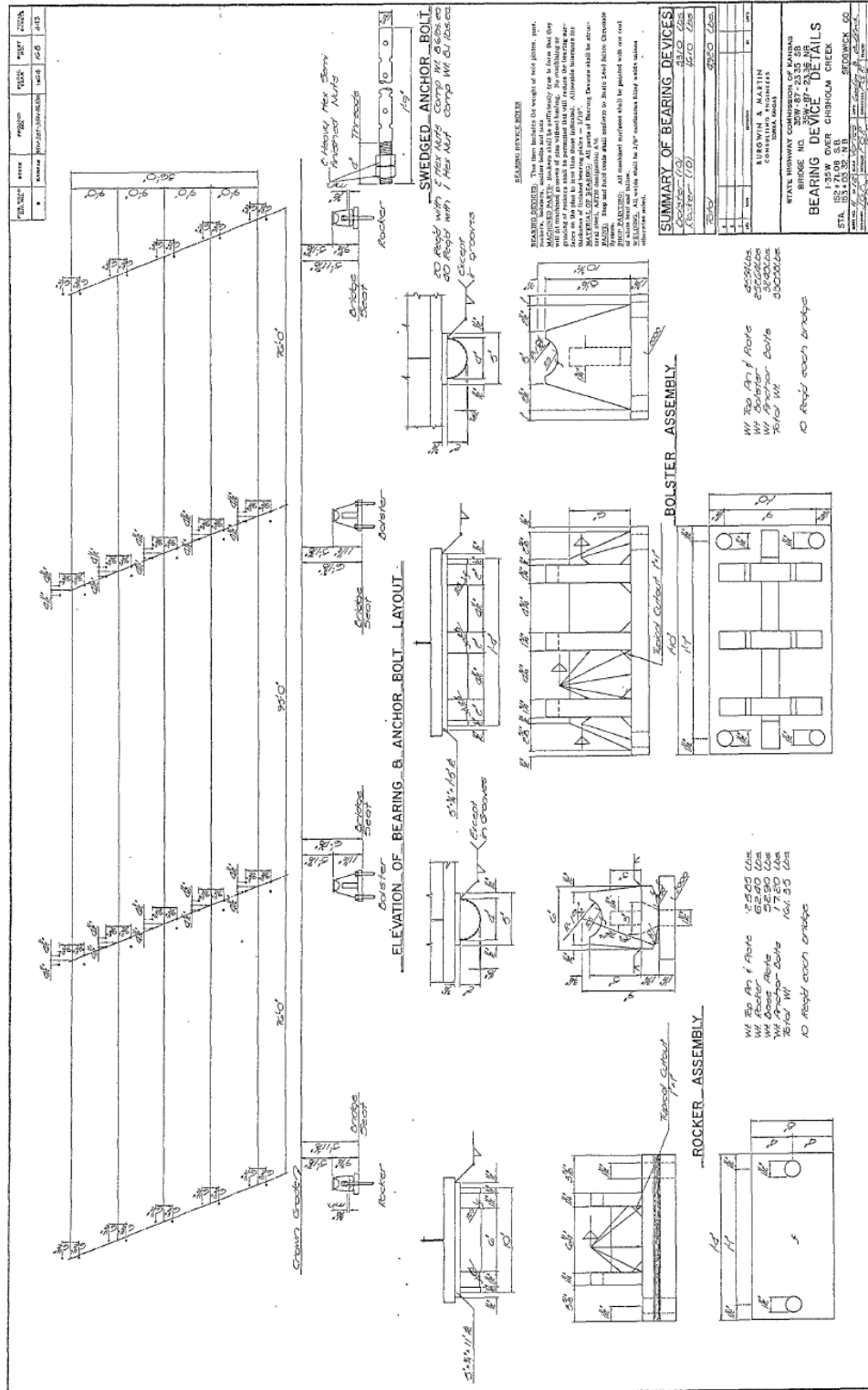


Figure F. 10: Bearing device details.

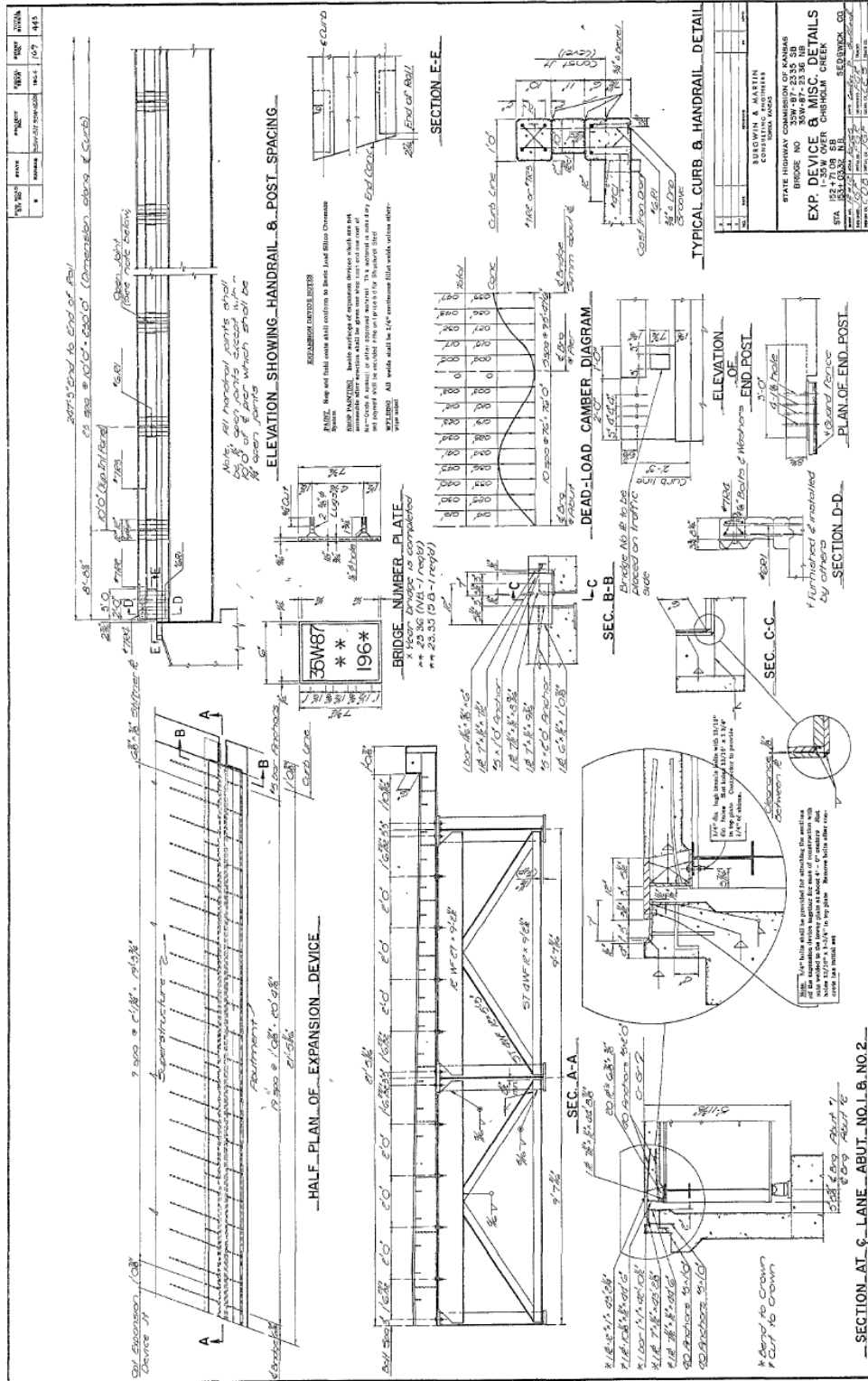


Figure F. 11: Expansion device and miscellaneous details.

Repair Plans

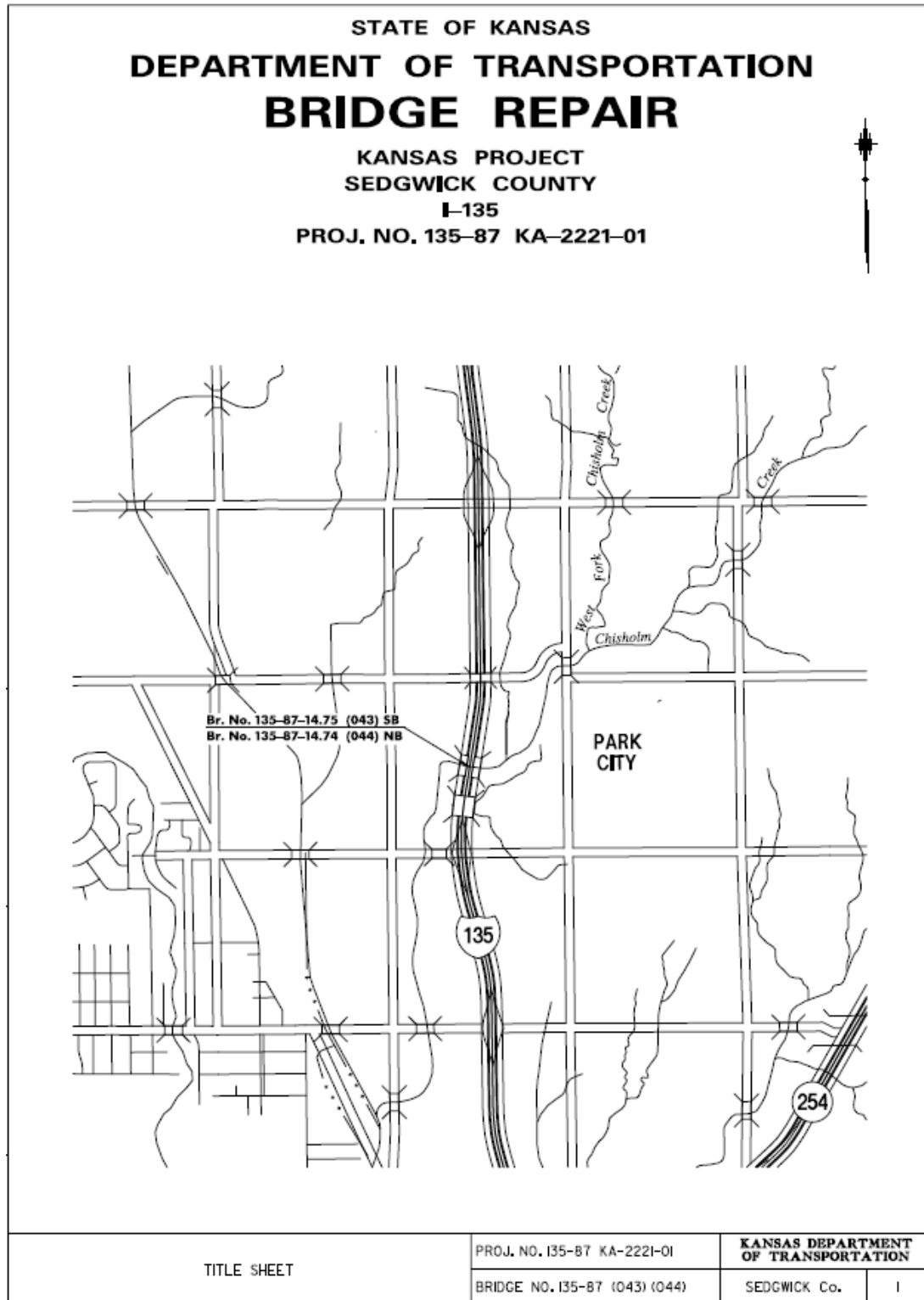


Figure F. 12: Title sheet.

SUMMARY OF STRUCTURAL STEEL QUANTITIES (For Information only)						
Bridge Number	Connection Angle 6" x 6" x 3/4" x 3/2" (Each)	* Plate 1" x 7/4" x 10/2" (Each)	* Plate 3/4" x 3/4" x 7/4" (Each)	Backing Plate 1" x 7/4" x 1'-10" (Each)	Fill Plate 3/8" x 3/2" x 7/4" (Each)	Fill Plate 3/8" x 3/2" x 3/2" (Each)
(043)	160	60	60	50	60	80
(044)	320	120	120	100	120	160
Total	480	180	180	150	180	240

* To be used in 'Fabricated Backing Plate Angle'.

POUNDS OF STRUCTURAL STEEL:

Single Web Stiffener Locations
Br. No. (043)....3,300 lbs.
Br. No. (044)....6,600 lbs.

Double Web Stiffener Locations
Br. No. (043)....2,354 lbs.
Br. No. (044)....4,708 lbs.

TOTAL:
Br. No. (043)....5,654 lbs
Br. No. (044)....11,308 lbs.
TOTAL.....16,962 lbs.

3/4" A325 Bolts:
3/2" - 960 Total
3/4" - 330 Total

INDEX TO DRAWINGS	
Sheet No.	Drawing
1	Title Sheet
2-3	General Notes and Quantities
4	Construction Layout
5	Framing Plan
6	Existing Girder Details at Cross Frames
7-8	Proposed Girder Web Repair Details at Cross Frames (Single Web Stiffener Locations)
9-10	Proposed Girder Web Repair Details at Cross Frames (Double Web Stiffener Locations)
11	Structural Steel Details

SUMMARY OF QUANTITIES		
ITEM	UNITS	QUANTITY
Bridge Repair	Lump Sum	Lump Sum
Flagger (Set)	Hour	1
Mobilization	Lump Sum	Lump Sum

ID #1: 150 Single Web Stiffener Locations
ID #2: 90 Double Web Stiffener Locations

Note: On Bridge (043), repair connections at the bottom flanges only.
On Bridge (044), repair connections at both the bottom and top flanges.

GENERAL NOTES AND QUANTITIES	PROJ. NO. I35-87 KA-2221-01	KANSAS DEPARTMENT OF TRANSPORTATION	
	BRIDGE NO. I35-87 (043) (044)	SEDGWICK Co.	2

Figure F. 13: General notes and quantities.

GENERAL NOTES

EXISTING DIMENSION VERIFICATION: Dimensions of the existing structure are based on old plans. Verify, by field measurement, the as-built dimensions of the existing structure and submit such verification in writing to the Engineer. The verification will include sketches, drawings, photographs and descriptions as needed to clearly define the as-built dimensions that will be incorporated in the new construction.

EXISTING STRUCTURE: Plans of the existing structure are on file and available for inspection by qualified bidders at the State Bridge Office, KDOT, Eisenhower State Office Building, 700 SW Harrison, Topeka, KS.

BRIDGE REPAIR: The bid item "Bridge Repair (Lump Sum)" shall be full compensation for materials, labor and equipment necessary to perform the work as shown.

STRUCTURAL STEEL: Structural steel shall be ASTM A709 Gr. 36. The structural steel shall be shipped unpainted.

BOLTS: All bolts, nuts and hardened flat washers shall conform to the heavy hex structural requirements of ASTM A325, Type 1, and KDOT Specifications unless otherwise noted. Direct Tension Indicators (DTIs) are to comply with the requirements of the latest edition of ASTM F959. No allowance will be made for high strength bolts used for permanent or temporary connections. This work is subsidiary to the bid item, "Bridge Repair" (Lump Sum). The number of bolts is shown for the convenience of the Contractor.

BOLTED CONNECTIONS: Use $\frac{3}{4}$ " diameter heavy hex structural bolts for all connections. Use $\frac{13}{16}$ " diameter bolt holes. Slotted holes require one additional standard hardened washer or plate washer.

Use Direct Tension Indicators (DTIs) on all high strength bolts. Place the DTI under the bolt head and turn the nut to tighten. This method is preferred whenever possible. Face the protrusions on the DTI to the underside of the bolt head. Place a hardened flat washer under the nut. See KDOT Specifications.

PAINTING: Paint all surfaces that have been exposed by repair procedures. Paint all new structural steel. The surfaces to be painted shall be cleaned to meet Steel Structures Painting Council Specifications SSPC-SP6. The field coats applied shall conform to an organic zinc primer with a waterborne acrylic finish coat. The finish coat will be Kansas dark green. The color shall match Federal Standard #34102. Painting shall be subsidiary to the bid item "Bridge Repair (Lump Sum)".

QUANTITIES: Items not listed separately in the Summary of Quantities are subsidiary to other items in the proposal.

GENERAL NOTES AND QUANTITIES	PROJ. NO. I35-87 KA-2221-01	KANSAS DEPARTMENT OF TRANSPORTATION	
	BRIDGE NO. I35-87 (043) (044)	SEDGWICK Co.	3

Figure F. 14: General notes and quantities.

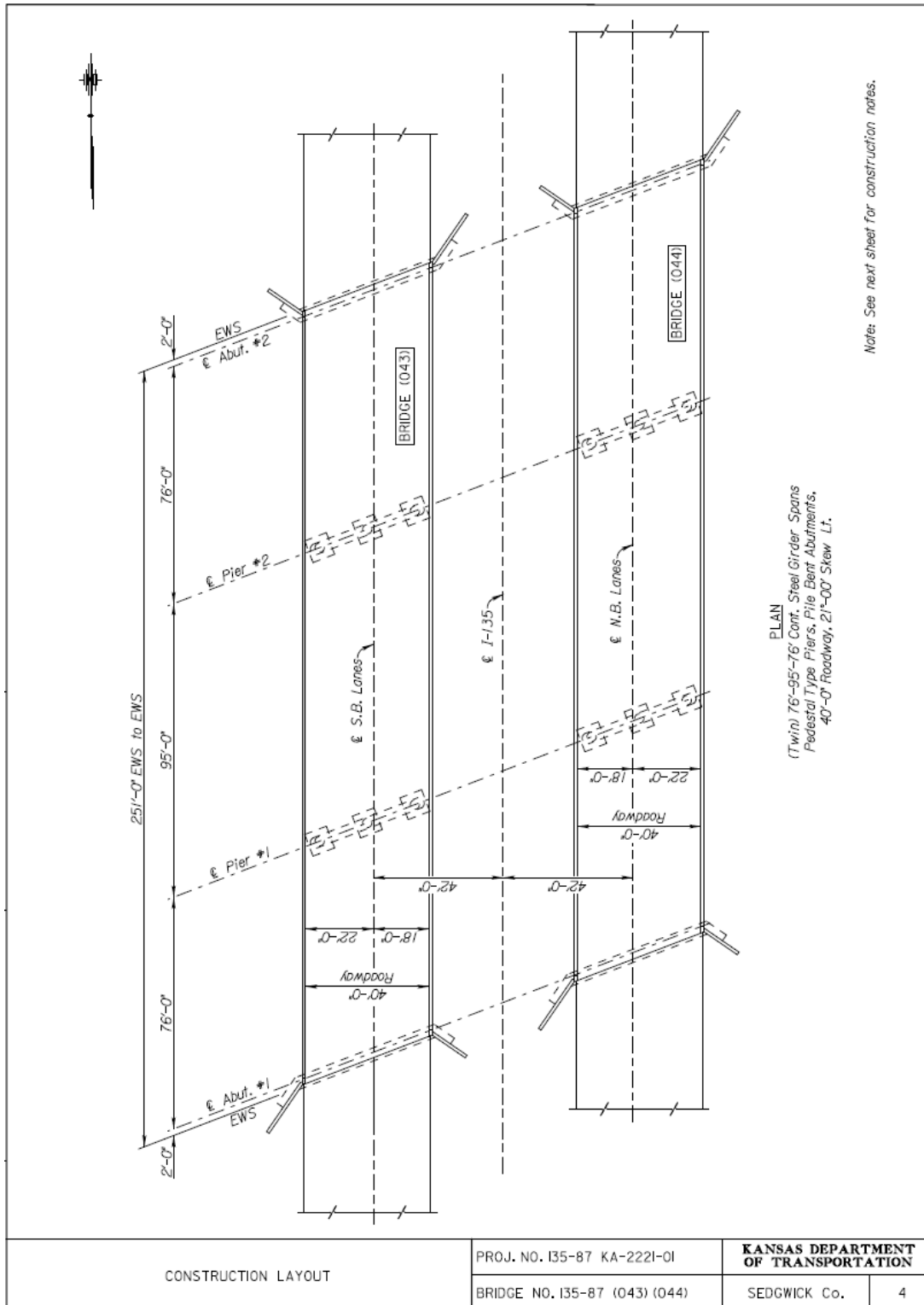


Figure F. 15: Construction layout.

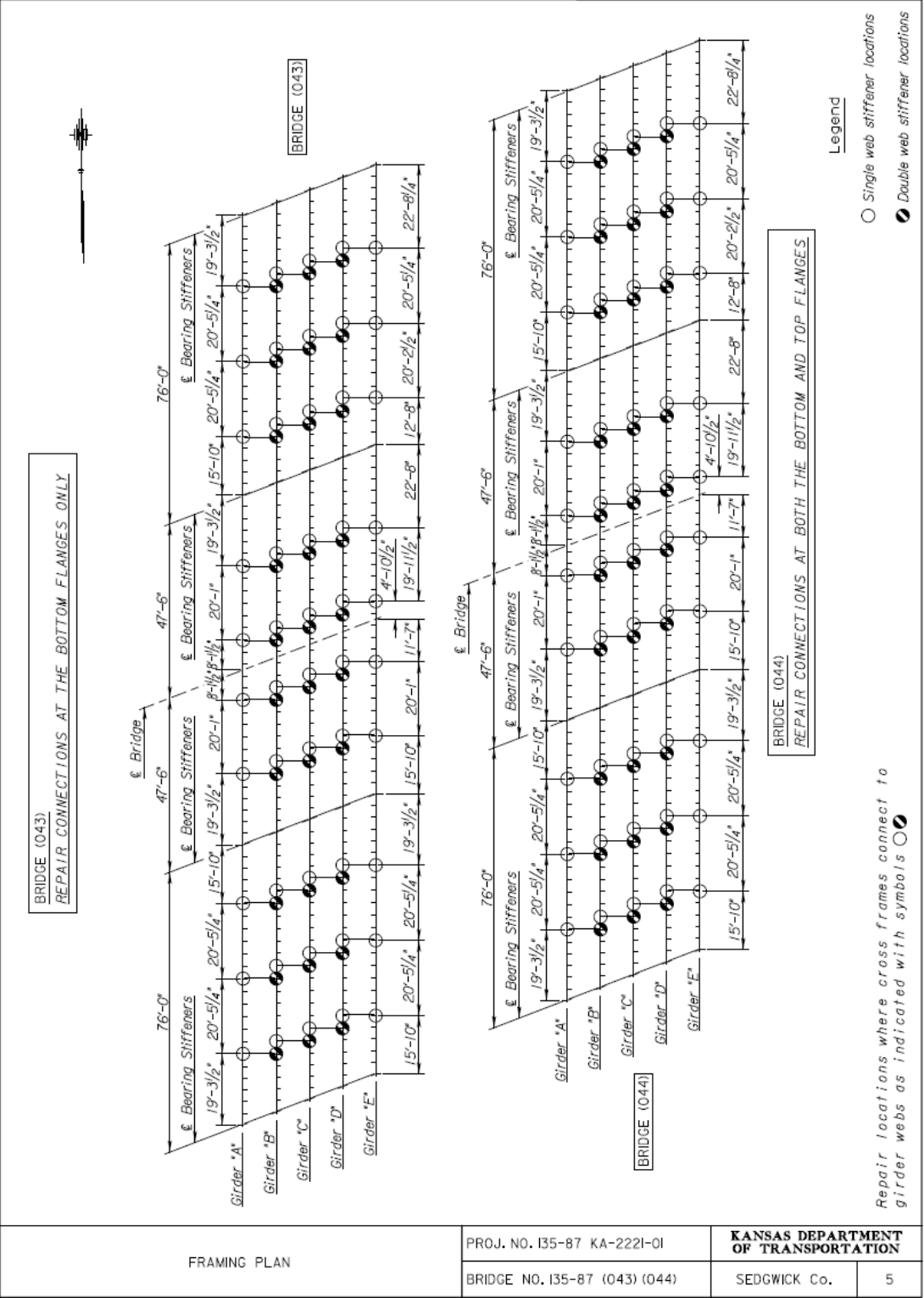
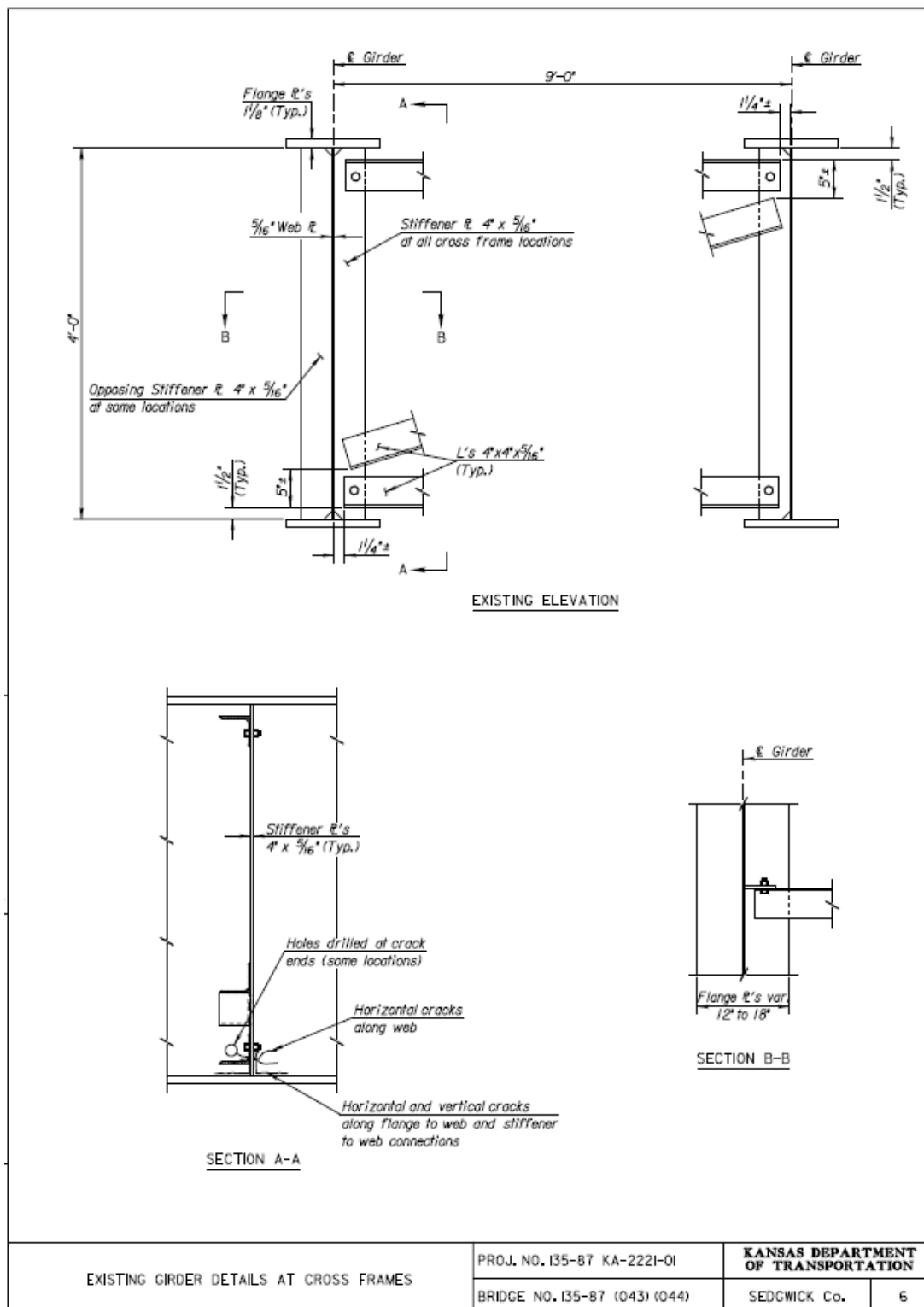
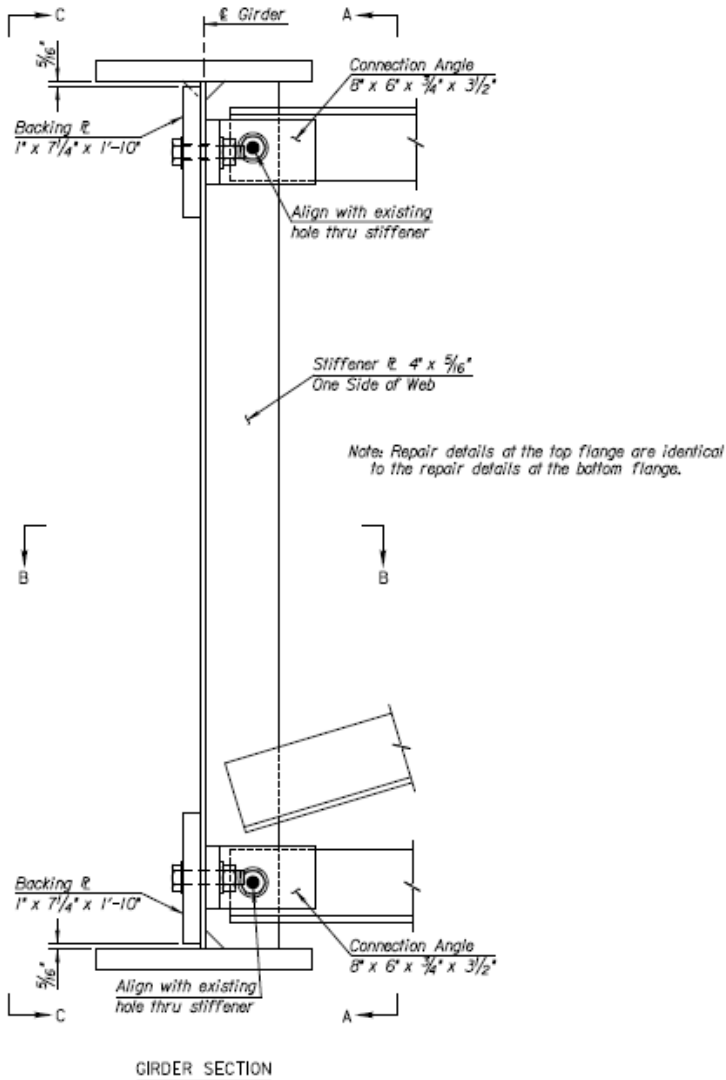


Figure F. 16: Framing plan.



SUGGESTED REPAIR PROCEDURES:

- 1) Remove bolt thru existing cross frame and stiffener.
- 2) Place Connection Angles and Fill Plate as shown in the details and use existing hole as a template to drill a $\frac{13}{16}$ " hole thru the Connection Angles, Fill Plate, existing cross frame and stiffener. Attach with a $\frac{3}{4}$ " A325 bolt.
- 3) Drill $\frac{13}{16}$ " holes thru existing web using shop drilled holes in the Connection Angles as a template.
- 4) Attach the Backing \bar{r} as shown in the details with a $\frac{3}{4}$ " A325 bolt using the shop drilled slotted hole.
- 5) Drill the remaining $\frac{13}{16}$ " holes in the Backing \bar{r} using the previously drilled holes in the existing web as a template. Complete attachment with $\frac{3}{4}$ " A325 bolts.
- 6) Paint all surfaces in the repair area with a waterborne acrylic finish coat.



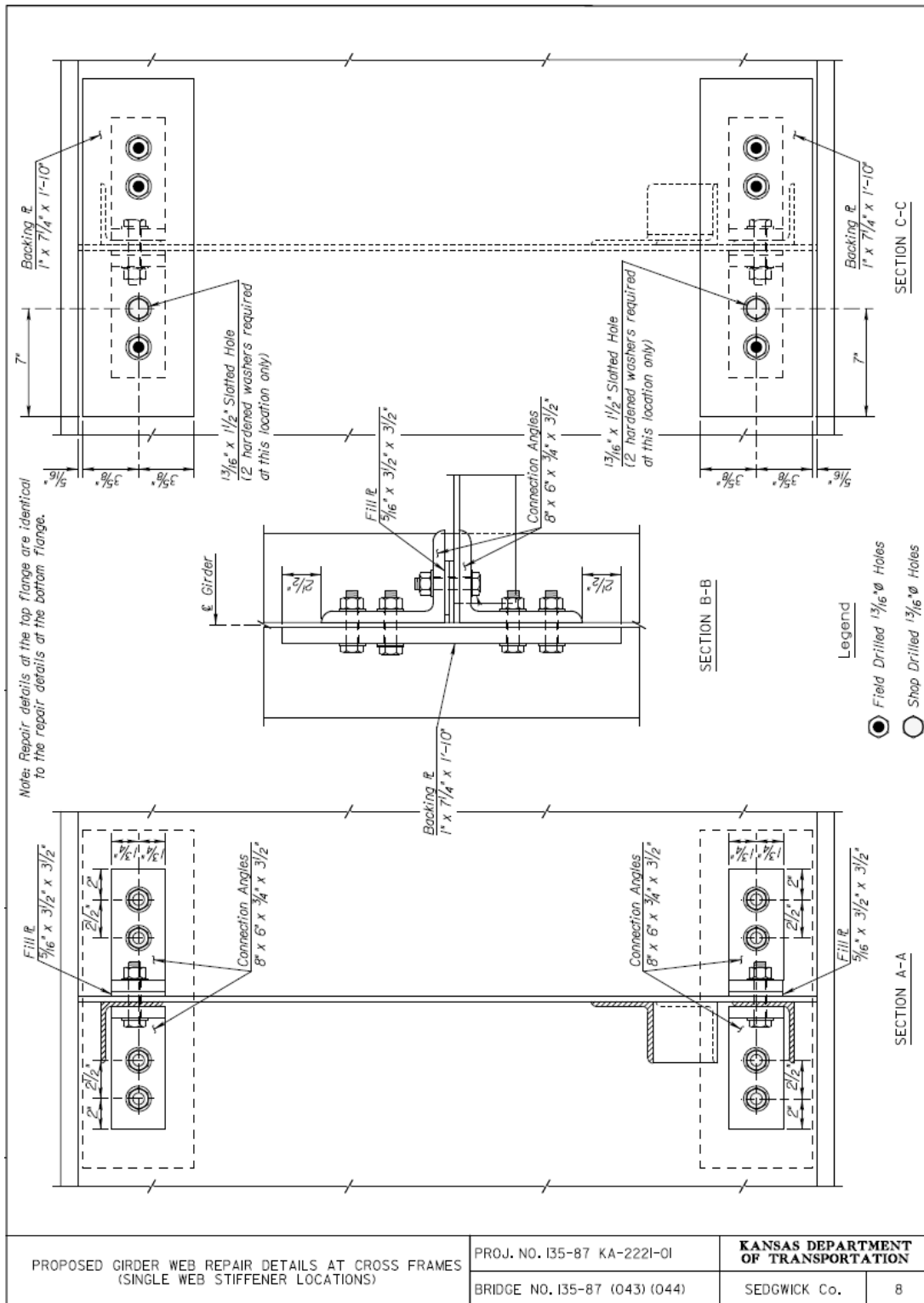
Note: See next sheet for "Section A-A", "Section B-B" and "Section C-C".

Legend

- Field Drilled $\frac{13}{16}$ " Holes
- Shop Drilled $\frac{13}{16}$ " Holes

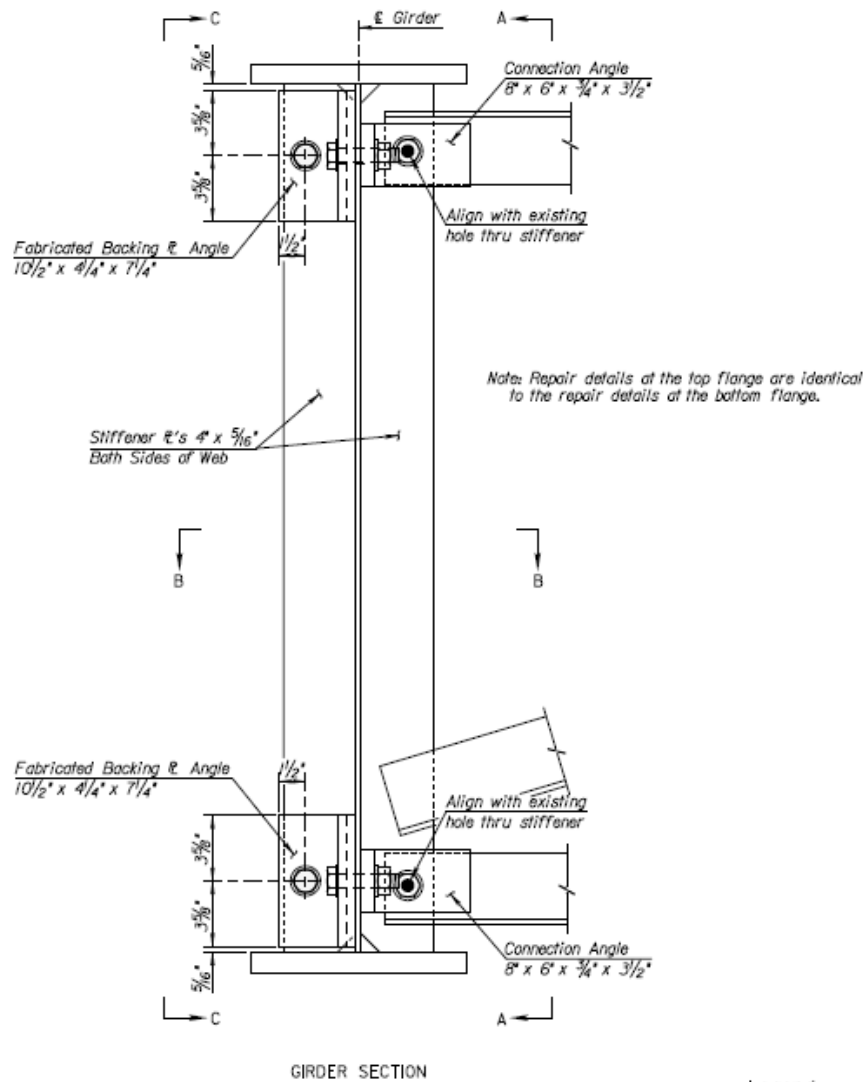
PROPOSED GIRDER WEB REPAIR DETAILS AT CROSS FRAMES (SINGLE WEB STIFFENER LOCATIONS)	PROJ. NO. 135-87 KA-2221-01 BRIDGE NO. 135-87 (043) (044)	KANSAS DEPARTMENT OF TRANSPORTATION SEDGWICK Co. 7	
--	--	--	--

Figure F. 18: Proposed girder web repair details at cross frames (single web stiffener locations).



SUGGESTED REPAIR PROCEDURES:

- 1) Remove bolt thru existing cross frame and stiffener.
- 2) Place Connection Angles and Fill Plate as shown in the details and use existing hole as a template to drill a $\frac{13}{16}$ " hole thru the Connection Angles, Fill Plate, existing cross frame and stiffener. Attach with a $\frac{3}{4}$ " A325 bolt.
- 3) Drill $\frac{13}{16}$ " holes thru existing web using shop drilled holes in the Connection Angles as a template.
- 4) Place Fabricated Backing \angle Angles and Fill \angle 's as shown in the details. Drill $\frac{13}{16}$ " hole thru the existing stiffener using the shop drilled holes in the Fabricated Backing \angle Angles and Fill \angle 's as a template. Attach with a $\frac{3}{4}$ " A325 bolt.
- 5) Drill remaining $\frac{13}{16}$ " holes in the Fabricated Backing \angle Angles using the previously drilled holes in the existing web as a template. Complete attachment with $\frac{3}{4}$ " A325 bolts.
- 6) Paint all surfaces in the repair area with a waterborne acrylic finish coat.



Note: See next sheet for "Section A-A", "Section B-B" and "Section C-C".

Legend

- Field Drilled $\frac{13}{16}$ " Holes
- Shop Drilled $\frac{13}{16}$ " Holes

PROPOSED GIRDER WEB REPAIR DETAILS AT CROSS FRAMES (DOUBLE WEB STIFFENER LOCATIONS)	PROJ. NO. I35-87 KA-2221-01 BRIDGE NO. I35-87 (043) (044)	KANSAS DEPARTMENT OF TRANSPORTATION SEDGWICK Co. 9	
---	--	---	--

Figure F. 20: Proposed girder web repair details at cross frames (double web stiffener locations).

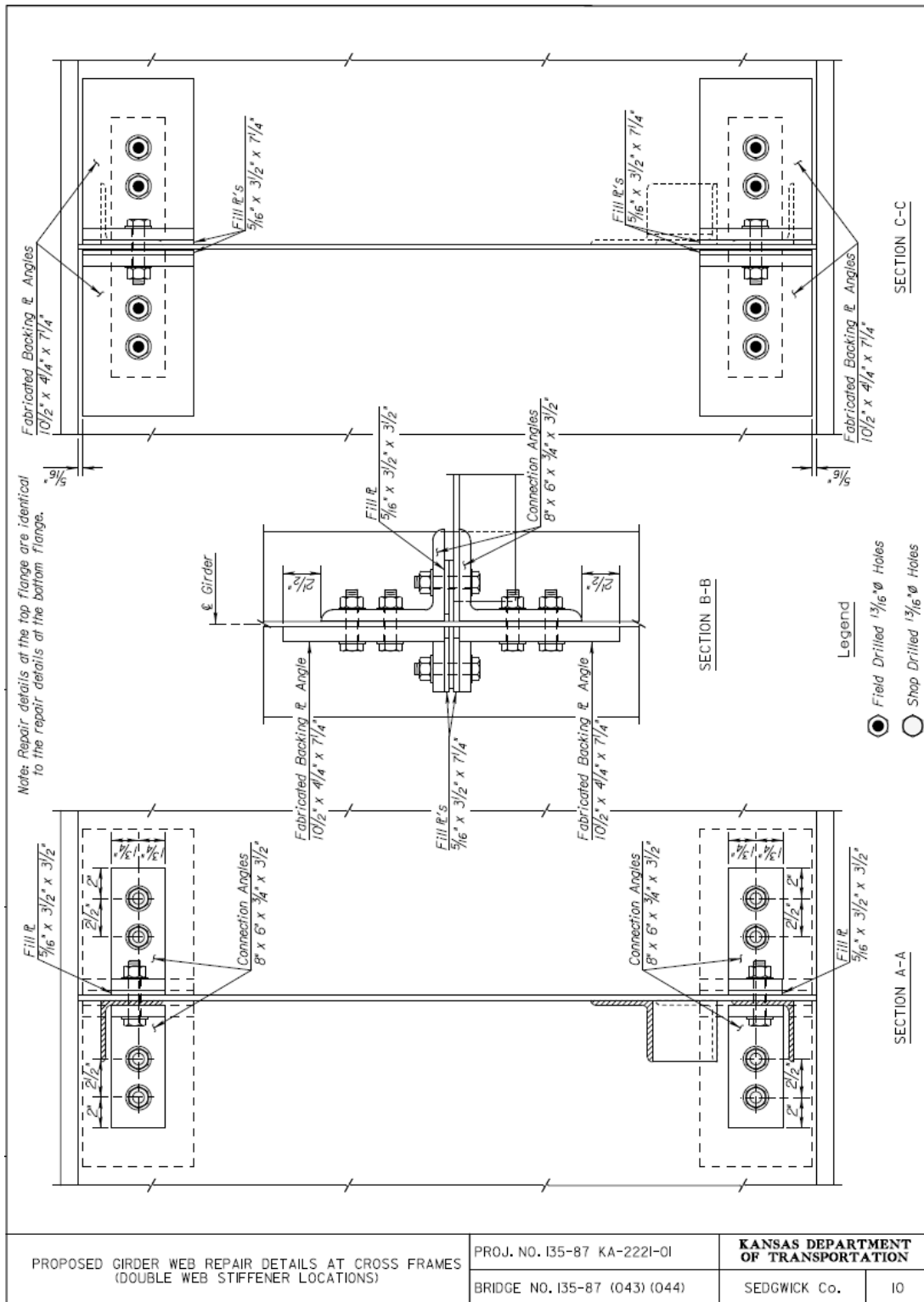


Figure F. 21: Proposed girder web repair details at cross frames (double web stiffener locations).

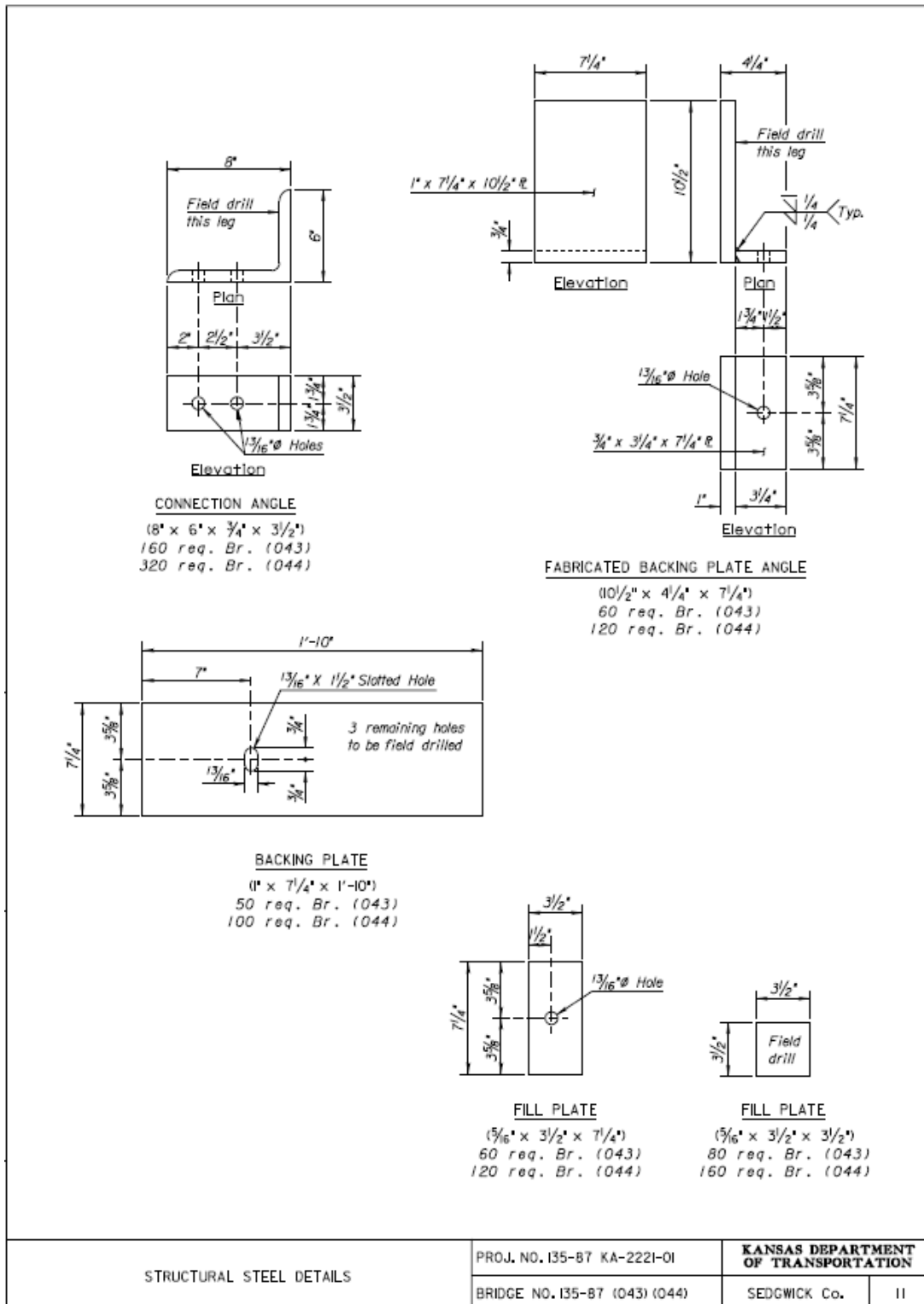


Figure F. 22: Structural steel details.

Appendix G: Filtered Field Test Data

Before Retrofit

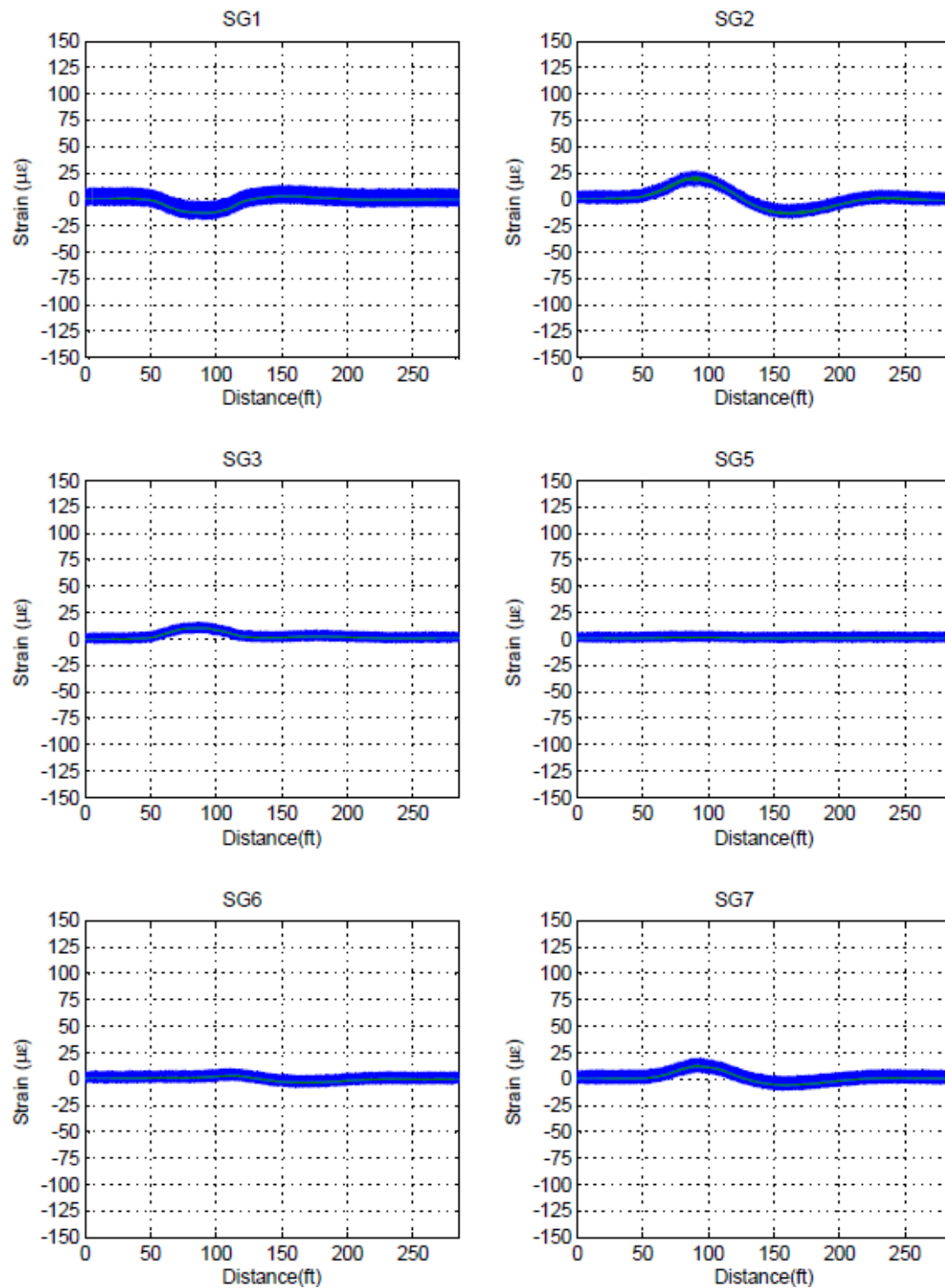


Figure G. 1: West Truck Load Placement 8-16 km/h (5-10 mph).

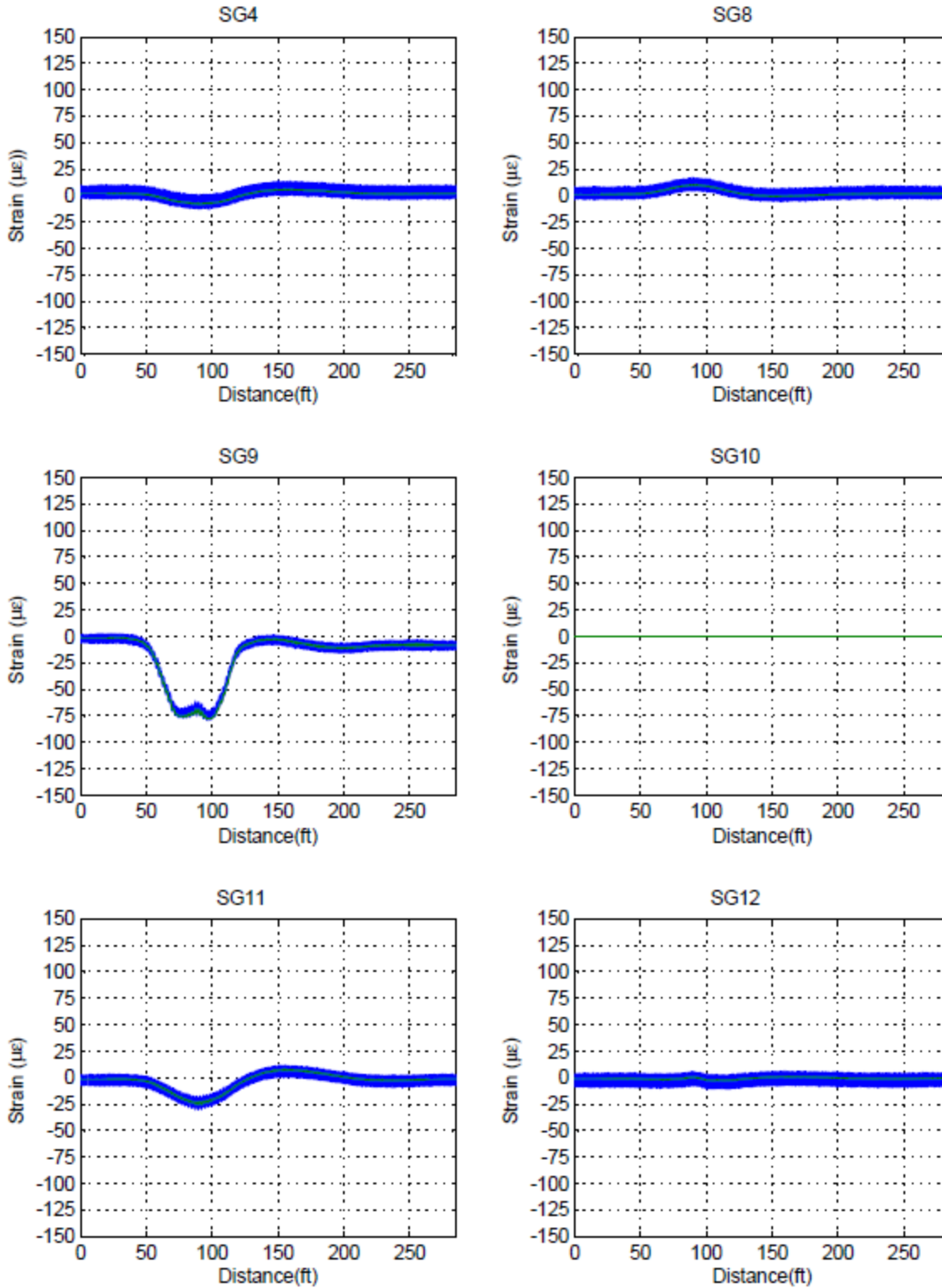


Figure G. 2: West Truck Load Placement 8-16 km/h (5-10 mph).

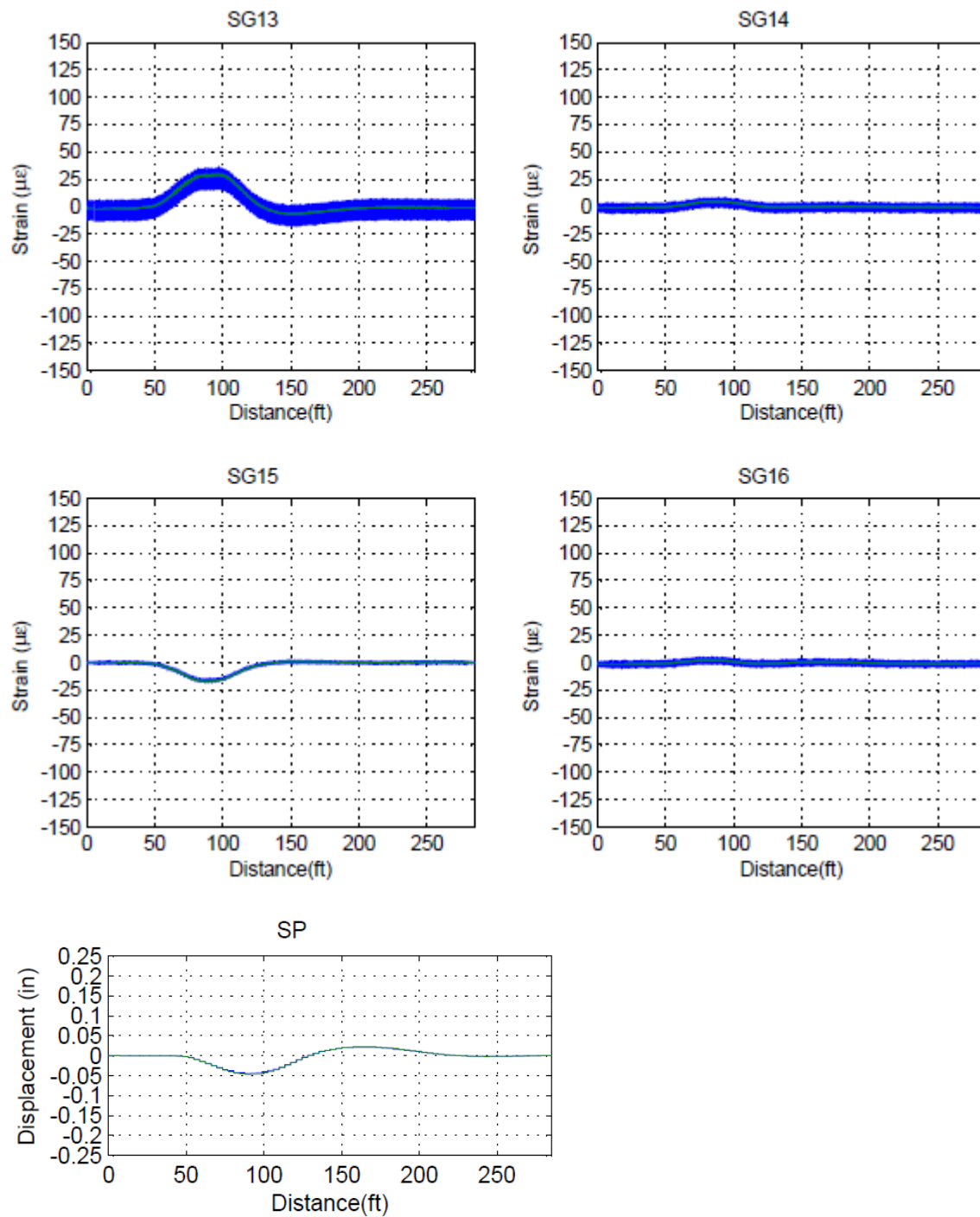


Figure G. 3: West Truck Load Placement 8-16 km/h (5-10 mph).

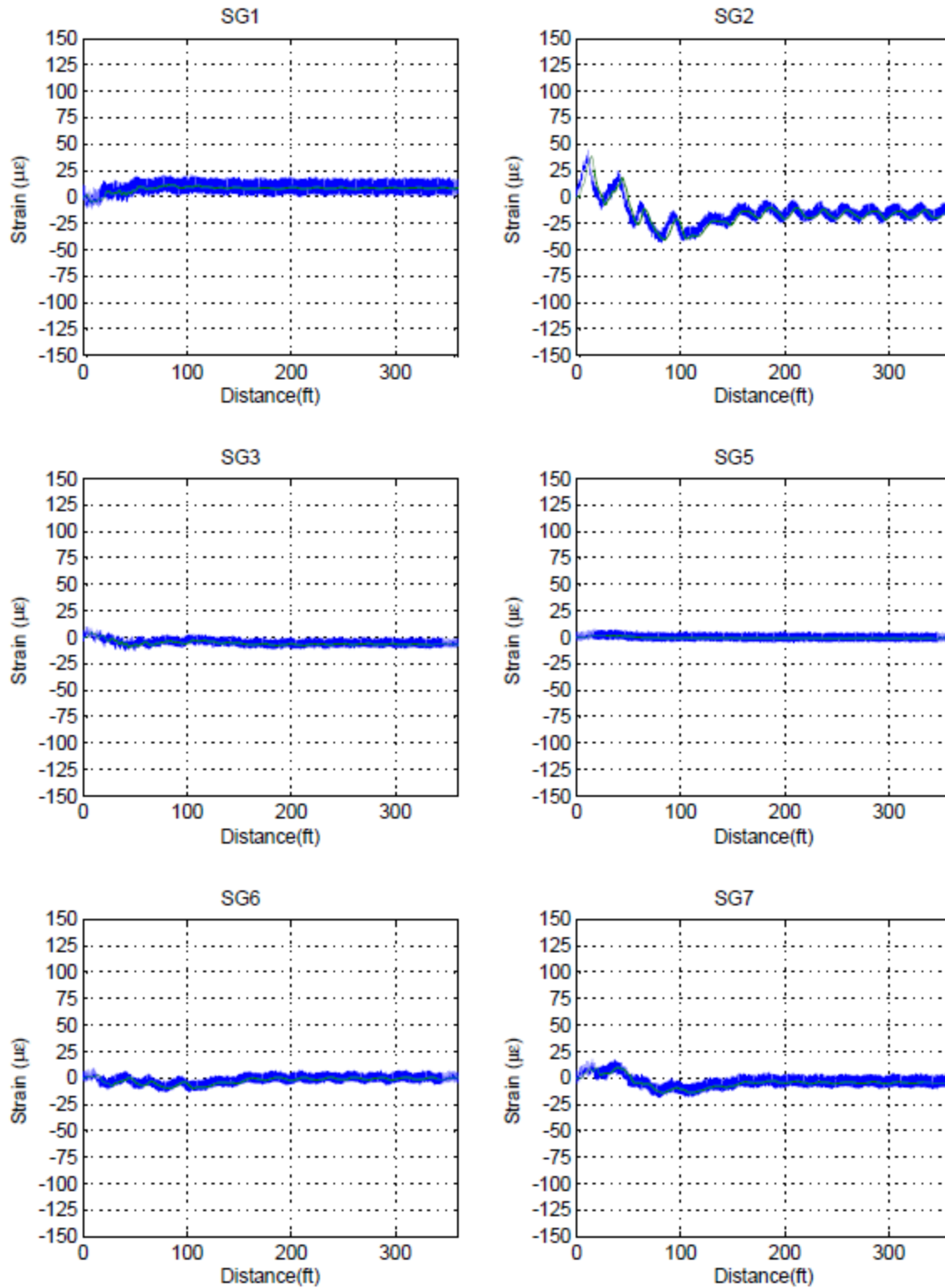


Figure G. 4: West Truck Load Placement 105-121 km/h (65-75 mph).

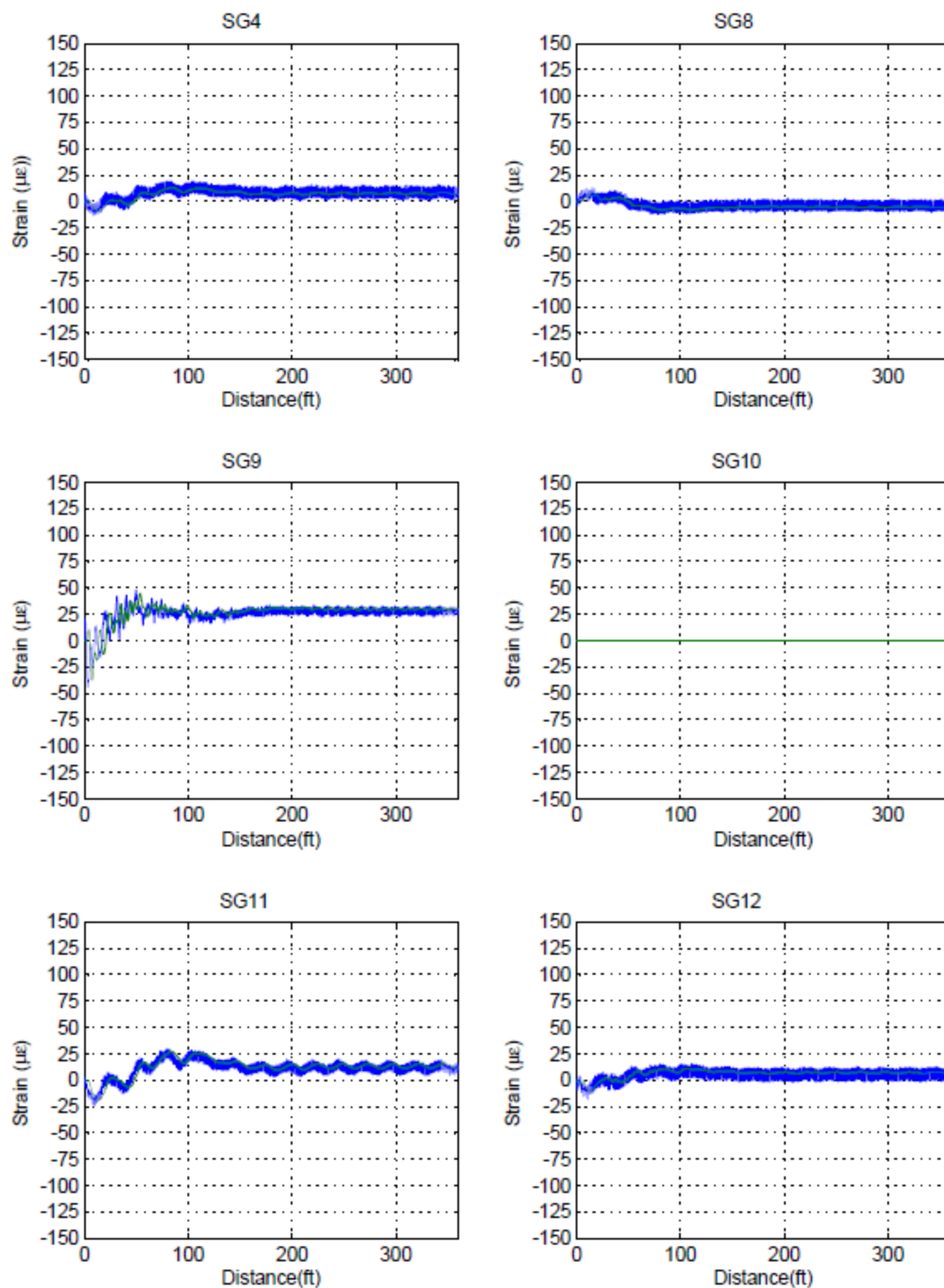


Figure G. 5: West Truck Load Placement 105-121 km/h (65-75 mph).

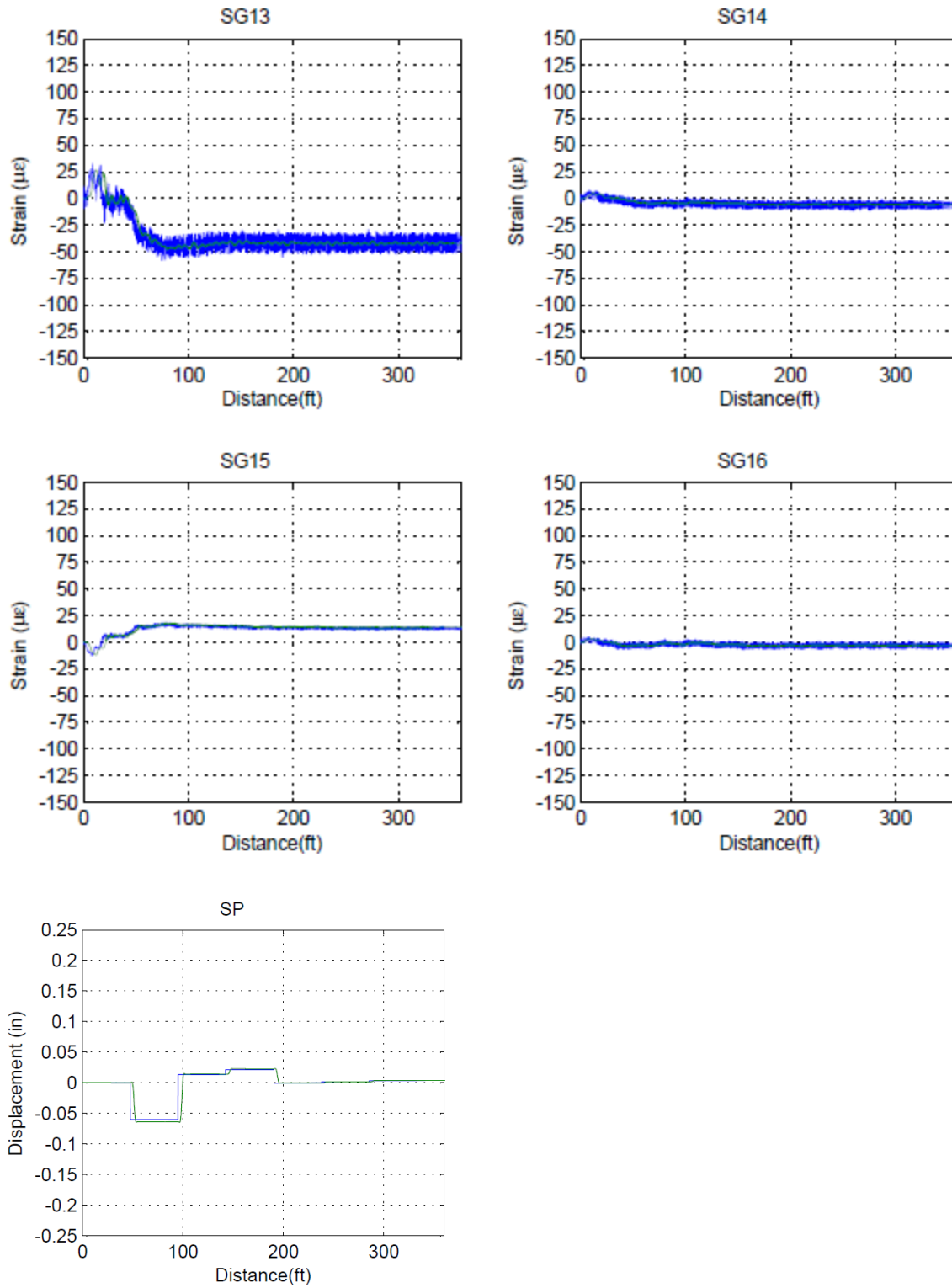


Figure G. 6: West Truck Load Placement 105-121 km/h (65-75 mph).

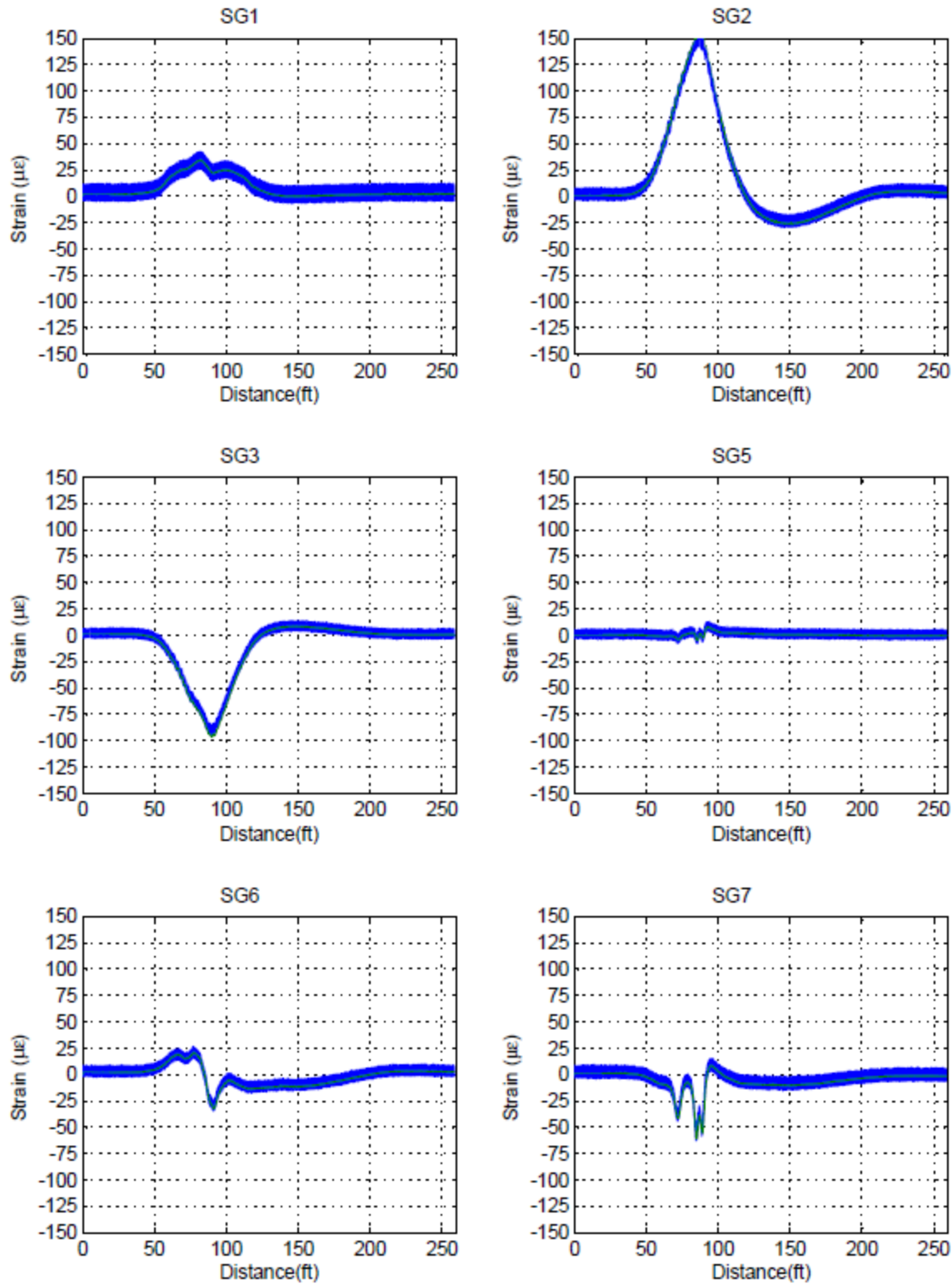


Figure G. 7: Center Truck Load Placement 8-16 km/h (5-10 mph).

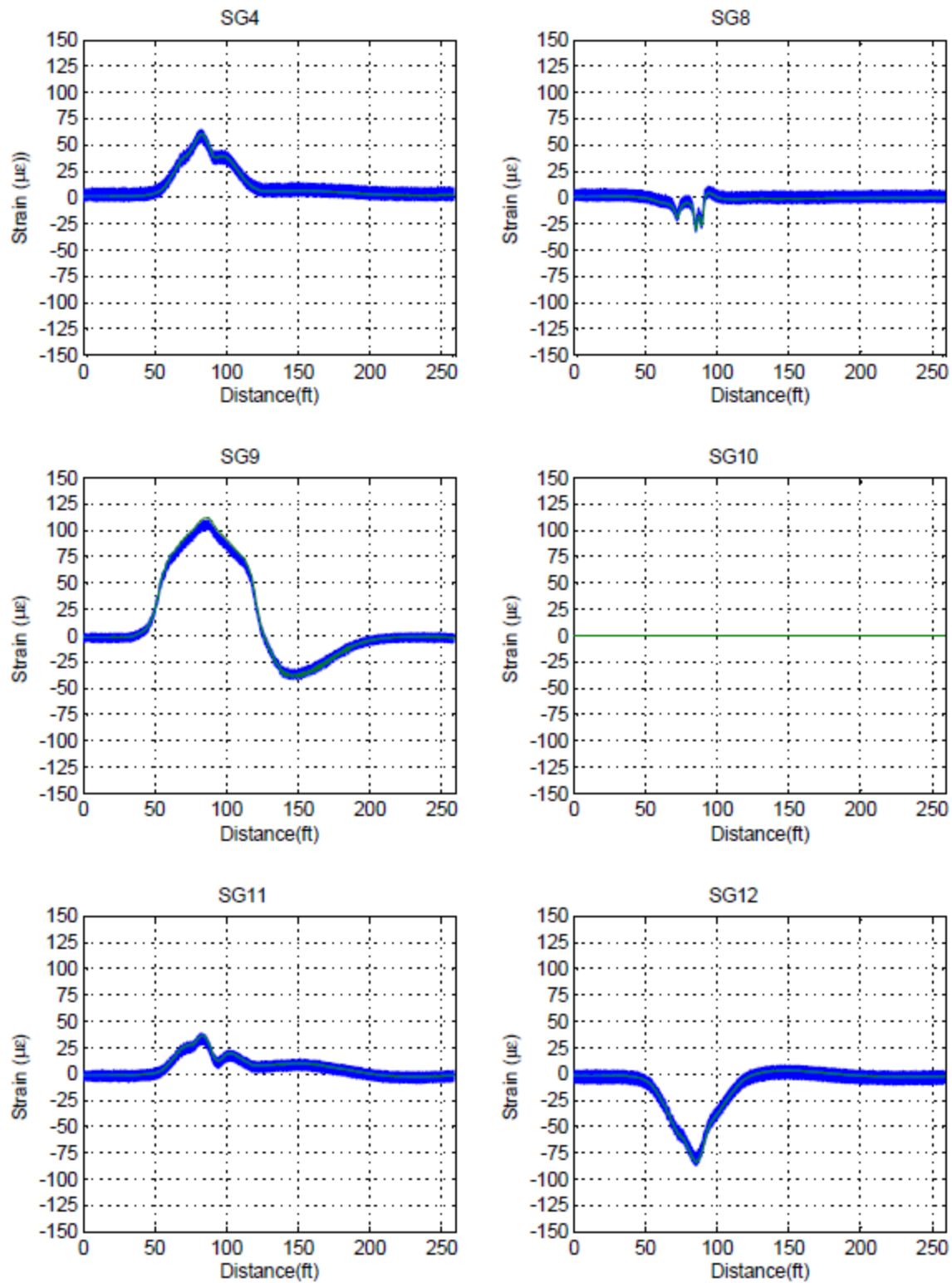


Figure G. 8: Center Truck Load Placement 8-16 km/h (5-10 mph).

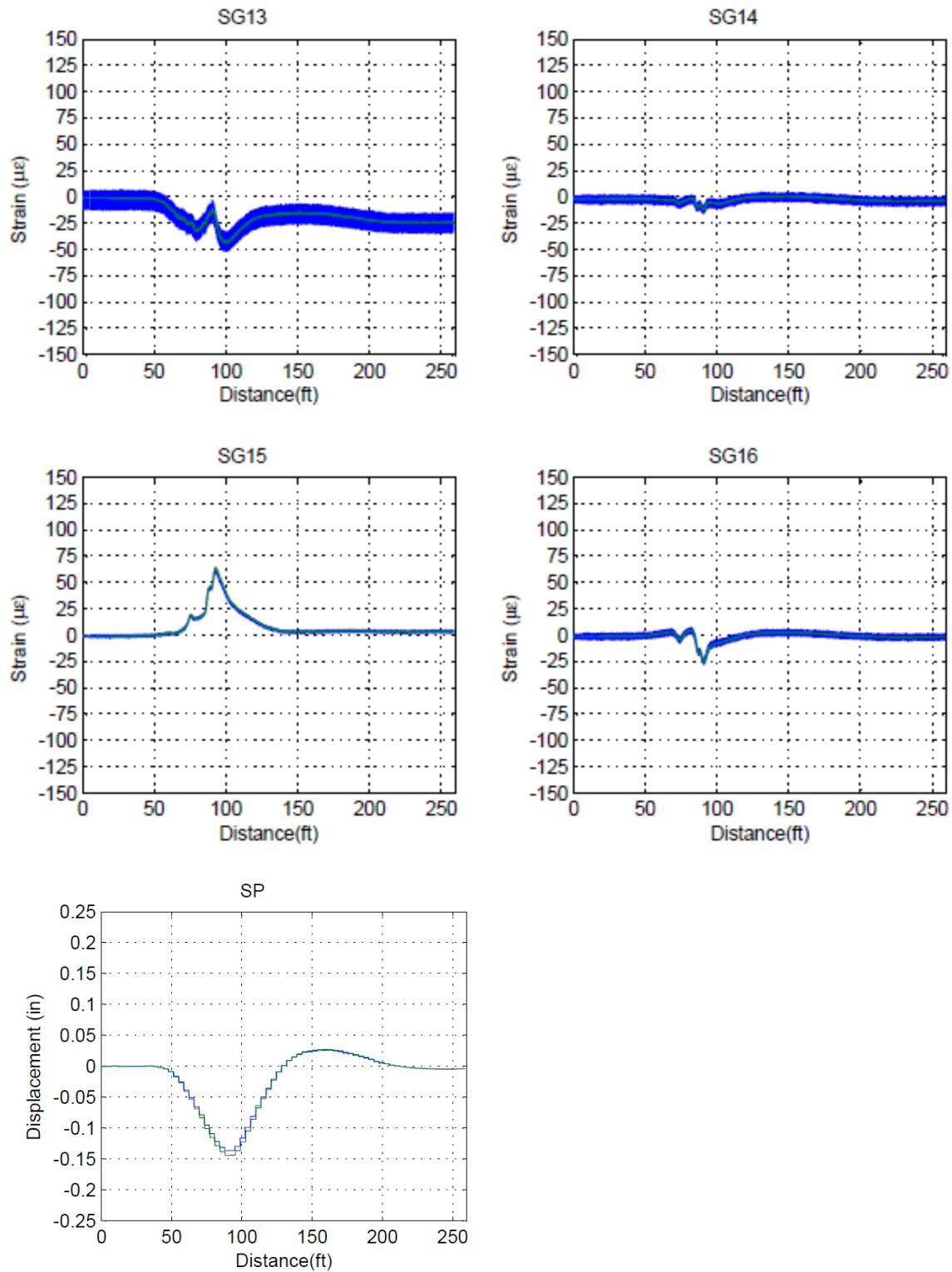


Figure G. 9: Center Truck Load Placement 8-16 km/h (5-10 mph).

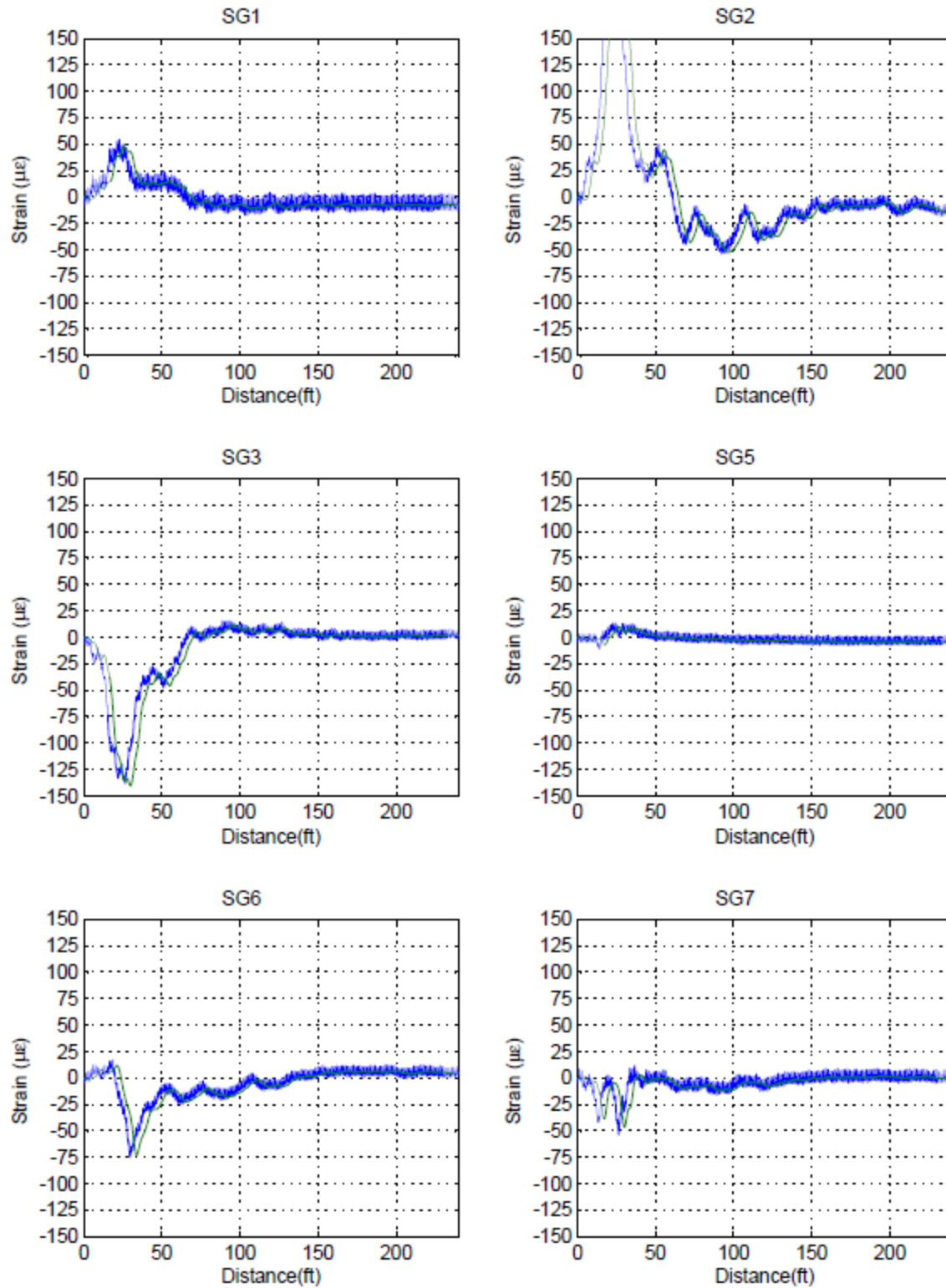


Figure G. 10: Center Truck Load Placement 105-121 km/h (65-75 mph).

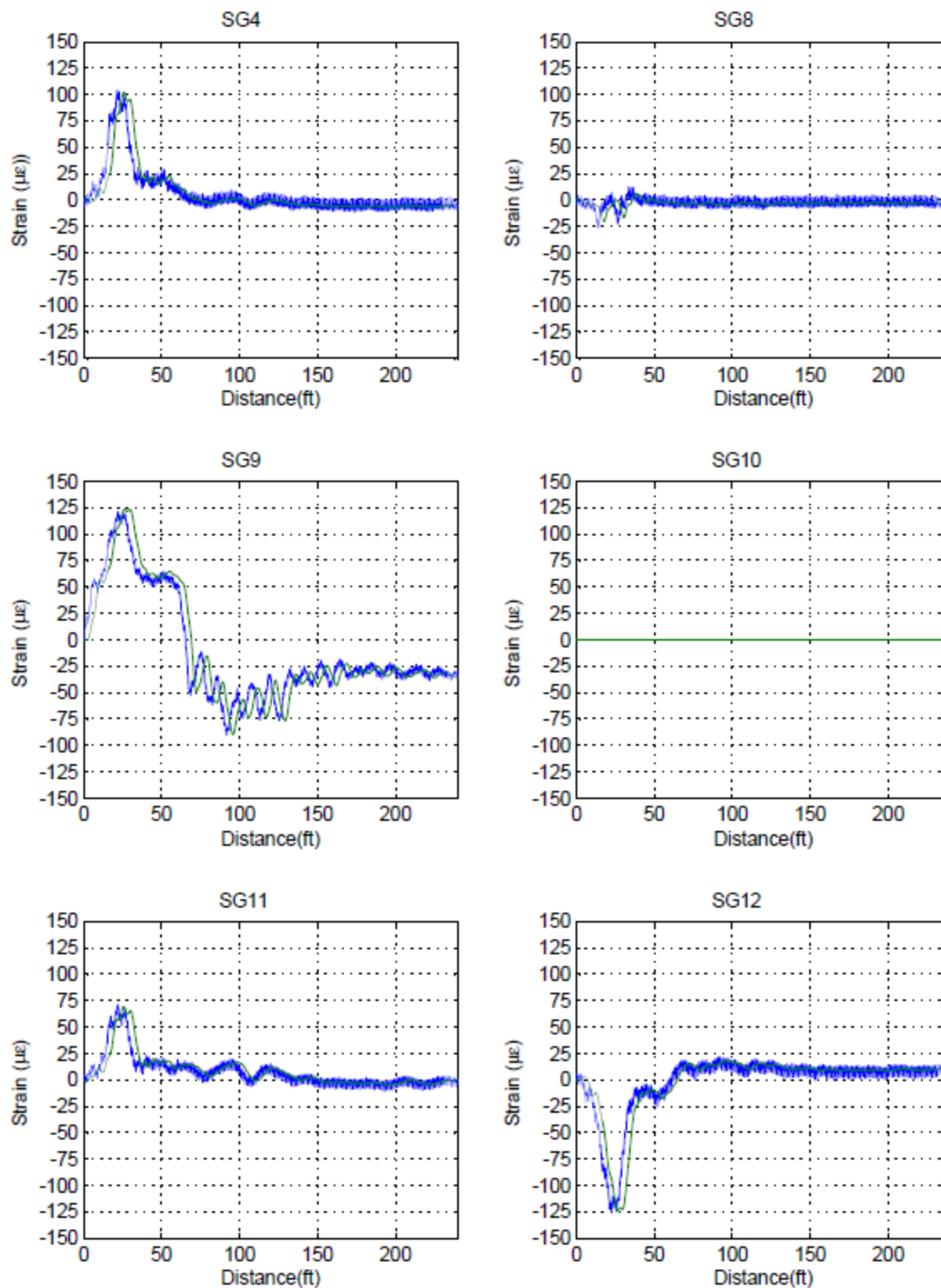


Figure G. 11: Center Truck Load Placement 105-121 km/h (65-75 mph).

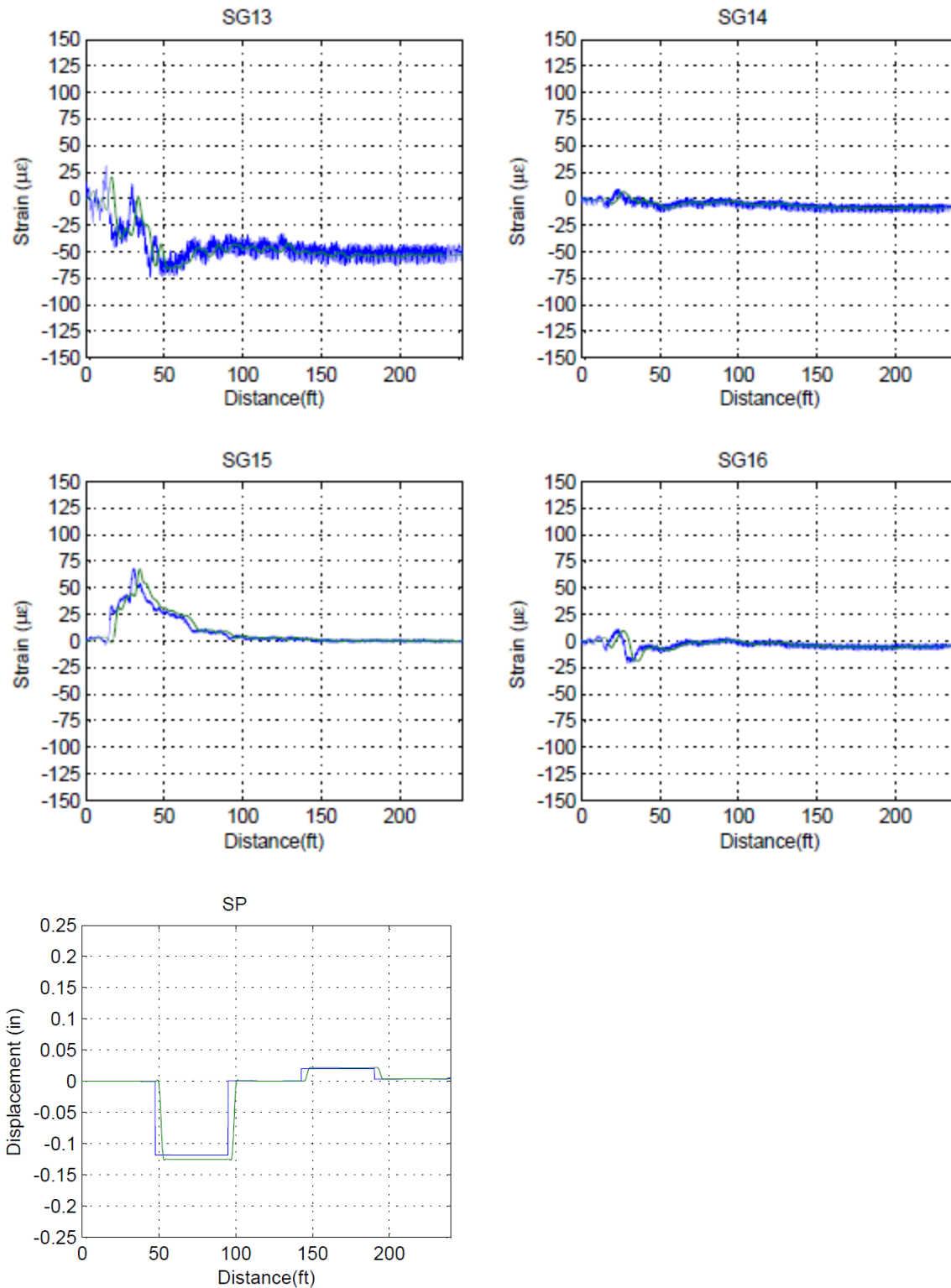


Figure G. 12: Center Truck Load Placement 105-121 km/h (65-75 mph).

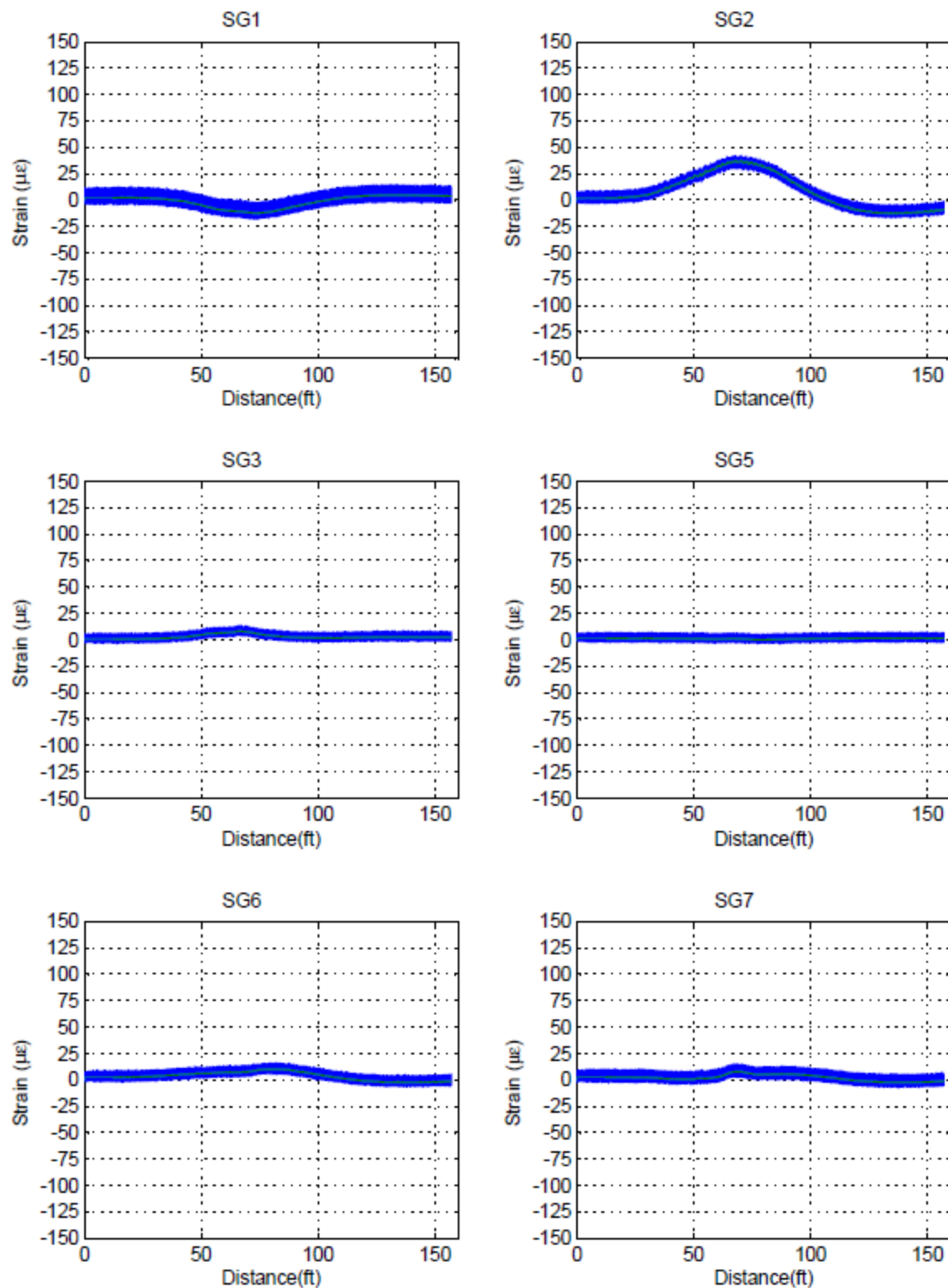


Figure G. 13: East Truck Load Placement 8-16 km/h (5-10 mph).

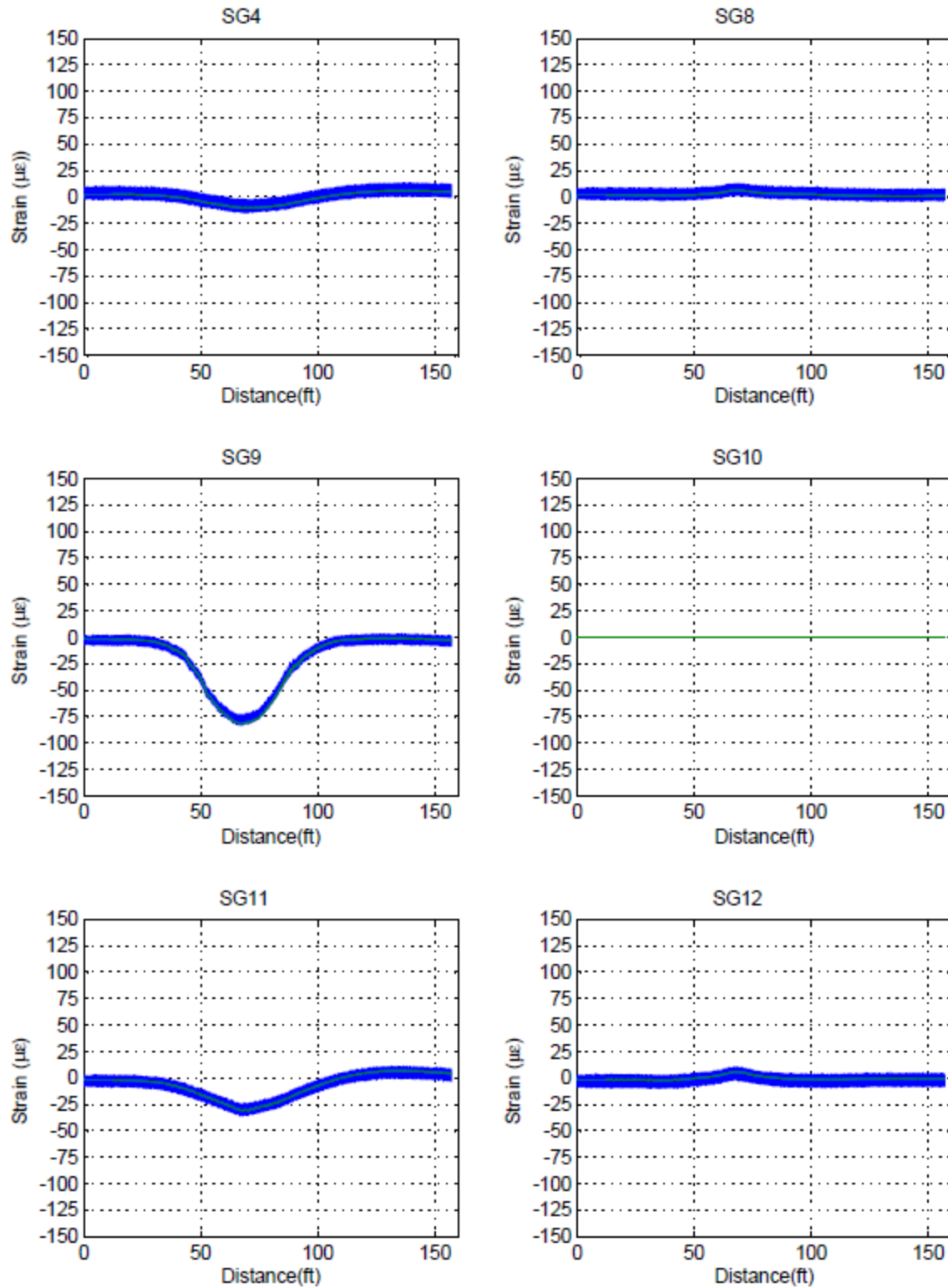


Figure G. 14: East Truck Load Placement 8-16 km/h (5-10 mph).

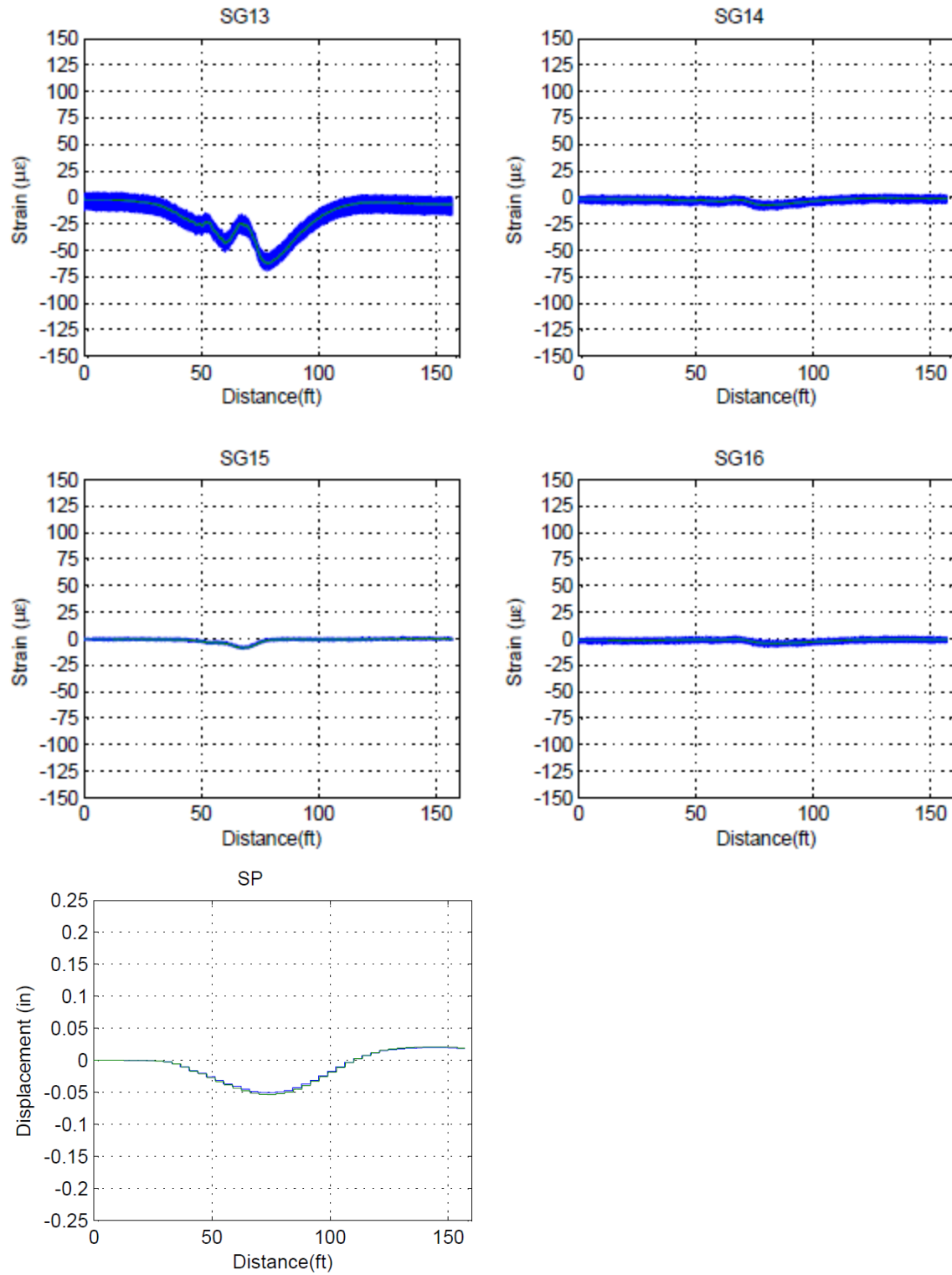


Figure G. 15: East Truck Load Placement 8-16 km/h (5-10 mph).

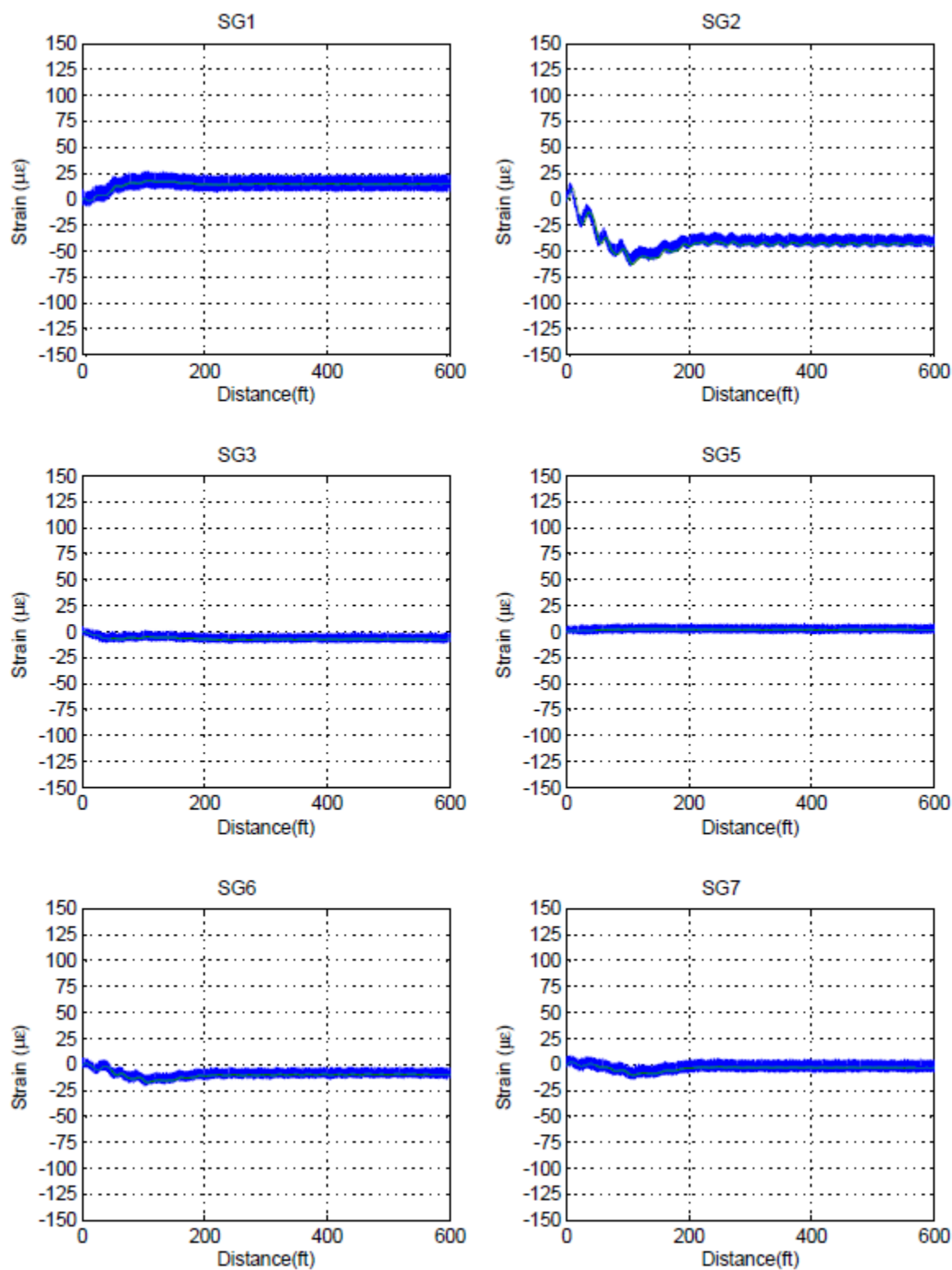


Figure G. 16: East Truck Load Placement 105-121 km/h (65-75 mph).

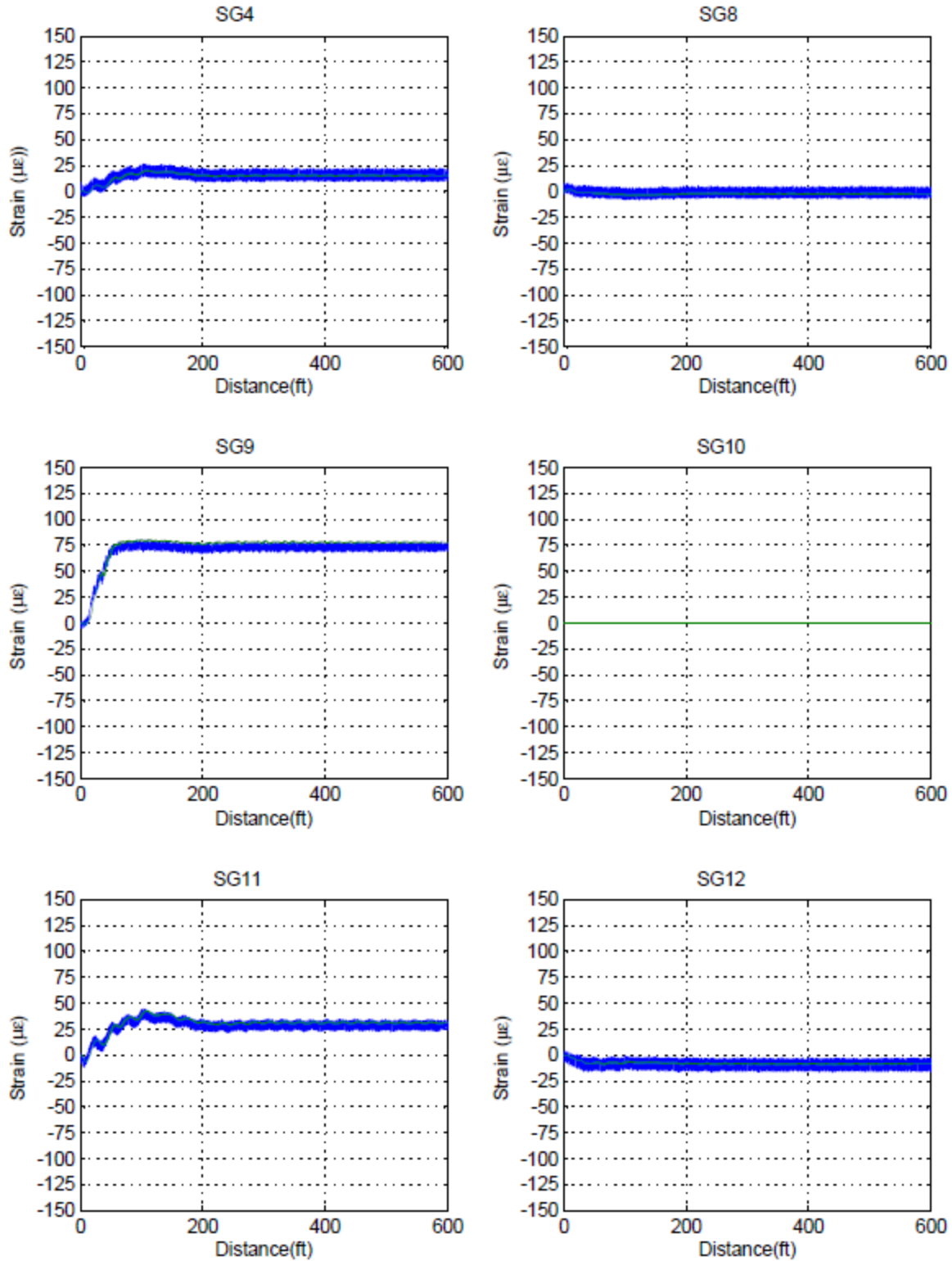


Figure G. 17: East Truck Load Placement 105-121 km/h (65-75 mph).

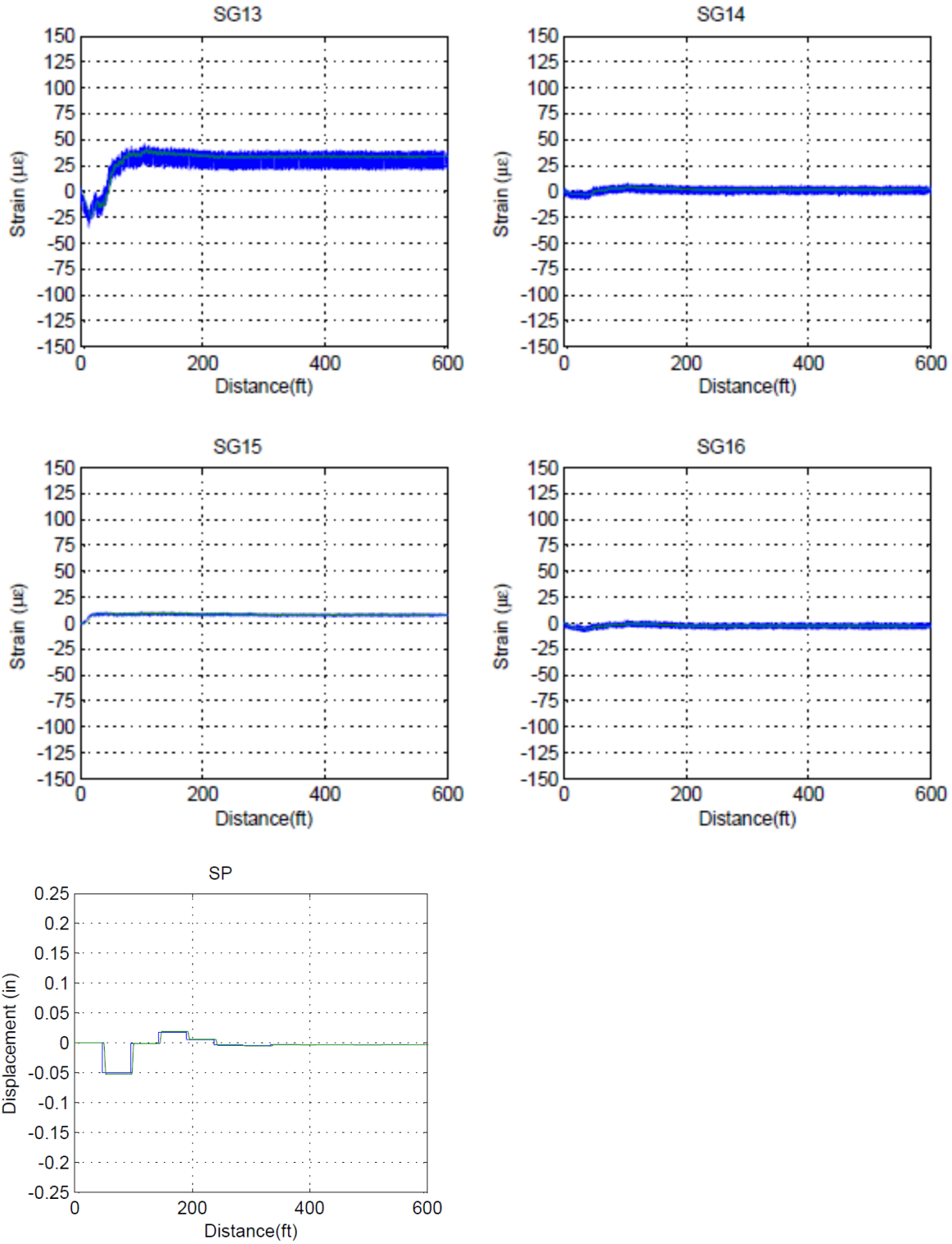


Figure G. 18: East Truck Load Placement 105-121 km/h (65-75 mph).

After Retrofit

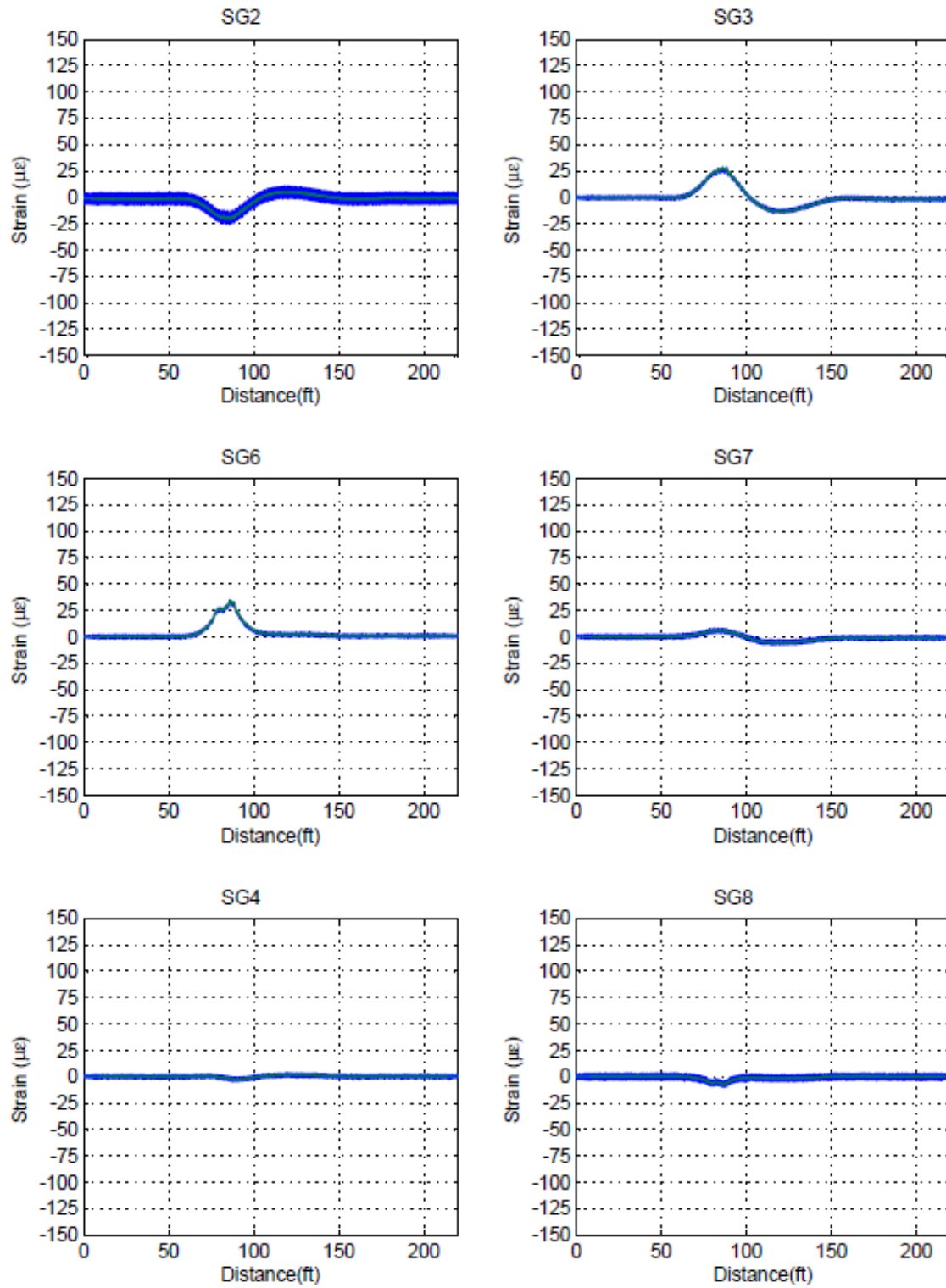


Figure G. 19: West Truck Load Placement 8-16 km/h (5-10 mph).

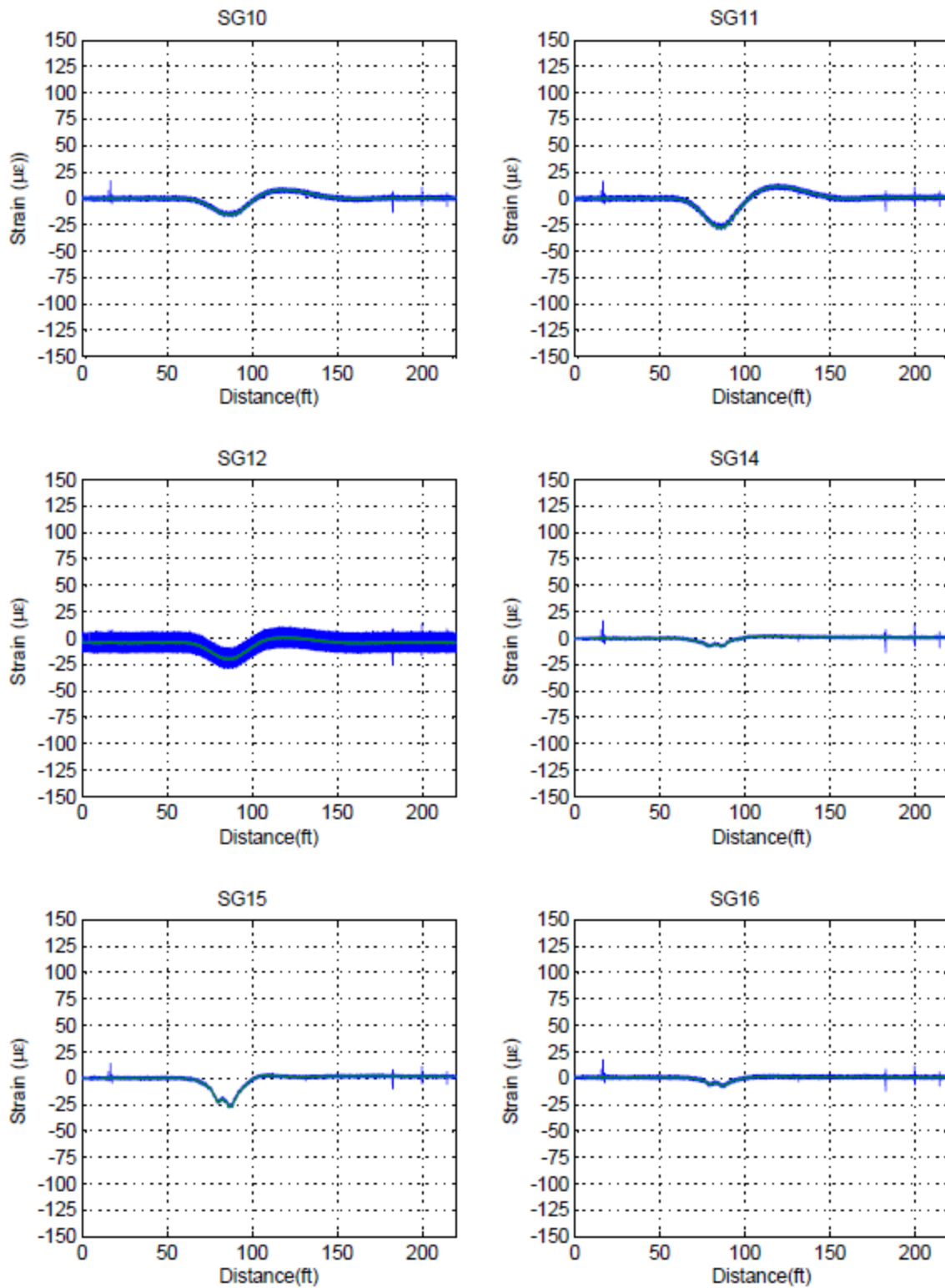


Figure G. 20: West Truck Load Placement 8-16 km/h (5-10 mph).

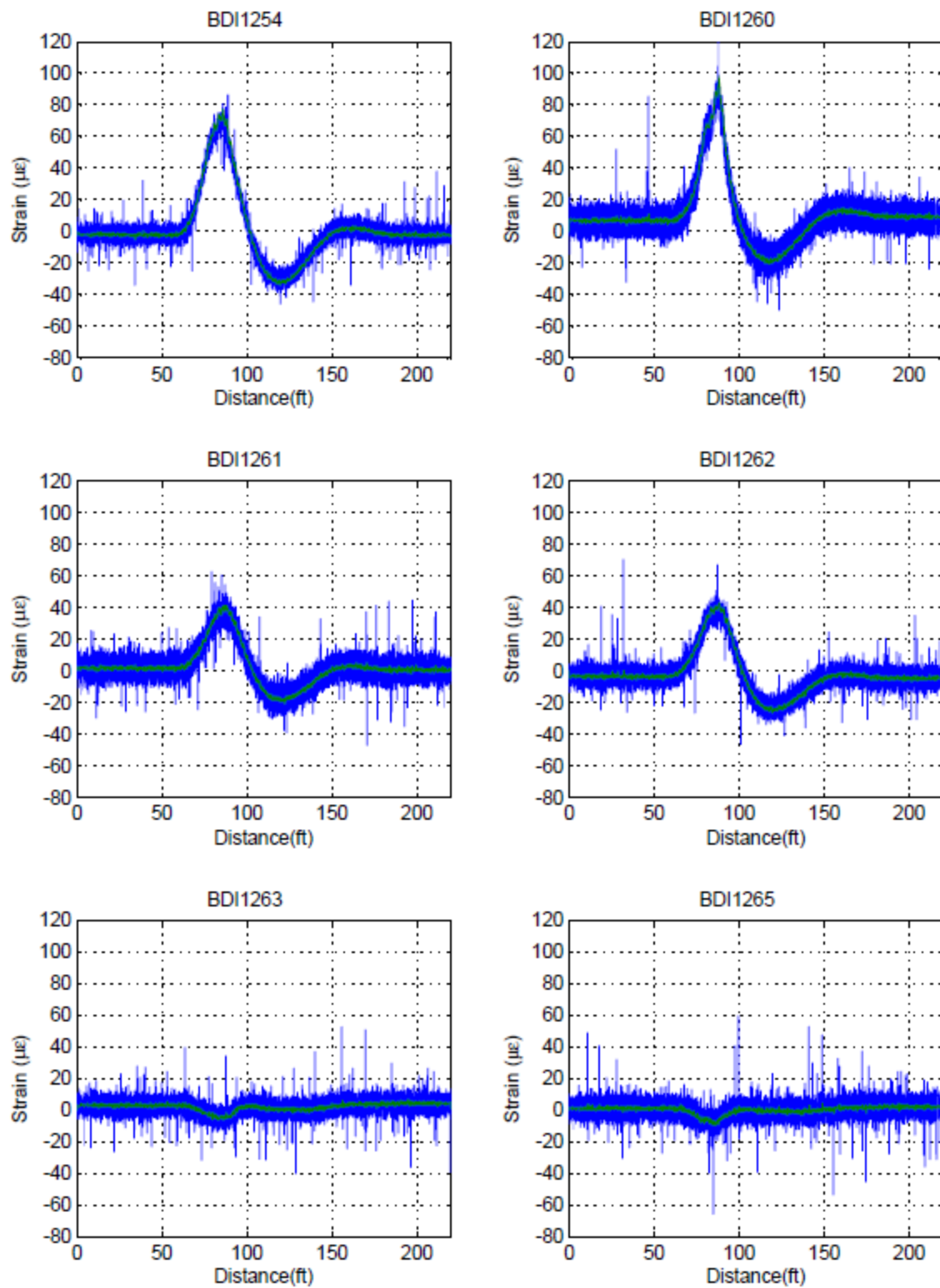


Figure G. 21: West Truck Load Placement 8-16 km/h (5-10 mph).

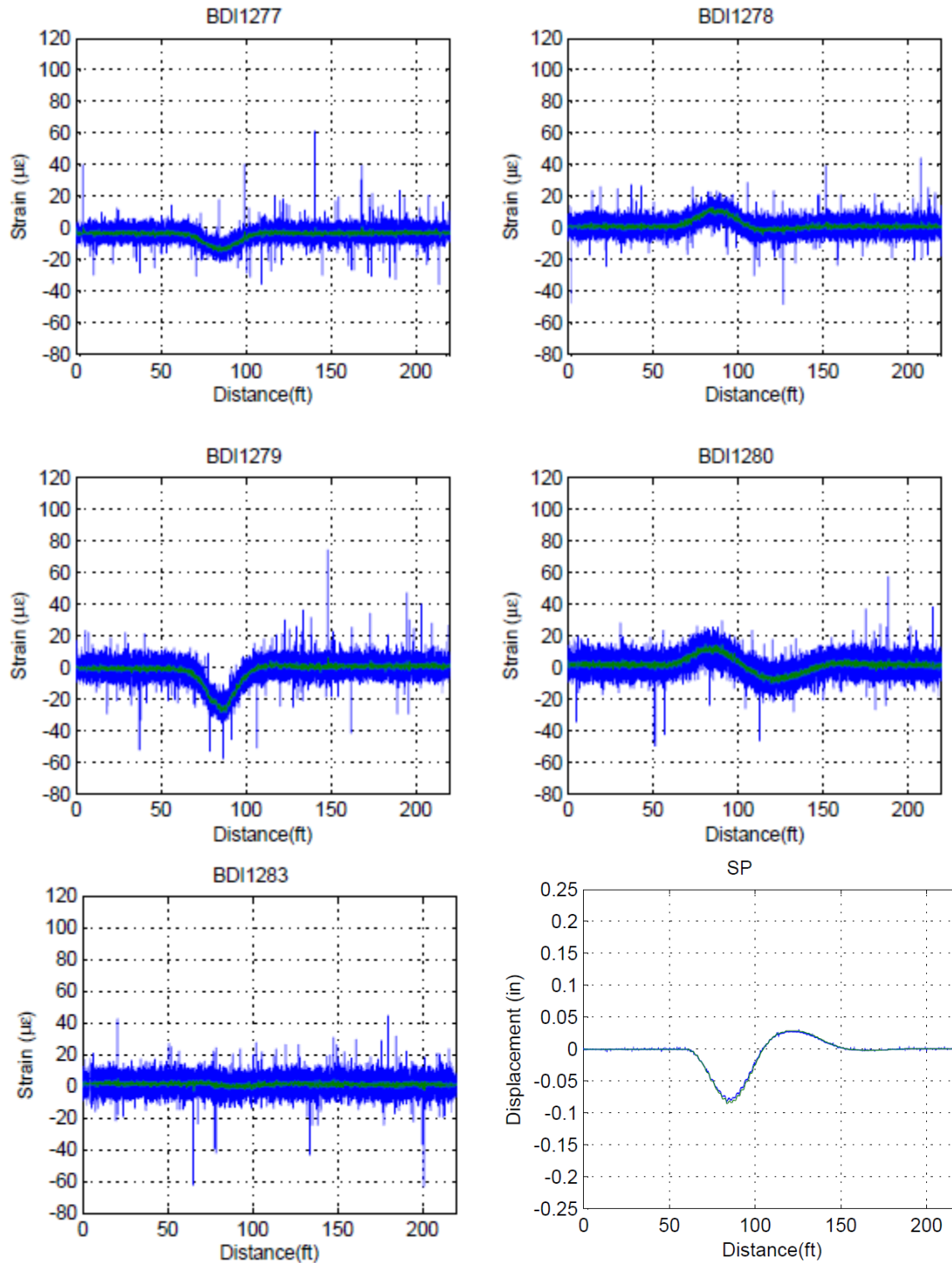


Figure G. 22: West Truck Load Placement 8-16 km/h (5-10 mph).

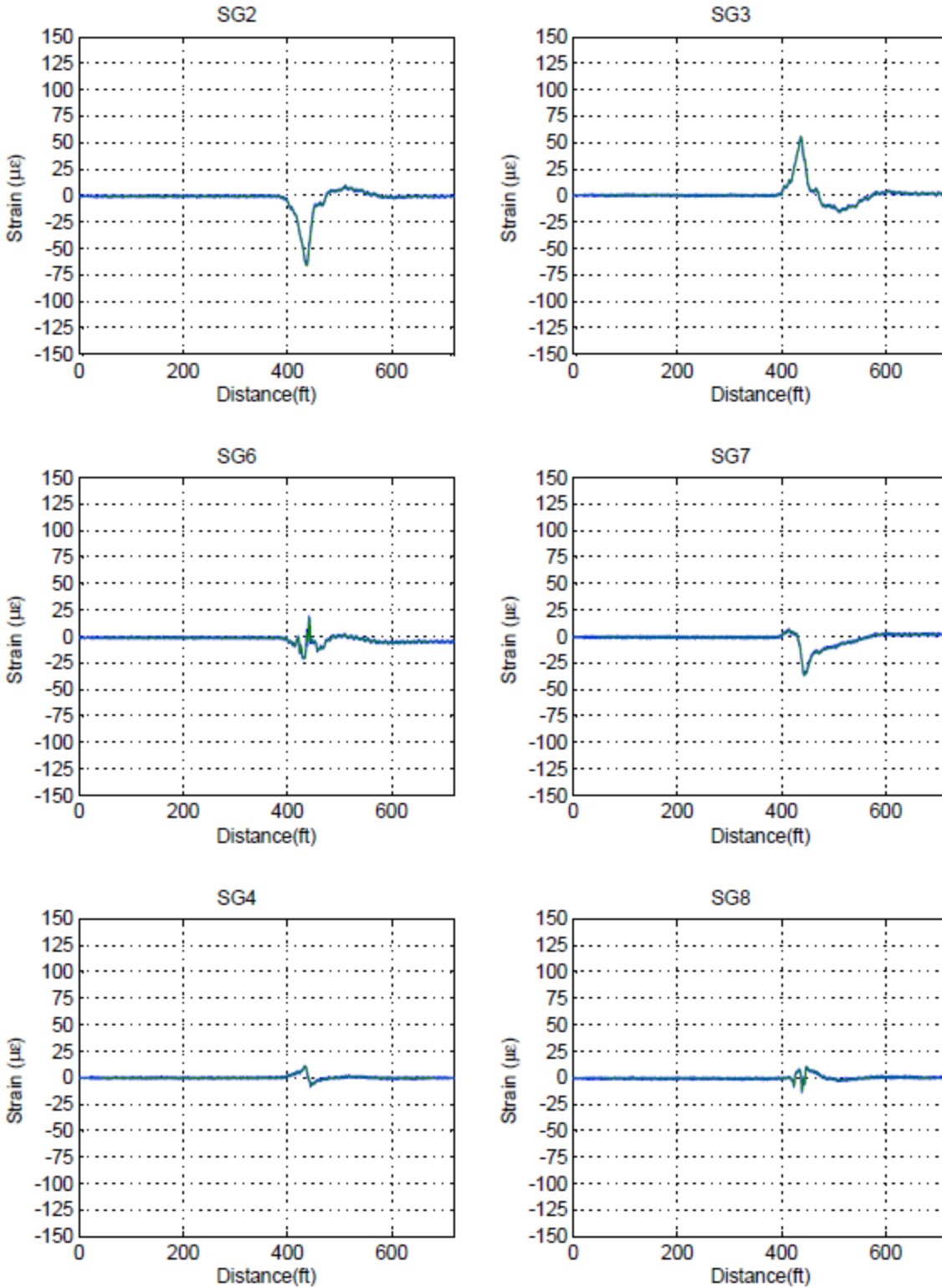


Figure G. 23: West Truck Load Placement 105-121 km/h (65-75 mph).

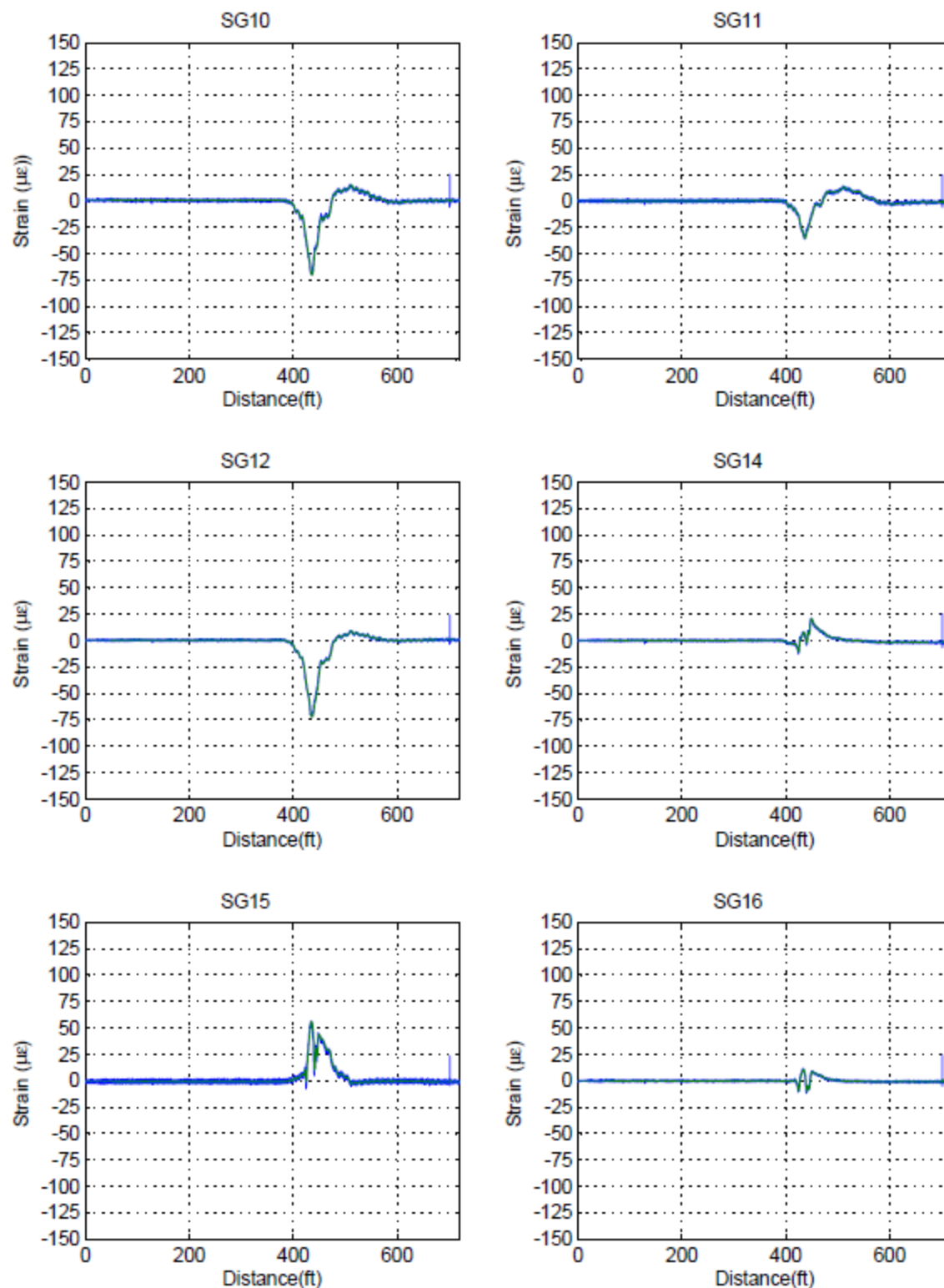


Figure G. 24: West Truck Load Placement 105-121 km/h (65-75 mph).

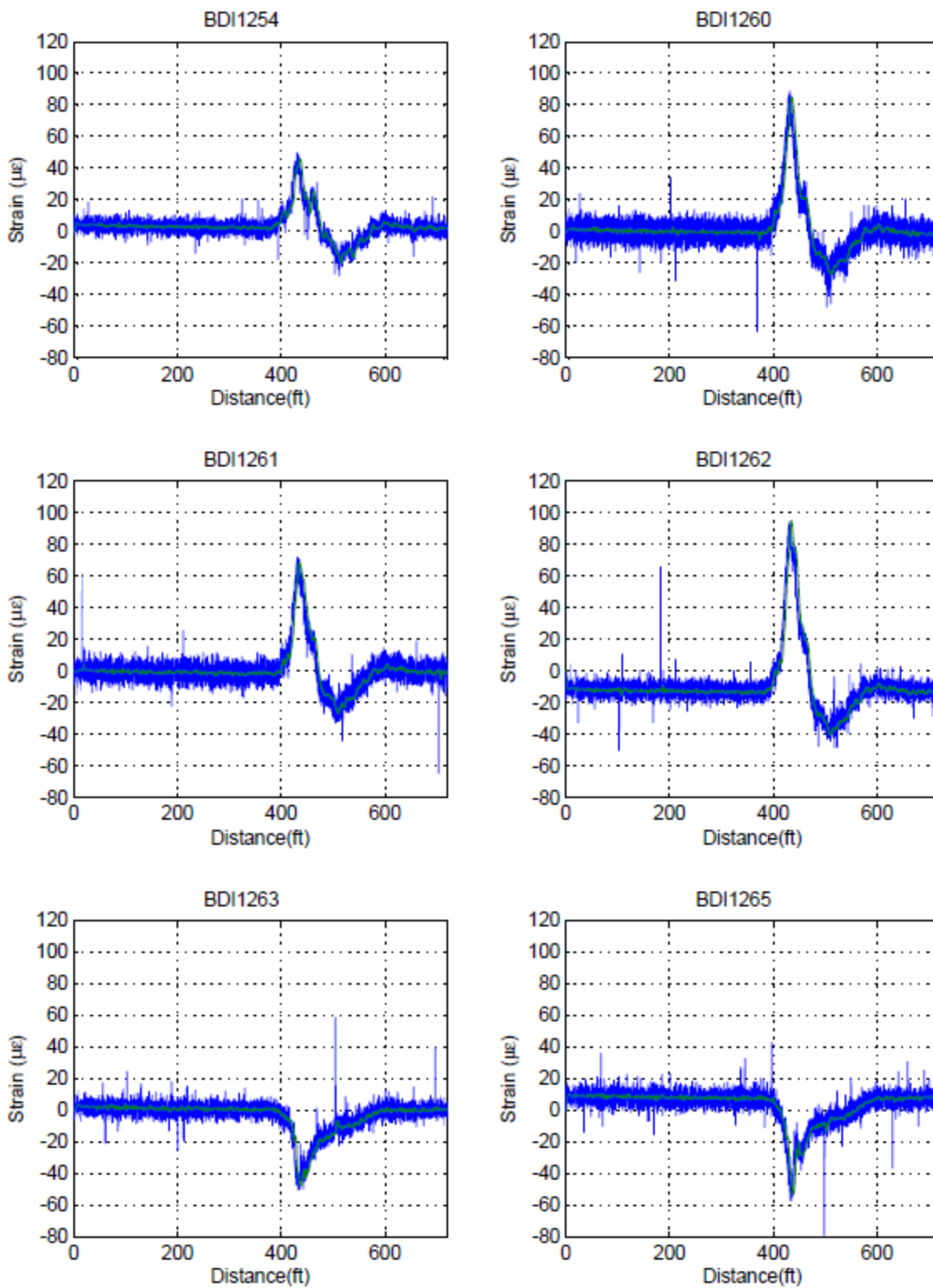


Figure G. 25: West Truck Load Placement 105-121 km/h (65-75 mph).

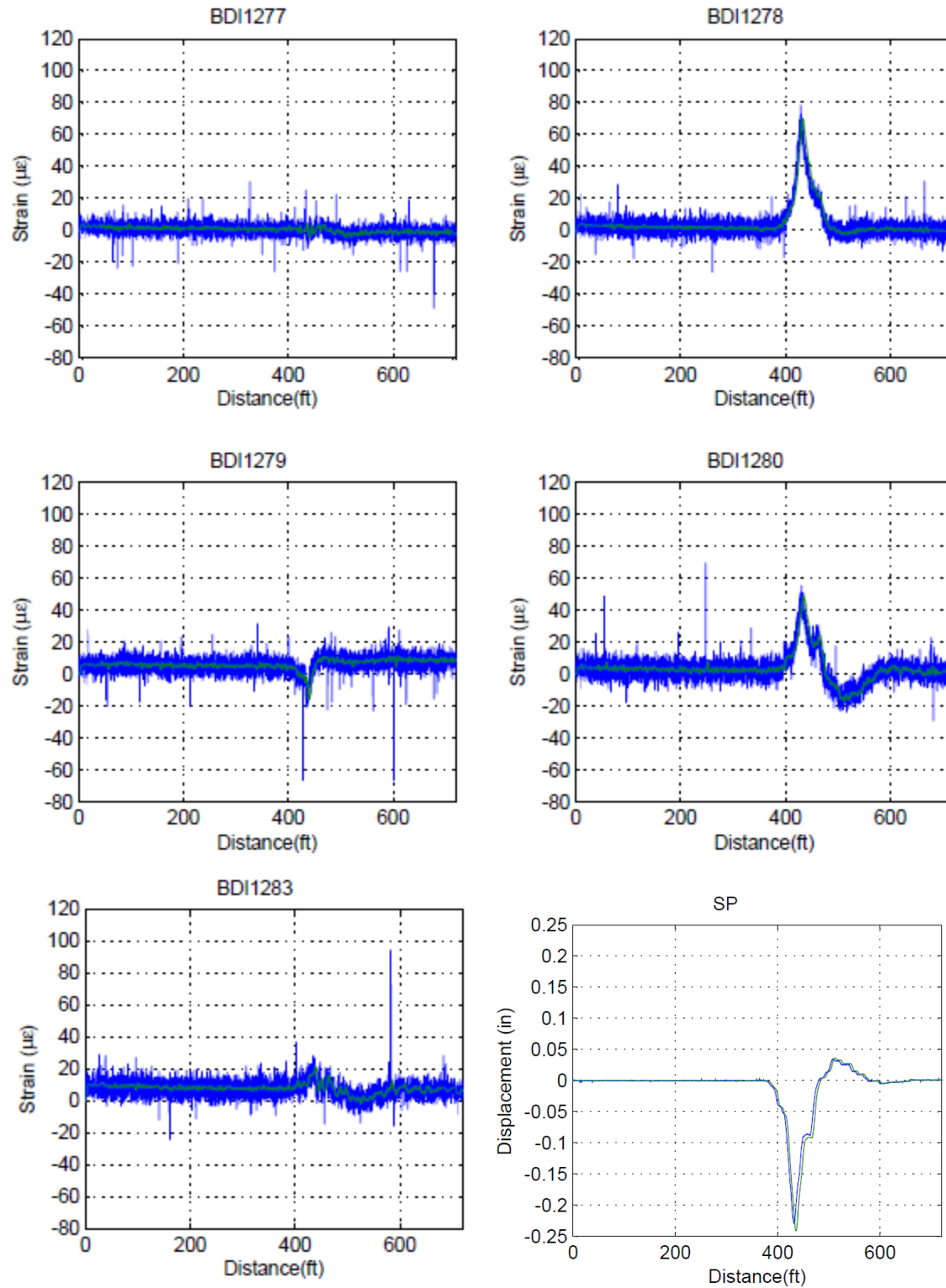


Figure G. 26: West Truck Load Placement 105-121 km/h (65-75 mph).

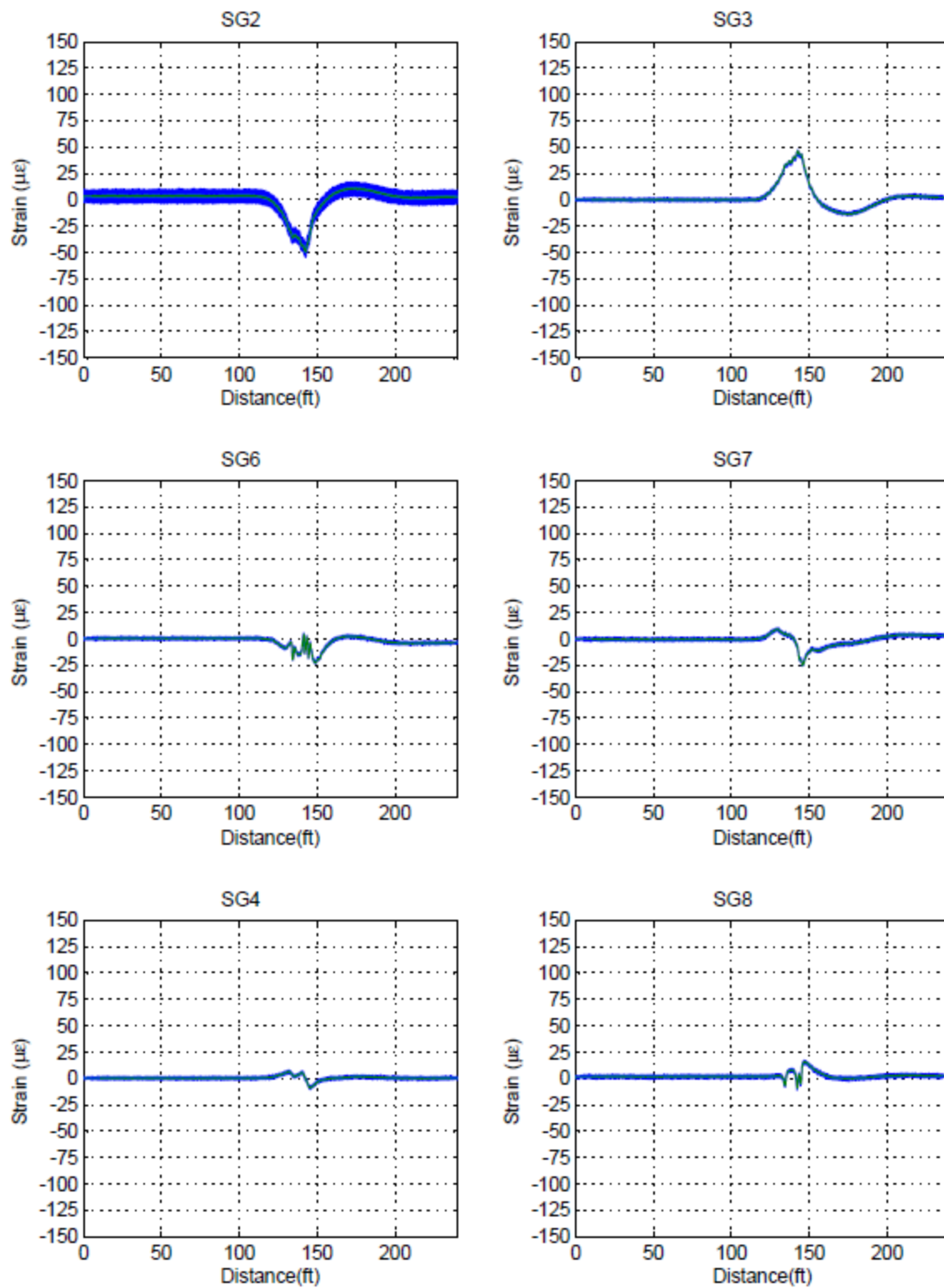


Figure G. 27: Center Truck Load Placement 8-16 km/h (5-10 mph).

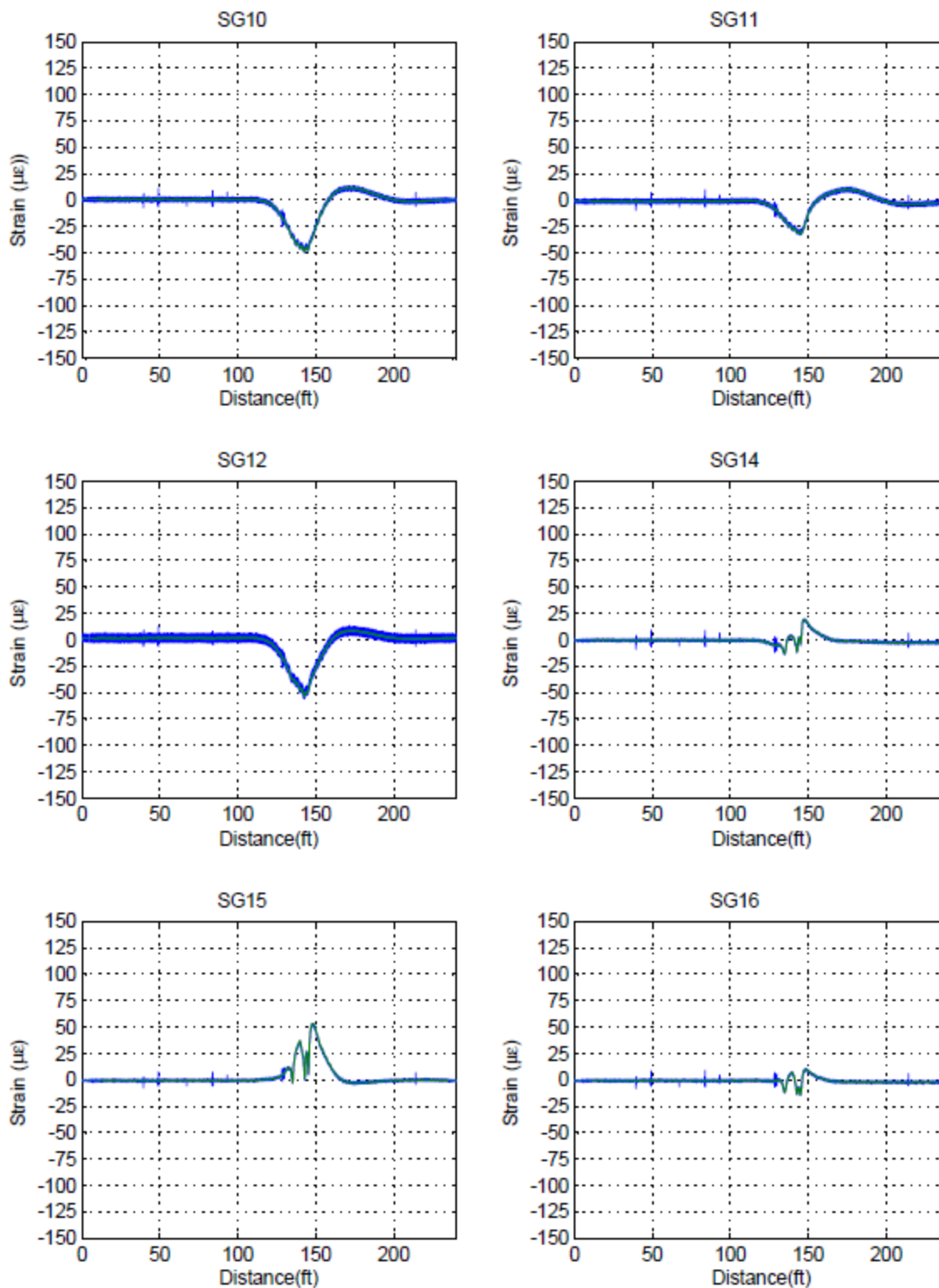


Figure G. 28: Center Truck Load Placement 8-16 km/h (5-10 mph).

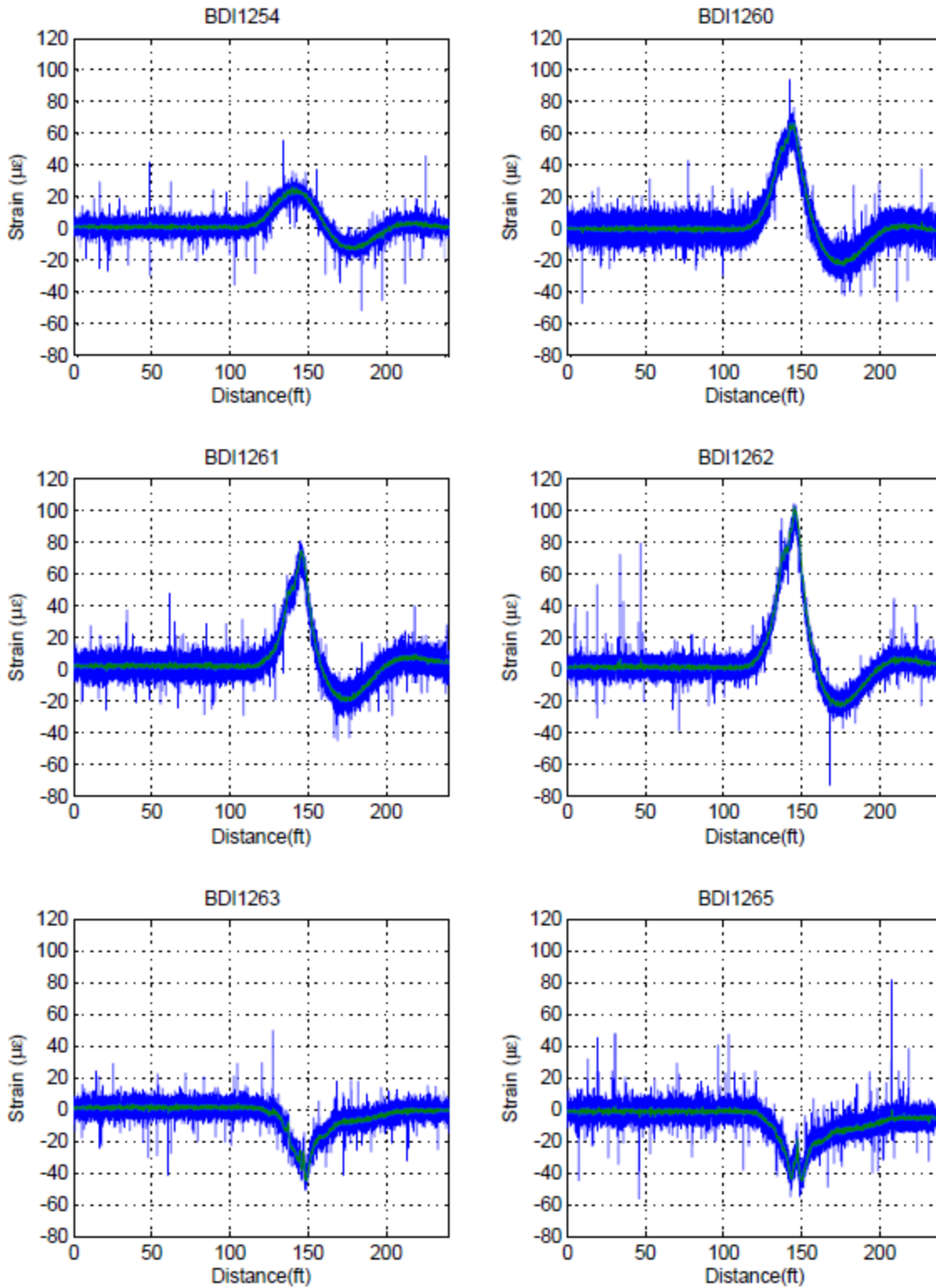


Figure G. 29: Center Truck Load Placement 8-16 km/h (5-10 mph).

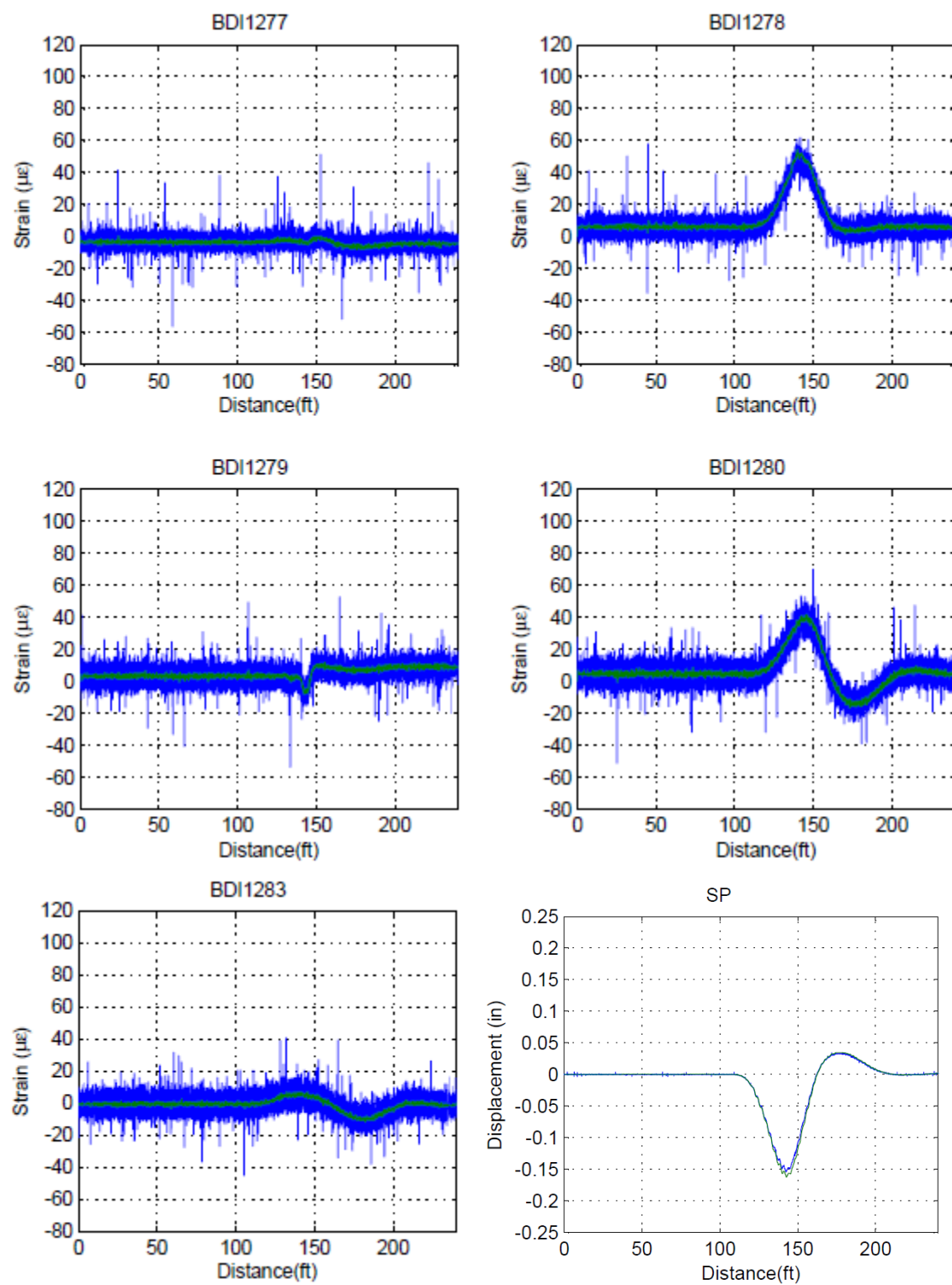


Figure G. 30: Center Truck Load Placement 8-16 km/h (5-10 mph).

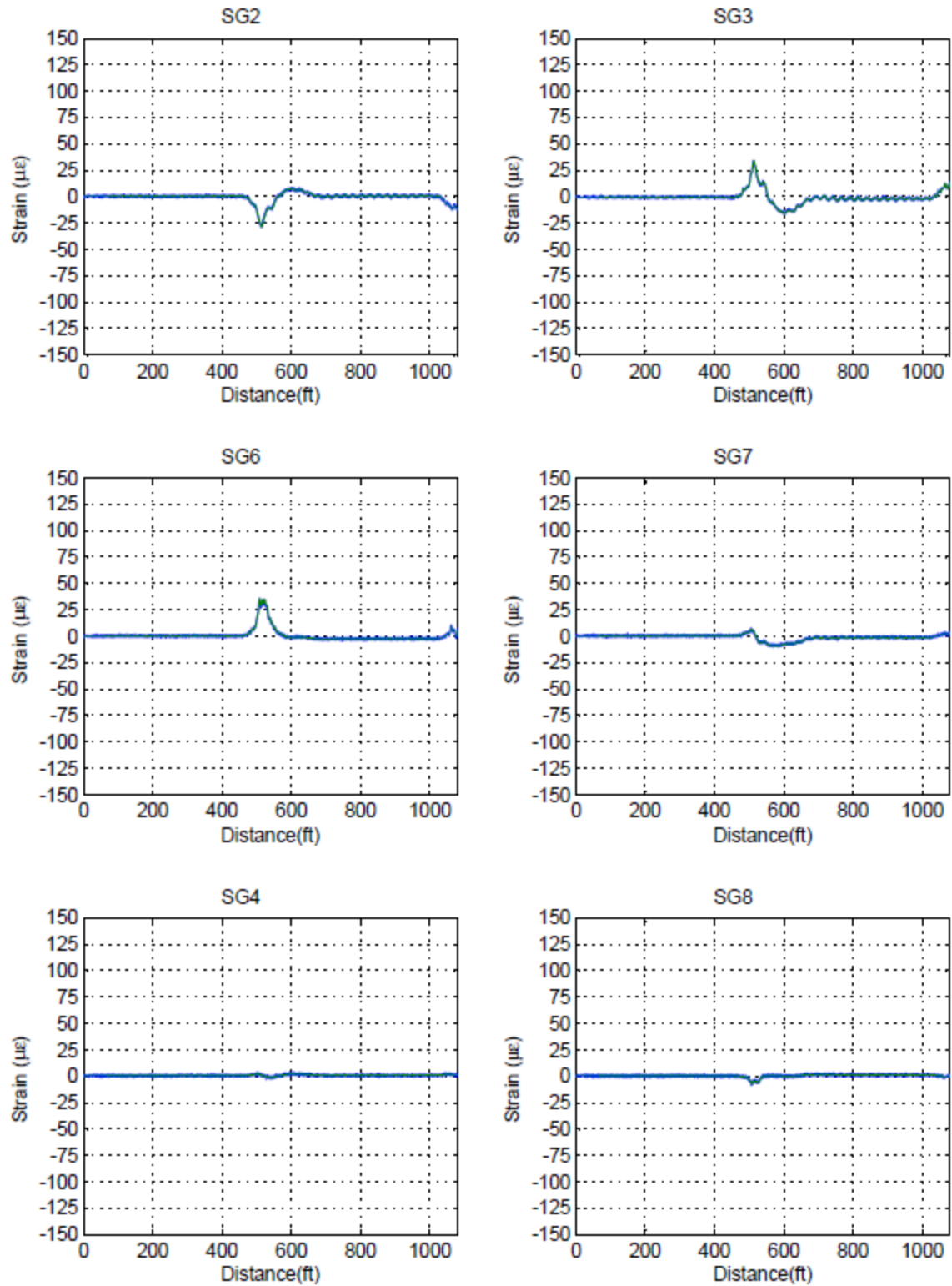


Figure G. 31: Center Truck Load Placement 105-121 km/h (65-75 mph).

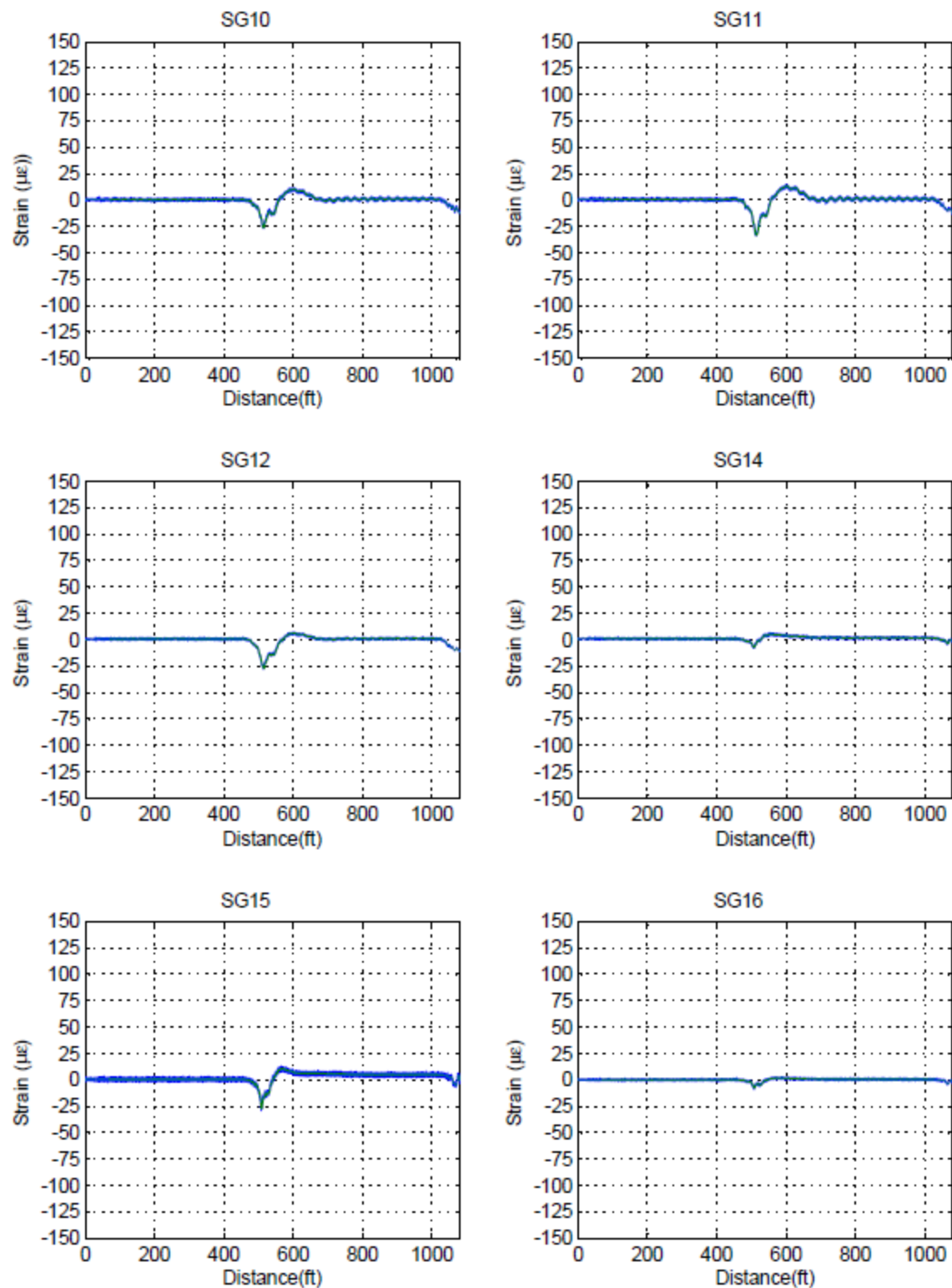


Figure G. 32: Center Truck Load Placement 105-121 km/h (65-75 mph).

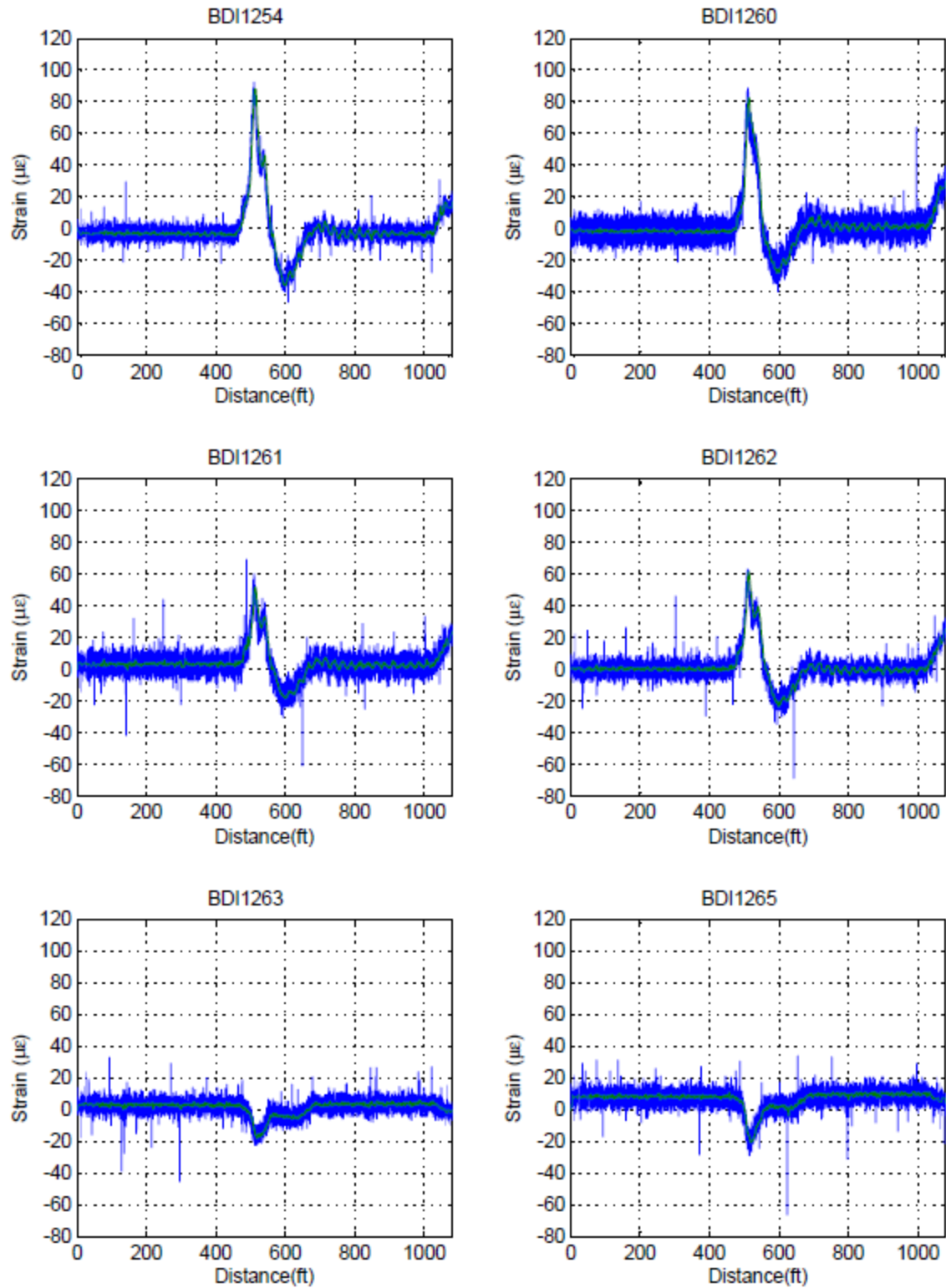


Figure G. 33: Center Truck Load Placement 105-121 km/h (65-75 mph).

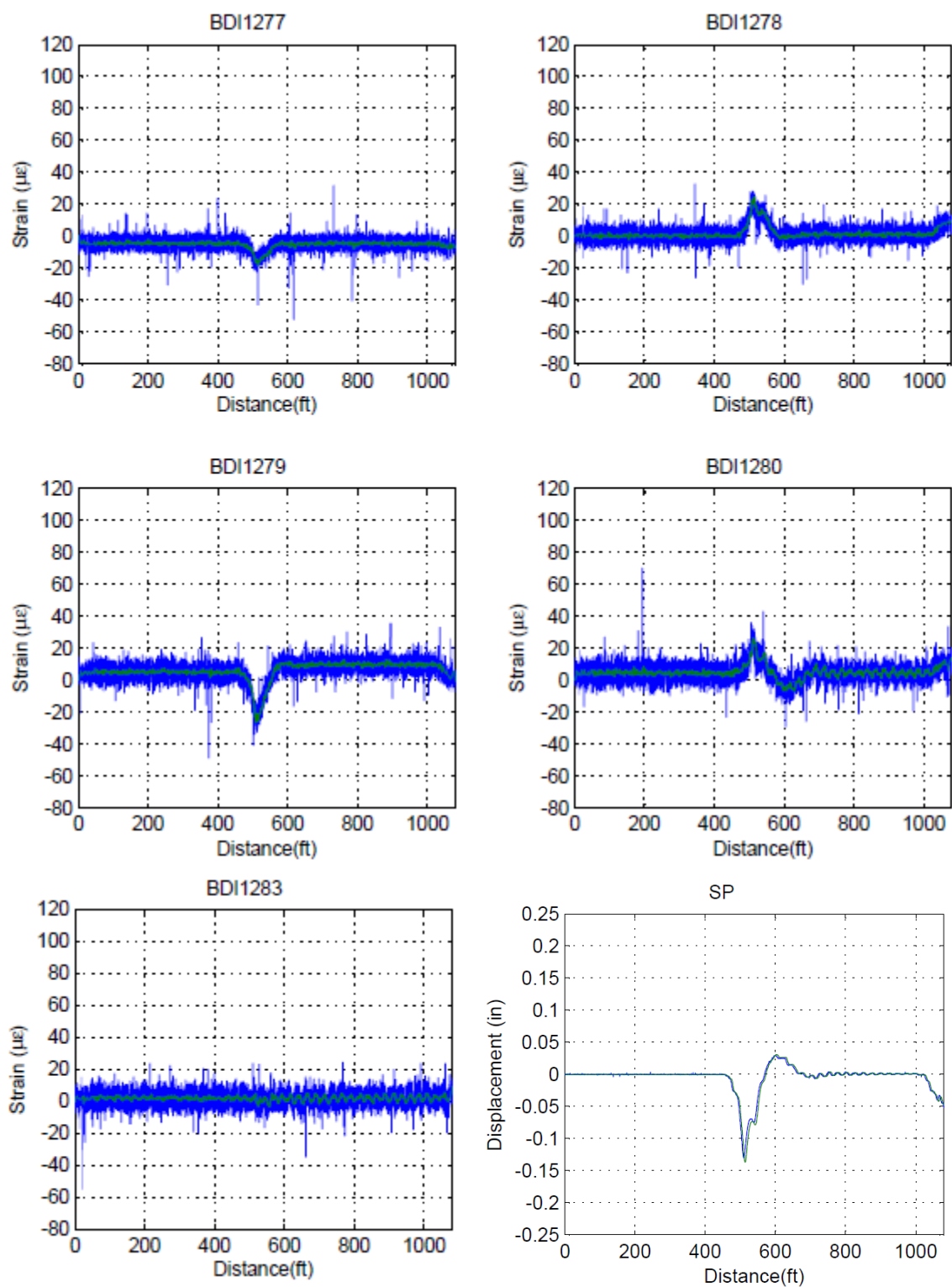


Figure G. 34: Center Truck Load Placement 105-121 km/h (65-75 mph).

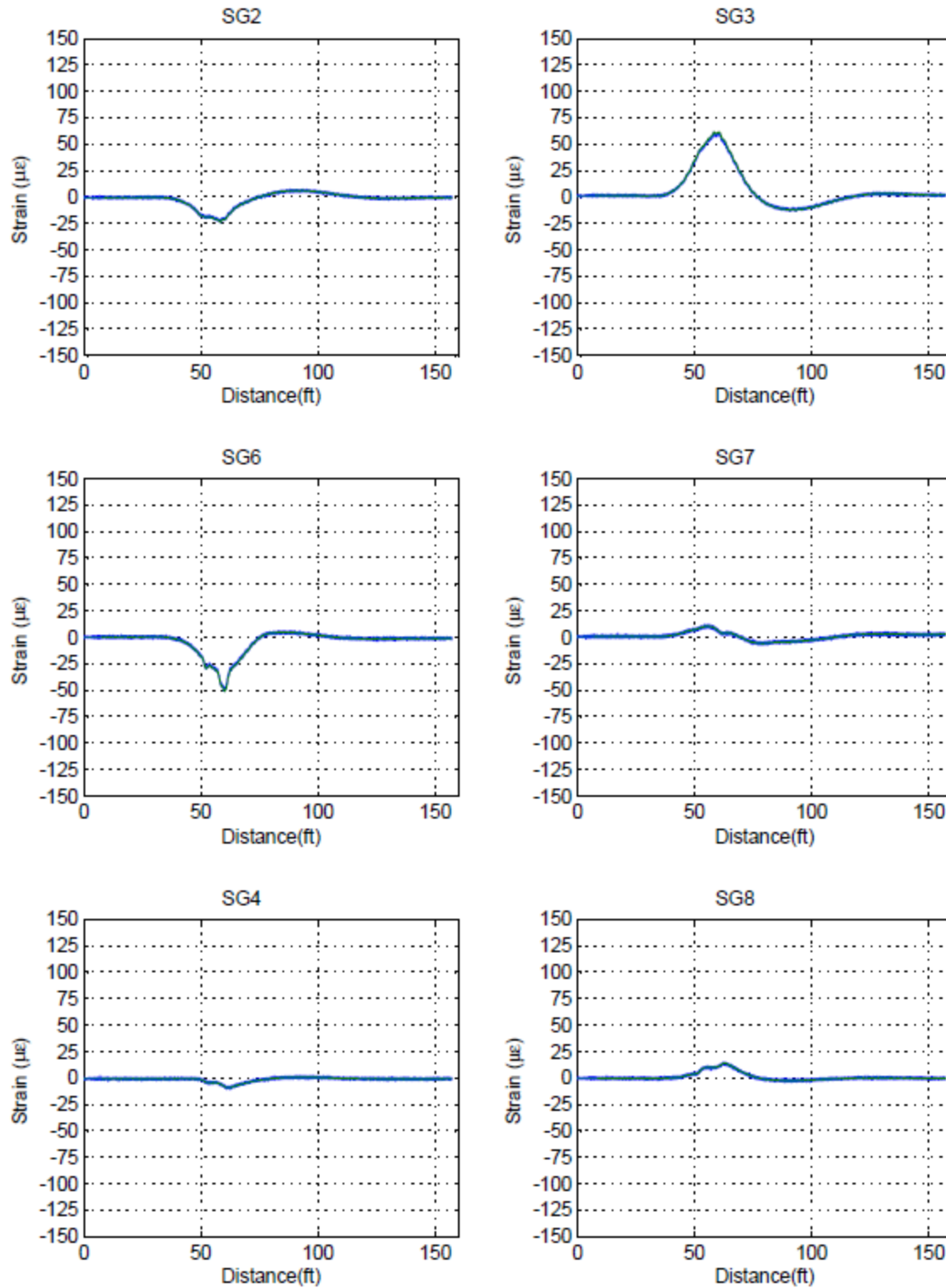


Figure G. 35: East Truck Load Placement 8-16 km/h (5-10 mph).

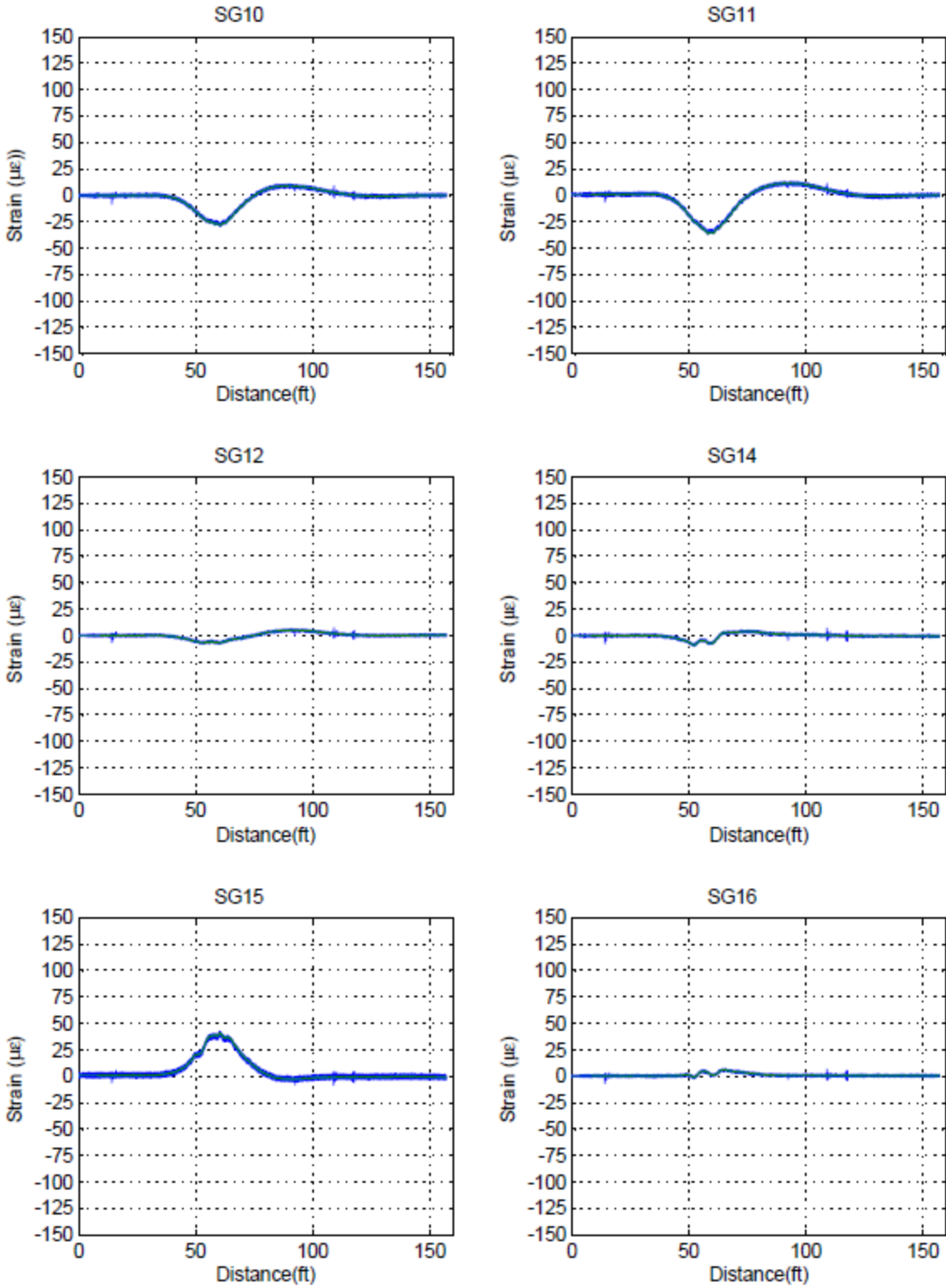


Figure G. 36: East Truck Load Placement 8-16 km/h (5-10 mph).

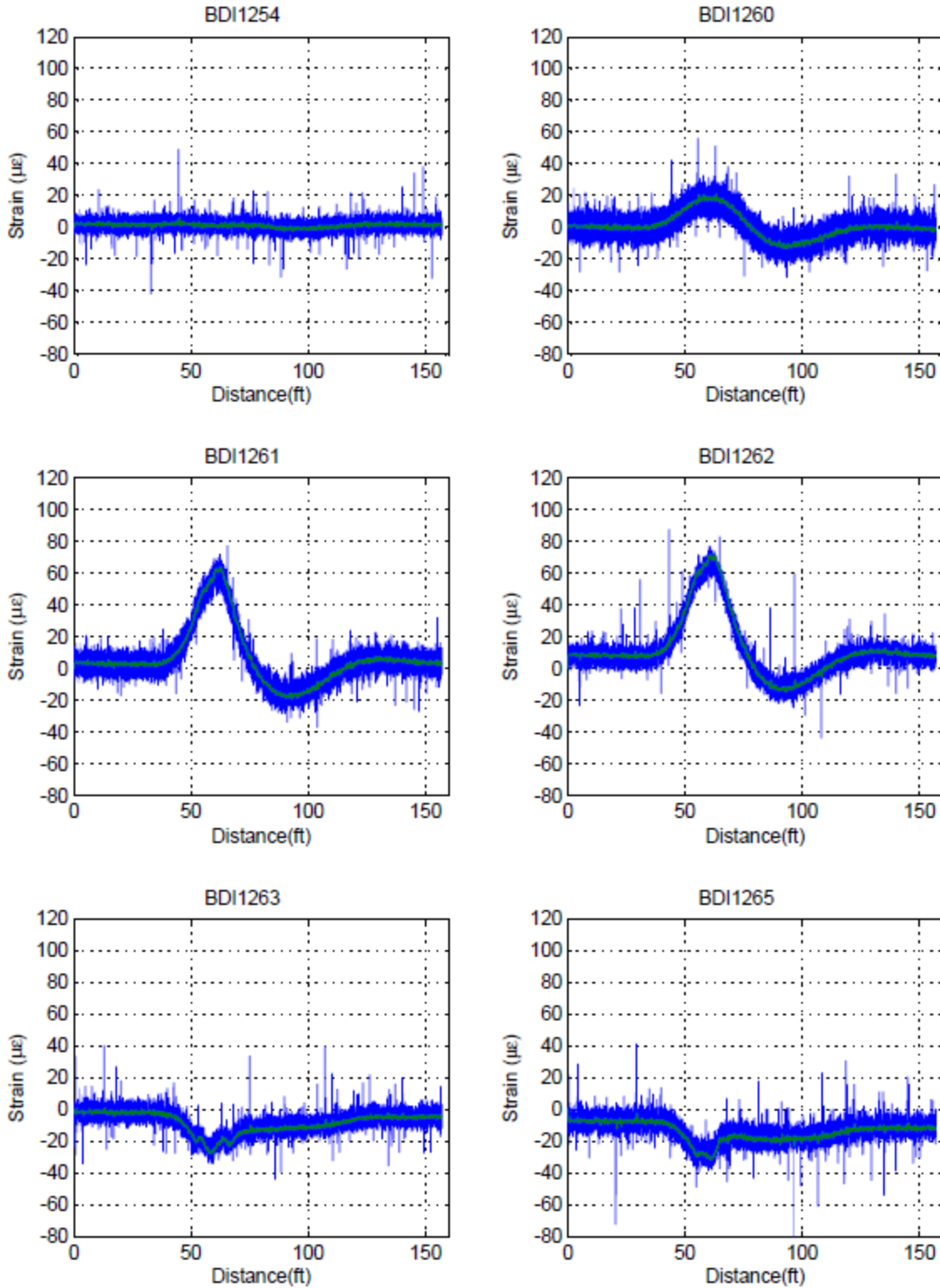


Figure G. 37: East Truck Load Placement 8-16 km/h (5-10 mph).

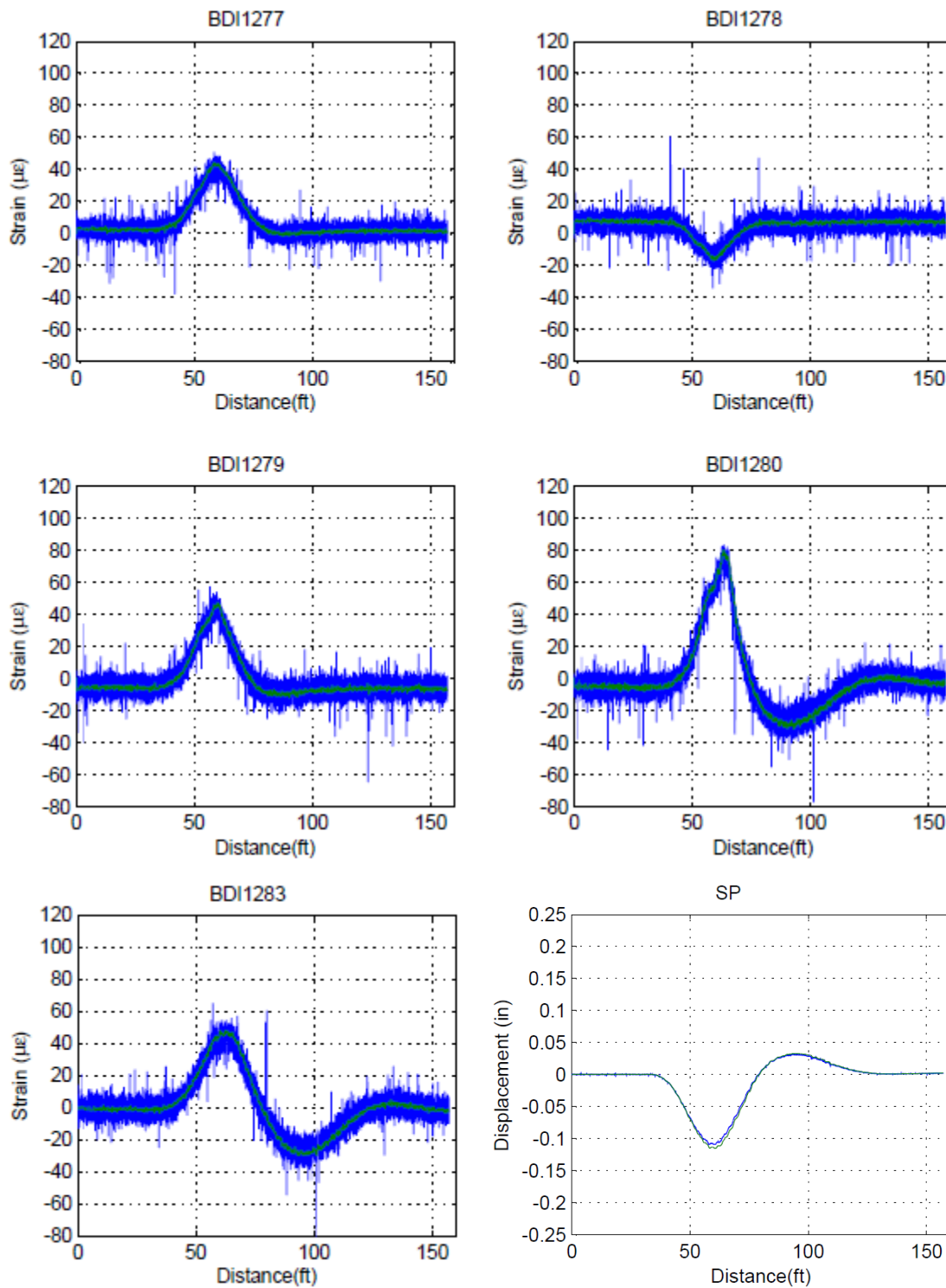


Figure G. 38: East Truck Load Placement 8-16 km/h (5-10 mph).

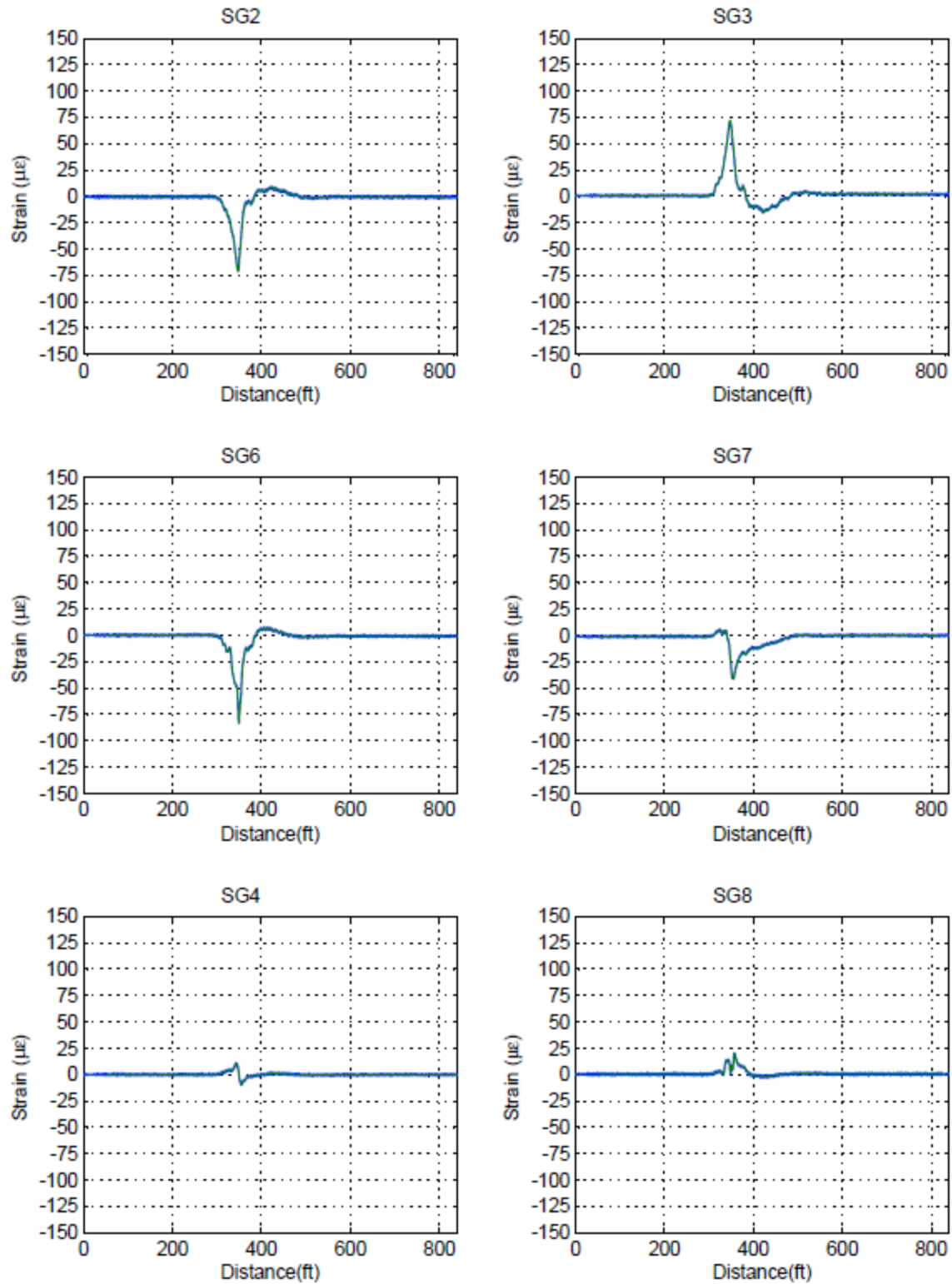


Figure G. 39: East Truck Load Placement 105-121 km/h (65-75 mph).

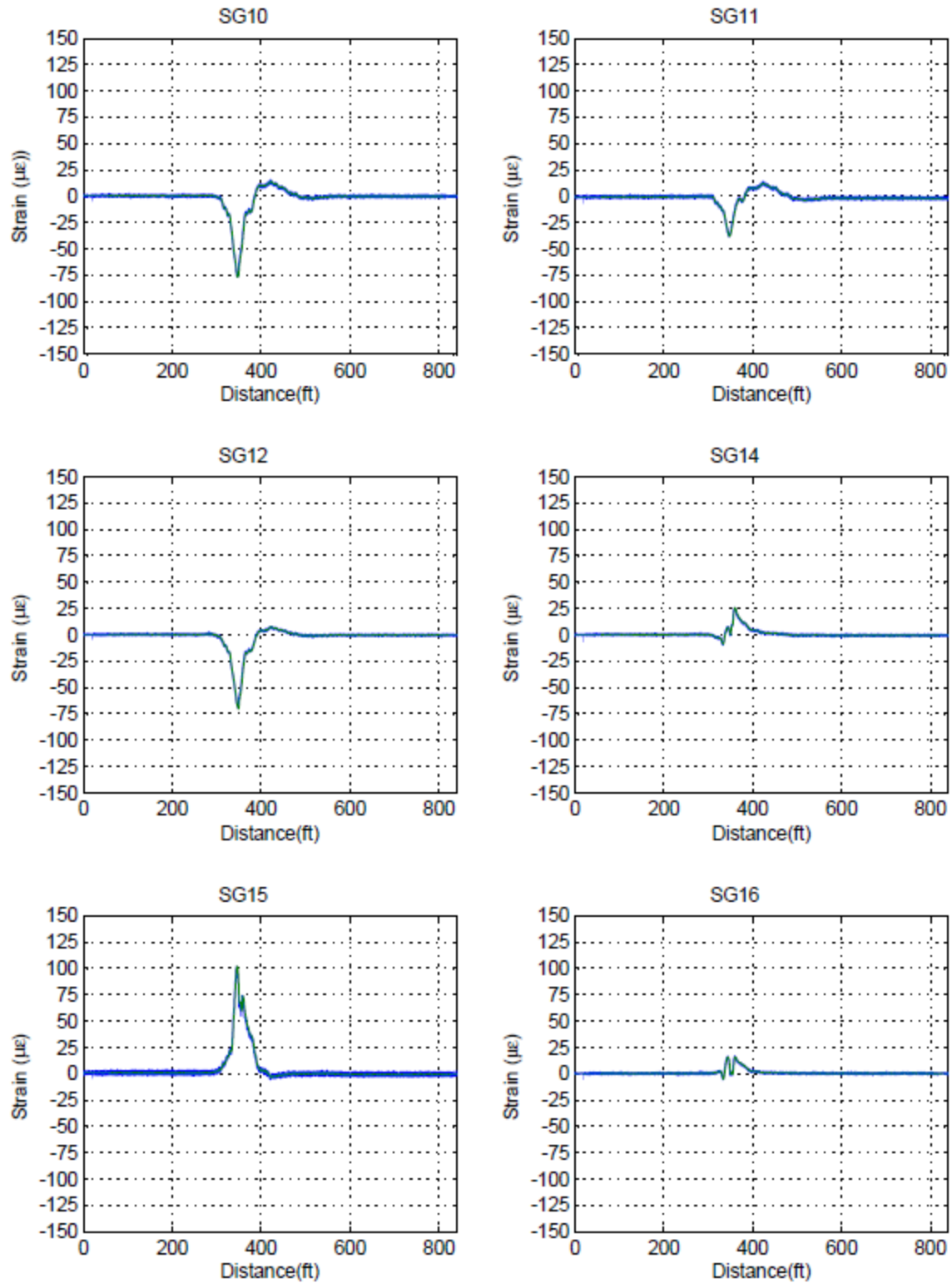


Figure G. 40: East Truck Load Placement 105-121 km/h (65-75 mph).

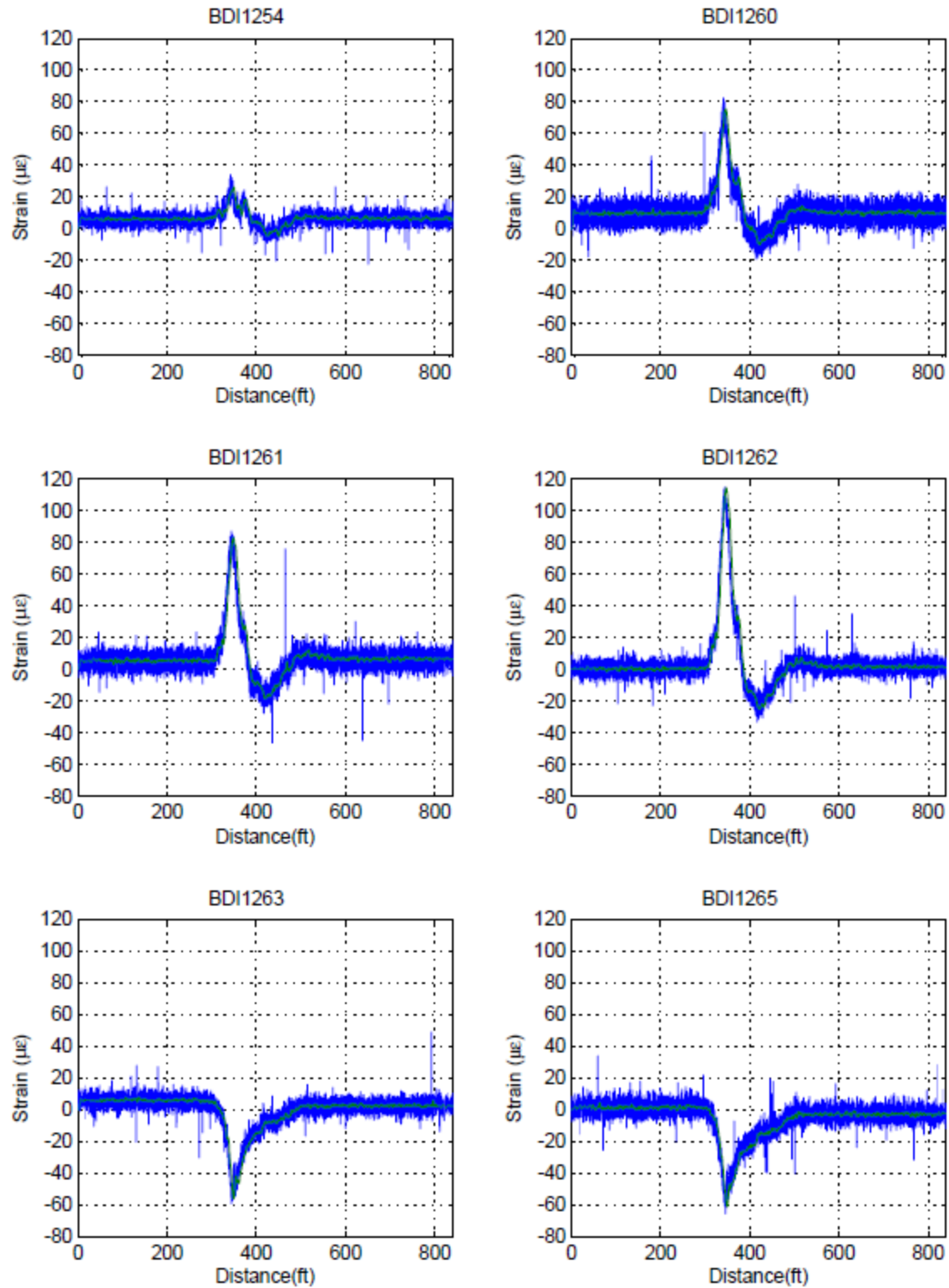


Figure G. 41: East Truck Load Placement 105-121 km/h (65-75 mph).

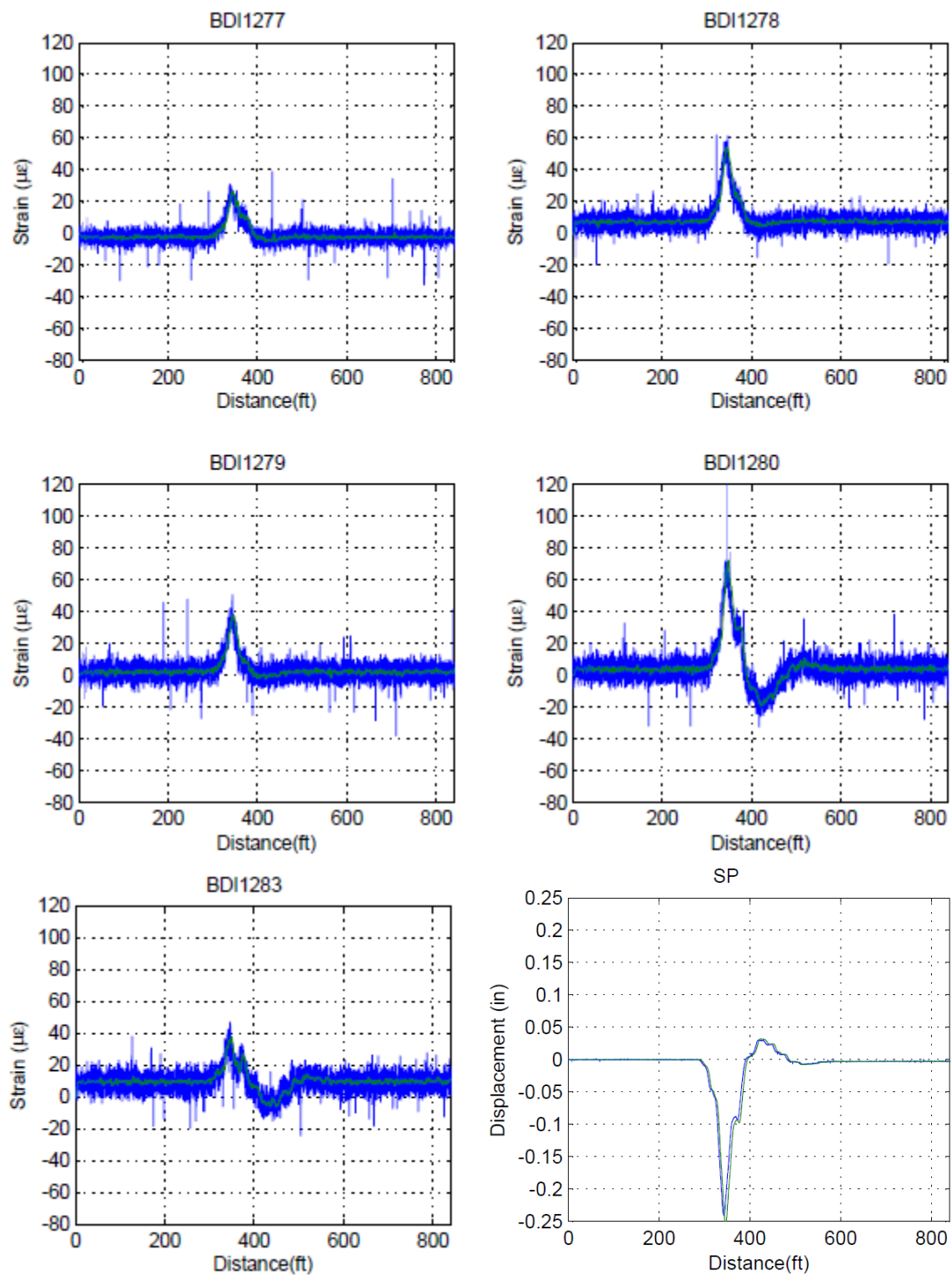


Figure G. 42: East Truck Load Placement 105-121 km/h (65-75 mph).

Appendix H: Field Test and Finite Element Analyses Results

Field Test and Complementary Finite Element Analyses

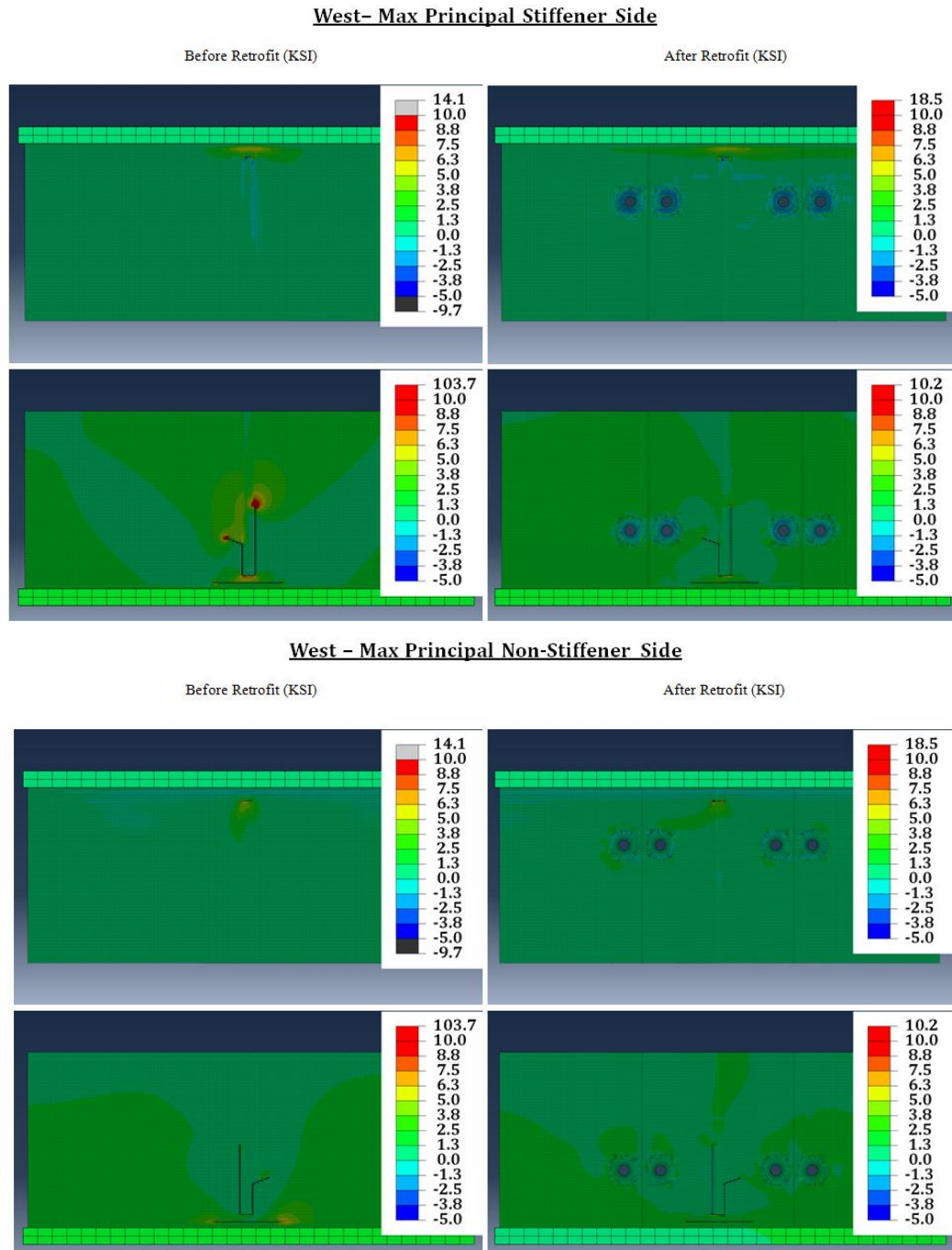
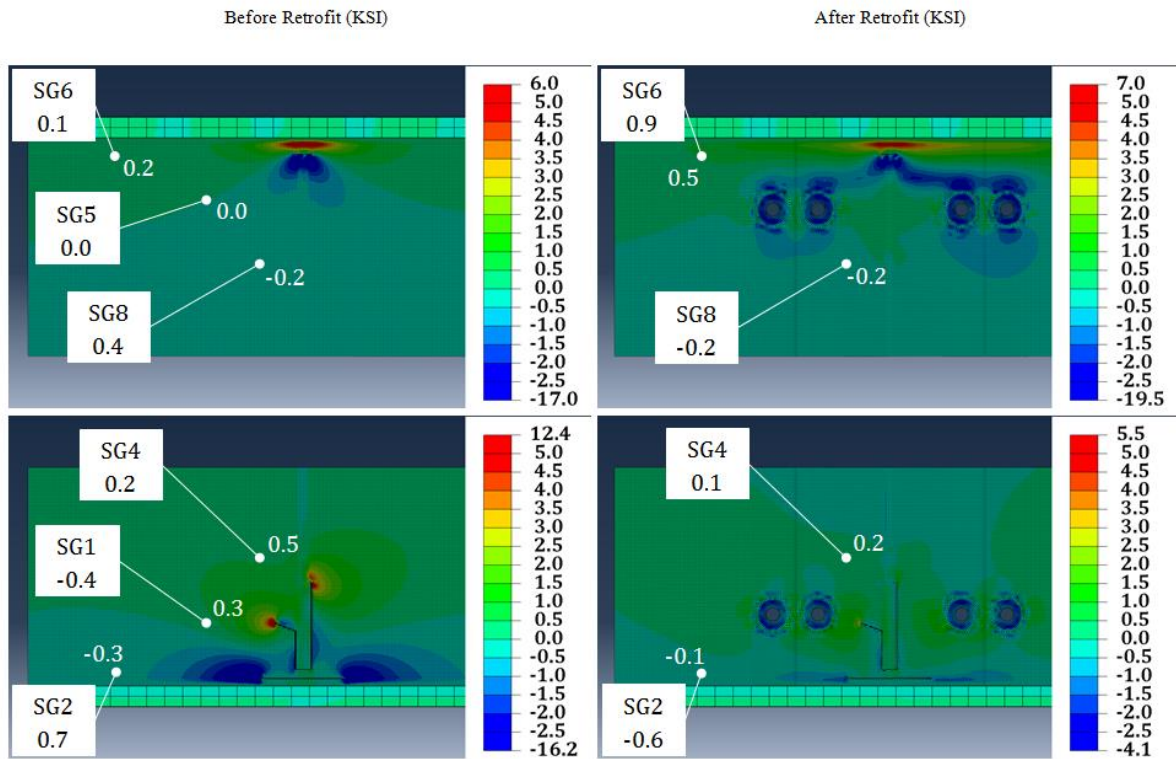


Figure H. 1: West Truck Load Placement Maximum Principal Web Gap Stresses Before and After Retrofit.

West – S22 Stiffener Side



West – S22 Non-Stiffener Side

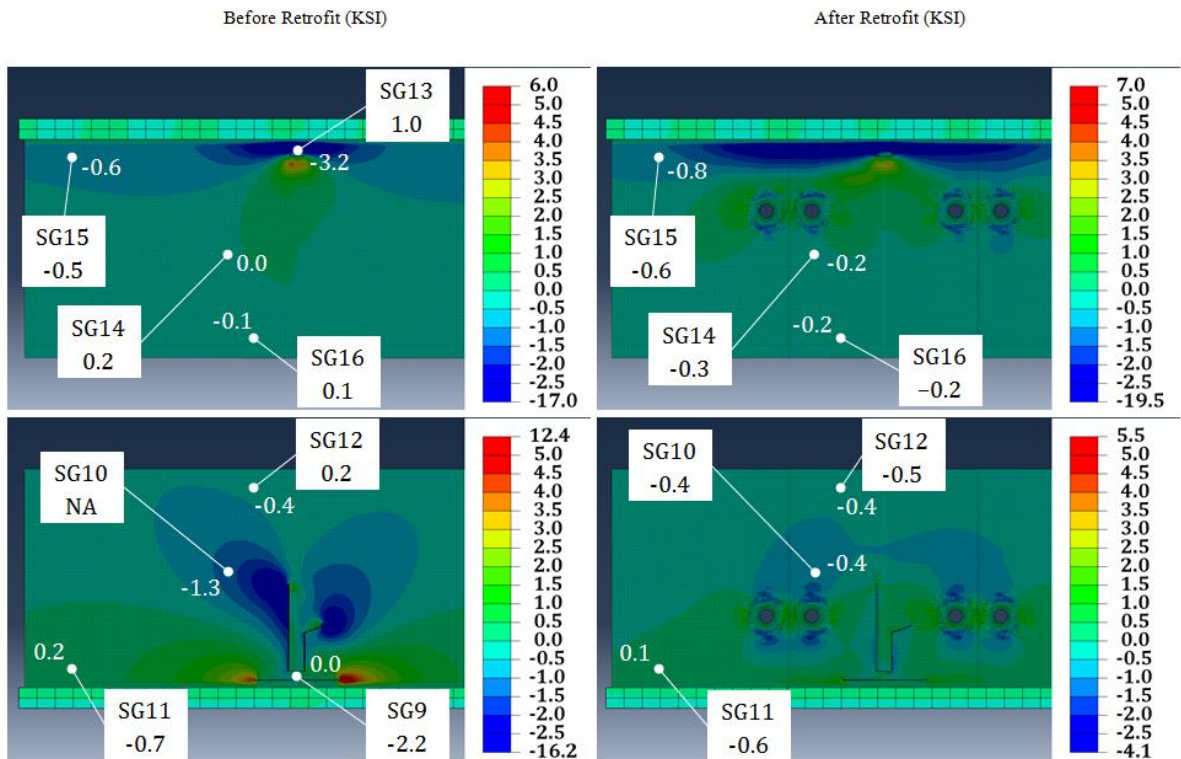
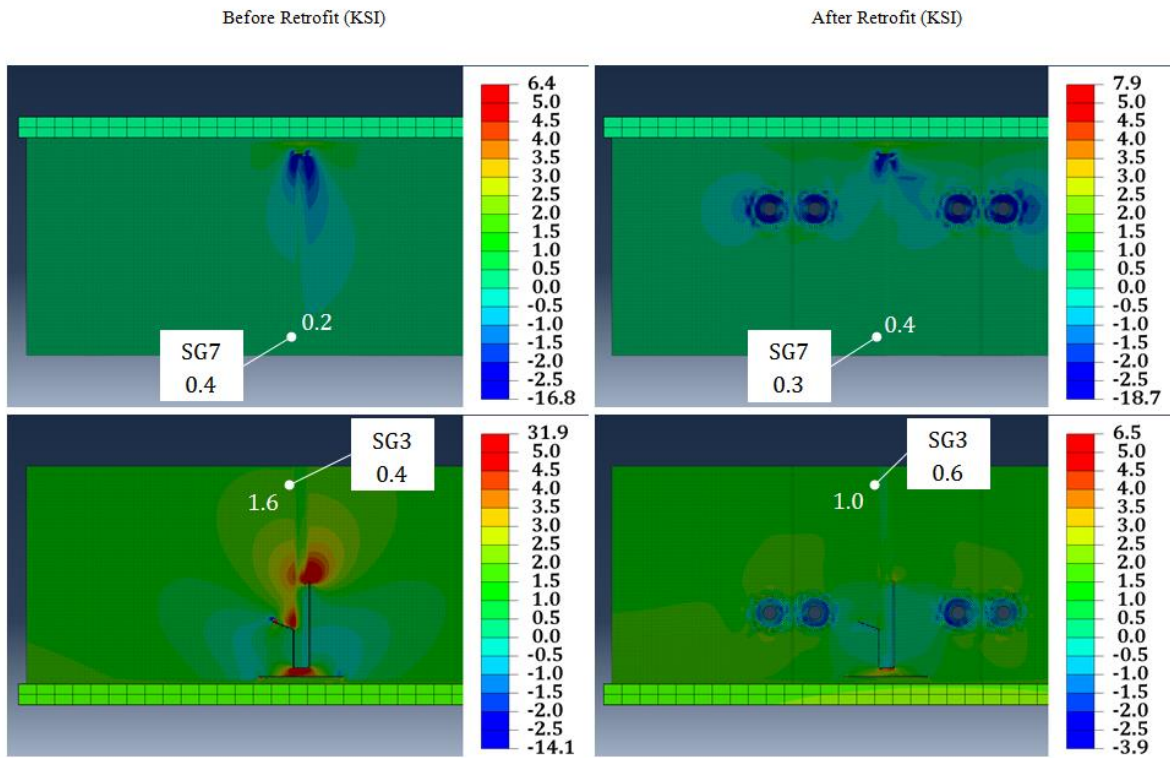
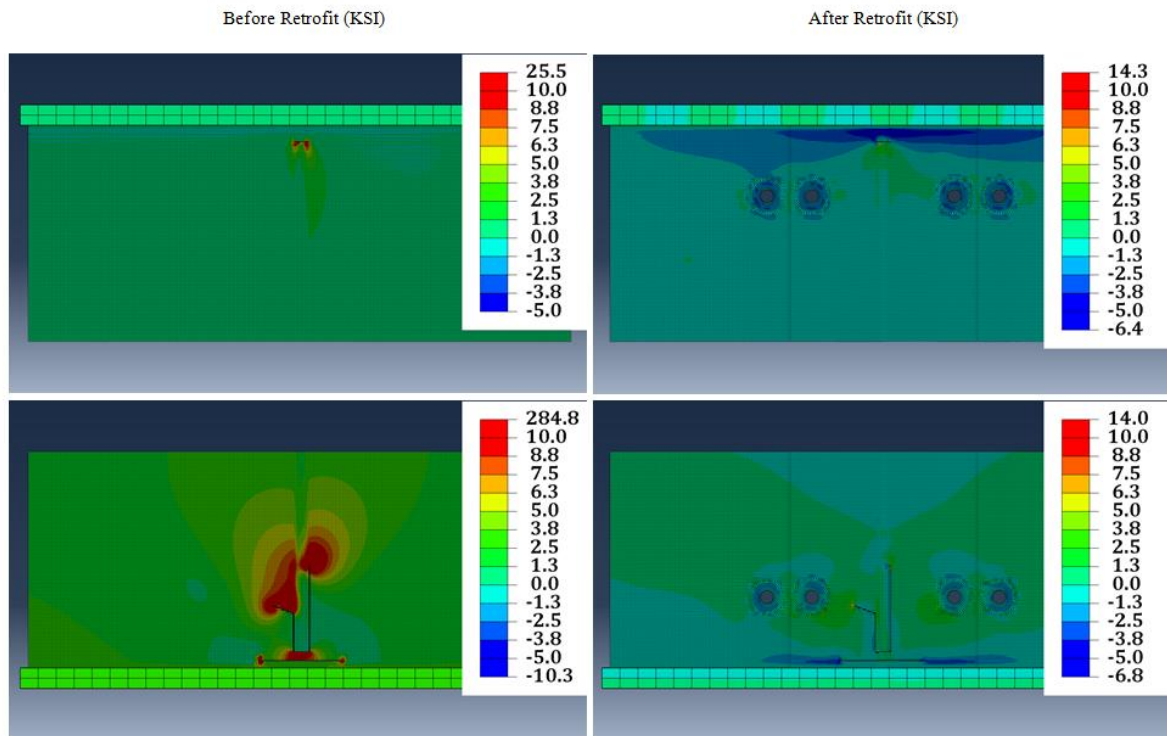


Figure H. 2: West Truck Load Placement Directional Web Gap Stresses Before and After Retrofit.

West – S11 Stiffener Side



Center – Max Principal Stiffener Side



Center – Max Principal Non-Stiffener Side

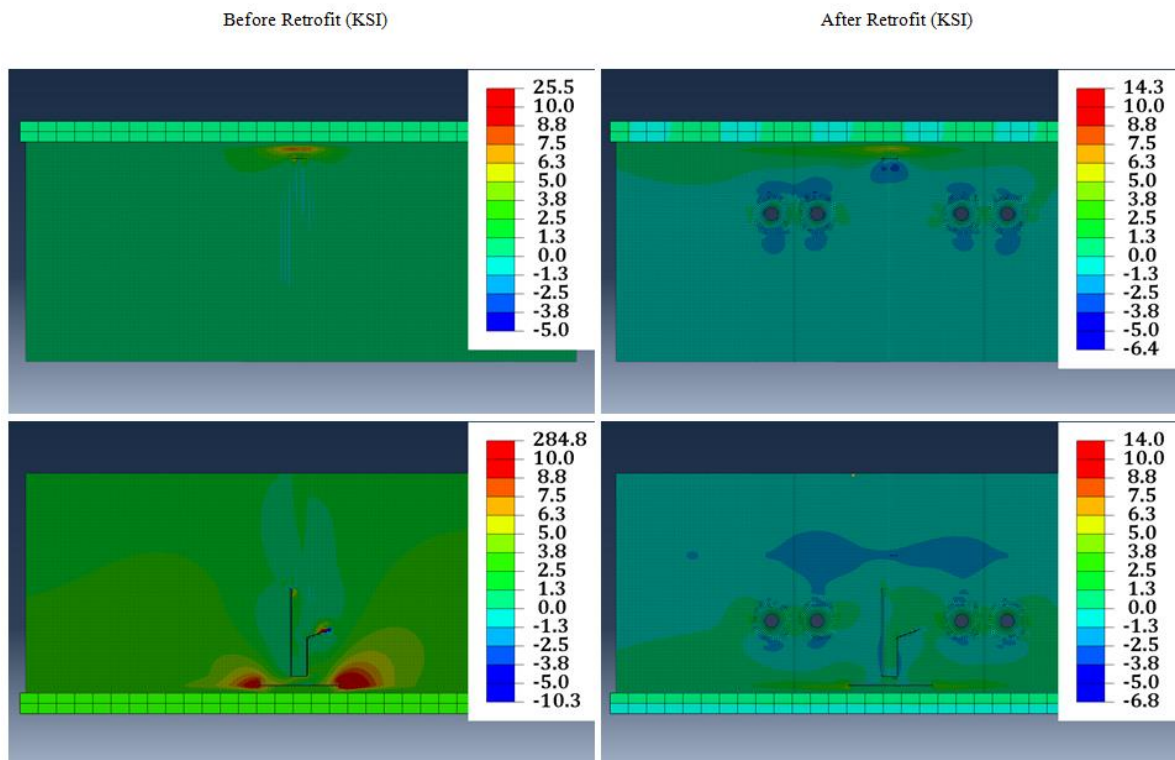


Figure H. 4: Center Truck Load Placement Maximum Principal Web Gap Stresses Before and After Retrofit.

Center – S22 Stiffener Side

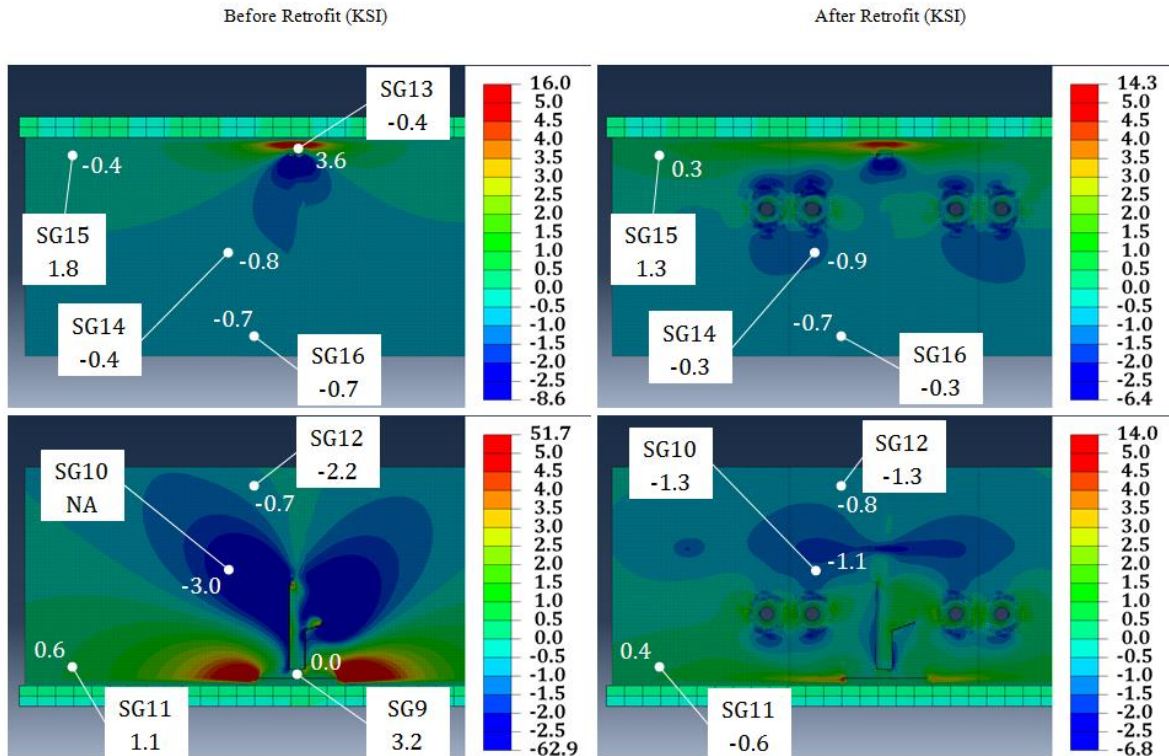
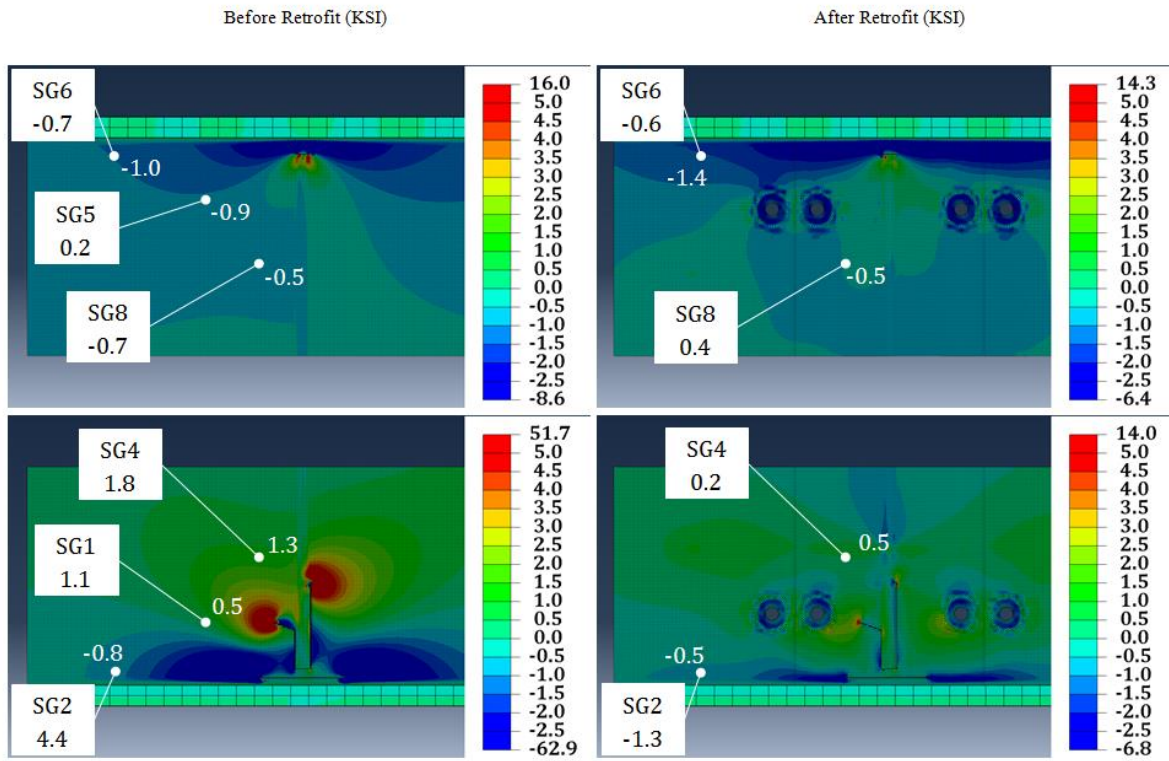


Figure H. 5: Center Truck Load Placement Directional Web Gap Stresses Before and After Retrofit.

Center – S11 Stiffener Side

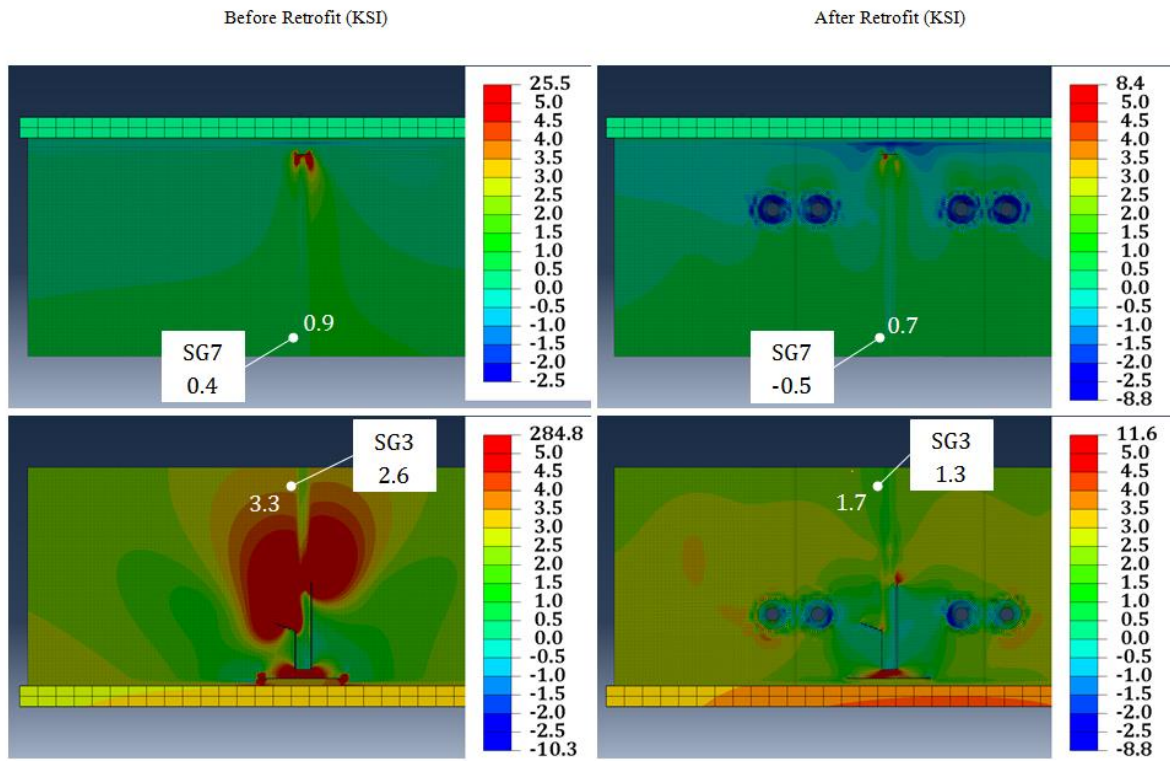
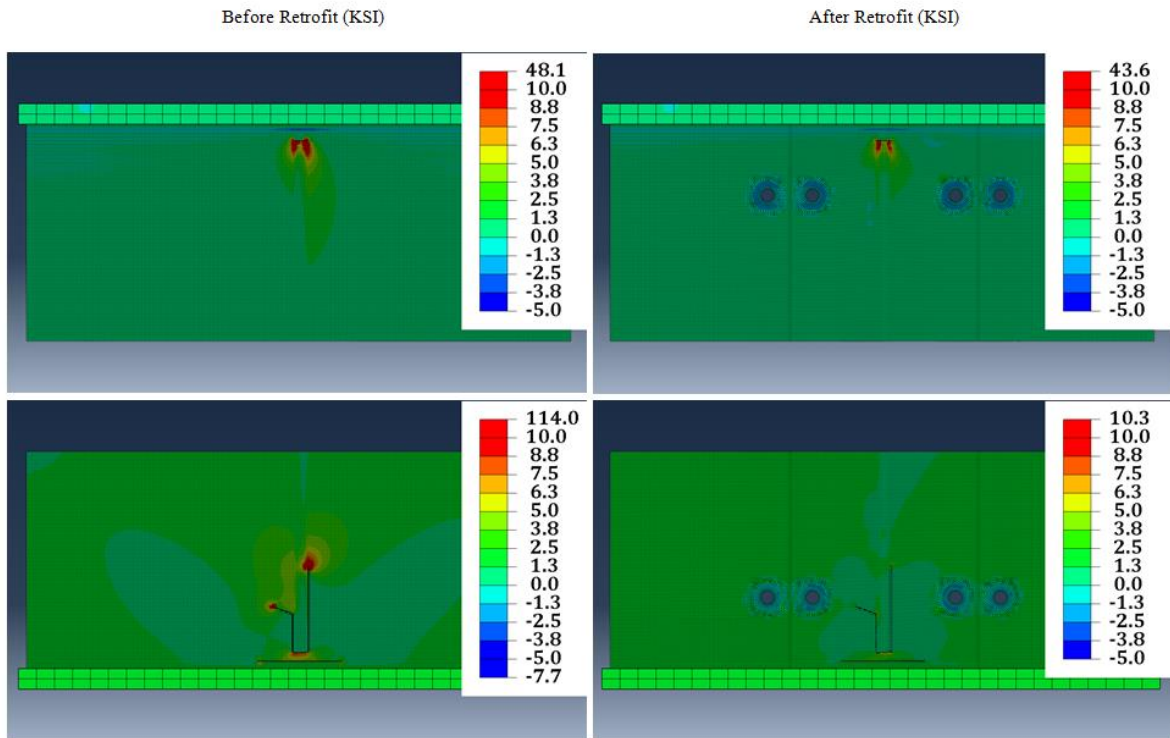


Figure H. 6: Center Truck Load Placement Directional Web Gap Stresses Before and After Retrofit.

East- Max Principal Stiffener Side



East - Max Principal Non-Stiffener Side

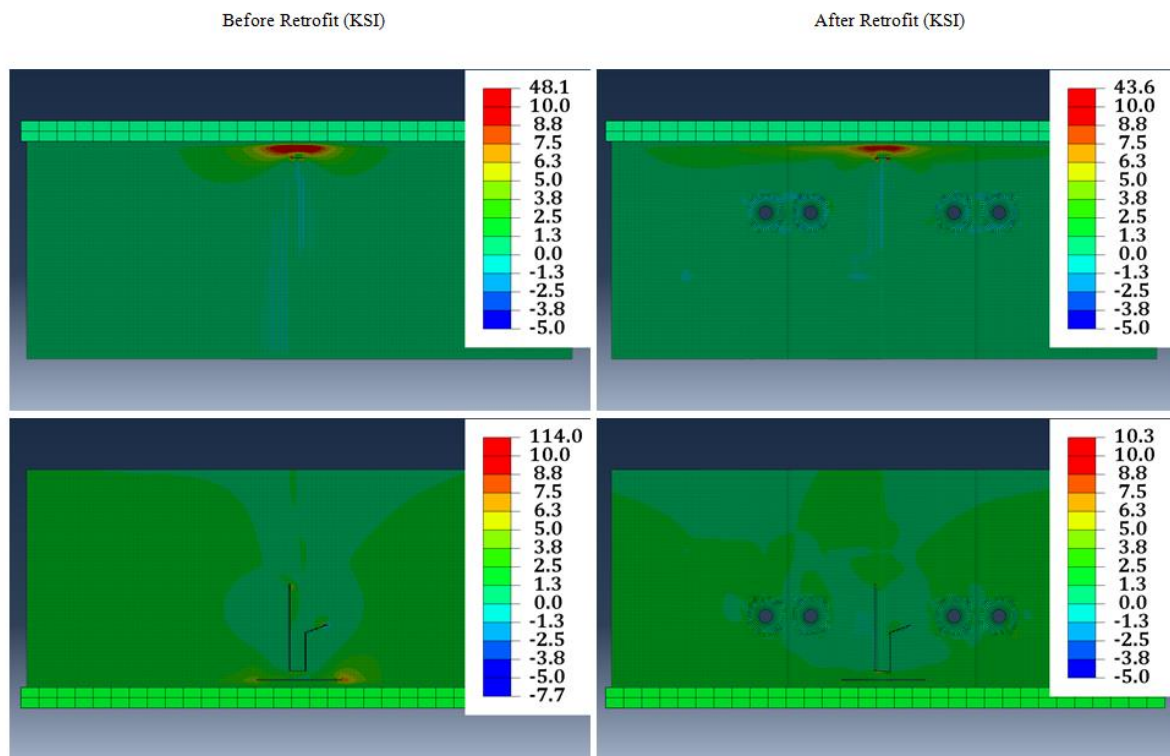
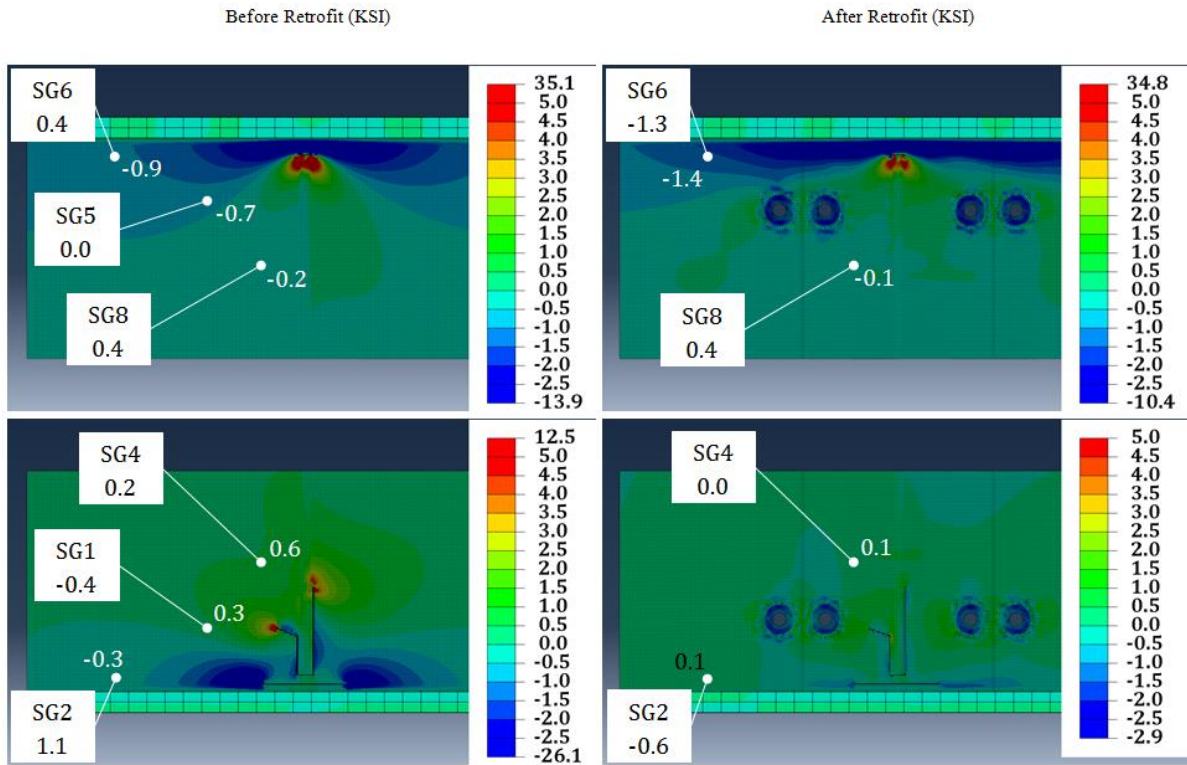


Figure H. 7: East Truck Load Placement Maximum Principal Web Gap Stresses Before and After Retrofit.

East - S22 Stiffener Side



East - S22 Non-Stiffener Side

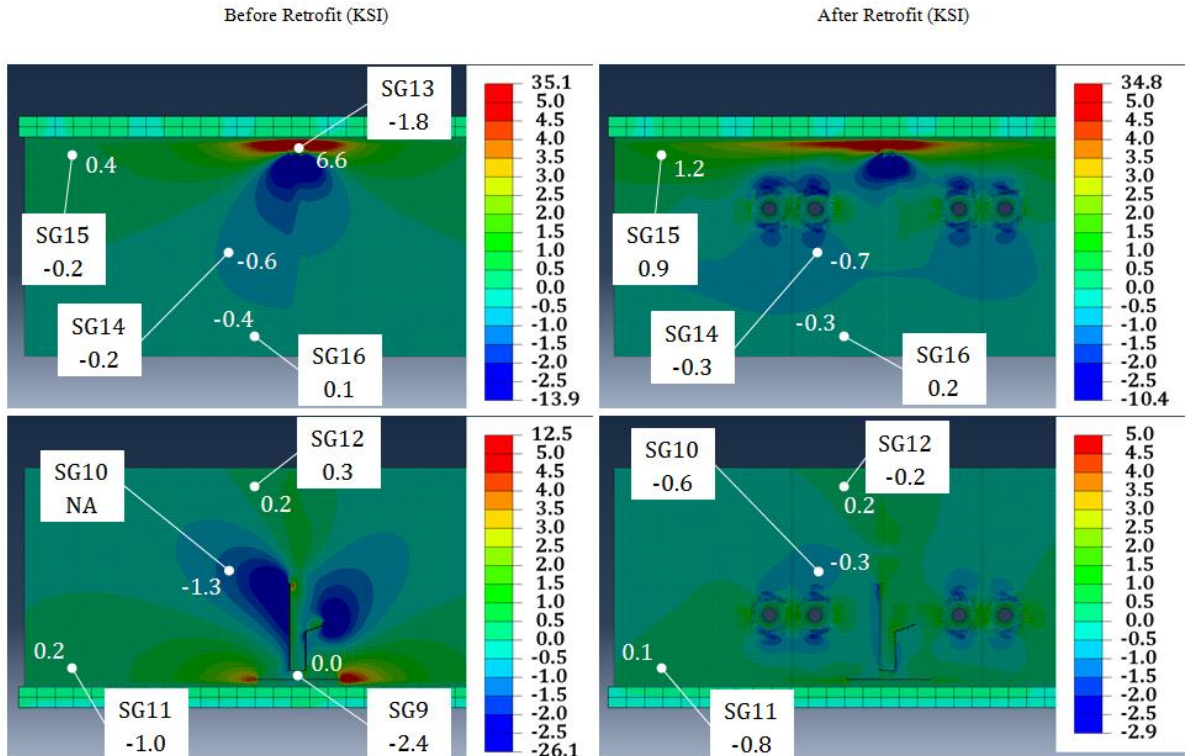


Figure H. 8: East Truck Load Placement Directional Web Gap Stresses Before and After Retrofit.

East – S11 Stiffener Side

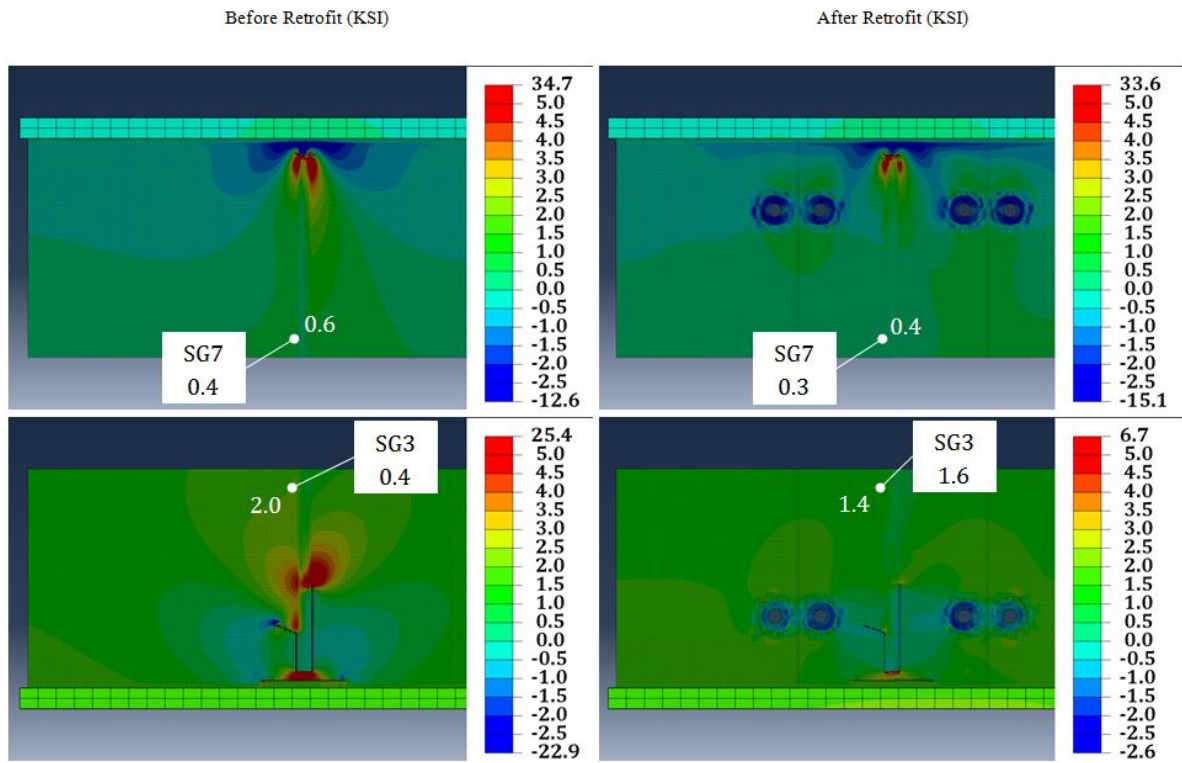


Figure H. 9: East Truck Load Placement Directional Web Gap Stresses Before and After Retrofit.

Top Web Gap Behavior Finite Element Analyses

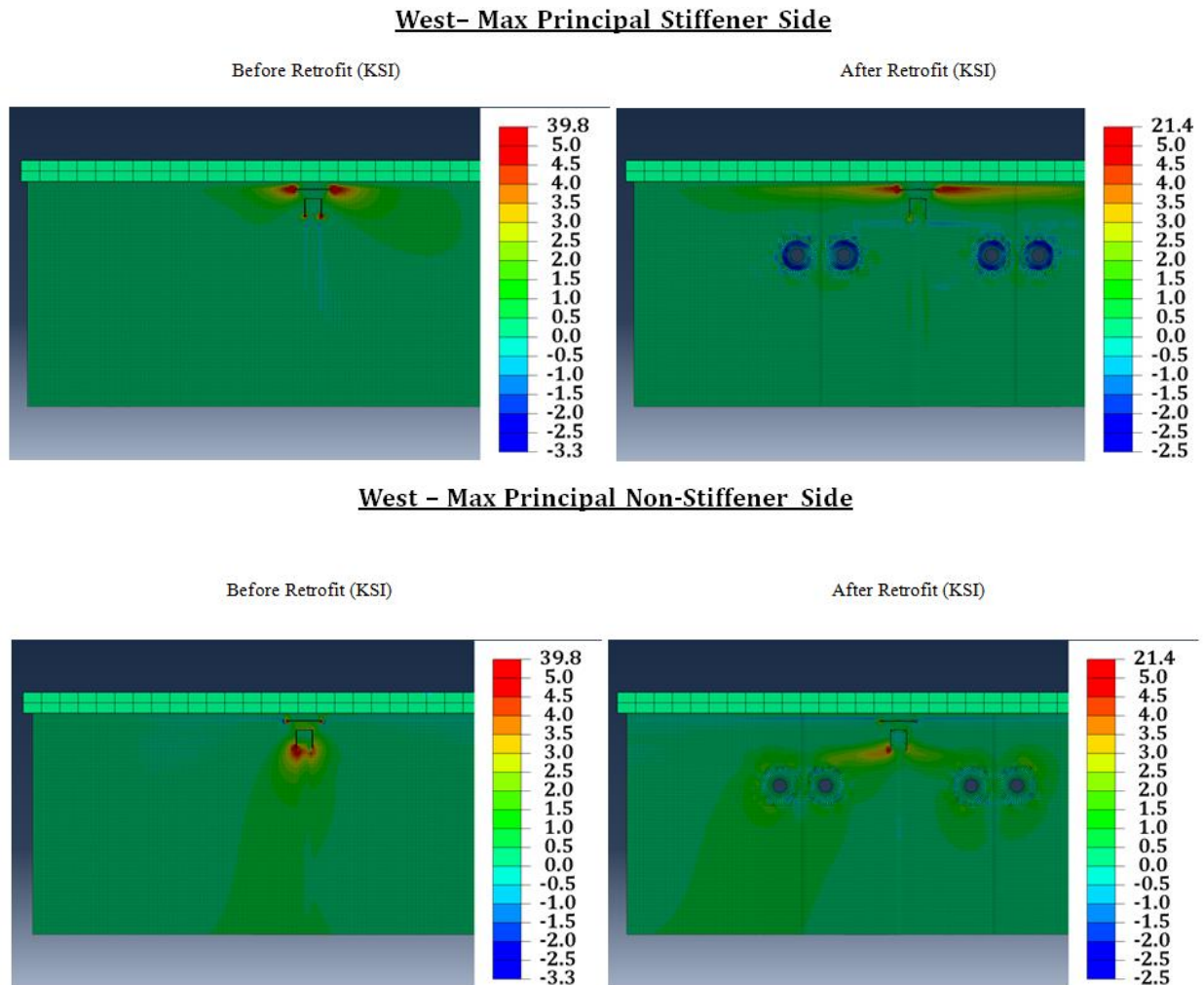
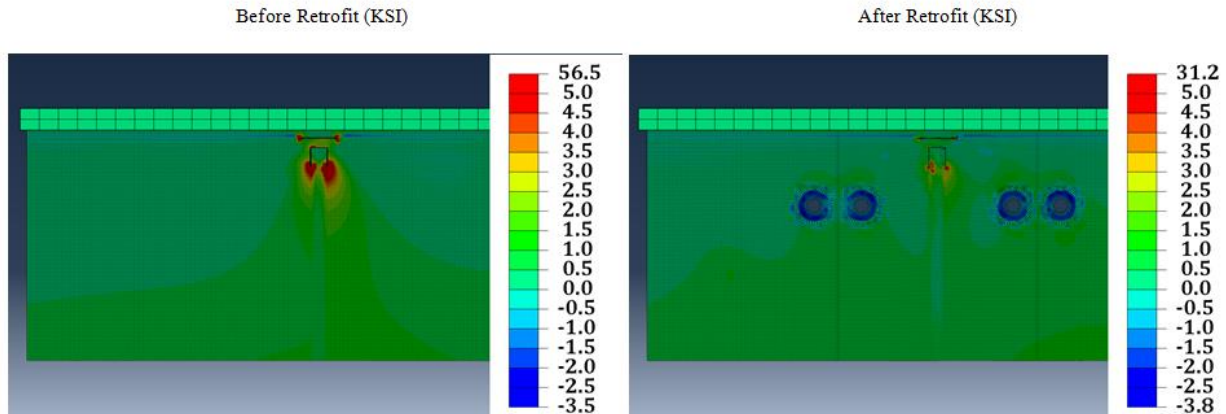


Figure H. 10: Maximum Principal Stresses at Top Web Gap for West Load Truck Placement with Connection Plate-To-Web and Flange-To-Web Weld Cracks Present.

Center- Max Principal Stiffener Side



Center - Max Principal Non-Stiffener Side

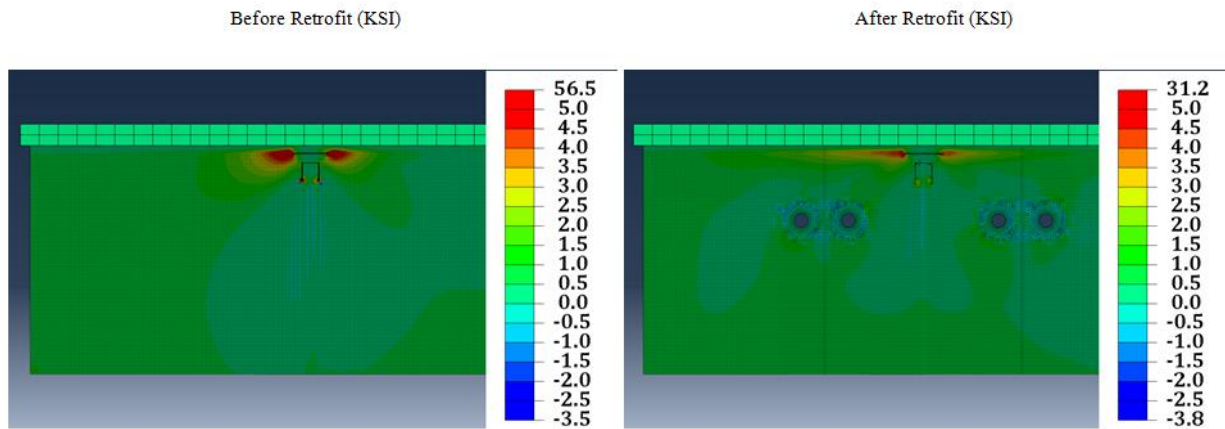
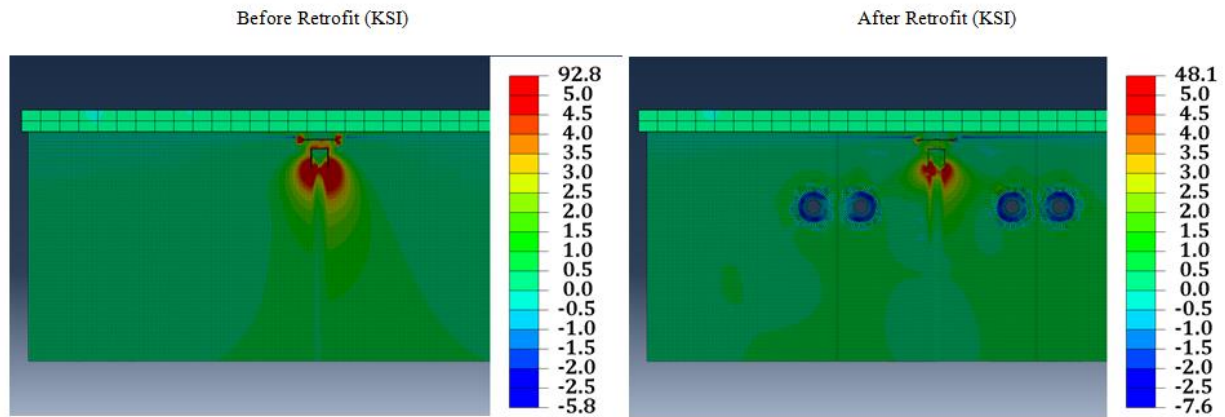


Figure H. 11: Maximum Principal Stresses at Top Web Gap for Center Load Truck Placement with Connection Plate-To-Web and Flange-To-Web Weld Cracks Present.

East- Max Principal Stiffener Side



East - Max Principal Non-Stiffener Side

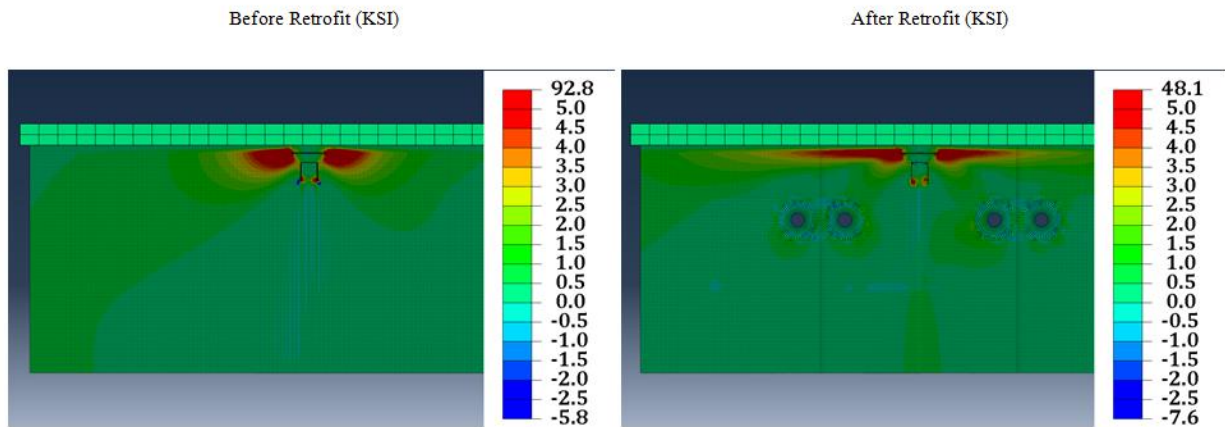
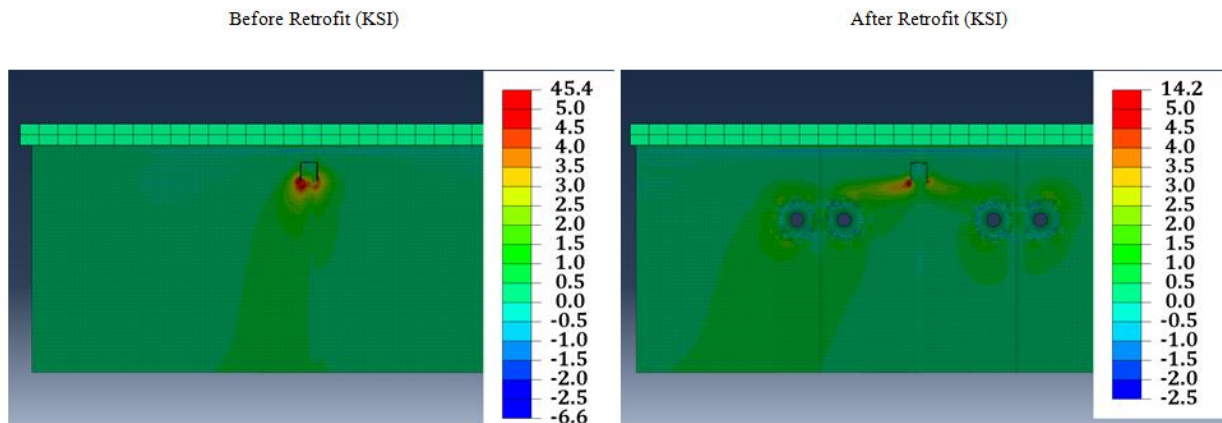
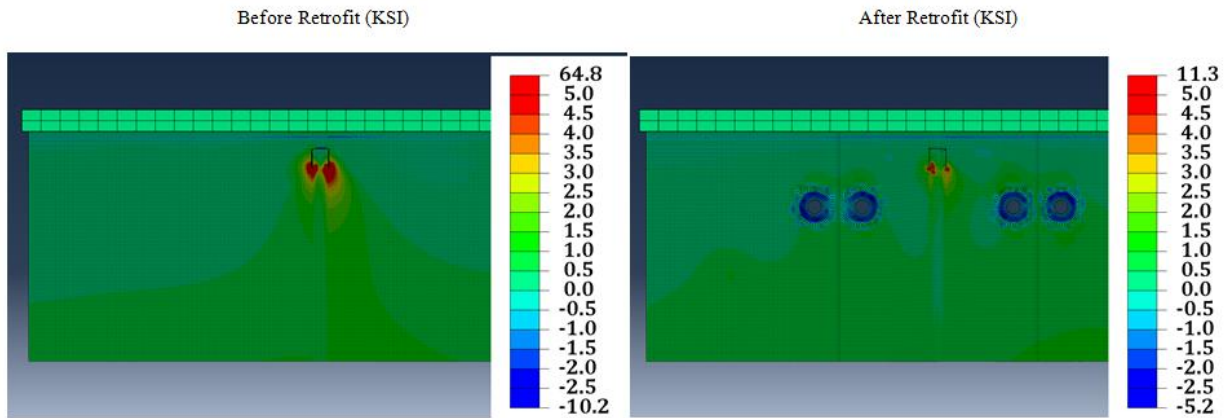


Figure H. 12: Maximum Principal Stresses at Top Web Gap for East Load Truck Placement with Connection Plate-To-Web and Flange-To-Web Weld Cracks Present.

West – Max Principal Non-Stiffener Side



Center– Max Principal Stiffener Side



East– Max Principal Stiffener Side

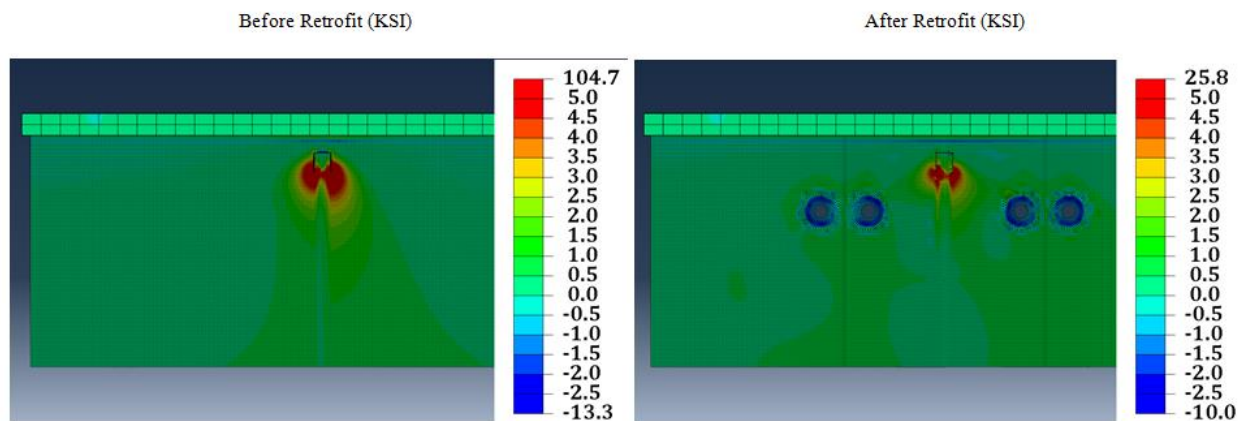
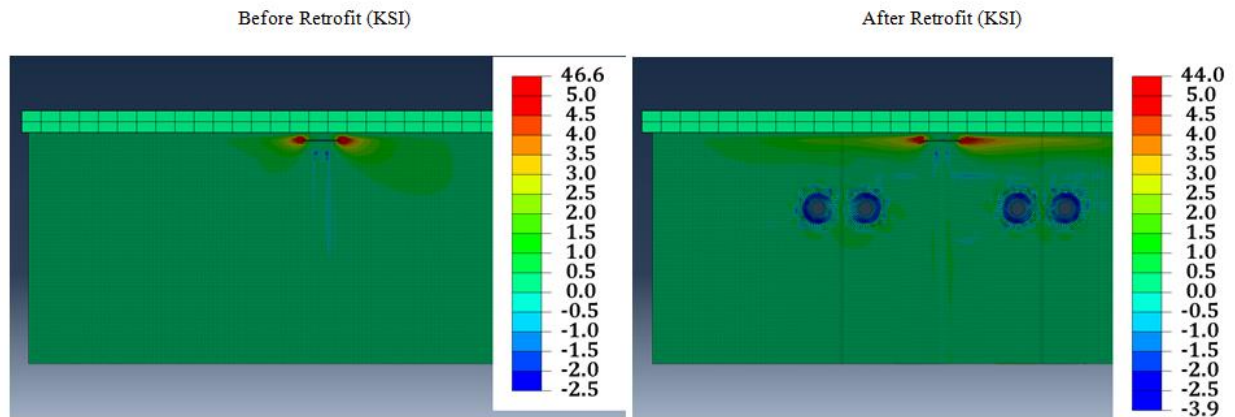
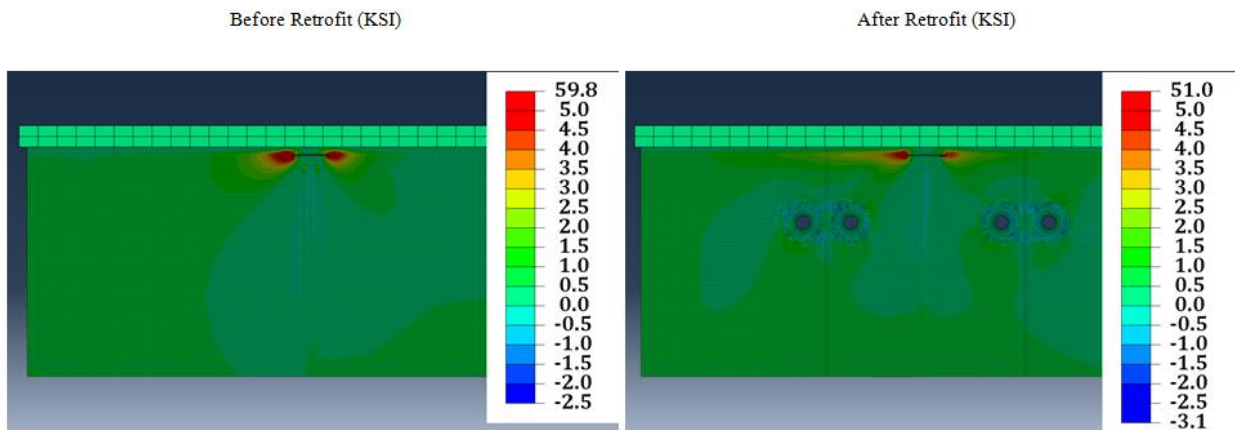


Figure H. 13: Maximum Principal Stresses at Top Web Gap for All Load Truck Placements with Only Connection Plate-To-Web Weld Crack Present.

West- Max Principal Stiffener Side



Center - Max Principal Non-Stiffener Side



East - Max Principal Non-Stiffener Side

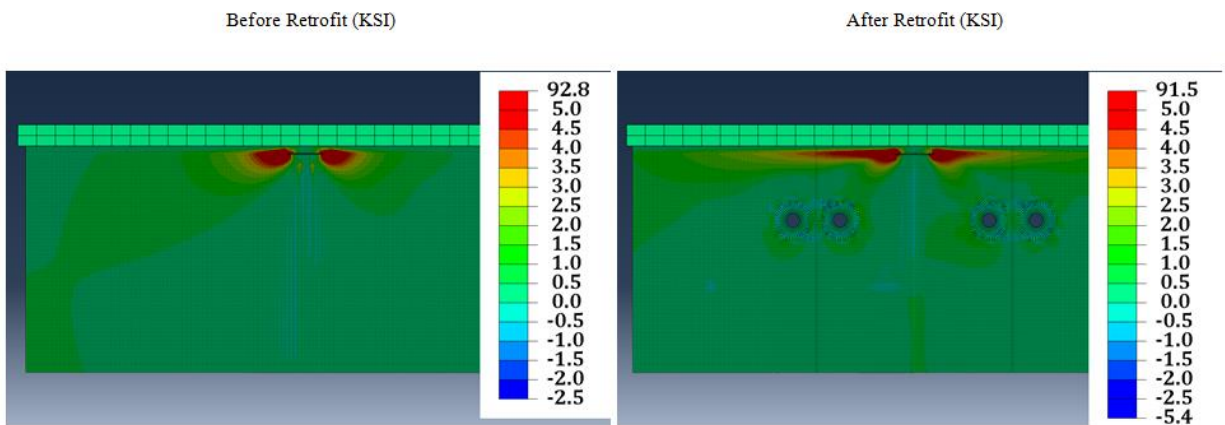


Figure H. 14: Maximum Principal Stresses at Top Web Gap for All Load Truck Placements with Only Flange-To-Web Weld Crack Present.

Appendix References

Nagati, D. (2012). "Repair of Steel Bridge Girders Damaged by Distortion-Induced Fatigue."
Master's Thesis, University of Kansas.